Die approbierte Originalversion dieser Dissertation ist in der Hauptbibliothek der Technischen Universität Wien aufgestellt und zugänglich.
http://www.ub.tuwien.ac.at

The approved original version of this thesis is available at the main library of the Vienna University of Technology.
http://www.ub.tuwien.ac.at/eng

DISSERTATION

Rapid and Controlled Bioorthogonal Ligations and Their Application in Molecular Imaging

ausgeführt zum Zwecke der Erlangung des akademischen Grades eines Doktors der technischen Wissenschaften
unter der Leitung von

Günter Allmaier

E164

Institut für Chemische Technologien und Analytik

eingereicht an der **Technischen Universität Wien**
Fakultät für Technische Chemie

von
Dipl.-Ing. Dennis **Svatunek**, BSc.
0725292
Neustiftgasse 60/2, 1070, Wien

Wien, am 26. November 2016

Scientific progress goes “BOINK”?

Hobbes, Calvin and Hobbes

Contents

Danksagung 1

Highlights 2

Abstract 3

Kurzfassung 5

Aims and Structure of the Thesis 7

Collaborations 8

1 Brief Introduction 9

1.1 Bioorthogonal Ligations 10

1.1.1 Staudinger Ligation 10

1.1.2 Strain-Promoted Alkyne Azide Cycloaddition (SPAAC) 12

1.1.3 Tetrazine Ligations 14

1.2 Bioorthogonal Ligations in PET Imaging 19

1.2.1 Rapid Radiolabeling 19

1.2.2 Pretargeted PET Imaging 21

1.3 Literature 24

2 Results and Discussion 29

2.1 Overview of Contributions 30

I. Strain-Promoted Alkyne Azide Cycloaddition 30

II. Tetrazine Ligation 30

2.2 Context of Contributions 31

I. Strain-Promoted Alkyne Azide Cycloaddition 31

II. Tetrazine Ligations 34

2.3 Conclusion 36

2.4 Literature 37

2.5 Original Works 38

Manuscript #1 39

Manuscript #2 44

Manuscript #3 49

Manuscript #4 72

Manuscript #5 79

Manuscript #6 106

Manuscript #7 113

Manuscript #8 123

3 Statement of Contribution 131

4 Appendix 134

Supporting Information - Manuscript #1 135

Supporting Information - Manuscript #2 146

Supporting Information - Manuscript #3 160

Supporting Information - Manuscript #4 182

Supporting Information - Manuscript #5 215

Supporting Information - Manuscript #6 266

Supporting Information - Manuscript #7 304

Supporting Information - Manuscript #8 339

5 Curriculum Vitae 343

Danksagung

Vielen Dank an meinen Doktorvater, Günter Allmaier, für die Möglichkeit diese Arbeit unter seiner Betreuung im Rahmen des MEIBio Doktoratskollegs durchführen zu können. Ebenfalls Danke an das ganze MEIBio Team, allen voran Martina Marchetti-Deschmann, als Leiterin des Kollegs, sowie den Faculty-Mitgliedern Ulrich Dodt, Herbert Hutter, Bernhard Lendl, Andreas Limbeck, Robert Sablatnig, Gerhard Schütz, Bernhard Seiboth und Christina Streli und vor allen meinen Kollegen Anna Balbekova, Maximilian „Max“ Bonta, Florian Brenner, Jonas Ramoni, Alexander „Ali“ Reismann, Anastasiya Svirkova, Maliheh Assadpour Tehrani und Anna Turyanskaya.

Vielen Dank ebenfalls an meinen Mitbetreuer Johannes Fröhlich für die Unterstützung und die Möglichkeit den Großteil dieser Arbeit in seinem Labor durchführen zu können. Größter Dank an meinen Mentor und auch Freund Hannes Mikula, der mich all die Jahre unterstützt, gefördert und gefordert hat und ohne den ich nicht da wäre wo ich jetzt bin. Vielen Dank auch an die Leute, die diese Arbeit durch ihren Einsatz und ihre harte Arbeit ermöglicht haben, allen voran an meinen Kollegen Christoph Denk sowie den Kooperationspartnern am AIT, Claudia Kunter-Hannes und Thomas Wanek. Bei Nicole „Nici“ Houszka möchte ich mich für die großartige Arbeit und die lustigen Stunden bedanken. Christian Hametner möchte ich für die Unterstützung in den letzten Jahren, vor allem in NMR-Fragen, danken.

Ganz besonders möchte ich mich auch bei meinen Laborkollegen Stefan Kronister, Stefan Lexmüller, Markus Schwarz und Barbara „Babsi“ Sohr für die Unterstützung, das angenehme Arbeitsklima und die vielen lustigen Stunden im „G10“ (und „H18“) und außerhalb bedanken. Den übrigen Mitgliedern der FGHF, Johannes Bintinger, Florian Glöcklhofer, Maximilian Haider, Brigitte Holzer, Ernst Horkel, Thomas Kader, Paul Kautny, Walter Kuba, Thomas Schwartz, Philipp Skrinjar, Julia Weber und Martin Wilkovitsch, danke ich für das angenehme Arbeitsklima und eine schöne gemeinsame Zeit.

Dank gebührt ebenfalls den allgemeinen Mitarbeitern des IAS sowie der TU Wien, im Besonderen Sabine Stiedry, Gerhard Seebauer, Florian Untersteiner, Tanja Halbarth und Jan Zabloudil für all die Dinge ohne die ein reibungsloser Forschungsablauf nicht möglich wäre.

Auch meinen Studienkollegen Felix Biegger, Daniel Bomze, Christoph Gasser, Charlotte „Lilo“ Leeb und Paul Gauss möchte ich an dieser Stelle für die wundervollen Jahre an der TU und die vielen schönen Erinnerungen danken.

Großer Dank geht auch an die österreichische Marshall Plan Foundation für die Möglichkeit eines Forschungsaufenhaltes in den USA. I also want to thank Prof. Joseph Fox for support and the opportunity to work in his lab, Samantha “Sam” Boyd, Robert “Rob” Panish and Natalee Smith for the nice welcome and all the help as well as the whole Fox group, Ram Selvaraj, Han Zhang, Li Yi, Srinvasa “Sri” Chintala, Yinshi Fang, Katarina Rohlfing and Yu Liu, for the nice working atmosphere. Also a big thank you to Zibo Li and his group for the good collaboration.

Meinen Eltern, Rudolf und Margit, möchte ich auf diesem Weg für die letzten 28 Jahre danken. Vielen Dank für eure Unterstützung und dass ihr immer für mich da wart. Ohne euch wäre das Studium und diese Arbeit nicht möglich gewesen. Vielen Dank auch an meine Schwester Nadine für die Unterstützung in den letzten Jahren.

Highlights

I. Strain-Promoted Alkyne Azide Cycloaddition

1. Investigations on the kinetics of strain-promoted alkyne azide cycloadditions
2. Investigation of small, ^{18}F-labeled alkylazides for *in vivo* chemistry and rapid radiolabeling

II. Tetrazine Ligation

1. Development of fluorine-18 and carbon-11 labeled tetrazines for pretargeted PET imaging and rapid radiolabeling
2. Rapid radiolabeling using an ultrafast tetrazine *trans*-cyclooctene ligation
3. Development of a low-cost setup for efficient photoisomerization of *cis*-cyclooctenes to *trans*-cyclooctenes

Abstract

Bioorthogonal reactions are powerful tools for the formation of covalent linkages, even in complex systems like living organisms, and have found applications in fields ranging from material sciences to biological chemistry. Important characteristics of such reactions are the (metabolic) stability of reactants and the products, high selectivity of the reactants towards each other, and high reactivity. This is of particular interest, since reactions in biological environments are commonly performed at very low concentration, especially in the case of radiolabeled probes. High reaction rates ensure good yields within an appropriate time span. While several of those reactions have been introduced only two are commonly used: (1) strain-promoted alkyne azide cycloadditions (SPAACs), and (2) tetrazine ligations. This thesis focuses on the kinetics of those two reactions and their application in pretargeted PET-imaging.

Due to the ring strain of cyclooctynes a Huisgen-cycloaddition with azides can be performed at room temperature without any catalyst. These strain-promoted alkyne azide cycloadditions show high reaction rates with second order rate constants of up to 4 $M^{-1}s^{-1}$. In the last decade several improvements of the kinetics of this reaction were achieved, mainly through structural alterations of the cyclooctyne. Only few studies were conducted focusing on the influence of different azides in SPAACs.

Within this thesis NMR kinetic experiments were conducted to study the influence of primary, secondary and tertiary aliphatic azides on the reaction rates with different cyclooctynes. It could be shown that tertiary azides show a significantly lower reactivity with steric demanding cyclooctynes compared with both primary and secondary azides. A computational study on these systems confirmed that this lower reactivity is caused by steric effects. Kinetics of SPAACs are usually assessed by NMR experiments, and solvents are therefore limited to deuterated substances. As part of this thesis a new method was developed that enables the measurement of strain-promoted alkyne azide cycloadditions under more complex reaction conditions and even in biological media like human blood plasma, using an in-line ATR-IR probe in combination with a custom made reaction vessel.

Bioorthogonal reactions are of high interest in the field of radiochemistry. To achieve rapid radiolabeling bioorthogonal ligations are used for fast and clean attachment of a radioisotope to the tracer molecule by using a radiolabeled bioorthogonal reagent. In pretargeted imaging approaches a non-radiolabeled marker molecule bearing a bioorthogonal reactive group is first administered in vivo. After accumulation in target tissue a radiolabeled compound with the complementary bioorthogonal reactive group is used as a secondary agent, which selectively reacts with the pre-administered marker forming a stable covalent linkage. This allows for prolonged accumulation of marker molecules in target tissue while using short-lived radioisotopes for imaging.

Several ^{18}F-labeled low-molecular-weight alkylazides were prepared and evaluated in regards to their suitability as secondary agents in pretargeted PET imaging. However, these compounds were not sufficiently stable *in vivo* but were shown to be useful and versatile reagents for rapid radiolabeling applications.

Due to the extremely low concentrations as used in the field of radiochemistry the tetrazine ligation is considered to be superior over SPAAC, since second order rate constants of up to 3 000 000 $M^{-1}s^{-1}$ can be reached. 1,2,4,5-Tetrazines react with strained dienophiles, such as *trans*-cyclooctenes, in an inverse electron-demand Diels-Alder cycloaddition, followed by a retro Diels-Alder reaction forming dihydropyridazines.

The ultrafast reaction between a conformationally strained *trans*-cyclooctene and tetrazines was utilized to develop a method for rapid radiolabeling of a tetrazine-tagged RGD-peptide using an ^{18}F-labeled *trans*-cyclooctene. This strategy afforded imaging probes with improved metabolic stability and pharmacokinetic properties compared to previously developed and reported rapid radiolabeling or direct labeling strategies, resulting in prolonged blood circulation and thus better accumulation.

Furthermore, several radiolabeled tetrazines for pretargeted PET imaging and rapid radiolabeling were prepared and evaluated. Computational investigations of the kinetics of tetrazine ligations suggested, that the combination of less reactive dialkyltetrazines and highly reactive *trans*-cyclooctenes leads to reaction rates similar to the commonly used combination of highly reactive tetrazines and less reactive

trans-cyclooctenes. However, while highly reactive tetrazines are not sufficiently stable under commonly used direct ^{18}F-labeling conditions the use of dialkyltetrazines allows for effective radiolabeling and led to the development of the first reported ^{18}F-tetrazine. This secondary agent showed promising *in vivo* stability and homogeneous biodistribution. On the basis of these results several second generation ^{18}F-labeled tetrazines with improved Diels-Alder reactivity were developed. In addition, an ^{11}C-labeled tetrazine based on a similar dialkyl scaffold could be prepared and successfully used in a pretargeted PET imaging experiment using *trans*-cyclooctene-tagged mesoporous silica nanoparticles that were shown to accumulate in the lungs (Figure 1).

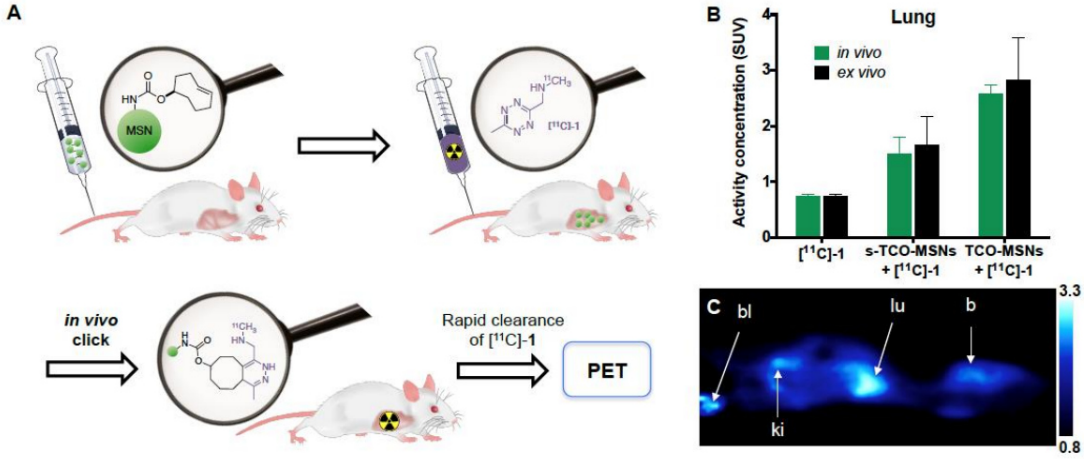

Figure 1: Pretargeted PET imaging using TCO-modified silica nanoparticles and an ^{11}C-tetrazine. Taken with permission from Bioconjugate Chem. 2016, 27, 1707–1712, Copyright 2016 American Chemical Society.

Furthermore, a low-cost flow setup for photoisomerization of *cis*-cyclooctenes to *trans*-cyclooctenes, the most commonly used dienophiles for tetrazine ligation, was designed and characterized.

In summary, valuable insights in the kinetics of the two most common bioorthogonal ligations were obtained, and new analytical and computational methods for monitoring these reactions and predicting reactivities, respectively, were developed. These ligations were also successfully used in the field of radiochemistry leading to new radiolabeled tetrazines for pretargeted PET imaging and new methods for rapid radiolabeling.

Kurzfassung

Bioorthogonale Reaktionen ermöglichen die Bildung kovalenter Bindungen in hochkomplexen Umgebungen wie etwa lebenden Organismen und haben daher breite Anwendung in vielen Bereichen der Wissenschaft gefunden. Derartige Reaktionen müssen hochselektiv ablaufen und die Reaktionspartner sowie das Produkt müssen hohe Stabilität aufweisen. Des Weiteren sind hohe Reaktionsgeschwindigkeiten vorteilhaft und teilweise sogar essentiell, da speziell in biologischen Umgebungen die Konzentration der Reaktanden stark limitiert ist. Eine hohe Reaktionsgeschwindigkeit gewährleistet, dass ein ausreichender Umsatz in kurzer Zeit erreicht werden kann. Während in den letzten Jahren mehrere bioorthogonale Reaktionen entwickelt wurden, finden nur zwei Varianten breite Anwendung: (1) die *strain-promoted alkyne azide cycloaddition* (SPAAC; Deutsch: durch Ringspannung begünstigte Alkin-Azid Cycloaddition) und (2) Tetrazin-Ligationen. Der Fokus dieser Arbeit liegt auf der kinetischen Untersuchung dieser beiden Reaktionen, der Beschreibung bislang unbekannter Selektivitäten sowie Anwendungen bioorthogonaler Chemie im Bereich der Radiochemie, im speziellen der zweistufigen Bildgebung mittels Positronen-Emissions-Tomographie (PET).

Als SPAAC-Reaktionen versteht man Huisgen-Cycloadditionen zwischen Cyclooctinen und organischen Aziden zu 1,2,3-Triazolen. Aufgrund der hohen Ringspannung der Cyclooctine laufen diese Reaktionen auch ohne Verwendung eines Katalysators bei Raumtemperatur mit beachtlichen Geschwindigkeitskonstanten zweiter Ordnung von bis zu 4 $M^{-1}s^{-1}$ ab. Große Anstrengungen zur Verbesserung dieser Reaktion, vor allem in Bezug auf die Reaktionsgeschwindigkeit, wurden unternommen, wobei jedoch hauptsächlich strukturelle Veränderungen des Cyclooctins untersucht wurden. Der Einfluss struktureller Eigenschaften des Azids auf die Reaktionsgeschwindigkeit und Selektivität von SPAAC-Reaktionen wurde nur in wenigen Studien untersucht.

Mit dem Ziel den Einfluss unterschiedlicher Azide besser beschreiben zu können, wurde die Kinetik von SPAAC-Reaktionen primärer, sekundärer und tertiärer Azide mit verschiedenen Cyclooctinen untersucht. Im Gegensatz zu primären als auch sekundären Aziden konnte festgestellt werden, dass die Reaktion von tertiären Aziden mit sterisch anspruchsvollen Cyclooctin-Derivaten mit signifikant geringerer Reaktionsgeschwindigkeit abläuft –. Dieses Verhalten wurde anschließend mittels quantenchemischer Berechnungen untersucht, wobei festgestellt werden konnte, dass die erniedrigte Reaktivität in der Tat auf sterische Effekte zurückzuführen ist.

Die kinetische Untersuchung von SPAAC-Reaktionen wird üblicherweise mittels ^{1}H-NMR Methoden durchgeführt, was jedoch zu einer starken Limitierung der zu untersuchenden Reaktionsbedingungen führt, da ausschließlich deuterierte Lösungsmittel ohne zusätzliche Additive verwendet werden können. Reaktionskinetische Untersuchungen unter komplexen Bedingungen können auf diese Weise nicht durchgeführt werden. Im Rahmen dieser Arbeit ist es gelungen, eine neuartige Methode basierend auf ATR/IR-Messungen zu entwickeln, welche die Untersuchung von SPAAC in komplexen und auch biologischen Medien, bis hin zu humanem Blutplasma, ermöglicht.

Bioorthogonale Reaktionen sind von großem Interesse für die Entwicklung neuer Methoden im Bereich der Radiomarkierung und Positronen-Emissions-Tomographie. Die hohe Reaktionsgeschwindigkeit und Selektivität bioorthogonaler Chemie ermöglichen die Entwicklung von Methoden im Bereich „Rapid Radiolabeling“ (Deutsch:.schnelle Radiomarkierung) Des Weiteren ist eine bioorthogonale *in vivo* Ligation entscheidend für Anwendungen im Bereich „Pretargeted Imaging“ (Deutsch: vormarkierte Bildgebung). Dieses zweistufige Verfahren zur Bildgebung stellt eine äußerst vielsprechende Methode für diagnostische Anwendungen dar. Hierbei wird in einem ersten Schritt ein nicht radiomarkierter Marker verabreicht, der mit einer bioorthogonal reaktiven Gruppe modifiziert ist. Nach Anreicherung dieses Markers im Zielgewebe wird in einem zweiten Schritt ein radiomarkiertes Agens verabreicht, welches eine komplementäre bioorthogonal reaktive Gruppe trägt und nun *in vivo* an den zuvor angereicherten Marker bindet. Dies erlaubt die Verwendung von kurzlebigen Radioisotopen für die Bildgebung und Lokalisation von langsam akkumulierenden Wirkstoffen und Substanzen.

Im Rahmen dieser Arbeit konnten mehrere ^{18}F-markierte Alkylazide hergestellt werden, welche auf ihre Eignung als sekundäres Agens für die zweistufige Bildgebung mittels PET untersucht sowie erfolgreich für Rapid Radiolabeling angewendet wurden.

Aufgrund der üblicherweise geringen Konzentrationen bei der Herstellung und Anwendung von Radiopharmazeutika wird die Tetrazin Ligation im Vergleich zu SPAAC bevorzugt angewendet, da bei Reaktionen mit gespannten Dienophilen wesentlich höhere Reaktionsgeschwindigkeiten von bis zu 3 000 000 $M^{-1}s^{-1}$ erreicht werden können. Das Tetrazin reagiert hierbei mit einem gespannten Cycloocten, üblicherweise ein *trans*-Cyclooctenderivat, in einer Diels-Alder Cycloaddition gefolgt von einer Retro-Diels-Alder Reaktion (Cycloreversion) zu einem stabilen Dihydropyridazin.

Die extrem schnell ablaufende Reaktion zwischen gespannten *trans*-Cyclooctenen und Tetrazinen wurde genutzt, um ein neues Verfahren für die Radiomarkierung von Proteinen zu entwickeln. Hierbei wurde die Reaktion eines Tetrazin-markierten RGD-Peptids mit einem radiomarkierten *trans*-Cycloocten (TCO) verwendet, um innerhalb weniger Minuten ^{18}F-markierte RGD-Peptide zu erzeugen, welche im Vergleich mit direkt markierten oder mit zuvor beschriebenen Methoden hergestellten Radio-Peptiden verbesserte *in vivo* Eigenschaften aufweisen.

Des Weiteren konnten mehrere radiomarkierte Tetrazine für die Radiomarkierung sowie die bioorthogonale zweistufige Bildgebung mittels PET hergestellt und evaluiert werden. Theoretische Studien zeigten, dass mit der Kombination aus relativ weniger reaktiven Dialkyltetrazinen und hochreaktiven *trans*-Cyclooctenen ähnliche Reaktionsgeschwindigkeiten erreicht werden können wie mit üblicherweise angewendeten hochreaktiven Tetrazinen in Kombination mit weniger reaktiven *trans*-Cyclooctenen. Dieser reaktionskinetische Kompromiss ermöglichte die Verwendung von stabileren Tetrazinen, welche mittelsdirekter Radiofluorierung mit ^{18}F modifiziert werden konnten. Dies führte zum ersten bekannten ^{18}F-markierten Tetrazin. Dieses sekundäre Agens zeigte vielversprechende *in vivo* Eigenschaften wie hohe Stabilität und homogene Biodistribution und stellt daher einen wichtigen Meilenstein auf dem Weg zu neuen diagnostischen Methoden dar. Basierend auf diesen Resultaten konnte eine Reihe weiterer ^{18}F-markierten Tetrazine entwickelt werden, wobei die Reaktivität des Tetrazins durch Optimierung der Methode zur Radiofluorierung schrittweise erhöht werden konnte. Darüber hinaus wurde ein Kohlenstoff-11 markiertes Tetrazin entwickelt, welches ebenfalls auf einem Dialkyltetrazin Grundgerüst aufbaut. Dieses wurde erfolgreich in einem ersten Modell-Experiment zur zweistufigen Bildgebung mittels PET angewandt.Dazu wurden *trans*-Cycloocten derivatisierte Nanopartikel verwendet, welche durch bioorthogonale *in vivo* Reaktion mit dem erwähnten ^{11}C-Tetrazin visualisiert werden konnten (Abbildung 1).

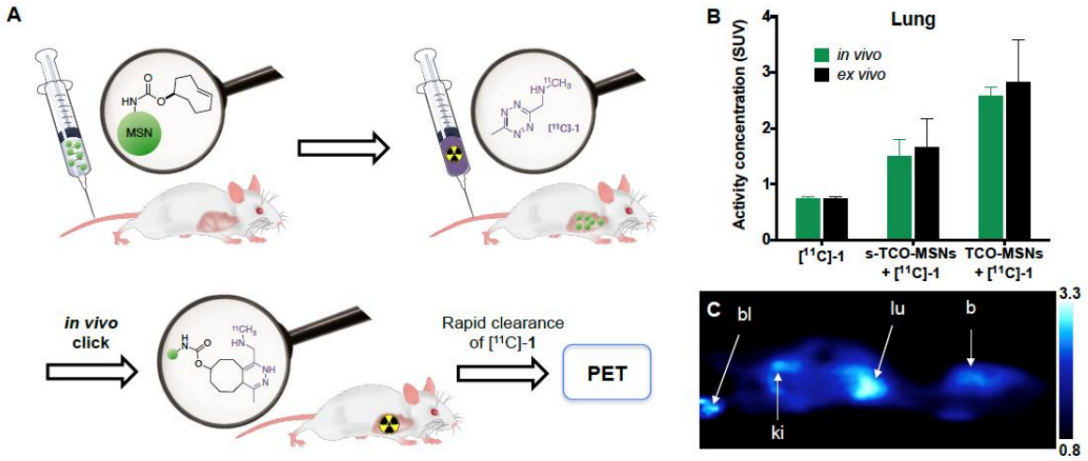

Abbildung 1: Zweistufige Bildgebung mittels PET unter Verwendung von *trans*-Cycloocten derivatisierten Nanopartikel (welche sich in der Lunge anreichern) und eines ^{11}C-markierten Tetrazins. Mit Erlaubnis von Bioconjugate Chem. 2016, 27, 1707–1712, Copyright 2016 American Chemical Society.

Im Rahmen dieser Arbeit konnte zudem ein Photoflussreaktor entwickelt werden, welcher die kostengünstige Photoisomerisierung von *cis*-Cyclooctenen erlaubt, um auf diese Weise eine Vielzahl von TCO-Verbindungen herstellen zu können.

Zusammenfassend konnte die Kinetik der zwei herausragendsten bioorthogonaler Reaktionen auf vielfältige Weise untersucht und signifikante neue Erkenntnisse gewonnen werden. Basierend auf diesen Resultaten konnten bioorthogonale Ligationen erfolgreich angewendet werden, um neue Methoden in den Bereichen Rapid Radiolabeling und Pretargeted PET Imaging zu entwickeln.

Aims and Structure of the Thesis

The main objective of this doctoral research was the investigation of the reactivity and kinetics of the two most commonly used bioorthogonal ligations and their use in the development of bioorthogonal tools for molecular imaging, in particular for positron emission tomography.

This thesis is written as a cumulative work and consists of two parts: (1) a brief introduction to the overall topic and (2) the main part including original works (manuscripts #1 to #8, already published, submitted or in preparation). Supporting information of these manuscripts can be found in the Appendix of the thesis and contains most of the experimental details and data.

The applicant (D. Svatunek) is first author of 3 and co-author of 5 of these publications. 3 Manuscripts were written and composed predominantly by D. Svatunek. Contributions of the applicant to the other manuscripts were manifold and essential for successful completion of the respective research projects.

The thesis is thematically divided into two main topics:

I. Strain-Promoted Alkyne Azide Cycloaddition and
II. Tetrazine Ligation.

Topic I consists of: (1) the investigation of the reactivity of secondary and tertiary azides in the strain-promoted alkyne azide cycloaddition (SPAAC), which can be used to control reactions in a semiorthogonal manner, and (2) the development of a method to investigate SPAAC reactivities by ATR-IR, even in complex media like human blood plasma. In addition, investigations on small ^{18}F-labeled alkyl azides have been carried out. These click agents can be used for rapid radiolabeling via SPAAC.

The focus of topic II was the use of tetrazine ligations the development of radiopharmaceutical methods. Several new radiolabeled tetrazines were developed and investigated towards reactivity and *in vivo* behavior. Furthermore, a system for rapid radiolabeling featuring highly reactive s-TCO was developed, pushing the limits of reactivity and allowing extremely short reaction times in radiolabeling. In addition, a simple and cheap system for the photoisomerization of cyclooctenes was introduced.

Collaborations

The following collaborations were essential for a successful completion and the scientific outcome of this PhD thesis:

- PD Dr. Claudia Kuntner-Hannes, Dr. Thomas Wanek, Austrian Institute of Technology (AIT), Biomedical Systems, Forschungscenterstraße 1, 2444 Seibersdorf, Austria
- Prof. Joseph M. Fox, University of Delaware, Department of Chemistry and Biochemistry, 272 Lammot Dupont Laboratory, Newark, DE 19715, USA
- Assoc. Prof. Zibo Li, University of North Carolina School of Medicine, Biomedical Research Imaging Center, Department of Radiology, 125 Mason Farm Road, Chapel Hill, NC 27599, USA

1 Brief Introduction

1.1 Bioorthogonal Ligations

Bioorthogonal ligations are reactions that proceed selectively even in highly complex environments, like living organisms forming covalent linkages. Therefore, both reaction partners need to exhibit exceptional high selectivity towards each other. Furthermore, the reaction partners, and the ligation products need to be reasonable stable under *in vivo* conditions and not interfere with the bio-chemical systems in any form, reasoning the term 'bioorthogonality'.

Since their first introduction by Saxon and Bertozzi in 2000, who used a modified Staudinger reaction for ligation of biotin to glycans,[1] several bioorthogonal ligations have been introduced.[2–7] The two most prominent ones are the strain-promoted alkyne azide cycloadditions (SPAAC) and the group of tetrazine ligations.

Due to the low concentrations usually present in biological environments high reaction rates are mandatory. Known bioorthogonal reactions show rates from 0.001 $M^{-1}s^{-1}$ as reported for the Staudinger ligation up to several million $M^{-1}s^{-1}$ as reported for the tetrazine ligation, spanning a range of reactivity of over nine orders of magnitude.[8,9]

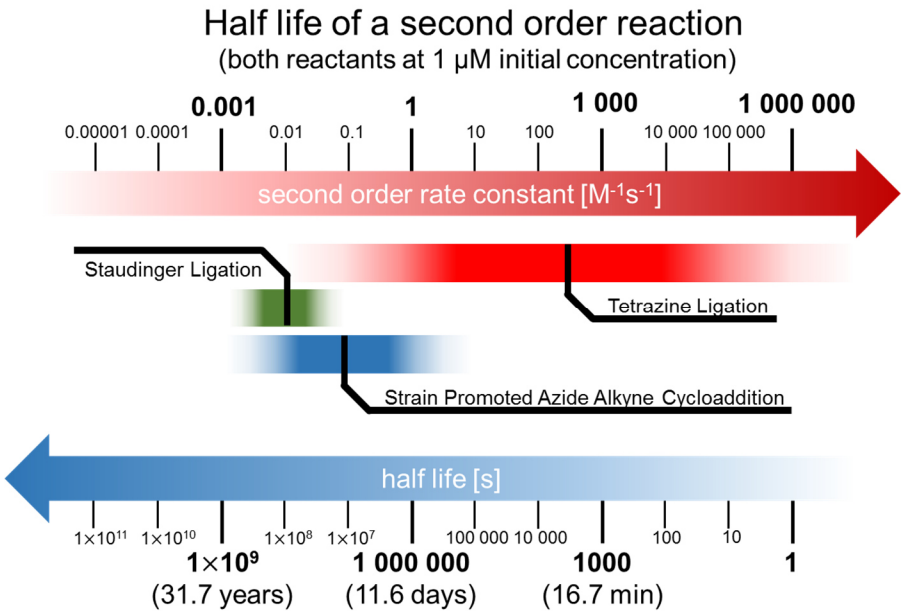

Figure 1: Relationship between second order rate constants and half-life at 1 µM concentration

To highlight the importance of high reactivity at low concentrations Figure 1 shows the relationship between second order rate constant and first half-life of these reactions with both reagents at 1 µM concentration. In addition, the ranges of second order rate constants of the three most prominent bioorthogonal ligations are outlined.

1.1.1 Staudinger Ligation

The Staudinger Ligation is based on the Staudinger reaction, which is the reaction between a phosphine, usually triphenylphosphine, and an azide, forming an iminophosphorane in the first step.[10] After hydrolysis an amine and a phosphine oxide are obtained (Scheme 1).

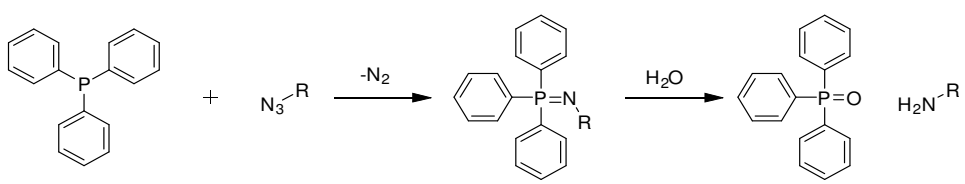

Scheme 1: Staudinger reaction

The nitrogen in the iminophosphorane is highly nucleophilic. This is used in the Staudinger ligation where an ester is introduced, usually directly attached to the substituents of the phosphine, which is attacked by the nitrogen.[1] After hydrolysis a stable amide bond between both reagents is formed.

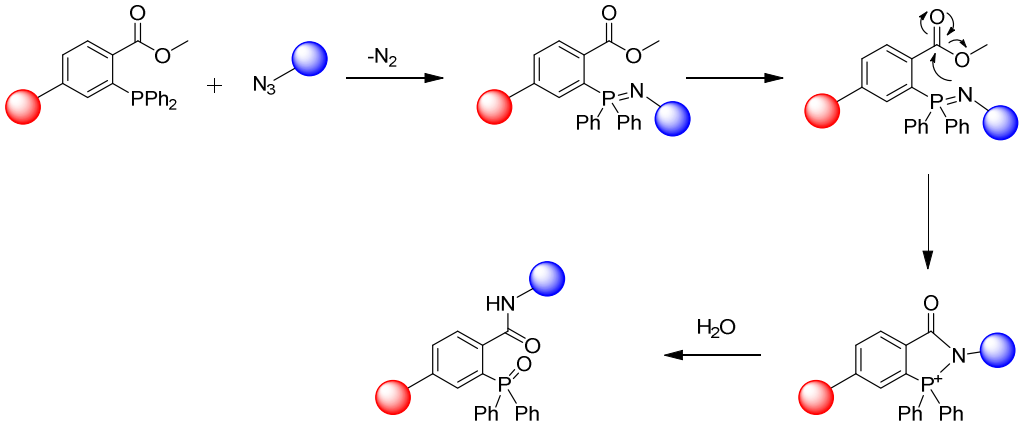

Scheme 2: Mechanism of the Staudinger ligation

The big disadvantage of this ligation is the presence of the large triphenylphosphine oxide structure in the product. To tackle this problem, the so-called traceless staudinger ligation was developed.[11] In this modified version a native amide bond can be formed. Therefore, phosphines like diphenylphosphinemethanethiol are used. The bioorthogonal reagent is first synthesized by acylation forming the thioester also called Raines ligation reagent. This is then used in a Staudinger reaction with an azide. After hydrolysis the phosphine oxide moiety is cleaved off.

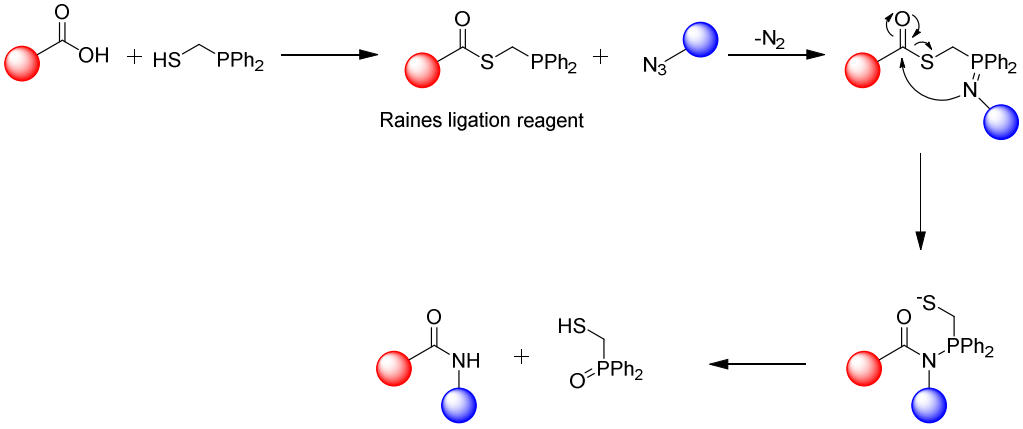

Scheme 3: Traceless Staudinger ligation

The Staudinger ligation was used in a range of applications ranging from new methods in chemical biology like glycan imaging in developing zebrafish,[1] protein labeling,[12–15] lipid labeling[16] or DNA labeling[17] to synthetic applications like surface modification.[18] A comprehensive overview is given in the review of van Berkel *et al.*[19]

Reaction rates of Staudinger ligations are rather low compared to other bioorthogonal reactions. The non-traceless Staudinger ligation has rates of about 3.8 x 10^{-3} $M^{-1}s^{-1}$ (aqueous KH_2PO_4 (10 mM)/acetonitrile 1:1)[8] while the traceless version is reported to have similar rates of 7.7 x 10^{-3} $M^{-1}s^{-1}$ (DMF/D_2O 6:1).[11] Due to these low reaction rates, other bioorthogonal ligations, mainly SPAAC and tetrazine ligations, are commonly used nowadays. However, the Staudinger ligation remains a highly robust method for *in vitro* and *in vivo* labeling in non-time-critical applications.

1.1.2 Strain-Promoted Alkyne Azide Cycloaddition (SPAAC)

More than 50 years ago, Rolf Huisgen presented a specific type of cycloaddition, the 1,3-dipolar cycloaddition, which was published in 1961.[20] In these (3+2) or [4+2] cycloadditions a 1,3-dipole reacts with a dipolarophile, such as an alkyne or alkene, forming a 5-membered ring (Figure 2).

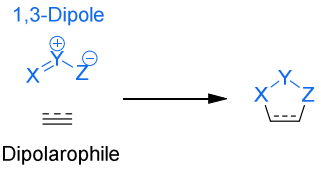

Figure 2: 1,3-Diploar cycloaddition

One of the most prominent 1,3-diploar cycloadditions is the reaction of azides with alkynes forming 1,2,3-triazoles (example shown in Figure 3a), usually called Huisgen cycloaddition. This reaction requires quite long reaction times at elevated temperatures and usually produces a mixture of isomers.

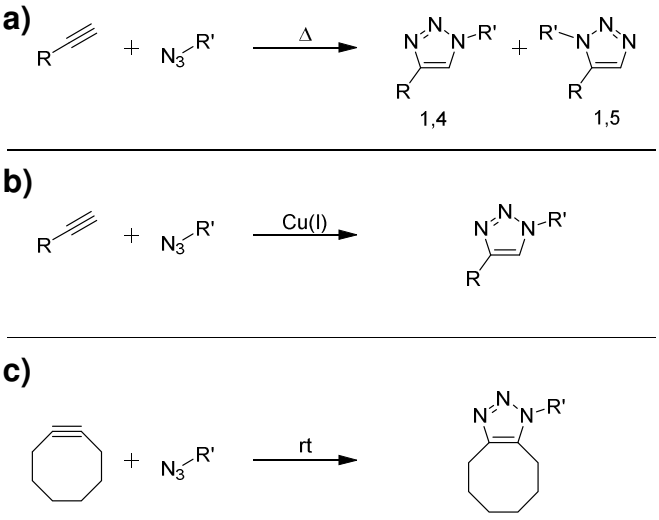

Figure 3: a) Huisgen cycloaddition; **b)** Copper(I) catalyzed alkyne azide cycloaddition; **c)** Strain-promoted alkyne azide cycloaddition

In 2001 Barry Sharpless introduced the concept of 'click chemistry', a term to describe high yielding reactions with a broad scope, good atom economy, no or easy separable byproducts and high stereo specificity.[21] In addition, such reactions need to be easy to carry out and should tolerate easily removable or green solvents. Several click reactions were developed, most notably the copper-catalyzed alkyne azide cycloaddition (CuAAC), which is commonly called "click chemistry". This reaction is a modified version of the Huisgen cycloaddition with a terminal alkyne. By adding Cu(I) to the reaction mixture this cycloaddition can be performed at low temperature only yielding 1,4-substituted triazoles (Figure 3b). The 1,5-triazole can be selectively obtained by ruthenium catalysis.[22]

Due to the cytotoxic nature of copper or ruthenium these reactions are only conditionally qualified for ligations *in vivo*.[23] In 2004 Bertozzi and coworkers reported a copper-free version of this click reaction,[24] based on work by Wittig *et al.*, who reported in 1961 that cyclooctyne and phenyl azide react "explosionsartig" (like an explosion) to form a single product (Figure 3c).[25] This high reactivity of cyclooctynes towards organic azides is based on the high strain on the triple bond. While a strain-free triple bond is straight with an angle of 180° the bond angle in cyclooctyne is about 158° (M06-2X/6-311+G(d,p), gas phase). This lowers the activation energy of this cycloaddition substantially, since the alkyne is already distorted towards transition state geometry. Calculations showed that the energy of activation is lowered from 20.9 kcal/mol for the strain-free addition between 2-propyne and methyl azide to 10.4 kcal/mol for the strain-promoted reaction of cyclooctyne and methyl azide.[26]

Bertozzi *et al.* applied this reaction for covalent modifications *in vivo*, using a cyclooctyne derivative with a handle for further modification, called **OCT** (Figure 4).[24]

In recent years several cyclooctyne derivatives were developed, mainly aiming to improve reactivity. Starting from **OCT**, which shows rate constants similar to the Staudinger ligation, first attempts focused on introducing electron withdrawing groups adjacent to the triple bond. Fluorine was introduced in propargylic position yielding a mono-fluorinated species usually abbreviated as **MOFO**,[27] which already showed substantially higher reactivity. This led to the development of **DIFO**, a cyclooctyne that features a difluoromethylene in propargylic position.[28] **DIFO** pushed the reactivity of SPAAC by more than an order of magnitude to 0.076 $M^{-1}s^{-1}$ and was also studied extensively by computational methods by Houk and coworkers.[36] This cyclooctyne is of particular interest, as it not only uses strain as the driving force for high reactivity but also electronic effects. It was also the first cyclooctyne used in *in vivo* applications for the fluorescence imaging in living developing zebra fish,[37] and *Caenorhabditis elegans* (roundworm).[38]

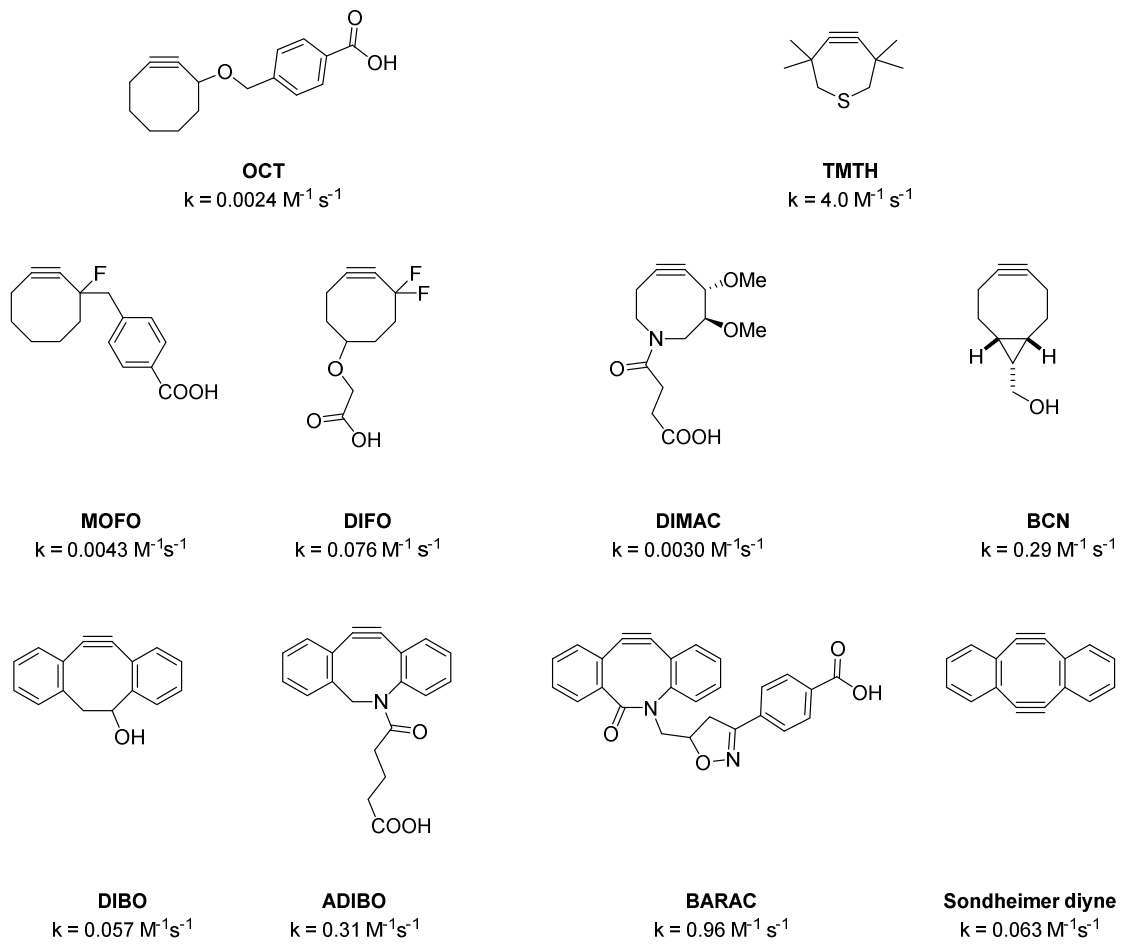

Figure 4: Selected cyclooctyne derivatives and their second order rate constants measured with benzyl azide in acetonitrile: OCT,[24] MOFO,[27] DIFO,[28] BARAC,[29] DIMAC,[30] TMTH[31] ; methanol: DIBO,[32] Sondheimer diyne,[33] ADIBO[34]; CD_3CN/D_2O (1:2): BCN[35]

However, despite the promising reaction rates in model reactions **DIFO** performed poorly in a mouse model and was outperformed by the Staudinger ligation, due to unselective binding to murine serum albumin.[39] This led to the development of the more hydrophilic derivative **DIMAC**.[30] While it shows better water solubility the reactivity is considerably lower (k = 0.003 $M^{-1}s^{-1}$) than the one of **DIFO**, which is negating the positive features of this cyclooctyne.

Another approach of improving cyclooctyne reactivity is the use of dibenzocyclooctyne structures, which increases the strain by introducing sp^2-centers. In 2008 Boons *et al.* introduced the class of **DIBO** cyclooctynes[40] that show similar reactivity to **DIFO**. Bertozzi and coworkers could push the reactivity of dibenzocyclooctynes even further by introducing a lactam structure into the cyclooctyne ring leading to **BARAC**, which showed a 10-fold higher reactivity.[29] However, this reagent shows only limited stability, as it "should be stored as a solid at 0 °C protected from light and oxygen". Another dibenzo derivative is **ADIBO** (also called DIBAC or DBCO), which was introduced by van Delft and coworkers in 2010.[34] While showing slightly lower reactivity than **BARAC,** it exhibits higher stability and better synthetic accessibility.

Also in 2010 van Delft *et al.* introduced another cyclooctyne, bicyclononyne or **BCN**.[35] By introducing a *cis*-fused cyclopropane ring attached to the backbone of the cyclooctyne core structure the reaction rate could be pushed to a similar level compared to **ADIBO**, while using a smaller and less lipophilic reagent.

In addition to 8-membered rings also 7-membered rings were studied. Since the carbocycle cycloheptyne is not stable, one carbon was substituted by a sulfur atom, which led to a stable, 7-membered cycloalkyne. 3,3,6,6-Tetramethylthiacycloheptyne (**TMTH**) was reported in 1970 by Krebs and coworker[41] and investigated in 2012 by Bertozzi *et al.* as reagent for copper-free click chemistry.[31] It showed exceptional high reaction rates of 4.0 $M^{-1}s^{-1}$ with benzyl azide in CD_3CN, however, **TMTH** or derivatives of this reagent have not been used in any further studies.

While several cyclooctynes have been developed only two, **BCN** and **ADIBO**, found wide use and are commercially available at the time of writing this work.

In addition to the above described cyclooctynes the **Sondheimer diyne** was used as a bi-functional dipolarophile in SPAAC reactions by Hosoya *et al.*[33] They could show that sterically hindered aryl azides react faster with dibenzo cyclooctyne derivatives than sterically non-hindered aryl azides due to "pre-distortion", which lowers the energy needed to reach the transition state geometry. This work presents the first thorough investigation of different azides to further push and tune reaction rates in SPAAC.

Another impressive work on the reactivity of different azides in SPAAC was presented by van Delft and coworkers in 2014.[42] They presented that highly electron deficient azides react very rapidly with steric non-demanding alkyl cyclooctynes like **BCN**, with second order rate constants up to 3 $M^{-1}s^{-1}$, the highest reported values for a cyclooctyne-based SPAAC to date.

1.1.3 Tetrazine Ligations

In 1928 Diels and Alder published their work on [2+4] cycloadditions between dienes and dienophiles (one example shown in Scheme 4).[43] These reactions are now commonly known as Diels-Alder (DA) reactions. In the normal electron demand Diels-Alder reaction an electron rich diene reacts with an electron poor dienophile. The main interaction is between the HOMO of the diene and the LUMO of the dienophile. In the inverse electron demand DA reaction the interaction between LUMO of the diene and HOMO of the dienophile has the highest impact on the reaction. In addition, there are cases where both normal and inverse interactions are in the same range.

The DA reaction is a powerful tool in organic synthesis. One of the first applications of a Diels-Alder reaction as synthetic key step was the synthesis of cortisone and cholesterol by Woodward and coworkers in 1952.[44] DA was used extensively in a vast number of groundbreaking projects.[45]

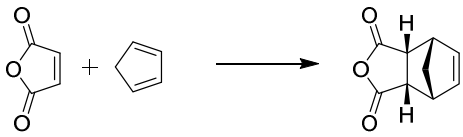

Scheme 4: [2+4] cycloaddition between Maleic anhydride and cyclopentadiene as reported by Diels and Alder, one of the most prominent examples of a DA reaction

In 1990 Sauer *et al.* described the kinetics of an inverse electron demand DA reaction between 1,2,4,5-tetrazines (Tz) and dienophiles, which proceed at very high reaction rates (Scheme 5).[46,47]



Scheme 5: Inverse electron demand DA initiated reaction between 1,2,4,5-tetrazines and dienophiles

This reaction proceeds in two steps. In the first rate-determining step the tetrazine and the dienophile react in an inverse electron demand DA addition to a bicyclic product, which then reacts in a second step in a retro Diels-Alder reaction under the loss of nitrogen to the dihydropyridazine species. This product usually tautomerizes or is oxidized to the pyridazine. Figure 5 shows a typical energy diagram of such a reaction as well as a detailed overview of the reaction. This inverse electron demand DA (IEDDA) reaction was introduced by the groups of Fox[48] and Weissleder[49] independently as a bioorthogonal reaction in 2008. Weissleder *et al.* used the reaction between norbornenes and a 3-aryl substituted 1,2,4,5-tetrazine, which has a rather low rate constant of 1.9 $M^{-1}s^{-1}$ in aqueous solution, comparable to very fast SPAAC reactions. For pretargeted live cell imaging the group of Joseph Fox took a different route. They used diaryl-tetrazines and a *trans*-cyclooctene (TCO), which was identified by Sauer and coworkers as the dienophile with the highest reactivity towards tetrazines by several orders of magnitude,[46] and were able to reach a second order rate constant of 2 000 $M^{-1}s^{-1}$ in methanol:water 9:1 at 25 °C.[48] This made the tetrazine ligation very interesting for several applications, since ligation times decreased substantially allowing for reaction at very low

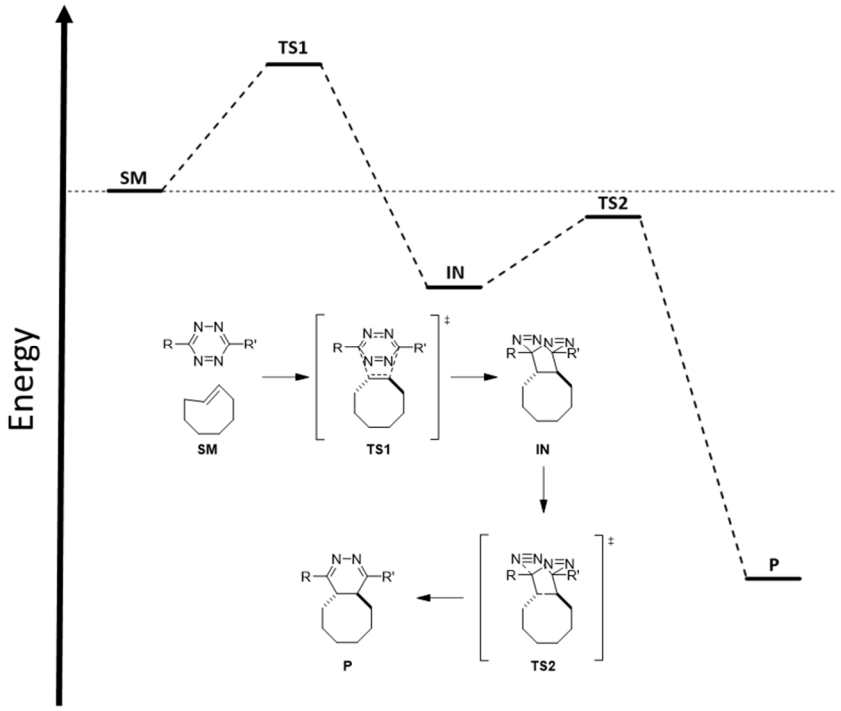

Figure 5: Typical energy diagram of the reaction between a trans-cyclooctene and a 1,2,4,5-tetrazine; SM=starting material, TS=transition state, IN=intermediate, P=product

concentration while still obtaining good yield in reasonable time. A very promising recent application is the use of this reaction in radiolabeling, where high reaction rates are mandatory due to very low concentrations and short half-lifes of the most commonly used radionuclides with high specific activity. The use of bioorthogonal ligations for radio-applications is explained in more detail in chapter 1.2.

The kinetics and mechanism of the inverse electron demand DA reactions of tetrazines were studied extensively using both experimental and theoretical methods.[50–56] Due to the pink color of the tetrazine and the colorless or slightly yellow products, tetrazine ligations can be followed very well by photometric methods, enabling the study of these ultrafast reactions by stopped-flow methodology. Due to the broad availability and simplicity of this method rate constants are frequently reported. However, since the rate of the tetrazine reaction is highly influenced by the solvent, as it is the case for most Diels-Alder reactions, reported values in different solvents cannot readily be compared. As an example, the group of Fox reported a rate of 2 000 $M^{-1}s^{-1}$ for the reaction of 3,6-dipyridyl-1,2,4,5-tetrazine (**1**) with **TCO** at 25°C in methanol:water 9:1,[48] while Karver *et al.* reported a value of 26 000 $M^{-1}s^{-1}$ for tetrazine **2** with **TCO** in PBS at 37°C,[57] a 13-fold difference in reactivity (Figure 6). Since Diels-Alder reactions are highly accelerated in aqueous media,[58,59] it is likely that the difference between rates would be much lower, if measured in the same solvent. In fact, the bispyridyl substituted Tz might even show a higher reactivity than **2**. Measurements of the reactivity of 3,6-dipyridyl-1,2,4,5-tetrazine and the Boc-protected derivative of **2** towards **TCO** in 1,4-dioxane at 25°C revealed that the bispyridyl-derivative shows a more than 50% higher reactivity than the mono-substituted Tz (226 $M^{-1}s^{-1}$ vs. 146 $M^{-1}s^{-1}$, unpublished results). Therefore, there are ongoing efforts from our group to harmonize kinetic measurements of tetrazine ligations, in an attempt to make the reported results comparable. Nevertheless, this data is important for the respective application and, keeping solvent effects in mind, one can determine the approximate relative reactivity quite well in most cases.

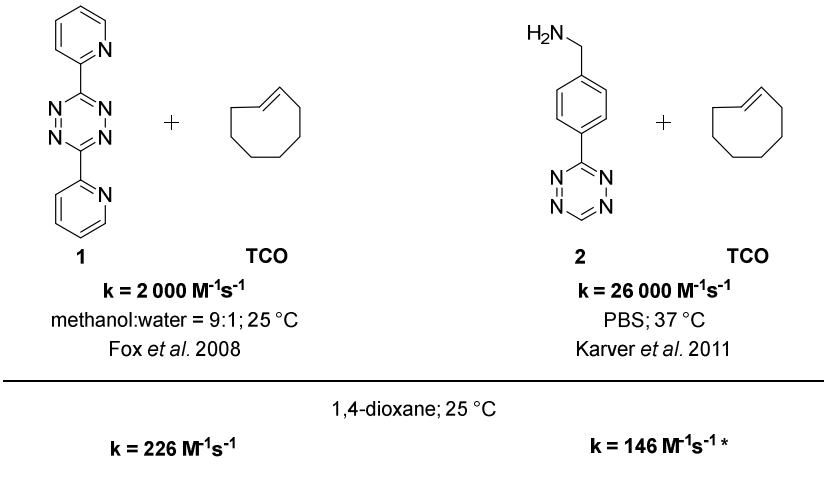

Figure 6: Discrepancy between reported second order rate constants due to solvent effects; * measured for the Boc-protected derivative

The reported rate constants of tetrazine ligations span more than nine orders of magnitude, from low reactive norbornenes, which have rate constants of 0.001 $M^{-1}s^{-1}$ even with highly reactive bispyridyl

tetrazines,[50] up to 3 300 000 $M^{-1}s^{-1}$ for highly reactive *trans*-cyclooctenes with highly reactive bispyridyl tetrazines in water.[9]

The high reactivity of tetrazines towards dienophiles also sparked the interest of computational chemists. Talbot *et al.* investigated the origin of the high IEDDA reactivity of 1,2,4,5-tetrazines compared to other nitrogen containing 6-membered heterocycles.[55] They concluded that the high reactivity of 1,2,4,5-tetrazines compared to pyridine, 1,2-diazine or 1,2,3- and 1,2,4-triazines does not originate from more favorable frontier molecular orbital (FMO) interactions but rather in a decreased open-shell Pauli repulsion between the reactants. Houk and coworkers did extensive work on cycloadditions and performed several studies on the tetrazine ligation in recent years. Most notably they investigated the effect of dienophile strain on the tetrazine ligation[52] as well as the effect of different substitution patterns on the tetrazine.[53]

Two different approaches were taken for improving the tetrazine ligation, with the first one, mainly led by Fox and coworkers, focusing on further accelerating the reaction. In 2011 Fox *et al.* published a highly reactive *trans*-cyclooctene derivative, which is two orders of magnitude more reactive than *trans*-cyclooctene or the before used *trans*-cyclooctene-5-ol (**TCO-OH**) derivatives (Figure 7).[60] Similar to van Delft's **BCN**, this compound features a *cis*-fused cyclopropane ring in the backbone. This cyclopropane locks the cyclooctene from a low-energy crown formation into a higher energy half-chair conformation, resulting in more strain, a higher HOMO and therefore higher reactivity. It is usually referred to as strained TCO, or abbreviated as **s-TCO.** The highest reported rate constants for the tetrazine ligation, up to 3 300 000 $M^{-1}s^{-1}$, were reached using this TCO in combination with bispyridyl tetrazine.

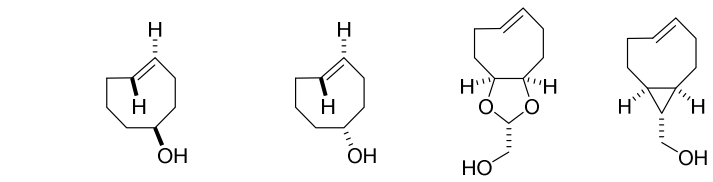

Figure 7: Commonly used TCO derivatives; rates taken from [9]

In 2014 the Fox group expanded this concept of conformationally strained cyclooctenes by using *cis*-fused dioxolan rings in the backbone of the cyclooctene, leading to **d-TCO**.[9] While this cyclooctene has a 10-fold lower reactivity compared to **s-TCO**, it is still 4-14 times more reactive than commonly used **TCO-OH** and shows higher water solubility and stability than **s-TCO.**

The second effort in improving tetrazine ligations was to find what can be seen as an "azide-like" tag for the tetrazine ligation. The big advantage of SPAAC over the tetrazine ligation is the use of azides. This functionality is highly stable under *in vivo* conditions and, in general, very well accepted by metabolism.[61] This makes metabolic labeling, using azide-tagged building blocks, possible. In contrast, both reactive groups in tetrazine ligation are rather big and suffer from either *in vivo* instability or low reactivity. Thus, there was and still is a desire for a small, stable tag that exhibits high reactivity and can be used for metabolic labeling. Such a reactive group was introduced in 2012 by Devaraj *et al.* in the form of cyclopropenes.[62] Based on the work of Sauer *et al.*,[46] who reported that the unstable cyclopropene and the stable 3-methylcyclopropene show high reaction rates with highly reactive tetrazines, they were able to develop cyclopropene derivatives with sufficient stability while still obtaining reasonable high reaction rates of up to 13 $M^{-1}s^{-1}$ (12% DMSO in water, 37°C) by using 1-methyl substituted cyclopropenes.[62] They were able to use cyclopropenes for tagging phospholipides for live cell labeling in combination with a fluorogenic dye containing a tetrazine for ligation (Figure 8).

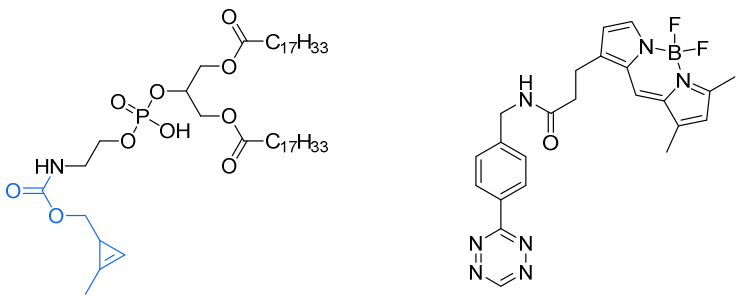

cyclopropene tagged phospholipide

fluorogenic tetrazine probe

Figure 8: Cyclopropene tagged phospholipide and flurogenic tetrazine probe used by Devaraj and coworkers; Cyclopropene tag highlighted in blue

Design of this cyclopropene tag is crucial for reactivity as well as stability. Using 3,3-disubstituted derivatives leads to a substantial drop in reaction rate, as already noted by Sauer,[46] due to steric hindrance. Introducing a methyl group in position 2 in addition to position 1 also leads to reduced reactivity.[63] Unfortunately the reaction rates are not as high as for other dienophiles like *trans*-cyclooctenes. Devaraj *et al.* noticed that the nature of the substituent in 3-position of the cyclopropene has a large impact on the reactivity as well as the stability in aqueous media. They were able to nearly double the reaction rate of this ligation by changing the substituent from a carbamate based linker to an amide (Figure 9).[56] However, low rates of cyclopropenes compared to *trans*-cyclooctenes limit the applicability of this tetrazine reaction.

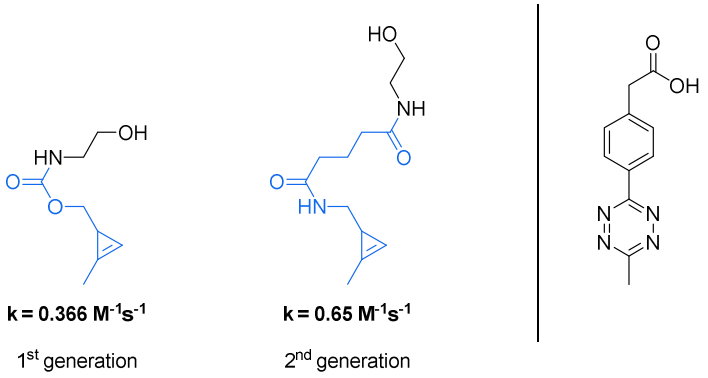

Figure 9: First and second generation cyclopropene tags for Tz ligation; Indicated reaction rates are reported for reaction with tetrazine shown on the right in 50 mM MOPS buffer, pH = 7.5, 250 mM NaCl at room temperature

Another interesting development in tetrazine chemistry is the idea of not only ligating two structures but also releasing structures by bioorthogonal reactions. One might understand this as bioorthogonal elimination or even substitution reaction and the basic principle is often referred to as “click and release” chemistry. Figure 10 shows the concept of such a reaction in comparison to classic ligation.

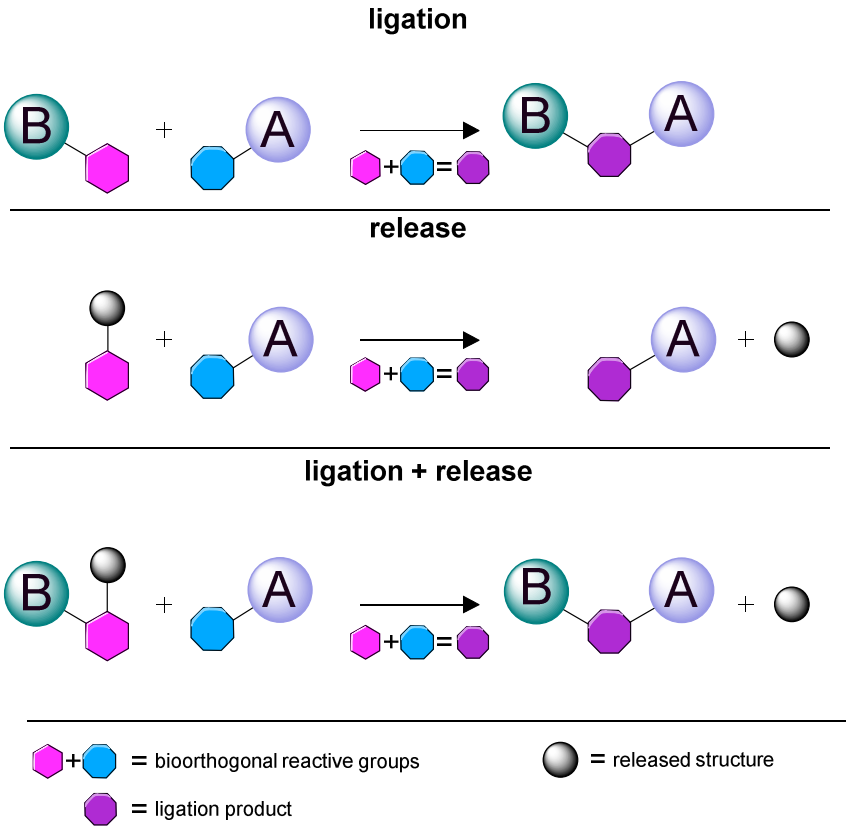

Figure 10: Possible modes of bioorthogonal ligations including “click and release” chemistry

In 2013 Rossin, Robillard and coworkers introduced a release TCO (**r-TCO**), which releases a molecule upon conjugation with a tetrazine.[64] This is realized by using a carbamate-linked molecule of interest in allylic position to the *trans*-configured double bond of TCO. After conjugation with a tetrazine (Scheme 6 Structure **4**) the authors proposed that the carbamate can eliminate either by direct route (**I**) or after tautomerization to **5** to structure **7** (route **II**), and furthermore that tautomer **6** will not release the molecule of interest.

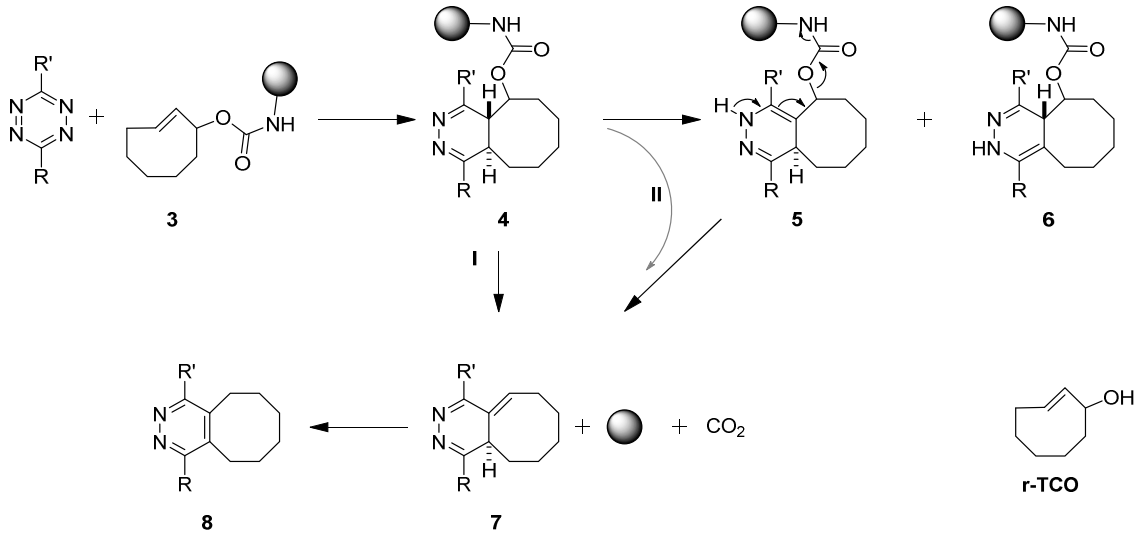

Scheme 6: Mechanism of the tetrazine ligation triggered release reaction

In 2016 Rossin, Robillard and coworkers introduced another release TCO, however in contrast to **r-TCO**, this bifunctional *trans*-cyclooctene **9** enables conjugation as well as release (Figure 11).[65]

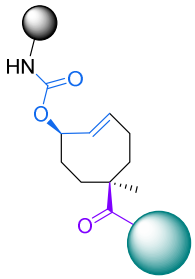

Figure 11: Structure of a release TCO with functional handle for ligation; release functionality shown in blue, handle for stable modification shown in purple

1.2 Bioorthogonal Ligations in PET Imaging

Positron emission tomography (PET) is a widely used and highly sensitive functional imaging technique. Hereby a molecule of interest is labeled with a β^+-decaying radionuclide, also called tracer, and applied to the patient. After decay of the radionuclide a positron is emitted. Depending on the radionuclide this positron has a different kinetic energy and needs to be slowed down before being able to recombine with its antiparticle an electron. The path range, the distance between location of decay and recombination with an electron, is in the range of tenths of a millimeter up to several mm. The positron then annihilates with an electron forming two gamma rays with 511 keV energy. Both photons are emitted at an angle of nearly 180° due to conservation of momentum. By placing a detector ring around the patient so-called coincidence events can be measured and recorded. Using reconstruction one can use this data to determine a three-dimensional distribution of decay- or, to be precise, annihilation-events. This can be directly converted into a three-dimensional concentration distribution of the applied tracer.[66]

The most commonly used tracer molecule is ^{18}F-2-fluorodeoxyglucose (^{18}F-**FDG**), a D-glucose derivative in which the 2-OH is substituted by a bioisosteric fluorine-18. **FDG** is actively transported into cells and metabolically trapped after phosphorylation of 6-OH, since the resulting 6-phosphate of FDG cannot be further metabolized. Therefore, glucose uptake can be imaged by PET using FDG.[67]

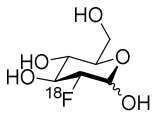

Figure 12: ^{18}F-**FDG**

Fluorine-18 is the most common radionuclide in PET imaging. It exhibits β^+-decay with low positron decay energy and a half-life of 109.8 minutes and can be produced in a cyclotron by an $^{18}O(p,n)^{18}F$ nuclear reaction. Hereby nucleophilic ^{18}F-fluoride can be produced by bombardment of $[^{18}O]H_2O$ while electrophilic $[^{18}F]F_2$ is accessible by irradiation of $[^{18}O]O_2$ gas.[68]

Another common radionuclide in PET is carbon-11. It can be produced using a $^{14}N(p,\alpha)^{11}C$ nuclear reaction and has a half-life of 20.38 minutes. If the reaction is carried out in presence of oxygen $[^{11}C]CO_2$ is produced, which is a useful building block in organic chemistry. In the presence of hydrogen $[^{11}C]CH_4$ is produced, which can be converted into [^{11}C]methyl iodide or triflate and used in methylation reactions.[68]

Other used PET radionuclides include nitrogen-13 and oxygen-15. In addition to covalently bound nuclides also radiometals, such as zirconium-89, copper-64, gallium-68 or scandium-44, are extensively used in PET imaging.[68] Those metals are usually introduced into tracers by using chelating ligands for the corresponding cations, like 1,4,7,10-tetraazacyclododecane-1,4,7,10-tetraacetic acid (**DOTA**).[69]

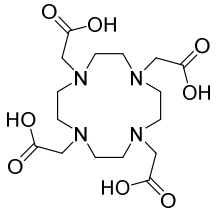

Figure 13: DOTA chelator

There are two main applications of bioorthogonal chemistry in PET imaging: (1) rapid radiolabeling (chapter 1.2.1) and (2) pretargeted PET imaging (chapter 1.2.2).

1.2.1 Rapid Radiolabeling

Rapid radiolabeling is a technique for synthesis of radiolabeled tracer molecules using a fast click reaction in the last step to attach the radionuclide to the molecule of interest (Figure 14). This method has several advantages compared to conventional syntheses. Radiosynthesis has only to be established and optimized once. This leads to fast and efficient labeling of different structures, as shown by Bejot *et al.*, who used copper(I) catalyzed alkyne azide cycloadditions for the synthesis of six different hypoxia probes.[70] The use of a prosthetic group also eliminates several difficulties when dealing with radiolabeling. For example, Fluorine-18, the most common PET isotope, is usually introduced by nucleophilic substitution using ^{18}F-fluoride. However, fluoride itself is only a weak nucleophile thus these reactions usually require elevated temperatures and quite long reaction times. The use of highly selective click reactions also eliminates the need for protecting groups during radiolabeling. In addition, depending on the used click reaction and protocol, purification can be omitted after rapid radiolabeling, making rapid click reactions particularly attractive for labeling of large peptides and proteins.

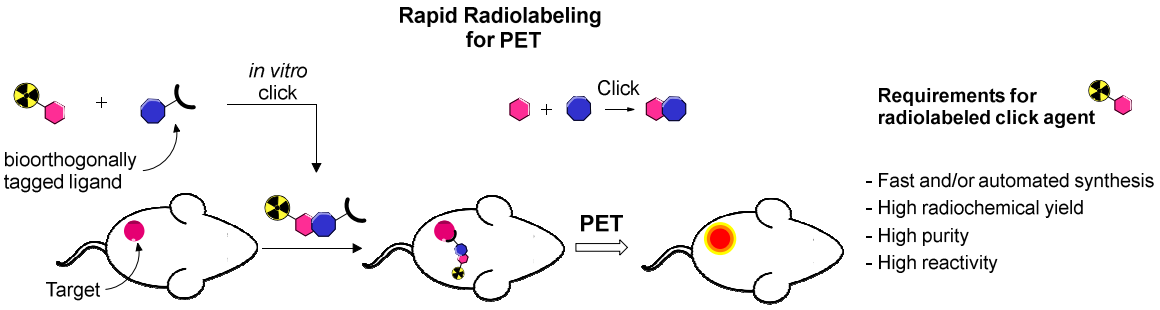

Figure 14: Concept of rapid radiolabeling using a radiolabeled tetrazine

Copper(I) catalyzed alkyne azide cycloadditions have been used for the synthesis of PET tracers.[70–76] However, the use of cytotoxic copper in the labeling step raises safety concerns and demands extensive purification of the tracer. Therefore, the copper-free click reaction has proven to be an efficient tool for rapid radiolabeling.[75–77] Several radiolabeled cyclooctynes have been developed based on **ADIBO** and used in radiosynthesis (Scheme 7). Arumugam *et al.* used ^{18}F-**11**, which was directly labeled with ^{18}F-fluoride by nucleophilic substitution of tosylate **10**, for labeling of an azide-tagged model peptide,[78] while Sutcliffe and coworkers used a two-step procedure wherein they first produced [^{18}F]N-succinimidyl 4-fluorobenzoate ([^{18}F]**SFB**) which was then used for radiolabeling of an ADIBO-amine to produce radiolabeled cyclooctyne **15**.[79] This [^{18}F]**ADIBO** was successfully used in labeling of an integrin αvβ6-specific peptide.[80] Bouvet *et al.* used [^{18}F]**SFB** for labeling of commercially available ADIBO-amine **16** to produce **17**, which was subsequently used in radiolabeling of different azides, including a geldanamycin azide.[81] Several radiolabeled azides found use in CuAAC labeling and were also used in rapid radiolabeling by SPAAC. Campbell-Verduyn *et al.* used different ^{18}F-labeled azides for radiolabeling of ADIBO-tagged bombesin.[82] Using rapid radiolabeling they were able to vary the used azide and therefore fine-tune lipophilicity for optimal pharmacokinetics of the tracer. Kim *et al.* applied an ^{18}F-labeled mini-PEG azide for labeling of an **ADIBO**-tagged cRGD peptide.[83] For a more comprehensive overview about CuAAC and SPAAC in rapid radiolabeling see [75,76].

High reaction rates are important in rapid radiolabeling, since it allows for shorter reaction times or even lower concentration. This is very important especially in case of the radiolabeling of proteins, since an excess of radiolabeled bioorthogonal reagent would require purification after the labeling step to get rid of unreacted reagent, while an excess of protein would lower the specific activity, due to unreacted substrate. The tetrazine ligation between tetrazines and TCOs is the fasted reported bioorthogonal reaction and was consequently used in rapid radiolabeling. In 2010, two

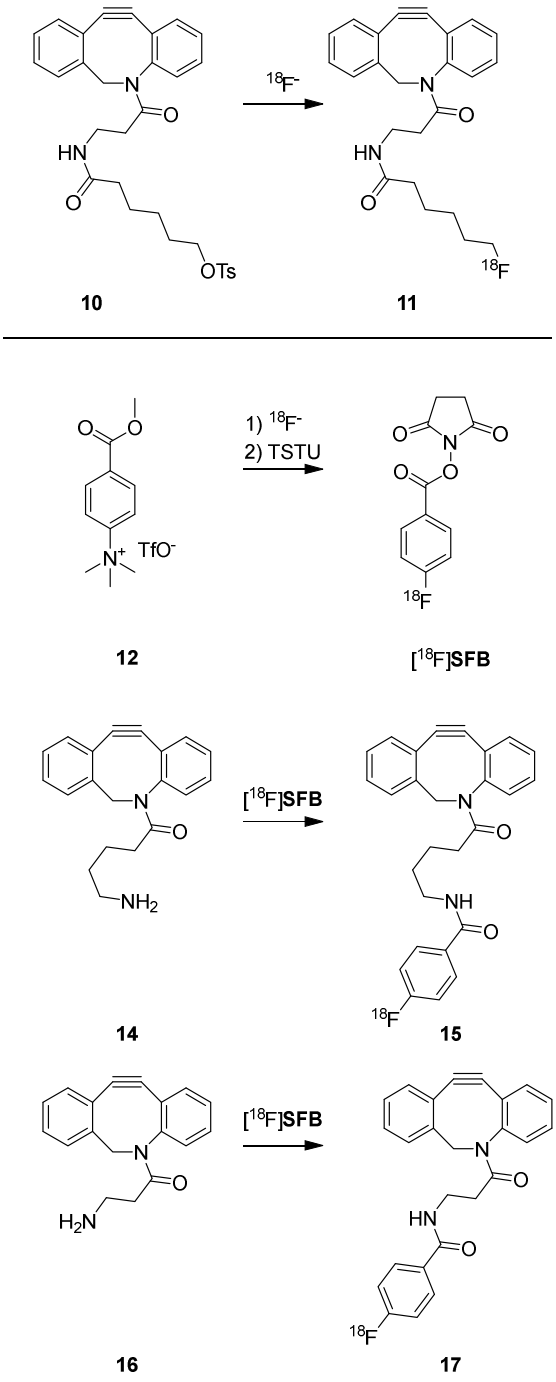

Scheme 7: ^{18}F-labeled **ADIBO** derivatives

years after introduction of the Tz-ligation, the Fox group reported the use of this reaction in the “Rapid Construction of Fluorine-18 Labeled Probes”.[84] Using an ^{18}F-labeled TCO they were able to radiolabel bispyridyl tetrazine within minutes. Attempts for synthesizing an ^{18}F-labeled tetrazine have failed. Just one year later the same group reported the use of this exact reaction for the labeling of a cRGD peptide, which was then used for PET imaging in an U87MG mouse tumor model.[85] The labeling could be achieved in shorter time and in higher yield compared to CuAAC-based labeling or labeling *via* [^{18}F]**SFB**. In this case the tetrazine was introduced to the peptide by lysine acylation. In 2013 Fox and coworkers reported a tetrazine tag for labeling of cysteine groups, which can then be used for rapid radiolabeling using their previously described system of an [^{18}F]TCO and dipyridyl tetrazine.[86,87] However, it was noticed, that the ligation product of dipyridyl tetrazines and TCO does not show sufficient *in vivo* stability. In 2015 Fox *et al.* reported on a modified labeling system, which improved the *in vivo* stability of the ligation product by using a CF_3-substituted 3,6-diphenyl-tetrazine instead of a bispyridyl derivative.[88] We were able to further improve this technique by using an ^{18}F-**s-TCO** derivative that improved the reaction rate drastically. Furthermore, the use of mini-PEG linkers led to better biodistribution of the tracer molecules (Manuscript #7).[89]

Up to 2014 only ^{18}F-labeled TCOs were known, until we reported on the development of the first ^{18}F-labeled Tz based on a dialkyl-scaffold, which lowered inverse electron demand DA reactivity but made direct radiolabeling possible (Manuscript #4).[90] In 2015, Schirrmacher and coworkers introduced another ^{18}F-labeled tetrazine, however, no kinetic data was given and this tetrazine is expected to have a rather low reactivity.[91]

Another interesting radionuclide for PET imaging is carbon-11. In 2013, Herth *et al.* reported on the development of an ^{11}C-labeled tetrazine.[92] In 2016, we introduced another ^{11}C-Tz intended for rapid radiolabeling and pretargeted imaging (Manuscript #6).[93]

Ploegh and coworkers took advantage of the already known and optimized synthesis of ^{18}F-2-fluorodeoxyglucose (^{18}F-**FDG**) and developed a method for conjugating a tetrazine moiety to **FDG**, which was subsequently used in rapid radiolabeling of a TCO-tagged single domain antibody fragment.[94] In 2016 they reported the synthesis of an ^{18}F-labeled tetrazine using [^{18}F]**SFB** as prosthetic group, which was again used for rapid radiolabeling of single domain antibody fragments.[95]

Tetrazine ligation was also used in radiolabeling using radiometals. Zeglis *et al.* were able to label peptides with ^{89}Zr by using tetrazine-tagged amino acids in combination with a TCO-tagged chelator for ^{89}Zr.[96] Similarly, Spivey and coworkers employed a DOTA conjugated tetrazine for labeling of norbornene-tagged target compounds, and compared this method to rapid radiolabeling using SPAAC and considered the tetrazine ligation to be superior.[97] In addition, several iodine-125 labeled tetrazines were developed.[98–100]

1.2.2 Pretargeted PET Imaging

Pharmacokinetics and pharmacodynamics of the PET tracers have high influence on the imaging quality. Slow accumulation of the tracer at the target, in respect to the half-life of the used radionuclide, can limit target-to-background ratio of the signal. Likewise, binding affinity of the tracer to the target needs to be high and unbound tracer needs to be excreted fast, to limit non-specific signal and provide high target-to-background ratios. Therefore, usually only fast accumulating and clearing tracers are used in standard PET imaging protocols, using short-lived radionuclides like fluorine-18.

For this reason, slow accumulating agents, like antibodies and other nanomedicines or even small molecules, cannot be used in combination with short-lived radionuclides, and labeling with nuclides with longer half-life, like ^{89}Zr, result in an undesirable high radiation dose for the patient.

Pretargeted PET imaging can enable the use of short-lived radionuclides in combination with slow accumulating/clearing agents. This involves a two-step imaging process. First, a non-radioactive labeled marker molecule is applied and allowed to accumulate in target tissue. Then a radiolabeled secondary agent, usually called pulldown reagent, is applied, that selectively binds to the preadministered marker molecule *in vivo* (Figure 15).[101,102]

The first example of pretargeting in nuclear medicine was the use of “anti-metal-chelate” antibodies in combination with radiometals bound to chelating ligands.[103–105] Later developed strategies used the

stronger avidin-biotin binding for *in vivo* linkage of a pulldown reagent to the marker.[106] However, the size of the involved ligation partners as well as the allergic potential of avidin limited the use of this pretargeting technique. Bioorthogonal reactions provide the advantages of low-molecular-weight ligation partners, high reactivity and the formation of covalent bonds and are therefore well suited for pretargeting strategies.

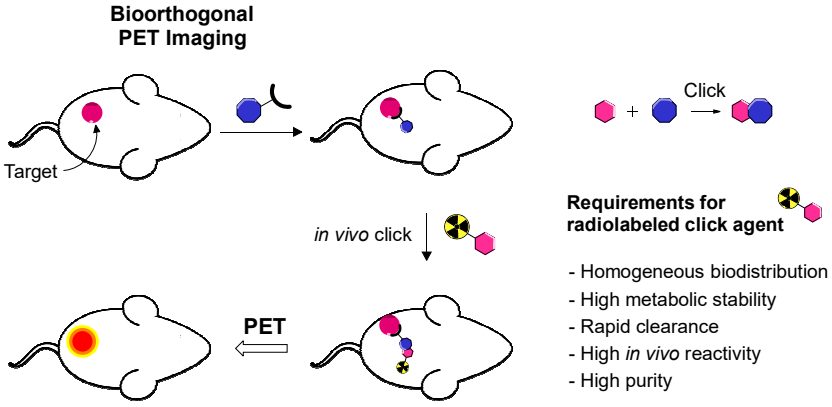

Figure 15: Concept of pretargeted PET imaging

For pretargeted PET imaging the requirements on the bioorthogonal ligations are even higher than for rapid radiolabeling applications. While the reaction still needs to proceed reasonably fast and the ligation products need to be stable and biocompatible in pretargeting experiments, the used bioorthogonal reagents also have to be stable and biocompatible and the reaction should proceed at exceptional high rates, since concentrations are even lower *in vivo*.

SPAAC was proposed by Spivey and coworkers as a tool for pretargeted PET imaging. They evaluated the biodistribution of ^{18}F-2-fluoroethyl azide and investigated the reaction of this radiolabeled azide with different cyclooctynes.[107] They concluded that this reaction should be suitable for pretargeted experiments and announced that they will perform further investigations on this topic. However, no further reports have been published so far. Furthermore, the *in vivo* stability was revised by our group and we could show that ^{18}F-2-fluoroethyl azide readily defluorinates *in vivo* (Manuscript #3). In general, SPAAC is now believed to have insufficient reaction kinetics for pretargeted PET experiments. Nevertheless, in 2013 Kim *et al.* reported pretargeted PET experiments using an ^{18}F-labeled PEG-azide in combination with **ADIBO**-tagged nanoparticles.[108] However, this is the only reported case of a successful pretargeting experiment using SPAAC.

Due to the exceptional high reaction rates the tetrazine ligation is considered the best suited bioorthogonal reaction for this kind of application and was successful used in several experiments. In 2012 Weissleder and coworkers reported the first application of *in vivo* Tz ligation for PET imaging using ^{18}F-labeled, tetrazine-tagged polymers for *in vivo* labeling of TCO-conjugated monoclonal antibodies.[109] Zeglis and coworkers used a TCO-labeled A33 antibody in combination with a ^{64}Cu-labeled tetrazine for pretargeted PET imaging of human colorectal carcinoma xenografts in mice.[110] Within this study they could demonstrate that the pretargeting approach, rather than conventional antibody labeling, leads to highly reduced off-target doses. In 2016 the same group reported on pretargeted PET imaging using an ^{18}F-labeled tetrazine based on an Al[^{18}F]-NOTA-approach for imaging of a TCO-tagged antibody.[111]

Efforts to develop an inverse approach by using a radiolabeled TCO-derivative (Figure 16) have not been successful so far, due to the instability of TCO in tracer concentrations.[112]

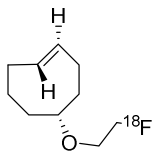

Figure 16: Radiolabeled TCO for *in vivo* imaging

While not using PET but rather SPECT as imaging modality the pretargeting systems developed by Robillard, Rossin and coworkers are worth mentioning here, since they can easily be adopted for PET imaging, using different radiometals. Rossin *et al.* used DOTA as chelator for indium-111 SPECT measurements, a ligand that can also be applied to the PET isotope gallium-68, scandium-44 or yttrium-86.[69] In 2010 Rossin, Robillard and coworkers reported on the pretargeted SPECT imaging of colocteral cancer xenografts in mice, using a TCO-

labeled antibody, which was allowed to accumulate for 24h, and was then labeled *in vivo* with an indium-111-labeled chelator-based tetrazine.[113] However, tumor-to-background ratio was limited by free circulating TCO-labeled antibody in blood, which reacted with the radiolabeled tetrazine. To prevent this *in vivo* side reaction Rossin *et al.* used a three step protocol which boosted the tumor-to-blood ratio by 250-fold.[114] In the first step the TCO-labeled antibody was administered. After accumulation, non-bound antibody-TCO conjugate was efficiently removed from blood by injecting tetrazine-modified clearing agents, based on albumin. In the final step the radiolabeled Tz was injected to perform selective *in vivo* click chemistry with on-target TCO-antibodies.

In addition, Rossin *et al.* investigated the stability of **TCO-5-OH** tags used for labeling of antibodies. They concluded that TCO is probably deactivated by isomerization to unreactive *cis*-alkene by copper-containing proteins and therefore stability can be increased when using a short linker.[115] Due to the higher stability based on the used linker they were also able to use higher reactive **axially configured TCO-5-OH**, further boosting tumor-to-background ratio.

1.3 Literature

[1] E. Saxon, C. R. Bertozzi, *Science* **2000**, *287*, 2007–2010.

[2] D. M. Patterson, L. a Nazarova, J. a Prescher, *ACS Chem. Biol.* **2014**, *9*, 592–605.

[3] C. S. McKay, M. G. Finn, *Chem. Biol.* **2014**, *21*, 1075–1101.

[4] E. M. Sletten, C. R. Bertozzi, *Angew. Chem. Int. Ed.* **2009**, *48*, 6974–98.

[5] E. M. Sletten, C. R. Bertozzi, *Acc. Chem. Res.* **2011**, *44*, 666–76.

[6] A.-C. Knall, C. Slugovc, *Chem. Soc. Rev.* **2013**, *42*, 5131–42.

[7] J. M. Fox, M. S. Robillard, *Curr. Opin. Chem. Biol.* **2014**, *21*, v–vii.

[8] M. J. Hangauer, C. R. Bertozzi, *Angew. Chem. Int. Ed.* **2008**, *47*, 2394–2397.

[9] A. Darko, S. Wallace, O. Dmitrenko, M. M. Machovina, R. a. Mehl, J. W. Chin, J. M. Fox, *Chem. Sci.* **2014**, *5*, 3770.

[10] J. Clayden, *Organic Chemistry*, Oxford University Press, **2001**.

[11] M. B. Soellner, B. L. Nilsson, R. T. Raines, *J. Am. Chem. Soc.* **2006**, *128*, 8820–8.

[12] K. L. Kiick, E. Saxon, D. A. Tirrell, C. R. Bertozzi, *Proc. Natl. Acad. Sci. U. S. A.* **2002**, *99*, 19–24.

[13] S. A. Slavoff, I. Chen, Y.-A. Choi, A. Y. Ting, *J. Am. Chem. Soc.* **2008**, *130*, 1160–1162.

[14] A. S. Raghavan, H. C. Hang, *Drug Discov. Today* **2009**, *14*, 178–184.

[15] K. Tanaka, K. Minami, T. Tahara, E. R. O. Siwu, K. Koyama, S. Nozaki, H. Onoe, Y. Watanabe, K. Fukase, *J. Carbohydr. Chem.* **2010**, *29*, 118–132.

[16] H. C. Hang, E.-J. Geutjes, G. Grotenbreg, A. M. Pollington, M. J. Bijlmakers, H. L. Ploegh, *J. Am. Chem. Soc.* **2007**, *129*, 2744–2745.

[17] A. Baccaro, S. Weisbrod, A. Marx, *Synthesis* **2007**, *2007*, 1949–1954.

[18] M. Köhn, *J. Pept. Sci.* **2009**, *15*, 393–397.

[19] S. S. Van Berkel, M. B. Van Eldijk, J. C. M. Van Hest, *Angew. Chem. Int. Ed.* **2011**, *50*, 8806–8827.

[20] R. Huisgen, *Proc. Chem. Soc.* **1961**, 357.

[21] H. C. Kolb, M. G. Finn, K. B. Sharpless, *Angew. Chem. Int. Ed.* **2001**, *40*, 2004–2021.

[22] B. C. Boren, S. Narayan, L. K. Rasmussen, L. Zhang, H. Zhao, Z. Lin, G. Jia, V. V Fokin, *J. Am. Chem. Soc.* **2008**, *130*, 8923–8930.

[23] M. Meldal, C. W. Tornøe, *Chem. Rev.* **2008**, *108*, 2952–3015.

[24] N. J. Agard, J. A. Prescher, C. R. Bertozzi, *J. Am. Chem. Soc.* **2004**, *126*, 15046–15047.

[25] G. Wittig, A. Krebs, *Chem. Ber.* **1961**, *94*, 3260–3275.

[26] C. G. Gordon, J. L. MacKey, J. C. Jewett, E. M. Sletten, K. N. Houk, C. R. Bertozzi, *J. Am. Chem. Soc.* **2012**, *134*, 9199–9208.

[27] N. J. Agard, J. M. Baskin, J. A. Prescher, A. Lo, C. R. Bertozzi, *ACS Chem. Biol.* **2006**, *1*, 644–648.

[28] J. M. Baskin, J. A. Prescher, S. T. Laughlin, N. J. Agard, P. V Chang, I. A. Miller, A. Lo, J. A. Codelli, C. R. Bertozzi, *Proc. Natl. Acad. Sci. U. S. A.* **2007**, *104*, 16793–16797.

[29] J. C. Jewett, E. M. Sletten, C. R. Bertozzi, *J. Am. Chem. Soc.* **2010**, *132*, 3688–3690.

[30] E. M. Sletten, C. R. Bertozzi, *Org. Lett.* **2008**, *10*, 3097–3099.

[31] G. De Almeida, E. M. Sletten, H. Nakamura, K. K. Palaniappan, C. R. Bertozzi, *Angew. Chem. Int. Ed.* **2012**, *51*, 2443–2447.

[32] N. E. Mbua, J. Guo, M. A. Wolfert, R. Steet, G.-J. Boons, *ChemBioChem* **2011**, *12*, 1912–1921.

[33] S. Yoshida, A. Shiraishi, K. Kanno, T. Matsushita, K. Johmoto, H. Uekusa, T. Hosoya, *Sci. Rep.* **2011**, *1*, 82.

[34] M. F. Debets, S. S. van Berkel, S. Schoffelen, F. P. J. T. Rutjes, J. C. M. van Hest, F. L. van Delft, *Chem. Commun.* **2010**, *46*, 97–99.

[35] J. Dommerholt, S. Schmidt, R. Temming, L. J. a Hendriks, F. P. J. T. Rutjes, J. C. M. Van Hest, D. J. Lefeber, P. Friedl, F. L. Van Delft, *Angew. Chem. Int. Ed.* **2010**, *49*, 9422–9425.

[36] D. H. Ess, G. O. Jones, K. N. Houk, *Org. Lett.* **2008**, *10*, 1633–1636.

[37] S. T. Laughlin, J. M. Baskin, S. L. Amacher, C. R. Bertozzi, *Science* **2008**, *320*, 664–667.

[38] S. T. Laughlin, C. R. Bertozzi, *ACS Chem. Biol.* **2009**, *4*, 1068–1072.

[39] P. V Chang, J. A. Prescher, E. M. Sletten, J. M. Baskin, I. A. Miller, N. J. Agard, A. Lo, C. R. Bertozzi, *Proc. Natl. Acad. Sci.* **2010**, *107*, 1821–1826.

[40] X. Ning, J. Guo, M. A. Wolfert, G. J. Boons, *Angew. Chem. Int. Ed.* **2008**, *47*, 2253–2255.

[41] A. Krebs, H. Kimling, *Tetrahedron Lett.* **1970**, *11*, 761–764.

[42] J. Dommerholt, O. van Rooijen, A. Borrmann, C. F. Guerra, F. M. Bickelhaupt, F. L. van Delft, *Nat. Commun.* **2014**, *5*, 5378–5384.

[43] O. Diels, K. Alder, *Justus Liebig's Ann. der Chemie* **1928**, *460*, 98–122.

[44] R. B. Woodward, F. Sondheimer, D. Taub, K. Heusler, W. M. McLamore, *J. Am. Chem. Soc.* **1952**, *74*, 4223–4251.

[45] K. C. Nicolaou, S. a. Snyder, T. Montagnon, G. Vassilikogiannakis, *Angew. Chem. Int. Ed.* **2002**, *41*, 1668–1698.

[46] F. Thalhammer, U. Wallfahrer, J. Sauer, *Tetrahedron Lett.* **1990**, *31*, 6851–6854.

[47] A. Meier, J. Sauer, *Tetrahedron Lett.* **1990**, *31*, 6855–6858.

[48] M. L. Blackman, M. Royzen, J. M. Fox, *J. Am. Chem. Soc.* **2008**, *130*, 13518–9.

[49] N. K. Devaraj, R. Weissleder, S. a Hilderbrand, *Bioconjug. Chem.* **2008**, *19*, 2297–9.

[50] A.-C. Knall, M. Hollauf, C. Slugovc, *Tetrahedron Lett.* **2014**, *55*, 4763–4766.

[51] Y. Liang, J. L. Mackey, S. a Lopez, F. Liu, K. N. Houk, *J. Am. Chem. Soc.* **2012**, *134*, 17904–7.

[52] F. Liu, R. S. Paton, S. Kim, Y. Liang, K. N. Houk, *J. Am. Chem. Soc.* **2013**, *135*, 15642–9.

[53] F. Liu, Y. Liang, K. N. Houk, *J. Am. Chem. Soc.* **2014**, *136*, 11483–93.

[54] J. a. Wagner, D. Mercadante, I. Nikić, E. a. Lemke, F. Gräter, *Chem. - A Eur. J.* **2015**, *21*, 12431–12435.

[55] A. Talbot, D. Devarajan, S. J. Gustafson, I. Fernández, F. M. Bickelhaupt, D. H. Ess, *J. Org. Chem.* **2015**, *80*, 548–558.

[56] J. Yang, Y. Liang, J. Šečkutė, K. N. Houk, N. K. Devaraj, *Chemistry* **2014**, *20*, 3365–75.

[57] M. R. Karver, R. Weissleder, S. A. Hilderbrand, *Bioconjug. Chem.* **2011**, *22*, 2263–2270.

[58] O. Sijbren, Catalysis of Diels-Alder Reactions in Water, **1998**.

[59] J. W. Wijnen, S. Zavarise, J. B. F. N. Engberts, M. Charton, *J. Org. Chem.* **1996**, *61*, 2001–2005.

[60] M. T. Taylor, M. L. Blackman, O. Dmitrenko, J. M. Fox, *J. Am. Chem. Soc.* **2011**, *133*, 9646–9.

[61] M. F. Debets, C. W. J. Van Der Doelen, F. P. J. T. Rutjes, F. L. Van Delft, *ChemBioChem* **2010**, *11*, 1168–1184.

[62] J. Yang, J. Šečkutė, C. M. Cole, N. K. Devaraj, *Angew. Chem. Int. Ed.* **2012**, *51*, 7476–9.

[63] D. M. Patterson, L. a Nazarova, B. Xie, D. N. Kamber, J. a Prescher, *J. Am. Chem. Soc.* **2012**, *134*, 18638–43.

[64] R. M. Versteegen, R. Rossin, W. ten Hoeve, H. M. Janssen, M. S. Robillard, *Angew. Chem. Int. Ed.* **2013**, *52*, 14112–6.

[65] R. Rossin, S. M. J. van Duijnhoven, W. ten Hoeve, H. M. Janssen, L. H. J. Kleijn, F. J. M. Hoeben, R. M. Versteegen, M. S. Robillard, *Bioconjug. Chem.* **2016**, *27*, 1697–1706.

[66] S. R. Cherry, M. Dahlbom, in *PET*, Springer New York, New York, NY, **n.d.**, pp. 1–117.

[67] T. Ido, C.-N. Wan, V. Casella, J. S. Fowler, A. P. Wolf, M. Reivich, D. E. Kuhl, *J. Label. Compd. Radiopharm.* **1978**, *14*, 175–183.

[68] International Atomic Energy Agency., *Cyclotron Produced Radionuclides : Principles and Practice*, International Atomic Energy Agency, **2009**.

[69] E. W. Price, C. Orvig, *Chem. Soc. Rev.* **2014**, *43*, 260–90.

[70] R. Bejot, L. Carroll, K. Bhakoo, J. Declerck, V. Gouverneur, *Bioorganic Med. Chem.* **2012**, *20*, 324–329.

[71] D. Zhou, W. Chu, C. S. Dence, R. H. Mach, M. J. Welch, *Nucl. Med. Biol.* **2012**, *39*, 1175–1181.

[72] M. Glaser, E. Arstad, *Bioconjug. Chem.* **2007**, *18*, 989–993.

[73] L. Iddon, J. Leyton, B. Indrevoll, M. Glaser, E. G. Robins, A. J. T. George, A. Cuthbertson, S. K. Luthra, E. O. Aboagye, *Bioorganic Med. Chem. Lett.* **2011**, *21*, 3122–3127.

[74] G. Smith, M. Glaser, M. Perumal, Q. De Nguyen, B. Shan, E. Årstad, E. O. Aboagye, *J. Med. Chem.* **2008**, *51*, 8057–8067.

[75] K. Kettenbach, H. Schieferstein, T. L. Ross, *Biomed Res. Int.* **2014**, *2014*, DOI 10.1155/2014/361329.

[76] M. Pretze, D. Pietzsch, C. Mamat, *Molecules* **2013**, *18*, 8618–8665.

[77] J. Y. Choi, B. C. Lee, *Nucl. Med. Mol. Imaging (2010).* **2015**, *49*, 258–267.

[78] S. Arumugam, J. Chin, R. Schirrmacher, V. V. Popik, A. P. Kostikov, *Bioorganic Med. Chem. Lett.* **2011**, *21*, 6987–6991.

[79] R. D. Carpenter, S. H. Hausner, J. L. Sutcliffe, *ACS Med. Chem. Lett.* **2011**, *2*, 885–889.

[80] S. H. Hausner, R. D. Carpenter, N. Bauer, J. L. Sutcliffe, *Nucl. Med. Biol.* **2013**, *40*, 233–239.

[81] V. Bouvet, M. Wuest, F. Wuest, *Org. Biomol. Chem.* **2011**, *9*, 7393.

[82] L. S. Campbell-Verduyn, L. Mirfeizi, A. K. Schoonen, R. A. Dierckx, P. H. Elsinga, B. L. Feringa, *Angew. Chem. Int. Ed.* **2011**, *50*, 11117–11120.

[83] H. L. Kim, K. Sachin, H. J. Jeong, W. Choi, H. S. Lee, D. W. Kim, *ACS Med. Chem. Lett.* **2015**, *6*, 402–407.

[84] Z. Li, H. Cai, M. Hassink, M. L. Blackman, R. C. D. Brown, P. S. Conti, J. M. Fox, *Chem. Commun.* **2010**, *46*, 8043–5.

[85] R. Selvaraj, S. Liu, M. Hassink, C.-W. Huang, L.-P. Yap, R. Park, J. M. Fox, Z. Li, P. S. Conti, *Bioorg. Med. Chem. Lett.* **2011**, *21*, 5011–4.

[86] S. Liu, M. Hassink, R. Selvaraj, L. Yap, R. Park, H. Wang, X. Chen, J. M. Fox, Z. Li, P. S. Conti, *Mol. Imaging* **2013**, *12*, 121–128.

[87] Z. Wu, S. Liu, M. Hassink, I. Nair, R. Park, L. Li, I. Todorov, J. M. Fox, Z. Li, J. E. Shively, et al., *J. Nucl. Med.* **2013**, *54* , 244–251.

[88] R. Selvaraj, B. C. Giglio, S. Liu, H. Wang, M. Wang, H. Yuan, S. R. Chintala, L. Yap, P. S. Conti, J. M. Fox, et al., *Bioconjug. Chem.* **2015**, 150213112416009.

[89] M. Wang, D. Svatunek, K. Rohlfing, Y. Liu, H. Wang, B. Giglio, H. Yuan, Z. Wu, Z. Li, J. Fox, *Theranostics* **2016**, *6*, 887–895.

[90] C. Denk, D. Svatunek, T. Filip, T. Wanek, D. Lumpi, J. Fröhlich, C. Kuntner, H. Mikula, *Angew. Chem. Int. Ed.* **2014**, *53*, 9655–9659.

[91] J. Zhu, S. Li, C. Wängler, B. Wängler, R. B. Lennox, R. Schirrmacher, *Chem. Commun.* **2015**, DOI 10.1039/C5CC03623B.

[92] M. M. Herth, V. L. Andersen, S. Lehel, J. Madsen, G. M. Knudsen, J. L. Kristensen, *Chem. Commun.* **2013**, *49*, 3805–7.

[93] C. Denk, D. Svatunek, S. Mairinger, J. Stanek, T. Filip, D. Matscheko, C. Kuntner, T. Wanek, H. Mikula, *Bioconjug. Chem.* **2016**, *27*, 1707–1712.

[94] M. Rashidian, E. J. Keliher, M. Dougan, P. K. Juras, M. Cavallari, G. R. Wojtkiewicz, J. T. Jacobsen, J. G. Edens, J. M. J. Tas, G. Victora, et al., *ACS Cent. Sci.* **2015**, 150603073029009.

[95] M. Rashidian, L. Wang, J. G. Edens, J. T. Jacobsen, I. Hossain, Q. Wang, G. D. Victora, N. Vasdev, H. Ploegh, S. H. Liang, *Angew. Chem. Int. Ed.* **2016**, *55*, 528–533.

[96] B. M. Zeglis, F. Emmetiere, N. Pillarsetty, R. Weissleder, J. S. Lewis, T. Reiner, *ChemistryOpen* **2014**, *3*, 48–53.

[97] H. L. Evans, L. Carroll, E. O. Aboagye, A. C. Spivey, *J. Label. Compd. Radiopharm.* **2013**, DOI 10.1002/jlcr.3153.

[98] A. R. Genady, J. Tan, M. E. El-Zaria, A. Zlitni, N. Janzen, J. F. Valliant, *J. Organomet. Chem.* **2015**, *791*, 204–213.

[99] J. P. K. Dzandzi, D. R. Beckford Vera, A. R. Genady, S. a. Albu, L. J. Eltringham-Smith, A. Capretta, W. P. Sheffield, J. F. Valliant, *J. Org. Chem.* **2015**, *80*, 7117–7125.

[100] S. a. Albu, S. A. Al-Karmi, A. Vito, J. P. K. Dzandzi, A. Zlitni, D. Beckford-Vera, M. Blacker, N. Janzen, R. M. Patel, A. Capretta, et al., *Bioconjug. Chem.* **2016**, *27*, 207–216.

[101] C. Chang, R. M. Sharkey, E. A. Rossi, H. Karacay, W. McBride, H. J. Hansen, J.-F. Chatal, J. Barbet, D. M. Goldenberg, *Mol. Cancer Ther.* **2002**, *1*, 553–63.

[102] D. M. Goldenberg, C. H. Chang, E. A. Rossi, W. J. McBride, R. M. Sharkey, *Theranostics* **2012**, *2*, 523–540.

[103] D. A. Goodwin, C. F. Meares, M. J. Mccall, M. Mctigue, W. Chaovapong, *J. Nucl. Med.* **1988**, *29*, 226–234.

[104] D. A. Goodwin, C. F. Meares, G. F. David, M. McTigue, M. J. McCall, J. M. Frincke, M. R. Stone, R. M. Bartholomew, J. P. Leung, *Int. J. Radiat. Appl. Instrumentation. Part B. Nucl. Med. Biol.* **1986**, *13*, 383–391.

[105] D. T. Reardan, C. F. Meares, D. A. Goodwin, M. McTigue, G. S. David, M. R. Stone, J. P. Leung, R. M. Bartholomew, J. M. Frincke, *Nature* **1985**, *316*, 265–268.

[106] J. B. Chem, **2003**, *30*, 776–780.

[107] H. L. Evans, R. L. Slade, L. Carroll, G. Smith, Q.-D. Nguyen, L. Iddon, N. N. Kamaly, H. Stöckmann, F. J. Leeper, E. O. Aboagye, et al., *Chem. Commun.* **2012**, *48*, 991–3.

[108] S. B. Lee, H. L. Kim, H.-J. Jeong, S. T. Lim, M.-H. Sohn, D. W. Kim, *Angew. Chem. Int. Ed.* **2013**, *52*, 10549–52.

[109] N. K. Devaraj, G. M. Thurber, E. J. Keliher, B. Marinelli, R. Weissleder, *Proc. Natl. Acad. Sci. U. S. A.* **2012**, *109*, 4762–4767.

[110] B. M. Zeglis, K. K. Sevak, T. Reiner, P. Mohindra, S. D. Carlin, P. Zanzonico, R. Weissleder, J. S. Lewis, *J. Nucl. Med.* **2013**, *54*, 1389–1396.

[111] J. P. Meyer, J. L. Houghton, P. Kozlowski, D. Abdel-Atti, T. Reiner, N. V. K. Pillarsetty, W. W. Scholz, B. M. Zeglis, J. S. Lewis, *Bioconjug. Chem.* **2016**, *27*, 298–301.

[112] L. Wyffels, D. Thomae, A.-M. Waldron, J. Fissers, S. Dedeurwaerdere, P. Van der Veken, J. Joossens, S. Stroobants, K. Augustyns, S. Staelens, *Nucl. Med. Biol.* **2014**, *41*, 513–23.

[113] R. Rossin, P. Renart Verkerk, S. M. van den Bosch, R. C. M. Vulders, I. Verel, J. Lub, M. S. Robillard, *Angew. Chem. Int. Ed.* **2010**, *49*, 3375–3378.

[114] R. Rossin, T. Läppchen, S. M. van den Bosch, R. Laforest, M. S. Robillard, *J. Nucl. Med.* **2013**, *54* , 1989–1995.

[115] R. Rossin, S. M. van den Bosch, W. Ten Hoeve, M. Carvelli, R. M. Versteegen, J. Lub, M. S. Robillard, *Bioconjug. Chem.* **2013**, *24*, 1210–7.

2 Results and Discussion

2.1 Overview of Contributions

I. Strain-Promoted Alkyne Azide Cycloaddition

Manuscript #1

Dennis Svatunek, Nicole Houszka, Christoph Denk, Christian Hametner, Günter Allmaier and Hannes Mikula*; Reactivity of Secondary and Tertiary Azides in Strain-Promoted Alkyne Azide Cycloadditions, manuscript draft.

Manuscript #2

Dennis Svatunek, Gottfried Eilenberger, Christoph Denk, Daniel Lumpi, Christian Hametner, Günter Allmaier and Hannes Mikula*; Monitoring of Strain-Promoted Alkyne Azide Cycloadditions in Biological Media by Inline ATR-IR spectroscopy, manuscript draft.

Manuscript #3

Christoph Denk, Martin Wilkovitsch, Philipp Skrinjar, Dennis Svatunek, Severin Mairinger, Claudia Kuntner, Thomas Filip, Johannes Fröhlich, Thomas Wanek, Hannes Mikula*; Investigation of Small [^{18}F]-Fluoroalkylazides for Rapid Radiolabeling and *In Vivo* Click Chemistry, *Bioconjugate Chemistry* **2016**, submitted manuscript.

II. Tetrazine Ligation

Manuscript #4

Christoph Denk, Dennis Svatunek, Thomas Filip, Thomas Wanek, Daniel Lumpi, Johannes Fröhlich, Claudia Kuntner*, Hannes Mikula*; Development of a ^{18}F-Labeled Tetrazine with Favorable Pharmacokinetics for Bioorthogonal PET Imaging, *Angew. Chem. Int. Ed.* **2014**, 53, 9655–9659.

Manuscript #5

Christoph Denk, Dennis Svatunek, Severin Mairinger, Claudia Kuntner, Thomas Filip, Michael Sauberer, Johannes Fröhlich, Thomas Wanek, Hannes Mikula*; A Tale of 3-[^{18}F]Fluoropropyl-1,2,4,5-tetrazines, manuscript draft

Manuscript #6

Christoph Denk, Dennis Svatunek, Severin Mairinger, Johann Stanek, Thomas Filip, Dominik Matscheko, Claudia Kuntner, Thomas Wanek, Hannes Mikula*; Design, Synthesis, and Evaluation of a Low-Molecular-Weight ^{11}C-Labeled Tetrazine for Pretargeted PET Imaging Applying Bioorthogonal *in Vivo* Click Chemistry, *Bioconjugate Chem.* **2016**, 27, 1707-1712.

Manuscript #7

Mengzhe Wang, Dennis Svatunek, Katarina Rohlfing, Yu Liu, Hui Wang, Ben Giglio, Hong Yuan, Zhanghong Wu, Zibo Li*, Joseph Fox*; Conformationally Strained *trans*-Cyclooctene (sTCO) Enables the Rapid Construction of ^{18}F-PET Probes *via* Tetrazine Ligation, *Theranostics* **2016**, 6, 887-895.

Manuscript #8

Dennis Svatunek, Christoph Denk, Veronika Rosecker, Barbara Sohr, Christian Hametner, Günter Allmaier, Johannes Fröhlich, Hannes Mikula*; Efficient low-cost preparation of *trans*-cyclooctenes using a simplified flow setup for photoisomerization, *Monatsh Chem* **2016**, 147, 579–585.

2.2 Context of Contributions

In this chapter the context of the subsequently introduced manuscripts or paper drafts will be outlined. The next paragraphs will briefly explain the focus of research in the single topics, refer to theoretical fundamentals and reveal how these contribute to the main topic of the thesis. For detailed background information and respective references see Chapter 2.5.

The main topic of this work is the understanding and improvement of bioorthogonal reactions as well as the development of bioorthogonal applications in PET imaging. We focused on two different types of bioorthogonal ligations: (1) the strain-promoted alkyne azide cycloaddition and (2) tetrazine ligations. Therefore, this chapter is thematically divided into two sections, each focusing on a different ligation, while the overall objective is the same.

I. Strain-Promoted Alkyne Azide Cycloaddition

In recent years several cyclooctyne derivatives have been introduced and investigated towards increased reactivity. However, only few studies, most notable the work of Yoshida *et al.*[1] and van Delft and coworkers,[2] investigated the impact of structural alteration of the azide on the kinetics of SPAAC. We were interested in how steric hindrance can influence the reactivity of alkyl azides in this reaction and conducted experimental and computational investigations to get detailed mechanistic insight leading to a better molecular understanding (Manuscript #1). We hypothesized that primary, secondary and tertiary azides will show very similar reactivity in a reaction with a sterically non-demanding cyclooctyne, like **BCN**, while in reaction with a sterically hindered cyclooctyne, like **ADIBO**, the tertiary azide should not be able to interact well with the triple bond causing a significant drop in reactivity.

First, kinetic NMR measurements were performed, which confirmed our hypothesis. Figure 1 shows the measured rate constants of both **BCN** and **ADIBO** with a primary, secondary and tertiary azide in $CDCl_3$ as determined by ^{1}H-NMR measurements. A tertiary azide reacts about 2500-fold slower with **ADIBO** than it does with **BCN**, and 200 000 times slower than the primary azide with **ADIBO**.

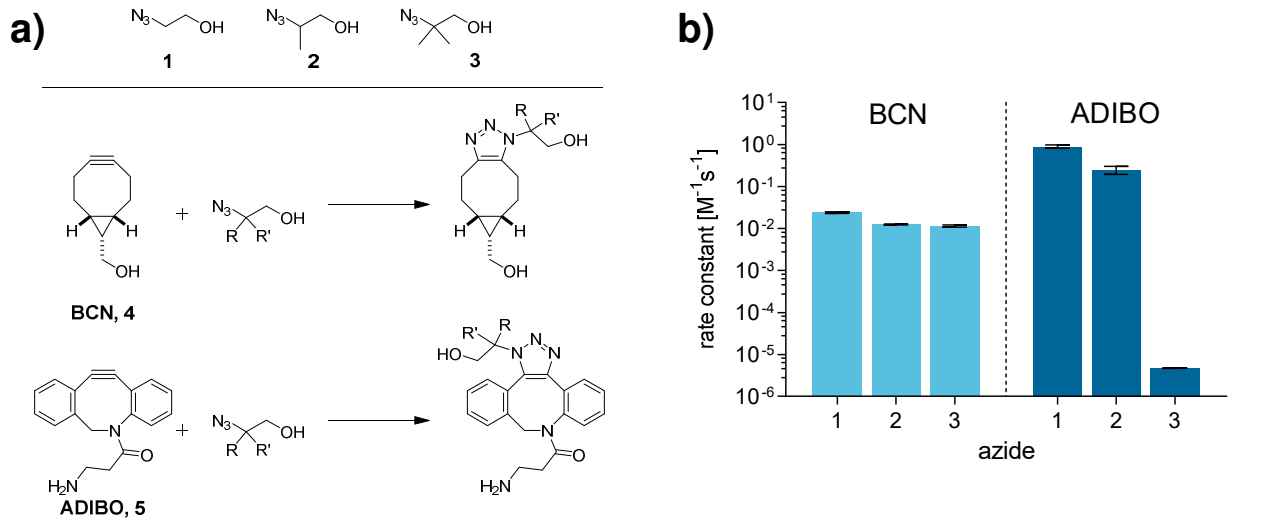

Figure 1: a) Used reaction for comparison of the reactivity of primary, secondary and tertiary azides; **b)** Measured second order rate constants.

The origin of this low reactivity was further investigated using computational methods. Interaction/distortion analysis, as introduced by Houk[3] and Bickelhaupt,[4] was applied using computational methods proposed by van Delft and coworkers.[5] We could show that the low reactivity of tertiary azides with sterically demanding **ADIBO** indeed originates from increased steric hindrance as indicated by a substantially higher distortion energy (Figure 2).

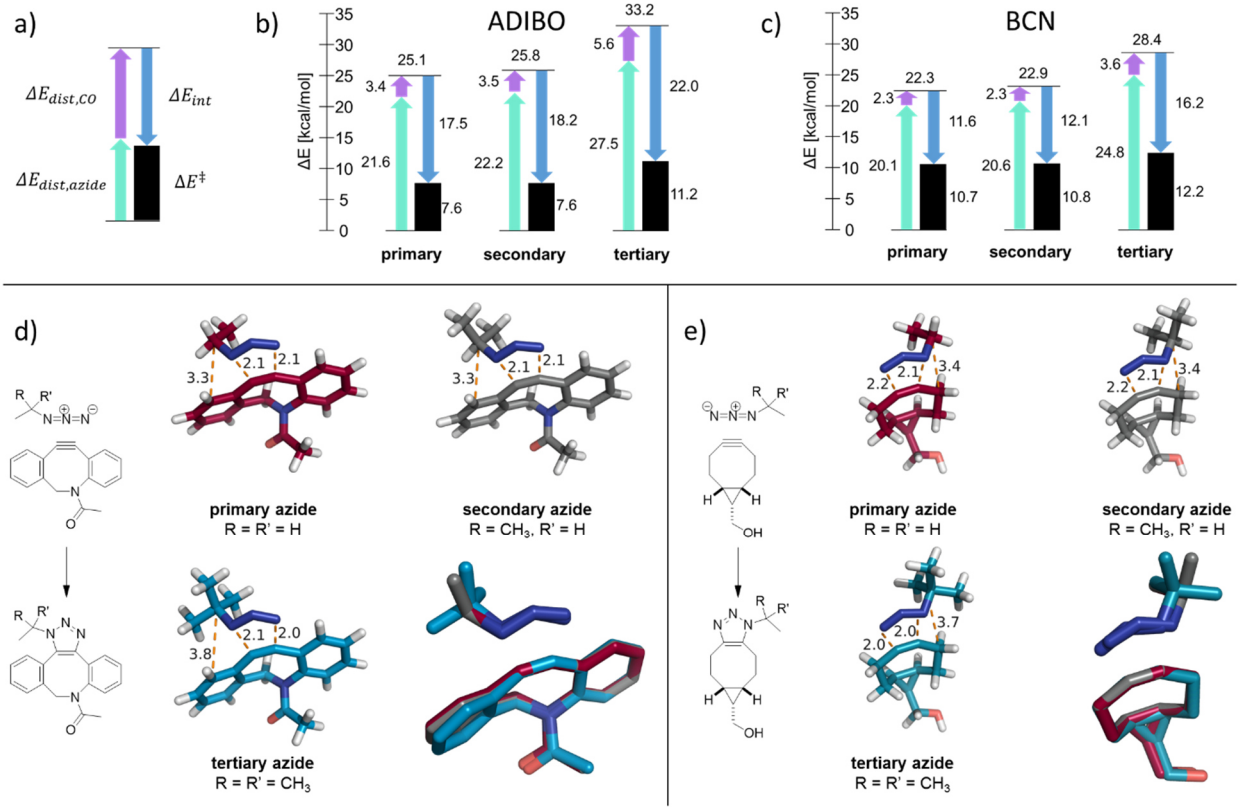

Figure 2: a) Relation of different energies calculated using distortion/interaction analysis (DIA); **b)** Results of DIA for cyclooctyne ADIBO; **c)** Results of DIA for cyclooctyne BCN; **d)** SCS-MP2/6-311++G(2d,p)//6-311+G(d,p) calculated transition states of reactions of ADIBO with primary, secondary and tertiary azides and overlay of all three transition states **c)** SCS-MP2/6-311++G(2d,p)//6-311+G(d,p) calculated transition states of reactions of BCN with primary, secondary and tertiary azides and overlay of all three transition states.

As described and done in manuscript #1, kinetics of strain-promoted alkyne azide cycloadditions are usually investigated by kinetic NMR experiments. However, there are several drawbacks of this method. Reagents have to be mixed outside of the NMR instrument, resulting in a delay between start of the reaction and first data points. This also results in the need of an internal standard. In addition, temperature control is difficult and only possible with expensive equipment. Most importantly, this method is limited to deuterated solvents. However, evaluation of the kinetics of bioorthogonal ligations under more complex reaction conditions, for example in biological media, is of utmost importance. We therefore opted for the development of a method that allows for monitoring of such reactions in aqueous solutions. By using an in-line ATR-IR probe and a custom made reaction flask, as shown in Figure 3, which allows for accurate temperature control and stirring, using less than 1 mL of reaction volume, we have been able to measure rate constants of SPAAC reactions at different temperatures and in different solvents, including human blood plasma.

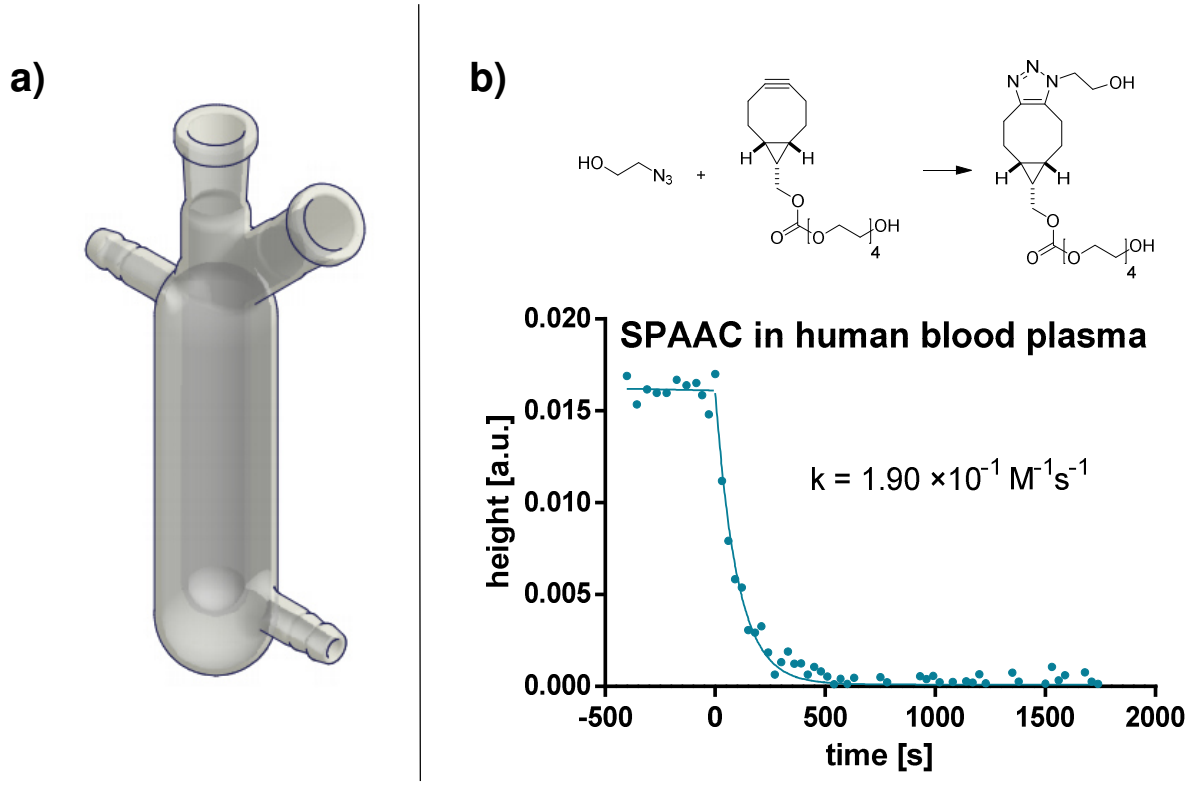

Figure 3: a) Used, custom-made reaction flask; **b)** Strain-promoted alkyne azide cycloaddition measured in human blood plasma

In addition to reaction kinetics investigations low-molecular-weight ^{18}F-labeled alkyl azides have been developed for their use in *in vivo* chemistry (manuscript #3). [^{18}F]2-Fluoroethylazide was proposed by Evans *et al.* as suitable reagent for pretargeted PET imaging.[6] Within this contribution we were able to improve the radiosynthesis of this reagent by introduction of a novel, crystalline precursor for radiolabeling. However, during our experiments we noticed rapid degradation of this alkyl azide causing generation of free [^{18}F]fluoride, which accumulates in bones. Derivatives of this compound, [^{18}F]1-azido-3-fluoropropane and [^{18}F]2-azido-1-fluoropropane, showed similar behavior *in vivo*. Nonetheless, these radiolabeled azides can be used for rapid radiolabeling using SPAAC or copper-catalyzed click chemistry. The latter was used in this work for radiolabeling of alkyne-tagged endomorphine-1 using [^{18}F]2-fluoroethylazide as radio-click agent (Figure 4).

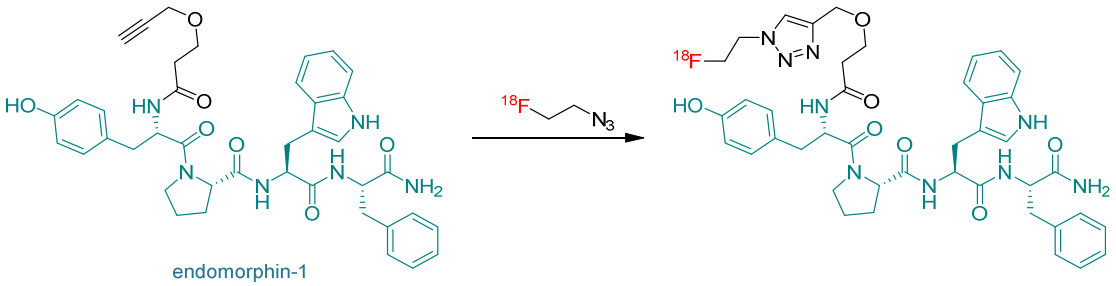

Figure 4: Rapid radiolabeling of endomorphin-1 using [^{18}F]fluoroethylazide

II. Tetrazine Ligations

Due to the very high reaction rates encountered in tetrazine ligations, this kind of bioorthogonal ligation is the perfect reaction for radiolabeling and pretargeted PET applications, especially if short lived isotopes, such as positron emitters ^{18}F and ^{11}C, are involved. Before 2014 no ^{18}F-labeled tetrazines were known and there were only two reports about a failed radiolabeling attempt of a highly reactive tetrazines by Fox *et al.*[7] As described in manuscript #4 we focused on the development of an ^{18}F-labeled tetrazine based on a less reactive dialkyl-tetrazine scaffold. This structure was chosen, since we hypothesized that lower reactivity of the tatrazine should lead to higher stability during radiolabeling via direct radiofluorination. Computational prediction of reaction kinetics using DFT methods suggested, that the combination of such a Tz with highly reactive s-TCO will lead to similar reaction rates as commonly used highly reactive tetrazines achieve in combination with low reactivity TCOs substituted at C5. This was also confirmed by stopped-flow measurements.

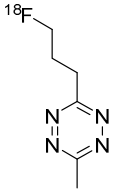

6

^{18}F-Tetrazine **6** showed homogenous biodistribution in mice, including the brain, and good *in vivo* stability.

Having a first ^{18}F-labeled Tz available we started to investigate derivatives (Figure 6) with the aim to improve the reactivity while maintaining sufficient stability for direct radiolabeling also by further improvement of the radiofluorination procedure (manuscript #5). Seven additional aryl-alkyl tetrazines were investigated, starting with prediction of kinetics using computational methods. Based on calculated $\Delta G^{\ddagger}$ values, proposed tetrazines were expected to have relative rates compared to **6** of 1.8 to 70-fold. However, stopped-flow measurements revealed that calculated $\Delta E^{\ddagger}$ values show a much better correlation to the measured rate constants, in case of aryl-alkyl substituted tetrazines, and can be used as for reliable prediction of the reactivity of such systems.

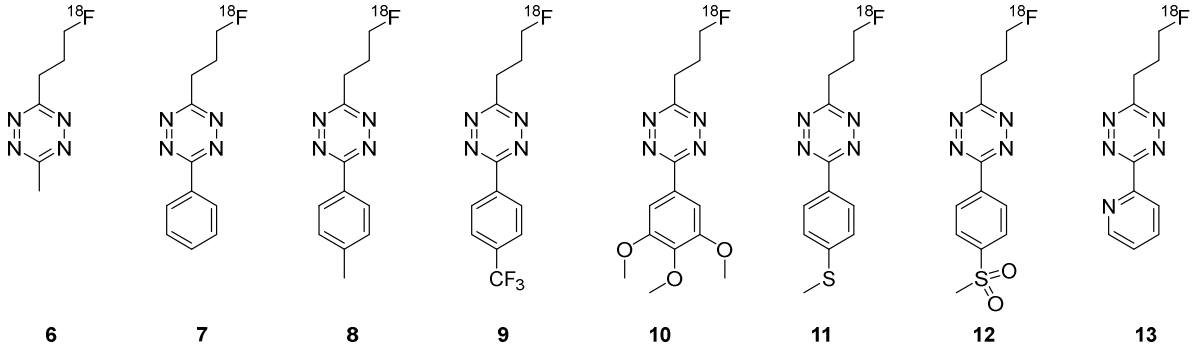

6 **7** **8** **9** **10** **11** **12** **13**

Figure 5: Second generation ^{18}F-labeled tetrazines

Radiolabeling of the four less reactive tetrazines **7**, **8**, **10** and **11** was possible, while the higher reactive compounds **9**, **12** and **13** were not stable under labeling conditions. However, tetrazine **12** could be prepared by oxidation of **11** using dimethyldioxirane in acetone (post-radiolabeling modification). **11** and **12** both showed homogeneous biodistribution and good *in vivo* stability, however, **11** got oxidized to the sulfoxide and **12** *in vivo*. Since **12** is significantly more reactive than **11**, this in vivo oxidation is a first example of a metabolic turn-on of radiolabeled click agents.

In comparison to **6**, we were able to increase the reactivity by a factor of 4, while still obtaining good radiochemical yields, homogeneous biodistribution and good *in vivo* stability.

In addition to ^{18}F-tetrazines ^{11}C-labeled click imaging agents are of high interest. In Manuscript #6 we describe the successful development of a small ^{11}C-tetrazine. Selected structures (similar to the previously discovered ^{18}F-labeled dialkyltetrazine) were first investigated by DFT to estimate their reactivity with *trans*-cyclooctenes. Compound **14** was finally excluded, due to extremely low predicted reaction rates, whereas **15** was chosen for further investigations. Stopped-flow measurements revealed reaction rates comparable to **6** and radiolabeling was possible in good yield within only 5 minutes. PET measurements of **15** in mice showed homogeneous biodistribution and rapid renal

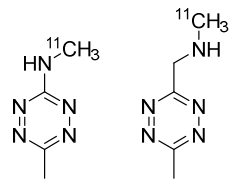

14 **15**

excretion. A proof-of-concept experiment for pretargeted PET imaging using this tetrazine was conducted, using TCO labeled nanoparticles, which accumulate in the lungs. Using this approach, the ability of this ^{11}C-tetrazine to act as a pull-down reagent in pretargeted PET imaging could be successfully demonstrated.

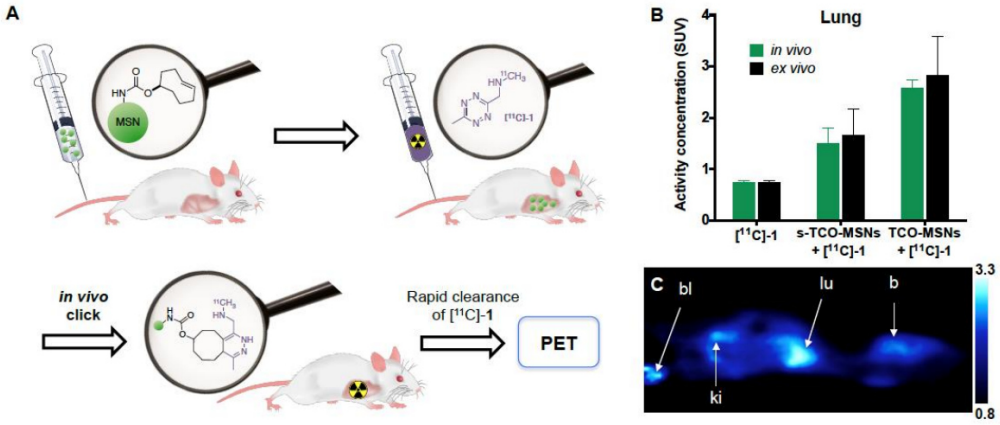

Figure 6: Pretargeted PET imaging using TCO modified nanoparticles and ^{11}C-**15**. Taken with permission from Bioconjugate Chem. 2016, 27, 1707−1712, Copyright 2016 American Chemical Society.

The high reaction rates of tetrazine ligations make this kind of bioorthogonal reactions attractive for rapid radiolabeling. In manuscript #7 we describe the development of the highly reactive ^{18}F-tagged s-TCO (**16**) and show its application in rapid radiolabeling of tetrazine-labeled cRGDyK peptide **17**. Due to the extremely high reactivity of the used reaction partners, labeling was possible within minutes at low µM concentration, even if ^{18}F-labeled compound was used in excess. The produced probe (**18**) showed improved pharmacokinetic properties compared to conventionally labeled RGD peptides or previously used rapid labeling protocols based on tetrazine ligations leading to a better signal-to-background ratio in PET imaging of U87 xenografts in mice (Figure 7).

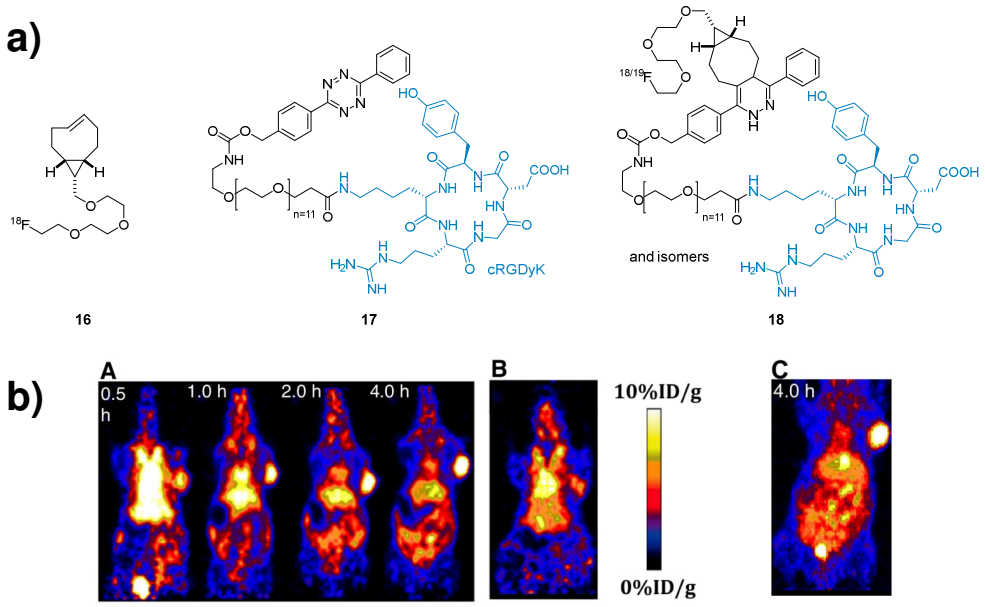

Figure 7: a) Structures used in manuscript #7; **b)** (A) Small animal PET images of mice bearing U87 xenografts, injected with ^{18}F-**18** and imaged 0.5 h, 1.0 h, 2.0 h and 4.0 h post injection, respectively. (B) A 'blocking' experiment in which cyclic RGDyK peptide (200 µg) was injected prior to the injection of ^{18}F-**15**, with imaging at 1.0 h post injection. (C) Two-dimensional maximum intensity projection at 4.0 h post injection of ^{18}F-**18**. [Reprinted with permission from Theranostics, 2016, 6, 887−895; Copyright 2016 Ivyspring Int. Publ.]

Furthermore, we have been able to develop a simple, low-cost setup for photoisomerization of cyclooctenes (manuscript #8). *Trans*-cyclooctenes are the most commonly used dienophiles in tetrazine ligations, due to their extremely high reactivity in bioorthogonal reactions with tetrazines. However, to date only one derivative, (E)-cyclooct-4-enol, is commercially available, but even this one only in low quantities and at a relatively high price. In 2008 Fox and coworkers introduced a method for producing *trans*-cyclooctenes in amounts of up to grams per batch using a photo isomerization approach.[8] This method, which was used in the Fox lab as described in manuscript #7, involves a rather expensive commercial setup and exhibits limited batch size based on the size of available quartz glass flasks. In manuscript #8 we describe a modified system, featuring a flow-photoreactor, constructed from readily available and low-cost components. This flexible setup allows for the synthesis of TCOs on small to large scale and was tested and used for the synthesis of several functionalized TCO-derivatives, such as s-TCO and d-TCO. The performance in regard to yield and kinetics was investigated and we were able to show that this setup can compete and even, in some cases, outperform reported methods. Figure 8 shows a comparison between the setup introduced by Fox and coworkers and the system featured in manuscript #8.

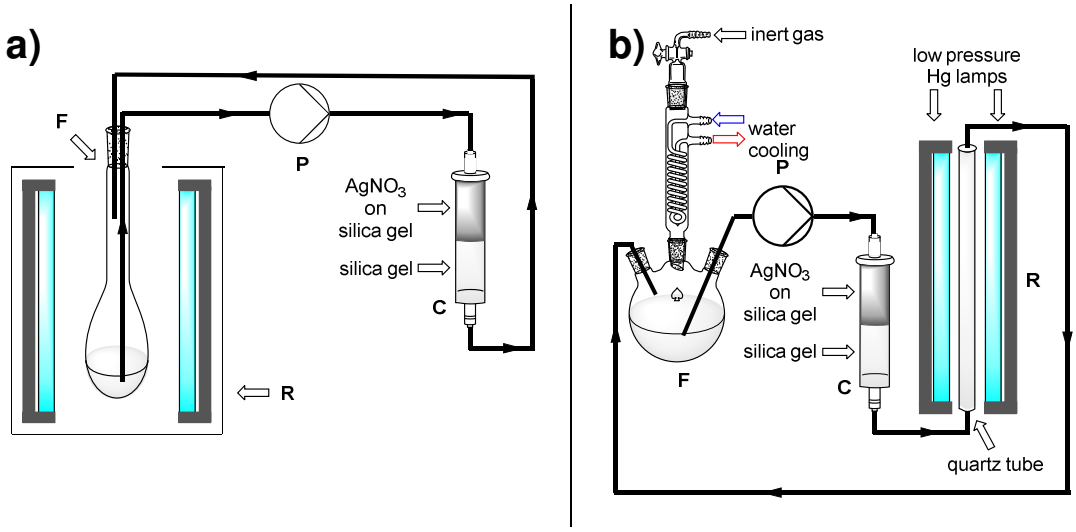

Figure 8: a) Setup as developed and used by the Fox group (also used within the study as described in manuscript #7); **b)** Setup presented in manuscript #8; **R**=reactor, **P**=pump, **F**=reservoir flask, **C**=column. [Reprinted with permission from Monatsh. Chem. 2016, 147, 579–585; Copyright 2016 Springer Nature]

2.3 Conclusion

In summary, within this thesis valuable insight in kinetics of the strain-promoted alkyne azide cycloaddition as well as tetrazine ligations was obtained, and new methods for prediction of reactivities and monitoring of bioorthogonal reactions have successfully been developed. Furthermore, these bioorthogonal ligations were successfully used for the development of new radiochemical methods focusing on pretargeted PET imaging and rapid radiolabeling, featuring several new radiolabeled tetrazines and an ^{18}F-tagged s-TCO derivative. In addition, a simple and versatile setup for the synthesis of TCOs was presented.

We are convinced that the methods, tools and insights presented in this work will find broad application in the fields of bioorthogonal chemistry, pretargeted PET imaging and rapid radiolabeling.

2.4 Literature

[1] S. Yoshida, A. Shiraishi, K. Kanno, T. Matsushita, K. Johmoto, H. Uekusa, T. Hosoya, *Sci. Rep.* **2011**, *1*, 82.

[2] J. Dommerholt, O. van Rooijen, A. Borrmann, C. F. Guerra, F. M. Bickelhaupt, F. L. van Delft, *Nat. Commun.* **2014**, *5*, 5378–5384.

[3] D. H. Ess, K. N. Houk, *J. Am. Chem. Soc.* **2007**, *129*, 10646–10647.

[4] A. Diefenbach, F. M. Bickelhaupt, *J. Phys. Chem. A* **2004**, *108*, 8460–8466.

[5] J. Garcia-Hartjes, J. Dommerholt, T. Wennekes, F. L. Van Delft, H. Zuilhof, *Eur. J. Org. Chem.* **2013**, *6*, 3712–3720.

[6] H. L. Evans, R. L. Slade, L. Carroll, G. Smith, Q.-D. Nguyen, L. Iddon, N. N. Kamaly, H. Stöckmann, F. J. Leeper, E. O. Aboagye, et al., *Chem. Commun.* **2012**, *48*, 991–3.

[7] Z. Li, H. Cai, M. Hassink, M. L. Blackman, R. C. D. Brown, P. S. Conti, J. M. Fox, *Chem. Commun.* **2010**, *46*, 8043–5.

[8] M. Royzen, G. P. a Yap, J. M. Fox, *J. Am. Chem. Soc.* **2008**, *130*, 3760–1.

2.5 Original Works

In the following section, all manuscripts (published; submitted; drafts) are included. Permissions for the reprint of already published articles were kindly given by John Wiley and Sons (manuscript #4), the American Chemical Society (manuscript #6), Ivyspring Int. Publ. (manuscript #7) and Springer Nature (manuscript #8). Supporting Information for all manuscripts, containing most of experimental details and data is included in the appendix of this thesis.

Manuscript #1

Dennis Svatunek, Nicole Houszka, Christoph Denk, Christian Hametner, Günter Allmaier and Hannes Mikula*; Reactivity of Secondary and Tertiary Azides in Strain-Promoted Alkyne Azide Cycloadditions, manuscript draft.

COMMUNICATION

Reactivity of Secondary and Tertiary Azides in Strain-Promoted Alkyne Azide Cycloadditions

Dennis Svatunek, Nicole Houszka, Christoph Denk, Christian Hametner, Günter Allmaier and Hannes Mikula*[a]

Abstract: The strain-promoted alkyne azide cycloaddition (SPAAC) is the most prominent bioorthogonal reaction and finds broad application. Over the years several different cyclooctyne derivatives have been developed and investigated in regards to their reactivity towards azides. However, only few studies examined the influence of different azides on the reaction rates. Within this work we investigated the reactivity of secondary and tertiary azides with cyclooctynes BCN and ADIBO, both experimentally and by computational methods. Primary, secondary and tertiary azides show comparable reaction rates with steric non-demanding cyclooctyne BCN. If steric hindrance is introduced, as by the aryl substituents of ADIBO, reactivity of tertiary azides drops several orders of magnitude in comparison to primary and secondary azides. Computational methods revealed, that this drop in reactivity indeed originates in steric hindrance between the tertiary alkyl residue and the aryl structures of ADIBO.

Since the introduction of bioorthogonal chemistry in 2000 by Saxon and Bertozzi, who showed that a modified staudinger reaction can be used to ligate two molecules within a biologic environment,[1] several bioorthogonal reactions have been developed.[2–7] The two most important ones are the strain-promoted alkyne azide cycloadditions (SPAAC) as well as the tetrazine ligations,[2,8] with commercially available reagents for both types of reactions.

SPAAC reactions are based on the 1,3-dipolar cycloaddition between azides and alkynes to form 1,2,3-triazoles, commonly known as Huisgen cycloadditions. These reactions usually have to be performed at elevated temperatures, due to sluggish kinetics. In 2002 the groups of Sharpless[9] and Meldal[10] independently reported on a copper(I) catalyzed version of this reaction, which allows for rapid formation of triazoles at room temperature. However, the use of copper can be problematic in several applications, for example in case of *in vivo* chemistry, due to the cytotoxic nature of copper. This reaction can be performed at room temperature without the need for a catalyst if cyclooctynes are used as 1,3-dipolarophiles. Due to the strain on the alkyne, the triple bond is already distorted towards transition state geometry, which significantly lowers the energy of activation, allowing for fast reactions (reported second order rate constants between 0.002 – 4.0 $M^{-1}s^{-1}$)[11,12] at room temperature without any catalyst. While tetrazine ligations show much higher reaction rates (up to 3 300 000 $M^{-1}s^{-1}$),[13] which is of utmost importance in applications like *in vivo* radiolabeling using short-lived radioisotopes,[14,15] SPAAC can be used in non time critical applications. It has the advantage of higher stability of the bioorthogonal reactive groups, and the small size of the azide tag. This enables metabolic labeling, since the azide group is generally well accepted by biological processes.[16]

Because of this, SPAACs has found broad applications as a tool for producing covalent linkages in a range of different fields, ranging from materials sciences to chemical biology and biomedical research, and big effort went into optimiziation of these cycloadditions. Several studies were conducted examining the reactivity of cyclooctynes.[12,17–22] Reactivities of new derivatives were investigated extensively both experimentally and theoretically,[23–25] leading to a series of improved cyclooctynes like BCN (**4**)[26] or ADIBO (**5**),[27] which are both commercially available to date. However, only few investigations were done regarding the nature of the azide. In 2011 Hosoya and coworkers reported that sterically hindered 2,6-substituted phenyl azides show higher reactivity with dibenzo cyclooctyne derivatives than sterically non hindered phenyl azides, due to "predistortion" of the azide and therefore lowered activation energy.[28] In 2014 van Delft and coworkers showed, that SPAAC can be accelerated by using electron deficient aryl azides in combination with the less sterically hindered alkyl cyclooctyne BCN.[11]

In general, primary alkyl azides or steric non-demanding aryl azides are used in strain-promoted alkyne azide cycloadditions. Only few reactions with secondary alkyl azides are reported and to the best of our knowledge only one reaction between a tertiary azide, 1-azidoadamantane, and cyclooctynes was described.[29] However, no kinetic data was provided yer.

We were interested in how secondary and tertiary azides perform in strain-promoted alkyne-azide cycloadditions, especially with different cyclooctynes like alkyl cyclooctynes and diaryl derivatives. We hypothesized that primary, secondary and tertiary azides will show similar reactivity if no steric hindrance is present, as it is with less sterically hindered cyclooctynes like BCN. In contrast a drop in reactivity is expected for tertiary azides in combination with steric demanding cyclooctynes like ADIBO, due to steric hindrance at the transition state.

Kinetic NMR experiments using commercially available cyclooctynes BCN (**4**) and ADIBO (**5**), and the homologous series 2-azidoethanol (**1**), 2-azidopropanol (**2**) and 2-azido-2-methylpropanol (**3**) as representatives for primary, secondary and tertiary azides were conducted. These studies were performed on a Bruker Avance III HD 600 MHz spectrometer equipped with a Prodigy BBO cryo probe using ^{1}H-NMR spectroscopy. Solutions of azides and cyclooctynes in $CDCl_3$ were mixed in the NMR tubes, transferred into the NMR machine and multiple ^{1}H-spectra were recorded over a time of 30 to 360 minutes, depending on the reaction rate. Reactions were conducted in triplicates at 298 K. Using an internal standard, the concentration of starting materials over time was monitored and second order rate constants were calculated. Detailed experimental description and selected data sets can be found in the supporting information. As expected all three azides show very similar reaction rates with BCN, ranging from 0.012 to 0.024 $M^{-1}s^{-1}$ (Figure 1). Relative rates, in comparison to the reaction between BCN (**4**) and primary azide **1**, are 0.54 and 0.50 for secondary (**2**) and tertiary azide (**3**) respectively (Table 1). In case of the reaction with ADIBO (**5**), the rate of the tertiary azide, 4.7×10^{-6} $M^{-1}s^{-1}$ (relative rate 0.0002), is five orders

[*] D. Svatunek, N. Houszka, Dr. C. Denk, Dr. C. Hametner, Dr. H. Mikula
Institut für Angewandte Synthesechemie
Technische Universität Wien (TUW) (Austria)
E-mail: hannes.mikula@tuwien.ac.at

D. Svatunek, Prof. G. Allmaier
Institut für Chemische Technologie und Analytik
Technische Universität Wien (TUW) (Austria)

Supporting information for this article is given via a link at the end of the document.

of magnitude lower than that of the primary and the secondary azide **2** and **3**, which showed rates of 0.90 and 0.25 $M^{-1}s^{-1}$, respectively. This corresponds to relative rates of 38 for the combination of **1** and **5**, and 10 for the reaction between **2** and **5**.

Table 1. Rate constants determined by ^{1}H-NMR kinetic measurements of reactions between azides **1**, **2** and **3** and cyclooctynes **4** and **5** in $CDCl_3$ at 298K.

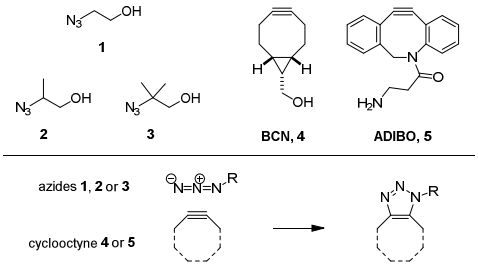

	second order rate constants [$M^{-1}s^{-1}$]		relative reactivity values [a] [ ]	
azide	+ 4	+ 5	+ 4	+ 5
1	0.024 ± 0.001	0.90 ± 0.09	1.0	38
2	0.013 ± 0.0003	0.25 ± 0.05	0.54	10
3	0.012 ± 0.001	0.0000047 ± 0.00000004	0.50	0.00020

[a] relative to reaction between **1** and **4**

To further investigate the origin of the low reactivity of the tertiary azide **3** with ADIBO (**5**) a computational study was conducted. SCS-MP2/6-311+G(2d,2p)//MP2/6-311G(d,p) was used, as suggested by van Delft and coworkers,[30] with the modification of adding counter poise correction to the transition state energy. All calculations were performed using NWChem 6.6. Avogadro and PyMol were used for data analysis.

Distortion/interaction analysis (DIA, also known as activation strain model), as introduced by Houk[31] and Bickelhaupt,[32] was applied for in depth investigation of steric and electronic effects during these reactions. Hereby the energy of activation is dissected in distortion energy, ΔE_{dist} (energy needed for distorting reactants to transition state geometry) and interaction energy, ΔE_{int} (energy released by interaction between the reagents). ΔE_{dist} can be determined by comparing energies of isolated reactants at transition state geometries to their energy at ground state geometry. Interaction energy is the difference of the sum of energies of all isolated reactants at transition state geometry and the energy of the transition state structure (Figure 2a).

Model structures were used for calculations (Figure 2d for ADIBO and 2e for BCN). Results of DIA for the reaction between ADIBO and ethyl azide, isopropyl azide and t.-butyl azide is shown in Figure 2b. In this case the reaction with tertiary azide showed a higher energy of activation with a $\Delta\Delta E^{\ddagger}$ of 3.6 kcal/mol compared to primary and secondary azide. This can be attributed to an 8.1 kcal/mol (32 %) increase in total distortion energy in case of the tertiary azide, with a 2.2 kcal/mol (65 %) increase in cyclooctyne distortion energy and a 5,9 kcal/mol (27 %) increase in azide distortion energy. Interaction energy increases by about 26 % (4.5 kcal/mol), not beeing able to compensate the increased distortion energy.

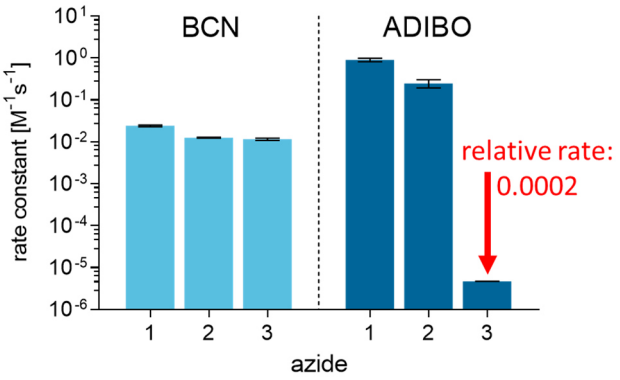

Figure 1. Second order rate constants of reaction between azides 1, 2 and 3 and cyclooctynes 4 and 5

DIA for the reaction of BCN with different azides is shown in Figure 2c. In this case the difference in energy of activation between reaction of primary and tertiary azide is significantly lower with a $\Delta\Delta E^{\ddagger}$ of only 1.5 kcal/mol (12 %). The overall distortion energy is increased by 6.1 kcal/mol (27 %), whereas azide distortion energy is increased by 4.7 kcal/mol (23 %) and cyclooctyne distortion energy by 1.4 kcal/mol (56 %). In contrast to the reaction with ADIBO this increased distortion energy is mostly compensated by the 4.6 kcal/mol (40 %) higher interaction energy.

A comparison of transition state geometries (Figure 2d) shows that in case of the tertiary azide and ADIBO the distance between the aromatic ring and the azide is increased, as indicated by an additional length of 0.5 Å between the alpha-carbon atom of the azide and the nearest carbon of the aromatic ring. An overlay of these three structures demonstrates that this increase in distance originates in bending of the tert.-butyl group and the benzo group in opposite directions. This also explains the high increase in distortion energy of both cyclooctyne and azide in this reaction of 5.9 and 2.2 kcal/mol, respectively. In contrast, in case of BCN (Figure 2e) the difference in distance between the alpha-carbon atom of the azide and the propargylic carbon atom of BCN changes only by 0.3 Å, while the distance between the triple bond and the azide decreases by 0.1-0.2 Å, which, in general, leads to a better overlap of the involved molecular orbitals and therefore higher interaction energy, which is substantially increased, in relation to ADIBO. An overlay of all three transition state structures (Figure 2c) shows that the t.-butyl group of the tertiary azide is only slightly bent away in comparison to primary and secondary azide, explaining the moderate increase in azide distortion energy in the reaction of BCN and tertiary azides. Distortion/interaction analysis confirms that the low reactivity of tertiary azides with ADIBO is indeed caused by steric hindrance.

This reactivity difference allows for an interesting application. Since tertiary azides react extremly slow with ADIBO, but not with BCN, they can be used for semiorthogonal SPAAC reactions. If both primary and tertiary azides are present in the reaction mixture, and ADIBO is added, it is expected to predominately react with the primary azide. If all primary azide is consumed, added BCN can only react with available tertiary azide. This order dependent selectivity is described as semiorthogonality. A possible application would be the site specific labeling of different parts of a protein (Figure 3).

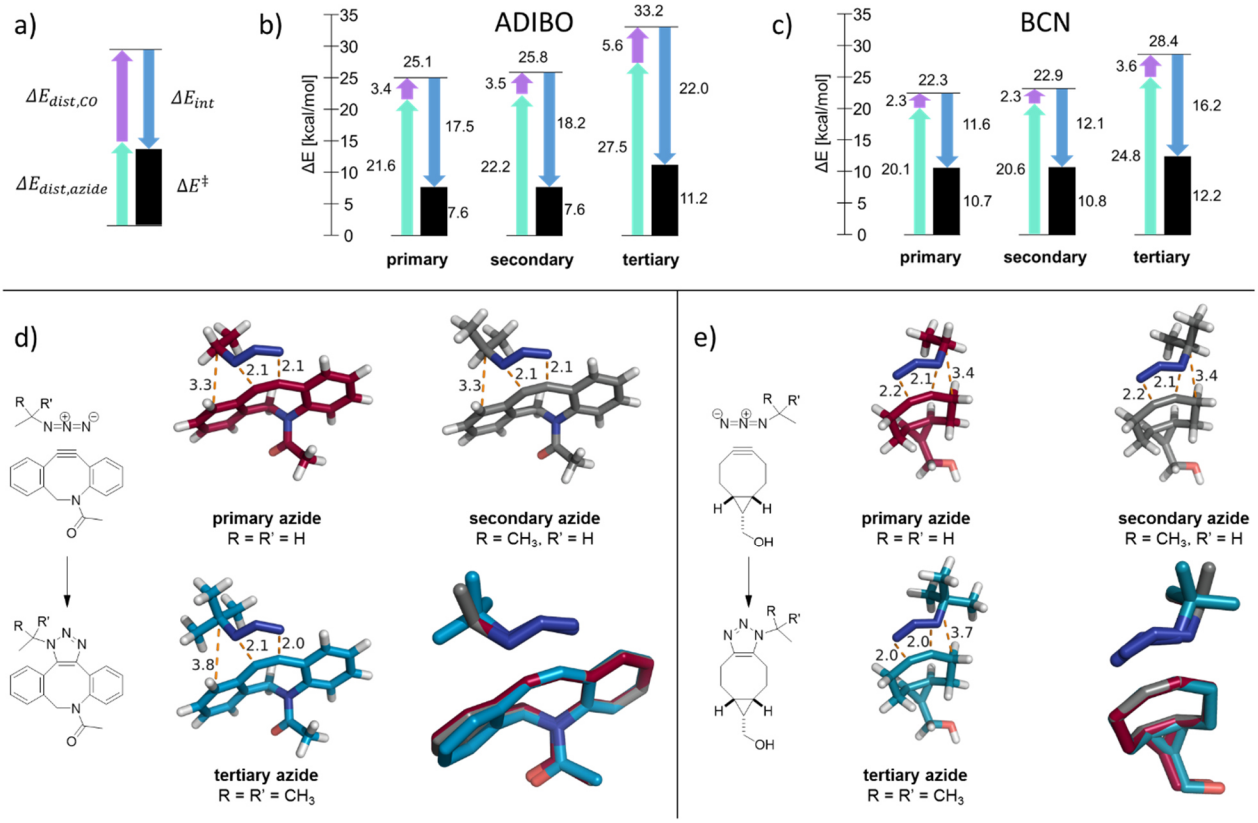

Figure 2. a) Connection between different energies calculated during Distortion/Interaction Analysis; **b)** Results of DIA for cyclooctyne ADIBO; **c)** Results of DIA for cyclooctyne BCN; **d)** SCS-MP2/6-311++G(2d,p)//6-311+G(d,p) calculated transition states of reaction between ADIBO and primary, secondary and tertiary azides and overlay of all three transition states **c)** SCS-MP2/6-311++G(2d,p)//6-311+G(d,p) calculated transition states of reaction between BCN and primary, secondary and tertiary azides and overlay of all three transition states.

Reactions beeing not only bioorthogonal but also mutually orthogonal are of high interest, since it allows for selective labeling of two or more targets simultaniously. While there are such orthogonal click schemes described in literature, they utilize a combination of tetrazine ligation and the strain-promoted alkyne azide cycloaddition.[33,34] Another approach for (semi)orthogonal labeling was the use of SPAAC in combination with copper(I) catalyzed alkyne azide cycloadditions (CuAAC).[35,36] However, CuAAC is only conditionally qualified for ligation *in vivo* due to the use of cytotoxic copper.[37] In contrast the here proposed combinations of tertiary and primary azides with BCN and ADIBO allows for semiorthogonal and bioorthogonal click reactions using SPAAC and commercially available building blocks exclusively. A proof of concept studies, exploiting this semiorthogonal behavior, is currently ongoing in our laboratories.

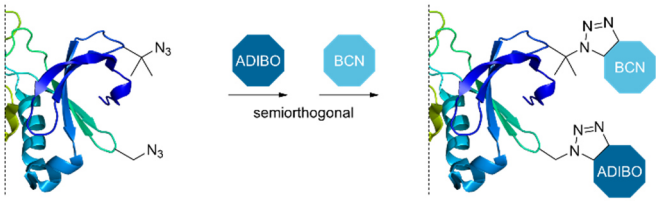

Figure 3. Possible application of the reactivity difference of tertiary azides towards cyclooctynes BCN and ADIBO in site-specific labeling of proteins.

In summary, we were able to assess the reactivity of primary, secondary and tertiary azides towards alkyl cyclooctyne BCN and diaryl cyclooctyne ADIBO. Due to steric hindrance reaction rates between tertiary azides and ADIBO are several orders of magnitude lower than in case of the reaction between tertiary azides with BCN or primary and secondary azides with either cyclooctyne. Therefore, secondary azides can be used in SPAAC reactions, without significant loss of reactivity. Tertiary azides can be used in combination with sterically non-demanding cyclooctynes like BCN. In addition, the difference in reactivity of tertiary azides with BCN and ADIBO leads to possible semiorthogonal applications.

Acknowledgements

We thank the doctoral program 'Molecular and Elemental Imaging in Biosciences (MEIBio)' of TU Wien for funding. Quantum-chemical calculations were performed using the Vienna Scientific Cluster (VSC).

Keywords: Click Chemistry • Kinetics • Strained Molecules • Semiorthogonality • Bioorthogonality

[1] E. Saxon, C. R. Bertozzi, *Science* **2000**, *287*, 2007–2010.
[2] D. M. Patterson, L. a Nazarova, J. a Prescher, *ACS Chem. Biol.* **2014**, *9*, 592–605.
[3] C. S. McKay, M. G. Finn, *Chem. Biol.* **2014**, *21*, 1075–1101.
[4] E. M. Sletten, C. R. Bertozzi, *Angew. Chem. Int. Ed.* **2009**, *48*, 6974–98.
[5] E. M. Sletten, C. R. Bertozzi, *Acc. Chem. Res.* **2011**, *44*, 666–76.
[6] A.-C. Knall, C. Slugovc, *Chem. Soc. Rev.* **2013**, *42*, 5131–42.
[7] J. M. Fox, M. S. Robillard, *Curr. Opin. Chem. Biol.* **2014**, *21*, v–vii.
[8] J. C. Jewett, C. R. Bertozzi, *Chem. Soc. Rev.* **2010**, *39*, 1272–9.

[9] V. V. Rostovtsev, L. G. Green, V. V. Fokin, K. B. Sharpless, *Angew. Chem. Int. Ed.* **2002**, *41*, 2596–2599.
[10] C. W. Tornøe, C. Christensen, M. Meldal, *J. Org. Chem.* **2002**, *67*, 3057–3064.
[11] J. Dommerholt, O. van Rooijen, A. Borrmann, C. F. Guerra, F. M. Bickelhaupt, F. L. van Delft, *Nat. Commun.* **2014**, *5*, 5378–5384.
[12] N. J. Agard, J. A. Prescher, C. R. Bertozzi, *J. Am. Chem. Soc.* **2004**, *126*, 15046–15047.
[13] A. Darko, S. Wallace, O. Dmitrenko, M. M. Machovina, R. a. Mehl, J. W. Chin, J. M. Fox, *Chem. Sci.* **2014**, *5*, 3770.
[14] R. Rossin, P. Renart Verkerk, S. M. van den Bosch, R. C. M. Vulders, I. Verel, J. Lub, M. S. Robillard, *Angew. Chem. Int. Ed.* **2010**, *49*, 3375–3378.
[15] N. K. Devaraj, R. Weissleder, *Acc. Chem. Res.* **2011**, *44*, 816–27.
[16] M. F. Debets, C. W. J. Van Der Doelen, F. P. J. T. Rutjes, F. L. Van Delft, *ChemBioChem* **2010**, *11*, 1168–1184.
[17] N. E. Mbua, J. Guo, M. A. Wolfert, R. Steet, G.-J. Boons, *ChemBioChem* **2011**, *12*, 1912–1921.
[18] G. De Almeida, E. M. Sletten, H. Nakamura, K. K. Palaniappan, C. R. Bertozzi, *Angew. Chem. Int. Ed.* **2012**, *51*, 2443–2447.
[19] E. M. Sletten, C. R. Bertozzi, *Org. Lett.* **2008**, *10*, 3097–3099.
[20] J. C. Jewett, E. M. Sletten, C. R. Bertozzi, *J. Am. Chem. Soc.* **2010**, *132*, 3688–3690.
[21] J. M. Baskin, J. A. Prescher, S. T. Laughlin, N. J. Agard, P. V Chang, I. A. Miller, A. Lo, J. A. Codelli, C. R. Bertozzi, *Proc. Natl. Acad. Sci. U. S. A.* **2007**, *104*, 16793–16797.
[22] N. J. Agard, J. M. Baskin, J. A. Prescher, A. Lo, C. R. Bertozzi, *ACS Chem. Biol.* **2006**, *1*, 644–648.
[23] C. G. Gordon, J. L. MacKey, J. C. Jewett, E. M. Sletten, K. N. Houk, C. R. Bertozzi, *J. Am. Chem. Soc.* **2012**, *134*, 9199–9208.
[24] D. H. Ess, G. O. Jones, K. N. Houk, *Org. Lett.* **2008**, *10*, 1633–1636.
[25] B. Gold, N. E. Shevchenko, N. Bonus, G. B. Dudley, I. V Alabugin, *J. Org. Chem.* **2012**, *77*, 75–89.
[26] J. Dommerholt, S. Schmidt, R. Temming, L. J. a Hendriks, F. P. J. T. Rutjes, J. C. M. Van Hest, D. J. Lefeber, P. Friedl, F. L. Van Delft, *Angew. Chem. Int. Ed.* **2010**, *49*, 9422–9425.
[27] M. F. Debets, S. S. van Berkel, S. Schoffelen, F. P. J. T. Rutjes, J. C. M. van Hest, F. L. van Delft, *Chem. Commun.* **2010**, *46*, 97–99.
[28] S. Yoshida, A. Shiraishi, K. Kanno, T. Matsushita, K. Johmoto, H. Uekusa, T. Hosoya, *Sci. Rep.* **2011**, *1*, 82.
[29] M. Müller, C. Maichle-Mössmer, H. F. Bettinger, *J. Org. Chem.* **2014**, *79*, 5478–83.
[30] J. Garcia-Hartjes, J. Dommerholt, T. Wennekes, F. L. Van Delft, H. Zuilhof, *European J. Org. Chem.* **2013**, *6*, 3712–3720.
[31] D. H. Ess, K. N. Houk, *J. Am. Chem. Soc.* **2007**, *129*, 10646–10647.
[32] ‡ and Axel Diefenbach†, §. F. Matthias Bickelhaupt*, **2004**, DOI 10.1021/jp047986+.
[33] J. a. Wagner, D. Mercadante, I. Nikić, E. a. Lemke, F. Gräter, *Chem. - A Eur. J.* **2015**, *21*, 12431–12435.
[34] Y. Liang, J. L. Mackey, S. a Lopez, F. Liu, K. N. Houk, *J. Am. Chem. Soc.* **2012**, *134*, 17904–7.
[35] J. Schoch, M. Staudt, A. Samanta, M. Wiessler, A. Jäschke, *Bioconjug. Chem.* **2012**, *23*, 1382–1386.
[36] N. Münster, P. Nikodemiak, U. Koert, *Org. Lett.* **2016**, *18*, 4296–4299.
[37] M. Meldal, C. W. Tornøe, *Chem. Rev.* **2008**, *108*, 2952–3015.

Manuscript #2

Dennis Svatunek, Gottfried Eilenberger, Christoph Denk, Daniel Lumpi, Christian Hametner, Günter Allmaier and Hannes Mikula*; Monitoring of Strain-Promoted Alkyne Azide Cycloadditions in Biological Media by Inline ATR-IR spectroscopy, manuscript draft.

COMMUNICATION

Monitoring of Strain-Promoted Alkyne Azide Cycloadditions in Biological Media by Inline ATR-IR spectroscopy

Dennis Svatunek, Gottfried Eilenberger, Christoph Denk, Daniel Lumpi, Christian Hametner, Günter Allmaier and Hannes Mikula*

Abstract: The strain-promoted alkyne azide cycloaddition (SPAAC) is a powerful tool for forming covalent bonds between molecules, even *in vivo,* and therefore found broad application in fields ranging from materials sciences to biological chemistry and biomedical research. For many applications, knowledge about reaction kinetics of these ligations is of utmost importance. Kinetics are usually assessed and studied by NMR measurements. However, these experiments are quite elaborate, require expensive equipment, and reaction conditions are limited in terms of temperature and restricted to deuterated solvents. Herein we present a method for monitoring SPAACs in different solvents, including human blood plasma, and at different temperatures, using an inline ATR-IR probe.

In 1960 Rolf Huisgen reported on 1,3-dipolar cycloadditions including the reaction of organic azides and alkynes forming triazoles.[1] This reaction, commonly known as Huisgen cycloaddition, has found broad attention after the introduction of a copper-catalyzed alternative by Sharpless *et al.*[2] and Meldal *et al.*,[3] which is also often just referred to as "click chemistry". In contrast to Huisgen's protocol only one isomer is formed and the activation energy is significantly lowered, allowing for efficient conversion even at room temperature. However, due to the use of cytotoxic copper, these reactions are only conditionally qualified for *in vivo* applications.[4] Already in 1961 Wittig and coworkers reported that cyclooctyne and phenyl azide react extremely fast at room temperature forming a single product.[5] This reaction was used and modified by Bertozzi and coworkers to develop a bioorthogonal click ligation in 2004.[6] Due to the strain on the triple bond, cyclooctyne it is already distorted towards transition state geometry, which significantly lowers the activation energy and allows for rapid ligation at room temperature without the use of a copper catalyst. Therefore, this reaction is commonly known as strain-promoted alkyne azide cycloaddition (SPAAC) or copper free click (CFC) chemistry.

Several different cyclooctyne derivatives have been developed in the last decade to improve both reactivity and stability of these bioorthogonal compounds.[7–10] Furthermore, the influence of different azides was investigated.[6–9,11–14] Reported second order rate constants range from 2.4×10^{-3} $M^{-1}s^{-1}$ [6] up to 34 $M^{-1}s^{-1}$.[15] Reaction kinetics are usually assessed by NMR experiments. In this case reaction partners are mixed in deuterated solvents in an NMR tube and the reaction is monitored by consecutive scans at defined time points. Using the decrease in starting material signals or increase of product signals the rate constants can be determined. The advantage of this method is the ability to easily follow every involved species, assuming separated signals. However, there are several drawbacks. The first measurement can only be acquired minutes after mixing the compounds, missing the most valuable part of the reaction progress. Moreover, an internal standard is required, since calculations of rate constants demand knowledge of concentrations, which cannot be accurately determined without using a reference. Furthermore, temperature control of the sample is difficult and limited and expensive high frequency spectrometers might be required to separate the desired signals. Most importantly, only deuterated solvents can be used. This leads to the exclusion of biological media as solvent for kinetic measurements. However, knowledge about the kinetics of bioorthogonal ligations under more complex reaction conditions is of utmost importance considering respective applications *in vitro* and *in vivo*.

Another approach for monitoring SPAAC is the use of IR spectroscopy. Azides show a characteristic absorption at around 2100 cm^{-1}, which can be followed over time to determine kinetics. Since azide signals are usually separated from other signals, including solvent signals, it is possible to monitor the reaction progress in several solvents and in presence of other substances. Figure 1a shows the IR spectra of phenylacetylene (**1**), benzyl azide (**2**) and their click product **3**, with a separated azide band at 2100 cm^{-1}. Since the sample in an IR spectrometer is usually easily accessible, it is possible to monitor the reaction solution during the addition of the reaction partner enabling measurements with no delay between the start of the reaction and the first data point. In addition, spectra can be acquired in very short intervals, allowing for observation of fast reactions. Rate determination of cycloadditions including azides by IR spectroscopy was already performed by Huisgen *et al.* in 1967.[16] They were able to determine the reactivity of over 40 different alkynes and alkenes in the 1,3-diploar cycloaddition with azides and also assessed solvent effects to a certain extend.[16] In their 2014 study on the "highly accelerated inverse electron-demand cycloaddition of electron-deficient azides with aliphatic cyclooctynes" van Delft and coworkers also used transmission-FTIR measurements for determination of reaction kinetics.[13] However, while they were able to use a 9:1 mixture of THF:H_2O, measurements failed at higher water content or with other solvents like methanol.

Herein we present a method for rate determination of SPAAC ligations at different temperatures and in various solvents, even including human blood plasma, using ATR-IR spectroscopy. A ReactIR 15 system (Mettler Toledo) equipped with an ATR-IR SiComp probe, which was designed for *in situ* reaction monitoring, was used. This SiComp probe features a silicon crystal for ATR, that exhibits low absorption around 2100 $cm^{-1,}$ in contrast to diamond crystals used in DiComp Probes. This setup allows for temperature control and the use of inert gas atmosphere and stirring, by simply immerging the probe into a reaction solution within a tempered (and sealed) vessel. In this study a special flask (Figure 1b) was used, allowing for temperature-controlled measurements in low reaction volumes.

[*] D. Svatunek, G. Eilenberger, Dr. C. Denk, Dr. D. Lumpi, Dr. C. Hametner, Dr. H. Mikula
Institut für Angewandte Synthesechemie
Technische Universität Wien (TUW) (Austria)
E-mail: hannes.mikula@tuwien.ac.at

D. Svatunek, Prof. G. Allmaier
Institut für Chemische Technologie und Analytik
Technische Universität Wien (TUW) (Austria)

Supporting information for this article is given via a link at the end of the document.

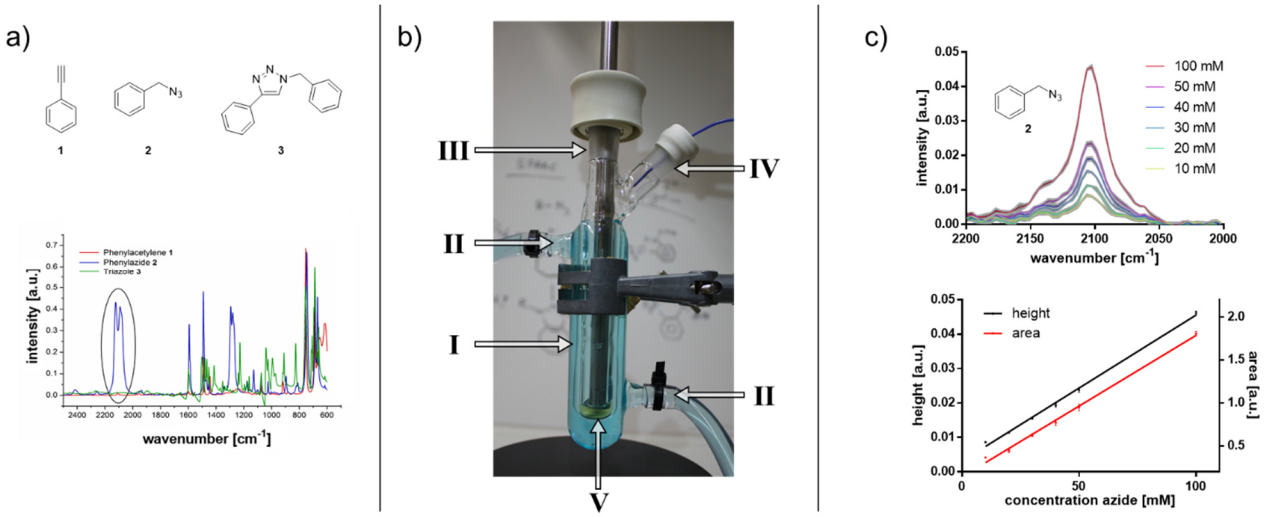

Figure 1. a) Comparison of IR spectra of phenylacetylene (**1**), benzyl azide (**2**) and their click-product **3**, highlighted with a black circle is the azide signal of **2**; **b)** used flask for ATR-IR measurements: **I** shows the double walled tube with the connections to the thermostat (**II**). The ATR-IR probe is inserted by the NS14 glass joint on top (**III**), reagents can be added over joint **IV**. A small magnetic stirring bar is used for stirring in 0.5 mL of reaction volume (**V**); **c)** azide signal in acetonitrile at 37 °C in DMSO at different concentrations, gray areas indicate standard deviation (n=3), and the corresponding height and area based calibration curves.

It consists of a double-walled tube (**I**), which was connected to a thermostat for heating or cooling (**II**), as well as two NS14 glass joints arranged in a 45° angle, one on top for inserting the ATR-IR probe (**III**) and a second one for addition of reagents or additional temperature sensors (**IV**). With this setup a volume of 0.5 mL is sufficient for effective monitoring, even while stirring (**V**). If no stirring is needed even lower volumes can be used. This system was first evaluated by measurement of a calibration curve of benzyl azide in acetonitrile with concentrations ranging from 10 mM to 100 mM (Figure 1c). Very good linear correlation was obtained. In the next step this setup was applied to monitoring of a SPAAC reaction. Therefore, 1 mL of reaction volume was used. Before starting the measurement, the background of pure solvent was acquired. Then 0.9 mL of azide solution was placed in the flask and waited for temperature equilibration. Then 0.1 mL of a 10-fold concentrated 1,3-dipolarophile solution was added to obtain an equimolar mixture of both reagents. Monitoring of the reaction was started before adding the second reactant and reaction was followed by consecutive ATR-IR spectroscopy. The interval between the scans was based on reaction rate, ranging from 20 s for fast reactions to 1 min for slower conversions. For detailed description of the used settings see supporting information. For evaluation of this setup the reaction between benzyl azide **2** and cyclooctyne 4 in DMSO at 37 °C was monitored (Figure 2a). Data was recorded using the iC IR™ 4.3.27 software (Mettler Toledo). Data pretreatment was performed in iC IR™ and Prism 6 (GraphPad Software Inc.) was used for data analysis. First, the background spectrum was subtracted followed by baseline correction. Then a peak region was assigned to the area of the azide signal (2100 cm^{-1}). Peak area and peak height were analyzed over time. Rate constants were determined by linearization and subsequent linear fit. Reaction monitoring using the signal height showed less noise and better linear relationship in the linearized form than data obtained using peak area. In addition, the peak height is not dependent on the width of the assigned peak region. Therefore, peak height was chosen for further measurements. A representative example of the different curves determined by peak height and peak area is shown in Figure 2a. Despite the different signal-to-noise ratios similar results were obtained for the calculated rate constants (peak height: 1.52×10^{-2} $M^{-1}s^{-1}$ vs. peak area: 1.46×10^{-2} $M^{-1}s^{-1}$). Measurements at different concentrations, ranging from 10 mM to 100 mM were conducted (see Supporting information). While measurement at low mM concentrations (<25 mM) is possible, the signal-to-noise ratio is reaching the limit for accurate analysis. Therefore, a starting concentration of 50 mM or higher is recommended for reliable and reproducible measurements.

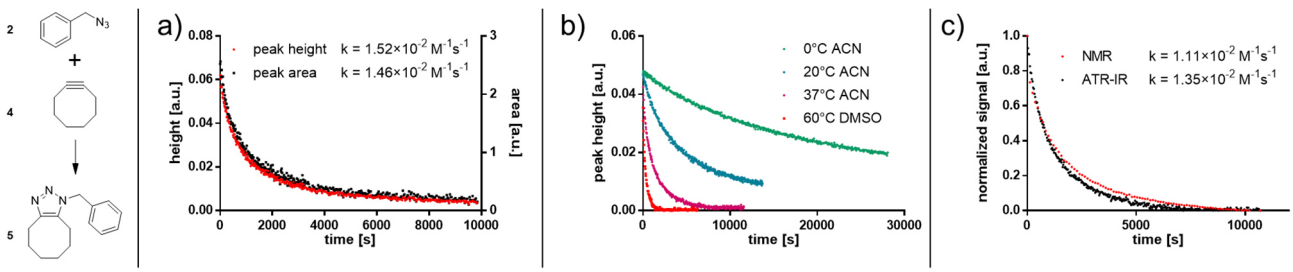

Figure 2. a) Comparison between height and area based method for reaction monitor of the reaction between **2** and **4** in DMSO at 37 °C and at 100 mM starting concentration; **b)** Reaction between **2** and **4** at different temperatures at 100 mM starting concentration; **c)** Comparison between NMR and ATR-IR reaction monitoring of reaction between **2** and **4** in acetonitrile at 37 °C.

A big advantage of the used setup is the ability to easily monitor reactions at different temperatures. After establishing this method, the reaction of benzyl azide and cyclooctyne was followed successfully at different temperatures, ranging from 0°C to 60°C (Figure 2b). Reaction rates were determined to be between 4.99×10^{-4} $M^{-1}s^{-1}$ at 0 °C and 7.32×10^{-2} $M^{-1}s^{-1}$ at 60 °C. In addition, this method was compared to commonly used ^{1}H-NMR measurements (Figure 2c). by studying the reaction between benzyl azide and cyclooctyne in acetonitrile at 37 °C. Both methods show very similar curves and the calculated rate constants are comparable (1.11×10^{-2} $M^{-1}s^{-1}$ determined by NMR and 1.35×10^{-2} $M^{-1}s^{-1}$ determined by ATR-IR). To test this method for following faster ligations, measurements of the reaction between the highly reactive cyclooctyne BCN (**6**)[10] and benzyl azide were performed at 37 °C in DMSO (Figure 3).

We were able to use this method for determinations of rate constants of different reactions, using various azides, cyclooctynes and solvents. Full experimental data and results can be found in the supporting information. To assess the applicability of our method for monitoring SPAAC in water and biological media, calibration curves of water-soluble 2-azidoethanol in both water (see supporting information) and human blood plasma (Figure 4a) were measured. Both peak height and peak area show very good linear correlation for concentration ranging from 20 to 200 mM in both solvents.

Since the results were very promising and did not reveal a significant difference between the azide signal in water and blood plasma we proceeded to directly monitor SPAAC in human blood plasma. Measurement of the reaction between PEGylated BCN **8** and 2-azidoethanol **7** at 100 mM and 20 °C was conducted (Figure 4b). The signal-to-noise ratio was determined to be lower than in organic solvents. Nevertheless. the decrease of azide signal could reliably be used for determination of the rate constant. As for measurements in organic solvents, analyzing the peak height gave better signal-to-noise ratios than using peak area (height: 1.90×10^{-1} $M^{-1}s^{-1}$ vs. area: 2.12×10^{-1} $M^{-1}s^{-1}$). Data for an additional measurement of the reaction at 37 °C and 50 mM concentration can be found in the supporting information.

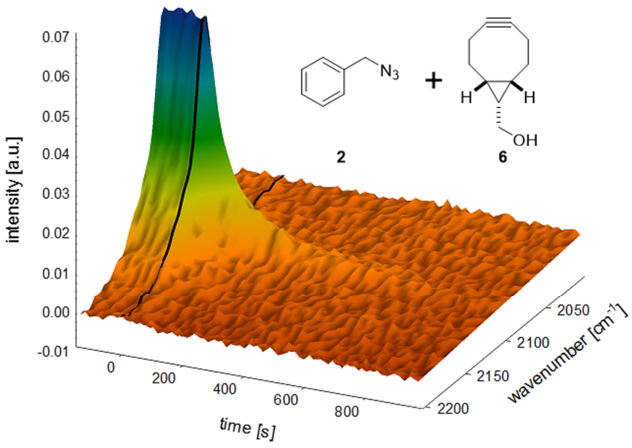

Figure 3. 3D-plot of azide signal during the reaction between benzyl azide (**2**) and BCN (**6**), the black lines indicates t=0.

In summary, we have developed a method for in-line ATR-IR kinetic measurements of strain-promoted azide alkyne cycloadditions, which allows for reaction monitoring in several solvents, even including blood plasma. The used setup allows for measurements at different temperatures in less than 1 mL reaction volume. Data acquisition is possible during the addition of the reaction partner, and therefore first data points are obtained right after the start of the reaction. All this grants the possibility of performing kinetic investigations of fast bioorthogonal SPAACs at conditions similar to those used in respective applications, for example in biological media at 37 °C, providing important information on reactivity of the used reaction partners. Hence, we expect this method to find application in the emerging field of bioorthogonal chemistry and provide valuable insight regarding kinetics of strain-promoted alkyne azide cycloadditions under complex reaction conditions.

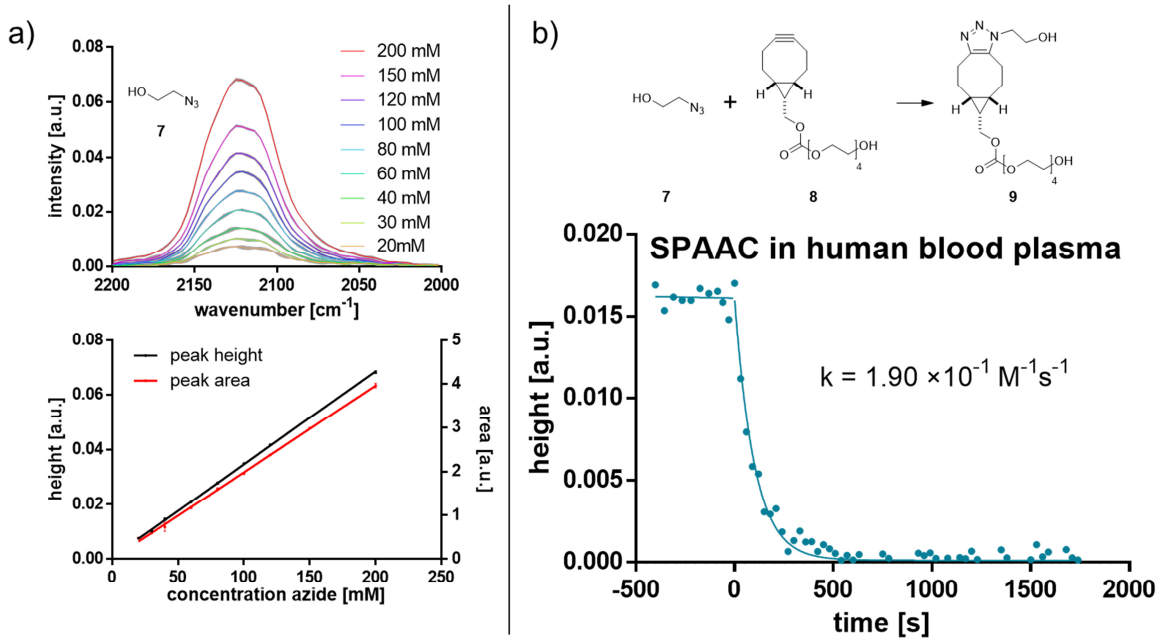

Figure 4. a) Azide signal in human blood plasma at 37 °C at different concentrations, gray areas indicate standard deviation (n=3), and the corresponding height and area based calibration curves; **b)** Monitoring of the reaction between PEGylated BCN **8** and water soluble azide **7** in human blood plasma at 20 °C and 100 mM starting concentration; Time 0 indicates addition of BCN **8**; Linear fit (t<0) and exponential fit (t>0) were added for better visualization.

Acknowledgements

We thank Rudolf Svatunek for the design drawings and the doctoral program 'Molecular and Elemental Imaging in Biosciences (MEIBio)' of TU Wien for funding.

Keywords: Click Chemistry • Kinetics • Strained Molecules • ATR-IR • Bioorthogonality

[1] R. Huisgen, *Proc. Chem. Soc.* **1961**, 357.

[2] V. V. Rostovtsev, L. G. Green, V. V. Fokin, K. B. Sharpless, *Angew. Chem. Int. Ed.* **2002**, *41*, 2596–2599.

[3] C. W. Tornøe, C. Christensen, M. Meldal, *J. Org. Chem.* **2002**, *67*, 3057–3064.

[4] M. Meldal, C. W. Tornøe, *Chem. Rev.* **2008**, *108*, 2952–3015.

[5] G. Wittig, A. Krebs, *Chem. Ber.* **1961**, *94*, 3260–3275.

[6] N. J. Agard, J. A. Prescher, C. R. Bertozzi, *J. Am. Chem. Soc.* **2004**, *126*, 15046–15047.

[7] J. M. Baskin, J. A. Prescher, S. T. Laughlin, N. J. Agard, P. V Chang, I. A. Miller, A. Lo, J. A. Codelli, C. R. Bertozzi, *Proc. Natl. Acad. Sci. U. S. A.* **2007**, *104*, 16793–16797.

[8] E. M. Sletten, C. R. Bertozzi, *Org. Lett.* **2008**, *10*, 3097–3099.

[9] M. F. Debets, S. S. van Berkel, S. Schoffelen, F. P. J. T. Rutjes, J. C. M. van Hest, F. L. van Delft, *Chem. Commun.* **2010**, *46*, 97–99.

[10] J. Dommerholt, S. Schmidt, R. Temming, L. J. a Hendriks, F. P. J. T. Rutjes, J. C. M. Van Hest, D. J. Lefeber, P. Friedl, F. L. Van Delft, *Angew. Chem. Int. Ed.* **2010**, *49*, 9422–9425.

[11] J. C. Jewett, E. M. Sletten, C. R. Bertozzi, *J. Am. Chem. Soc.* **2010**, *132*, 3688–3690.

[12] N. J. Agard, J. M. Baskin, J. A. Prescher, A. Lo, C. R. Bertozzi, *ACS Chem. Biol.* **2006**, *1*, 644–648.

[13] J. Dommerholt, O. van Rooijen, A. Borrmann, C. F. Guerra, F. M. Bickelhaupt, F. L. van Delft, *Nat. Commun.* **2014**, *5*, 5378–5384.

[14] S. Yoshida, A. Shiraishi, K. Kanno, T. Matsushita, K. Johmoto, H. Uekusa, T. Hosoya, *Sci. Rep.* **2011**, *1*, 82.

[15] D. A. Sutton, V. V. Popik, *J. Org. Chem.* **2016**, *81*, 8850–8857.

[16] R. Huisgen, G. Szeimies, L. Möbius, *Chem. Ber.* **1967**, *100*, 2494–2507.

Manuscript #3

Christoph Denk, Martin Wilkovitsch, Philipp Skrinjar, Dennis Svatunek, Severin Mairinger, Claudia Kuntner, Thomas Filip, Johannes Fröhlich, Thomas Wanek, Hannes Mikula*; Investigation of Small [^{18}F]-Fluoroalkylazides for Rapid Radiolabeling and *In Vivo* Click Chemistry, *Bioconjugate Chemistry* **2016**, submitted manuscript.

Investigation of Small [^{18}F]-Fluoroalkylazides for Rapid Radiolabeling and *In Vivo* Click Chemistry

Christoph Denk[a], Martin Wilkovitsch[a], Philipp Skrinjar[a], Dennis Svatunek[a], Severin Mairinger[b], Claudia Kuntner[b], Thomas Filip[b], Johannes Fröhlich[a], Thomas Wanek[b] and Hannes Mikula[a*]

a) Institut für Angewandte Synthesechemie, Technische Universität Wien (TUW) (Austria) E-mail: hannes.mikula@tuwien.ac.at b) Health and Environment Department, Biomedical Systems, Austrian Institute of Technology (AIT) Seibersdorf (Austria)

Graphical Abstract

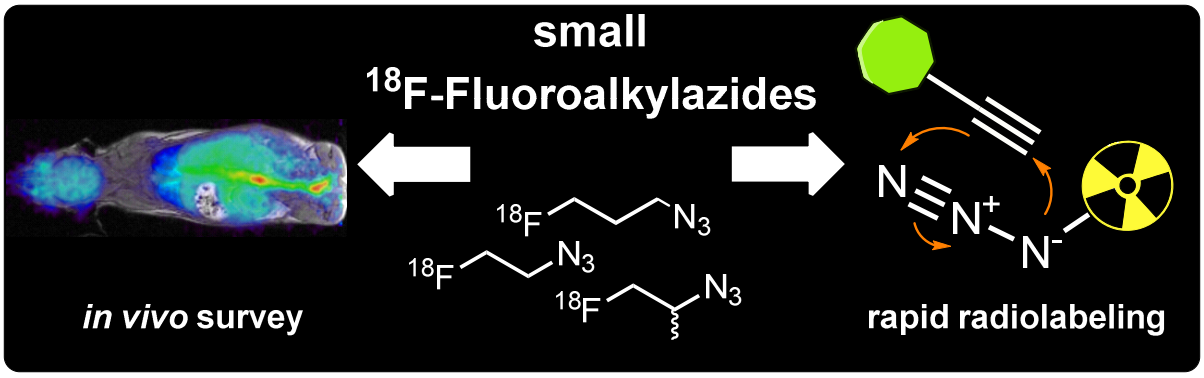

Abstract

Radiofluorinated alkylazides have been reported for *click* radiolabeling and pretargeted PET imaging. However, little data is available about their biodistribution and metabolism *in vivo*. Therefore, the synthesis of known 1-azido-2-[^{18}F]-fluoroethane was improved and it´s *in vivo* behavior investigated in detail. A panel of novel low-molecular-weight Fluoroalkylazides, that should exhibit beneficial properties, were developed and radiolabeled. Biodistribution, pharmacokinetic and *in vivo* stability data in mice were collected by PET/MR studies in mice. Reactivity in copper catalyzed cycloadditions was confirmed by labeling propargyl tagged peptide endomorphin-1 in high yields and short reaction times.

Introduction

Positron Emission Tomography (PET) allows non invasive molecular imaging and quantification of metabolic processes. High sensitivity, spatial and temporal resolution makes PET an indispensable diagnostic tool in clinic and biomedical research. The versatility of this imaging modality is highly dependent on the availability of specific radiolabeled probes. Short lived nuclides are generally preferred, due to low patient radiation dose and potentially high specific activity. However, sufficient time is still necessary for production, quality control, delivery and application of the probe. Fluorine-18 (t1/2 = 109.8 min) is thus considered the “ideal” PET radioisotope that enables the radiochemist to conduct multi-step synthesis and purifications using chromatographic methods.

[^{18}F]Fluoroethylazide ([^{18}F]FEA) is reported to be a highly versatile tool for PET imaging and radiochemistry. [^{18}F]FEA has frequently been used as prosthetic group for labeling applications, and has also been proposed as secondary agent in pretargeted (bioorthogonal) PET imaging.[1–3]

For its use as prosthetic group a precursor compound is modified to carry a terminal alkyne, and subsequently reacted with [^{18}F]FEA in a copper(I) catalyzed cycloaddition (CuAAC) (Figure 1a).[2–6] This methodology is highly selective and in contrast to direct ^{18}F-labeling no protecting groups are required.[7] Furthermore, this technique is fast, high-yielding and applicable to sensitive molecules like peptides and other biomolecules.[7,8]

[^{18}F]FEA was moreover reported as secondary agent for bioorthogonal PET imaging.[1] This two-step pre-targeting process allows imaging of long circulating nanomedicines with short half-life nuclides like fluorine-18. In a first step the probe modified with a reactive tag (chemical reporter) is administered and allowed to accumulate. In a second step a fast clearing radiolabeled agent (pull down reagent, PDR) is given that ligates to the pre-administered compound *in vivo* (Figure 1b). The strain promoted alkyne-azide cycloaddition (SPAAC) using organic azides and cyclooctynes as reactants has been frequently applied *in vitro* and *in vivo*.[9–13]

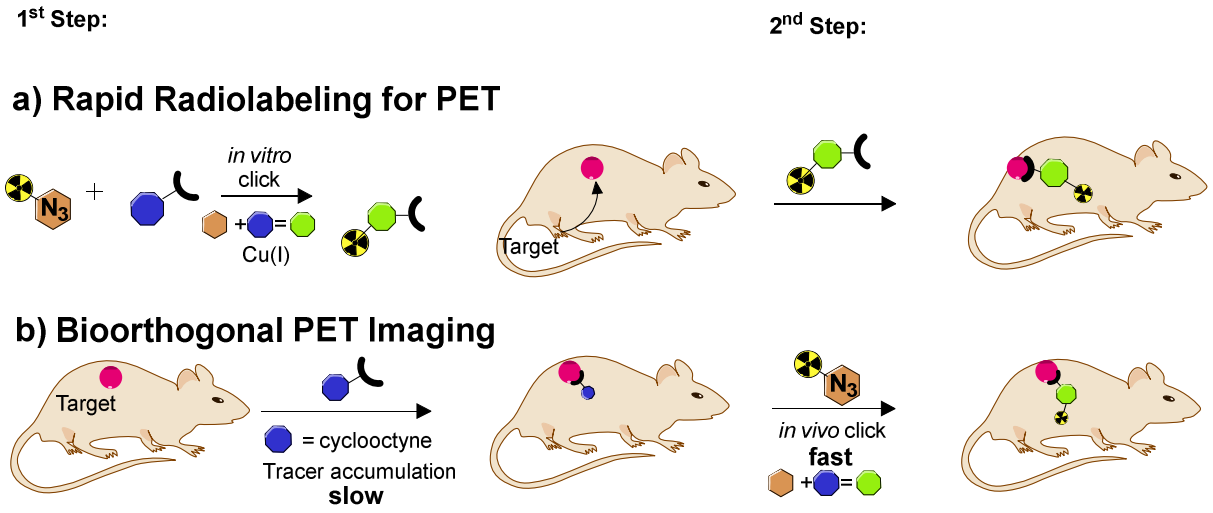

Figure 1: *Use of* [^{18}F]*fluorinated azides as prosthetic group for „click" radiolabeling (a) and as secondary agent in bioorthogonal PET imaging (b)*

Moreover, good results using pre-targeting in positron emission tomography (PET) with pre-administered cyclooctyne-labeled nanoparticles and an azide-functionalized fluorine-18 probe based on ethylene glycol were reported.[9] Due to its polarity this mini-PEG (polyethylene glycol) derived compound is unlikely to cross cell membranes and thus not suitable for internalizing chemical reporters. A metabolically stable probe with low molecular weight (fast pharmacokinetics) and medium polarity (crossing of biological membranes) is proposed to be of high versatility for SPAAC mediated pre-targeted PET imaging, but up to now no data on metabolic stability of ^{18}F-FEA was available.[1]

Despite the usefulness of [^{18}F]FEA several problems are associated with this low-molecular weight agent. [^{18}F]FEA is highly volatile and usually purified from the labeling reaction mixture by co-distillation with acetonitrile.[2] However, this purification is time consuming, since care must be taken not to exceed 90°C distillation temperature. Otherwise precursor is carried over, causing impurities

and interferences in subsequent cycloaddition reactions.[14] Moreover, the tosylated precursor is highly viscous making it difficult to handle in small quantities. Stable 2-fluoroethylazide, required for synthesis of cold reference materials, is potentially explosive, gaseous and difficult to handle in substance.[2]

Within this paper we aim to shed light on the applicability of [^{18}F]FEA and related compounds as PDR by studying the biodistribution and metabolism of this low molecular weight compounds. Furthermore, we present new tools that circumvent problems associated with [^{18}F]FEA. A novel crystalline precursor for [^{18}F]FEA that allows higher yields and also eliminates distillation carry-over is introduced. In addition two novel low-molecular-weight ^{18}F-fluoroalkylazides (1-azido-3-[^{18}F]fluoropropane and 2-Azido-1-[^{18}F]fluoropropane) are presented as prosthetic groups with beneficial properties, and further investigated towards their usability as pull down reagents for pretargeted PET imaging and rapid radiolabeling.

Results and discussion

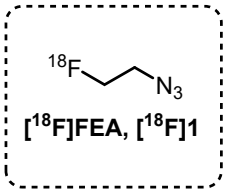

When our group started working on PET radiochemistry we required a multifunctional tool that allows for rapid radiolabeling and bioorthogonal imaging based on the azide-alkyne click cycloaddition (SPAAC). Moreover small molecular weight (to achieve fast pharmacokinetics and migration between compartments) as well as medium polarity (to allow for membrane diffusion) were key attributes of the sought for radiolabeled agent. In addition to numerous reported successful examples in rapid radiolabeling, a promising biodistribution study reported for 1-Azido-2-[^{18}F]fluoroethane ([^{18}F]FEA, [^{18}F]**1**) prompted us to pursue further evaluation of this compound.[1]

Radiosynthesis of [^{18}F]**1** is based on the K_2CO_3/K222 system for nucleophilic substitution on tosylated precursor 2-azidoethyl 4-methylbenzenesulfonate.[2,7,15] After short reaction time at elevated temperature (80-110°C) the product is isolated by co-distillation with acetonitrile. However different measures, including time consuming distillation at low temperature, reduced pressure and the use of low precursor mass, are required to minimize carry-over of the volatile tosylate. Codistilled precursor causes chemical impurities and furthermore competes with [^{18}F]**1** for alkyne groups.

To circumvent this problem, 2-azidoethyl 4-nitrobenzenesulfonate (**2**) was synthesized as novel precursor material from 2-azidoethanol and nosyl chloride in 67% yield (Scheme I). The nosylate was obtained as crystalline solid, thus making handling of small quantities easier as compared to the highly viscous 2-azidoethyl 4-methylbenzenesulfonate. [^{18}F]**1** for click radiolabeling applications was obtained by reacting **2** with azeotropically dried ^{18}F-fluoride and K_2CO_3/K222 in acetonitrile for 5 min at 105°C. Time efficient distillation at 105-110°C in a stream of argon afforded [^{18}F]**1** in 75% decay corrected yield and >99% radiochemical purity. Most noteworthy, no precursor was detectable in the distilled product by HPLC due to reduced volatility of **2** in comparison with 2-azidoethyl 4-methylbenzenesulfonate.

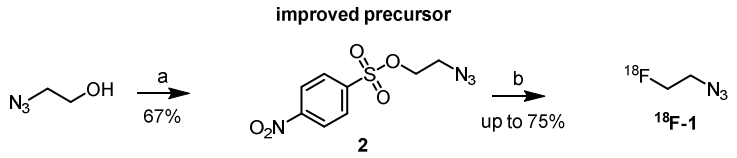

Scheme I: *Synthesis of precursor materials **2** and subsequent radiolabeling, a) NsCl, N(Et)$_3$ b) ^{18}F-HF, K_2CO_3, Kryptofix-222*

For biodistribution and metabolic studies another method of purification had to be chosen due to toxicity associated with acetonitrile. [^{18}F]FEA for animal experiments was synthesized from **2** using an

automated GE TRACERlab FX_{FDG} module with integrated HPLC purification system. A water/ethanol gradient in combination with a reversed phase column was used for isolation to yield the product in biocompatible media. [^{18}F]FEA was obtained in 48% decay corrected radiochemical yield (non-optimized) and in radiochemical purity exceeding 99.6%. Identity of [^{18}F]**1** was confirmed by comparison of HPLC retention times with authentic standard, and stability of the formulation was assessed by radio HPLC six hours post tracer synthesis that still revealed > 97% purity

However, our findings from the murine metabolic study of [^{18}F]**1** revealed high bone uptake indicating metabolic instability and liberation of free ^{18}F-anions (details see *in vivo* section). Noteworthy, probes synthesized by rapid radiolabeling using [^{18}F]**1** are not generally known to exhibit metabolic instability *in vivo*. We reasoned that a possible pathway for this degradation is the abstraction of hydrogen alpha to the azide resulting in elimination of fluoride (Scheme II a). To minimize this effect, we designed a series of close analogs, with the aim to improve *in vivo* stability while retaining high versatility of the probe (Scheme II b).

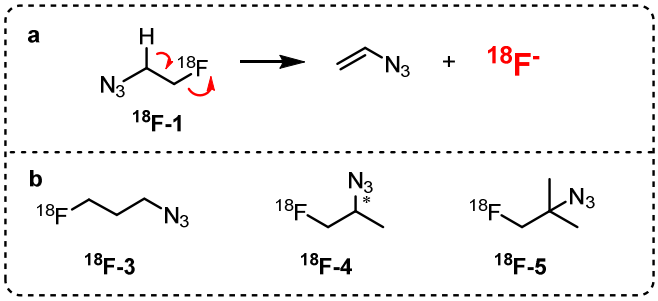

Scheme II: a) *Possible degradation pathway of [^{18}F]**1***
b) *Derivatives considered to increase metabolic stability*

We assumed that 1-azido-3-[^{18}F]fluoropropane ([^{18}F]**3**) might show reduced tendency to liberate fluorine ions due to diminished electronic interactions between the azide functionality and hydrogens in beta position to fluorine. Still, essential properties such as low molecular weight and medium polarity are retained in this molecule. In 2-azido-1-[^{18}F]fluoropropane ([^{18}F]**4**) the approach of branching, thus introducing steric bulk was followed. Introduction of a methyl group in alpha position to the azide functionality limits H-acidity (inductive effects) and accessibility (steric effects) of the adjacent hydrogen. Finally, replacing all alpha-hydrogens by methyl groups gives 2-azido-2-methy-1-[^{18}F]fluoropropane ([^{18}F]**5**). If the liberation of fluorine ions *in vivo* follows an elimination mechanism as depicted in Scheme II a, this form of degradation should no longer be possible in [^{18}F]**5**.

To access these compounds the nosylate approach, already successfully applied in the synthesis of [^{18}F]**1**, was followed. Precursor substance for [^{18}F]**2**, 3-azidopropyl 4-nitrobenzenesulfonate **(6)** was synthesized in two steps from 3-chloropropan-1-ol which was reacted at 50°C with sodium azide in DMF. The crude product was further treated with p-nitrobenzenesulfonyl chloride and triethylamine in anhydrous dichloromethane. Subsequent purification by column chromatography afforded **6** as crystalline solid in 33% overall yield (Scheme III). Radiolabeling using conditions described above for the radiolabeling of [^{18}F]**1** afforded [^{18}F]**3** after co-distillation with acetonitrile in 39.3% decay corrected radiochemical yield and in > 98% radiochemical purity. Preparative HPLC (using water/ethanol as eluent system) was used to obtain a product free of

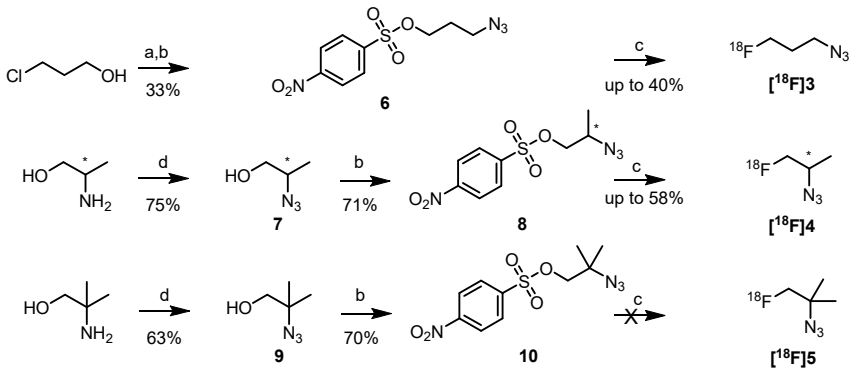

Scheme III: *Synthesis of precursor materials **6, 8, 10** and subsequent radiolabeling: a) NaN_3 b) NsCl, $N(Et)_3$ c) ^{18}F-HF, K_2CO_3, Kryptofix-222 d) 1H-Imidazole-1-sulfonyl azide, K_2CO_3, $CuSO_4$*

acetonitrile for murine biodistribution experiments. The experiment was conducted using a GE Tracerlab FX_{FDG} module with integrated HPLC purification system. [^{18}F]**3** was obtained in 23.5% decay corrected radiochemical yield (non-optimized) and radiochemical purity exceeding 94%. Identity of [^{18}F]**3** was confirmed by comparison of HPLC retention times with authentic standard, and stability of the formulation was assessed by radio HPLC three hours post tracer synthesis that still revealed > 89% radiochemical purity.

[^{18}F]**4** was synthesized from crystalline precursor **8**. Commercially available racemic alaninol was subjected to copper catalyzed diazotransfer conditions using 1*H*-imidazole-1-sulfonyl azide to obtain 2-azidopropan-1-ol (**7**) in 75% yield.[16,17] Nosylation, using conditions described for **2**, followed by column chromatography gave rise to racemic **8** in 71% yield (Scheme III). Noteworthy, alaninol is also available as *R* or *S* isomer, making enantiopure [^{18}F]**4** accessible whenever required. However, in this study we decided to investigate racemic [^{18}F]**4** for ethnic reasons thus limiting the number of required animals. When **8** was reacted with azeotropically dried ^{18}F-K222 complex in anhydrous acetonitrile for 7 min at 100°C followed by distillation in a stream of argon [^{18}F]**4** was yielded as solution in anhydrous acetonitrile in 58% decay-corrected yield and 99.7% radiochemical purity. For biodistribution studies acetonitrile-free [^{18}F]**4** was synthesized on an automated GE Tracerlab FX module followed by preparative HPLC purification in 27% decay-corrected radiochemical yield and >96% radiochemical purity.

Applying a similar synthetic strategy for [^{18}F]**5,** 2-amino-2-methylpropan-1-ol was subjected to copper catalyzed diazotransfer conditions to obtain 2-azido-2-methylpropanol (**9**) in 63% isolated yield. The nosylated compound **10** was obtained in 70% yield by reaction of alcohol **9** with nosyl chloride and triethylamine in anhydrous DCM (Scheme III). Unfortunately radiolabeling attempts using the K_2CO_3/K222 method resulted in formation of an unknown radiolabeled species of unexpected lipophilicity in 70% radiochemical yield. HPLC retention times did not match retention times of authentic standard. Although the identity of the formed compound could not be clarified, modeling the labeling reaction in deuterated acetonitrile using “cold” potassium fluoride followed by ^{19}F-NMR spectroscopy indicated the absence of a primary alkylfluoride (shift -220 ppm). Instead signals at -105 ppm indicated formation of re-arrangement or elimination products.

Access to non-radioactive (“cold”) reference compounds is essential for identification of the radiolabeled agent by comparison of HPLC retention times. Furthermore, when *click* radiolabeling is intended the stable (fluorine-19) azides are required as building blocks for synthesis of cold click-cycloaddition reference compounds. 1-Azido-2-fluoroethane (**1**) is highly volatile and potentially explosive and should thus not be isolated *in substance*.[2] The already reported tosylation of 2-fluoroethan-1-ol followed by reaction with sodium azide and subsequent filtration yielded a 1.36 M solution of **1** in DMF

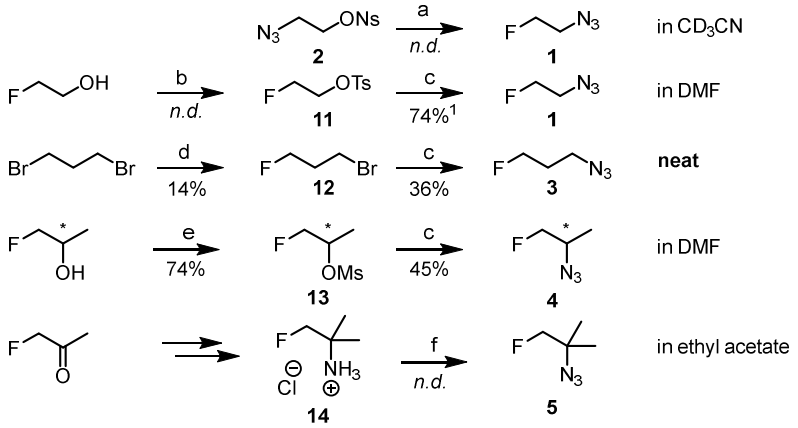

Scheme IV: *Synthesis of reference compounds **1, 3, 4** and **5**. a) KF, Kryptofix-222, b) TsCl, pyridine, c) NaN_3, d) KF e) DMAP, MsCl, $N(Et)_3$, f) 1H-Imidazole-1-sulfonyl azide, K_2CO_3, $CuSO_4$*
n.d.= not determined; [1])overall yield over steps b+c

that was successfully used in cycloaddition reactions.[18] In addition **1**, free of DMF, was obtained by reacting **2** with anhydrous potassium fluoride and Kryptofix-222 in CD_3CN followed by evaporation at low pressure and trapping of volatiles in a liquid nitrogen trap (Scheme IV).

1-Azido-3-fluoropropane (**3**) was synthesized starting from 1,3-dibromopropane to form 1-bromo-3-fluoropropane (**12**). Although **12** was isolated in only 14% yield its synthesis from cheap starting materials is still economically favorable.[19] Nucleophilic substitution with sodium azide in DMF afforded **3** in 36% yield. Due to a higher boiling point compared to **1** we were able to isolate neat **3** as colorless liquid by careful distillation; a clear benefit when onward use for chemical modification is intended. Although we did not encounter any problems, safety precautions like blast shields as well as performing reactions in small scale are highly recommended. 2-azido-1-fluoropropane (**4**) was also obtained as solution in DMF (1.05 M) by mesylation of commercially available 1-fluoropropan-2-ol followed by reaction with sodium azide in anhydrous DMF and subsequent filtration.[20] No attempts were made to isolate neat **4**. Tertiary azide **5** was obtained as a solution in ethyl acetate applying diazotransfer conditions on 2-amino-2-methyl-1-fluoropropane hydrochloride (**14**).[17] Amine **14** was prepared following a published sequence starting from fluoroacetone.[21]

HPLC retention times of radiolabeled species (as distillate in acetonitrile for rapid radiolabeling or in aqueous medium for *in vivo* use) were compared with retention times of cold compounds to proof identity of the radiolabeled agent (see ESI for chromatographic data). Compounds that were not isolated in substance (**1, 4** and **5**) were ligated with cyclooctyne (1*R*,8*S*,9s)-Bicyclo[6.1.0]non-4-yn-9-ylmethanol (BCN)[22] in a strain promoted alkyne-azide cycloaddition and resulting triazoles **15**, **16** and **17** were isolated and fully characterized by NMR and MS. [^{18}F]**1** and [^{18}F]**4** were also treated with BCN resulting in rapid ligation. HPLC retention times of resulting ^{18}F-triazoles ([^{18}F]**15** and [^{18}F]**16**) were compared with their non-radioactive counterparts to further ensure identity of investigated compounds (Scheme V). When the labeling product arising from tertiary azide precursor **10,** was reacted with BCN, HPLC retention times with **17** did not match, confirming formation of an undesired re-arrangement or elimination product during the labeling reaction.

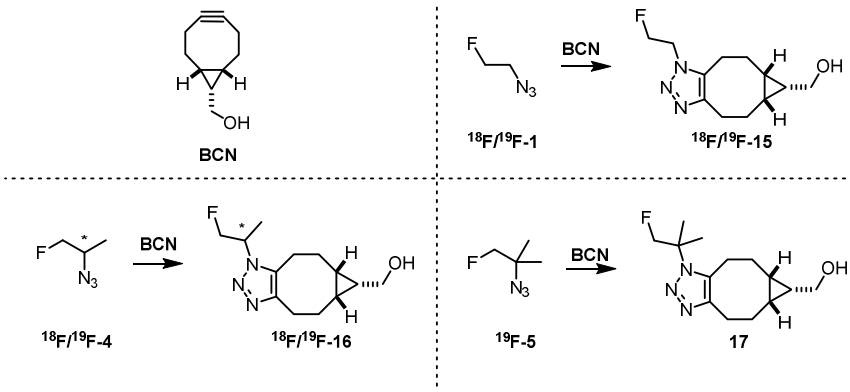

Scheme V: *Synthesis of* BCN ligation products **15, 16** and **17**

Application of [^{18}F]**1** as prosthetic group for rapid "click" radiolabeling is well documented.[2–8,23] Several modifications of the original procedure from Arstad and Glaser were reported to shorten reaction times and eliminate the need for heating. Especially noteworthy, addition of the water soluble copper-ligand bathophenanthroline sodium sulfonate reduces the required amount of copper and sodium ascorbate while maintaining, or even enhancing ligation rates at room temperature.[3]

To test and compare [^{18}F]**3** and [^{18}F]**4** as prosthetic group against already established [^{18}F]**1** we chose the tetrapeptide endomorphin-1 (EM-1) as substrate. EM-1 is a endogenous substance and powerful μ-opioid receptor agonist (K_i = 360 pM), that is of potential interest for imaging purposes.[24] In addition EM-1 is commercially available and possesses only one nucleophilic amine to allow for site specific

modification. EM-1 was treated with commercially available 2,5-dioxopyrrolidin-1-yl-3-(prop-2-yn-1-yloxy)propanoate and triethylamine in anhydrous DMF to introduce an alkyne functional group (Scheme VI). Propargyl modified endomorphin-1 **18** was obtained in 42% yield following HPLC purification. Ligation products **19, 20** and **21** formed by reaction of propargylated EM-1 **18** with **1, 3** and **4** were prepared using the copper(II)sulfate/sodium ascorbate/bathophenantroline system in DMF, and isolated by RP-HPLC. [^{18}F]**19, [**^{18}F]**20** were formed in good radiochemical yields within 10 minutes by reacting 1 mg of **18** with the according ^{18}F-fluoroalkylazide ([^{18}F]**1** and [^{18}F]**3**) using the copper(II)sulfate/sodium ascorbate/bathophenanthroline system in a mixture of acetonitrile and DMF (Scheme VI).

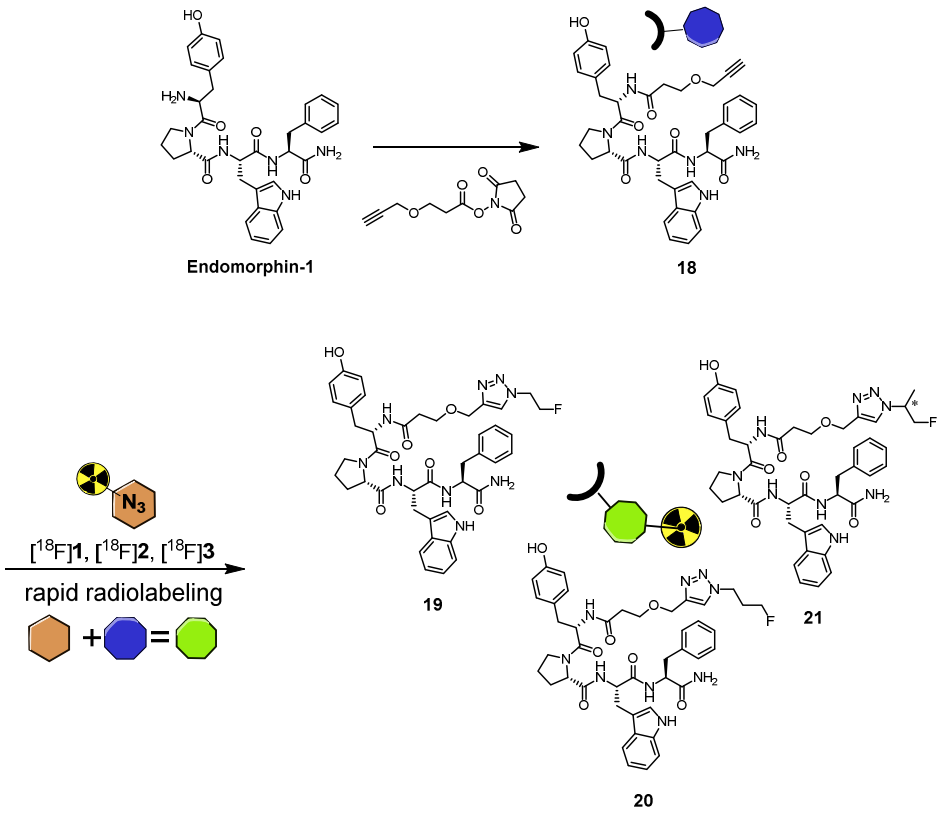

Scheme VI: *Synthesis of* propargyl modified endomorphin-1 **18,** Ligation products of **18** with **1** (**19**), **3** (**20**) and **4** (**21**)

Subjecting [^{18}F]**4** to similar experimental conditions yielded [^{18}F]**21** in excellent radiochemical yield of 98%. Retention times of ligation products were compared by radio-HPLC with authentic standards **19**-**21**. In addition, plasma stability of ligation products was assayed by incubation in human blood plasma for 120 minutes followed by radio-TLC analysis. Similar stabilities (~80-86%) were observed for all ligation products further indicating the applicability of [^{18}F]**3** and [^{18}F]**4** as prosthetic group equal or better compared to frequently used [^{18}F]**1**.

In vivo investigation

The test substances ([^{18}F]**1**, [^{18}F]**3**, [^{18}F]**4**) were injected into female BALB/c mice and dynamic PET (n=4 for [^{18}F]**1**, n = 2 for [^{18}F]**3** and [^{18}F]**4**) or PET/MR, n=1 for all test substances) scanning was performed for 120 minutes. Coronal PET/MR images are shown in Graph I. Analysis of organ time activity curves (Graph II) reveals a uniform uptake of all agents in most analyzed organs that slowly decreases from ~1.5 to ~1 SUV (standardized uptake value) during the course of the experiment. High uptake in the urinary bladder suggests renal elimination as main excretion route for all investigated substances.

Secondary azide **4** exhibits the fastest clearance, a clear benefit when use as PDR in bioorthogonal PET imaging is intended (Graph II e). Interestingly brain uptake shows a slight but steady increase for all analyzed tracers (Graph II a).

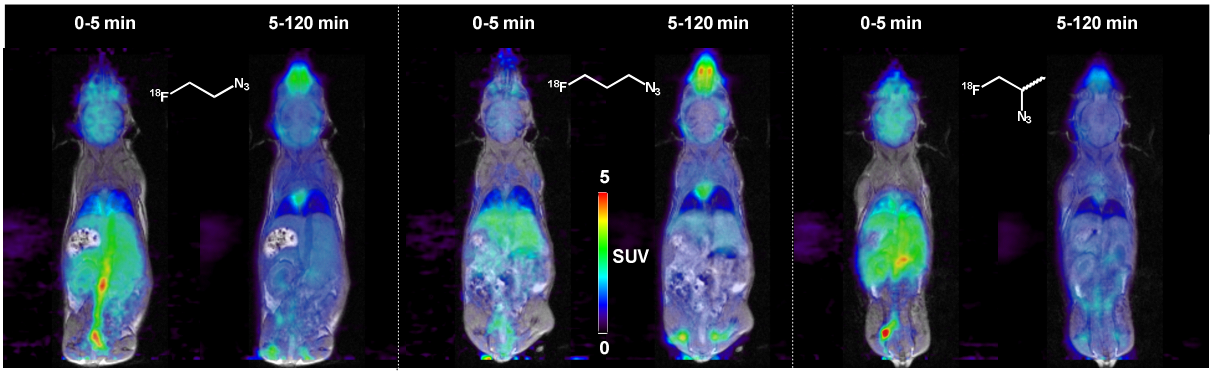

Graph I**: Coronal PET/MR slices of test substances [^{18}F]**1**, [^{18}F]**3** and [^{18}F]**4

[^{18}F]**3** exhibits a higher muscular uptake compared to [^{18}F]**1** and [^{18}F]**4** that increased throughout the experiment (Graph II c). Most noteworthy, an increase of radioactivity concentration in bone was observed – a good indicator for metabolic instability and *in vivo* defluorination of the tracer molecules. Activity concentration in bone peaked at 3.6 SUV for [^{18}F]**1** and 6.5 SUV for [^{18}F]**3**, thus showing that *in vivo* stability could not be improved by insertion of one extra methylene group. [^{18}F]**4** showed lowest bone uptake (peak SUV = 2.7), compared to [^{18}F]**1** and [^{18}F]**3**, indicating improved *in vivo* stability over [^{18}F]**1** and [^{18}F]**3** (Graph II f). In addition, coronal PET/MR images (Graph I) show skull uptake in the 5-120 min summation images, that is least pronounced in [^{18}F]**4** while [^{18}F]**3** exhibits the most pronounced uptake. Placing a "total box" ROI over the entire animal revealed constant activity over the entire imaging period, showing that [^{18}F]**1,** [^{18}F]**3** and [^{18}F]**4** are not lost by respiration.

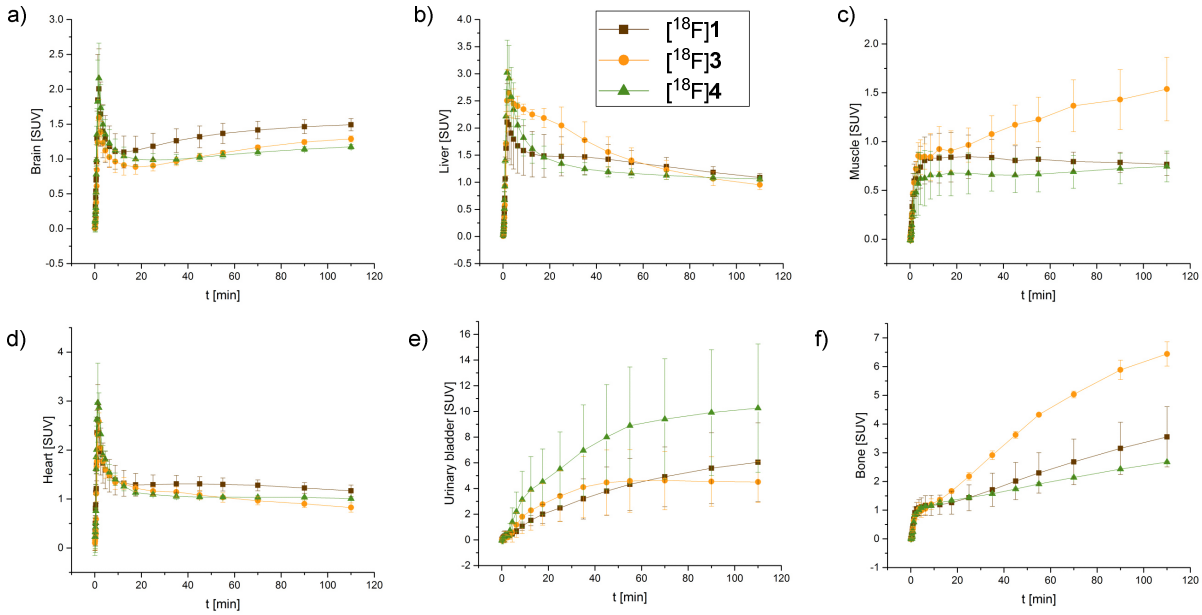

***Graph II**: Time activity curves of analyzed tracers in a) brain, b) liver, c) muscle, d) heart, e) urinary bladder, f) bone in female BALB/c mice.*

Following imaging, blood and urine samples were collected and the mice were sacrificed. Organ samples were collected and measured for radioactivity in a gamma counter. Data obtained by gamma counting at 120 min post injection of the tracers reflect data obtained in the PET experiment (Graph III). Radio-HPLC was chosen for analysis of metabolites due to the volatile nature of the test substances that renders radio-TLC uncertain. Murine plasma was obtained by centrifugation of whole blood in heparin tubes, and plasma proteins were precipitated by addition of an equal volume of acetonitrile. Following centrifugation, the supernatant was injected into the HPLC system for analysis of plasma metabolites. Urine samples were injected after dilution with water. Data obtained from HPLC injections show diminutive (<4% of total radioactivity) amounts of intact compounds while the main fraction of radioactivity (> 90%) was detected as highly polar compound, most likely free ^{18}F-fluoride ions, confirming the metabolic instability of [^{18}F]**1**, [^{18}F]**3** and [^{18}F]**4**. Taking the rate of bone uptake into consideration (Graph II f) [^{18}F]**4** shows increased stability compared to [^{18}F]**1** and especially [^{18}F]**3** that exhibits the least *in vivo* stability. This data is also reflected in plasma metabolite HPLC analysis, wherein [^{18}F]**4** displayed the highest percentage (up to 4%) of intact tracer 120 min post administration. Despite nuances in metabolic stability, degradation seems to happen on a time scale that is not compatible with reaction kinetics of the SPAAC ligation. In addition, high bone uptake will contribute to background signal hindering image interpretation.

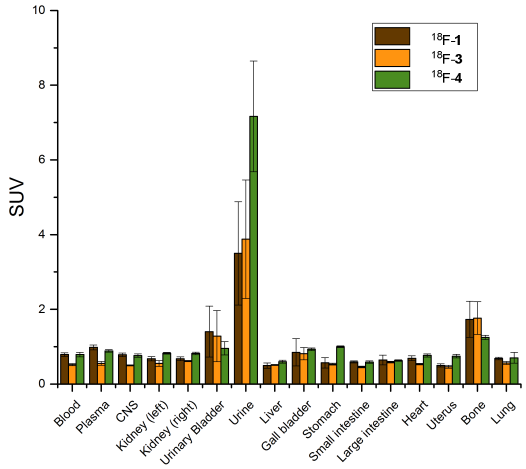

Graph III: *Biodistribution of [^{18}F]**1**, [^{18}F]**3** and [^{18}F]**4** obtained by γ-counting of organ samples 120 min post tracer administration*

In summary, we present an improved synthesis of [^{18}F]-fluoroethylazide based on novel precursor substance **2**, that is crystalline, easier to handle, and less volatile thus preventing the problem of distillative carry-over. In addition, two novel [^{18}F]-fluoroalkylazide agents ([^{18}F]**3,** [^{18}F]**4)** were developed, expanding the library of prosthetic groups for ^{18}F-labeling. Rapid radiolabeling was demonstrated on endogenous μ-opioid agonistic peptide endomorphin-1, and biodistribution and metabolism data on all compounds was collected. Our findings demonstrate that [^{18}F]**3** and [^{18}F]**4** are valuable tools for click radiolabeling coequal to [^{18}F]**1**. Application of [^{18}F]**1,** [^{18}F]**3** and [^{18}F]**4** as PDRs for *in vivo* click chemistry is not promising due to metabolic instability of all analyzed probes.

Experimental

General

Unless otherwise noted, all reagents were purchased from commercial suppliers and used without further purification. DCM was dried using PURESOLV-columns (Innovative Technology Inc.). Dry acetonitrile (Merck) and *N,N*-Dimethylformamide (Acros) was commercially obtained and stored under argon. All other solvents were distilled prior to use. BCN was synthesized following published procedures.[22] Imidazol-1-sulfonyl azide hydrochloride was prepared following known procedures.[17] Drying of organic solvents after extraction was performed using anhydrous Na_2SO_4 or $MgSO_4$ (Sigma Aldrich) and subsequent filtration. Reactions were carried out under an atmosphere of argon in air-dried glassware with magnetic stirring. Sensitive liquids were transferred via syringe. Thin layer chromatography was performed using TLC alumina plates (Merck, silica gel 60, fluorescence indicator F254, or Merck RP18 fluorescence indicator F254). Detection in radio-TLC was performed by placing the TLC plates on multisensitive phosphor screens (Perkin-Elmer Life Sciences, Waltham, MA). The screens were scanned at 300 dpi resolution using a PerkinElmer Cyclone® Plus Phosphor Imager (Perkin-Elmer Life Sciences). Preparative column chromatography was performed using a Büchi Sepacore Flash System (2 x Büchi Pump Module C-605, Büchi Pump Manager C-615, Büchi UV Photometer C-635, Büchi Fraction Collector C-660) or a Reveleris Grace system using silica gel 60 (40-63 µm) as obtained from Merck and distilled or redistilled solvents. Preparative HPLC was done on a Reveleris Grace system. ^{1}H, ^{13}C and ^{19}F NMR spectra were recorded on a Bruker Avance IIIHD 600 MHz spectrometer equipped with a Prodigy BBO cryo probe, on a Bruker Avance UltraShield 400 spectrometer or on a Bruker AC200 spectrometer at 20 °C. Chemical shifts are reported in ppm (δ) relative to tetramethylsilane and calibrated using solvent residual peaks. Data are shown as follows: Chemical shift, multiplicity (s = singlet, d = doublet, t = triplet, q = quartet, quin = quintet, m = multiplet, br = broad signal) and integration. [^{18}F]Fluoride was produced *via* the $^{18}O(p, n)^{18}F$ nuclear reaction by irradiating oxygen-18 enriched water (IASON, Austria) using a PETtrace cyclotron equipped with high yield liquid target system (GE Healthcare, Uppsala, Sweden). HPLC analysis was performed on a 1200 series system (Agilent Technologies) using a reversed phase columns and acetonitrile/water or phosphate buffer gradients. Analytical HPLC Conditions A: Agilent ZORBAX SB-Aq 5 µm, 4.6 x 250 mm, water / acetonitrile , 1.2 ml/min, 0-2 min 5% acetonitrile, 2→10 min 5%→20% acetonitrile, 10-16 min 20%→90%, 16-20 min 90% acetonitrile, B: Agilent Extend-C18 3.5 µm, 3 x 100 mm, gradient water/acetonitrile (+0.1 vol% TFA), 1.3 ml/min, 0-1 min 10%, 1→8 min 10%→60%, 8-9 min 60%. For radio-HPLC a GABI* radioactivity detector (raytest Isotopenmessgeraete GmbH, Straubenhardt, Germany) was used. Preparative HPLC separations were done on the built in HPLC system on the synthesis module (TRACERlab™ FX_{FDG}, General Electric Healthcare, Uppsala, Sweden) using a Macherey-Nagel EP 250/16 100-7 C-18 (10 µm, 16 x 250 mm) column and ethanol/water-gradients (flow rate: 4 mL/min) in combination with a K-2001 UV detector (Knauer) and radioactivity detector. LC-MS measurements were carried out on a HPLC system of Agilent Technologies with the following components: Agilent 1200 Series G1367B HiP ALS Autosampler, Agilent 1100 Series G1311A Quat Pump, Agilent 1100 Series G1379A Degasser, Agilent 1200 Series G1316B TCCSL, Agilent 1260 Infinity G1315D DAD as well as an Esquire HCT Ion Trap MS of Bruker as detectors. A Phenomenex Luna 10 µm, C18, 250 x 4.6 mm column eluted with a gradient of 10-90% acetonitrile in water was used at a flowrate of 1ml/min.

1-azido-2-fluoroethane (1)

2-Fluorethanol (1 eq., 1.0 g, 15.6 mmol) in 5 ml dry pyridine was cooled to 0°C and treated dropwise with a solution of TsCl (2 eq., 5.95 g, 31.2 mmol) in 8 ml of pyridine. The reaction mixture was stirred at 0°C for 3 hours and poured onto ice which caused the product to precipitate. Extraction with ethyl acetate, washing of the organic phase with 2N HCl, half-saturated Na_2CO_3 solution and brine, followed by drying over Na_2SO_4 and removal of the solvent yielded crude 2-fluoroethyl 4-methylbenzenesulfonate as colorless liquid. The tosylate was further stirred in 10 ml of anhydrous DMF with sodium azide (1.08 eq., 1.1 g, 16.9 mmol) for 48 hours at room temperature. Filtration of solids yielded a pale yellow solution containing 1.43 mmol/g (8.1 g, 74% of theory) **1** as investigated by ^{1}H NMR. **1** free of DMF was obtained by heating a mixture of 2-Azidoethyl 4-nitrobenzenesulfonate(**4**) (1 eq., 136 mg, 0.5 mmol) , Kryptofix-222 (0.95 eq., 136 mg, 0.47 mmol) and anhydrous potassium fluoride (1 eq., 30 mg, 0.5 mmol) in 1.5ml CD_3CN to 80°C for 10 minutes using a laboratory microwave. After cooling to room temperature vacuum (10 mbar) was applied and volatiles were collected in a trap cooled with liquid nitrogen resulting in a solution of **1** in deuterated acetonitrile. ^{1}H NMR (400 MHz, MeCN-d_3) δ = 3.53 (dt, *J*=28.9, 4.7 Hz, 2 H) 4.57 (dt, *J*=47.6, 4.7 Hz, 2 H) ppm ^{13}C NMR (50.32 MHz, MeCN-d_3) δ = 51.9 (d, *J*=19.3 Hz) 83.8 (d, *J*=166.8 Hz) ppm ^{19}F NMR (376.5 MHz, MeCN-d_3) δ = -223.2 ppm

2-Azidoethyl 4-nitrobenzenesulfonate (2)

2-azidoethanol (1 eq., 2.0 g, 23 mmol) and triethylamine (2.04 eq., 4.78 g, 47 mmol) in 20 ml absolute methylene chloride were cooled to 0°C and p-nitrobenzenesulfonyl chloride (2.04 eq., 10.4 g, 47 mmol) in 30 ml abs. methylene chloride was added during 20 minutes. After finished addition the mixture was gradually warmed to room temperature and stirred for additional 2 h. The reaction mixture was diluted with 100 ml DCM, washed twice with 2N HCl, followed by brine. Drying over Na_2SO_4, filtration and evaporation gave 10 g crude product which was subjected to column chromatography (10-20% ethyl acetate in hexanes). Stripping of solvents yielded nosylate **2** (4.2 g, 67% of theory) as yellow crystals. Recrystallization from toluene yielded **2** (3.93 g, 63% of theory) as slightly yellow crystals. ^{1}H NMR (200 MHz, $CDCl_3$): δ = 3.55 (t, *J*=4.9 Hz, 2 H) 4.27 (t, *J*=5.3 Hz, 2 H) 8.14 (dt, *J*=8.8, 2.3 Hz, 2 H) 8.42 (dt, *J*=8.8, 2.0 Hz, 2 H) ppm ^{13}C NMR (50 MHz, $CDCl_3$): δ = 49.4, 69.2, 124.5, 129.2, 141.2, 150.8 ppm

1-azido-3-fluoropropane (3)

1-bromo-3-fluoropropane (**12**, 1 eq., 2.5 g, 17.7 mmol) and sodium azide (3 eq., 3.45 g, 53.1 mmol) were stirred in 10 ml anhydrous DMF at 50°C for 4 days. The reaction mixture was diluted with 150 ml H_2O and extracted three times with diethyl ether. Pooled extracts were washed twice with sat. NH_4Cl and once with brine, dried over $MgSO_4$ and the solvent removed on the rotary evaporator. The raw product was distilled at 46-48°C/100 mbar to yield 650 mg **3** (35.5% of theory) as colorless liquid**.** ^{1}H NMR (400 MHz, CD_3CN): δ = 1.63 - 1.78 (m, 2 H) 3.20 (t, *J*=6.83 Hz, 2 H) 4.29 (dt, *J*=47.22, 5.90 Hz, 2 H) ppm ^{13}C NMR (101 MHz, CD_3CN): δ = 30.1 (d, *J*=19.78 Hz) 48.0 (d, *J*=5.65 Hz) 81.9 (d, *J*=162.48 Hz) ppm ^{19}F NMR (376.5 MHz, CD_3CN): δ = 222.9 ppm IR ν= 2092 cm^{-1} among others

3-azidopropyl 4-nitrobenzenesulfonate (6)

3-Chloropropan-1-ol (1 eq., 3.0 g, 31.7 mmol) and sodium azide (3 eq., 6.17 g, 95 mmol) were stirred in 25 ml anhydrous DMF at 50°C for 4 days. The reaction mixture was diluted with 200 ml H_2O and extracted three times with diethyl ether. Pooled extracts were washed with brine, dried over $MgSO_4$

and the solvent distillied off. The crude residue was taken up in 40 ml anhydrous DCM, treated with triethylamine (1.25 eq., 4.0 g, 39.6 mmol) and cooled to 0°C. A solution of nosyl chloride (1.25 eq., 8.8 g, 39.6 mmol) in 100 ml absolute DCM was added dropwise and the reaction stirred at room temperature for 16 hours. The reaction mixture was extracted twice with ice cold 2N HCl followed by sat. $NaHCO_3$. After drying over $MgSO_4$ and removal of solvent the crude product was purified over 90g SiO_2 eluting with 5 – 15% ethyl acetate in petrol ether yielding 2.95 g (33 % of theory) yellowish oil that crystallized in the freezer. ^{1}H NMR (400 MHz, $CDCl_3$): δ = 1.93 (quin, *J*=6.24 Hz, 2 H) 3.40 (t, *J*=6.24 Hz, 2 H) 4.21 (t, *J*=6.05 Hz, 2 H) 8.11 (dt, *J*=8.98, 2.00 Hz, 2 H) 8.40 (dt, *J*=9.37, 2.30 Hz, 2 H) ppm ^{13}C NMR (101 MHz, $CDCl_3$): δ = 28.3, 47.0, 68.2, 124.5, 129.2, 141.4, 150.8 ppm IR v= 2099 cm^{-1} among others

2-azidopropan-1-ol (7)

Potassium carbonate (1.21 eq., 4.52 g, 32.7 mmol) and copper sulfate pentahydrate (0.01 eq., 0.07 g, 0.27 mmol) were added to a stirring solution of 2-aminopropanol (1 eq., 2 g, 26.63 mmol) in 135 mL anhydrous methanol under argon atmosphere. Imidazole-1-sulfonyl azide hydrochloride (1.2 eq., 6.7 g, 57.25 mmol) was added and the mixture stirred for 3.5 h at room temperature. Afterwards methanol was removed *in vacuo*, the residue diluted with water (400 mL), acidified with conc. HCl until pH 5, extracted with ethyl acetate (3x200 mL), dried over $MgSO_4$, filtered and concentrated. The crude product was filtered over a pad of silica (hexanes:diethyl ether, 2:1) to obtain **7** (2.03 g, 75% of theory) as a yellowish oil. Rf (PE:Et_2O = 2:1) = 0.16; NMR data matched previously reported values.[19]

2-azidopropyl -4-nitrobenzenesulfonate (8)

7 (1 eq., 1 g, 9.89 mmol) and triethylamine (1.2 eq., 1.2 g, 11.87 mmol) were dissolved in 25 mL anhydrous DCM. After cooling to 0°C 4-nitrobenzenesulfonyl chloride (1.2 eq., 2.63 g, 11.87 mmol) was added and the mixture stirred for 100 min during which contents gradually warmed to room temperature. The reaction mixture was diluted with 120 mL DCM, extracted with 2 N HCl (2x100 mL), the combined organic layers were washed with brine, dried over $MgSO_4$, filtered and the solvent stripped. The product was purified by column chromatography over 90 g silica-gel (3-25% EE in hexanes) to afford **8** (2 g, 71% of theory) as a yellow powder. Rf (PE:EE = 4:1) = 0.23; ^{1}H NMR (400 MHz, $CDCl_3$): δ = 1.27 (d, *J*=6.63 Hz, 3 H) 3.80 (quind, *J*=6.78, 6.78, 6.78, 6.78, 4.10 Hz, 1 H) 4.03 (dd, *J*=10.15, 7.02 Hz, 1 H) 4.15 (dd, *J*=10.34, 4.10 Hz, 1 H) 8.15 (dt, *J*=8.98, 2.00 Hz, 2 H) 8.43 (dt, *J*=8.98, 2.00 Hz, 2 H) ppm ^{13}C NMR (101 MHz, $CDCl_3$): δ = 15.6, 55.5, 72.9, 124.5, 129.3, 141.4, 150.9 ppm

2-azido-2-methylpropan-1-ol (9)

To a stirred mixture of 2-amino-2-methyl-propan-1-ol (1 eq., 4.25 g, 47.7 mmol), potassium carbonate (1.2 eq., 8.0 g, 58 mmol) and $CuSO_4$ x 5 H_2O (0.01 eq., 119 mg, 0.48 mmol) in 200 ml methanol was added imidazol-1-sulfonyl azide hydrochloride (1.2 eq., 10 g, 57.25 mmol) in portions. The mixture was stirred overnight at room temperatureand the majority of MeOH was carefully removed on the rotary evaporator. The residue was taken up in 500 ml water, acidified (pH 4) with HCl, and the solution was extracted three times with ethyl acetate. Combined extracts were dried over $MgSO_4$ and the solvent was removed on the rotary evaporator (50 mbar). The residue was purified by filtration over a plug of SiO2 using PE:Et_2O = 2:1 as eluent. Stripping of solvent afforded 3.47 g tertiary azide **9** as colorless liquid (63% of theory). TLC-Rf (PE:Et_2O = 2:1) = 0.4, ^{1}H NMR (200 MHz, $CDCl_3$) δ = 1.27 (s, 6 H) 2.54 (br. s, 1 H) 3.42 (s, 2 H) ppm, ^{13}C NMR (50.32 MHz, $CDCl_3$): δ = 22.5, 62.4, 70.0 ppm

2-azido-2-methylpropyl 4-nitrobenzenesulfonate (10)

9 (1 eq., 1 g, 8.69 mmol) and triethylamine (1.2 eq., 1.05 g, 10.42 mmol) were dissolved in 10 mL anhydrous DCM. After cooling to 0°C 4-nitrobenzenesulfonyl chloride (1.2 eq., 2.31 g, 10.42 mmol) was added dropwise as a solution in 15 ml anhydrous DCM. The mixture was stirred for 100 min during which contents gradually warmed to room temperature. The reaction mixture was diluted with 100 mL DCM and washed twice with 2 N HCl and once with brine. Drying over $MgSO_4$ and stripping of the solvent afforded the crude product which was purified over 90g SiO_2 eluting with 3-28% EE in PE. **10** was obtained as off-white crystalline solid in 70.5% yield. Rf (PE:EE = 2:1) = 0.75; ^{1}H NMR (400 MHz, $CDCl_3$): δ = 1.29 - 1.33 (m, 6 H) 3.96 (s, 2 H) 8.15 (dt, *J*=8.98, 2.30 Hz, 2 H) 8.44 (dt, *J*=8.98, 2.30 Hz, 2 H) ppm ^{13}C NMR (101 MHz, $CDCl_3$): δ = 22.9, 59.5, 76.2, 124.5, 129.3, 141.1, 150.9 ppm

1-fluoropropan-2-yl methanesulfonate (13)

1-fluorpropan-2-ol (1 eq., 300 mg, 3.84 mmol) triethylamine (1.1 eq., 426 mg, 4.2 mmol) and N,N-dimethylaminopyridine (0.1 eq., 47 mg, 0.384 mmol) in 7 ml anhydrous DCM were cooled to 0°C. Mesyl chloride (1.1 eq., 324 µl, 4.2 mmol) was added dropwise and the mixture was allowed to reach room temperature and stirred for 1 additional hour. The reaction mixture was partitioned between 100 ml DCM and saturated NH_4Cl solution, the organic phase was dried over sodium sulphate and the solvent removed to obtain **13** as yellow oil that crystallized in the freezer into slightly yellow needles (440 mg, 74% of theory). The product was sufficiently pure for carrying it into the next synthetic step. ^{1}H NMR (400 MHz, $CDCl_3$) δ = 1.41 (dd, *J*=6.63, 1.56 Hz, 3 H) 3.05 (s, 3 H) 4.33 - 4.56 (m, 2 H) 4.90 - 5.03 (m, 1 H) ppm ^{13}C NMR (100.61 MHz, $CDCl_3$) δ = 16.3 (d, *J*=7.1 Hz) 48.4 (d, *J*=2.8 Hz) 77.1 (d, *J*=21.2 Hz) 84.3 (d, *J*=175.2 Hz) ppm ^{19}F NMR (376.5 MHz, $CDCl_3$) δ = -223.7 ppm

2-azido-1-fluoropropane (4)

1-fluoropropan-2-yl methanesulfonate (**13**, 1 eq., 211 mg, 1.35 mmol) and sodium azide (1.05 eq., 92 mg, 1.42 mmol) was stirred in anhydrous DMF at 50°C overnight. Additional NaN_3 (0.11 eq., 10 mg, 0.15 mmol) was added and the heating continued for further 24 hours after which ^{1}H-NMR indicated full conversion. The reaction mixture was centrifuged (13.4 krpm, 5 min) to remove insolubles. A solution of **4** in DMF was obtained (550 mg, 1.1 mmol/g as determined by ^{1}H-NMR, corresponding to 45% of theory). ^{1}H NMR (400 MHz, $CDCl_3$) δ = 1.16 (dd, *J*=6.80, 1.56 Hz, 3 H) 3.56 - 3.81 (m, 1 H) 4.18 (dd, *J*=9.76, 6.63 Hz, 0.5 H) 4.25 - 4.34 (m, 1 H) 4.40 (dd, *J*=9.56, 3.71 Hz, 0.5 H) ppm ^{13}C NMR (100.61 MHz, $CDCl_3$) δ = 14.4 (d, *J*=6.4 Hz) 56.4 (d, *J*=19.1 Hz) 85.6 (d, *J*=174.5Hz) ppm ^{19}F NMR (376.5 MHz, $CDCl_3$) δ = -223.5 ppm

((5aR,6S,6aS)-1-(2-fluoroethyl)-1,4,5,5a,6,6a,7,8-octahydrocyclopropa[5,6]cycloocta[1,2-d][1,2,3]triazol-6-yl)methanol, BCN-1-Conjugate (15)

BCN (1.7 eq., 23.2 mg, 0.155 mmol) and 1-Azido-2-fluoroethane (**1**, 1 eq., 8 mg, 0.09 mmol) were stirred in 2.2 ml acetonitrile for 4 hours. The solvent was removed and volatiles removed on the rotary evaporator. The residue was dissolved in 1ml DCM and loaded onto 8 g of silica that were eluted with 20-100% ethyl acetate in light petroleum. The product (Rf = 0.15 in EE) was obtained in 85% yield. ^{1}H NMR (400 MHz, $CDCl_3$) δ = 0.97 - 1.12 (m, 2 H) 1.16 - 1.28 (m, 1 H) 1.50 - 1.65 (m, 2 H) 1.76 (br. s, 1 H) 2.20 - 2.34 (m, 2 H) 2.66 - 2.78 (m, 1 H) 2.85 - 3.02 (m, 2 H) 3.08 - 3.20 (m, 1 H) 3.73 (qd, *J*=11.40, 7.87 Hz, 2 H) 4.55 (dt, *J*=25.61, 4.80 Hz, 2 H) 4.78 (dt, *J*=46.84, 4.80 Hz, 2 H) ppm ^{13}C NMR (100.61 MHz,

$CDCl_3$) δ = 19.4, 19.9, 21.3, 22.2, 22.6, 23.0, 23.03, 25.9, 48.1 (d, *J*=20.7 Hz), 59.8, 82.3 (d, *J*=173.3 Hz), 134.5, 144.6 ppm. LC/MS data see SI. ESI-MS: $[M+H]^+$ calcd. for $C_{12}H_{19}FN_3O^+$: 240.2 found: 240.5

((5aR,6S,6aS)-1-(2-fluoropropyl)-1,4,5,5a,6,6a,7,8-octahydrocyclopropa[5,6]cycloocta[1,2-d][1,2,3]triazol-6-yl)methanol, BCN-4-Conjugate (16)

BCN (1 eq., 25 mg, 0.160 mmol) and 1-Azido-1-fluoropropane (**4**, 1.04 eq., 17.1 mg, 0.166 mmol) were stirred in 150 µl DMF overnight. The reaction mixture was diluted with 1 ml water and 1 ml DMSO and loaded onto 30 g C18-SiO_2, which was eluted with 5-85% acetonitrile in water. The product containing fractions were combined and lyophilized to obtain 35 mg (83% of theory) of inseperable diastereomers as a colorless oil. ^{1}H NMR (600 MHz, $CDCl_3$) δ = 0.95 - 1.10 (m, 2 H) 1.16 - 1.24 (m, 1 H) 1.54 - 1.65 (m, 5 H) 2.21 - 2.31 (m, 2 H) 2.64 - 2.77 (m, 1 H) 2.87 - 3.00 (m, 2 H) 3.12 (dddd, *J*=15.74, 11.77, 7.85, 3.96 Hz, 1 H) 3.67 - 3.79 (m, 2 H) 4.61 - 4.83 (m, 3 H) ppm ^{13}C NMR (150.91 MHz, $CDCl_3$) δ = 16.06 (d, *J*=6.54 Hz), 16.1 (d, *J*=6.54 Hz), 16.2 (d, *J*=6.54 Hz),19.1, 19.2, 19.4, 19.9, 21.0, 21.2, 22.0, 22.2, 22.4, 22.7, 22.75, 23.1, 53.5, 53.6, 59.7, 59.8, 85.3 (d, *J*=175.48 Hz), 85.34 (d, *J*=175.48 Hz), 133.7, 133.9, 144.3, 144.4 ppm ^{19}F NMR (376.5 MHz, $CDCl_3$) δ = -218.9, -219.0 ppm. LC/MS data see SI. ESI-MS: $[M+H]^+$ calcd. for $C_{13}H_{21}FN_3O^+$: 254.2 found: 254.2

((5aR,6S,6aS)-1-(2-fluoro-2-methylpropyl)-1,4,5,5a,6,6a,7,8-octahydrocyclopropa[5,6]cycloocta[1,2-d][1,2,3]triazol-6-yl)methanol, BCN-5-Conjugate (17)

A mixture of 1-fluoro-2-methylpropan-2-amine hydrochloride (**14**, 1 eq., 340 mg, 2.66 mmol), potassium carbonate (2.2 eq., 808 mg, 5.8 mmol) and copper(II)sulphate pentahydrate (0.01 eq., 7 mg, 30 µmol) in 5 ml MeOH was treated with imidazol-1-sulfonyl azide hydrochloride (1.2 eq., 670 mg, 3.2 mmol) in one portion. The reaction mixture was stirred at room temperature overnight, diluted with 30 ml brine and extracted two times with ethyl acetate. Pooled extracts were washed with 2N HCl and brine and dried over $MgSO_4$. Following filtration an aliquot of the EE solution containing **5** was treated with BCN (30 mg, 200 µmol) and stirred for three hours at room temperature. Evaporation to dryness followed by column chromatography (60-100% EE in PE) afforded 35.8 mg **17** as white solid (68% of theory based on BCN). TLC-Rf (EE) = 0.17, ^{1}H NMR (400 MHz, $CDCl_3$) δ = 0.84 - 0.99 (m, 2 H) 1.07 - 1.18 (m, 1 H) 1.40 - 1.55 (m, 2 H) 1.67 (d, *J*=1.95 Hz, 6 H) 2.14 - 2.28 (m, 2 H) 2.75 - 2.88 (m, 2 H) 2.91 - 3.00 (m, 1 H) 3.05 - 3.14 (m, 1 H) 3.57 - 3.64 (m, 1 H) 3.65 - 3.71 (m, 1 H) 4.67 (d, *J*=47.61 Hz, 2 H) ppm ^{13}C NMR (100.61 MHz, $CDCl_3$) δ = 19.0, 19.7, 21.5, 23.6 (d, J = 2.83 Hz), 24.4 (d, J = 3.53 Hz), 25.3, 59.7, 62.1 (d, J = 19.78 Hz), 88.0 (d, J = 178.73 Hz), 134.0, 146.8 ppm, ^{19}F NMR (376.5 MHz, $CDCl_3$) δ = -221.46 ppm LC/MS data see SI. ESI-MS: $[M+H]^+$ calcd. for $C_{14}H_{23}FN_3O^+$: 268.2 found: 268.0

(S)-N-((S)-1-(((S)-1-amino-1-oxo-3-phenylpropan-2-yl)amino)-3-(1H-indol-3-yl)-1-oxopropan-2-yl)-1-((3-(prop-2-yn-1-yloxy)propanoyl)-D-tyrosyl)pyrrolidine-2-carboxamide, Propargyl-EM-1 (18)

25 mg endomorphin-1 (1 eq., 25 mg, 41 µmol) was dissolved in 1.2 ml DMSO:DMF = 1:1 (v/v) and triethylamine (5 eq., 28 µl, 205 µmol) was added. 2,5-Dioxopyrrolidin-1-yl 3-(prop-2-ynyloxy)propanoate (1.5 eq., 13.8 mg, 61 µmol) in 280 µl DMF was added in one portion, and the reaction mixture was stirred at 4°C overnight. LC/MS indicated quantitative transformation. The reaction mixture was diluted with 2 ml 0.1% TFA in water, loaded onto a preparative HPLC column (Phenomenex Luna C18, 21.2x250 mm, 10 µm) and eluted using a gradient of 10-90% acetonitrile + 0.1% TFA (v/v) in water. The product containing fraction was lyophilized to obtain **18** as yellow oil (42% of theory, 12.4 mg). ^{1}H NMR (600 MHz) and ^{13}C-NMR (150.91MHz) data see ESI. LC/MS data see ESI. ESI-MS: $[M-H]^-$ m/z calcd. for $C_{40}H_{43}N_6O_7^-$: 719.3 found: 719.8

(S)-N-((S)-1-(((S)-1-amino-1-oxo-3-phenylpropan-2-yl)amino)-3-(1H-indol-3-yl)-1-oxopropan-2-yl)-1-((3-((1-(2-fluoroethyl)-1H-1,2,3-triazol-4-yl)methoxy)propanoyl)-D-tyrosyl)pyrrolidine-2-carboxamide, EM-1-1 Conjugate (19)

Copper(II)sulfate pentahydrate (0.92 eq., 560 µg, 2.24 µmol) was mixed with sodium ascorbate (3.1 eq., 1500 µg, 7.6 µmol) in 10 µl water. After the mixture turned from black to yellow bathophenanthrolinedisulfonic acid disodium salt (0.76 eq., 1 mg, 1.86 µmol) in 20 µl water was added causing dark green coloration. The catalyst mixture was added to a solution of propargyl-endomoprphin-1 **18** (1 eq., 2 mg, 2.44 µmol) and **1** (10 eq., 2.17 mg, 24.4 µmol) in 220 µl DMF. The mixture was stirred for 2 hours at room temperature and kept at 4°C overnight. The reaction was quenched by addition of 500 µl 1% TFA in water, and loaded onto a preparative HPLC column (Phenomenex Luna C18(2), 10x250 mm, 10 µm). The column was eluted with a gradient of 10% to 90% acetonitrile in H_2O (+ 0.1% v/v TFA). The product containing fraction was lyophilized to obtain **19** as a white solid. A meaningful yield could not be determined due to the scale of the reaction. ^{19}F NMR (376.5 MHz, DMSO-*d6*) δ = -73.6 (residual TFA), -222.1 ppm**.** LC/MS data see ESI. ESI-MS: $[M-H]^-$ m/z calcd. for $C_{42}H_{47}FN_9O_7^-$: 808.4 found: 808.8

(S)-N-((S)-1-(((S)-1-amino-1-oxo-3-phenylpropan-2-yl)amino)-3-(1H-indol-3-yl)-1-oxopropan-2-yl)-1-((3-((1-(3-fluoropropyl)-1H-1,2,3-triazol-4-yl)methoxy)propanoyl)-D-tyrosyl)pyrrolidine-2-carboxamide, EM-1-2 Conjugate (20)

$CuSO_4$ pentahydrate (0.92 eq., 560 µg, 2.24 µmol) was mixed with sodium ascorbate (3.1 eq., 1500 µg, 7.6 µmol) in 10 µl water. After the mixture turned from black to yellow bathophenanthrolinedisulfonic acid disodium salt (0.76 eq., 1 mg, 1.86 µmol) in 20 µl water was added causing dark green coloration. The catalyst mixture was added to a solution of propargyl-endomoprphin-1 **18** (1 eq., 2 mg, 2.44 µmol) and **3** (10 eq., 2.5 mg, 24.4 µmol) in 200 µl DMF. The mixture was stirred for 2 hours at room temperature and kept at 4°C overnight. The reaction was quenched by addition of 500 µl 1% TFA in water, and loaded onto a preparative HPLC column (Phenomenex Luna C18(2), 10x250 mm, 10 µm). The column was eluted with a gradient of 10% to 90% acetonitrile in H_2O (+ 0.1% v/v TFA). The product containing fraction was lyophilized to obtain **20** as a white solid. A meaningful yield could not be determined due to the scale of the reaction. ^{19}F NMR (376.5 MHz, DMSO-*d6*) δ = -73.8 (residual TFA), -220.4 ppm LC/MS data see ESI. ESI-MS: $[M-H]^-$ m/z calcd. for $C_{43}H_{49}FN_9O_7^-$: 822.4 found: 822.8

(2S)-N-((S)-1-(((S)-1-amino-1-oxo-3-phenylpropan-2-yl)amino)-3-(1H-indol-3-yl)-1-oxopropan-2-yl)-1-((3-((1-(1-fluoropropan-2-yl)-1H-1,2,3-triazol-4-yl)methoxy)propanoyl)-D-tyrosyl)pyrrolidine-2-carboxamide, EM-1-3 Conjugate (21)

$CuSO_4$ pentahydrate (0.92 eq., 560 µg, 2.24 µmol) was mixed with sodium ascorbate (3.1 eq., 1500 µg, 7.6 µmol) in 10 µl water. After the mixture turned from black to yellow bathophenanthrolinedisulfonic acid disodium salt (0.76 eq., 1 mg, 1.86 µmol) in 20 µl water was added causing dark green coloration. The catalyst mixture was added to a solution of propargyl-endomoprphin-1 **18** (1 eq., 2 mg, 2.44 µmol) and **4** (10 eq., 22 µl C= 1.1 mmol/g in DMF, 24.4 µmol) in 200 µl DMF. The mixture was stirred for 4 hours at room temperature and kept at 4°C overnight. The reaction was quenched by addition of 500 µl 1% TFA in water, and loaded onto a preparative HPLC column (Phenomenex Luna C18(2), 10x250 mm, 10 µm). The column was eluted with a gradient of 10% to 90% acetonitrile in H_2O (+ 0.1% v/v TFA). The product containing fraction was lyophilized to obtain **16** as a white solid. A meaningful yield could not be determined due to the scale of the reaction. C/MS data see ESI. ESI-MS: $[M-H]^-$ m/z calcd. for $C_{43}H_{49}FN_9O_7^-$: 822.4 found: 822.8

Radiosynthesis of [^{18}F]**1**

A Sep-Pak Accell Plus QMA Plus Light Cartridge (Waters) was preconditioned with 0.5M K_2CO_3 solution (7 ml) followed by 15 ml water. Cyclotron produced ^{18}F-fluoride (836 MBq) in 2.5 ml water was passed over the cartridge, and the cartridge was eluted with a solution of 3.5 mg K_2CO_3 (25.3 µmol) and 14.1 mg [2.2.2]cryptand (37.5 µmol) in 1000 µl acetonitrile:H_2O = 9:1 (v/v). Volatiles were removed in a stream of argon at 105°C and residual water was removed by addition and subsequent evaporation of 700 µl anhydrous acetonitrile. The azeotropic drying step was repeated two times. 14.5 mg (53.2 µmol) of nosylate **2** in 500 µl dry acetonitrile was added, and the reaction mixture heated to 105°C for 5 min. Volatiles were distilled into 1 ml cooled (-20°C) acetonitrile in a slow stream of argon using a short polyethylene tubing with two attached needles. Two Sep-Pak AC2 Plus activated carbon cartridges (Waters) were connected in series to the outlet of the receiving vial as a safety measure. [^{18}F]**1** was obtained in 75.4% decay corrected yield. HPLC (Conditions A): [^{18}F]**1** has a retention time of 5.26 min. Radiochemical purity as determined by radio-HPLC exceeded 99%.

Conjugation of [^{18}F]**1** with BCN

300 µl of acetonitrile solution containing [^{18}F]**1** (126 MBq) was treated with cyclooctyne BCN (2 mg, 13.3 µmol), and the reaction mixture was stirred at room temperature. 108 minutes post cyclooctyne addition the reaction mixture was investigated by radio-HPLC (HPLC conditions A, 230 nm) to reveal 98.5% conversion to the ligation product [^{18}F]**15.** The retention time of [^{18}F]**15** (14.6 min) matched the retention time of **15**.

Radiosynthesis of [^{18}F]**3**

Cyclotron produced ^{18}F-fluoride (947 MBq) in 0.4 ml water was trapped on a PS-HCO_3^- (Cromafix) cartridge and was eluted with a solution of 1.75 mg K_2CO_3 (12.7 µmol) and 8.5 mg [2.2.2]cryptand (22.6 µmol) in 1000 µl acetonitrile:H_2O = 9:1 (v/v). Volatiles were removed in a stream of argon at 110°C and residual water was removed by addition and subsequent evaporation of 700 µl anhydrous acetonitrile. The azeotropic drying step was repeated twice. 7 mg (24.5 µmol) of nosylate **6** in 250 µl dry acetonitrile was added, and the reaction mixture heated to 90°C for 8 min. Volatiles were distilled into 200 µl cooled (-20°C) acetonitrile in a slow stream of argon using a short polyethylene tubing with two

attached needles. Two Sep-Pak AC2 Plus activated carbon cartridges were connected in series to the outlet of the receiving vial as a safety measure. [^{18}F]**3** was obtained in 39.3% decay corrected yield. HPLC conditions A (216 nm) were used, where [^{18}F]**3** has a retention time of 12.1 min that matched the retention time of reference compound **3**. Radiochemical purity exceeded 98%.

Radiosynthesis of [^{18}F]4

Cyclotron produced ^{18}F-fluoride (1.65 GBq) in 1.5 ml water was trapped on a PS-HCO_3^- (Cromafix) cartridge and was eluted with a solution of 3.5 mg K_2CO_3 (25.3 µmol) and 14.1 mg [2.2.2]cryptand (37.5 µmol) in 1000 µl acetonitrile:H_2O = 9:1 (v/v). Volatiles were removed in a stream of argon at 110°C and residual water was removed by addition and subsequent evaporation of 700 µl anhydrous acetonitrile. The azeotropic drying step was repeated twice. 14 mg (48.9 µmol) of nosylate **8** in 300 µl dry acetonitrile was added, and the reaction mixture heated to 100°C for 7 min. Volatiles were distilled into 200 µl cooled (-20°C) acetonitrile in a slow stream of argon using a short polyethylene tubing with two attached needles. Two Sep-Pak AC2 Plus activated carbon cartridges were connected in series to the outlet of the receiving vial as a safety measure. [^{18}F]**4** was obtained in 58.1% decay corrected yield. HPLC conditions A were used, where [^{18}F]**4** has a retention time of 11.8 min that matched the retention time of reference compound **4**. Radiochemical purity exceeded 99%.

Conjugation of [^{18}F]4 with cyclooctyne BCN

500 µl of acetonitrile solution containing [^{18}F]**4** (80 MBq) was treated with cyclooctyne BCN (0.5 mg, 3.3 µmol), and the reaction mixture was stirred at room temperature. The reaction was analyzed by radio-HPLC (HPLC Conditions A, 230 nm) 47 min and 134 min post cyclooctyne addition revealing 72% and 87% conversion to triazole [^{18}F]**16**. The retention time of [^{18}F]**16** (8.53 min) matched the retention time of reference compound **16**.

Synthesis of [^{18}F]19: Rapid radiolabeling of endomorphin-1 using [^{18}F]1

In a 1.5 ml tube $CuSO_4$ pentahydrate (1.2 mg, 4.48 µmol) was mixed with sodium ascorbate (3 mg, 15.2 µmol) in 20 µl water. After the mixture turned from black to yellow bathophenanthrolinedisulfonic acid disodium salt (2 mg, 3.72 µmol) in 40 µl water:DMF (4:1 v/v) was added causing dark green coloration. Propargylated endomorphin-1 **18** (1 mg, 2.22 µmol) in 100 µl DMF followed by [^{18}F]**1** (73 MBq) was added to the catalyst. Following homogenization the mixture was allowed to react for 10 min at room temperature followed by quenching with 500 µl 0.1% TFA in acetonitrile:H_2O = 1:1 (v/v). Radio-HPLC analysis (conditions B, 280 nm) revealed 65% yield of [^{18}F]-**19**. Using the same conditions with reduced catalyst amount (50%) afforded 63% incorporation yield. The retention time of [^{18}F]**19** (5.95 min) matched that of reference material **14**. (Chromatograms see ESI) A aliquot of purified [^{18}F]**19** (2.2 MBq) was collected from the analytical HPLC for stability testing in human blood plasma.

Synthesis of [^{18}F]20: Rapid radiolabeling of endomorphin-1 using [^{18}F]3

In a 1.5 ml tube $CuSO_4$ pentahydrate (1.2 mg, 4.48 µmol) was mixed with sodium ascorbate (3 mg, 15.2 µmol) in 20 µl water. After the mixture turned from black to yellow bathophenanthrolinedisulfonic acid disodium salt (2 mg, 3.72 µmol) in 40 µl water:DMF (4:1 v/v) was added causing dark green coloration. Propargylated endomorphin-1 **18** (1 mg, 2.22 µmol) in 100 µl DMF followed by [^{18}F]**3** (37 MBq) was added to the catalyst. Following homogenization the mixture was allowed to react for 10

min at room temperature followed by quenching with 500 µl 0.1% TFA in acetonitrile:H_2O = 1:1 (v/v). Radio-HPLC analysis (conditions B, 280 nm) revealed 64% yield of [^{18}F]**20**. The retention time of [^{18}F]**20** (6.12 min) matched that of reference material **20.** (Chromatograms see ESI) An aliquot of purified [^{18}F]**20** (1.4 MBq) was collected from the analytical HPLC for stability testing in human blood plasma.

Synthesis of [^{18}F]21: Rapid radiolabeling of endomorphin-1 using [^{18}F]4

In a 1.5 ml tube $CuSO_4$ pentahydrate (1.2 mg, 4.48 µmol) was mixed with sodium ascorbate (3 mg, 15.2 µmol) in 20 µl water. After the mixture turned from black to yellow bathophenanthrolinedisulfonic acid disodium salt (2 mg, 3.72 µmol) in 40 µl water:DMF (4:1 v/v) was added causing dark green coloration. Propargylated endomorphin-1 **18** (1 mg, 2.22 µmol) in 100 µl DMF followed by [^{18}F]**4** (70.7 MBq) in 50 µl acetonitrile was added to the catalyst. Following homogenization the mixture was allowed to react for 10 min at room temperature followed by quenching with 500 µl 0.1% TFA in acetonitrile:H_2O = 1:1 (v/v). Radio-HPLC analysis (conditions B, 280 nm) revealed 98% yield of [^{18}F]**21**. The retention time of [^{18}F]**21** (6.08 min) matched that of reference material **16.** (Chromatograms see ESI) An aliquot of purified [^{18}F]**21** (1.8 MBq) was collected from the analytical HPLC for stability testing in human blood plasma.

Plasma stability of [^{18}F] endomorphin-1 conjugates [^{18}F]19, [^{18}F]20 and [^{18}F]21

100-150 kBq of [^{18}F]**19**, [^{18}F]**20** or [^{18}F]**21** were incubated in 500 µl human blood plasma at 37°C for 120 minutes. To assess plasma stability, the solutions were spotted on reversed phase TLC plates. [^{18}F]**14**, [^{18}F]**15** and [^{18}F]**16** were spotted as reference. The plates were developed using acetonitrile:H_2O = 1:1 (v/v + 0.1vol% TFA) as mobile phase. Radioactivity was quantified using a Hewlett Packard Cyclone Phosphor Imager autoradiography system (see ESI). Analysis revealed 81% intact [^{18}F]**19,** 82% intact [^{18}F]**20** and 86% intact [^{18}F]**21.**

Synthesis of [^{18}F]1, [^{18}F]3 and [^{18}F]4 using a automated synthesis module (for *in vivo* study)

A remote controlled synthesis module (TRACERlab™ FXFDG, General Electric Healthcare, Uppsala, Sweden) with 3 mL glass reactor housed in a hot cell was used for automated labeling experiments. In general cyclotron produced no carrier added [^{18}F] fluoride was trapped on a preconditioned (5 ml 0.5 M K_2CO_3 followed by 15 ml water) Waters QMA light cartridge. The radioactivity was eluted with a solution of [2.2.2]cryptand (15 mg, 40 µmol) in acetonitrile (900 µl) to which a 3.5% aq. K_2CO_3 (100 µL, 25 µmol) solution had been added. After addition of dry acetonitrile (500 µL) volatiles were removed in vacuo at a temperature of 60-120 °C. After cooling to 60 °C a solution of precursor (12.5 mg, 46 µmol **2** for [^{18}F]**1**, 13.1 mg, 46 µmol **6** for [^{18}F]**3** and 13.7 mg, 48 µmol **8** for [^{18}F]**4**) in dry acetonitrile (650-700 µl) was added. The reaction mixture was heated to 100-105°C for 5 minutes followed by cooling to 35°C to prevent activity loss when venting the reactor. The reactor contents were loaded onto a preparative HPLC column (Macherey-Nagel EP 250/16 100-7 C-18, 10 µm, 16 x 250 mm) and eluted using a gradient of ethanol/water at a flow rate of 4 ml/min (0-10m 2% EtOH, 10m→50m 2%→30% EtOH for [^{18}F]**1**, 0-6m 3% EtOH, 6m→40m 3%→40% for [^{18}F]**3** and 0-10m 5% EtOH, 10m→50m 5%→50% EtOH for [^{18}F]**4**. 9.9 GBq [^{18}F]**1** was obtained from 36.2 GBq starting activity (48% decay corrected radiochemical yield), 16.7 GBq [^{18}F]**3** was obtained from 117 GBq starting activity (23.5% decay corrected radiochemical yield) and 18.6 GBq [^{18}F]**4** was obtained from 122 GBq starting activity (27% decay corrected radiochemical yield). The products were diluted with physiological saline to a

activity concentration of ~370 MBq/ml for iv administration. pH was between 5 and 7 for all formulations and osmolarity was within physiological range (300-500 mmol/kg). ^{18}F-species prepared by automated labeling matched HPLC retention times of authentic standards.

PET/MR Imaging – Biodistribution study

Mice underwent PET scanning on a dual animal bed in a dedicated small-animal PET scanner (n=4 for [^{18}F]**1**, n= 2 for [^{18}F]**3** and [^{18}F]**4**) and one mouse per test substance underwent sequential PET/MRI on two stand-alone scanners. Prior imaging, mice were pre-anesthetized in an induction chamber using isoflurane (2.5% in oxygen), placed in prone position on a heated animal bed (38°C) and the lateral tail vein was cannulated using a custom made tail vein catheter. Animal respiratory rate and body temperature were constantly monitored (SA Instruments Inc., Stony Brook, NY, USA) and the isoflurane level was adjusted (1.5-2.5% on oxygen) to achieve a constant depth of anesthesia. Anesthesia was maintained for the whole imaging period. A humidifier was used to moisten the gas mixture before supplying it to the animal(s). For anatomical magnetic resonance imaging (MRI) a single mouse body bed mounted with a mouse whole body RF coil was used. The whole body coil covers an axial field of view (FOV) of about 8 cm that is very similar to the axial FOV of the PET scanner (7.6 cm). Images were acquired on a 1 Tesla benchtop MRI (ICON, Bruker Biospin GmbH, Ettlingen, Germany) using a modified 3D T_1-weighted gradient echo sequence (T1-FLASH) with the following imaging parameters: echo time (TE) = 4.7 ms; repetition time (TR) = 25 ms; flip angle (FA) = 25 °; field of view (FOV) = 7.6 x 2.6 x 2.4 cm; matrix = 253 x 93; 32 slices; slice thickness = 750 µm; 5 repetitions; total imaging time = 6 min 15 sec. After MRI, the animal bed was transferred into the gantry of a microPET scanner (Focus 220, Siemens Medical Solutions, Knoxville, TN, USA). Total anesthesia time prior start of PET scanning for mice that underwent PET scanning only was similar to that of the PET/MRI examined animal. Direct after positioning of the animal bed in the gantry of the PET scanner a 10 min transmission scan using a rotating ^{57}Co point source was recorded. Simultaneously with intravenous injection of 6.1 ± 0.9 MBq [^{18}F]-**1**, 4.7 ± 0.2 MBq [^{18}F]-**3** or 6.5 ± 0.6 MBq [^{18}F]-**4** dynamic PET imaging was initiated for 120 min using an energy window of 250-750 keV and a timing window of 6 ns. After completion of the imaging procedure, a terminal blood sample was withdrawn under isoflurane anesthesia from the retro-orbital sinus vein and the animals were sacrificed by cervical dislocation. Blood was centrifuged (17000 *g*, 4°C, 4 min) to obtain plasma, and organ samples as well as urine were collected. Aliquots of blood, plasma and urine as well as organ samples were transferred into pre-weighted tubes and measured for radioactivity in a gamma counter (Wizard 1470, Perkin-Elmer, Wellesley, MA, USA). The measured radioactivity data were corrected for radioactive decay and expressed as standardized uptake value ((radioactivity per g/injected radioactivity) x body weight). The 60 min dynamic emission PET data were sorted into 26 frames, which incrementally increased in time length from 5 seconds to 20 min. Images were reconstructed using Fourier rebinning of the 3D sonograms followed by two-dimensional filtered back projection with a ramp filter, resulting in an image voxel size of 0.4 x 0.4 x 0.796 mm^3. A standard data correction protocol (normalization, attenuation and decay correction) was applied to the PET data. The PET units were converted into units of radioactivity concentration by applying a calibration factor derived from imaging of a cylindrical phantom with a known ^{18}F-radioactivity concentration. Corresponding PET/MRI images were aligned using a pre-calculated, fixed transformation matrix. Using the image analysis software Amide,[25] different volumes of interest (brain, liver, kidneys, urinary bladder, heart, bone (left humerus), muscle (right lower arm muscle)) were manually outlined on multiple planes and time-radioactivity concentration curves (TACs), expressed in standardized uptake values, were derived.

Analysis of murine metabolites – *in vivo* stability of small [^{18}F]-fluoroalkylazides

Blood and urine samples harvested directly after imaging experiments (120 min post administration) were used for metabolite studies. Murine plasma was obtained by centrifugation (17000 *g*, 4°C, 4 min), and plasma proteins were precipitated by addition of an equal volume acetonitrile and removed by centrifugation (17000 *g*, 4°C, 1 min). Supernatant solution was diluted with water and injected into a HPLC system using a lead shielded Berthold LB 507B radioactivity detector. [^{18}F]**1**, [^{18}F]**3** and [^{18}F]**4** were injected as reference materials. Urine was directly injected after dilution with water (1:10 v/v). Analysis revealed < 2% intact [^{18}F]**1**, < 3% intact [^{18}F]**3** and < 4% intact [^{18}F]**4** in plasma while the fraction of unchanged tracers was < 1% in urine for all test substances. The majority of activity (>90%) was detected as highly polar metabolites proofing the metabolic instability of the test substances.

References

(1) Evans, H. L., Slade, R. L., Carroll, L., Smith, G., Nguyen, Q.-D., Iddon, L., Kamaly, N. N., Stöckmann, H., Leeper, F. J., Aboagye, E. O., Spivey, A. C., and Aboagye, O. (2012) Copper-free click--a promising tool for pre-targeted PET imaging. *Chem. Commun. (Camb). 48*, 991–3.

(2) Glaser, M., and Arstad, E. (2007) "Click labeling" with 2-[F-18]fluoroethylazide for positron emission tomography. *Bioconjug. Chem. 18*, 989–993.

(3) Zhou, D., Chu, W., Dence, C. S., Mach, R. H., and Welch, M. J. (2012) Highly efficient click labeling using 2-[18F]fluoroethyl azide and synthesis of an 18FN-hydroxysuccinimide ester as conjugation agent. *Nucl. Med. Biol. 39*, 1175–1181.

(4) Bejot, R., Carroll, L., Bhakoo, K., Declerck, J., and Gouverneur, V. (2012) A fluorous and click approach for screening potential PET probes: Evaluation of potential hypoxia biomarkers. *Bioorganic Med. Chem. 20*, 324–329.

(5) Glaser, M., Solbakken, M., Turton, D. R., Pettitt, R., Barnett, J., Arukwe, J., Karlsen, H., Cuthbertson, A., Luthra, S. K., and Årstad, E. (2009) Methods for 18F-labeling of RGD peptides: Comparison of aminooxy [18F]fluorobenzaldehyde condensation with "click labeling" using 2-[18F]fluoroethylazide, and S-alkylation with [18F] fluoropropanethiol. *Amino Acids 37*, 717–724.

(6) Jia, L., Cheng, Z., Shi, L., Li, J., Wang, C., Jiang, D., Zhou, W., Meng, H., Qi, Y., Cheng, D., and Zhang, L. (2013) Fluorine-18 labeling by click chemistry: Multiple probes in one pot. *Appl. Radiat. Isot. 75*, 64–70.

(7) Iddon, L., Leyton, J., Indrevoll, B., Glaser, M., Robins, E. G., George, A. J. T., Cuthbertson, A., Luthra, S. K., and Aboagye, E. O. (2011) Synthesis and in vitro evaluation of [18F]fluoroethyl triazole labelled [Tyr3]octreotate analogues using click chemistry. *Bioorganic Med. Chem. Lett. 21*, 3122–3127.

(8) Kettenbach, K., Schieferstein, H., Ross, T. L., Kettenbach, K., Schieferstein, H., and Ross, T. L. (2014) 18F-Labeling Using Click Cycloadditions. *Biomed Res. Int. 2014*, 1–16.

(9) Lee, S. B., Kim, H. L., Jeong, H.-J., Lim, S. T., Sohn, M.-H., and Kim, D. W. (2013) Mesoporous Silica Nanoparticle Pretargeting for PET Imaging Based on a Rapid Bioorthogonal Reaction in a Living Body. *Angew. Chemie Int. Ed. 52*, 10549–10552.

(10) Prescher, J. A., and Bertozzi, C. R. (2005) Chemistry in living systems. *Nat. Chem. Biol. 1*, 13–21.

(11) Sletten, E. M., and Bertozzi, C. R. (2009) Bioorthogonal chemistry: fishing for selectivity in a sea of functionality. *Angew. Chem. Int. Ed. Engl. 48*, 6974–98.

(12) Baskin, J. M., Prescher, J. A., Laughlin, S. T., Agard, N. J., Chang, P. V, Miller, I. A., Lo, A., Codelli, J. A., and Bertozzi, C. R. (2007) Copper-free click chemistry for dynamic in vivo imaging. *Proc. Natl. Acad. Sci. U. S. A. 104*, 16793–7.

(13) Plass, T., Milles, S., Koehler, C., Schultz, C., and Lemke, E. A. (2011) Genetically Encoded Copper-Free Click Chemistry. *Angew. Chemie Int. Ed. 50*, 3878–3881.

(14) Pretze, M., Pietzsch, D., and Mamat, C. (2013) Recent trends in bioorthogonal click-radiolabeling reactions using fluorine-18. *Molecules 18*, 8618–8665.

(15) Kobus, D., Giesen, Y., Ullrich, R., Backes, H., and Neumaier, B. (2009) A fully automated two-step synthesis of an 18F-labelled tyrosine kinase inhibitor for EGFR kinase activity imaging in tumors. *Appl. Radiat. Isot. 67*, 1977–1984.

(16) Goddard-Borger, E. D., and Stick, R. V. (2007) An Efficient, Inexpensive, and Shelf-Stable Diazotransfer Reagent: Imidazole-1-sulfonyl Azide Hydrochloride. *Org. Lett. 9*, 3797–3800.

(17) Goddard-Borger, E. D., and Stick, R. V. (2011) An Efficient, Inexpensive, and Shelf-Stable Diazotransfer Reagent: Imidazole-1-sulfonyl Azide Hydrochloride. *Org. Lett. 13*, 2514–2514.

(18) Li, J., Shi, L., Jia, L., Jiang, D., Zhou, W., Hu, W., Qi, Y., and Zhang, L. (2012) Radiolabeling of RGD peptide and preliminary biological evaluation in mice bearing U87MG tumors. *Bioorg. Med. Chem. 20*, 3850–3855.

(19) HOFFMANN, F. W. (1949) ALIPHATIC FLUORIDES. I. w,w´-DIFLUOROALKANES. *J. Org. Chem. 14*, 105–110.

(20) Jean-Damien, C., Haley, M., and Binch, D. (2011) Compounds useful as inhibitors of atr kinase.

(21) Ok, D., Fisher, M. H., Wyvratt, M. J., and Meinke, P. T. (1999) Improved syntheses of fluorinated tertiary butylamines. *Tetrahedron Lett. 40*, 3831–3834.

(22) Dommerholt, J., Schmidt, S., Temming, R., Hendriks, L. J. A., Rutjes, F. P. J. T., Van Hest, J. C. M., Lefeber, D. J., Friedl, P., and Van Delft, F. L. (2010) Readily accessible bicyclononynes for bioorthogonal labeling and three-dimensional imaging of living cells. *Angew. Chemie - Int. Ed. 49*, 9422–9425.

(23) Gaeta, A., Woodcraft, J., Plant, S., Goggi, J., Jones, P., Battle, M., Trigg, W., Luthra, S. K., and Glaser, M. (2010) Use of 2-[(18)F]fluoroethylazide for the Staudinger ligation - Preparation and characterisation of GABA(A) receptor binding 4-quinolones. *Bioorg. Med. Chem. Lett. 20*, 4649–52.

(24) Horvath, G. (2000) Endomorphin-1 and endomorphin-2: pharmacology of the selective endogenous mu-opioid receptor agonists. *Pharmacol. Ther. 88*, 437–63.

(25) Loening, A. M., and Gambhir, S. S. (2003) AMIDE: A Free Software Tool for Multimodality Medical Image Analysis. *Mol. Imaging 2*, 131–137.

Manuscript #4

Christoph Denk, Dennis Svatunek, Thomas Filip, Thomas Wanek, Daniel Lumpi, Johannes Fröhlich, Claudia Kuntner*, Hannes Mikula*; Development of a ^{18}F-Labeled Tetrazine with Favorable Pharmacokinetics for Bioorthogonal PET Imaging, *Angew. Chem. Int. Ed.* **2014**, 53, 9655–9659.

(with permission from John Wiley & Sons)

Svatunek, D. (2016)

A Journal of the Gesellschaft Deutscher Chemiker

Angewandte Chemie

GDCh

International Edition

www.angewandte.org

2014–53/36

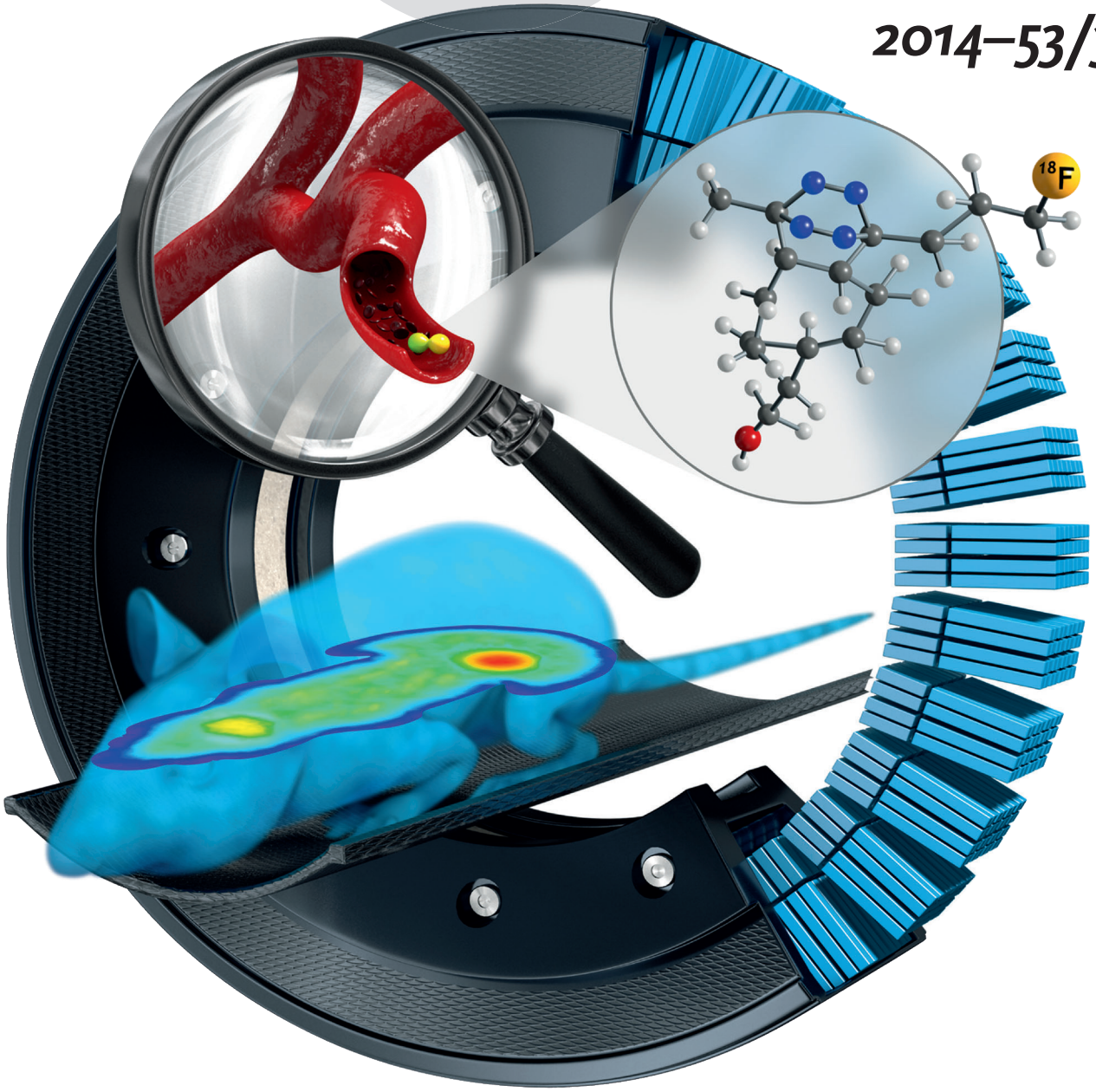

Bioorthogonal PET probes ...

... serve as highly valuable tools in the field of pretargeted molecular imaging. In their Communication on page 9655 ff., H. Mikula, C. Kuntner, and co-workers describe the development, synthesis, and characterization of a low-molecular-weight ^{18}F-labeled tetrazine derivative that can be used for bioorthogonal PET imaging of dienophile-tagged (bio)molecules through the application of in vivo chemistry.

WILEY-VCH

Angewandte International Edition Chemie

DOI: 10.1002/anie.201404277

Bioorthogonal Imaging

Development of a ^{18}F-Labeled Tetrazine with Favorable Pharmacokinetics for Bioorthogonal PET Imaging**

Christoph Denk, Dennis Svatunek, Thomas Filip, Thomas Wanek, Daniel Lumpi, Johannes Fröhlich, Claudia Kuntner, and Hannes Mikula**

Abstract: *A low-molecular-weight ^{18}F-labeled tetrazine derivative was developed as a highly versatile tool for bioorthogonal PET imaging. Prosthetic groups and undesired carrying of ^{18}F through additional steps were evaded by direct ^{18}F-fluorination of an appropriate tetrazine precursor. Reaction kinetics of the cycloaddition with trans-cyclooctenes were investigated by applying quantum chemical calculations and stopped-flow measurements in human plasma; the results indicated that the labeled tetrazine is suitable as a bioorthogonal probe for the imaging of dienophile-tagged (bio)molecules. In vitro and in vivo investigations revealed high stability and PET/MRI in mice showed fast homogeneous biodistribution of the ^{18}F-labeled tetrazine that also passes the blood–brain barrier. An in vivo click experiment confirmed the bioorthogonal behavior of this novel tetrazine probe. Due to favorable chemical and pharmacokinetic properties this bioorthogonal agent should find application in bioimaging and biomedical research.*

Bioorthogonal imaging applying in vivo chemistry has emerged as a highly versatile tool in chemical biology and biomedicine.[1] Since the development of copper-free click chemistry for bioimaging using the strain-promoted azide–alkyne cycloaddition (SPAAC),[2] this bioorthogonal ligation has been used for a wide variety of applications with the aim to examine the molecular details of biological processes.[3] Although reaction kinetics were successively improved during the last years,[4] rate constants of SPAAC ligations are still limited ($< 5\,M^{-1}s^{-1}$, acetonitrile, 20 °C) and therefore this chemistry is not fully suitable for bioconjugations in vivo. Nevertheless, in vivo SPAAC has recently been applied for the development of a pretargeted imaging approach using positron emission tomography (PET).[5] To circumvent problems in terms of (relatively) low reaction rates of SPAAC ligations, Fox et al. and Weissleder et al. have independently introduced the inverse-electron-demand Diels–Alder (IEDDA)-initiated conjugation between 1,2,4,5-tetrazines (Tz) and strained cycloalkenes as a highly efficient bioorthogonal ligation.[6] Since then, this reaction has attracted broad attention and has been extensively used in many biomedical applications including the development of bioorthogonal probes, live-cell imaging, protein labeling, and the synthesis of PET imaging agents.[7] Furthermore, IEDDA was successfully applied in combination with SPAAC for simultaneous multitarget imaging.[8] Recently, Carlson et al. reported the development of advanced bioorthogonal turn-on probes that apply through-bond energy transfer leading to fluorescence quenching within boron dipyrromethene (BODIPY)-tetrazine derivatives.[9] Reaction kinetics of IEDDA ligations were further improved by the development and application of the bicyclo[6.1.0]non-4-ene (s-TCO) moiety, an even more strained *trans*-cyclooctene derivative, as a highly reactive dienophile leading to tetrazine ligations with rate constants of up to approximately $20000\,M^{-1}s^{-1}$ (MeOH, 25 °C).[10] In addition to commonly used *trans*-cyclooctenes (TCO) and s-TCO,[11] cyclopropene (CP) tags have recently been reported as useful dienophiles with lower steric demand and have successfully been applied in live-cell imaging.[12]

Despite many applications of IEDDA ligations in the field of fluorescence imaging, the development of bioorthogonal PET approaches is still restricted due to a lack of efficient radiolabeled agents that distribute homogenously and show fast in vivo reaction kinetics, high stability, and adequate clearance. ^{18}F-Labeling of dienophiles such as TCO and norbornene was preferred in terms of pretargeting approaches applying IEDDA bioconjugations so far due to the previously observed and reported insufficient stability of tetrazines during direct fluorination.[13] Yet, this approach is still cumbersome due to the fact that instead of readily available cycloalkene tags the tetrazine moiety has to be attached to the pretargeting probe. Furthermore, a tetrazine-type radiolabeled agent would be capable of being applied for bioorthogonal imaging of various dienophiles and thus provide high versatility. A ^{11}C-labeled tetrazine was initially developed by Herth et al.[14] and metal radionuclides such as ^{64}Cu and ^{89}Zr were attached to tetrazines using chelating ligands resulting in relatively large and complex bioorthogonally imaging agents.[15] Furthermore, polymer-modified tetrazines were developed and used for pretargeted PET imaging.[16] However, the development of a readily accessible radiolabeled low-molecular-weight tetrazine taking advantage of the high specific radioactivity of ^{18}F (allowing admin-

[*] C. Denk, D. Svatunek, Dr. D. Lumpi, Prof. J. Fröhlich, Dr. H. Mikula
Institut für Angewandte Synthesechemie
Technische Universität Wien (TUW) (Austria)
E-mail: hannes.mikula@tuwien.ac.at
Dr. T. Filip, Dr. T. Wanek, Priv.-Doz. Dr. C. Kuntner
Health and Environment Department, Biomedical Systems
Austrian Institute of Technology (AIT)
Seibersdorf (Austria)
E-mail: claudia.kuntner@ait.ac.at

[**] Financial support from the Vienna Anniversary Foundation for Higher Education (H-2500/2012) is gratefully acknowledged. We thank Prof. Wolfgang Linert (VUT), Dr. Roland Müller (Seibersdorf Laboratories), Dominik Matscheko (VUT), and Walter Kuba (VUT) for their kind support during this work. PET = positron emission tomography.

Supporting information for this article is available on the WWW under http://dx.doi.org/10.1002/anie.201404277.

 © 2014 Wiley-VCH Verlag GmbH & Co. KGaA, Weinheim

istration of low-mass dosages and shorter radiation exposures) is still significant, which inspired us to focus on this particular problem in the field of bioorthogonal PET imaging.

Herein we report our results on the synthesis and characterization of a low-molecular-weight ^{18}F-labeled tetrazine with favorable pharmacokinetics that is applicable as a versatile tool for pretargeted PET imaging using in vivo IEDDA chemistry.

During the development of improved procedures for the synthesis of 1,2,4,5-tetrazines, the characterization of a variety of these compounds revealed an inverse correlation between their stability in fetal bovine serum and the reaction rates of their cycloaddition with dienophiles.[17] Therefore, we hypothesized that stability problems during direct tetrazine fluorination can be avoided or minimized by using less reactive 3,6-dialkyltetrazines that still possess sufficiently high reaction rates for pretargeted in vivo applications. The availability of physiologically stable radiolabeled tetrazines is crucial for the development of reliable PET imaging approaches. In addition to this trade-off (reactivity vs. stability), we intended to develop water-soluble low-molecular-weight compounds with the aim to obtain imaging agents with favorable pharmacokinetic properties. These considerations led to the chemical structure of tetrazine **1**. The two alkyl substituents were chosen to be as small as reasonable. A derivative with a methyl group was preferred since it is more stable than an unsubstituted tetrazine, and a three-methylene spacer was considered between the fluorine and the tetrazine moiety to avoid the undesired high reactivity of benzyl-type precursors (Tz-CH_2-X) as well as possible elimination during nucleophilic fluorination (Tz-CH_2CH_2-X → Tz-CH=CH_2). Quantum chemical calculations on the basis of a recently reported computational approach (DFT, M06-2X/6-31G(d,p), Gaussian 09)[18] were applied to estimate the reaction kinetics (Table 1) of **1** in comparison to that of phenyl-substituted tetrazines (e.g. **2**),[19] which are commonly used in combination with TCO tags for various bioorthogonal ligation applications.[20] As expected, modeling of IEDDA reactions with *trans*-cyclooctene (**3**) showed an increased activation free energy for **1** (18.8 kcal mol^{-1}) relative to that for **2** (15.0 kcal mol^{-1}), but this difference is compensated when s-TCO **4** is used for cycloaddition with **1** (15.3 kcal mol^{-1}). Thus, applying the bioorthogonal reaction pair **1**/**4** should result in reasonable rate constants similar to those of the frequently applied ligation between **2** and **3**. This assumption was verified by stopped-flow measurements after preparation of **1** starting from 4-hydroxypropanenitrile (**6**) applying metal-catalyzed tetrazine synthesis[21] followed by DAST-mediated fluorination of the intermediate **7** (Scheme 1). Furthermore, a significantly increased reaction rate was observed for the cycloaddition of **1** with the water-soluble s-TCO derivative **5** in human plasma ($k_2 > 8000\ M^{-1}s^{-1}$, 37 °C), which is in agreement with previously reported studies on the effect of water on IEDDA reaction kinetics (Table 1).[22]

Regarding the preparation of compound **7**, we have studied the impact of different reaction parameters on tetrazine synthesis and have mainly focused on the reagent grade of hydrazine. Finally, we did not observe significantly decreased yields of **7** when the monohydrate (18%) was used instead of anhydrous hydrazine (21%) that was originally used for the metal-catalyzed preparation of 3,6-dialkyltetrazines.[21] This is of particular interest, since the availability of anhydrous hydrazine has been restricted in Europe since 2011 due to the REACH regulation of the European Chemicals Agency.[23] Although commercially available hydrazine cyanurate can be used as a reagent for the safe preparation of anhydrous hydrazine of high purity,[24] reliable synthetic methods using the monohydrate or other forms (e.g. hydrazine salts) should be preferred.

The in vitro stability of **1** in human plasma was assessed by spectrophotometric measurements and HPLC. Almost no degradation was observed after incubation at 37 °C for 12 h (99% recovery) further revealing the capability of **1** as a promising scaffold for the development of a radiolabeled agent for pretargeted PET imaging. Although the excellent stability of **4** (no degradation in human serum, 30 mM butylamine in MeOH or 5 mM ethanethiol in MeOH) was shown by Taylor et al.,[10] they also observed isomerization (58% after 3.5 h) to the unreactive *cis* isomer at a high concentration of ethanethiol (30 mM in MeOH). Furthermore, Rossin et al. have recently reported that *trans*-cyclooctenes are probably isomerized by interactions with copper-containing proteins; they also presented strategies to circumvent this problem by increasing the steric bulk of the tag.[25]

Table 1: Reaction kinetics of IEDDA cycloadditions obtained by computational methods (M06-2X/6-31G(d,p), Gaussian 09) and stopped-flow measurements.

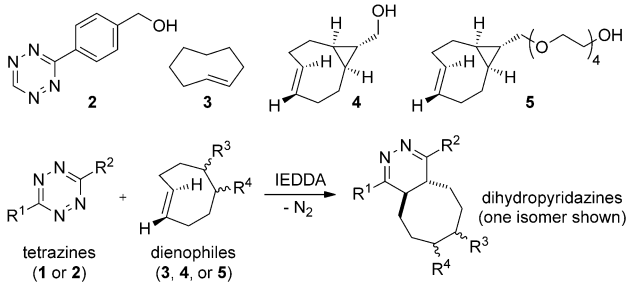

Tetrazine	DP[a]	Solvent	$\Delta G^{\ddagger}_{calcd}$[b]	$\Delta G^{\ddagger}$[c]	k_2 [$M^{-1}s^{-1}$][d]
1	**3**	1,4-dioxane	18.7	17.5	1.49 ± 0.01
1	**4**	1,4-dioxane	15.3	15.0	85.5 ± 2.3
1	**5**	human plasma	n.d.[e]	n.d.	8200 ± 300
2	**3**	1,4-dioxane	15.0	15.1	79.2 ± 1.3

[a] DP = dienophile. [b] Calculated activation free energies (kcal mol^{-1}; 25 °C). [c] Activation free energies determined by stopped-flow measurements (kcal mol^{-1}; 25 °C). [d] Second-order rate constants (measurements at 37 °C). [e] n.d. = not determined.

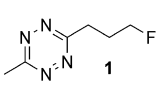

1

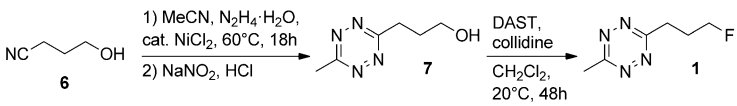

Scheme 1. Synthesis of tetrazine **1** (DAST = diethylaminosulfur trifluoride).

© 2014 Wiley-VCH Verlag GmbH & Co. KGaA, Weinheim

The stability of compound **5** was assessed by incubation in human plasma at 37 °C for 24 h leading to a recovery of >80 %, a significantly higher value than those previously reported for reactive tetrazines.[17] Hence, the combination of radiolabeled tetrazines as pull-down reagents and (s-)TCO labeling should be advantageous for bioorthogonal in vivo imaging in contrast to inverse strategies involving tetrazine tags and radiolabeled dienophiles.

Radiosynthesis affording [^{18}F]-**1** was successfully carried out by direct fluorination of the tosylated intermediate **8** in a radiochemical yield of up to 18 % (Figure 1). Cycloaddition of [^{18}F]-**1** with s-TCO **4** occurred rapidly forming the conjugate [^{18}F]-**9** that slowly isomerized to [^{18}F]-**10** (both products as a mixture of regio- and stereoisomers).

In vivo studies were performed by administration of [^{18}F]-**1** to female BALB/c mice followed by dynamic PET ($n=4$) and PET/MR ($n=2$) imaging (MR = magnetic resonance tomography). A very homogenous biodistribution of [^{18}F]-**1** was observed in all regions in the body including the brain, which clearly indicates the ability of [^{18}F]-**1** to pass the blood–brain barrier (Figure 2). Furthermore, PET/MR revealed no significant extent of in vivo defluorination of [^{18}F]-**1**, since no enhanced radioactivity uptake in bone was observed.[26] Time–activity curves were similar for all analyzed organs

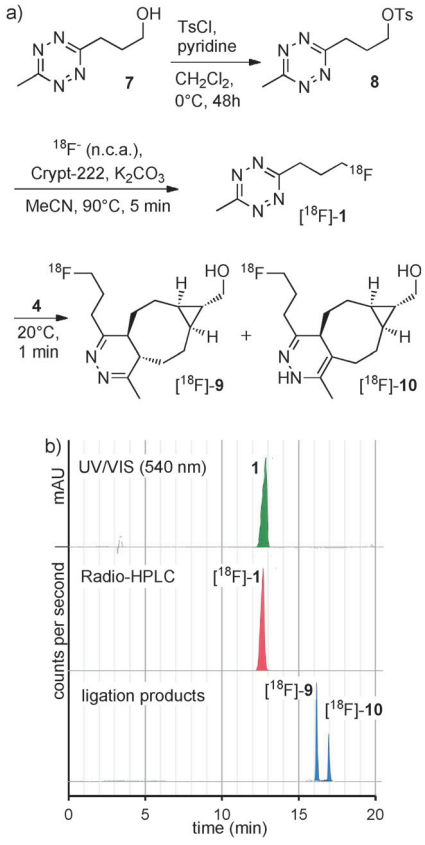

Figure 1. a) Radiosynthesis of [^{18}F]-**1** and IEDDA cycloaddition with s-TCO **4** (n.c.a. = no carrier added; only one isomer shown for [^{18}F]-**9** and [^{18}F]-**10**). b) HPLC of **1** (UV/Vis, 540 nm), radio-HPLC of purified [^{18}F]-**1** and ligation products after click reaction with s-TCO **4**. HPLC conditions: Zorbax SB-Aq reversed phase, H_2O/MeCN gradient elution.

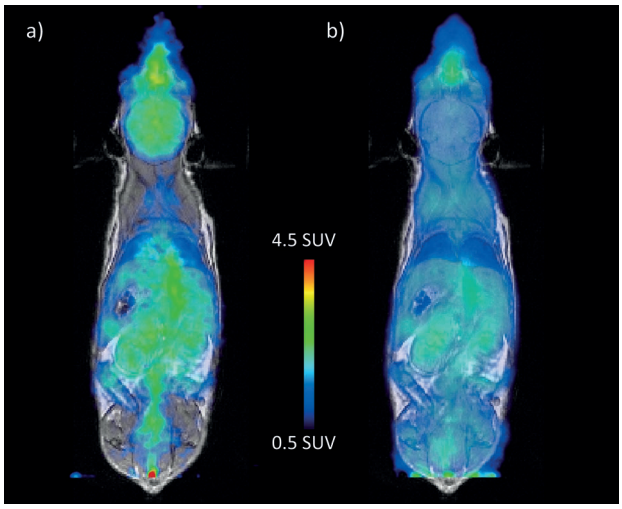

Figure 2. Combined PET/MRI summation images: 0–5 min (a) and 5–120 min (b) after injection of [^{18}F]-**1**.

(Figure 3a). After the initial perfusion directly after intravenous administration of [^{18}F]-**1** a very uniform uptake steadily decreasing from 2 to 1.5 SUV (standardized uptake value) was observed in all organs (except the urinary bladder) during the onset of the PET scan. Conversely, SUV in the urinary bladder increased from 2 to 10 SUV, suggesting

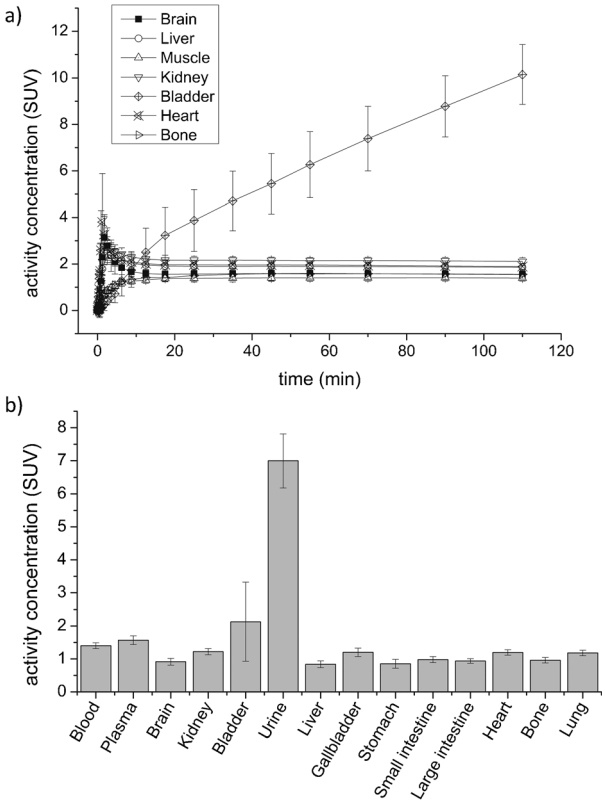

Figure 3. a) Mean organ time–activity curves obtained in BALB/c mice ($n=6$; for bone $n=2$). b) Ex vivo biodistribution of [^{18}F]-**1** in indicated organs 2 h after intravenous administration in mice ($n=6$). Data are presented as mean SUV ± standard deviation. All organs (apart from the bladder) displayed similar radioactivity concentration values.

 © 2014 Wiley-VCH Verlag GmbH & Co. KGaA, Weinheim

a rapid renal clearance of [^{18}F]-**1**. Evaluation of the ex vivo biodistribution determined 120 min after [^{18}F]-**1** injection gave values ranging from 1 SUV to 1.5 SUV with the exception of the urinary bladder (Figure 3b), which is in good agreement with the PET results. The in vivo stability of [^{18}F]-**1** was further examined by radio-TLC of mouse plasma obtained immediately after the imaging experiments (120 min after administration). We observed only a low degree of metabolic degradation (approximately 15%) as shown by the formation of more polar metabolites, which is assumed to occur via enzyme-catalyzed oxidation of the methyl group of [^{18}F]-**1** thus leading to xenobiotic metabolization similar to toluene and related compounds.[27]

Furthermore, the bioconjugation of [^{18}F]-**1** and the water-soluble dienophile **5** was performed in vivo to verify the bioorthogonal behavior of this novel tetrazine-type PET probe.[^{18}F]-**1** was administered to female BALB/c mice ($n = 4$) followed by **5** after an initial period of 20 min. In this experiment an inverse approach was used to allow for the homogenous biodistribution of the radiolabeled tetrazine prior to in vivo reaction. After 5, 15, and 30 min retroorbital blood was collected and the click reaction was quenched by addition of the more reactive tetrazine **2**. Murine plasma was obtained and analyzed using radio-TLC (Figure 4). Finally, we observed >90% conversion after 5 min and complete in vivo reaction 30 min after administration of **5** (see the Supporting Information, Figure S4). These results clearly indicate and confirm the capability of [^{18}F]-**1** as a highly valuable and versatile bioorthogonal probe for pretargeted PET imaging.

In summary, we have developed a fast and reliable procedure for the synthesis of a low-molecular-weight and water-soluble radiolabeled tetrazine; direct [^{18}F]-fluorination was applied to avoid additional steps and the need for prosthetic groups. Furthermore, [^{18}F]-**1** was prepared using readily accessible and/or commercially available reagents without the use of anhydrous hydrazine and [^{18}F]-**1** was shown to possess highly favorable pharmacokinetic properties. Although high stability of [^{18}F]-**1** was observed, its metabolic behavior has still to be verified in further studies. In vivo investigations clearly indicate the suitability of this radiolabeled tetrazine as a pull-down reagent for pretargeted PET imaging. Hence, we expect this highly versatile and readily accessible compound, which enables in vivo detection of dienophile-tagged (bio)molecules, to find many applications and lead to further investigations in the fields of bioorthogonal imaging and biomedical research.

Received: April 13, 2014
Revised: May 9, 2014
Published online: July 2, 2014

Keywords: bioorthogonal chemistry · click chemistry · imaging agents · kinetics · tetrazines

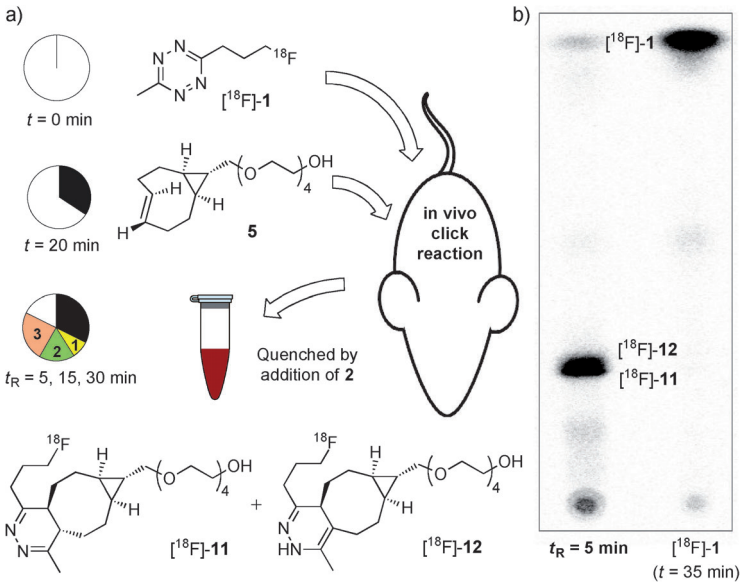

Figure 4. a) Bioorthogonal in vivo reaction of [^{18}F]-**1** and dienophile **5** leading to the formation of [^{18}F]-**11** and [^{18}F]-**12** (one isomer shown). b) Radio-TLC (SiO_2) of plasma obtained after 5 min of reaction time (left) and blank obtained 35 min after administration of [^{18}F]-**1** (right).

[1] a) L. Carroll, H. L. Evans, E. O. Aboagye, A. C. Spivey, *Org. Biomol. Chem.* **2013**, *11*, 5772–5781; b) N. K. Devaraj, R. Weissleder, *Acc. Chem. Res.* **2011**, *44*, 816–827; c) E. M. Sletten, C. R. Bertozzi, *Acc. Chem. Res.* **2011**, *44*, 666–676.

[2] J. M. Baskin, J. A. Prescher, S. T. Laughlin, N. J. Agard, P. V. Chang, I. A. Miller, A. Lo, J. A. Codelli, C. R. Bertozzi, *Proc. Natl. Acad. Sci. USA* **2007**, *104*, 16793–16797.

[3] a) S. T. Laughlin, J. M. Baskin, S. L. Amacher, C. R. Bertozzi, *Science* **2008**, *320*, 664–667; b) A. B. Neef, C. Schultz, *Angew. Chem.* **2009**, *121*, 1526–1529; *Angew. Chem. Int. Ed.* **2009**, *48*, 1498–1500; c) T. Plass, S. Milles, C. Koehler, C. Schultz, E. A. Lemke, *Angew. Chem.* **2011**, *123*, 3964–3967; *Angew. Chem. Int. Ed.* **2011**, *50*, 3878–3881; d) R. Xie, S. Hong, X. Chen, *Curr. Opin. Chem. Biol.* **2013**, *17*, 747–752; e) J. C. Jewett, C. R. Bertozzi, *Chem. Soc. Rev.* **2010**, *39*, 1272–1279; f) J. C. Jewett, E. M. Sletten, C. R. Bertozzi, *J. Am. Chem. Soc.* **2010**, *132*, 3688–3690.

[4] G. de Almeida, E. M. Sletten, H. Nakamura, K. K. Palaniappan, C. R. Bertozzi, *Angew. Chem.* **2012**, *124*, 2493–2497; *Angew. Chem. Int. Ed.* **2012**, *51*, 2443–2447.

[5] S. B. Lee, H. L. Kim, H.-J. Jeong, S. T. Lim, M.-H. Sohn, D. W. Kim, *Angew. Chem.* **2013**, *125*, 10743–10746; *Angew. Chem. Int. Ed.* **2013**, *52*, 10549–10552.

[6] a) M. L. Blackman, M. Royzen, J. M. Fox, *J. Am. Chem. Soc.* **2008**, *130*, 13518–13519; b) N. K. Devaraj, R. Weissleder, S. A. Hilderbrand, *Bioconjugate Chem.* **2008**, *19*, 2297–2299.

[7] a) G. Budin, K. S. Yang, T. Reiner, R. Weissleder, *Angew. Chem.* **2011**, *123*, 9550–9553; *Angew. Chem. Int. Ed.* **2011**, *50*, 9378–9381; b) K. Lang, L. Davis, J. Torres-Kolbus, C. Chou, A. Deiters, J. W. Chin, *Nat. Chem.* **2012**, *4*, 298–304; c) K. S. Yang, G. Budin, T. Reiner, C. Vinegoni, R. Weissleder, *Angew. Chem.* **2012**, *124*, 6702–6707; *Angew. Chem. Int. Ed.* **2012**, *51*, 6598–6603; d) D. S. Liu, A. Tangpeerachaikul, R. Selvaraj, M. T. Taylor, J. M. Fox, A. Y. Ting, *J. Am. Chem. Soc.* **2011**, *134*, 792–795; e) J. L. Seitchik, J. C. Peeler, M. T. Taylor, M. L. Blackman, T. W. Rhoads, R. B. Cooley, C. Refakis, J. M. Fox, R. A. Mehl, *J. Am. Chem. Soc.* **2012**, *134*, 2898–2901; f) E. Kim, K. S. Yang, R. Weissleder, *PLoS One* **2013**, *8*, e81275; g) T. Reiner, E. J.

© 2014 Wiley-VCH Verlag GmbH & Co. KGaA, Weinheim

Keliher, S. Earley, B. Marinelli, R. Weissleder, *Angew. Chem.* **2011**, *123*, 1963 – 1966; *Angew. Chem. Int. Ed.* **2011**, *50*, 1922 – 1925.
[8] M. R. Karver, R. Weissleder, S. A. Hilderbrand, *Angew. Chem.* **2012**, *124*, 944 – 946; *Angew. Chem. Int. Ed.* **2012**, *51*, 920 – 922.
[9] J. C. T. Carlson, L. G. Meimetis, S. A. Hilderbrand, R. Weissleder, *Angew. Chem.* **2013**, *125*, 7055 – 7058; *Angew. Chem. Int. Ed.* **2013**, *52*, 6917 – 6920.
[10] M. T. Taylor, M. L. Blackman, O. Dmitrenko, J. M. Fox, *J. Am. Chem. Soc.* **2011**, *133*, 9646 – 9649.
[11] R. Selvaraj, J. M. Fox, *Curr. Opin. Chem. Biol.* **2013**, *17*, 753 – 760.
[12] J. Yang, J. Šečkutė, C. M. Cole, N. K. Devaraj, *Angew. Chem.* **2012**, *124*, 7594 – 7597; *Angew. Chem. Int. Ed.* **2012**, *51*, 7476 – 7479.
[13] a) J. Šečkutė, N. K. Devaraj, *Curr. Opin. Chem. Biol.* **2013**, *17*, 761 – 767; b) Z. Li, H. Cai, M. Hassink, M. L. Blackman, R. C. D. Brown, P. S. Conti, J. M. Fox, *Chem. Commun.* **2010**, *46*, 8043 – 8045; c) J. C. Knight, S. Richter, M. Wuest, J. D. Way, F. Wuest, *Org. Biomol. Chem.* **2013**, *11*, 3817 – 3825.
[14] M. M. Herth, V. L. Andersen, S. Lehel, J. Madsen, G. M. Knudsen, J. L. Kristensen, *Chem. Commun.* **2013**, *49*, 3805 – 3807.
[15] a) R. Rossin, P. R. Verkerk, S. M. van den Bosch, R. C. M. Vulders, I. Verel, J. Lub, M. S. Robillard, *Angew. Chem.* **2010**, *122*, 3447 – 3450; *Angew. Chem. Int. Ed.* **2010**, *49*, 3375 – 3378; b) B. M. Zeglis, K. K. Sevak, T. Reiner, P. Mohindra, S. D. Carlin, P. Zanzonico, R. Weissleder, J. S. Lewis, *J. Nucl. Med.* **2013**, *54*, 1389 – 1396.
[16] N. K. Devaraj, G. M. Thurber, E. J. Keliher, B. Marinelli, R. Weissleder, *Proc. Natl. Acad. Sci. USA* **2012**, *109*, 4762 – 4767.
[17] M. R. Karver, R. Weissleder, S. A. Hilderbrand, *Bioconjugate Chem.* **2011**, *22*, 2263 – 2270.
[18] F. Liu, R. S. Paton, S. Kim, Y. Liang, K. N. Houk, *J. Am. Chem. Soc.* **2013**, *135*, 15642 – 15649.
[19] S. A. Lang, B. D. Johnson, E. Cohen, *J. Heterocycl. Chem.* **1975**, *12*, 1143 – 1153.
[20] a) E. J. Keliher, T. Reiner, G. M. Thurber, R. Upadhyay, R. Weissleder, *ChemistryOpen* **2012**, *1*, 177 – 183; b) E. J. Keliher, T. Reiner, A. Turetsky, S. A. Hilderbrand, R. Weissleder, *ChemMedChem* **2011**, *6*, 424 – 427; c) B. M. Zeglis, P. Mohindra, G. I. Weissmann, V. Divilov, S. A. Hilderbrand, R. Weissleder, J. S. Lewis, *Bioconjugate Chem.* **2011**, *22*, 2048 – 2059; d) H.-S. Han, N. K. Devaraj, J. Lee, S. A. Hilderbrand, R. Weissleder, M. G. Bawendi, *J. Am. Chem. Soc.* **2010**, *132*, 7838 – 7839; e) J. B. Haun, N. K. Devaraj, S. A. Hilderbrand, H. Lee, R. Weissleder, *Nat. Nanotechnol.* **2010**, *5*, 660 – 665.
[21] J. Yang, M. R. Karver, W. Li, S. Sahu, N. K. Devaraj, *Angew. Chem.* **2012**, *124*, 5312 – 5315; *Angew. Chem. Int. Ed.* **2012**, *51*, 5222 – 5225.
[22] J. W. Wijnen, S. Zavarise, J. B. F. N. Engberts, M. Charton, *J. Org. Chem.* **1996**, *61*, 2001 – 2005.
[23] Inclusion of Substances of Very High Concern in the Candidate List (2011). ED/31/2011 published in accordance with Article 59(10) of the Regulation No 1907/2006 of the European Parliament and of the Council of 18 December 2006 concerning the Registration, Evaluation, Authorisation and Restriction of Chemicals (REACH).
[24] E. Nachbaur, G. Leiseder, *Monatsh. Chem.* **1971**, *102*, 1718 – 1723.
[25] R. Rossin, S. M. van den Bosch, W. ten Hoeve, M. Carvelli, R. M. Versteegen, J. Lub, M. S. Robillard, *Bioconjugate Chem.* **2013**, *24*, 1210 – 1217.
[26] a) R. A. Hawkins, Y. Choi, S.-C. Huang, C. K. Hoh, M. Dahlbom, C. Schiepers, N. Satyamurthy, J. R. Barrio, M. E. Phelps, *J. Nucl. Med.* **1992**, *33*, 633 – 642; b) E. Even-Sapir, E. Mishani, G. Flusser, U. Metser, *Semin. Nucl. Med.* **2007**, *37*, 462 – 469.
[27] D. E. Chapman, T. J. Moore, S. R. Michener, G. Powis, *Drug Metab. Dispos.* **1990**, *18*, 929 – 936.

 © 2014 Wiley-VCH Verlag GmbH & Co. KGaA, Weinheim

Manuscript #5

Christoph Denk, Dennis Svatunek, Severin Mairinger, Claudia Kuntner, Thomas Filip, Michael Sauberer, Johannes Fröhlich, Thomas Wanek, Hannes Mikula*; A Tale of 3-[^{18}F]Fluoropropyl-1,2,4,5-tetrazines, manuscript draft

A Tale of 3-[^{18}F]Fluoropropyl-1,2,4,5-Tetrazines

Christoph Denk[a], Dennis Svatunek[a], Severin Mairinger[b], Claudia Kuntner[b], Thomas Filip[b], Michael Sauberer[b], Johannes Fröhlich[a], Thomas Wanek[b] and Hannes Mikula[a*]

a) Institute of Applied Synthetic Chemistry, Vienna University of Technology (TUW), (Austria) E-mail: hannes.mikula@tuwien.ac.at b) Health and Environment Department, Biomedical Systems, Austrian Institute of Technology (AIT) Seibersdorf (Austria)

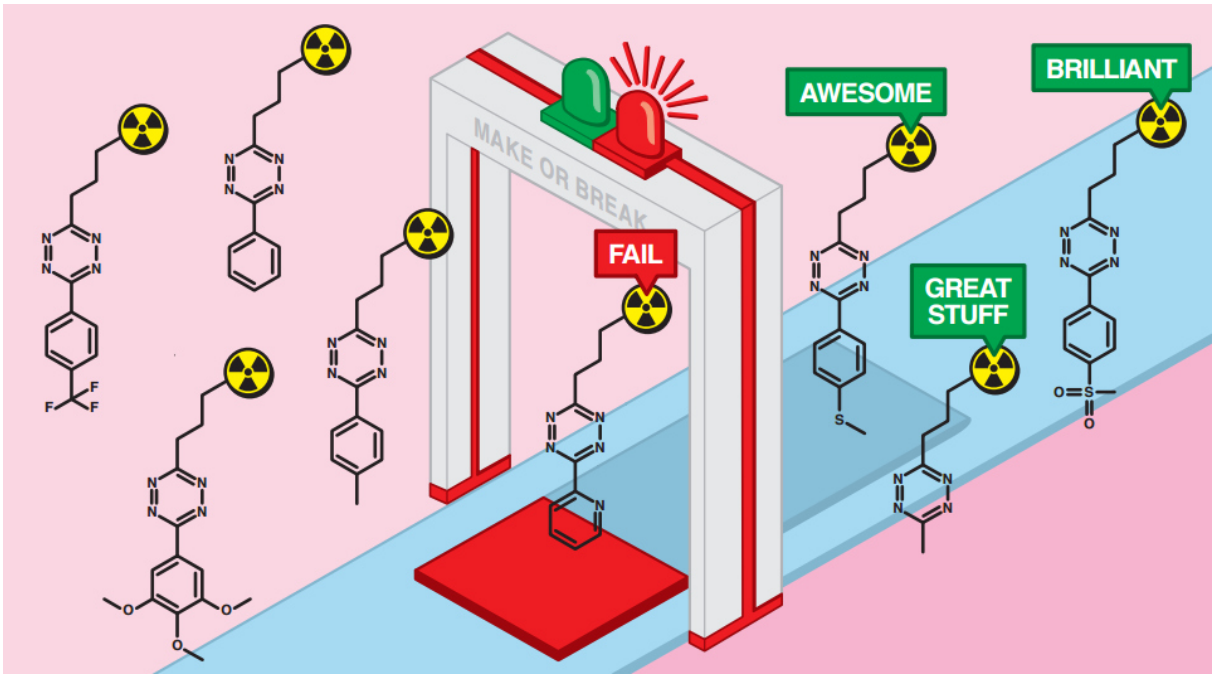

Radiolabeled 1,2,4,5-tetrazines are promising agents for bioorthogonal PET imaging. Derivatives based on the 3-fluoropropyl moiety are accessible by direct nucleophilic ^{18}F-fluorination. Building on previous results[1] a series of eight novel 3-fluoropropyl-tetrazines was designed, aiming for improved reactivity while retaining beneficial pharmacological properties. Reactivity was investigated *in silico* and by stopped flow measurements with dienophile *trans*-cyclooctene. Radiolabeling was optimized and the biodistribution, metabolic stability and pharmacokinetics of labeled compounds were investigated by PET/MR scanning in a murine model. One promising compound for pretargeted PET imaging was identified, and its cycloaddition reactivity was furthermore enhanced post-labeling by DMDO mediated oxidation of the fluorine-18 species.

Introduction

Bioorthogonal ligations have emerged as valuable tool for a variety of applications.[2,3] In positron emission tomography (PET) imaging, pretargeting strategies decouple accumulation kinetics from the physical half-life of radionuclides: A tagged marker compound is administered and given sufficient time to accumulate in the desired target tissues. Following accumulation and subsequent excretion of non-bound marker, a radiolabeled agent is administered that rapidly binds to the preadministered compound *via* a bioorthogonal reaction.[2,4–7] In particular for nuclear medicine applications rapid ligation rates are crucial due to diminutive concentrations used commonly and radioactive decay of involved agents. Although a variety of bioorthogonal reactions has been reported, the ligation between

1,2,4,5-tetrazines (Tz) and strained dienophiles proved especially suitable for radiolabeled agents due to particular high ligation rates of up to 10^7 $M^{-1}s^{-1}$.[6,8] In these inverse electron demand Diels Alder (IEDDA) cycloadditions, that were reported by Fox and co-workers and Weissleder and co-workers in 2008, electron deficient 1,2,4,5-tetrazines react with electron rich dienophiles under liberation of nitrogen forming dihydropyridazines.[9,10] Cyclooctynes, cyclopropenes and trans-cyclooctenes (TCOs) offer adequate stability and reactivity to be used as bioorthogonal tags, but straight forward synthetic accessibility and highest rates made TCO the most frequently employed dienophile.[11–13] Fox and co-workers furthermore reported TCO-derivatives with enhanced reaction rates and increased polarity and stability.[8,13] Tetrazine derivatives are accessible by metal catalyzed tetrazine synthesis and other methods.[14,15] IEDDAs potential as pretargeting tool in SPECT and PET imaging was recognized as early as 2010 by Rossin, Robilliard and coworkers.[7] Studies investigating ^{18}F-labeled TCO as bioorthogonal PET probe revealed a very inhomogenous biodistribution profile as well as rapid metabolism of this highly lipophilic probe.[16] For this reason, research was focused on the development of radiolabeled tetrazine agents to be used in combination with TCO-tagged marker compounds. Fluorine-18 was considered the “gold standard” isotope for imaging, due to favourable decay characteristics, high specific activity, straight forward radiochemistry and broad availability in and around facilities with in-house cyclotron. Early radiofluorination attempts conducted by Fox and co-workers resulted in degradation and led to the conclusion that 1,2,4,5-tetrazines are unstable under typical ^{18}F labeling conditions.[17] Therefore research focused on chelator modified tetrazines, labelled with radiometals like lutetium-177, copper-64 and indium-111.[5,7,18] Pretargeted immunoimaging with high signal-to-background ratios using these derivatives was demonstrated by Zeglis *et al.* and Robilliard, Rossin and co-workers thus proofing the abilities of pretargeted (bioorthogonal) imaging.[5,6] Nevertheless, the use of chelators results in highly polar compounds that are restricted to extracellular targets. In 2013 Herth and co-workers reported the development of a carbon-11 labeled Tz probe, but no *in vivo* data of this compound was collected.[19] In 2014 the first radiofluorinated Tz was developed in our lab by utilization of a dialkyl-scaffold that renders the Tz moiety less reactive in IEDDA reactions, but on the other hand improves stability to allow for direct fluorine-18 labeling. The compound 3-(3-[^{18}F]fluoropropyl)-6-methyl-1,2,4,5-tetrazine (**1**) was prepared by nucleophilic displacement of a tosylate group by non-carrier-added fluoride in moderate radiochemical yield. The derivative exhibited very uniform biodistribution as well as good metabolic stability, both key factors for successful application as secondary agent in imaging.[1] However, the dialkyl-scaffold, although shown to be sufficiently fast for pretargeting in mice, is limiting reactivity and therefore the *in vivo* applicability of this probe. Although ^{18}F-tetrazine probes prepared by a two-step radiochemical procedure based on labeled carbohydrates were reported, direct labelling is still advantageous due to shorter overall synthesis time and easier purification.[20,21] We hypothesized that replacing the 6-methyl group in **1** with aryl groups would lead to derivatives with increased reactivity that are still suitable for direct labelling with fluorine-18. Furthermore we aimed to explore the chemical space between reactivity and stability of the probes.

Synthesis of Reference Compounds

Based on structure **1,** we aimed to exchange the 6-methyl group by an aryl group (compounds **2-8**, Figure 1) to enhance reactivity. For this reason phenyl-derivative **2** was considered. For compound **1** very favourable *in vivo* properties (homogenous biodistribution, good metabolic stability) were noted.[1] Renal excretion took place in form of several polar metabolites, which we hypothesized arise from oxidation and conjugation at the 6-methyl position. To explore the influence of such a metabolic handle, derivatives with oxidizable groups (compounds **3** and **6**) were included in this study. In addition, compound **4** seemed interesting due to a blockage of the oxidative metabolism at the methyl-group combined with increased reactivity caused by the electron withdrawing properties of the trifluoromethyl group. Furthermore, the 3,4,5-trimethoxy **5** and methylsulfone **7** derived compounds were selected due to higher polarity as compared to compounds **2** – **4** that is likely to facilitate renal rather than hepatobiliary excretion. Hepatobiliary excretion would contribute to a high background signal in liver, gall bladder and intestines thus limiting the diagnostic utility of the probe. To address the top end of the IEDDA reactivity scale of alkyl-aryl-tetrazines electron deficient pyridyl-tetrazine **8** was included in our study**.**

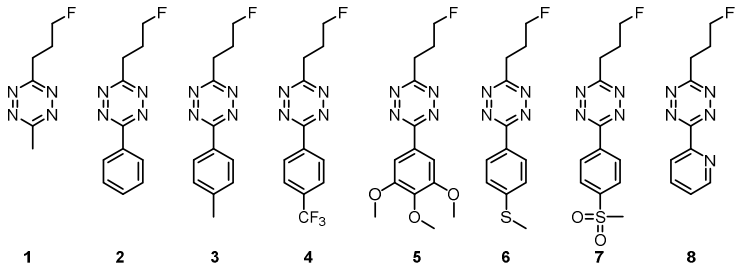

Figure 1: *3-(3-Fluoropropyl)tetrazines considered in this work*

Instead of applying the published procedure using deoxofluorination reagents (such as DAST) on hydroxypropyl-tetrazine derivatives,[1] we directly employed 4-fluorobutyronitrile (**9**) in the metal catalyzed tetrazine synthesis yielding reference compounds **1**-**6** and **8** directly (Scheme 1). 4-Fluorobutyronitrile was synthesized by reacting 3-bromo-1-fluoropropane with sodium cyanide in tetraethylene glycol followed by distillation in 63% yield.[22] Although 3-bromo-1-fluoropropane is commercially available, its preparation from low priced 1,3-dibromopropane is highly recommended.[23] Employing the fluoroalkylnitrile **9** and acetonitrile in a metal catalyzed tetrazine synthesis with $NiCl_2$ and anhydrous hydrazine, **1** could be prepared in significantly improved 37% yield compared to previously published procedures.[1] We noticed that the use of anhydrous hydrazine is advantageous for dialkyl derivatives, but aryl-alkyl substituted 1,2,4,5-tetrazines are also accessible using hydrazine monohydrate, thus eliminating the need for preparation and handling of anhydrous hydrazine. Yields of the metal catalyzed Tz synthesis varied from substrate to substrate ranging from 1.3 to 16.5%. An optimization towards reaction stochiometry, reaction time and temperature for each individual substrate would be necessary to achieve optimum yield. Within this work we focused on “target oriented synthesis” and did not optimize reaction parameters beyond the point where sufficient material for the study could

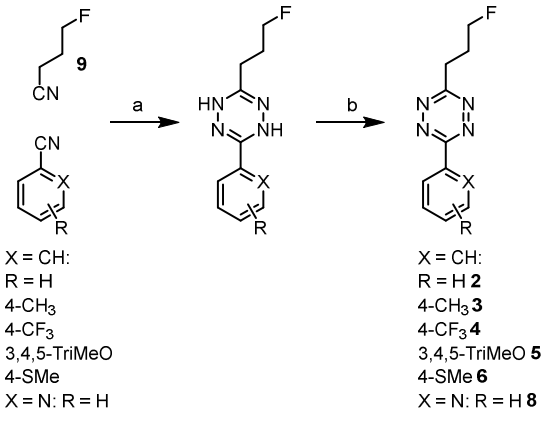

Scheme 1: *Synthesis of 3-fluoropropyl tetrazines*
a) N_2H_2 x H_2O, $NiCl_2$ b) $NaNO_2$ / HCl

be obtained. **2** was synthesized from 4-fluorobutyronitrile and benzonitrile using nickel(II)chloride and hydrazine monohydrate followed by oxidation of the dihydrotetrazine by the $NaNO_2$/HCl system in 16.5% overall yield. The *p*-tolyl derivative **3** was obtained from *p*-methylbenzonitrile and 4-fluorobutyronitrile using comparable conditions in 6.4% yield. Tetrazine **4** (4.7%), trimethoxy derivative **5** (12.5%), thiomethyl-tetrazine **6** (1.3%) and pyridyl-Tz **8** (10.8%) were prepared using similar synthetic procedures on substituted benzonitriles and 4-fluorobutyronitrile. Oxygen must be excluded from syntheses of sulfide **6**, since the compound readily oxidizes in air to the methylsulfoxide-derivative **26**, that we could isolate as by-product in 16% yield. Methylsulfone Tz derivative **7** was synthesized from **6** by dimethyldioxirane (DMDO) mediated oxidation.[24] All substances appeared as deep purple to red crystalline solids that did not show signs of decomposition, even after prolonged storage (-20°C, > 1 yr).

Kinetic investigations

Relative reactivity values (RRVs) of tetrazines **2** through **8** were predicted using a previously described computational method.[1] Therefore ΔG of activation of the IEDDA reaction with *trans*-cyclooctene **10** was determined by DFT calculations using the Minnesota density functional M06-2X in combination with the 6-311G+(d,p) basis set in the gas phase. $\Delta G^{\ddagger}$ was then used to calculate relative reaction rates. RRVs were predicted to be in the range of 1.8 to 9.8 in comparison to **1** for tetrazine **2-7**, while pyridyl derivative **8** was predicted to show a 70-fold enhanced reactivity as compared to **1** (detailed data see supporting information, Section 6).

Reactivity of tetrazines **1-8** towards *trans*-cyclooctene (**10**) in 1,4-dioxane was then investigated using stopped-flow photometry. Measured rates, relative reactivity values as well as ΔG of activation are shown in Table 1. A comparison of experimental second order rate constants is furthermore shown in Figure 2. As expected for IEDDA reactions, electron donating substituents, like methoxy- or methyl-groups on the aryl substituent lower the reactivity towards dienophiles such as TCO in comparison with electron withdrawing groups, like the trifluoromethyl-group. Interestingly, the trimethoxy substituted derivative **5** showed a lower reactivity (0.9 RRV) as the dialkyl substituted Tz **1**. While tetrazines **2** to **4** show elevated reactivities, ranging from 1.2 – 3.6 RRV, the methyl sulfone compound **7** and pyridyl substituted Tz **8** showed a considerably higher value of 4.5 and 13.6 RRVs respectively.

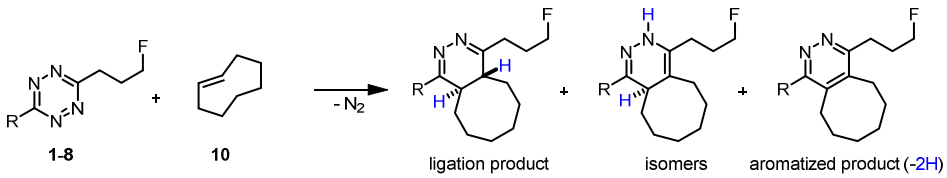

Reactant Pair	Second order rate constants [$M^{-1}s^{-1}$] 25°C	37°C	50°C	ΔG‡ [kcal/mol]	RRV
1 + 10	1.11	1.57	2.20	17.39	1.00
2 + 10	1.58	2.30	3.18	17.18	1.44
3 + 10	1.26	1.90	2.91	17.32	1.22
4 + 10	3.87	5.72	8.05	16.65	3.60
5 + 10	1.00	1.44	1.96	17.45	0.90
6 + 10	1.30	1.97	2.53	17.28	1.19
7 + 10	5.10	7.51	8.84	16.47	4.47
8 + 10	14.63	20.90	31.08	15.87	13.55

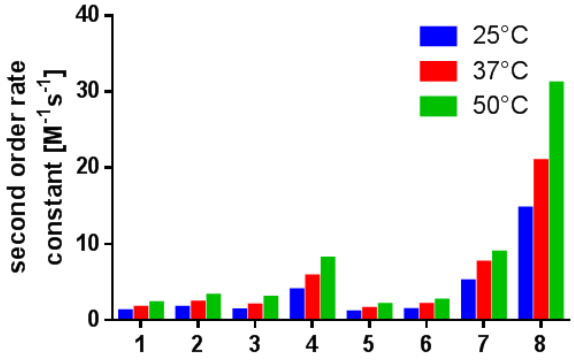

Table 2 and Figure 2: *Measured rates (stopped flow) of tetrazines **1-8** with dienophile TCO (**10**) (RRV =mean relative reactivity value compared to **1** + **10**)*

These experimental results are in agreement with the prediction that tetrazines **2**-**7** will show a comparable rate to **1** while **8** displays enhanced IEDDA reactivity. However, this computational method was not able to predict the correct increase of reactivity for **8** and furthermore failed to predict the order of reactivities for tetrazines **2-7**.

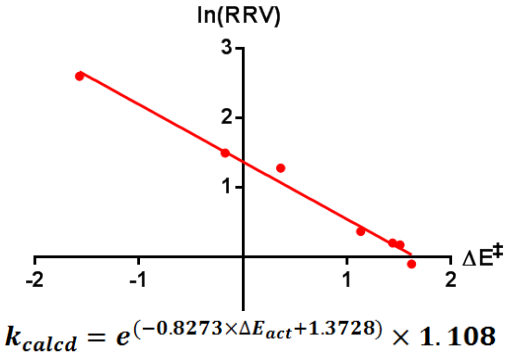

$$k_{calcd} = e^{(-0.8273 \times \Delta E_{act} + 1.3728)} \times 1.108$$

***Figure 3** and **Formula 1:** Correlation between relative rates and ΔE‡ found for alkyl-aryl substituted tetrazines*

However, using ΔE‡ calculated using the M06-2X density functional in combination with the 6-311+G(d,p) basis set, was found to show an excellent correlation with the logarithm of the relative reactivities (Figure 3). ΔE‡ can therefore be used to predict reactivities of alkyl-aryl substituted tetrazines in the IEDDA reaction with *trans*-cyclooctene. Formula 1 describes the found relation between calculated ΔE‡ and second order rate constants at 25°C in dry 1,4-dioxane.

Precursor Synthesis & Radiolabeling

To obtain precursor substances suitable for fluorine-18 radiolabeling, the according alcohols (**11**-**16**, **23**) were synthesized followed by installation of a suitable leaving group. 3-Hydroxypropyl tetrazine derivatives (**11**-**16**) were obtained by nickel catalyzed Tz synthesis with hydrazine monohydrate from according benzonitriles and 4-hydroxybutanenitrile followed by oxidation (Scheme 2a). In the case of phenyl-Tz **11** a yield of 42% was achieved, while p-tolyl-derivative **12** was isolated in 31% yield. Furthermore, using the same methodology *p*-trifluoromethylphenyl-Tz **13** (27.2%), 3,4,5-trimethoxyphenyl-Tz **14** (12.5%), 4-thiomethylphenyl-Tz **15** (5.4%) and pyridyl Tz **16** (6.2%) were obtained as pink to red crystalline materials.

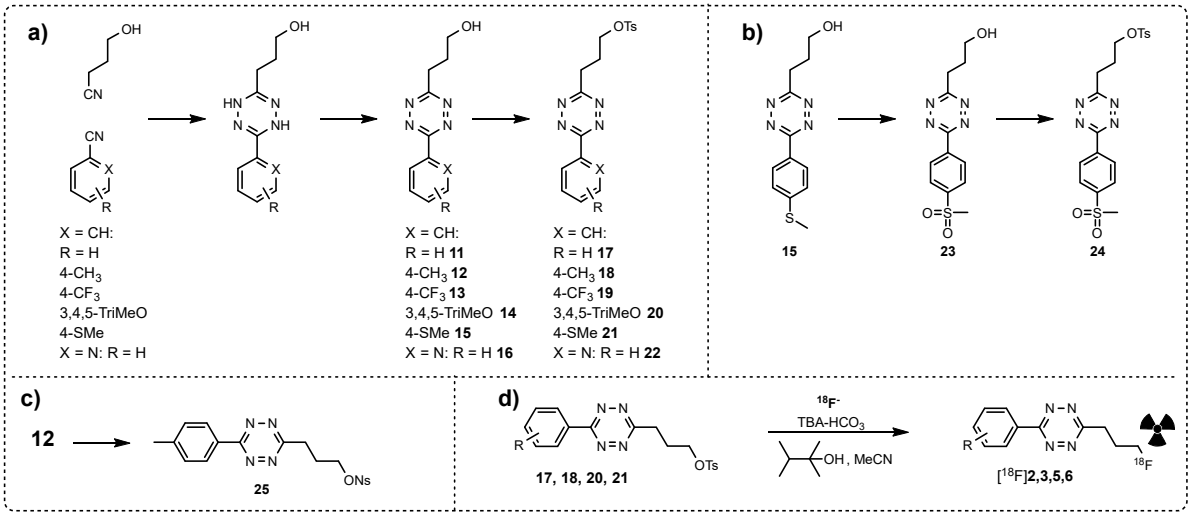

Scheme 2: *a) Synthesis of radiolabeling precursors **17**-**22*** b-c) synthesis of radiolabeling precursors **24** and **25** and d) radiolabeling using thexyl alcohol and TBA-HCO_3

In general, we noticed higher yields for tetrazine synthesis involving hydroxybutyronitrile compared to synthesis applying the fluorinated alkyl nitrile **9**. Sulfon derivative **23** was synthesized from thiomethyl tetrazine **15** by oxidation using dimethyl dioxirane (Scheme 2b). All alcohols were subjected to tosylation using *p*-tosyl chloride and pyridine in anhydrous dichloromethane giving tosylates **17**-**22** and **24** in good yields (see Scheme 2a+b). In case of the p-tolyl-tetrazine **12** also the nosylate **25** was prepared due to better reactivity in nucleophilic substitutions (Scheme 2c). However, poor solubility as well as stability problems prompted us to focus on tosylated species. The p-tolyl tosylate **18** was used for optimization of the radiofluorination reaction. When the standard [2.2.2]cryptand/K_2CO_3 method, that proved most suitable in the preparation of [^{18}F]**1**, was applied, around 11.2% incorporation yield into [^{18}F]**3** (determined by radio-HPLC) was observed. DMSO as solvent, nosylate **25** as precursor or the use of $KHCO_3$ instead of potassium carbonate resulted in reduced incorporation yields to values below 6%. When tetrabutylammonium hydrogencarbonate in anhydrous acetonitrile was used for labeling a significantly improved radiochemical yield of [^{18}F]**3** (22.9%) was noted. Further optimization of the reaction solvent revealed a very good incorporation yield of 56% when a 1:1 (v/v) mixture of acetonitrile and 2,3-dimethyl-2-butanol (thexyl alcohol) was used as labeling solvent, which is in agreement with previous reports documenting the positive influence of tertiary alcohols on fluorine-18 radiolabeling.[25,26] This method was transferred onto an automated synthesis module (TRACERlab FX_{FDG} synthesis module (GE Healthcare) housed in a shielded hot cell, where in a non-optimized sequence 10 GBq of [^{18}F]**3** could be obtained from 181 GBq cyclotron produced fluorine-18 (9.5% decay corrected radiochemical yield). In automated synthesis, purification of the compounds was achieved by preparative RP-HPLC using 10 mM PO_4-puffer (pH 6) and acetonitrile as eluents. The HPLC eluate was monitored in series for radioactivity and UV absorption, the product fraction was collected, diluted with water and passed over a preactivated C18 Sep-Pak Plus cartridge (Waters, Milford, MA, USA). The cartridge was then eluted with 2.5 ml ethanol to obtain the [^{18}F]tetrazine. The ethanolic solution was diluted with saline to < 10% ethanol content at an approximate activity concentration of 370MBq/mL for intravenous (iv) administration into mice. Applying the optimized radiolabeling conditions to phenyl-Tz-Precursor **17**, 40% of radioactivity was incorporated into the precursor as investigated by radio-TLC and radio-HPLC. 8.9 GBq of [^{18}F]**2** with a specific activity of 99 GBq/µmol ready for i.v. administration were obtained using the automated synthesizer (6.3% isolated radiochemical yield). All attempts of nucleophilic fluorination using 3-(6-(4-

(trifluoromethyl)phenyl)-1,2,4,5-tetrazin-3-yl)propyl 4-methylbenzenesulfonate **(19)** as precursor failed to produce > 1% incorporation yield of [^{18}F]**4**. A variety of reaction conditions and two individual batches of **19** were tested, but mainly unreacted [^{18}F]-fluoride was present in the reaction mixture as investigated by radio-HPLC. No signs of base promoted decomposition was noted, so the inaccessibility of [^{18}F]**4** by nucleophilic fluorination remains an enigma. [^{18}F]**5** could be isolated in 15.8% decay corrected radiochemical yield from **20** (18% incorporation yield as investigated by HPLC) using the TBA/thexyl alcohol/acetonitrile system. Attempts to further optimize conditions for this particular derivative (solvent, stochiometry, temperature and duration) all resulted in diminished incorporation yields. Using the automated synthesizer, 7.0 GBq of formulated [^{18}F]**5** could be obtained, corresponding to 4.9% decay corrected radiochemical yield. For the thiomethyl derivative [^{18}F]**6** up to 47.5% incorporation yield were measured by radio-HPLC. For animal experiments, 11.5 GBq [^{18}F]**6** (8.6% decay corrected radiochemical yield) in excellent (230 GBq/µmol) specific activity were obtained using the automated TRACERlab FX$_{FDG}$ synthesis module. Attempts of preparing sulfone [^{18}F]**7** by direct radiofluorination of tosylate **24** failed to give practical yields. Decomposition was noted using HPLC analysis of the reaction mixture. We assume that the high reactivity of this particular tetrazine derivative renders direct ^{18}F-labeling impossible.

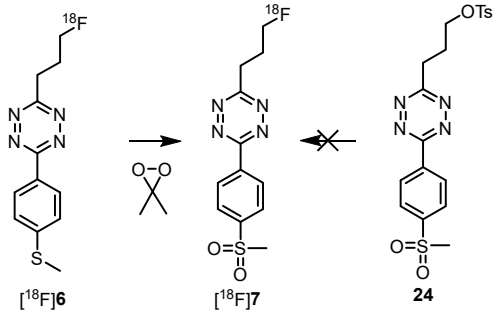

Scheme 3: *Radiosynthesis of [^{18}F]**7** by DMDO mediated oxidation of [^{18}F]**6***

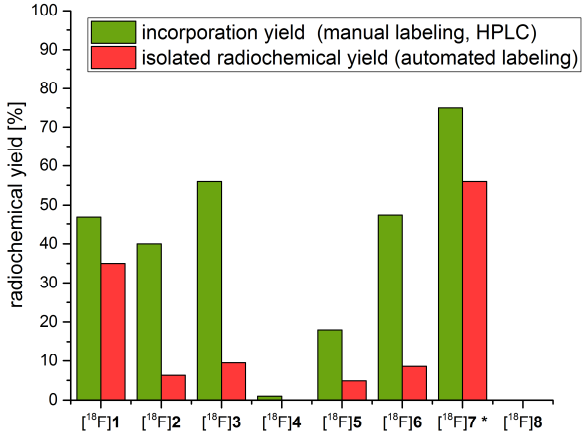

Figure 4: *Overview of incorporation yields (evaluated by radio-HPLC) and isolated radiochemical yields for tetrazines 1-8. *) two-step labelling, yield based on [^{18}F]**6***

Instead a two step radiochemical synthesis sequence was chosen to access [^{18}F]**7** by DMDO mediated oxidation of sulfide [^{18}F]**6**. For this reason [^{18}F]**6** in ethanol, as obtained by automated radiosynthesis, was concentrated to dryness and redissolved in 1 ml acetone containing dimethyldioxirane (~40 mM). After short reaction time (60-80 seconds) volatiles were removed on the rotary evaporator and the residue was purified using RP-HPLC to obtain [^{18}F]**7** in 56% radiochemical yield and good specific activity of 56 GBq/µmol thus bypassing the inaccessibility by direct radiolabeling (Scheme 3). Despite optimization attempts, we were not able to prepare pyridyl tetrazine derivative [^{18}F]**8** by nucleophilic fluorination of precursor **22**. In all cases radiofluoride incorporation into [^{18}F]**8** was below 1%, while the major product was a highly apolar compound, whose identity could not be clarified. In addition to successful preparation of novel radiotetrazines [^{18}F]**2**, [^{18}F]**3** and [^{18}F]**5**-**7**, the radiosynthesis of already described dialkyltetrazine [^{18}F]**1** could also be significantly improved to 35% decay corrected isolated radiochemical yield (vs. previously reported 5%)[1] using the TBA, thexyl alcohol and acetonitrile labeling system. An overview of incorporation and isolated radiochemical yields is shown in Figure 4.

In vivo evaluation

Compounds [^{18}F]**2**, [^{18}F]**3** and [^{18}F]**5**-**7** were administered to female BALB/c mice *via* a tail vein catheter. Anatomic MR imaging (n= 1 for [^{18}F]**2**, [^{18}F]**3**, [^{18}F]**5** and [^{18}F]**6**) followed by a 120 min dynamic PET (n=3 for [^{18}F]**2**, [^{18}F]**3**, [^{18}F]**5** and [^{18}F]**6**, n=2 for [^{18}F]**7**) scan was performed. At the end of PET a terminal blood sample was withdrawn under isoflurane anesthesia from the retroorbital sinus vein and animals were sacrificed by cervical dislocation. Urine samples were collected and organs were harvested. Aliquots of blood and plasma and all organ samples were measured for radioactivity in a y counter (Wizard 1470; Perkin-Elmer). Plasma and urine proteins were precipitated by addition of acetonitrile and consequently removed by centrifugation. Each supernatant and diluted radiotracer solution as reference was spotted on thin-layer chromatography (TLC) plates (silica gel 60F 254 nm, 10 x 20 cm; Merck, Darmstadt, Germany) and plates were developed in an appropriate solvent system. Detection was performed by placing the TLC plates on multisensitive phosphor screens (Perkin-Elmer Life Sciences, Waltham, MA). The screens were scanned at 300 dpi resolution using a PerkinElmer Cyclone® Plus Phosphor Imager (Perkin-Elmer Life Sciences) to obtain metabolism data.

Organ time activity curves (TACs) for phenyl tetrazine [^{18}F]**2**, p-tolyl tetrazine[^{18}F]**3** and 3,4,5-trimethoxy phenyl tetrazine derivative [^{18}F]**5** (shown in supporting information) show rapid renal clearance as indicated by a steep rise of activity concentration within the urinary bladder. The liver shows high initial uptake of these three substances, but activity is cleared rapidly from most organs despite bone, where a steady increase of activity concentration throughout the experiment is observed. These findings are a good indicator for metabolic instability and liberation of free fluoride from the test substances. Bone uptake of these derivatives is also visible in PET/MR summation images (see ESI), that is especially pronounced in the well perfused nasal bone. Metabolite analysis of [^{18}F]**2,** [^{18}F]**3** and [^{18}F]**5** using radio-TLC (see ESI) indicate the presence of free fluoride (Rf = 0) and polar metabolites, while the amount of unchanged tetrazine in plasma and urine are below the limit of detection, furthermore confirming rapid degradation of this probes *in vivo*.

In contrast to above mentioned compounds, data obtained from thiomethyl-tetrazine derivative [^{18}F]**6** does not indicate *in vivo* defluorination. PET/MR images show homogenous biodistribution with slightly elevated uptake in the liver (see Figure 5a-b). After initial perfusion [^{18}F]**6** exhibits very uniform uptake in all analyzed organs but the urinary bladder, wherein a steady increase of activity concentration indicates rapid renal clearance (see Figure 5c, for TACs without urinary bladder signal see ESI). PET data also clearly demonstrates the ability of [^{18}F]**6** to pass the blood brain barrier.

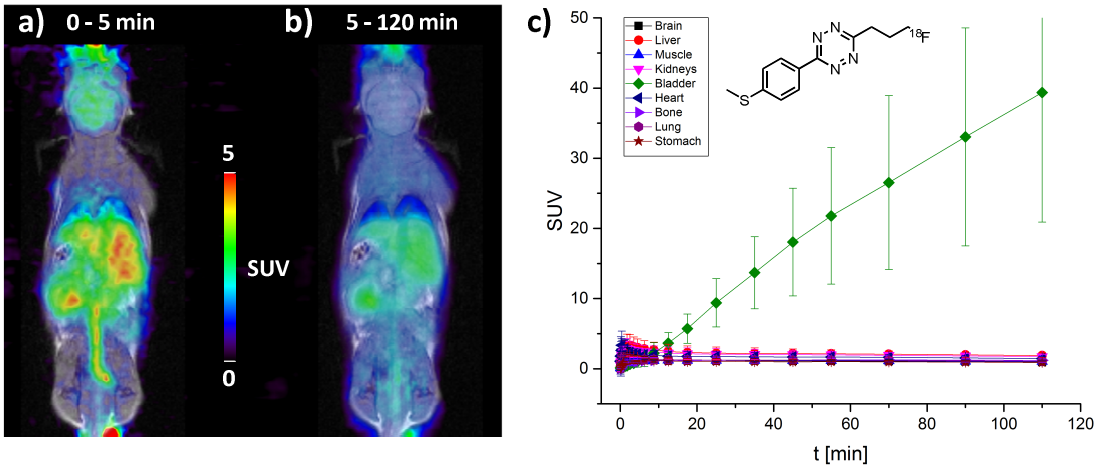

Figure 5: *Coronal PET/MR slices showing time frames 0-5 min (a) and 5-120 min (b) post administration of [^{18}F]**6**. c) Dynamic PET data obtained for [^{18}F]**6** showing homogenous biodistribution and renal excretion*

TLC metabolite analysis revealed oxidative metabolism of [^{18}F]**6** (see Figure 6). As seen in Figure 6b the radiofluorinated reference compound (left lane) already contains 5% impurity in form of the sulfoxide-derivative **26**, most likely due to air oxidation during work-up and formulation of the radiotracer. Identity of the sulfoxide was determined by TLC-Rf comparison with authentic standard (Figure 6c). Two hours post administration < 1% of [^{18}F]**6** is detected in plasma, while 13.9 (±3.2)% of plasma radioactivity is attributed to the sulfone [^{18}F]**7**, and 61.8 (±4.9)% to the sulfoxide-species [^{18}F]**26**, both active "clickable" metabolites of [^{18}F]**6** that exhibit accelerated bioorthogonal cycloaddition reactivity as compared to the parent compound (calculated rate relative to reaction of **1** + **10** is 2.51 for **26** and 4.47 for **7**, see ESI for details). The compound is excreted renally mainly as sulfoxide metabolite (up to 45% in urine), accompanied by more polar metabolites.

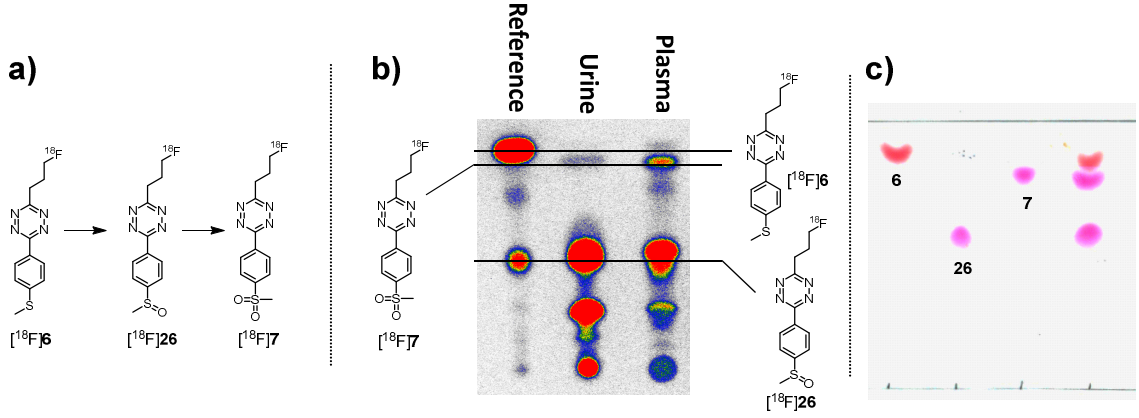

Figure 6: *a) Oxidative metabolism of [^{18}F]**6**, b)Radio-TLC (SiO_2, 5% MeOH in DCM) showing reference compound [^{18}F]**6** (left lane), urine (middle lane) and plasma samples 120 min post [^{18}F]**6** administration to native BALB/c mice c) TLC showing retention behaviour of compounds **6**, **7** and **26** (SiO_2, 5% MeOH in DCM)*

To further shed light on the metabolism of [^{18}F]**6,** the compound was administered to BALB/c mice (n=3), and the animals were sacrificed 60 minutes post radiotracer administration. Organs and blood were harvested for gamma counter analysis to obtain biodistribution data. In addition, plasma, urine, bile, as well as liver and brain extracts were analyzed using radio-TLC (see ESI for TLC lanes). At the 60 min time point [^{18}F]**6** is already absent in plasma (< 1%) while the active metabolite composition resembles the 120 min time point. Within the central nervous system 18.8 (±4.6) % of native [^{18}F]**6** is

still intact, 49.3 (±9.0) % of activity is attributed to the sulfoxide and 11.5 (±1.6) % to the sulfone metabolite, clearly showing that this bioorthogonal imaging agent is also suitable for neuro-targets inside the brain. Within the liver the main fraction of activity (39.9 ± 0.3%) is attributed to unchanged [^{18}F]**6**, while 14.5 (±4.2) % and 11.3 (±0.5) % are the fractions of sulfoxide and sulfone metabolites respectively. The urine composition one hour post tracer administration resembles the urine composition after two hours of uptake time. Beside highly polar radiometabolites, the sulfoxide is the main active species (17.3 ± 2.0%) in bile. The metabolism of [^{18}F]**6** is in good agreement with previously reported data describing the metabolism of organic sulfides.[27]

PET scanning of the sulfone tetrazine derivative [^{18}F]**7** revealed renal excretion as well as homogenous biodistribution, that is clearly visible in PET images and organ time activity curves shown in Figure 7b-c. The main mode of excretion for [^{18}F]**7** is renal (as visible in the time activity curve of the urinary bladder), but also to a certain extent hepatobiliar, as indicated by uptake in the intestines (Figure 7). TACs without the urinary bladder signal can be found in the supporting information of this manuscript. Similar to the thioether [^{18}F]**6**, also the sulfone [^{18}F]**7** penetrates the blood-brain-barrier, and is thus applicable for pretargeting tasks within the central nervous system.

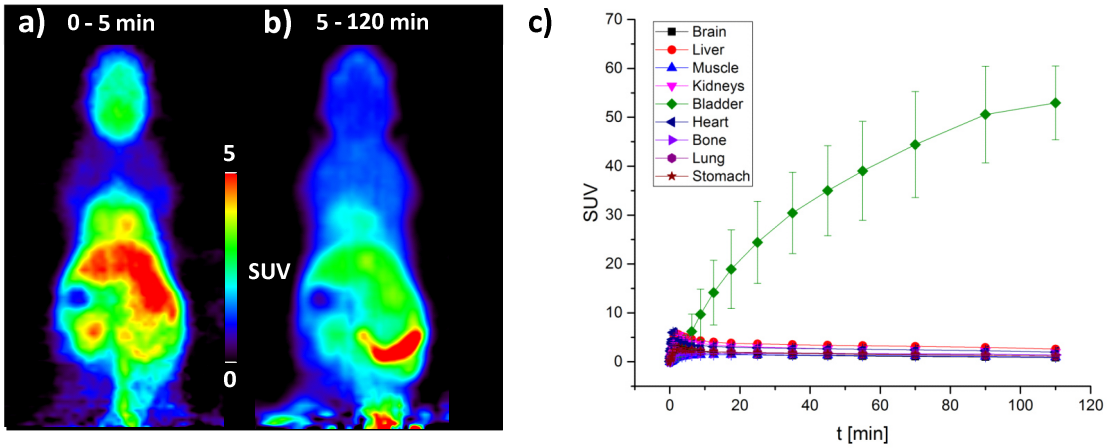

Figure 7: *Coronal PET slices showing time frames 0-5 min (a) and 5-120 min (b) post administration of [^{18}F]**7**. c) Dynamic PET data obtained for [^{18}F]**7** showing homogenous biodistribution and mainly renal excretion*

Plasma metabolite analysis 2 hours post tracer administration revealed a high fraction (65%) of unchanged tetrazine probe, rendering [^{18}F]**7** nearly as metabolically stable as previously published [^{18}F]**1**. Although not common, literature reports also reductive metabolism of sulfur[28] compounds in higher animals.[29] 18.2-19.9% of radioactivity in plasma is, according to radio-TLC, attributed to the reduced sulfoxide tetrazine species. Analysis of urine radioactivity revealed that 10.4-13.7% [^{18}F]**7** is excreted unmetabolized, while the majority of radioactivity in the urine arises from polar metabolites, whose identity has not been further investigated.

Data from the *ex vivo* biodistributions is summarized in Figure 8. In general *ex vivo* biodistribution data for all analyzed compounds is in good agreement with data obtained from the PET experiments.

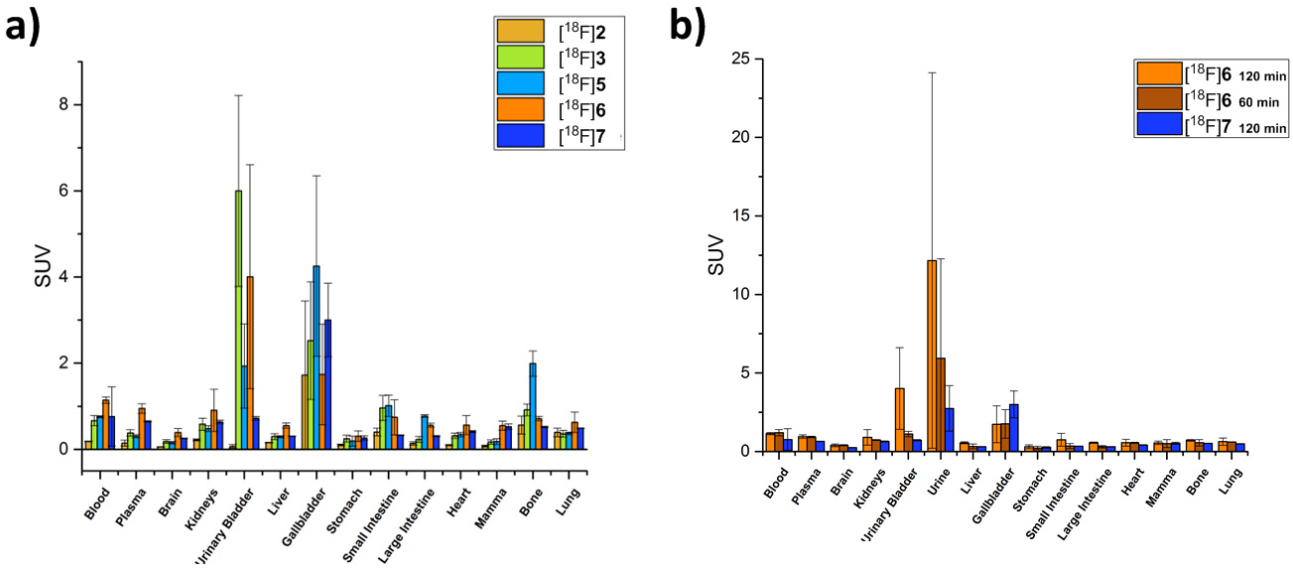

Figure 8: *Ex vivo biodistribution data for compounds a) [^{18}F]**2**, **3**, **5-7** 120 min post administration and b) [^{18}F]**6** (120 & 60 min post injection) and [^{18}F]**7** 120 min post administration*

The biodistribution of [^{18}F]**6** at the 60 min and 120 min terminal time points is compared in Figure 8b. Beside excretion organs only minor changes in the biodistribution pattern of [^{18}F]**6** are visible between those time points, indicating that 60 – 120 min post tracer administration would be a beneficial time window for image acquisition in actual bioorthogonal PET pretargeting experiments.

Conclusion

A series of 3-fluoropropyl-aryl-tetrazines was designed based on the structure of **1**. The compounds were successfully synthesized and their reactivity towards the dienophile *trans*-cyclooctene was investigated using stopped flow photometry. Furthermore, a simple computational method was established, that allows reactivity prediction for aryl-alkyl-tetrazines.

Direct nucleophilic radiofluorination, using an optimized protocol, enabled the synthesis of four novel ^{18}F-fluoropropyl tetrazines ([^{18}F]**2**, [^{18}F]**3**, [^{18}F]**5**, [^{18}F]**6**). In addition, using this modified procedure, the isolated yield of [^{18}F]**1** was increased 7-fold. Still, the most reactive derivatives ([^{18}F]**4,** [^{18}F]**7,** [^{18}F]**8**) could not be prepared using this methodology. However, we were able to prepare [^{18}F]**7** by fast post-labeling oxidation of [^{18}F]**6** in high yield using dimethyl dioxirane (DMDO), thus boosting bioorthogonal reactivity of this compound.

In vivo evaluation using PET and MR imaging as well as radiometabolite analysis revealed highly promising properties for compounds [^{18}F]**6** and [^{18}F]**7** to be used as secondary probe in bioorthogonal PET imaging. Both agents exhibit homogenous biodistribution in the mouse model and are renally excreted. In addition, both tetrazines are capable of penetrating the blood-brain-barrier, and should thus allow pretargeted imaging within the central nervous system.

[^{18}F]**6**, that is accessible by direct radiofluorination, acts as a pro-drug, which is metabolically activated to more reactive sulfoxide and sulfone species [^{18}F]**7**. Administration of [^{18}F]**7** revealed high metabolic stability of this oxidized probe.

Within this contribution we further explored the chemical space of ^{18}F-tetrazines and present two derivatives that show improved kinetics and beneficial pharmacokinetic properties as compared to previously published dialkyltetrazine [^{18}F]**1**.

Experimental

Materials and Methods

Unless otherwise noted, all reagents were purchased from commercial suppliers and used without further purification. DCM and 1,4-dioxane were dried using PURESOLV-columns (Innovative Technology Inc.). Dry acetonitrile (Sigma Aldrich) was commercially obtained and stored under argon. Dienophile TCO (**10**) and DMDO were prepared following known procedures.[30,31] Anhydrous hydrazine was prepared by the vacuum thermolysis of hydrazine cyanurate.[32] All other solvents were distilled prior to use. Drying of organic solvents after extraction was performed using anhydrous Na_2SO_4 or $MgSO_4$ (Sigma Aldrich) and subsequent filtration. Reactions were carried out under an atmosphere of argon in air-dried glassware with magnetic stirring. Sensitive liquids were transferred via syringe. Thin layer chromatography was performed using TLC alumina plates (Merck, silica gel 60, fluorescence indicator F254, or Merck, aluminium oxide neutral, fluorescence indicator F254). Detection in radio-TLC was performed by placing the TLC plates on multisensitive phosphor screens (Perkin-Elmer Life Sciences, Waltham, MA). The screens were scanned at 300 dpi resolution using a PerkinElmer Cyclone® Plus Phosphor Imager (Perkin-Elmer Life Sciences). Preparative column chromatography was performed using a Büchi Sepacore Flash System (2 x Büchi Pump Module C-605, Büchi Pump Manager C-615, Büchi UV Photometer C-635, Büchi Fraction Collector C-660) using silica gel 60 (40-63 µm) as obtained from Merck and distilled or redistilled solvents. ^{1}H, ^{13}C and ^{19}F NMR spectra were recorded on a Bruker Avance IIIHD 600 MHz spectrometer equipped with a Prodigy BBO cryo probe or on a Bruker Avance UltraShield 400 spectrometer at 20 °C. Chemical shifts are reported in ppm (δ) relative to tetramethylsilane and calibrated using solvent residual peaks. Data are shown as follows: Chemical shift, multiplicity (s = singlet, d = doublet, t = triplet, q = quartet, quin = quintet, m = multiplet, br = broad signal) and integration. A temperature-controlled Applied Photophysics SX20 (535 nm LED light source) stopped flow photometer systems (Applied Photophysics, Surrey, UK) was used for stopped flow measurements. HR-MS analysis was carried out from methanol solutions (concentration: 10 ppm) by using an HTC PAL system autosampler (CTC Analytics AG, Zwingen, Switzerland), an Agilent 1100/1200 HPLC with binary pumps, degasser and column thermostat (Agilent Technologies, Waldbronn, Germany) and Agilent 6230 AJS ESI–TOF mass spectrometer (Agilent Technologies, Palo Alto, United States). [^{18}F]Fluoride was produced *via* the ^{18}O(p,n)^{18}F nuclear reaction by irradiating oxygen-18 enriched water (IASON, Austria) using a PETtrace cyclotron equipped with high yield liquid target system (GE Healthcare, Uppsala, Sweden). HPLC analysis was performed on a 1200 series system (Agilent Technologies) using a reversed phase columns and acetonitrile / water or acetonitrile / phosphate buffer gradients. Analytical conditions: (A): Agilent Extend-C18 3.5 µm, 3 x 100 mm, gradient 10mM PO4-puffer pH=6/ acetonitrile, 1.3 ml/min, 0-1 min 15% acetonitrile, 1→8 min 15%→85% acetonitrile, 8-9 min 85% acetonitrile. (B): Agilent ZORBAX SB-Aq 5 µm, 4.6 x 250 mm, water / acetonitrile , 1.2 ml/min, 0-2 min 5% acetonitrile, 2→10 min 5%→20% acetonitrile, 10-16 min 20%→90%, 16-20 min 90% acetonitrile. For radio-HPLC a GABI star radioactivity detector (raytest Isotopenmessgeraete GmbH, Straubenhardt, Germany) was used. Preparative HPLC separations were done on the built in HPLC system on a synthesis module (TRACERlab™ FX_{FDG}, General Electric Healthcare, Uppsala, Sweden) using a Macherey-Nagel EP 250/16 100-7 C-18 (10 µm, 16 x 250 mm) column and phosphate puffer (10mM, pH = 6) / acetonitrile-gradient (flow rate: 5 mL/min, 0-6 min

10% acetonitrile, 6.01 min 30% acetonitrile, 6.01→40 min 30%→80% acetonitrile) in combination with a K-2001 UV detector (Knauer) and radioactivity detector.

Chemical Synthesis

3-(3-fluoropropyl)-6-methyl-1,2,4,5-tetrazine (1)

4-fluorobutanenitrile (**9**, 1 eq., 100 mg, 1.15 mmol) and zinc triflate (0.46 eq., 192 mg, 0.528 mmol) in anhydrous acetonitrile (7 eq., 330 mg, 8 mmol) were treated dropwise with anhydrous hydrazine (36 eq., 1.3 g, 41.1 mmol) at 0°C (Caution: gas evolution, exothermic!). The reaction mixture was heated to 42°C for 24 hours. The reaction mixture was cooled to room temperature and diluted with a 10% aqueous solution of sodium nitrite (7 eq., 0.55 g, 8 mmol). 5% HCl was added slowly until gas evolution ceased. The red solution was extracted five times with diethyl ether. Pooled extracts were dried over $MgSO_4$ and the solvent was removed on the rotary evaporator. Column chromatography over 40 g SiO_2 (5-12% diethyl ether in petroleum ether) afforded **1** (67.3 mg, 37.5% of theory) as red oil. Spectroscopic data matched previously reported values.

3-(3-fluoropropyl)-6-phenyl-1,2,4,5-tetrazine (2)

A mixture of benzonitrile (1 eq., 237 mg, 2.3 mmol), 4-fluorobutanenitrile (2 eq., 400 mg, 4.6 mmol) and anhydrous $NiCl_2$ (0.15 eq., 45 mg, 0.345 mmol) was treated dropwise with hydrazine monohydrate (9 eq., 1.1 g, 21 mmol) (Caution: gas evolution, exothermic!). The purple reaction mixture was kept at 52°C for 16 hours. After returning to room temperature the reaction mixture was diluted with a solution of sodium nitrite (8 eq., 2.54 g, 37 mmol) in 25 ml water and cooled with an ice bath. 1N HCl was added slowly until gas evolution ceased, and the intense red mixture was extracted three times with ethyl acetate. Pooled extracts were washed with brine, dried over $MgSO_4$ and concentrated on the rotary evaporator. Purification by column chromatography over 40 g SiO_2 (3-12% EE in PE) yielded **2** as purple solid (83 mg, 16.5% of theory). TLC-Rf (DCM) = 0.77, ^{1}H NMR (400 MHz, $CDCl_3$) δ = 2.36 - 2.50 (m, 2 H) 3.53 (t, *J*=7.80 Hz, 2 H) 4.65 (dt, *J*=47.22, 5.90 Hz, 2 H) 7.57 - 7.66 (m, 3 H) 8.57 - 8.63 (m, 2 H) ppm ^{13}C NMR (100.61 MHz, $CDCl_3$) δ = 28.5 (d, *J*=20.49Hz), 30.9 (d, *J*=4.94Hz), 82.8 (d, *J*=166.72Hz), 127.9, 129.2, 131.7, 132.6, 164.3, 169.2 ppm ^{19}F NMR (376.5 MHz, $CDCl_3$) δ = -219.9 ppm HR-ESI-MS: calcd. for $[M+H]^+$ $C_{11}H_{12}FN_4^+$: 219.1041, found: 219.1048.

3-(3-fluoropropyl)-6-(p-tolyl)-1,2,4,5-tetrazine (3)

A mixture of 4-methylbenzonitrile (1 eq., 404 mg, 3.44 mmol), 4-fluorobutanenitrile (1.87 eq., 560 mg, 6.43 mmol) and anhydrous $NiCl_2$ (0.15 eq., 68 mg, 0.52 mmol) was treated dropwise with hydrazine monohydrate (9 eq., 1.55 g, 31 mmol) (Caution: gas evolution, exothermic!) and heated to 65°C for 20 hours. After returning to room temperature the reaction mixture was diluted with a solution of sodium nitrite (12 eq., 2.85 g, 41.3 mmol). 2N HCl was added slowly until gas evolution ceased, and the deep red mixture was extracted three times with ethyl acetate. Pooled extracts were washed with brine, dried over Na_2SO_4 and concentrated on the rotary evaporator. Column chromatography over 40 g SiO_2 afforded **3** (51 mg, 6.4% of theory) as red crystalline solid. TLC-Rf (DCM) = 0.73, ^{1}H NMR (400 MHz, $CDCl_3$) δ = 2.33 - 2.50 (m, 5 H) 3.51 (t, *J*=7.60 Hz, 2 H) 4.64 (dt, *J*=47.06, 5.60 Hz, 2 H) 7.39 (d, *J*=8.18 Hz, 2 H) 8.48 (d, *J*=8.18 Hz, 2 H) ppm ^{13}C NMR (100.61 MHz, $CDCl_3$) δ = 21.6, 28.5 (d, *J*=20.70 Hz), 30.8 (d, *J*=5.37 Hz), 82.9 (d, *J*=166.39 Hz), 127.9, 128.9, 130.0, 143.3, 164.3, 168.9 ppm ^{19}F NMR (376.5 MHz, $CDCl_3$) δ = -219.9 ppm HR-ESI-MS: calcd. for $[M+H]^+$ $C_{12}H_{14}FN_4^+$: 233.11970, found: 233.11922.

3-(3-fluoropropyl)-6-(4-(trifluoromethyl)phenyl)-1,2,4,5-tetrazine (4)

A mixture of 4-trifluoromethylbenzonitrile (1 eq., 500 mg, 2.92 mmol), 4-fluorobutanenitrile (2 eq., 509 mg, 5.84 mmol) and anhydrous $NiCl_2$ (0.15 eq., 56.8 mg, 0.44 mmol) was treated dropwise with hydrazine monohydrate (9 eq., 1.32 g, 26.2 mmol) (Caution: gas evolution, exothermic!) and heated to 65°C for 24 hours. After returning to room temperature the reaction mixture was diluted with a solution of sodium nitrite (6 eq., 1.2 g, 17.5 mmol) in 15 ml water. 2N HCl was added slowly until gas evolution ceased. The purple solution was extracted three times with ethyl acetate. Pooled extracts were washed with water, dried over $MgSO_4$ and the solvent was removed on the rotary evaporator. Column chromatography over 90 g SiO_2 (3-10% ethyl acetate in petroleum ether) afforded **4** (39 mg, 4.7% of theory) as purple crystalline solid. TLC-Rf (PE:EE =3:1) = 0.79 ^{1}H NMR (400 MHz, $CDCl_3$) δ = 2.38 - 2.53 (m, 2 H) 3.58 (t, *J*=7.80 Hz, 2 H) 4.67 (dt, *J*=46.83, 5.50 Hz, 2 H) 7.87 (d, *J*=8.20 Hz, 2 H) 8.75 (d, *J*=8.20 Hz, 2 H) ppm ^{13}C NMR (100.61 MHz, $CDCl_3$) δ = 28.5 (d, *J*=19.80 Hz), 31.1 (d, *J*=4.94 Hz), 82.8 (d, *J*=166.01 Hz), 123.7 (q, *J*=272.68 Hz), 126.2 (q, *J*=3.53 Hz), 128.3, 134.2 (q, *J*=33.20 Hz), 163.5, 169.9 ppm, ^{19}F NMR (376.5 MHz, $CDCl_3$) δ = -219,9 (1 F), -63.1 (3 F) ppm, HR-ESI-MS: calcd. for $[M+H]^+$ $C_{12}H_{11}F_4N_4^+$: 287.09144, found: 287.09058.

3-(3-fluoropropyl)-6-(3,4,5-trimethoxyphenyl)-1,2,4,5-tetrazine (5)

A mixture of 3,4,5-trimethoxybenzonitrile (1 eq., 444 mg, 2.3 mmol), 4-fluorobutanenitrile (2 eq., 400 mg, 4.6 mmol) and anhydrous $NiCl_2$ (0.15 eq., 45 mg, 0.345 mmol) was treated dropwise with hydrazine monohydrate (9 eq., 1.1 g, 21 mmol) (Caution: gas evolution, exothermic!). The purple reaction mixture was kept at 52°C for 16 hours. After returning to room temperature the reaction mixture was diluted with a solution of sodium nitrite (8 eq., 2.54 g, 37 mmol) in 25 ml water and cooled with an ice bath. 1N HCl was added slowly until gas evolution ceased, and the intense red was extracted three times with ethyl acetate. Pooled extracts were washed with brine, dried over $MgSO_4$ and concentrated on the rotary evaporator. Purification by column chromatography over 40 g SiO_2 (10-50% EE in PE) yielded **5** as red solid (13 mg, 1.8% of theory). TLC-Rf (DCM) = 0.12 ^{1}H NMR (400 MHz, $CDCl_3$) δ = 2.35 - 2.51 (m, 2 H) 3.53 (t, *J*=7.80 Hz, 2 H) 3.98 (s, 3 H) 4.00 (s, 6 H) 4.66 (dt, *J*=46.83, 5.90 Hz, 2 H) 7.90 (s, 2 H) ppm ^{13}C NMR (100.61 MHz, $CDCl_3$) δ = 28.4 (d, *J*=20.49 Hz), 30.8 (d, *J*=4.94 Hz), 56.3, 61.0, 82.9 (d, *J*=166.01 Hz), 105.1, 126.6, 142.1, 153.9, 163.8, 168.9 ppm ^{19}F NMR (376.5 MHz, $CDCl_3$) δ = -219.9 ppm HR-ESI-MS: calcd. for $[M+H]^+$ $C_{14}H_{18}FN_4O_3^+$: 309.1357, found: 309.1359

3-(3-fluoropropyl)-6-(4-(methylthio)phenyl)-1,2,4,5-tetrazine (6) & 3-(3-fluoropropyl)-6-(4-(methylsulfinyl)phenyl)-1,2,4,5-tetrazine (26)

A mixture of 4-thiomethylbenzonitrile (1 eq., 343 mg, 2.3 mmol), 4-fluorobutanenitrile (2 eq., 400 mg, 4.6 mmol) and anhydrous $NiCl_2$ (0.15 eq., 45 mg, 0.345 mmol) was treated dropwise with hydrazine monohydrate (9 eq., 1.1 g, 21 mmol) (Caution: gas evolution, exothermic!). The purple reaction mixture was kept at 42°C for 18 hours. After returning to room temperature the reaction mixture was diluted with a solution of sodium nitrite (8 eq., 2.54 g, 37 mmol) in 25 ml water and cooled with an ice bath. 1N HCl was added slowly until gas evolution ceased, and the intense red was extracted three times with ethyl acetate. Pooled extracts were washed with brine, dried over $MgSO_4$ and concentrated on the rotary evaporator. Purification by column chromatography over 40 g SiO_2 (20-50% DCM in PE) yielded **6** as red solid (8 mg, 1.3% of theory). TLC-Rf (DCM:PE = 1:1) = 0.15, ^{1}H NMR (400 MHz, $CDCl_3$) δ = 2.35 - 2.51 (m, 2 H) 2.58 (s, 3 H) 3.52 (t, *J*=7.80 Hz, 2 H) 4.66 (dt, *J*=47.22, 5.50 Hz, 2 H) 7.42 (dt, *J*=8.59, 2.00 Hz, 2 H) 8.52 (dt, *J*=8.98, 2.00 Hz, 2 H) ppm ^{13}C NMR (100.61 MHz, $CDCl_3$) δ = 14.9, 28.5 (d, *J*=20.49Hz), 30.6 (d, *J*=5.65Hz), 82.9 (d, *J*=166.72Hz), 125.9, 127.8, 128.1, 145.4, 164.1, 168.9 ppm ^{19}F

NMR (376.5 MHz, $CDCl_3$) δ = -219.9 ppm HR-ESI-MS: calcd. for $[M+H]^+$ $C_{12}H_{14}FN_4S^+$: 265.0918, found: 265.0923. Eluting from the same column with 2% MeOH in DCM 105 mg (16.3% of theory) of sulfoxide 3-(3-fluoropropyl)-6-(4-(methylsulfinyl)phenyl)-1,2,4,5-tetrazine (**26**) was obtained as oxidated byproduct. ^{1}H NMR (600 MHz, $CDCl_3$) δ = 2.40 - 2.50 (m, 2 H) 2.83 (s, 3 H) 3.58 (t, *J*=7.60 Hz, 2 H) 4.67 (dt, *J*=46.95, 5.60 Hz, 2 H) 7.89 (dt, *J*=8.80, 1.80 Hz, 2 H) 8.79 (dt, *J*=8.80, 1.80 Hz, 2 H) ppm ^{13}C NMR (150.91 MHz, $CDCl_3$) δ = 28.4 (d, *J*=19.62 Hz), 31.0 (d, *J*=5.45 Hz), 43.9, 82.9 (d, *J*=166.76 Hz), 124.4, 128.8, 134.3, 150.6, 163.6, 169.8 ppm ^{19}F NMR (376.5 MHz, $CDCl_3$) δ = -219.9 ppm

3-(3-fluoropropyl)-6-(4-(methylsulfonyl)phenyl)-1,2,4,5-tetrazine (7)

3-(3-fluoropropyl)-6-(4-(methylsulfinyl)phenyl)-1,2,4,5-tetrazine (**6**, 1 eq., 20 mg, 0.07 mmol) was treated with a ice cold solution of dimethyl dioxirane (DMDO) in 10 ml acetone (~40 mM). The pink reaction mixture was allowed to reach room temperature and stirred for additional 40 minutes. Volatiles were removed on the rotary evaporator and the residue was purified by column chromatography over 8 g SiO_2 (10-50% EE in PE). **7** was obtained as pink solid in (13 mg, 63 % of theory). TLC-Rf (5% MeOH in DCM) = 0.77, ^{1}H NMR (400 MHz, $CDCl_3$) δ = 2.39 - 2.54 (m, 2 H) 3.14 - 3.17 (m, 3 H) 3.60 (t, *J*=7.80 Hz, 2 H) 4.67 (dt, *J*=46.83, 5.50 Hz, 2 H) 8.20 (dt, *J*=8.50, 2.00 Hz, 2 H) 8.84 (dt, *J*=8.59, 2.00 Hz, 2 H) ppm ^{13}C NMR (100.61 MHz, $CDCl_3$) δ = 28.5 (d, *J*=20.49Hz), 31.2 (d, *J*=5.65Hz), 44.4, 82.8 (d, *J*=166.72Hz), 128.3, 128.8, 136.7, 144.1, 163.25, 170.1 ppm ^{19}F NMR (376.5 MHz, $CDCl_3$) δ = -219.8 ppm, HR-ESI-MS: calcd. for $[M+H]^+$ $C_{12}H_{14}FN_4O_2S^+$: 297.0816, found: 297.0816

3-(3-fluoropropyl)-6-(pyridin-2-yl)-1,2,4,5-tetrazine (8)

A mixture of 2-pyridinecarbonitrile (1 eq., 561 mg, 5.4 mmol), 4-fluorobutanenitrile (1 eq., 470 mg, 5.4 mmol) and anhydrous $NiCl_2$ (0.1 eq., 70 mg, 0.54 mmol) was treated dropwise with hydrazine monohydrate (6 eq., 1.62 g, 32.4 mmol) at 0°C (Caution: gas evolution, exothermic!). The inhomogenous reaction mixture was heated to 60°C for 24 hours. The reaction mixture was cooled and diluted with a 10% aqueous solution of sodium nitrite (4 eq., 1.52 g, 22 mmol). 2N HCl was added slowly until gas evolution ceased. The red solution was extracted three times with ethyl acetate. Pooled extracts were washed with brine, dried over Na_2SO_4 and the solvent was removed on the rotary evaporator. Column chromatography over 40 g SiO_2 (20-70% ethyl acetate in petroleum ether) afforded **8** (128 mg, 10.8% of theory) as red oil. TLC-Rf (EE) = 0.78, ^{1}H NMR (400 MHz, $CDCl_3$) δ = 2.29 - 2.44 (m, 2 H) 3.52 (t, *J*=7.70 Hz, 2 H) 4.58 (dt, *J*=47.20, 5.90 Hz, 2 H) 7.46 - 7.52 (m, 1 H) 7.92 (td, *J*=7.87, 1.83 Hz, 1 H) 8.56 (d, *J*=7.68 Hz, 1 H) 8.87 (d, *J*=4.03 Hz, 1 H) ppm ^{13}C NMR (100.61 MHz, $CDCl_3$) δ = 28.3 (d, *J*=20.70Hz), 30.9 (d, *J*=4.60 Hz), 82.7 (d, *J*=166.39 Hz), 123.8, 126.2, 137.3, 150.0, 150.7, 163.6, 169.9 ppm, ^{19}F NMR (376.5 MHz, $CDCl_3$) δ = -219.9 ppm, HR-ESI-MS: calcd. for $[M+H]^+$ $C_{10}H_{11}FN_5^+$: 220.09930, found: 220.09865.

4-Fluorobutanenitrile (9)

Warning: Alkylfluorides are potentially highly toxic! NaCN is highly toxic! A mixture of 1-bromo-3-fluoropropane (1 eq., 14.1 g, 100 mmol), powdered NaCN (1.25 eq., 6.12 g, 125 mmol) and triethylene glycol was slowly heated to 130°C. Care must be taken due to a exothermic reaction setting in at ~40°C. The mixture was kept between 120°C and 140°C for 120 minutes. After cooling to room temperature the mixture was distilled at 125 mbar to obtain 3.8 g **9** as colorless liquid. Another fraction (1.7 g) of product was obtained at 60°C/25 mbar. Combined yield: 5.5 g (63% of theory) ^{1}H NMR (200 MHz, $CDCl_3$) δ = 1.86 - 2.14 (m, 2 H) 2.47 (t, *J*=7.00 Hz, 2 H) 4.51 (dt, *J*=46.95, 5.50 Hz, 2 H) ppm, ^{13}C NMR (50.32 MHz, $CDCl_3$) δ = 13.2 (d, *J*=5.06 Hz), 26.2 (d, *J*=20.68 Hz), 81.2 (d, *J*=166.84 Hz), 118.7 ppm

3-(6-phenyl-1,2,4,5-tetrazin-3-yl)propan-1-ol (11)

A mixture of benzonitrile (1 eq., 4 g, 38.8 mmol), 4-hydroxybutanenitrile (2 eq., 6.6 g, 77.6 mmol) and anhydrous $NiCl_2$ (0.15 eq., 753 mg, 5.8 mmol) was treated dropwise with hydrazine monohydrate (9 eq., 17.5 g, 350 mmol) (Caution: gas evolution, exothermic!). The purple reaction mixture was heated to 42°C for 72 hours. After returning to room temperature the reaction mixture was diluted with a solution of sodium nitrite (6 eq., 16 g, 233 mmol) in 150 ml water and cooled with an ice bath. 2N HCl was added slowly until gas evolution ceased, and the intense red mixture was extracted three times with ethyl acetate. Pooled extracts were washed with brine, dried over Na_2SO_4 and concentrated on the rotary evaporator. Raw material (7 g) was purified by column chromatography over 90 g SiO_2 (30-75% EE in PE). **11** was obtained as purple solid (3.55 g, 42.3% of theory). TLC-Rf (PE:EE =1:1) = 0.42 ^{1}H NMR (400 MHz, $CDCl_3$) δ = 1.73 (br. s., 1 H) 2.24 - 2.33 (m, 2 H) 3.52 (t, *J*=7.41 Hz, 2 H) 3.85 (t, *J*=6.05 Hz, 2 H) 7.57 - 7.67 (m, 3 H) 8.58 - 8.63 (m, 2 H) ppm ^{13}C NMR (100.61 MHz, $CDCl_3$) δ = 30.6, 31.5, 61.8, 127.9, 129.2, 131.8, 132.6, 164.2, 169.9 ppm HR-ESI-MS: calcd. for $[M+H]^+$ $C_{11}H_{13}N_4O^+$: 217.1084, found: 217.1089.

3-(6-(p-tolyl)-1,2,4,5-tetrazin-3-yl)propan-1-ol (12)

A mixture of 4-methylbenzonitrile (1 eq., 1 g, 8.54 mmol), 4-hydroxybutanenitrile (2 eq., 1.45 g, 17.1 mmol) and anhydrous $NiCl_2$ (0.15 eq., 166 mg, 1.28 mmol) was treated dropwise with hydrazine monohydrate (9 eq., 3.85 g, 77 mmol) (Caution: gas evolution, exothermic!). The purple solution was heated to 65°C for 23 hours. After returning to room temperature the reaction mixture was diluted with a solution of sodium nitrite (6 eq., 3.5 g, 51 mmol) in 30 ml water and cooled with a ice bath. 2N HCl was added slowly until gas evolution ceased, and the intense red mixture was extracted three times with ethyl acetate. Pooled extracts were washed with brine, dried over Na_2SO_4 and concentrated on the rotary evaporator. Column chromatography over 90 g SiO_2 (15-50% EE in PE) afforded **12** (620 mg, 31.5% of theory) as purple crystalline solid. TLC-Rf (PE:EE =1:1) = 0.42 ^{1}H NMR (400 MHz, $CDCl_3$) δ = 2.25 (quin, *J*=7.30 Hz, 2 H) 2.41 (br. s., 1 H) 2.44 (s, 3 H) 3.46 (t, *J*=7.45 Hz, 2 H) 3.82 (t, *J*=6.14 Hz, 2 H) 7.36 (d, *J*=8.18 Hz, 2 H) 8.43 (d, *J*=8.18 Hz, 2 H) ppm ^{13}C NMR (100.61 MHz, $CDCl_3$) δ = 21.6, 30.6, 31.4, 61.6, 127.8, 128.9, 129.9, 143.2, 164.2, 169.5 ppm HR-ESI-MS: calcd. for $[M+H]^+$ $C_{12}H_{15}N_4O^+$: 231.12404, found: 231.12349.

3-(6-(4-(trifluoromethyl)phenyl)-1,2,4,5-tetrazin-3-yl)propan-1-ol (13)

A mixture of 4-trifluoromethylbenzonitrile (1 eq., 500 mg, 2.92 mmol), 4-hydroxybutanenitrile (2 eq., 497 mg, 5.84 mmol) and anhydrous $NiCl_2$ (0.15 eq., 56.8 mg, 0.44 mmol) was treated dropwise with hydrazine monohydrate (9 eq., 1.31 g, 26.2 mmol) (Caution: gas evolution, exothermic!). The purple solution was heated to 60°C for 24 hours. After returning to room temperature the reaction mixture was diluted with a solution of sodium nitrite (6 eq., 1.20 g, 17.5 mmol) and cooled with a ice bath. 2N HCl was added slowly until gas evolution ceased, and the intense purple mixture was extracted twice with ethyl acetate. Pooled extracts were washed with brine, dried over $MgSO_4$ and concentrated on the rotary evaporator. Column chromatography over 40 g SiO_2 (35% EE in PE) afforded **13** (226 mg, 27.2% of theory) as purple crystalline solid. TLC-Rf (PE:EE =3:1) = 0.09 ^{1}H NMR (400 MHz, $CDCl_3$) δ = 1.74 (br. s., 1 H) 2.30 (quin, *J*=6.72 Hz, 2 H) 3.55 (t, *J*=7.45 Hz, 2 H) 3.86 (t, *J*=5.99 Hz, 2 H) 7.86 (d, *J*=8.18 Hz, 2 H) 8.73 (d, *J*=8.18 Hz, 2 H) ppm ^{13}C NMR (100.61 MHz, $CDCl_3$) δ = 30.6, 31.7, 61.7, 123.7 (q, *J*=272.20 Hz), 126.2 (q, *J*=3.83 Hz), 128.2, 134.1 (q, *J*=32.97 Hz), 135.1, 163.3, 170.5 ppm, ^{19}F NMR (376.5 MHz, $CDCl_3$) δ = -63.1 ppm, HR-ESI-MS: calcd. for $[M-H]^-$ $C_{12}H_{10}F_3N_4O^-$: 283.08122, found: 283.08203.

3-(6-(3,4,5-trimethoxyphenyl)-1,2,4,5-tetrazin-3-yl)propan-1-ol (14)

A mixture of 3,4,5-trimethoxybenzonitrile (1 eq., 1 g, 5.18 mmol), 4-hydroxybutanenitrile (2 eq., 881 mg, 10.35 mmol) and anhydrous $NiCl_2$ (0.15 eq., 100 mg, 0.77 mmol) was treated dropwise with hydrazine monohydrate (12.2 eq., 3.15 g, 63 mmol) (Caution: gas evolution, exothermic!). The inhomogenous reaction mixture was heated to 50°C for 72 hours. After returning to room temperature the reaction mixture was diluted with a solution of sodium nitrite (6 eq., 2.15 g, 31 mmol) in 20 ml water and cooled with an ice bath. 2N HCl was added slowly until gas evolution ceased, and the intense red mixture was extracted four times with ethyl acetate. Pooled extracts were washed with brine, dried over $MgSO_4$ and concentrated on the rotary evaporator. Column chromatography over 90 g SiO_2 (30-75% EE in PE) afforded **14** (198 mg, 12.5% of theory) as pink crystalline solid. ^{1}H NMR (400 MHz, $CDCl_3$) δ = 2.22 - 2.32 (m, 2 H) 3.50 (t, *J*=7.41 Hz, 2 H) 3.85 (t, *J*=6.05 Hz, 2 H) 3.97 (s, 3 H) 4.00 (s, 6 H) 7.89 (s, 2 H) ppm ^{13}C NMR (100.61 MHz, $CDCl_3$) δ = 30.6, 31.4, 56.3, 61.0, 61.8, 105.0, 126.7, 142.0, 153.9, 163.7, 169.6 ppm HR-ESI-MS: calcd. for $[M+H]^+$ $C_{14}H_{19}F_3N_4O_4^+$: 307.1401, found: 307.1406.

3-(6-(4-(methylthio)phenyl)-1,2,4,5-tetrazin-3-yl)propan-1-ol (15)

A mixture of 4-thiomethylbenzonitrile (1 eq., 1 g, 6.7 mmol), 4-hydroxybutanenitrile (2 eq., 1.14 g, 13.4 mmol) and anhydrous $NiCl_2$ (0.15 eq., 129 mg, 1 mmol) was treated dropwise with hydrazine monohydrate (9 eq., 3 g, 60.3 mmol) (Caution: gas evolution, exothermic!). The purple solution was heated to 52°C for 18 hours. After returning to room temperature the reaction mixture was diluted with a solution of sodium nitrite (8 eq., 4 g, 54 mmol) and cooled with a ice bath. 1N HCl was added slowly until gas evolution ceased, and the intense red mixture was extracted with ethyl acetate. A insoluble white solid was removed by filtration. Pooled extracts were washed with brine, dried over $MgSO_4$ and concentrated on the rotary evaporator. Column chromatography over 40 g SiO_2 (10-25% EE in PE) afforded **15** (95.6 mg, 5.4% of theory) as red solid. TLC-Rf (PE:EE =1:1) = 0.37 ^{1}H NMR (400 MHz, $CDCl_3$) δ = 2.26 (tt, *J*=7.41, 6.24 Hz, 2 H) 2.57 (s, 3 H) 3.48 (t, *J*=7.41 Hz, 2 H) 3.83 (t, *J*=6.05 Hz, 2 H) 7.40 (dt, *J*=8.59, 2.30 Hz, 13 H) 8.48 (dt, *J*=8.59, 2.30 Hz, 13 H) ppm ^{13}C NMR (100.61 MHz, $CDCl_3$) δ = 14.8, 30.6, 31.4, 61.7, 125.9, 128.0, 145.2, 163.9, 169.5 ppm HR-ESI-MS: calcd. for $[M+H]^+$ $C_{12}H_{15}N_4OS^+$: 263.0961, found: 263.0970

3-(6-(pyridin-2-yl)-1,2,4,5-tetrazin-3-yl)propan-1-ol (16)

A mixture of 2-pyridinecarbonitrile (1 eq., 1 g, 9.6 mmol), 4-hydroxybutanenitrile (2 eq., 1.63 g, 19.21 mmol) and anhydrous $NiCl_2$ (0.15 eq., 188 mg, 1.44 mmol) was treated dropwise with hydrazine monohydrate (9 eq., 4.3 g, 86.4 mmol) (Caution: gas evolution, exothermic!). The purple solution was heated to 45°C for 16 hours. After returning to room temperature the reaction mixture was diluted with a solution of sodium nitrite (6.25 eq., 4.14 g, 60 mmol) in 40 ml water and cooled with a ice bath. 1N HCl was added slowly until gas evolution ceased, and the red solution was extracted three times with ethyl acetate. Pooled extracts were washed with brine, dried over Na_2SO_4 and concentrated on the rotary evaporator. Column chromatography over 60 g SiO_2 (75-100% EE in PE) afforded **16** (129.5 mg, 6.2% of theory) as red crystalline solid. TLC-Rf (EE) = 0.22 ^{1}H NMR (400 MHz, $CDCl_3$) δ = 2.23 - 2.32 (m, 2 H) 3.55 (t, *J*=7.41 Hz, 2 H) 3.83 (t, *J*=6.05 Hz, 2 H) 7.55 (ddd, *J*=7.71, 4.78, 1.17 Hz, 1 H) 7.97 (td, *J*=7.80, 1.95 Hz, 1 H) 8.61 - 8.65 (m, 1 H) 8.90 - 8.96 (m, 1 H) ppm,^{13}C NMR (100.61 MHz, $CDCl_3$) δ = 30.7, 31.7, 61.6, 123.9, 126.4, 137.5, 150.2, 150.8, 163.5, 170.8 ppm HR-ESI-MS: calcd. for $[M+H]^+$ $C_{10}H_{12}N_5O^+$: 218.10364, found: 218.10316.

3-(6-phenyl-1,2,4,5-tetrazin-3-yl)propyl 4-methylbenzenesulfonate (17)

A mixture of 3-(6-phenyl-1,2,4,5-tetrazin-3-yl)propan-1-ol (**11**, 1 eq., 200 mg, 0.925 mmol) and tosyl chloride (2 eq., 353 mg 1.85 mmol) in 5 ml dry dichloromethane was cooled to 0°C and treated dropwise with anhydrous pyridine (2 eq., 146 mg, 1.85 mmol). The mixture was stirred for 24h at room temperature and diluted with 30 ml DCM. The organic layer was separated and washed with cold 1N HCl followed by cold half concentrated $NaHCO_3$ solution. Drying over Na_2SO_4, removal of solvent and column chromatography over 40 g SiO_2 eluting with 3-20% ethyl acetate in petrol ether afforded 250.4 mg **17** as purple crystalline solid (73% of theory). TLC-Rf (PE:EE =1:1) = 0.91, ^{1}H NMR (400 MHz, $CDCl_3$) δ = 2.36 - 2.44 (m, 5 H) 3.44 (t, *J*=7.41 Hz, 2 H) 4.25 (t, *J*=6.05 Hz, 2 H) 7.30 (d, *J*=8.20 Hz, 2 H) 7.57 - 7.68 (m, 3 H) 7.74 - 7.80 (m, 2 H) 8.56 - 8.60 (m, 2 H) ppm ^{13}C NMR (100.61 MHz, $CDCl_3$) δ = 21.6, 26.6, 30.7, 68.9, 127.9, 128.0, 129.3, 129.8, 131.6, 132.7, 132.8, 144.9, 164.3, 168.6 ppm

3-(6-(p-tolyl)-1,2,4,5-tetrazin-3-yl)propyl 4-methylbenzenesulfonate (18)

A mixture of 3-(6-(p-tolyl)-1,2,4,5-tetrazin-3-yl)propan-1-ol (**12**, 1 eq., 330 mg, 1.43 mmol) and tosyl chloride (2.5 eq., 681 mg 3.6 mmol) in 8 ml dry dichloromethane was cooled to 0°C and treated dropwise with anhydrous pyridine (3 eq., 350 µl, 4.3mmol). The mixture was stirred overnight at room temperature until TLC indicated consumption of starting material. The reaction mixture was diluted with 50 ml DCM, washed once with ice cold 1N HCl followed by half concentrated cold $NaHCO_3$ solution and brine. Drying over $MgSO_4$, removal of solvent and column chromatography over 40g SiO_2 eluting with 0-30% ethyl acetate in petrol ether afforded 430 mg **18** as red crystalline solid (78% of theory). TLC-Rf (PE:EE =3:1) = 0.62 ^{1}H NMR (400 MHz, $CDCl_3$) δ = 2.35 - 2.43 (m, 5 H) 2.48 (s, 3 H) 3.41 (t, *J*=7.45 Hz, 2 H) 4.24 (t, *J*=6.14 Hz, 2 H) 7.30 (d, *J*=8.18 Hz, 2 H) 7.40 (d, *J*=8.18 Hz, 2 H) 7.77 (d, *J*=8.18 Hz, 2 H) 8.46 (d, *J*=8.18 Hz, 2 H) ppm^{13}C NMR (100.61 MHz, $CDCl_3$) δ = 21.6, 21.7, 26.6, 30.7, 69.0, 127.8, 127.9, 128.8, 129.8, 130.0, 143.4, 144.9, 164.3, 168.3 ppm HR-ESI-MS: calcd. for $[M+H]^+$ $C_{19}H_{21}N_4O_3S^+$: 385.13289, found: 385.13181.

3-(6-(4-(trifluoromethyl)phenyl)-1,2,4,5-tetrazin-3-yl)propyl 4-methylbenzenesulfonate (19)

A mixture of 3-(6-(4-(trifluoromethyl)phenyl)-1,2,4,5-tetrazin-3-yl)propan-1-ol (**13**, 1 eq., 100 mg, 0.352 mmol) and tosyl chloride (2 eq., 134.2 mg 0.71 mmol) in 5 ml dry dichloromethane was cooled to 3°C and treated dropwise with anhydrous pyridine (2 eq., 55.6 mg, 0.71 mmol). The mixture was stirred for 168h at 3°C and poured onto a mixture of 0.5N HCl and ice. The organic layer was separated and washed with half concentrated cold $NaHCO_3$ solution and brine. Drying over $MgSO_4$, removal of solvent and column chromatography over SiO_2 eluting with 0-20% ethyl acetate in petrol ether afforded 124.8 mg **19** as purple crystalline solid (81% of theory). TLC-Rf (PE:EE =3:1) = 0.55, ^{1}H NMR (400 MHz, $CDCl_3$) δ = 2.37 - 2.47 (m, 5 H) 3.49 (t, *J*=7.45 Hz, 2 H) 4.26 (t, *J*=5.99 Hz, 2 H) 7.31 (d, *J*=7.89 Hz, 2 H) 7.77 (d, *J*=8.18 Hz, 2 H) 7.87 (d, *J*=8.18 Hz, 2 H) 8.71 (d, *J*=8.18 Hz, 2 H) ppm ^{13}C NMR (100.61 MHz, $CDCl_3$) δ = 21.6, 26.6, 31.0, 68.9, 123.7 (q, *J*=272.2Hz), 126.2 (q, *J*=3.1Hz), 127.9, 128.3, 129.9, 132.7, 134.2 (q, *J*=32.97Hz), 135.0, 144.9, 163.4, 169.3 ppm

3-(6-(3,4,5-trimethoxyphenyl)-1,2,4,5-tetrazin-3-yl)propyl 4-methylbenzenesulfonate (20)

A mixture of 3-(6-(3,4,5-trimethoxyphenyl)-1,2,4,5-tetrazin-3-yl)propan-1-ol (**14**, 1 eq., 100 mg, 0.326 mmol) and tosyl chloride (2 eq., 124 mg 0.653 mmol) in 2 ml dry dichloromethane was cooled to 0°C and treated dropwise with anhydrous pyridine (2 eq., 51 mg, 0.653 mmol). The mixture was stirred for 24h at room temperature and diluted with 20 ml DCM. The organic layer was separated and washed with cold 1N HCl followed by cold half-concentrated $NaHCO_3$ solution. Drying over Na_2SO_4, removal of solvent and column chromatography over 40 g SiO_2 eluting with 10-50% ethyl acetate in petrol ether afforded 142.2 mg **20** as red crystalline solid (95% of theory). TLC-Rf (PE:EE =1:1) = 0.65, ^{1}H NMR (400 MHz, $CDCl_3$) δ = 2.36 - 2.44 (m, 5 H) 3.43 (t, *J*=7.41 Hz, 2 H) 3.98 (s, 3 H) 3.99 - 4.03 (m, 6 H) 4.26 (t, *J*=6.05 Hz, 2 H) 7.32 (d, *J*=7.80 Hz, 2 H) 7.75 - 7.80 (m, 2 H) 7.87 (s, 2 H) ppm ^{13}C NMR (100.61 MHz, $CDCl_3$) δ = 21.6, 26.6, 30.7, 56.4, 61.0, 69.0, 105.1, 126.5, 127.9, 129.9, 132.8, 142.2, 144.9, 153.9, 163.8, 168.3 ppm HR-ESI-MS: calcd. for $[M+H]^+$ $C_{21}H_{25}N_4O_6S^+$: 461.1489, found: 461.1504

3-(6-(4-(methylthio)phenyl)-1,2,4,5-tetrazin-3-yl)propyl 4-methylbenzenesulfonate (21)

A mixture of 3-(6-(4-(methylthio)phenyl)-1,2,4,5-tetrazin-3-yl)propan-1-ol (**15**, 1 eq., 54 mg, 0.205 mmol) and tosyl chloride (4 eq., 156 mg 0.82 mmol) in 3 ml dry dichloromethane was cooled to 0°C and treated dropwise with anhydrous pyridine (4 eq., 65 mg, 0.82 mmol). The mixture was stirred overnight at 0°C and for 3 hours at room temperature. The reaction mixture was diluted with 20 ml DCM, washed once with ice cold 1N HCl followed by half concentrated cold $NaHCO_3$ solution and brine. Drying over $MgSO_4$, removal of solvent and column chromatography over SiO_2 eluting with 0-50% ethyl acetate in petrol ether afforded 57 mg **21** as red crystalline solid (66.7% of theory). TLC-Rf (PE:EE =1:1) = 0.75, ^{1}H NMR (400 MHz, $CDCl_3$) δ = 2.35 - 2.43 (m, 5 H) 2.58 (s, 3 H) 3.41 (t, *J*=7.41 Hz, 2 H) 4.25 (t, *J*=6.05 Hz, 2 H) 7.31 (d, *J*=7.81 Hz, 2 H) 7.42 (dt, *J*=8.59, 2.30 Hz, 2 H) 7.78 (dt, *J*=8.20, 2.00 Hz, 2 H) 8.49 (dt, *J*=8.98, 2.00 Hz, 2 H) ppm ^{13}C NMR (100.61 MHz, $CDCl_3$) δ = 14.9, 21.6, 26.6, 30.7, 69.0, 125.9, 127.7, 127.9, 128.1, 129.9, 132.8, 144.9, 145.5, 164.1, 168.3 ppm

3-(6-(pyridin-2-yl)-1,2,4,5-tetrazin-3-yl)propyl 4-methylbenzenesulfonate (22)

To a cooled (0°C) solution of 3-(6-(pyridin-2-yl)-1,2,4,5-tetrazin-3-yl)propan-1-ol (**16**, 1 eq., 64 mg, 0.29 mmol) and anhydrous pyridine (2 eq., 47 mg, 0.6 mmol) in 3 ml dry dichloromethane was added tosyl chloride (2 eq., 115 mg 0.60 mmol) in one portion. The reaction was stirred at 0°C until TLC indicated consumption of starting materials (3 days). The solution was poured onto a 40 ml ice cold 1% HCl. The organic layer was separated and the aqueous layer was extracted three times with DCM. Pooled extracts were washed with half concentrated cold $NaHCO_3$ solution and dried over Na_2SO_4. Removal of solvent and column chromatography over SiO_2 (8 g) eluting with 50-70% ethyl acetate in petrol ether afforded 72 mg **22** as pink crystalline solid (66.8% of theory). TLC-Rf (EE) = 0.75, ^{1}H NMR (400 MHz, $CDCl_3$) δ = 2.35 - 2.45 (m, 5 H) 3.48 (t, *J*=7.32 Hz, 2 H) 4.23 (t, *J*=6.04 Hz, 2 H) 7.30 (d, *J*=8.05 Hz, 2 H) 7.56 (dd, *J*=7.50, 4.94 Hz, 1 H) 7.76 (d, *J*=8.05 Hz, 2 H) 7.98 (t, *J*=7.50 Hz, 1 H) 8.61 (d, *J*=8.05 Hz, 1 H) 8.94 (d, *J*=4.76 Hz, 1 H) ppm ^{13}C NMR (100.61 MHz, $CDCl_3$) δ = 21.5, 26.6, 30.9, 68.9, 123.9, 126.4, 127.8, 129.8, 132.7, 137.4, 144.9, 150.1, 150.8, 163.7, 169.5 ppm, HR-ESI-MS: calcd. for $[M+H]^+$ $C_{17}H_{18}N_5O_3S^+$: 372.11249, found: 372.11156.

3-(6-(4-(methylsulfonyl)phenyl)-1,2,4,5-tetrazin-3-yl)propan-1-ol (23)

3-(6-(4-(methylthio)phenyl)-1,2,4,5-tetrazin-3-yl)propan-1-ol (**15**, 1 eq., 40 mg, 0.15 mmol) was treated with a ice cold solution of dimethyl dioxirane (DMDO) in 25 ml acetone (~40 mM). The pink reaction mixture was allowed to reach room temperature and stirred for additional 30 minutes. Volatiles were removed on the rotary evaporator and **25** was obtained in 75% yield following purification by column chromatography over 8 g SiO_2 (0-15% MeOH in DCM).^{1}H NMR (600 MHz, DMSO-d_6) δ = 2.06 - 2.13 (m, 2 H) 3.39 (t, *J*=7.60 Hz, 2 H) 3.55 - 3.60 (m, 2 H) 4.63 (t, *J*=5.14 Hz, 1 H) 8.22 (dt, *J*=8.51, 1.80 Hz, 2 H) 8.72 (dt, *J*=8.80, 2.10 Hz, 2 H) ppm ^{13}C NMR (150.91 MHz, DMSO-d_6) δ = 30.6, 31.3, 43.3, 60.0, 128.0, 128.4, 136.6, 143.8, 162.6, 170.3 ppm, HR-ESI-MS: calcd. for $[M+H]^+$ $C_{12}H_{15}N_4O_3S^+$: 295.0859, found: 295.0873

3-(6-(4-(methylsulfonyl)phenyl)-1,2,4,5-tetrazin-3-yl)propyl 4-methylbenzenesulfonate (24)

A mixture of 3-(6-(4-(methylsulfonyl)phenyl)-1,2,4,5-tetrazin-3-yl)propan-1-ol (**23**, 1 eq., 26.6 mg, 90 µmol) and tosyl chloride (4 eq., 69 mg, 0.36 mmol) in 4 ml dry dichloromethane was cooled to 0°C and treated with anhydrous pyridine (5 eq., 50 µl, 0.45 mmol). The mixture was stirred at 4°C until TLC indicated consumption of starting material. The reaction mixture was diluted with 20 ml DCM. The organic layer was separated and washed with cold 1N HCl followed by cold half-concentrated $NaHCO_3$ solution. Drying over Na_2SO_4, removal of solvent and column chromatography over 40 g SiO_2 eluting with 0-3% MeOH in DCM afforded 32 mg **24** as pink crystalline solid (79% of theory). ^{1}H NMR (600 MHz, $CDCl_3$) δ = 2.39 - 2.46 (m, 5 H) 3.15 (s, 3 H) 3.51 (t, *J*=7.48 Hz, 2 H) 4.26 (t, *J*=5.90 Hz, 2 H) 7.33 (d, *J*=7.92 Hz, 2 H) 7.77 (dt, *J*=8.51, 2.10 Hz, 2 H) 8.19 (dt, *J*=8.51, 1.80 Hz, 2 H) 8.81 (dt, *J*=8.80, 1.80 Hz, 2 H) ppm ^{13}C NMR (150.91 MHz, $CDCl_3$) δ = 21.6, 26.7, 31.1, 44.4, 68.9, 127.9, 128.3, 128.8, 129.9, 132.7, 136.6, 144.0, 145.0, 163.2, 169.5

3-(6-(p-tolyl)-1,2,4,5-tetrazin-3-yl)propyl 4-nitrobenzenesulfonate (25)

A mixture of 3-(6-(p-tolyl)-1,2,4,5-tetrazin-3-yl)propan-1-ol (**12**, 1 eq., 70 mg, 0.30 mmol) and nosyl chloride (2.07 eq., 140 mg 0.63 mmol) in 4 ml dry dichloromethane was cooled to 0°C and treated dropwise with anhydrous pyridine (2.07 eq., 50 mg, 0.63 mmol). The mixture was stirred for 48 hours at 0°C (conducting the reaction at room temperature causes elimination and sharply reduced yield). The reaction mixture was diluted with 100 ml DCM, washed once with ice cold 1N HCl followed by half concentrated cold $NaHCO_3$ solution and brine. Drying over $MgSO_4$, removal of solvent and column chromatography over 40g SiO_2 eluting with 0-20% ethyl acetate in petrol ether afforded 90.9 mg **25** as red crystalline solid (72% of theory). TLC-Rf (PE:EE =1:1) = 0.95 ^{1}H NMR (400 MHz, $CDCl_3$) δ = 2.40 - 2.51 (m, 5 H) 3.45 (t, *J*=7.16 Hz, 2 H) 4.36 (t, *J*=5.99 Hz, 2 H) 7.40 (d, *J*=7.89 Hz, 2 H) 8.10 (d, *J*=8.77 Hz, 2 H) 8.38 (d, *J*=8.77 Hz, 2 H) 8.44 (d, *J*=8.19 Hz, 2 H) ppm ^{13}C NMR (100.61 MHz, $CDCl_3$) δ = 21.7, 26.8, 30.7, 70.0, 124.5, 127.9, 129.2, 130.1, 141.5, 143.7, 150.8, 164.4, 168.2 ppm HR-ESI-MS: calcd. for $[M+H]^+$ $C_{18}H_{18}N_5O_5S^+$: 416.1023, found: 416.1040.

Radiolabeling

General procedure for manual radiolabeling

A QMA light cartridge (Waters) was preconditioned with 0.5M K_2CO_3 solution (7 ml) followed by 15 ml water. Cyclotron produced ^{18}F-fluoride in water (0.5-2.5 ml) was passed over the cartridge, and the cartridge was eluted with a solution 0.075M tetrabutylammonium hydrogen carbonate solution, followed by 1 ml of acetonitrile. Volatiles were removed in a stream of argon at 105°C and residual water was removed by addition and subsequent evaporation of 700 µl anhydrous acetonitrile. The azeotropic drying step was repeated two more times. Precursor was added in the labelling solvent, and the reaction mixture was heated to the indicated temperature for the indicated time span. After cooling of the reaction contents incorporation yield was investigated by radio-HPLC and/or radio-TLC. In several cases the fluorine-18 tetrazine derivatives were additionally isolated using preparative HPLC.

[^{18}F]1: 328 MBq ^{18}F fluoride, 430 µl TBA-HCO_3-Lsg (32.25 µmol), 10 mg (32.4 µmol) 3-(6-methyl-1,2,4,5-tetrazin-3-yl)propyl 4-methylbenzenesulfonate in 400 µl thexyl alcohol/anhydrous acetonitrile v/v = 1:1, 4.5 min; 95°C: incorporation yield (HPLC) = 46.5%, incorporation yield (TLC) = 48.3%, isolated yield (decay corrected) = 33.4%

[^{18}F]2: 356 MBq ^{18}F fluoride, 250 µl TBA-HCO_3-Lsg (18.75 µmol), 6.7 mg (18.1 µmol) **17** in 400 µl thexyl alcohol/anhydrous acetonitrile v/v = 1:1, 5 min; 95°C: incorporation yield (HPLC) = 40%, incorporation yield (TLC) = 40.5%

[^{18}F]3: 363 MBq ^{18}F fluoride, 500 µl TBA-HCO_3-Lsg (37.5 µmol), 12.7 mg (33.0 µmol) **18** in 500 µl thexyl alcohol/anhydrous acetonitrile v/v = 1:1, 5 min, 107°C: incorporation yield (HPLC) = 56.2%, isolated yield (decay corrected) = 41.7%

[^{18}F]5: 355 MBq ^{18}F fluoride, 250 µl TBA-HCO_3-Lsg (18.75 µmol), 9.0 mg (19.5 µmol) **20** in 400 µl thexyl alcohol/anhydrous acetonitrile v/v = 1:1, 5 min; 95°C: incorporation yield (HPLC) = 13.7%, incorporation yield (TLC) = 18%

[^{18}F]6: 481.7 MBq ^{18}F fluoride, 166 µl TBA-HCO_3-Lsg (12.5 µmol), 5.2 mg (12.5 µmol) **21** in 400 µl thexyl alcohol/anhydrous acetonitrile v/v = 1:1, 8 min; 97°C: incorporation yield (HPLC) = 47.7%

^{18}F-species prepared by manual labeling matched HPLC retention times with authentic standards (see supporting information)

General procedure for automated radiolabeling

A remote controlled synthesis module (TRACERlab™ FXFDG, General Electric Healthcare, Uppsala, Sweden) with 3 mL glass reactor housed in a hot cell was used for automated labeling experiments. In general cyclotron produced no carrier added [^{18}F] fluoride was trapped on a preconditioned (5 ml 0.5 M K_2CO_3 followed by 15 ml water) Waters QMA light cartridge. The radioactivity was eluted with 500 µl 0.075M TBA-HCO_3 solution followed by 1 ml acetonitrile. Volatiles were removed in vacuo at a temperature of 60-120 °C. After cooling to 50 °C a solution of precursor in a mixture of dry acetonitrile

and thexyl alcohol was added. The reaction mixture was heated to 93°C for 8 minutes followed by cooling to 45°C and consequent transfer into a vial. The reactor was rinsed with 2 ml DMSO:water = 1:1 (v/v). Combined solutions were injected into a preparative HPLC column (Macherey-Nagel EP 250/16 100-7 C-18, 10 µm, 16 x 250 mm) and eluted using a gradient of phosphate puffer (10 mM pH = 6) and acetonitrile at a flow rate of 5 ml/min (0-6 min 10% acetonitrile, 6.01 min 30% acetonitrile, 6.01→40 min 30%→80% acetonitrile) The product fraction was diluted with 50 ml water, prior to passage over a preconditioned (5 ml acetonitrile followed by 15 ml H_2O) tc18 plus SepPak cartridge (Waters). The cartridge was eluted with 1.5 ml ethanol, and the ethanolic solution was diluted with saline to < 10% EtOH for in vivo experiments. The products were further diluted with physiological saline to a activity concentration of ~370 MBq/ml for iv administration. pH was between 5 and 7 for all formulations and osmolarity was within physiological range (300-500 mmol/kg). ^{18}F-species prepared by automated labeling matched HPLC retention times with authentic standards.

[^{18}F]**2:** 246.4 GBq ^{18}F fluoride, 12.2 mg (33 µmol) **17** in a mixture of 200 µl thexyl alcohol and 300 µl anhydrous acetonitrile yielded 8.88 GBq [^{18}F]**2** (6.3% decay corrected), retention time on preparative HPLC: 29.0 min, radiochemical purity (analytical HPLC) = 95%. Specific activity (HPLC) = 99 GBq/µmol (see ESI for determination of SA).

[^{18}F]**3:** 181.3 GBq ^{18}F fluoride, 12.0 mg (31.2 µmol) **18** in a mixture of 300 µl thexyl alcohol and 300 µl anhydrous acetonitrile yielded 9.99 GBq [^{18}F]**3** (9.5% decay corrected), radiochemical purity (analytical HPLC) = 98.3%

[^{18}F]**5:** 233.2 GBq ^{18}F fluoride, 11.7 mg (25.4 µmol) **20** in a mixture of 200 µl thexyl alcohol and 300 µl anhydrous acetonitrile yielded 6.98 GBq [^{18}F]**5** (4.9% decay corrected), retention time on preparative HPLC: 28.1 min, radiochemical purity (analytical HPLC) = 94.4%

[^{18}F]**6:** 218.3 GBq ^{18}F fluoride, 11.0 mg (26.4 µmol) **21** in a mixture of 200 µl thexyl alcohol and 300 µl anhydrous acetonitrile yielded 11.5 GBq [^{18}F]**6** (8.6% decay corrected), retention time on preparative HPLC: 32.6 min, radiochemical purity (analytical HPLC) = 95.4% Specific activity (HPLC) = 229.5 GBq/µmol (see ESI for determination of SA).

Preparation of [^{18}F]7

5.3 GBq [^{18}F]**6** in 1.5 ml EtOH as obtained by automated labelling was evaporated to dryness on the rotary evaporator (40°C, 20 mbar) in a 8 ml vial. The residue was treated with 0.5 ml of an ice cold solution of dimethyldioxirane (DMDO) in acetone (~40 mM). After 60 seconds reaction time volatiles were removed on the rotary evaporator. The residue was re-dissolved in 2.5 ml DMSO:water = 1:1 (v/v) and injected into the preparative HPLC system described at the section automated labelling. 2.36 GBq [^{18}F]**7** (56% decay corrected yield) eluted with a retention time of 23.1 min. The product containing fraction was evaporated to dryness on the rotary evaporator and formulated in 0.9% saline to obtain a product ready for iv administration. Radiochemical purity (analytical HPLC) = 93.0%, specific activity (HPLC) = 56.2 GBq/µmol (see ESI for determination of SA). HPLC retention time of [^{18}F]**7** matched with the retention time of authentic standard.

PET/MR Imaging – Biodistribution study

Mice underwent PET scanning on a dual animal bed in a dedicated small-animal PET scanner (n=2 for [^{18}F]**2**, [^{18}F]**3**, [^{18}F]**5,** [^{18}F]**6** and [^{18}F]**7** and one mouse per test substance (except [^{18}F]**7)** underwent sequential PET/MRI on two stand-alone scanners. Prior imaging, mice were pre-anesthetized in an induction chamber using isoflurane (2.5% in oxygen), placed in prone position on a heated animal bed (38°C) and the lateral tail vein was cannulated using a custom made tail vein catheter. Animal respiratory rate and body temperature were constantly monitored (SA Instruments Inc, Stony Brook, NY, USA) and the isoflurane level was adjusted (1.5-2.5% on oxygen) to achieve a constant depth of anesthesia. Anesthesia was maintained for the whole imaging period. A humidifier was used to moisten the gas mixture before supplying it to the animal(s). For anatomical magnetic resonance imaging (MRI) a single mouse body bed mounted with a mouse whole body RF coil was used. The whole body coil covers an axial field of view (FOV) of about 8 cm that is very similar to the axial FOV of the PET scanner (7.6 cm). Images were acquired on a 1 Tesla benchtop MRI (ICON, Bruker Biospin GmbH, Ettlingen, Germany) using a modified 3D T_1-weighted gradient echo sequence (T1-FLASH) with the following imaging parameters: echo time (TE) = 4.7 ms; repetition time (TR) = 25 ms; flip angle (FA) = 25 °; field of view (FOV) = 7.6 x 2.6 x 2.4 cm; matrix = 253 x 93; 32 slices; slice thickness = 750 µm; 5 repetitions; total imaging time = 6 min 15 sec. After MRI, the animal bed was transferred into the gantry of a microPET scanner (Focus 220, Siemens Medical Solutions, Knoxville, TN, USA). Total anesthesia time prior start of PET scanning for mice that underwent PET scanning only was similar to that of the PET/MRI examined animals. Direct after positioning of the animal bed in the gantry of the PET scanner a 10 min transmission scan using a rotating ^{57}Co point source was recorded. Simultaneously with intravenous injection of 6.8 ± 3.4 MBq [^{18}F]-**2**, 4.2 ± 1.9 MBq [^{18}F]-**3**, 10.8 ± 0.3 MBq [^{18}F]-**5,** 13.1 ± 8.6 MBq [^{18}F]-**6** or 34.2 ± 7.0 MBq [^{18}F]-**7** dynamic PET imaging was initiated for 120 min using an energy window of 250-750 keV and a timing window of 6 ns. After completion of the imaging procedure, a terminal blood sample was withdrawn under isoflurane anesthesia from the retro-orbital sinus vein and the animals were sacrificed by cervical dislocation. Blood was centrifuged (17000 *g*, 4°C, 4 min) to obtain plasma, and organ samples as well as urine were collected. Aliquots of blood, plasma and urine as well as organ samples were transferred into pre-weighted tubes and measured for radioactivity in a gamma counter (Wizard 1470, Perkin-Elmer, Wellesley, MA, USA). The measured radioactivity data were corrected for radioactive decay and expressed as standardized uptake value ((radioactivity per g/injected radioactivity) x body weight). The 60 min dynamic emission PET data were sorted into 26 frames, which incrementally increased in time length from 5 seconds to 10 min. Images were reconstructed using Fourier rebinning of the 3D sinograms followed by two-dimensional filtered back projection with a ramp filter, resulting in an image voxel size of 0.4 x 0.4 x 0.796 mm^3. A standard data correction protocol (normalization, attenuation and decay correction) was applied to the PET data. The PET units were converted into units of radioactivity concentration by applying a calibration factor derived from imaging of a cylindrical phantom with a known ^{18}F-radioactivity concentration. Corresponding PET/MRI images were aligned using a pre-calculated, fixed transformation matrix. Using the image analysis software Amide, different volumes of interest (brain, liver, kidneys, urinary bladder, heart, bone (left humerus), muscle (right forearm muscle)), lung, stomach were manually outlined on multiple planes and time-radioactivity concentration curves (TACs), expressed in standardized uptake values, were derived.

Analysis of murine metabolites

Blood and urine samples harvested directly after imaging experiments (120 min post administration) were used for metabolity studies. Murine plasma was obtained by centrifugation (17000 *g*, 4°C, 4 min), and plasma proteins were precipitated by addition of a equal volume acetonitrile and centrifuged (17000 *g*, 4°C, 1 min). Urine was also diluted with acetonitrile (1:10 v/v) and briefly centrifuged. Supernatant solutions were spotted on silica TLC plates, and eluted using an appropriate solvent mixture (0-5% MeOH in DCM). For Details of used mobile phase and developed TLC plates see section 1 of the supporting information. The diluted test substances were spotted as reference materials. Three mice dosed with [^{18}F]**7** were sacrificed 60 min post tracer administration. Aliquots of blood, plasma and urine as well as organ samples were transferred into pre-weighted tubes and measured for radioactivity in a gamma counter (Wizard 1470, Perkin-Elmer, Wellesley, MA, USA). The measured radioactivity data were corrected for radioactive decay and expressed as standardized uptake value ((radioactivity per g/injected radioactivity) x body weight). Plasma and urine was prepared for TLC analysis as described above. The brain was homogenized with 300 µL acetonitrile using a IKA T10 basic Ultra-turrax (IKA Laboratory Equipment, Staufen, Germany). The same procedure was applied to the liver using 1500 µL acetonitrile. Bile was diluted 1: 10 (v/v) with acetonitrile. All samples were briefly centrifuged and the supernatants were spotted on silica TLC plates that were eluted with 5% MeOH in DCM. Radioactivity distribution on TLC plates was visualized using the procedure described in the materials and methods section.

References

(1) Denk, C., Svatunek, D., Filip, T., Wanek, T., Lumpi, D., Fröhlich, J., Kuntner, C., and Mikula, H. (2014) Development of a (18) F-Labeled Tetrazine with Favorable Pharmacokinetics for Bioorthogonal PET Imaging. *Angew. Chem. Int. Ed. Engl.* 1–6.

(2) Knight, J. C., and Cornelissen, B. (2014) Bioorthogonal chemistry: implications for pretargeted nuclear (PET/SPECT) imaging and therapy. *Am. J. Nucl. Med. Mol. Imaging 4*, 96–113.

(3) Patterson, D. M., Nazarova, L. A., and Prescher, J. A. (2014) Finding the right (bioorthogonal) chemistry. *ACS Chem. Biol. 9*, 592–605.

(4) Meyer, J. P., Houghton, J. L., Kozlowski, P., Abdel-Atti, D., Reiner, T., Pillarsetty, N. V. K., Scholz, W. W., Zeglis, B. M., and Lewis, J. S. (2016) 18F-Based Pretargeted PET Imaging Based on Bioorthogonal Diels-Alder Click Chemistry. *Bioconjug. Chem. 27*, 298–301.

(5) Zeglis, B. M., Sevak, K. K., Reiner, T., Mohindra, P., Carlin, S. D., Zanzonico, P., Weissleder, R., and Lewis, J. S. (2013) A Pretargeted PET Imaging Strategy Based on Bioorthogonal Diels – Alder Click Chemistry. *J. Nucl. Med.* 1389–1396.

(6) Rossin, R., and Robillard, M. S. (2014) Pretargeted imaging using bioorthogonal chemistry in mice. *Curr. Opin. Chem. Biol. 21*, 161–169.

(7) Rossin, R., Verkerk, P. R., Van Den Bosch, S. M., Vulders, R. C. M., Verel, I., Lub, J., and Robillard, M. S. (2010) In vivo chemistry for pretargeted tumor imaging in live mice. *Angew. Chemie - Int. Ed. 49*, 3375–3378.

(8) Darko, A., Wallace, S., Dmitrenko, O., Machovina, M. M., Mehl, R. A., Chin, J. W., and Fox, J. M. (2014) Conformationally Strained trans-Cyclooctene with Improved Stability and Excellent Reactivity in Tetrazine Ligation. *Chem. Sci. 5*, 3770–3776.

(9) Blackman, M. L., Royzen, M., and Fox, J. M. (2008) Tetrazine Ligation: Fast Bioconjugation Based on Inverse-Electron-Demand Diels−Alder Reactivity. *J. Am. Chem. Soc. 130*, 13518–13519.

(10) Devaraj, N. K., Weissleder, R., and Hilderbrand, S. a. (2008) Tetrazine-Based Cycloadditions : Application to Pretargeted Live Cell Imaging Tetrazine-Based Cycloadditions : Application to Pretargeted Live Cell Imaging. *Communications 19*, 2297–2299.

(11) Yang, J., Šečkute, J., Cole, C. M., and Devaraj, N. K. (2012) Live-cell imaging of cyclopropene tags with fluorogenic tetrazine cycloadditions. *Angew. Chemie - Int. Ed.*

(12) Royzen, M., Yap, G. P. A., and Fox, J. M. A Photochemical Approach to Functionalized trans - Cyclooctenes Driven by Metal Complexation 1–30.

(13) Taylor, M. T., Blackman, M. L., Dmitrenko, O., Fox, J. M., and Ligation, T. (2011) Design and Synthesis of Highly Reactive Dienophiles for the. *J. Am. Chem. Soc. 133*, 9646–9649.

(14) Yang, J., Karver, M. R., Li, W., Sahu, S., and Devaraj, N. K. (2012) Metal-catalyzed one-pot synthesis of tetrazines directly from aliphatic nitriles and hydrazine. *Angew. Chemie - Int. Ed. 51*, 5222–5225.

(15) Hu, W.-X., and Xu, F. (2008) Synthesis, structures of some unsymmetrical 3,6-disubstituted-1,2,4,5-tetrazines. *J. Heterocycl. Chem. 45*, 1745–1750.

(16) Wyffels, L., Thomae, D., Waldron, A. M., Fissers, J., Dedeurwaerdere, S., Van der Veken, P., Joossens, J., Stroobants, S., Augustyns, K., and Staelens, S. (2014) In vivo evaluation of 18F-labeled TCO for pre-targeted PET imaging in the brain. *Nucl. Med. Biol. 41*, 513–523.

(17) Li, Z., Cai, H., Hassink, M., Blackman, M. L., Brown, R. C. D., Conti, P. S., and Fox, J. M. (2010) Tetrazine-trans-cyclooctene ligation for the rapid construction of 18F labeled probes. *Chem. Commun. (Camb). 46*, 8043–5.

(18) Kumar, A., Hao, G., Liu, L., Ramezani, S., Hsieh, J. T., Öz, O. K., and Sun, X. (2015) Click-chemistry strategy for labeling antibodies with copper-64 via a cross-bridged tetraazamacrocyclic chelator scaffold. *Bioconjug. Chem. 26*, 782–789.

(19) Herth, M. M., Andersen, V. L., Lehel, S., Madsen, J., Knudsen, G. M., Kristensen, J. L., and Herth, M. M. (2013) Development of a (11)C-labeled tetrazine for rapid tetrazine-trans-cyclooctene ligation. *Chem. Commun. (Camb). 49*, 3805–7.

(20) Keinänen, O., Li, X. G., Chenna, N. K., Lumen, D., Ott, J., Molthoff, C. F. M., Sarparanta, M., Helariutta, K., Vuorinen, T., Windhorst, A. D., and Airaksinen, A. J. (2016) A New Highly Reactive and Low Lipophilicity Fluorine-18 Labeled Tetrazine Derivative for Pretargeted PET Imaging. *ACS Med. Chem. Lett. 7*, 62–66.

(21) Rashidian, M., Keliher, E. J., Dougan, M., Juras, P. K., Cavallari, M., Wojtkiewicz, G. R., Jacobsen, J. T., Edens, J. G., Tas, J. M. J., Victora, G., Weissleder, R., and Ploegh, H. L. (2015) Use of 18F-2-Fluorodeoxyglucose to Label Antibody Fragments for Immuno-Positron Emission Tomography of Pancreatic Cancer. *ACS Cent. Sci.* 150603073029009.

(22) Cott, W. J., Howell, C., and White, W. (1948) Toxic Fluorine Compounds. V. w-Fluoronitriles and w-Fluoro-w ’-nitroalkanes *3604*, 3484–3487.

(23) HOFFMANN, F. W. (1949) ALIPHATIC FLUORIDES. I. ι,ι’-DIFLUOROALKANES. *J. Org. Chem. 14*, 105–110.

(24) Hanson, P., Hendrickx, R. a a J., and Lindsay Smith, J. R. (2008) Kinetic studies on the oxidation of aryl methyl sulfides and sulfoxides by dimethyldioxirane; absolute rate constants and activation parameters for 4-nitrophenyl methyl sulfide and sulfoxide. *Org. Biomol. Chem. 6*, 762–71.

(25) Lee, S. J., Oh, S. J., Chi, D. Y., Lee, B. S., Ryu, J. S., and Moon, D. H. (2008) Comparison of synthesis yields of 3’-deoxy-3’-[18F]fluorothymidine by nucleophilic fluorination in various alcohol solvents. *J.*

Label. Compd. Radiopharm. 51, 80–82.

(26) Kim, D. W., Jeong, H. J., Lim, S. T., and Sohn, M. H. (2010) Recent trends in the nucleophilic [18F]-radiolabeling method with no-carrier-added [18F]fluoride. *Nucl. Med. Mol. Imaging (2010). 44*, 25–32.

(27) Williams, K. I. H., Burstein, S. H., and Layne, D. S. (1966) Metabolism of dimethyl sulfide, dimethyl sulfoxide, and dimethyl sulfone in the rabbit. *Arch. Biochem. Biophys. 117*, 84–87.

(28) (2009) So long sulphur. *Nat. Chem. 1*, 333–333.

(29) Angus, P. W., Mihaly, G. W., Morgan, D. J., and Smallwood, R. A. (1989) Oxygen dependence of omeprazole clearance and sulfone and sulfide metabolite formation in the isolated perfused rat liver. *J. Pharmacol. Exp. Ther. 250*, 1043–7.

(30) Mikula, H., Svatunek, D., Lumpi, D., Glöcklhofer, F., Hametner, C., and Fröhlich, J. (2013) Practical and Efficient Large-Scale Preparation of Dimethyldioxirane. *Org. Process Res. Dev. 17*, 313–316.

(31) Royzen, M., Yap, G. P. A., and Fox, J. M. (2008) A photochemical synthesis of functionalized trans-cyclooctenes driven by metal complexation. *J. Am. Chem. Soc. 130*, 3760–3761.

(32) Nachbaur, E., and Leiseder, G. (1971) Ueber eine einfache und gefahrlose Methode zur Darstellung von wasserfreiem Hydrazin. *Monatshefte fuer Chemie 102*, 1718–1723.

Manuscript #6

Christoph Denk, Dennis Svatunek, Severin Mairinger, Johann Stanek, Thomas Filip, Dominik Matscheko, Claudia Kuntner, Thomas Wanek, Hannes Mikula*; Design, Synthesis, and Evaluation of a Low-Molecular-Weight ^{11}C-Labeled Tetrazine for Pretargeted PET Imaging Applying Bioorthogonal *in Vivo* Click Chemistry, *Bioconjugate Chem.* **2016**, 27, 1707-1712.

(with permission from American Chemical Society. Copyright 2016 American Chemical Society)

Bioconjugate Chemistry

Article

pubs.acs.org/bc

Design, Synthesis, and Evaluation of a Low-Molecular-Weight ^{11}C-Labeled Tetrazine for Pretargeted PET Imaging Applying Bioorthogonal in Vivo Click Chemistry

Christoph Denk,[†] Dennis Svatunek,[†] Severin Mairinger,[‡] Johann Stanek,[‡] Thomas Filip,[‡] Dominik Matscheko,[†] Claudia Kuntner,[‡] Thomas Wanek,[‡] and Hannes Mikula*[,†]

[†]Institute of Applied Synthetic Chemistry, Vienna University of Technology, 1040 Wien, Austria

[‡]Health and Environment Department, Biomedical Systems, Austrian Institute of Technology, 2444 Seibersdorf, Austria

Supporting Information

ABSTRACT: A low-molecular-weight tetrazine labeled with the short-lived positron emitter carbon-11 was developed as a bioorthogonal PET probe for pretargeted imaging. A method for efficient and fast synthesis of this imaging agent is presented using radiolabeling of a readily available precursor. High reactivity with *trans*-cyclooctenes was observed and in vivo investigations including PET/MR scanning showed homogeneous biodistribution, good metabolic stability, and rapid excretion in naive mice. These properties are key to the success of bioorthogonal ^{11}C-PET imaging, which has been shown in a simple pretargeting experiment using TCO-modified mesoporous silica nanoparticles. Overall, this ^{11}C-labeled tetrazine represents a highly versatile and advantageous chemical tool for bioorthogonal PET imaging and enables pretargeting approaches using carbon-11 for the first time.

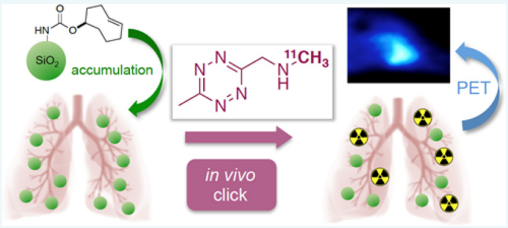

INTRODUCTION

Bioorthogonal ligations have emerged in recent years as versatile and efficient chemical tools for forming covalent linkages within highly complex environments such as living organisms. In 2004, Bertozzi and co-workers were first to use the catalyst-free strain-promoted alkyne azide cycloaddition (SPAAC) for two-step glycome imaging in live developing zebrafish and introduced the concept of bioorthogonality.[1−3] In such pretargeting approaches, a chemical reporter bearing a bioorthogonal reactive group (tag) is administered, allowed to accumulate, and (after clearance of unbound material) visualized using a labeled secondary agent that selectively reacts with the tag (in vivo chemistry).[4] This method has gained interest, especially in nuclear medicine wherein the short half-life of commonly used PET radioisotopes (^{18}F: 109.8 min, ^{11}C: 20.4 min) restricts their application for imaging of slow accumulation processes. Even though longer-lived PET isotopes (^{64}Cu: 12.7 h, ^{89}Zr: 78.4 h, ^{124}I: 100.2 h) can be used and applied for the development of slowly accumulating imaging agents (e.g., antibodies), their limited availability, high cost, and, most importantly, the resulting prolonged radiation exposure pose serious limitations.[5]

The very low concentrations of radiolabeled agents in vivo require rapid bioorthogonal click reaction to achieve effective ligation within a short time period. Even though the SPAAC ligation has recently been successfully applied for pretargeted PET imaging, second-order reaction rates of less than 5 M^{-1} s^{-1} (MeCN, 20 °C) are still a drawback, which limits further applications of this strategy.[6] Several other bioorthogonal reactions have been reported recently, of which the inverse electron demand Diels−Alder reaction (IEDDA) of 1,2,4,5-tetrazines (Tz) and strained alkene dienophiles such as *trans*-cyclooctenes (TCO) has superior kinetics with rate constants of up to 3.3 × 10^6 M^{-1} s^{-1} (water, 25 °C).[7−12] Alongside applications in live cell imaging, protein labeling, and rapid construction of PET probes, the tetrazine ligation has successfully been applied by Rossin, Robillard, and co-workers in a SPECT pretargeting study using a ^{177}Lu labeled Tz and a TCO−CC49 antibody leading to images with outstanding tumor-to-background ratios.[7,13−15] Even though still synthetically challenging, the metal-catalyzed tetrazine synthesis reported by Yang et al. made unsymmetrical 1,2,4,5-tetrazines accessible, and the flow photoisomerization process reported by Fox and co-workers gave rise to a straightforward preparation of *trans*-cyclooctenes.[16,17] Several tetrazine and TCO derivatives were developed to fine-tune the reactivity and stability of the reactants, and different modes of attachment of IEDDA tags to biomolecules were investigated to optimize bioorthogonal reactivity.[4,11,18−21] The use of radiolabeled Tz is believed to be advantageous over the use of radiolabeled TCO derivatives since the latter were shown to quickly metabolize when applied in tracer amounts.[5]

The first radiolabeled Tz were metal chelator bearing compounds labeled with long-lived radiometals such as ^{64}Cu, ^{177}Lu, and ^{111}In.[15,22,23] However, to take full advantage of the pretargeting approach, radiotetrazines with short-lived emitters

Received: May 10, 2016
Revised: June 15, 2016
Published: June 16, 2016

ACS Publications © 2016 American Chemical Society

DOI: 10.1021/acs.bioconjchem.6b00234
Bioconjugate Chem. 2016, 27, 1707−1712

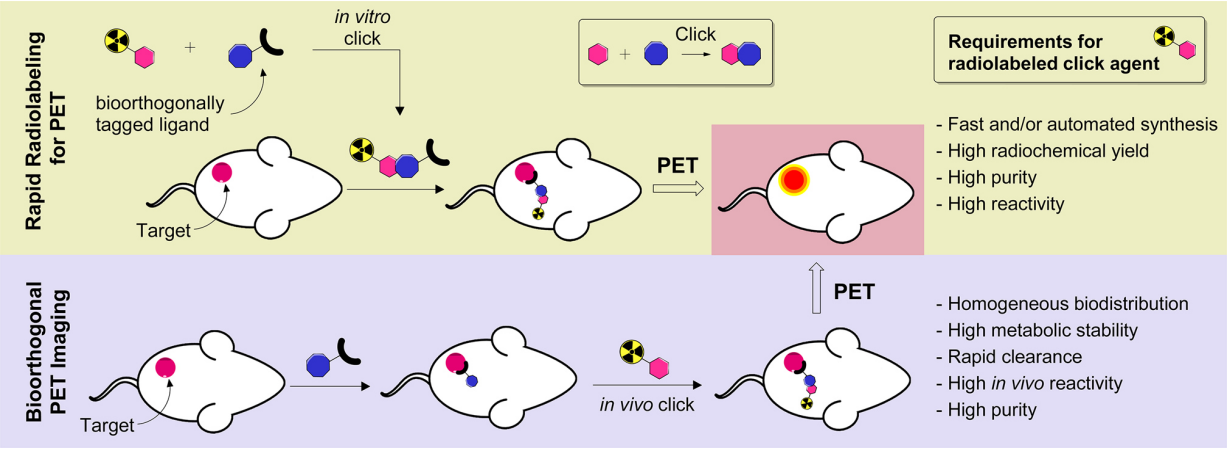

Figure 1. Two main applications of bioorthogonal ligations in the field of PET imaging: Rapid radiolabeling using in vitro click chemistry before administration (top); bioorthogonal PET imaging applying in vivo chemistry (bottom).

are beneficial due to reduced radiation dose delivered to the patient. ^{18}F was first used for in vivo click reactions in combination with dextrans.[24] This approach has recently been extended to ^{68}Ga-PET imaging.[25]

In 2014, we reported the development of the first fluorine-18 labeled low-molecular-weight Tz by bypassing the previously reported instability of tetrazines under fluorination conditions using a less reactive dialkyl-tetrazine scaffold that nonetheless possesses sufficient IEDDA reactivity for fast in vivo click chemistry.[26] This probe showed homogeneous biodistribution, rapid clearance, and high stability, thus fulfilling the requirements for in vivo click applications. However, due to the low radiochemical yield, this ^{18}F-Tz is not suitable for in vitro radiolabeling applications prior to administration and subsequent imaging. Recently, Zhu et al. and Rashidian et al. reported optimized procedures for the synthesis of ^{18}F-tetrazines enabling rapid radiolabeling,[27,28] but did not include any in vivo or stability data. Carbon-11 labeled Tz offer additional benefits such as a short half-life of 20.4 min and a high specific activity that potentially allows for pretargeting experiments at multiple time points, since each dosing of ^{11}C-Tz is likely to consume only a small fraction of available dienophile-tags. In addition, carbon-11 is produced from ^{14}N (99.6% abundance), thus reducing production costs, although an on-site cyclotron is required (due to the short half-life), limiting the application of ^{11}C-labeled compounds in general. The first carbon-11 tetrazine was reported by Herth et al. in 2013, but no in vivo, biodistribution, or stability data is available.[29] Moreover, the chemical structure of this ^{11}C-Tz, which consists of four aryl rings, is likely to limit water solubility and facilitate plasma protein binding and hepatic metabolization.

In addition to sufficient reaction rates, radiotetrazines intended to be used as in vivo imaging agents need to exhibit homogeneous biodistribution, metabolic stability, and fast excretion kinetics, which is exceptionally important for image contrast with short-lived isotopes such as ^{11}C. Overall, only a few radiolabeled tetrazines have been reported so far,[22,23,26−31] most are applicable to either in vitro or in vivo studies, whereas a multifunctional tool applicable to both principal uses of bioorthogonal ligations in the field of PET imaging (Figure 1) would be highly beneficial. Furthermore, to the best of our knowledge, not a single successful pretargeting approach has been reported so far using a small-molecule tetrazine that has been labeled with a covalently attached radionuclide (neither ^{18}F nor ^{11}C). Moreover, pretargeting has been impossible so far in the field of carbon-11 PET imaging in general due to the lack of a method that allows for fast in vivo labeling of a preadministered and accumulated compound. Consequently, we focused on the development of a low-molecular-weight ^{11}C-tetrazine with emphasis on favorable pharmacokinetic properties (homogeneous biodistribution, high stability, and fast clearance) for bioorthogonal PET imaging.

RESULTS AND DISCUSSION

Due to the in vivo properties of the previously described ^{18}F-dialkyltetrazine, we hypothesized that a ^{11}C-labeled compound with a similar structure is likely to be useful as a bioorthogonal PET probe. Hence, we aimed to keep the molecular weight of the compound to a minimum to facilitate fast pharmacokinetics. Furthermore, an NH_2 group was selected as nucleophilic labeling site for straightforward introduction of carbon-11 via ^{11}C-methylation. Thus, tetrazines **1** and **2** were considered (Table 1). Reactivity was estimated by computational methods (M06-2X/6-31G(d,p), 1,4-dioxane, Gaussian 09)[32] and compared to the ^{18}F-Tz **3** for which rapid in vivo ligation has already been demonstrated.[26] Free energies of activation ($\Delta G^{\ddagger}$) of the IEDDA-initiated reaction between the above-mentioned tetrazines and the dienophiles TCO (**4**) and s-TCO (**5**) were calculated and differences ($\Delta\Delta G^{\ddagger}$) were used to estimate reaction rates relative to those of **3**+**4** and **3**+**5** (Table 1). **1** was predicted to exhibit reactivity comparable to **3** (relative rates of 1.32−1.36) whereas **2** was predicted to show only low reactivity (relative rates of 0.00009−0.0006). Based on these considerations Tz **1** was selected for further investigations.

Metal-catalyzed tetrazine synthesis starting from Boc-protected *N*-methylaminoacetonitrile (**8**) followed by deprotection afforded Tz **1** (Figure 2A).[17] Rate constants and free activation energies obtained by stopped-flow measurements were in good agreement with calculated values. The water-soluble TCO derivatives **6** (using major TCO, i.e., equatorial substitution at C6 of the TCO moiety) and **7** (s-TCO) have been used for measurements in PBS showing rates of 175.4 M^{-1} s^{-1} and more than 40 000 M^{-1} s^{-1}, respectively, in the IEDDA reaction with tetrazine **1** (Table 1). Furthermore, good plasma stability was observed by absorbance measure-

DOI: 10.1021/acs.bioconjchem.6b00234
Bioconjugate Chem. 2016, 27, 1707−1712

Table 1. Reaction Kinetics of IEDDA Cycloadditions Obtained by Computational Methods (M06-2X/6-31G(d,p), 1,4-Dioxane (CPCM), Gaussian 09), and Stopped-Flow Measurements

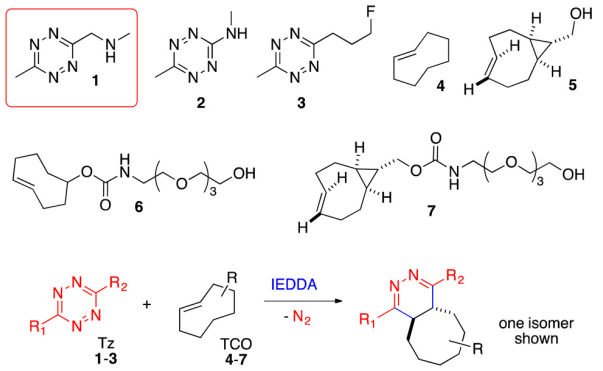

reaction	k_2 [M^{-1} s^{-1}]	calculated relative rate	relative rate
1 + **4**	1.04 ± 0.03[a]	1.32[c]	0.70[c]
2 + **4**	n.d.	0.00009[c]	n.d.
3 + **4**[26]	1.49 ± 0.01[a]	1.00[c]	1.00[c]
1 + **5**	89.5 ± 1.1[a]	1.36[d]	1.05[d]
2 + **5**	n.d.	0.0006[d]	n.d.
3 + **5**[26]	85.5 ± 2.3[a]	1.00[d]	1.00[d]
1 + **6**	175.4 ± 1.2[b]	n.d.	118[c]
1 + **7**	42 500 ± 3100[b]	n.d.	497[d]

[a]Measured in 1,4-dioxane at 37 °C. [b]Measured in PBS at 37 °C. [c]Relative to the reaction between **3** and **4**. [d]Relative to the reaction between **3** and **5**. n.d. = not determined.

ments and chromatography after incubation in human blood plasma at 37 °C (see Supporting Information, Figure S6). Although stable for at least 2 months at −20 °C, tetrazines **1** and desmethyl precursor **11**, which is accessible by deprotection of previously reported **10** (Figure 2B),[17] tend to slowly degrade and should be kept as Boc-protected compounds **9** and **10** if prolonged storage is intended. Alternatively, we have also prepared the trifluoroacetate salts of tetrazines **1** and **11** that show significantly improved stability.

Radiolabeling of **11** was successfully carried out using the [^{11}C]-CH_3OTf route on a GE Tracerlab FXC Pro synthesis module to obtain [^{11}C]-**1** in radiochemical purities exceeding 95% and in a decay-corrected radiochemical yield of 52 ± 6%, based on trapped [^{11}C]CH_3OTf (Figure 2C). The overall synthesis time was 30 min including purification by cation exchange chromatography. Hence, significant improvements in both radiochemical yield (52% vs 33%) and synthesis time (30 min vs 50−60 min) were obtained compared to the previously reported ^{11}C-labeled Tz.[29] The identity and radiochemical purity of [^{11}C]-**1** was verified by coelution with reference substance **1** (SCX-HPLC, Figure 2D). [^{11}C]-**1** readily reacted with s-TCO (**5**) to give conjugate [^{11}C]-**12** that slowly isomerized to the thermodynamically favored tautomer [^{11}C]-**13** (both products as a mixture of regio- and stereoisomers) as shown by radio-TLC (Figure 2E).

In vivo biodistribution of [^{11}C]-**1** was investigated by intravenous administration into female BALB/c mice (n = 3) and subsequent dynamic PET/MR scanning for 60 min (Figure 3A). Regions of interest were drawn for main organs in acquired PET/MR data to determine tissue specific time-radioactivity concentration curves (Figure 3B). After initial perfusion (0−5 min), [^{11}C]-**1** exhibited rapid renal clearance, as

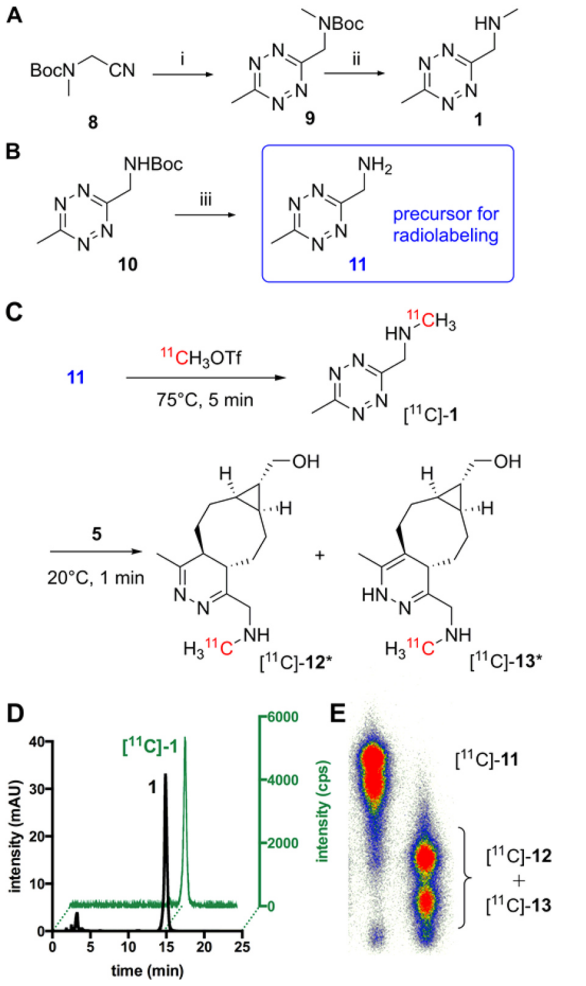

Figure 2. (A) Synthesis of tetrazine **1**: (i) MeCN, $NiCl_2$, NH_2NH_2, 42 °C, 18 h, then $NaNO_2$, aq. HCl, 20 °C, 20 min; (ii) TFA in DCM, 0 °C, 3 h. (B) Synthesis of precursor **11**: (iii) TFA in DCM, 20 °C, 26 h. (C) Radiosynthesis of [^{11}C]-**1** and further reaction with dienophile s-TCO (**5**); *only one isomer shown for [^{11}C]-**12** and [^{11}C]-**13**. (D) HPLC of **1** (UV/vis, 530 nm) and radio-HPLC of purified [^{11}C]-**1** (cps = counts per second). (E) Radio-TLC (10% MeOH and 1% NEt_3 in CH_2Cl_2) of [^{11}C]-**1** (left lane) and ligation products with s-TCO (**5**) (right lane).

indicated by a steep increase of radioactivity concentration to 96 ± 17 SUV (standardized uptake value) in the urinary bladder at 60 min, which is highly beneficial or even essential considering the short half-life of ^{11}C (20.4 min). All other organs analyzed displayed a very uniform uptake of 2−4 SUV, which slowly decreased to 0.6−2 SUV in the course of the imaging experiment (Figure 3A and B). It is noteworthy that the brain and medulla showed increased uptake, a good indicator for the ability of [^{11}C]-**1** to cross the blood brain barrier. Ex vivo biodistribution data (n = 3) was obtained 60 min post administration of [^{11}C]-**1** using a gamma counter showing uptake of 0.5−1.5 SUV in all analyzed organs, which is in good agreement with the last time frame of PET measurements (Figure 3C). In addition, in vivo stability and metabolism were investigated by radio-TLC analysis of plasma and urine samples that were taken after the imaging experiments (see Supporting Information, Figure S7). Due to the homogeneous biodistribution, high stability and low activity

DOI: 10.1021/acs.bioconjchem.6b00234
Bioconjugate Chem. 2016, 27, 1707−1712

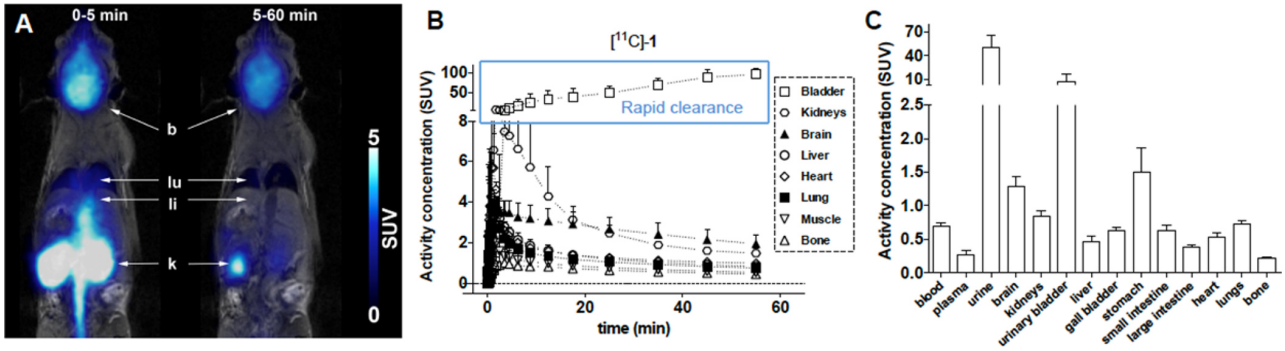

Figure 3. Biodistribution of [^{11}C]-**1**: (a) Combined coronal PET/MR images (b = brain, lu = lungs, li = liver, k = kidney). (b) Mean organ time vs activity curves in female BALB/c mice (n = 3) showing rapid clearance from the urinary bladder. (c) Ex vivo biodistribution data (obtained 60 min post administration of [^{11}C]-**1**).

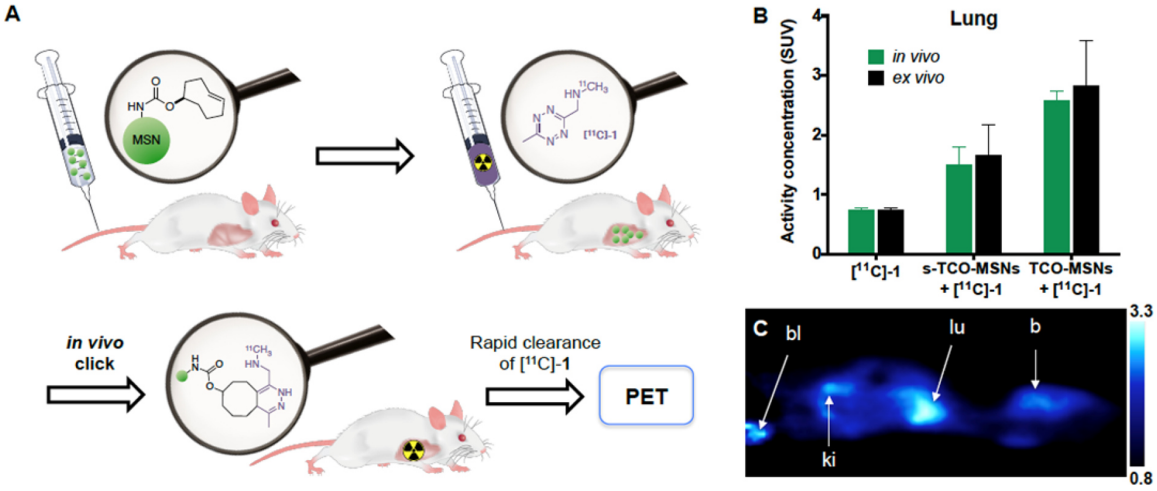

Figure 4. (A) In vivo click experiment using TCO- and s-TCO-modified silica nanoparticles (chemical structure shown for TCO). (B) Activity concentration measured in vivo by PET imaging (50−60 min) and ex vivo (after 60 min, gamma counter) showing increased lung uptake in female BALC/c mice when using s-TCO-MSNs (n = 5) and TCO-MSNs (n = 2). (C) Pretargeted PET image (sagittal view, 40−60 min): TCO-MSNs + [^{11}C]-**1** (scale bar unit: SUV; b = brain, bl = bladder, k = kidney, lu = lung).

concentrations after 60 min (beside excretion organs), any signal arising from in vivo conjugated [^{11}C]-**1** is expected to show good contrast, making this radiotetrazine a promising tool for pretargeted PET imaging.

Bioconjugation of [^{11}C]-**1** and the water-soluble dienophile **7** was performed in vivo to verify the bioorthogonal behavior of this novel click imaging agent. The s-TCO derivative **7** was administered to female BALB/c mice (n = 2) followed by [^{11}C]-**1** after an initial period of 5 min. Retroorbital blood was collected after 5 min and the click reaction was quenched. Murine plasma was obtained and analyzed using radio-TLC showing one major click product and an overall conversion of >98% after 5 min in vivo click reaction time (for details see Supporting Information, Figure S8).

To investigate the applicability of [^{11}C]-**1** for rapid radiolabeling and pretargeted PET imaging, mesoporous silica nanoparticles (MSNs) were prepared,[33] amino-functionalized,[34] and modified with TCO (major) and s-TCO, respectively. The reactive dienophile-loading was determined to be 115−120 μmol/g for both types of modified nanoparticles. s-TCO-MSNs were radiolabeled by fast click reaction with [^{11}C]-**1** (5 min reaction time) and administered to female BALB/c mice. In contrast to previously reported studies,[6,35] but also in accordance with recent findings,[36] we observed rapid and almost exclusive accumulation in the lung (see Supporting Information, Figure S9), most probably as a result of aggregation due to hydrophobic TCO surface modification. This behavior was further exploited to design a simple model for testing pretargeted carbon-11 PET imaging using [^{11}C]-**1**. MSNs labeled with TCO and s-TCO, respectively, were administered to female BALB/c mice in a first step. After sufficient time for accumulation of the MSNs in the lung (5 min, pretargeting step) [^{11}C]-**1** was injected and dynamic PET scanning was conducted. A significantly increased activity concentration in the lung was observed when using bioorthogonally labeled MSNs compared to biodistribution data of [^{11}C]-**1** as shown by PET imaging and ex vivo measurements (Figure 4). Notably, MSNs labeled with TCO (major) performed better than such labeled with the more reactive s-TCO tag. Although both modified MSNs were shown to be stable prior to imaging experiments with an almost identical dienophile-loading, we hypothesize that there is less uptake of [^{11}C]-**1** when using s-TCO-MSNs due to the lower stability of s-TCO under in vivo conditions. Nevertheless, these experiments clearly indicate the applicability of [^{11}C]-**1** for

DOI: 10.1021/acs.bioconjchem.6b00234
Bioconjugate Chem. 2016, 27, 1707−1712

pretargeted imaging using bioorthogonal in vivo click chemistry.

In summary, herein, we present the development of a carbon-11 labeled radiotetrazine as a secondary imaging agent for bioorthogonal PET applying in vivo click chemistry. The low-molecular-weight and water-soluble Tz **1** exihibits highly beneficial pharmacokinetic properties such as homogeneous biodistribution, rapid renal excretion, and sufficient metabolic stability strengthening the hypothesis that 3,6-dialkyltetrazines are well suited for the development of bioorthogonal tools for in vivo applications. Precursor **11** is readily accessible in two synthetic steps and can be efficiently labeled applying straightforward carbon-11 radiochemistry. The bioorthogonal behavior of [^{11}C]-**1** was demonstrated by selective in vivo click reaction with the water-soluble s-TCO derivative **7**. Furthermore, we were able to use [^{11}C]-**1** for rapid radiolabeling of silica nanoparticles that were shown by PET imaging to almost exclusively accumulate in the lung. Based on these results a pretargeting experiment was carried out showing that accumulated TCO-modified silica nanoparticles can be visualized by PET after in vivo click reaction with [^{11}C]-**1**. To the best of our knowledge, this represents the first reported example of pretargeted ^{11}C-PET imaging. Nevertheless, there is still a need for radiolabeled tetrazines with higher reactivity and sufficient stability to enable in vivo click at less accessible sites (compared to lung-localized nanoparticles), e.g., tumor-receptor bound antibody−TCO conjugates.

■ ASSOCIATED CONTENT

Supporting Information

The Supporting Information is available free of charge on the ACS Publications website at DOI: 10.1021/acs.bioconjchem.6b00234.

Materials and methods; synthetic procedures and compound characterization data (incl. copies of NMR spectra); synthesis, modification and characterization of mesoporous silica nanoparticles; reaction kinetics; radiolabeling; quantum-chemical calculations (incl. Cartesian coordinates of all structures); in vitro plasma stability; in vivo investigations (PDF)

■ AUTHOR INFORMATION

Corresponding Author

*E-mail: hannes.mikula@tuwien.ac.at.

Notes

The authors declare no competing financial interest.

■ ACKNOWLEDGMENTS

Financial support from the Vienna Anniversary Foundation for Higher Education (H-2500/2012) is gratefully acknowledged. We thank Dr. Roland Müller (Seibersdorf Laboratories), Prof. Wolfgang Linert, Prof. Christian Edtmaier, and Elisabeth Eitenberger (all TU Wien) for their kind support of this work. Quantum-chemical calculations were performed using the Vienna Scientific Cluster (VSC).

■ REFERENCES

(1) Dehnert, K. W., Baskin, J. M., Laughlin, S. T., Beahm, B. J., Naidu, N. N., Amacher, S. L., and Bertozzi, C. R. (2012) Imaging the sialome during zebrafish development with copper-free click chemistry. *ChemBioChem 13*, 353−357.

(2) Agard, N. J., Prescher, J. A., and Bertozzi, C. R. (2004) A strain-promoted [3 + 2] azide-alkyne cycloaddition for covalent modification of biomolecules in living systems. *J. Am. Chem. Soc. 126*, 15046−15047.

(3) Prescher, J. A., Dube, D. H., and Bertozzi, C. R. (2004) Chemical remodelling of cell surfaces in living animals. *Nature 430*, 873−877.

(4) Rossin, R., van den Bosch, S. M., Ten Hoeve, W., Carvelli, M., Versteegen, R. M., Lub, J., and Robillard, M. S. (2013) Highly reactive trans-cyclooctene tags with improved stability for Diels-Alder chemistry in living systems. *Bioconjugate Chem. 24*, 1210−1217.

(5) Wyffels, L., Thomae, D., Waldron, A.-M., Fissers, J., Dedeurwaerdere, S., Van der Veken, P., Joossens, J., Stroobants, S., Augustyns, K., and Staelens, S. (2014) In vivo evaluation of ^{18}F-labeled TCO for pre-targeted PET imaging in the brain. *Nucl. Med. Biol. 41*, 513−523.

(6) Lee, S. B., Kim, H. L., Jeong, H.-J., Lim, S. T., Sohn, M.-H., and Kim, D. W. (2013) Mesoporous silica nanoparticle pretargeting for PET imaging based on a rapid bioorthogonal reaction in a living body. *Angew. Chem., Int. Ed. 52*, 10549−10552.

(7) Devaraj, N. K., Weissleder, R., and Hilderbrand, S. (2008) Tetrazine-based cycloadditions: application to pretargeted live cell imaging. *Bioconjugate Chem. 19*, 2297−2299.

(8) Sletten, E. M., and Bertozzi, C. R. (2011) A bioorthogonal quadricyclane ligation. *J. Am. Chem. Soc. 133*, 17570−17573.

(9) Stöckmann, H., Neves, A. A., Stairs, S., Brindle, K. M., and Leeper, F. J. (2011) Exploring isonitrile-based click chemistry for ligation with biomolecules. *Org. Biomol. Chem. 9*, 7303−7305.

(10) Ning, X., Temming, R. P., Dommerholt, J., Guo, J., Ania, D. B., Debets, M. F., Wolfert, M. A., Boons, G. J., and Van Delft, F. L. (2010) Protein modification by strain-promoted alkyne-nitrone cycloaddition. *Angew. Chem., Int. Ed. 49*, 3065−3068.

(11) Darko, A., Wallace, S., Dmitrenko, O., Machovina, M. M., Mehl, R. a., Chin, J. W., and Fox, J. M. (2014) Conformationally strained trans-cyclooctene with improved stability and excellent reactivity in tetrazine ligation. *Chem. Sci. 5*, 3770−3776.

(12) Blackman, M. L., Royzen, M., and Fox, J. M. (2008) Tetrazine ligation: fast bioconjugation based on inverse-electron-demand Diels-Alder reactivity. *J. Am. Chem. Soc. 130*, 13518−13519.

(13) Reiner, T., and Zeglis, B. M. (2014) The inverse electron demand Diels−Alder click reaction in radiochemistry. *J. Labelled Compd. Radiopharm. 57*, 285−290.

(14) Versteegen, R. M., Rossin, R., ten Hoeve, W., Janssen, H. M., and Robillard, M. S. (2013) Click to release: instantaneous doxorubicin elimination upon tetrazine ligation. *Angew. Chem., Int. Ed. 52*, 14112−14116.

(15) Rossin, R., Läppchen, T., van den Bosch, S. M., Laforest, R., and Robillard, M. S. (2013) Diels−Alder Reaction for Tumor Pretargeting: In Vivo Chemistry Can Boost Tumor Radiation Dose Compared with Directly Labeled Antibody. *J. Nucl. Med. 54*, 1989−1995.

(16) Royzen, M., Yap, G. P. a, and Fox, J. M. (2008) A photochemical synthesis of functionalized trans-cyclooctenes driven by metal complexation. *J. Am. Chem. Soc. 130*, 3760−3761.

(17) Yang, J., Karver, M. R., Li, W., Sahu, S., and Devaraj, N. K. (2012) Metal-Catalyzed One-Pot Synthesis of Tetrazines Directly from Aliphatic Nitriles and Hydrazine. *Angew. Chem., Int. Ed. 51*, 5222−5225.

(18) Taylor, M. T., Blackman, M. L., Dmitrenko, O., and Fox, J. M. (2011) Design and synthesis of highly reactive dienophiles for the tetrazine-trans-cyclooctene ligation. *J. Am. Chem. Soc. 133*, 9646−9649.

(19) Karver, M. R., Weissleder, R., and Hilderbrand, S. A. (2011) Synthesis and Evaluation of a Series of 1,2,4,5-Tetrazines for Bioorthogonal Conjugation. *Bioconjugate Chem. 22*, 2263−2270.

(20) Rossin, R., van Duijnhoven, S. M. J., Läppchen, T., van den Bosch, S. M., and Robillard, M. S. (2014) Trans-cyclooctene tag with improved properties for tumor pretargeting with the diels-alder reaction. *Mol. Pharmaceutics 11*, 3090−3096.

(21) Rahim, M. K., Kota, R., and Haun, J. B. (2015) Enhancing Reactivity for Bioorthogonal Pretargeting by Unmasking Antibody-Conjugated trans-Cyclooctenes. *Bioconjugate Chem. 26*, 352−360.

DOI: 10.1021/acs.bioconjchem.6b00234
Bioconjugate Chem. 2016, 27, 1707−1712

(22) Zeglis, B. M., Sevak, K. K., Reiner, T., Mohindra, P., Carlin, S. D., Zanzonico, P., Weissleder, R., and Lewis, J. S. (2013) A Pretargeted PET Imaging Strategy Based on Bioorthogonal Diels-Alder Click Chemistry. *J. Nucl. Med. 54*, 1389−1396.
(23) Rossin, R., Renart Verkerk, P., van den Bosch, S. M., Vulders, R. C. M., Verel, I., Lub, J., and Robillard, M. S. (2010) In Vivo Chemistry for Pretargeted Tumor Imaging in Live Mice. *Angew. Chem., Int. Ed. 49*, 3375−3378.
(24) Devaraj, N. K., Thurber, G. M., Keliher, E. J., Marinelli, B., and Weissleder, R. (2012) Reactive polymer enables efficient in vivo bioorthogonal chemistry. *Proc. Natl. Acad. Sci. U. S. A. 109*, 4762−4767.
(25) Nichols, B., Qin, Z., Yang, J., Vera, D. R., and Devaraj, N. K. (2014) ^{68}Ga chelating bioorthogonal tetrazine polymers for the multistep labeling of cancer biomarkers. *Chem. Commun. 50*, 5215−5217.
(26) Denk, C., Svatunek, D., Filip, T., Wanek, T., Lumpi, D., Fröhlich, J., Kuntner, C., and Mikula, H. (2014) Development of a ^{18}F-Labeled Tetrazine with Favorable Pharmacokinetics for Bioorthogonal PET Imaging. *Angew. Chem., Int. Ed. 53*, 9655−9659.
(27) Zhu, J., Li, S., Wängler, C., Wängler, B., Lennox, R. B., and Schirrmacher, R. (2015) Synthesis of 3-chloro-6-((4-(di-tert-butyl-[^{18}F]fluorosilyl)-benzyl)oxy)-1,2,4,5-tetrazine ([18F]SiFA-OTz) for Rapid Tetrazine-Based ^{18}F-Radiolabeling. *Chem. Commun. 51*, 12415−12418.
(28) Rashidian, M., Keliher, E. J., Dougan, M., Juras, P. K., Cavallari, M., Wojtkiewicz, G. R., Jacobsen, J. T., Edens, J. G., Tas, J. M. J., Victora, G., et al. (2015) Use of ^{18}F-2-Fluorodeoxyglucose to Label Antibody Fragments for Immuno-Positron Emission Tomography of Pancreatic Cancer. *ACS Cent. Sci. 1*, 142−147.
(29) Herth, M. M., Andersen, V. L., Lehel, S., Madsen, J., Knudsen, G. M., and Kristensen, J. L. (2013) Development of a (11)C-labeled tetrazine for rapid tetrazine-trans-cyclooctene ligation. *Chem. Commun. 49*, 3805−3807.
(30) Meyer, J. P., Houghton, J. L., Kozlowski, P., Abdel-Atti, D., Reiner, T., Pillarsetty, N. V. K., Scholz, W. W., Zeglis, B. M., and Lewis, J. S. (2016) ^{18}F-Based Pretargeted PET Imaging Based on Bioorthogonal Diels-Alder Click Chemistry. *Bioconjugate Chem. 27*, 298−301.
(31) Keinänen, O., Li, X. G., Chenna, N. K., Lumen, D., Ott, J., Molthoff, C. F. M., Sarparanta, M., Helariutta, K., Vuorinen, T., Windhorst, A. D., et al. (2016) A New Highly Reactive and Low Lipophilicity Fluorine-18 Labeled Tetrazine Derivative for Pretargeted PET Imaging. *ACS Med. Chem. Lett. 7*, 62−66.
(32) Liu, F., Liang, Y., and Houk, K. N. (2014) Theoretical elucidation of the origins of substituent and strain effects on the rates of Diels-Alder reactions of 1,2,4,5-tetrazines. *J. Am. Chem. Soc. 136*, 11483−11493.
(33) Ostafin, A., Nooney, R. I., Thirunavukkarasu, D., Chen, Y., Josephs, R., and Ostafin, A. E. (2002) Synthesis of Nanoscale Mesoporous Silica Spheres with Controlled Particle Size. *Chem. Mater. 14*, 4721−4728.
(34) Yokoi, T., Yoshitake, H., and Tatsumi, T. (2004) Synthesis of amino-functionalized MCM-41 via direct co-condensation and post-synthesis grafting methods using mono-, di- and tri-amino-organo-alkoxysilanes. *J. Mater. Chem. 14*, 951−957.
(35) Lu, J., Liong, M., Li, Z., Zink, J. I., and Tamanoi, F. (2010) Biocompatibility, biodistribution, and drug-delivery efficiency of mesoporous silica nanoparticles for cancer therapy in animals. *Small 6*, 1794−1805.
(36) Keinänen, O., Li, X.-G., Chenna, N. K., Lumen, D., Sarparanta, M., Helariutta, K., Vuorinen, T., and Airaksinen, A. J. (2015) Proceedings of the World Molecular Imaging Congress 2015, Honolulu, Hawaii. *Mol. Imaging Biol. 18* (Supplement 1), 1−1553.

DOI: 10.1021/acs.bioconjchem.6b00234
Bioconjugate Chem. 2016, 27, 1707−1712

Manuscript #7

Mengzhe Wang, Dennis Svatunek, Katarina Rohlfing, Yu Liu, Hui Wang, Ben Giglio, Hong Yuan, Zhanghong Wu, Zibo Li*, Joseph Fox*; Conformationally Strained *trans*-Cyclooctene (sTCO) Enables the Rapid Construction of ^{18}F-PET Probes via Tetrazine Ligation, *Theranostics* **2016**, 6, 887-895.

(with permission from Ivyspring Int. Publ.)

Theranostics 2016, Vol. 6, Issue 6 887

IVYSPRING INTERNATIONAL PUBLISHER

Theranostics

2016; 6(6): 887-895. doi: 10.7150/thno.14742

Research Paper

Conformationally Strained *trans*-Cyclooctene (sTCO) Enables the Rapid Construction of ^{18}F-PET Probes via Tetrazine Ligation

Mengzhe Wang[1], Dennis Svatunek[2,3], Katarina Rohlfing[2], Yu Liu[2], Hui Wang[1], Ben Giglio[1], Hong Yuan[1], Zhanghong Wu[1], Zibo Li[1]✉, and Joseph Fox[2]✉

1. Department of Radiology and Biomedical Research Imaging Center, University of North Carolina at Chapel Hill, Chapel Hill, North Carolina, 27599, United States.
2. Brown Laboratories, Department of Chemistry and Biochemistry, University of Delaware, Newark, Delaware 19716, United States.
3. Institute of Applied Synthetic Chemistry, TU Wien, Vienna, 1060, Austria.

✉ Corresponding authors: Zibo Li, PhD. Email: ziboli@med.unc.edu Phone: 919-962-5152 Fox, PhD. Email: jmfox@udel.edu Phone: 302-831-0191.

© Ivyspring International Publisher. Reproduction is permitted for personal, noncommercial use, provided that the article is in whole, unmodified, and properly cited. See http://ivyspring.com/terms for terms and conditions.

Received: 2015.12.17; Accepted: 2016.03.10; Published: 2016.04.12

Abstract

The bioorthogonal reaction between tetrazines and *trans*-cyclooctenes is a method for the rapid construction of F-18 probes for PET imaging. Described here is a second generation ^{18}F-labeling system based on a conformationally strained *trans*-cyclooctene (sTCO)—a dienophile that is approximately 2 orders of magnitude more reactive than conventional TCO dienophiles. Starting from a readily prepared tosylate precursor, an ^{18}F labeled sTCO derivative (^{18}F-sTCO) could be synthesized in 29.3 +/- 5.1% isolated yield and with high specific activity. Tetrazine ligation was carried out with a cyclic RGD-conjugate of a diphenyl-s-tetrazine analogue (RGD-Tz) chosen from a diene class with an excellent combination of fast reactivity and stability both for the diene as well as the Diels-Alder adduct. For both the tetrazine and the sTCO, mini-PEG spacers were included to enhance solubility and improve the *in vivo* distribution profile of the resulting probe. Extremely fast reactivity (up to 2.86 x 10^5 $M^{-1}s^{-1}$ at 25 °C in water) has been observed in kinetic studies in the reaction of sTCO with diphenyl-s-tetrazine derivatives. A kinetic study on sTCO diastereomers in 55:45 MeOH:water showed that the *syn*-diastereomer displayed slightly faster reactivity than the *anti*-diastereomer. An ^{18}F-sTCO conjugate with RGD-Tz demonstrated prominent and persistent tumor uptake *in vivo* with good tumor-to-background contrast. Unlike most radiolabeled RGD peptides, the tumor uptake of this PET agent increased from 5.3 +/- 0.2% ID/g at 1 h post injection (p.i.), to 8.9 +/- 0.5% ID/g at 4 h p.i., providing evidence for prolonged blood circulation. These findings suggest that tetrazine ligations employing ^{18}F-sTCO should serve as a powerful and general platform for the rapid construction of peptide or protein derived PET agents.

Key words: bioorthogonal reaction, strained trans-cyclooctene (sTCO), positron emission tomography (PET), ^{18}F, RGD peptide.

Introduction

Positron emission tomography (PET) is a non-invasive imaging modality with the capacity to track radiolabeled biomolecules *in vivo*. This imaging technique employs radionuclides that emit positrons that collide with electrons and result in two detectable γ-rays.[1, 2] Of the common radionuclides that are utilized in PET, F-18 is the most broadly utilized due to the high positron efficiency, high specific radioactivity and clinically attractive half-life (~110 min).[3] These properties can minimize the toxic effects and radiation exposure to the patient. However, the short half-life of F-18, the modest nucleophilicity of fluoride, and the low concentrations that are intrinsic to both biology and radiochemistry

render it challenging to incorporate F-18 in complex biomolecules. The simple relationship between biomolecular rate constant and concentration shown in Table 1 illustrates the importance of fast rates to the field of F-18 labeling. Accordingly, there is a high demand for methods that efficiently introduce F-18 to biological macromolecules.

Table 1. Illustration of the practical importance of fast, bimolecular reactivity for radiolabeling at 1 μM. Radionuclides such as F-18 are prepared in small quantity and low concentration (typically ≤ 1 μM). Proteins and other biological macromolecules are typically utilized at micromolar concentrations. As both reactants are present in low concentration, fast reaction rates are essential to efficient coupling. The bioorthogonality and fast rate of the tetrazine-TCO ligation make it unusually well suited for radiolabeling applications.

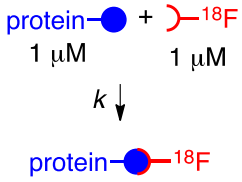

k (L/M•s)	$t_{1/2}$
10^6	1 sec
10^4	1.7 min
10^2	2.8 h
1	12 days
10^{-2}	3 years

The field of bioorthogonal chemistry is having a transformative influence on diverse fields including chemical biology, materials science, and nuclear medicine.[4-12] Since it was first introduced by us and others in 2008,[13-15] the tetrazine ligation has had a growing impact in biomedical research including radiolabeling, pretargeted imaging, *in vivo* reactions and other applications.[16-22] Our group has shown that the bioorthogonal reactions of tetrazines with *trans*-cyclooctene dienophiles proceed with exceptionally fast reaction rates (Figure 1).[23] The tetrazine-*trans*-cyclooctene ligation has become an important tool for biomolecular labeling because it is more rapid than other classes of bioorthogonal reactions.[24] Especially rapid reactivity has been observed for the conformationally strained dienophile, (1R,8S,E)-bicyclo[6.1.0]non-4-en-9-ylmethanol (sTCO),[25] for which rate constants as fast as 3.3 x 10^6 $M^{-1}s^{-1}$ have been measured (Figure 1c).[26] By comparison, strain driven reactions of azides with cyclooctynes typically proceed with rates constants < 1 $M^{-1}s^{-1}$.[24] Speed of labeling is a premium consideration for radiolabeling biological molecules, as both the radiolabel and the biomolecule are typically low in concentration. Recently, intracellular labeling of HaloTag fusion proteins has been used to compare the efficiency of bioorthogonal reactions involving tetrazine or azides with cyclopropenes, norbornenes, cycloalkenes and *trans*-cycloalkenes[10] In these studies, *trans*-cycloalkenes were identified as unique labeling reagents with sTCO-based reagents displaying the fastest reactivity. Moreover, while fluorescent reporters based on bicyclononyne (BCN) were prone to off-target labeling, TCO-based reporters were much more selective.[10] To date, radiolabeled analogs of sTCO have not yet been described.

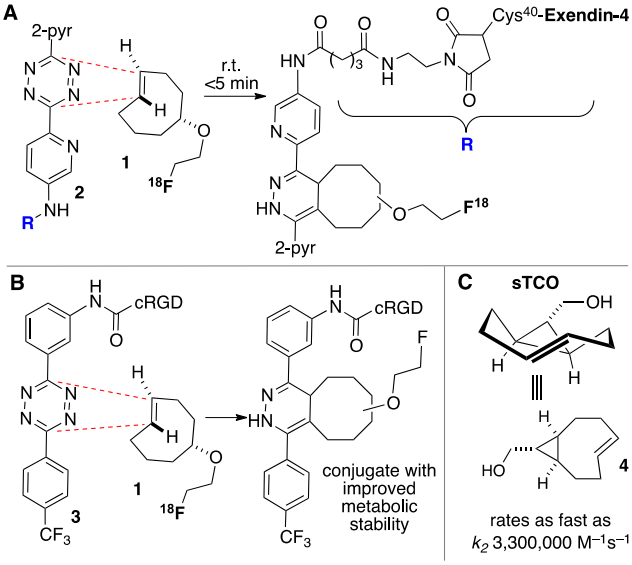

Figure 1. The tetrazine ligation with *trans*-cyclooctenes serves as a rapid method for the assembly of biomolecular-probe constructs. (A) The first generation system for F-18 labeling proceeds with fast kinetics but the Diels-Alder conjugate displays poor metabolic stability. (B) Diels-Alder conjugate from **1** and diphenyl-*s*-tetrazine derivative **3** displays improved metabolic stability. (C) The conformationally strained sTCO is the most reactive dienophile described to date, with rate constants of up to 3.3. x 10^6 $M^{-1}s^{-1}$ for room temperature conjugations in water.

In recent years several radiolabeled *trans*-cyclooctenes and *s*-tetrazines have been developed for applications in rapid radiolabeling. Previously we described an F-18 radiolabeling method that utilizes functionalized derivatives of di-2-pyridyl-*s*-tetrazine (**2**) and an ^{18}F-labeled *trans*-cyclooctene (**1**) (Figure 1a).[23, 27-30] Analogs of these compounds have been shown to combine with rapid kinetics,[26] thereby enabling probe construction for cancer imaging and diabetes monitoring within seconds.[28, 30] More recently, we have explored the probe **3** derived from diphenyl-*s*-tetrazine, which is less rapid but gives Diels-Alder adducts with improved *in vivo* stability relative to the first generation system.[29] ^{18}F-labeled trans-cyclooctene **1** has also been investigated for pretargeted PET imaging in the brain.[31]

To great effect, Robillard and coworkers have used the *trans*-cyclooctene/di-2-pyridyl-*s*-tetrazine system for pretargeted cancer imaging. In this case *trans*-cyclooctene was used as a tagging compound

while a DOTA modified tetrazine moiety was used to attach either ^{111}In or ^{177}Lu radiolabels.[20, 21, 32-34] Weissleder and coworkers have shown that polymer modified tetrazines can be used for *in vivo* bioorthogonal labeling and PET imaging using ^{18}F-labeled TCO **1**.[17] Weissleder, Lewis and coworkers reported a pretargeting approach for PET imaging based on this method and demonstrated dramatically reduced non-targeted organ uptake.[22] Spivey and coworkers used a ^{68}Ga-DOTA modified 3-methyl-6-phenyl-*s*-tetrazine to construct probes from norbornene-labeled compounds.[35] In 2014, Devaraj and coworkers demonstrated that tetrazine modified, ^{64}Ga-chelating polymers could be employed in a proof-of-principle experiment for pretargeted PET imaging of *trans*-cyclooctene tagged antibodies targeting cancer cells.[36] Zeglis et al. used tetrazine bearing amino acids for ^{89}Zr labeling of peptides applying a *trans*-cyclooctene which was modified with deferrioxamine, a chelating agent for zirconium.[37]

While **1** was the only known ^{18}F labeled *trans*-cyclooctene, there have been considerable efforts recently to produce ^{18}F-labeled tetrazines. In 2014, Kuntner, Mikula and coworkers described a practical synthesis of an ^{18}F-labeled *s*-tetrazine.[38] While this dialkyl-*s*-tetrazine showed lower reactivity than commonly used tetrazines, direct F-18 labeling was possible and the compound exhibit good pharmacokinetic properties as well as high *in vivo* stability.[38] More recently, an ^{18}F-labeled 3-chloro-6-benzyloxy-s-tetrazine was described,[39] and Weissleder, Ploegh and coworkers introduced an ^{18}F labeled tetrazine based on ^{18}F-2-deoxyfluoroglucose, linked to a methyl-phenyl-s-tetrazine by oxime ligation, which enabled rapid radiolabeling of a trans-cyclooctene labeled peptide.[40] Ploegh, Liang and coworkers also introduced an ^{18}F labeled SFB-tetrazine and successfully construct PET probes with *trans*-cyclooctene tagged antibody fragment.[41] Lewis and coworkers introduced another ^{18}F-tetrazine in 2015, which was radiolabeled by an aluminum-[^{18}F]fluoride-NOTA-complex and successfully applied in pretargeted PET imaging of pancreatic cancer xenografts using a *trans*-cyclooctene labeled antibody.[42] A dipyridyl-*s*-tetrazine labeled by ^{11}C was recently introduced by Herth and coworkers.[43]

While there has been a surge in recent activity directed toward the development of new ^{18}F-labeled tetrazines, we recognized that the fastest reactivity would be borne out with conformationally strained sTCO derivatives. Accordingly, we sought to develop an ^{18}F labeled *trans*-cyclooctene that would display superior kinetics in tetrazine ligation. Here, we describe ^{18}F-sTCO—a new radiotracer based on the most reactive trans-cyclooctene dienophile. It is shown that ^{18}F-sTCO rapidly combines with tetrazines and can be used to rapidly assemble probes for PET imaging. The kinetics in Diels-Alder reactions of the two diastereomers of sTCO were evaluated, and the more reactive *syn*-sTCO diastereomer was utilized for further study in PET probe construction. The tetrazine ligation with ^{18}F-sTCO was used to synthesize a radiolabeled RGD peptide and in a mouse tumor model was demonstrated to have a high level of tumor uptake relative to that in liver, kidney, and muscles. After 4 h post injection, the tumor was the most prominent image in the PET scan with tumor uptake that was 1.6–2.4 fold higher than other major organs.

Materials and methods

All commercially available analytical grade chemical reagents were purchased from Aldrich (St. Louis, MO) and used without further purification. Analytical reversed-phase HPLC using a Gemini 5µ C18 column (250 x 4.6mm) was performed on a SPD-M30A photodiode array detector (Shimadzu) and model 105S single-channel radiation detector (Carroll & Ramsey Associates). Radio HPLC analyses were carried out at 1 mL/min with water/acetonitrile eluent mixtures. For other HPLC analyses, the solvents were modified with 0.1% TFA.

Chemistry

Synthetic protocols, characterization details, and copies of ^{1}H NMR, ^{13}C NMR, and ^{19}F NMR spectra, the crude HPLC trace for ^{18}F labeling, and the HPLC data for the PBS stability study can be found in the Supplementary Material.

Stopped-Flow Kinetic Analysis

The second order rate constant was measured under pseudo-first order conditions using an excess of the appropriate sTCO diastereomer (**4** or **5**), and by following the exponential decay of absorbance due to the tetrazine chromophore of **11** at 298 nm using an SX 18MV-R stopped-flow spectrophotometer (Applied Photophysics Ltd.). For each run, equal volumes of 45:55 water:methanol solutions of sTCO and PEGylated tetrazine **11** were mixed in the stopped flow device. Reactions were carried out with tetrazine **11** at 0.05 mM and final concentrations of 0.245, 0.49, 0.98 and 1.47 mM for the *syn*-diastereomer **5**. Similarly, reactions were carried out with tetrazine **11** at 0.05 mM and final concentrations of 0.25, 0.50, 1.00 and 1.50 mM for the *anti*-diastereomer **4**. A total of 400 data points were recorded over a period of 1 second, and each sample was performed in sextuplicate at 298 K. The k_{obs} was determined by

nonlinear regression analysis of the data points using Prism software (v. 6.00, GraphPad Software Inc.). The results are reported in the Supporting Information.

Radiochemistry

The radiolabeling reactions were carried out using the following protocol unless specified. sTCO-tosylate **8** (9.1 µmol) was dissolved in MeCN (30 µL) and then allowed to react with ^{18}F-TBAF (200 mCi) at 85 °C for 10 min. The reaction was quenched by adding water (500 µL). The mixture was then passed through a Sep-Pak cartridge (Sep-Pak Plus light alumina) followed by HPLC purification. After HPLC purification, the fraction containing the desired product was diluted with 10 mL of water, trapped on C18 Sep-Pak, washed with 10 mL water, and eluted off with 0.5 mL EtOH. A portion of the solution containing **^{18}F-9** was reserved for the *in vitro* stability test. Then a fraction of the solution (10 mCi, estimated to be 4.8 nmol) was mixed with a DMSO solution of tetrazine-RGD conjugate **12** (ranging from 0.07 µmol to 3.3 nmol). After shaking for 10 seconds at room temperature, a portion of the reaction mixture (3 mCi) was loaded onto HPLC for further analysis. The HPLC eluent containing **^{18}F-15** was collected and organic solvent was removed using rotary evaporator. After carefully adjusting the pH to 7.5, **^{18}F-15** was reconstituted in 1x PBS for the stability test and small animal studies.

In Vitro Stability

^{18}F-9 and **^{18}F-15** was incubated in 1x PBS buffer at 37 °C. An aliquot of the solution (~25 µCi) was taken out and loaded on HPLC at 1 h and 2 h time point for analysis. **^{18}F-9** was also incubated in FBS at 37 °C and after 1 h, an aliquot of the solution (~25 µCi) was taken out and added to an equal volume of TFA. Similarly,**^{18}F-15** was also incubated in FBS at 37 °C, and at 2 and 4 h time points, aliquots of the solution (~25 µCi) were taken and added to an equal volume of TFA. For each sample, the mixture was centrifuged at 14000 rpm for 5 min. The supernatant was then diluted with 1 mL water and loaded on C18 Sep-Pak. After washing with 1 mL water, the cartridge was eluted with 0.5 mL acetonitrile. The water fraction and acetonitrile fraction were combined and loaded on HPLC for analysis

Small Animal PET Imaging

Animal procedures were performed according to a protocol approved by the UNC Institutional Animal Care and Use Committee. PET scans and image analysis were performed using a small animal PET scanner as previously reported.[44] Human U87MG tumor-bearing mice were anesthetized using 2% isoflurane and injected with 3.7 MBq (100 µCi) of **^{18}F-15** via the tail vein. At 0.5, 1.0, 2.0, and 4.0 h post injection, static emission scans were acquired for 10 min. Normal nude mice were injected with 3.7 MBq (100 µCi) of ^{18}F-sTCO-PEG-tetrazine (compound obtained by combining **^{18}F-9** and **11**) or **^{18}F-9** using the same protocol. Raw PET images were reconstructed using 2D ordered subset expectation maximization (OSEM) algorithm. No background correction was performed. Regions of interest (ROI) were manually drawn over the tumor and other organs on the decay corrected coronal images. Based on the assumption that the tissue density is 1 g/mL, the ROIs were converted to % ID/g by dividing dose per gram at ROI by injected dose.

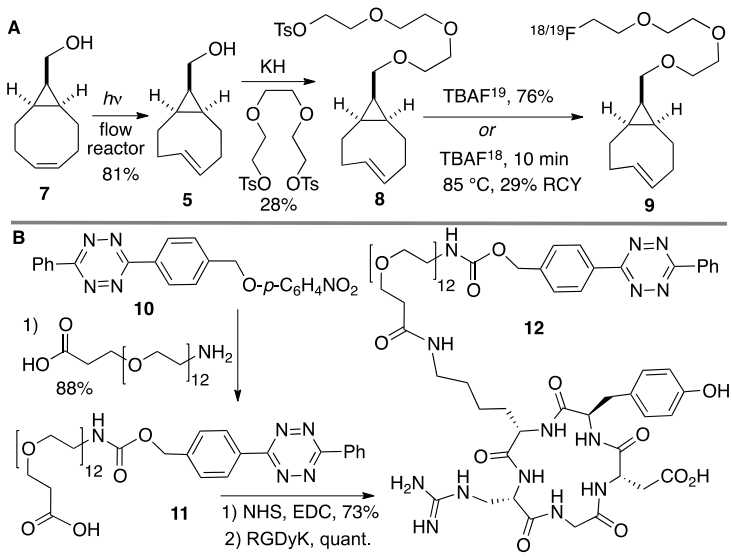

Figure 2. (A) Synthesis of *syn*-sTCO **5**, labeling precursor **8**, cold standard **^{19}F-9**, and radiotracer **^{18}F-9**. (B) Synthesis of a cyclic RGD-diphenyl-s-tetrazine conjugate **12**.

Statistical analysis

Quantitative data were expressed as mean ± SD. Means were compared using one-way ANOVA and Student's t test. *P* values <0.05 were considered statistically significant.

Results and Discussion

Chemistry

The *anti*-diastereomer of sTCO (**4**) was prepared as described previously, and the *syn*-diastereomer **5** was prepared as shown in Figure 2A. Thus, photoisomerization of **7** using our previously described flow reactor [14] gave *syn*-sTCO **5** in 81% yield. Our initial efforts to activate *syn*-sTCO **5** through reaction with NsCl or TsCl were unsuccessful, and lead only to skeletal rearrangement products. After

experimentation, we developed a synthesis that directly provided a tosylate product through alkylation of the alcohol **5** with a bis-tosylate that contained a mini-PEG linker. Thus, combination of this alcohol with KH and triethylene glycol ditosylate gave the sTCO tosylate **8** in 28% yield. To create the HPLC standard, the treatment of **8** with TBAF in anhydrous THF gave the ^{19}F-labeled derivative **9** in 76% yield. A diphenyl-*s*-tetrazine conjugate of a cyclic RGD was synthesized as shown Figure 2B. The nitrophenylcarbonate **10** was sequentially coupled with a "mini-PEG" amino acid to give **11**. Subsequent coupling with NHS and conjugation with the cyclic peptide RGDyK gave **12** in high yield.

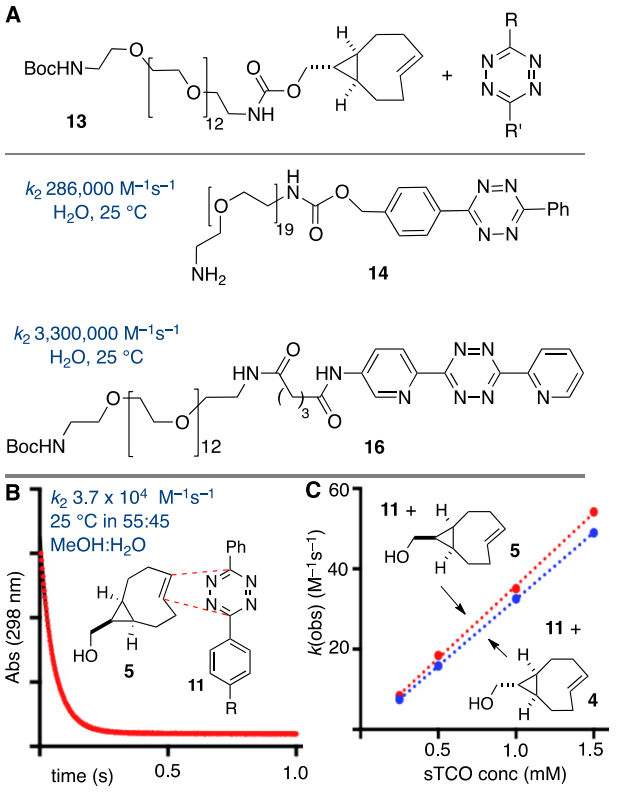

Figure 3. Rapid reactions of s-TCO derivatives with tetrazines. (A) Rate constants of *anti*-sTCO and tetrazine analogs in water. (B,C) Rate constants for the *syn*- and *anti*-diastereomers of sTCO were measured in mixed aqueous/organic media. (B) Kinetic data for the reaction of **5** (0.49 mM) and **11** (0.05 mM). The sTCO *syn*-diastereomer **5** is slightly more reactive than the *anti*-diastereomer **4**.

Stopped flow kinetic analysis was used to measure the rate of the Diels-Alder reaction between tetrazine derivative **11** and *anti*- and *syn*-diastereomers of sTCO (**4** and **5**, respectively). In a prior study with **13**, a mini-PEG derivative of the sTCO *anti*-diastereomer, it was found that the water soluble diphenyl-*s*-tetrazine analog **14** and the di-2-pyridyl-*s*-tetrazine analog **16** react with rate constants of 2.86 x 10^5 M^{-1}s^{-1} and 3.3 x 10^6 M^{-1}s^{-1} (Figure 3a). The latter is the fastest rate constant that has been described for a bioorthogonal reaction. For the present study, we used stopped flow analysis to compare the relative rate of the *syn*- and *anti*-diastereomers of sTCO with tetrazine **11** in mixed organic/aqueous media (55:45 MeOH:water at 25 °C). As expected, the rates in MeOH:water were ~9 fold slower than the measurements made in purely aqueous media, but still extremely rapid. The rate constant for the *syn*-diastereomer **5** with tetrazine **11** was k_2 3.7 x 10^4 (+/- 0.1 x 10^3) M^{-1}s^{-1}, and the *anti*-diastereomer **4** reacted with a rate constant k_2 3.3 x 10^4 (+/- 0.1 x 10^3) M^{-1}s^{-1}. Because the *syn*-diastereomer was more reactive it was chosen for further development in PET probe construction.

Radiochemistry

^{18}F-labeled sTCO (**^{18}F-9**) was produced using the protocol described in Figure 2. By treating tosylate precursor **8** (182 mM) with ^{18}F-TBAF in acetonitrile at 85 °C for 10 min, we were able to obtain the radiolabeled **^{18}F-9** in 29.3 +/- 5.1% isolated radiochemical yield with 99% radiochemical purity after HPLC purification (Figure 2a, Figure 5a). Here, the reaction concentration was determined to be important, as running the reaction at 91 mM gave **^{18}F-9** in only 9.3 +/- 2.4% isolated yield. The specific activity was determined to be 2.1 +/- 0.8 Ci/µmol. The product identity was confirmed by co-injection with an independently synthesized **^{19}F-9** standard. Prior to reacting with targeting molecules, we first tested the *in vitro* stability of **^{18}F-9**. After incubation in 1X PBS, the radiopurity remained at 97.5% and 97.3% at 1 hour and 2 hour time points, respectively (Figure S3). This result demonstrated that **^{18}F-9** is sufficiently stable to construct PET probes in aqueous solution. It was also observed that **^{18}F-9** was stable in fetal bovine serum for 1 hour with retention of 74% radiochemical purity (Figure S10).

As depicted in Figure 4, the conjugation of ^{18}**F-9** with RGD-tetrazine **12** (700 µM) produced conjugate ^{18}**F-15** as a mixture of isomers. The starting material ^{18}**F-9** was completely consumed upon initial assay (<5 minutes). Reducing the concentration of **12** to 33 µM lead to an inversion in stoichiometry, and the complete consumption of **12** and the observation of unreacted ^{18}**F-9**. This ability to achieve complete labeling when the ^{18}F-labeled substrate is used *in excess* speaks to the high efficiency and rate of bioorthgonal reaction using **^{18}F-9**.

Under ambient reaction conditions, a 91% radiochemical yield of ^{18}**F-15** was obtained with 99% purity (Figure S4) after HPLC purification. The crude radio-HPLC trace is displayed in Figure 5B. The specific activity was determined to be 0.91 +/- 0.20 Ci/µmol. An analog reaction with **^{19}F-9** produced the

isomeric "cold" Diels-Alder conjugates **^{19}F-15**. LC-MS analysis confirmed that the both of the major peaks from the conjugation had mass spectra matching the theoretical for **^{19}F-15** (Supporting Information). More rapidly eluting minor peaks also had correct mass data, and likely correspond to the aminal (hydrated) forms of the product.[25] The slowest eluting peak from the radio-HPLC trace of **^{18}F-15** was collected and the *in vitro* stability was studied. It was observed that the adduct was stable in PBS buffer for 2 hours with retention of 98.5% radiochemical purity (Figure 5C). Conjugate **^{18}F-15** was also found to be stable in fetal bovine serum with 96.7% and 94.5% purity at 2 and 4 hours post incubation respectively. (Figure S10)

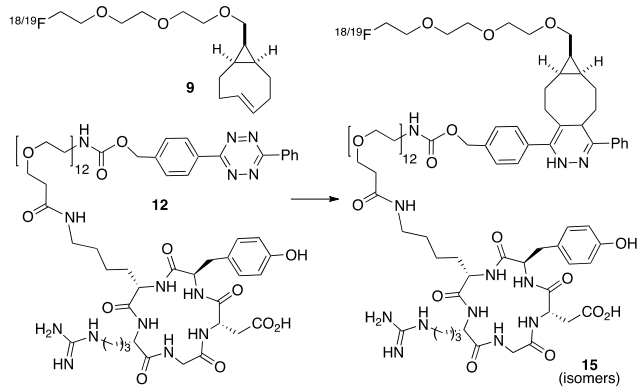

Figure 4. Conjugation of ^{18}**F-9** with RGD-tetrazine **12** to produce conjugate ^{18}**F-15** as a mixture of isomers. Cold standards were independently prepared.

Due to the low concentration and short time scale that is intrinsic to ^{18}F labeling of proteins, the fast kinetics and bioorthogonality of the tetrazine-TCO ligation provide a clear benefit over conventional radiolabeling methods. With our prior system, highly reactive tetrazines were required in order to obtain rapid reactivity at micromolar concentrations, but the resulting Diels-Alder conjugates had only moderate stability *in vivo* (Figure 1a).[30]The superior reactivity of ^{18}F-sTCO allows rapid kinetics (>10^4 $M^{-1}s^{-1}$) to be realized with more stable diphenyl-*s*-tetrazines, giving rise to Diels-Alder conjugates which are known to possess improved *in vivo* stability.[29] Moreover, the system described here leads to conjugates with improved blood circulation and higher levels of tumor uptake than observed using the previously described systems shown in Figure 1.

Small Animal PET imaging

The localization of **^{18}F-15** in human U87MG tumor-bearing mice (n=5) was performed by static microPET scans at multiple time-point post tail vein injection. Selected decay-corrected coronal images at different time points are shown in Figure 6 after injection of 3.7 MBq (100 µCi) of **^{18}F-15**. High and persistent tumor accumulation was observed with good tumor to background contrast as early as 30 min post injection. The 2D maximum intensity projection for the images displayed in Figure 6 and S9. The quantitative biodistribution derived from small-animal PET images are shown in Figure 7. The inclusion of mini-PEG spacers resulted in a biodistribution profile that was significantly improved relative to previously constructed TCO/tetrazine-based probes that lack a PEG spacer, and the blood circulation of this new construct was improved significantly compared with previously described constructs. The tumor uptake was 5.3 +/- 0.2, 6.9 +/- 0.5, 7.5 +/- 0.8 and 8.9 +/- 0.5 % ID/g at 0.5, 1.0, 2.0, and 4.0 h post injection, respectively. At 4.0 h post injection, the tumor became the brightest spot in PET scan, with a tumor-to-liver and tumor-to-kidney ratio of 1.6 and 2.4, respectively. Given the improved blood circulation and high levels of tumor uptake for this small peptide-based probe, we anticipate that ^{18}F-sTCO based probes should find broad utility for the labeling of larger peptides, proteins and other biomolecules.

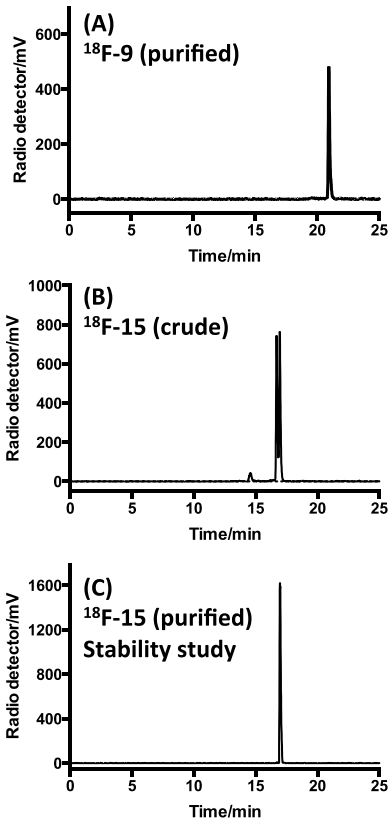

Figure 5. Radio-HPLC analyses. (A) Purified ^{18}**F-9** after incubation in PBS for 2 h at 37 °C. (B) Combination of ^{18}**F-9** with **12** gives two major isomeric adducts ^{18}**F-15**. (C) The slow eluting isomer of ^{18}**F-15** after purified by HPLC, incubation in PBS for 2 h at 37 °C, and reanalysis.

The specificity of **^{18}F-15** was confirmed by a blocking experiment in which the radiotracer was co-injected with an excess amount of cRGDyK. The RGD peptide is a well-established targeting molecule,[45-49] and as can be seen in Figure 6B, in the presence of non-radio labeled cRGDyK (200 µg), the tracer uptake in tumor dropped to 4.8 +/- 0.3% at 1 h post injection. As expected the cRGDyK peptide, which should be readily cleared than a PEGylated peptide, did not completely block the signal due to ^{19}F-**15**. However, the signal in the presence of blocking cRGDyK was significantly ($P<0.05$) lower than that observed without a blocking agent.

We also performed microPET imaging with a normal (non-tumor bearing) nude mouse that had been injected with **^{18}F-9**. The imaging data indicated that the compound was rapidly cleared by the gallbladder, kidney and liver within 2 hours (Figure S8). We also analyzed the clearance of the compound obtained by combining **^{18}F-9** with **11**. This Diels-Alder conjugate— an analog of **^{18}F-15** that lacks the RGD moiety— still remained in the blood circulatory system after 4 hours (Figure S7). The blood uptake was 2.4% ID/g at 4 h post injection. Previously, we have described ^{18}F-labeled RGD probes derived from *trans*-cyclooctene **1** (Figure 1). These probes which lack PEGylation are cleared much more rapidly.[29, 30] These results suggested that the entire PEGylated Diels-Alder moiety plays a role in enhancing the circulation time of the probe. Future experiments will aim to determine the respective contributions of the Diels-Alder conjugate and the PEG chains as factors in increasing the circulation lifetime. We believe that the rapid clearance of **^{19}F–9** and the long circulation lifetime of its PEGylated Diels-Alder conjugates may prove advantageous for future applications in pretargeted imaging, and we are currently pursuing these applications.

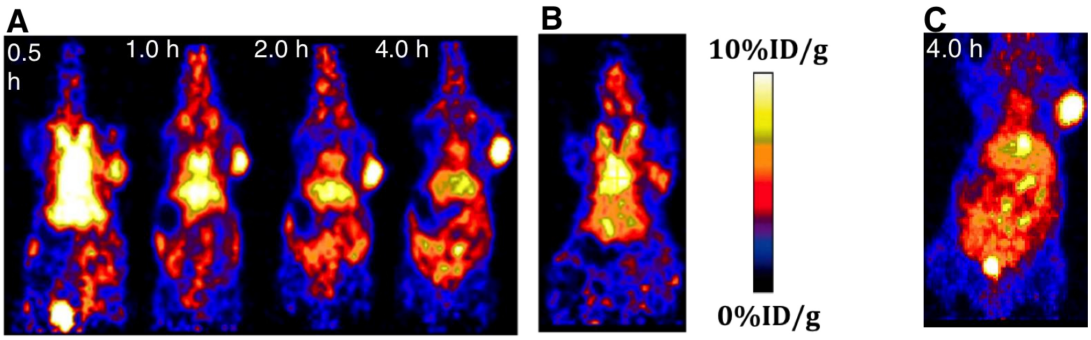

Figure 6. (A) Small animal PET images of mice bearing U87 xenograft, injected with ^{18}**F-15** and imaged 0.5 h, 1.0 h, 2.0 h and 4.0 h post injection, respectively. (B) A 'blocking' experiment in which cyclic RGDyK peptide (200 µg) was injected prior to the injection of ^{18}**F-15**, with imaging at 1.0 h post injection. (C) Two-dimensional maximum intensity projection at 4.0 h post injection of ^{18}**F-15**.

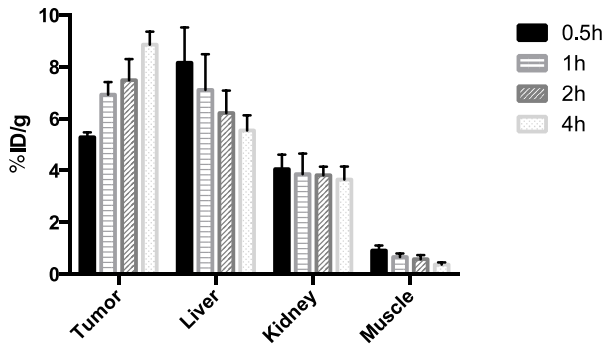

Figure 7. Tumor and major organ radioactivity accumulation quantification from a static scan at 0.5, 1, 2, and 4 h post injection of ^{18}**F-15** into U87MG tumor model. Data are expressed as average +/- SD.

Conclusions

A conformationally strained trans-cyclooctene, ^{18}F-sTCO (**9**), was prepared via a one-step fluorination. This new PET-tracer is based on the conformationally strained *trans*-cyclooctene (sTCO)—a dienophile that is approximately 2 orders of magnitude more reactive than conventional TCO dienophiles. In a model system, the rate constants for sTCO-diastereomers were compared, and the *syn*-diastereomer was found to be slightly more reactive and therefore was chosen for further development. The effectiveness of 9 for the construction of radiolabeled probes was demonstrated with the production of a cyclic RGD based probe **15**. Mini-PEG groups were included in the design of **15** to improve both the water solubility and the pharmacokinetic properties of the probe. In tumor-bearing mice, ^{18}F-**15** demonstrated a significantly improved blood half-life compared with monomeric RGD peptide analogs. As a result, increased tumor uptake of ^{18}F-**15** was observed at a late time point. Given the exceptional kinetics of ^{18}F-**9** and the improved tumor uptake and accumulation of the derived probe ^{18}F-**15**, we expect that this labeling system will be broadly applicable for attachment of F-18 to a host of applications in probe construction,

pretargeted imaging, and treatment applications.

Supplementary Material

Supplementary figures and information.
http://www.thno.org/v06p0887s1.pdf

Acknowledgment

This work was supported by NIBIB (5R01EB014354-03), P30-CA016086-35-37 from the National Cancer Institute, and UNC Radiology Department and BRIC. Spectra were obtained with instrumentation supported by NIH grants P20GM104316, P30GM110758, S10RR026962, S10OD016267 and NSF grants CHE-0840401, CHE-1229234. D.S. is grateful to the Austrian Marshall Plan Foundation for a fellowship and the MEIBio doctoral program of TU Wien for financial support.

Competing Interests

The authors have declared that no competing interest exists.

References

1. Sorensen J. How Does the Patient Benefit from Clinical PET? Theranostics. 2012; 2: 427-36.
2. Schlyer DJ. PET tracers and radiochemistry. Ann Acad Med Singapore. 2004; 33: 146-54.
3. Li Z, Conti PS. Radiopharmaceutical chemistry for positron emission tomography. Adv Drug Deliv Rev. 2010; 62: 1031-51.
4. Patterson DM, Prescher JA. Orthogonal bioorthogonal chemistries. Curr Opin Chem Biol. 2015; 28: 141-9.
5. King M, Wagner A. Developments in the field of bioorthogonal bond forming reactions-past and present trends. Bioconjug Chem. 2014; 25: 825-39.
6. McKay CS, Finn MG. Click chemistry in complex mixtures: bioorthogonal bioconjugation. Chem Biol. 2014; 21: 1075-101.
7. Patterson DM, Nazarova LA, Prescher JA. Finding the right (bioorthogonal) chemistry. ACS Chem Biol. 2014; 9: 592-605.
8. Kang SW, Lee S, Na JH, Yoon HI, Lee DE, Koo H, et al. Cell labeling and tracking method without distorted signals by phagocytosis of macrophages. Theranostics. 2014; 4: 420-31.
9. Fox JM, Robillard MS. Editorial overview: In vivo chemistry: Pushing the envelope. Curr Opin Chem Biol. 2014; 21: v-vii.
10. Murrey HE, Judkins JC, Am Ende CW, Ballard TE, Fang Y, Riccardi K, et al. Systematic Evaluation of Bioorthogonal Reactions in Live Cells with Clickable HaloTag Ligands: Implications for Intracellular Imaging. J Am Chem Soc. 2015; 137: 11461-75.
11. Zhang H, Dicker KT, Xu X, Jia X, Fox JM. Interfacial Bioorthogonal Cross-Linking. ACS Macro Lett. 2014; 3: 727-31.
12. Liu S, Zhang H, Remy RA, Deng F, Mackay ME, Fox JM, et al. Meter-long multiblock copolymer microfibers via interfacial bioorthogonal polymerization. Adv Mater. 2015; 27: 2783-90.
13. Blackman ML, Royzen M, Fox JM. The Tetrazine Ligation: Fast Bioconjugation based on Inverse-electron-demand Diels-Alder Reactivity. J Am Chem Soc. 2008; 130: 13518-9.
14. Royzen M, Yap GPA, Fox JM. A Photochemical Synthesis of Functionalized trans-Cyclooctenes Driven by Metal Complexation. J Am Chem Soc. 2008; 130: 3760-1.
15. Selvaraj R, Fox JM. trans-Cyclooctene—a stable, voracious dienophile for bioorthogonal labeling. Current Opinion in Chemical Biology. 2013; 17: 753-60.
16. Carroll L, Evans HL, Aboagye EO, Spivey AC. Bioorthogonal chemistry for pre-targeted molecular imaging - progress and prospects. Org Biomol Chem. 2013; 11: 5772-81.
17. Devaraj NK, Thurber GM, Keliher EJ, Marinelli B, Weissleder R. Reactive polymer enables efficient in vivo bioorthogonal chemistry. Proc Natl Acad Sci U S A. 2012; 109: 4762-7.
18. Devaraj NK, Upadhyay R, Haun JB, Hilderbrand SA, Weissleder R. Fast and Sensitive Pretargeted Labeling of Cancer Cells via Tetrazine/Trans-Cyclooctene Cycloaddition. Angew Chem Int Ed Engl. 2009; 48: 7013-6.
19. Reiner T, Zeglis BM. The inverse electron demand Diels–Alder click reaction in radiochemistry. J Labelled Comp Radiopharm. 2014; 57: 285-90.
20. Rossin R, Läppchen T, van den Bosch SM, Laforest R, Robillard MS. Diels–Alder Reaction for Tumor Pretargeting: In Vivo Chemistry Can Boost Tumor Radiation Dose Compared with Directly Labeled Antibody. J Nucl Med. 2013; 54: 1989-95.
21. Rossin R, Renart Verkerk P, van den Bosch SM, Vulders RCM, Verel I, Lub J, et al. In Vivo Chemistry for Pretargeted Tumor Imaging in Live Mice. Angew Chem Int Ed Engl. 2010; 49: 3375-8.
22. Zeglis BM, Sevak KK, Reiner T, Mohindra P, Carlin SD, Zanzonico P, et al. A Pretargeted PET Imaging Strategy Based on Bioorthogonal Diels–Alder Click Chemistry. J Nucl Med. 2013; 54: 1389-96.
23. Wu Z, Liu S, Hassink M, Nair I, Park R, Li L, et al. Development and Evaluation of ^{18}F-TTCO-Cys40-Exendin-4: A PET Probe for Imaging Transplanted Islets. J Nucl Med. 2013; 54 :244-51.
24. Lang K, Chin JW. Bioorthogonal Reactions for Labeling Proteins. ACS Chemical Biology. 2014; 9: 16-20.
25. Taylor MT, Blackman ML, Dmitrenko O, Fox JM. Design and synthesis of highly reactive dienophiles for the tetrazine-trans-cyclooctene ligation. J Am Chem Soc. 2011; 133: 9646-9.
26. Darko A, Wallace S, Dmitrenko O, Machovina MM, Mehl RA, Chin JW, et al. Conformationally Strained -Cyclooctene with Improved Stability and Excellent Reactivity in Tetrazine Ligation. Chem Sci. 2014; 5: 3770-6.
27. Li Z, Cai H, Hassink M, Blackman ML, Brown RCD, Conti PS, et al. Tetrazine-trans-cyclooctene ligation for the rapid construction of ^{18}F labeled probes. Chem Commun (Camb). 2010; 46: 8043-5.
28. Liu S, Hassink M, Selvaraj R, Yap L-P, Park R, Wang H, et al. Efficient ^{18}F labeling of cysteine containing peptides and proteins using the tetrazine-trans-cyclooctene ligation. Molecular imaging. 2013; 12: 121-8.
29. Selvaraj R, Giglio BC, Liu S, Wang H, Wang M, Yuan H, et al. Improved Metabolic Stability for ^{18}F PET Probes Rapidly Constructed via Tetrazine trans-Cyclooctene Ligation. Bioconjug Chem. 2015; 26: 435-42.
30. Selvaraj R, Liu S, Hassink M, Huang C-w, Yap L-p, Park R, et al. Tetrazine-tans-cyclooctene ligation for the rapid construction of integrin $\alpha_v\beta_3$ targeted PET tracer based on a cyclic RGD peptide. Bioorg Med Chem Lett 2011; 21: 5011-4.
31. Wyffels L, Thomae D, Waldron AM, Fissers J, Dedeurwaerdere S, Van der Veken P, et al. In vivo evaluation of ^{18}F-labeled TCO for pre-targeted PET imaging in the brain. Nucl Med Biol. 2014; 41: 513-23.
32. Rossin R, van den Bosch SM, Ten Hoeve W, Carvelli M, Versteegen RM, Lub J, et al. Highly reactive trans-cyclooctene tags with improved stability for Diels-Alder chemistry in living systems. Bioconjug Chem. 2013; 24: 1210-7.
33. Rossin R, van Duijnhoven SM, Lappchen T, van den Bosch SM, Robillard MS. Trans-cyclooctene tag with improved properties for tumor pretargeting with the diels-alder reaction. Mol Pharm. 2014; 11: 3090-6.
34. van Duijnhoven SM, Rossin R, van den Bosch SM, Wheatcroft MP, Hudson PJ, Robillard MS. Diabody Pretargeting with Click Chemistry In Vivo. J Nucl Med. 2015; 56: 1422-8.
35. Evans HL, Carroll L, Aboagye EO, Spivey AC. Bioorthogonal chemistry for ^{68}Ga radiolabelling of DOTA-containing compounds. J Labelled Comp Radiopharm. 2014; 57: 291-7.
36. Nichols B, Qin Z, Yang J, Vera DR, Devaraj NK. ^{68}Ga chelating bioorthogonal tetrazine polymers for the multistep labeling of cancer biomarkers. Chem Commun (Camb). 2014; 50: 5215-7.
37. Zeglis BM, Emmetiere F, Pillarsetty N, Weissleder R, Lewis JS, Reiner T. Building Blocks for the Construction of Bioorthogonally Reactive Peptides via Solid-Phase Peptide Synthesis. ChemistryOpen. 2014; 3: 48-53.
38. Denk C, Svatunek D, Filip T, Wanek T, Lumpi D, Frohlich J, et al. Development of a ^{18}F-labeled tetrazine with favorable pharmacokinetics for bioorthogonal PET imaging. Angew Chem Int Ed Engl. 2014; 53: 9655-9.
39. Zhu J, Li S, Wangler C, Wangler B, Lennox RB, Schirrmacher R. Synthesis of 3-chloro-6-((4-(di-tert-butyl[^{18}F]fluorosilyl)-benzyl)oxy)-1,2,4,5-tetrazine ([^{18}F]SiFA-OTz) for rapid tetrazine-based ^{18}F-radiolabeling. Chem Commun (Camb). 2015; 51: 12415-8.
40. Rashidian M, Keliher EJ, Dougan M, Juras PK, Cavallari M, Wojtkiewicz GR, et al. Use of ^{18}F-2-Fluorodeoxyglucose to Label Antibody Fragments for Immuno-Positron Emission Tomography of Pancreatic Cancer. ACS Central Science. 2015; 1: 142-7.
41. Rashidian M, Wang L, Eden JG, Jacobsen JT, Hossain I, Wang Q, et al. Enzyme-Mediated Modification of Single-Domain Antibodies for Imaging Modalities with Different Characteristics. Angewandte Chemie International Edition. 2015; 02142.
42. Meyer JP, Houghton JL, Kozlowski P, Abdel-Atti D, Reiner T, Pillarsetty NV, et al. F-Based Pretargeted PET Imaging Based on Bioorthogonal Diels-Alder Click Chemistry. Bioconjug Chem. 2015.
43. Herth MM, Andersen VL, Lehel S, Madsen J, Knudsen GM, Kristensen JL. Development of a ^{11}C-labeled tetrazine for rapid tetrazine-trans-cyclooctene ligation. Chem Commun (Camb). 2013; 49: 3805-7.
44. Deng H, Wang H, Wang M, Li Z, Wu Z. Synthesis and Evaluation of ^{64}Cu-DOTA-NT-Cy5.5 as a Dual-Modality PET/Fluorescence Probe to Image Neurotensin Receptor-Positive Tumor. Mol Pharm. 2015; 12: 3054-61.
45. Lang L LW, Jia HM, Fanng DC, Zhang S, Sun X, Zhu L, Ma Y, Shen B, Kiesewetter DO, Niu G, Chen X. New Methods for Labeling RGD Peptides With Bormine-76. Theranostics. 2011; 1: 341-53.
46. Chen X, Park R, Shahinian AH, Tohme M, Khankaldyyan V, Bozorgzadeh MH, et al. 18F-labeled RGD peptide: Initial evaluation for imaging brain tumor angiogenesis. Nuclear Medicine and Biology. 2004; 31: 179-89.

47. Chen H, Niu G, Wu H, Chen X. Clinical Application of Radiolabeled RGD Peptides for PET Imaging of Integrin αvβ3. Theranostics. 2016; 6: 78-92.
48. Zhang Y, Yang Y, Cai W. Multimodality Imaging of Integrin α(v)β(3) Expression. Theranostics. 2011; 1: 135-48.
49. Ye Y, Chen X. Integrin targeting for tumor optical imaging. Theranostics. 2011; 1: 102-26.

Manuscript #8

Dennis Svatunek, Christoph Denk, Veronika Rosecker, Barbara Sohr, Christian Hametner, Günter Allmaier, Johannes Fröhlich, Hannes Mikula*; Efficient low-cost preparation of *trans*-cyclooctenes using a simplified flow setup for photoisomerization, *Monatsh Chem* **2016**, 147, 579–585.

(with permission from Springer Nature)

Monatsh Chem (2016) 147:579–585
DOI 10.1007/s00706-016-1668-z

ORIGINAL PAPER

Efficient low-cost preparation of *trans*-cyclooctenes using a simplified flow setup for photoisomerization

Dennis Svatunek[1,2] · Christoph Denk[1] · Veronika Rosecker[1] · Barbara Sohr[1] · Christian Hametner[1] · Günter Allmaier[2] · Johannes Fröhlich[1] · Hannes Mikula[1]

Received: 15 November 2015 / Accepted: 24 December 2015 / Published online: 22 February 2016
© The Author(s) 2016. This article is published with open access at Springerlink.com

Abstract Bioorthogonal ligations have emerged as highly versatile chemical tools for biomedical research. The exceptionally fast reaction between 1,2,4,5-tetrazines and *trans*-cyclooctenes (TCOs), also known as tetrazine ligation, is frequently used in this regard. Growing numbers of applications for the tetrazine ligation led to an increased demand for TCO compounds, whose commercial availability is still very limited. Reported photochemical procedures for the preparation of TCOs using flow chemistry are straightforward and high yielding but require expensive equipment. Within this contribution, we present the construction and characterization of a low-cost flow photoreactor assembled from readily accessible components. Syntheses of all commonly used *trans*-cyclooctene derivatives were successfully carried out using the described system. We are convinced that the presented system for photoisomerization will promote access to bioorthogonally reactive TCO derivatives.

Graphical abstract

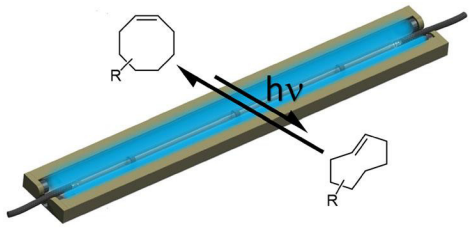

Keywords Photochemistry · Cycloadditions · Click chemistry · Alkenes · Isomerization · Bioorthogonal chemistry

Introduction

From a chemists perspective biological systems are extraordinarily complex. Each individual cell combines a broad range of functional groups, macromolecules, enzymes, and organelles with different pH values as well as sub-compartments with oxidizing or reducing conditions. Stepping up from the single cell level to a higher organism adds another magnitude of complexity to the "in vivo chemical space", which are far off simple mixtures usually present in a typical synthetic experiment.

Bioorthogonal chemistry, a term first introduced by Carolyn R. Bertozzi [1], is a tool that allows covalent bond formation within highly complex environments, using small molecule reaction partners. Those reactions (also referred to as "in vivo click chemistry") meanwhile found numerous applications in fluorescent imaging, drug delivery, PET and SPECT imaging, radionuclide therapy,

Electronic supplementary material The online version of this article (doi:10.1007/s00706-016-1668-z) contains supplementary material, which is available to authorized users.

✉ Hannes Mikula
hannes.mikula@tuwien.ac.at

[1] Institute of Applied Synthetic Chemistry, TU Wien, Vienna, Austria

[2] Institute of Chemical Technologies and Analytics, TU Wien, Vienna, Austria

radiochemistry or drug target identification among several others [2–6]. High selectivity and fast ligation rates of the involved bioorthogonal groups are as important as the metabolic stability of reaction partners and ligation products, as well as their biocompatibility (also in regards of toxicity). A prominent example is the reaction of organic azides with cyclooctynes to form 1,2,3-triazoles, wherein the strained conformation of the cyclooctyne eliminates the need for (cytotoxic) copper(I)-catalysis thus also referred to as the copper-free click (CFC) or strain-promoted alkyne azide cycloaddition (SPAAC) [7]. SPAAC ligation rates are highly dependent on substitution motifs on the cyclooctyne moiety, whose synthesis is often cumbersome and low-yielding. Several improved and more easily accessible cyclooctyne derivatives have been reported, but reaction rates of SPAAC ligations are still limited to $\sim 5\ M^{-1}\ s^{-1}$. Nevertheless, besides many in vitro applications SPAAC has been successfully used for in vivo fluorescent imaging in developing zebrafish [8] as well as for pretargeting in positron emission tomography (PET) [9].

A significant improvement was achieved by the groups of Joseph Fox [10] and Ralph Weissleder [11] in 2008, when they independently introduced the inverse electron demand Diels–Alder reaction (IEDDA) between 1,2,4,5-tetrazines (Tz) and strained dienophiles as highly efficient bioorthogonal reaction (Fig. 1a). When *trans*-cyclooctene (TCO) derivatives react with electron deficient Tz compounds second order rate constants of up to 3.3×10^6 $M^{-1}\ s^{-1}$ (25 °C, H_2O) [12] were observed, making the IEDDA reaction several orders of magnitude faster than SPAAC and the fastest bioorthogonal ligation discovered so far. Hence, rapid ligation can be achieved even at very high dilutions frequently encountered within living systems. IEDDA has successfully been applied in pretargeted PET imaging [13, 14]. The recent development of tetrazines labeled with short-lived fluorine-18 [15–17] also allows imaging of long-circulating nanomedicines with short-lived isotopes as well as rapid radiolabeling of dienophile-tagged (bio)molecules [18–22], avoiding further purification steps. In pharmaceutical and biomedical research dienophile-tagged small molecules were used in vitro in combination with fluorogenic tetrazines [23–26] to visualize sites of drug accumulation at sub-cellular resolution. Tz ligations were also applied for target identification studies [27] and the synthesis of biocompatible polymers and hydrogels [28, 29].

Ligation rates of IEDDA conjugations are strongly dependent on steric and electronic influences on the tetrazine and the dienophile employed [30–32]. Norbornene and terminal alkenes were used as dienophiles, but low rates even with highly reactive Tz derivatives limit their use [33–35]. Cyclopropenes were introduced as dienophiles with less steric demand and higher reactivity compared to norbornene [36–38]. However, the most reactive dienophiles are *trans*-cyclooctenes (TCOs) (Fig. 1b). The parent compound *trans*-cyclooctene (TCO, **1**) is useful as reagent for ligation rate measurements using spectrophotometric techniques, but lacks a site for further derivatization thus making it unusable for bioconjugation. Consequently TCO derivatives including a functional group for further modification have been developed, out of which *trans*-cycloocten-5-ol (TCO-5-OH, **2**), which exists in two diastereomers, is the most frequently used. The diastereomer with axially configured hydroxyl group is formed in smaller amounts using photoisomerization and is thus often referred to as the "minor" TCO-5-OH (**2a**). **2a** shows moderately elevated reactivity compared to "major" (equatorial configuration) TCO-5-OH (**2e**). Nevertheless, steric hindrance makes further modifications of **2a** difficult, which is why **2e** is the most commonly used TCO in literature so far. TCO-5-OH has been proven to be reactive in vivo for prolonged times ranging to several days, but the mode of attachment and the microenvironment of the functionality is reported to influence the half-life inside the living system [39]. Annihilation of a cyclopropane ring to the cyclooctene core structure led to the development of (rel-1*R*,8*S*,9*R*,4*E*)-bicyclo[6.1.0]non-4-en-9-ylmethanol (s-TCO, **4**), which is one order of magnitude more reactive than TCO-5-OH. This dienophile was reported in 2011 by the Fox group [40], and is by far the fastest reacting TCO derivative known so far. Unfortunately high reactivity

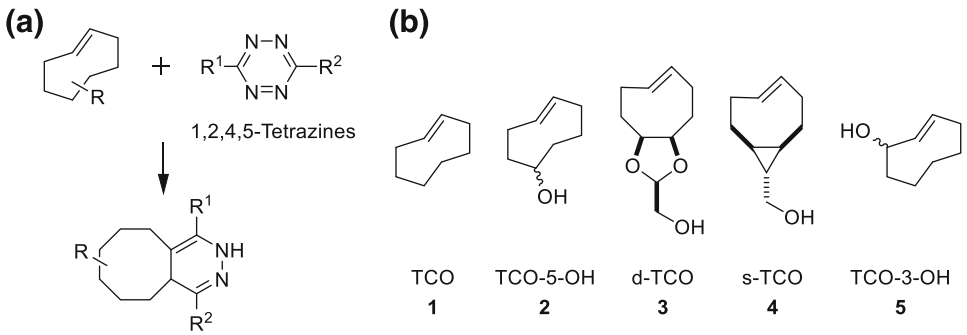

Fig. 1 **a** Inverse electron demand Diels–Alder (IEDDA) reaction between *trans*-cyclooctenes and 1,2,4,5-tetrazines; **b** selected known *trans*-cyclooctene derivatives

comes for the price of reduced stability, making s-TCO the choice whenever rapid reaction is more relevant than prolonged stability. Another highly reactive dienophile ((2*S*,3a*R*,9a*S*,*E*)-3a,4,5,8,9,9a-hexahydrocycloocta[*d*] [1, 3] dioxol-2-yl)methanol (d-TCO, **3**) [12], contains a dioxolane as structural motif enhancing its polarity and water solubility, which is a clear benefit when working in biological media. It exhibits IEDDA reactivity in between the rates for TCO-5-OH and s-TCO and is reported to display high stability. Another compound, *trans*-cycloocten-3-ol (TCO-3-OH, **5**), which also exists in an equatorial (**5e**) and axial configured (**5a**) isomer, deserves special attention due to its "click-to-release" behavior. The cytotoxic drug doxorubicin was conjugated to **5a** using a carbamate linkage on its 3-OH functionality leading to a pro-drug that can be activated by bioorthogonal click reaction with tetrazines [41]. This methodology gives rise to new therapeutic strategies, and the full potential of release chemistry is expected to unfold in years to come. The choice of which dienophile is suited best has to be made for every particular bioconjugation task depending on the necessities for ligation rate, stability, steric impact, and availability. Currently only the two isomers of TCO-5-OH, **2e** and **2a** are commercially available (**2e** also in activated form for conjugation reactions) and quite cost intensive when larger quantities are required.

State of the art TCO synthesis was introduced by Fox and coworkers in 2008 and made these useful small molecules more accessible [42]. When *cis*-cyclooctenes are irradiated with UV-C (254 nm) in the presence of a singlet sensitizer an equilibrium between *cis*- and *trans*-isomers is reached (photoisomerization) [43, 44]. The *trans*-isomers, in contrast to the *cis*-compounds, form stable complexes with silver cations. Hence, passing the reaction mixture through a cartridge filled with $AgNO_3$ on silica ($AgNO_3$/SiO_2) actively removes the TCO species from the equilibrium, allowing excellent reaction yields of TCOs from the respective *cis*-isomers in multigram quantities (Fig. 2a). Despite being broadly applicable for TCO synthesis the described setup uses a commercial UV reactor in which a quartz flask containing the reaction mixture has to be immersed (Fig. 2b). Both UV source and special glassware are cost intensive, and differently sized quartz flasks are necessary to maintain high flexibility regarding the scale of the reaction. Systems including flow photoreactors would eliminate this problem. Such reactors are commercially available (e.g. UV-150 photochemical reactor, Vapourtec Ltd.; Advanced-Flow™ G1 Photo Reactor, Corning®), but cost intensive and often require even more expensive flow chemistry equipment. We, therefore, aimed to develop and characterize an effective, versatile, and low-cost flow photoreactor using readily available components for the preparation of various TCO derivatives.

Results and discussion

The most promising design featured a quartz glass tube (Ø 16 mm, length 790 mm) connected to tubes at both ends and a total volume of 165 cm^3 as a flow cell. Two 55 W low-pressure mercury lamps (OSRAM, HNS 55 W OFR, T8, 90 cm) with a dominant wavelength of 254 nm were used for irradiation and placed alongside the quartz glass tube (Fig. 3). For a picture of the used setup see Electronic Supplementary Material (Fig. S1). This setup was mounted onto a back plate, covered with aluminum foil to prevent harmful radiation from exiting the system and aligned in vertical orientation. Solutions were pumped through the reactor upwards to allow for better filling of the reactor (see Electronic Supplementary Material). The total cost of this

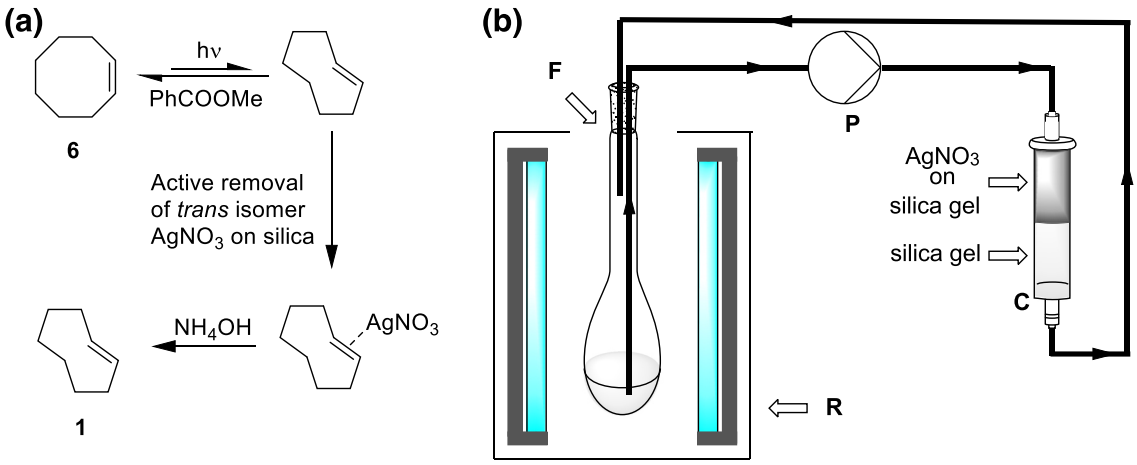

Fig. 2 **a** Photochemical isomerization of *cis*-cyclooctene with active removal of *trans* compound; **b** Reaction setup used by Fox et al.: ***C*** column, ***P*** metering pump, ***F*** quartz glass flask filled with reaction solution, ***R*** Rayonet photochemical reactor

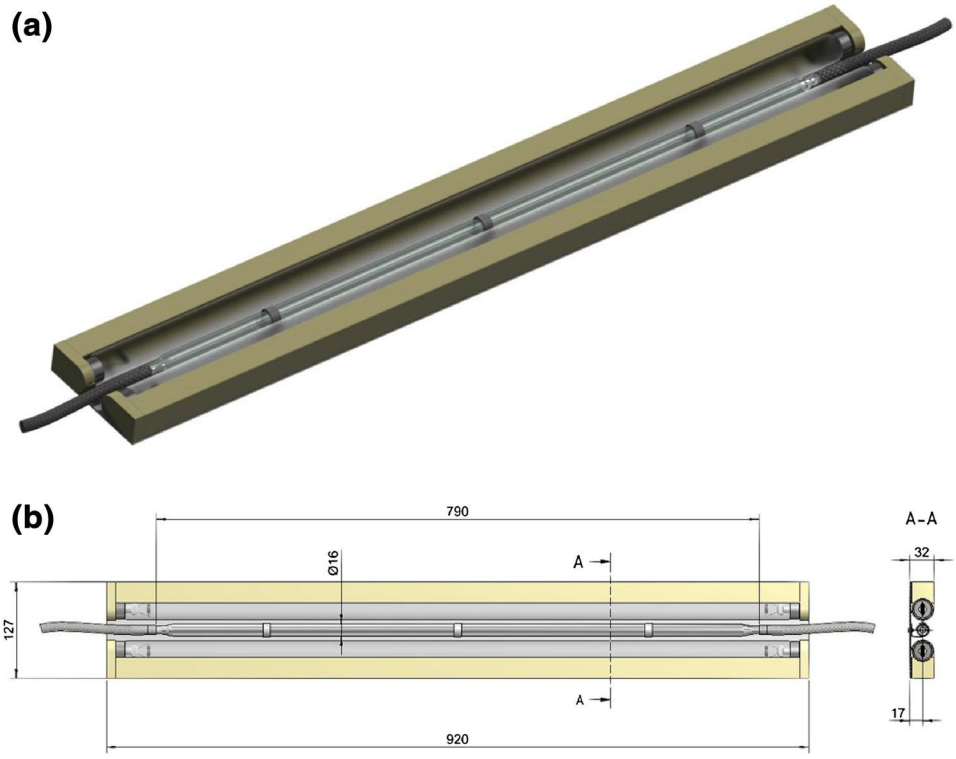

Fig. 3 **a** 3D view of the flow photoreactor; **b** dimensions in mm

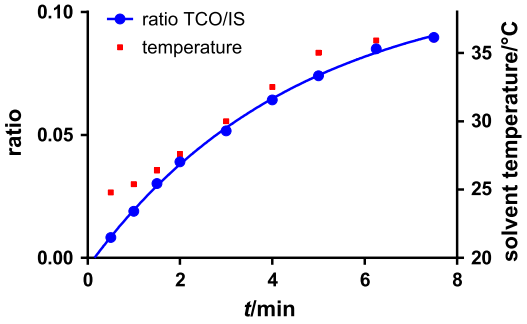

Fig. 4 Development of TCO/IS ratio and temperature during isomerization

device was below 300€ while the costs for commercially available systems (photoreactor including lamps and quartz glass flasks) are significantly higher (2000–5000€ or even more).

To determine the required time for reaching the equilibrium during photoisomerization a solution of *cis*-cyclooctene (**6**), methyl benzoate as singlet sensitizer and undecane as internal standard (IS, used for GC-FID measurements) in diethyl ether/hexanes (1/1) was irradiated without flow. Samples were taken after different irradiation times and analyzed by GC-FID. The temperature in the system reached 36 °C after about 6.5 min, which resulted in boiling of the solvent. The TCO/IS ratio was calculated over time and the data was fitted to a one phase association equation resulting in a predicted half-time of around 3.1 min (Fig. 4). The exact irradiation time for reaching the equilibrium could not be determined due to the rising temperature.

A flow rate of 100 cm^3/min was chosen for photoisomerization, which results in a rather short dwell time of 99 s. This is beneficial since the rate of isomerization is highest within the first minutes and the increase of temperature is only moderate.

For flow photoisomerization, the setup shown in Fig. 5a was used, for a picture see Electronic Supplementary Material (Fig. S2). An HPLC pump (**P**) was used to pass the reaction mixture from a reservoir flask (**F**) through a column (**C**) filled with silica and topped with $AgNO_3$-impregnated silica ($AgNO_3/SiO_2$) and covered with aluminum foil, then through the vertically aligned flow reactor (**R**) back to the reservoir. The column was placed right after the pump and prior to the photoreactor to prevent damage due to backpressure. The use of the reservoir flask enables simple scaling of the reaction without the use of expensive quartz glass flasks in different dimensions, since containers of any size and shape can be used for **F**. Implementation of cooling/heating of the solution as well as reactions under inert gas atmosphere can easily be realized in this setup. In this case a 3-neck round bottom flask equipped with a condenser was used, which was cooled and put under inert gas atmosphere.

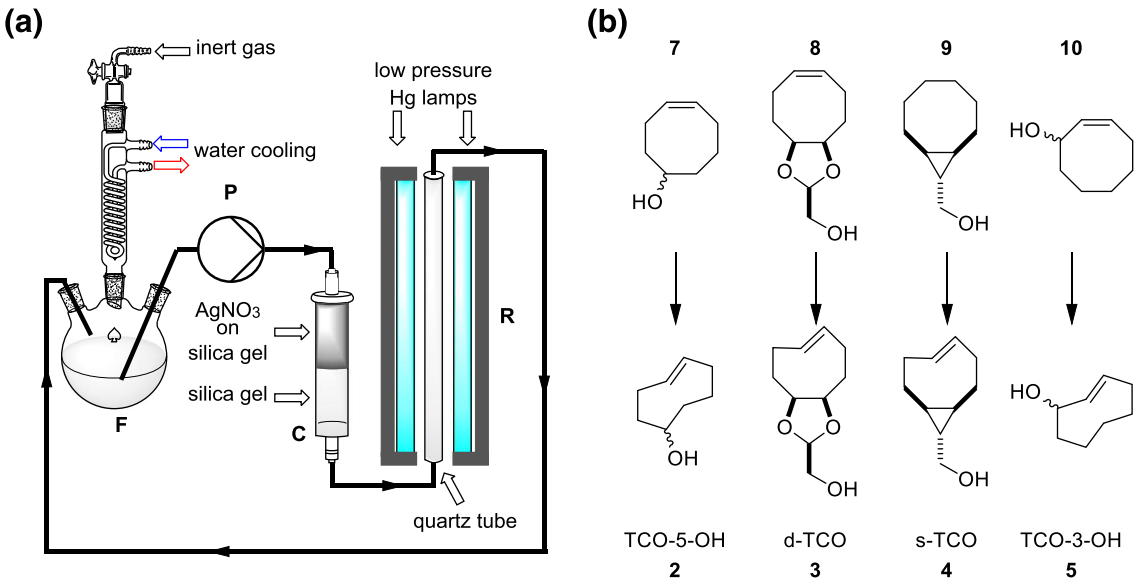

Fig. 5 **a** Flow photoisomerization setup; **b** isomerization of compounds **2**, **3**, **4**, and **5**

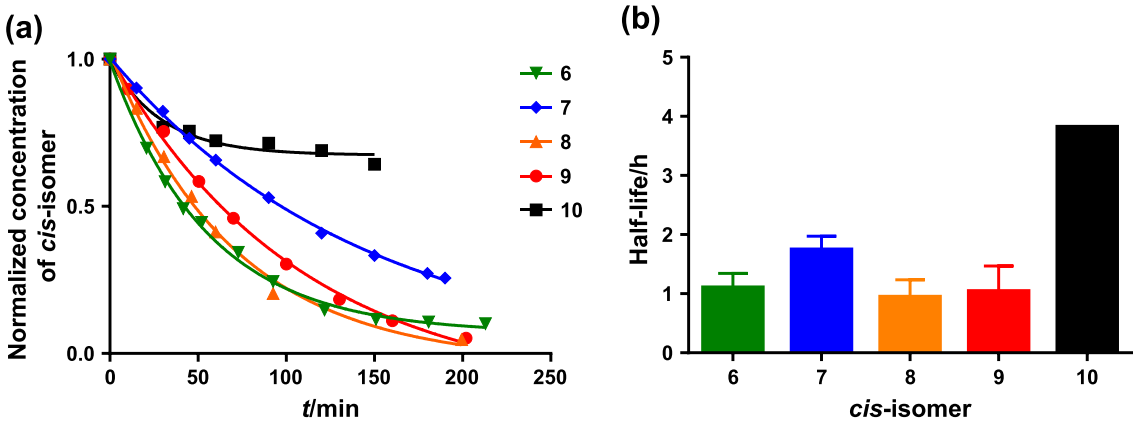

Fig. 6 **a** Decline of CCO derivatives during photoisomerization; **b** half-lifes of CCO compounds during photoisomerization

This setup was used for the synthesis of *trans*-cyclooctene (**1**) as a test substance followed by isomerization of *cis*-cycloocten-5-ol (**7**), ((2*S*,3a*R*,9a*S*,*Z*)-3a,4,5,8,9,9a-hexahydrocycloocta[*d*] [1, 3] dioxol-2-yl)methanol (**8**) and (1*R*,8*S*,9*R*,4*Z*)-bicyclo[6.1.0]non-4-en-9-ylmethanol (**9**) as well as *cis*-cycloocten-3-ol (**10**) to their corresponding *trans*-isomers (Fig. 5b). Reactions were monitored by measuring the remaining *cis*-configured starting material by GC (Fig. 6a). Isomerizations of **6**, **7**, **8**, and **9** were performed at least in duplicates and revealed similar isomerization times and a mean half-life of 72 ± 24 min for all 9 reactions (Fig. 6b). The isomerization of **10** to TCO-3-OH (mixture of **5a/5e**) was significantly slower with a half-life of 3.8 h, which is in good agreement with the reported reaction time of 32 h [41] for this derivative in comparison to 6-26 h reported for other TCOs [12, 40, 42]. Furthermore, isolated yields were compared with previously reported results (Table 1).

Conclusion

We were able to develop a low-cost and easy-to-build flow photoreactor that can be used for efficient synthesis of *trans*-cyclooctenes starting from respective *cis*-derivatives by photoisomerization. The setup was tested and characterized using different substituted and frequently used TCO derivatives. Isomerization was possible in relatively short time for all used substances with an average half-life of about 70 min with exception of **10** that showed a half-life of 3.8 h.

This simple design of a flow photoisomerization apparatus, which can easily be set up in any lab, enables the

Table 1 Comparison of yields for photoisomerization of **2**, **3**, **4**, and **5** reported in literature and those reached in this work

TCO	**2** (**2e**/**2a**)	**3**	**4**	**5** (**5e**/**5a**)
Literature	71 % [42] (47/24)	59 % [12]	74 % [40]	43 % [41] (25/18)
This work	47 % (32/15)	58 %	79 %	75 % (36/39)

efficient and cheap production of TCO derivatives up to multigram scale.

Experimental

Unless otherwise noted, all reagents were purchased from commercial suppliers and used without further purification. *Cis*-isomers **7** [42], **8** [12], **9** [40], and **10** [45] as well as $AgNO_3$-impregnated silica gel ($AgNO_3/SiO_2$) [42] were prepared following known procedures. GC-FID measurements were performed on a Trace™ 1310 GC chromatograph from Thermo Scientific equipped with TR-5MS columns (length 15 m, I.D. 0.25 mm, film 1.0 µm). ^1H and ^{13}C NMR spectra were recorded on a Bruker AC 200 or Bruker Avance UltraShield 400 spectrometer at 20 °C.

Kinetics of photoisomerization

The flow photoreactor as illustrated in Fig. 3 was closed at the bottom and filled with a 10 mM solution of 187 mg *cis*-cyclooctene (1.7 mmol), 231 mg methylbenzoate (1.7 mmol), and 265 mg *n*-undecane (1.7 mmol) in 170 cm^3 hexanes/Et_2O (1:1). A resistance thermometer was placed inside the tube to follow the temperature of the solvent. The lamps were turned on and samples were taken at different time points and analyzed by GC-FID.

Photoisomerization and synthesis of TCO compounds: general procedure

The setup shown in Fig. 5a was used. The column was filled with silica gel, topped with $AgNO_3/SiO_2$ (10 %) and flushed with solvent. Then the reservoir was filled with solvent and put under argon atmosphere. The pump was turned on and set to a flow rate of 100 cm^3/min. After the solvent had filled the whole system *cis*-cyclooctene (final concentration between 5 and 20 mM), methyl benzoate and, if applicable, *n*-undecane was slowly added to the reservoir over the course of several minutes to ensure homogeneous distribution of all reactants. Afterwards the solution was pumped through the system for another 20 min. The lamps were turned on and the reaction progress was monitored by GC-FID following the decline of the starting material in the reservoir flask using either methyl benzoate or *n*-undecane as internal standard. The reservoir flask was cooled with ice-water during isomerization. After the reaction was completed, as indicated by consumption of the starting material, the lamps were turned off. The column was flushed with generous amounts of the solvent as used during isomerization (>60 cm^3/mmol of *cis*-configured starting material) and then dried with compressed air. Silica and $AgNO_3/SiO_2$ were taken out of the column, stirred in a mixture of concentrated NH_4OH (37 %) and dichloromethane (each 10 cm^3/g $AgNO_3/SiO_2$) and filtrated. The filter cake was washed twice with concentrated NH_4OH (5 cm^3/g $AgNO_3/SiO_2$) and dichloromethane (5 cm^3/g $AgNO_3/SiO_2$). The organic layer was separated, washed twice with water, dried over Na_2SO_4, and concentrated. Column chromatography was used for further purification if needed.

trans-Cyclooctene (**1**)
Following the general procedure using 9.50 g **6** (86 mmol), 12.30 g methyl benzoate (91 mmol), 130 g $AgNO_3/SiO_2$ (10 %), 100 g SiO_2, and 3500 cm^3 Et_2O/hexanes (1:99); 5.50 g (50 mmol, 58 %) of pure **1** were obtained without further purification. Spectroscopic data matched those reported in the literature [42].

TCO-5-OH, rel-(1R,4E,pR)-cyclooct-4-enol (**2e**)
and *rel-(1R,4E,pS)-cyclooct-4-enol* (**2a**)
Following the general procedure using 2.03 g **7** (11.9 mmol), 2.00 g methyl benzoate (14.7 mmol), 27 g $AgNO_3/SiO_2$ (10 %), 18 g SiO_2, 700 cm^3 Et_2O/hexanes (9:1), 1.00 g *n*-undecane (6.4 mmol); the crude product was purified by column chromatography (90 g silica, hexanes/ethyl acetate, 4:1) to yield 658 mg (32 %, 5.2 mmol) of equatorial product (**2e**) and 313 mg (15 %, 2.5 mmol) of axial product (**2a**). Spectroscopic data matched that reported in the literature [42].

d-TCO, ((2 s,3aR,9aS,E)-3a,4,5,8,9,9a-hexahydrocyclooct a[d][1, 3]dioxol-2-yl)methanol (**3**)
Following the general procedure using 1.50 g **8** (8.2 mmol), 2.00 g methyl benzoate (14.7 mmol), 19 g $AgNO_3/SiO_2$ (10 %), 20 g SiO_2, 500 cm^3 Et_2O/hexanes (1:1), 1.00 g *n*-undecane (6.4 mmol); column chromatography (Et_2O/hexanes, 2:1) was performed to yield 875 mg (58 %, 4.8 mmol) of desired product **3**. Spectroscopic data matched that reported in the literature [12].

s-TCO, (rel-1R,8S,9R,4E)-bicyclo[6.1.0]non-4-en-9-ylmethanol (**4**)

Following the general procedure using 1.50 g **9** (9.9 mmol), 1.30 g methyl benzoate (9.5 mmol), 33 g $AgNO_3/SiO_2$ (10 %), 50 g SiO_2, 1000 cm^3 Et_2O/hexanes (1:1), 1.00 g *n*-undecane (6.4 mmol); 1.19 g (79 %, 7.8 mmol) of pure **4** were obtained without chromatographic purification. Spectroscopic data matched that reported in the literature [40].

TCO-3-OH, (1RS,2RS)-trans-cyclooct-2-enol (**5e**) and *(1SR,2RS)-trans-cyclooct-2-enol* (**5a**)

Following the general procedure using 2.00 g **10** (15.8 mmol), 2.15 g methyl benzoate (15.8 mmol), 35 g $AgNO_3/SiO_2$ (10 %), 40 g SiO_2, 800 cm^3 Et_2O/hexanes (1:1), 2.50 g *n*-undecane (15.8 mmol); the crude product was purified by column chromatography (90 g silica gel, 10-50 % ethyl acetate in hexanes) to yield 694 mg (35 %, 5.5 mmol) of axial isomer **5a**, 669 mg (33 %, 5.3 mmol) of equatorial isomer **5e** and 146 mg of a mixture (**5a**/**5e** = 1.3:1, 7 %, 1.2 mmol). NMR spectra matched those reported in the literature [41].

Acknowledgments We thank Rudolf Svatunek for the design drawings and the doctoral program 'Molecular and Elemental Imaging in Biosciences (MEIBio)' of TU Wien for funding.

Open Access This article is distributed under the terms of the Creative Commons Attribution 4.0 International License (http://creativecommons.org/licenses/by/4.0/), which permits unrestricted use, distribution, and reproduction in any medium, provided you give appropriate credit to the original author(s) and the source, provide a link to the Creative Commons license, and indicate if changes were made.

References

1. Sletten EM, Bertozzi CR (2009) Angew Chem Int Ed 48:6974
2. Devaraj NK, Weissleder R (2011) Acc Chem Res 44:816
3. Knall A-C, Slugovc C (2013) Chem Soc Rev 42:5131
4. Lang K, Chin JW (2014) ACS Chem Biol 9:16
5. Willems LI, van der Linden WA, Li N, Li K, Liu N, Hoogendoorn S, van der Marel GA, Florea BI, Overkleeft HS (2011) Acc Chem Res 44:718
6. Knight JC, Cornelissen B (2014) Am J Nucl Med Mol Imaging 4:96
7. Jewett JC, Bertozzi CR (2010) Chem Soc Rev 39:1272
8. Laughlin ST, Baskin JM, Amacher SL, Bertozzi CR (2008) Science 320:664
9. Lee SB, Kim HL, Jeong H-J, Lim ST, Sohn M-H, Kim DW (2013) Angew Chem Int Ed 52:10549
10. Blackman ML, Royzen M, Fox JM (2008) J Am Chem Soc 130:13518
11. Devaraj NK, Weissleder R, Hilderbrand SA (2008) Bioconjugate Chem 19:2297
12. Darko A, Wallace S, Dmitrenko O, Machovina MM, Mehl RA, Chin JW, Fox JM (2014) Chem Sci 5:3770
13. Rossin R, van Duijnhoven SMJ, Läppchen T, van den Bosch SM, Robillard MS (2014) Mol Pharm 11:3090
14. Nichols B, Qin Z, Yang J, Vera DR, Devaraj NK (2014) Chem Commun 50:5215
15. Denk C, Svatunek D, Filip T, Wanek T, Lumpi D, Fröhlich J, Kuntner C, Mikula H (2014) Angew Chemie Int Ed 53:9655
16. Zhu J, Li S, Wängler C, Wängler B, Lennox RB, Schirrmacher R (2015) Chem Commun 51:12415
17. Rashidian M, Keliher EJ, Dougan M, Juras PK, Cavallari M, Wojtkiewicz GR, Jacobsen JT, Edens JG, Tas JMJ, Victora G, Weissleder R, Ploegh H (2015) ACS Cent Sci 1:142
18. Wu Z, Liu S, Hassink M, Nair I, Park R, Li L, Todorov I, Fox JM, Li Z, Shively JE, Conti PS, Kandeel F (2013) J Nucl Med 54:244
19. Selvaraj R, Liu S, Hassink M, Huang C-W, Yap L-P, Park R, Fox JM, Li Z, Conti PS (2011) Bioorg Med Chem Lett 21:5011
20. Liu S, Hassink M, Selvaraj R, Yap L, Park R, Wang H, Chen X, Fox JM, Li Z, Conti PS (2013) Mol Imaging 12:121
21. Selvaraj R, Giglio BC, Liu S, Wang H, Wang M, Yuan H, Chintala SR, Yap L, Conti PS, Fox JM, Li Z (2015) Bioconjugate Chem 26:435
22. Li Z, Cai H, Hassink M, Blackman ML, Brown RCD, Conti PS, Fox JM (2010) Chem Commun 46:8043
23. Meimetis LG, Carlson JCT, Giedt RJ, Kohler RH, Weissleder R (2014) Angew Chem Int Ed 29:7531
24. Yang J, Šečkutė J, Cole CM, Devaraj NK (2012) Angew Chem Int Ed 51:7476
25. Devaraj NK, Hilderbrand S, Upadhyay R, Mazitschek R, Weissleder R (2010) Angew Chem Int Ed 49:2869
26. Carlson JCT, Meimetis LG, Hilderbrand SA, Weissleder R (2013) Angew Chem Int Ed 52:6917
27. Yang KS, Budin G, Tassa C, Kister O, Weissleder R (2013) Angew Chem Int Ed 52:10593
28. Zhang H, Dicker KT, Xu X, Jia X, Fox JM (2014) ACS Macro Lett 3:727
29. Liu S, Zhang H, Remy RA, Deng F, Mackay ME, Fox JM, Jia X (2015) Adv Mater 27:2783
30. Liu F, Liang Y, Houk KN (2014) J Am Chem Soc 136:11483
31. Liu F, Paton RS, Kim S, Liang Y, Houk KN (2013) J Am Chem Soc 135:15642
32. Karver M, Weissleder R, Hilderbrand SA (2011) Bioconjugate Chem 22:2263
33. Lang K, Davis L, Torres-Kolbus J, Chou C, Deiters A, Chin JW (2012) Nat Chem 4:298
34. Knall A-C, Hollauf M, Slugovc C (2014) Tetrahedron Lett 55:4763
35. Beckmann HSG, Niederwieser A, Wiessler M, Wittmann V (2012) Chem Eur J 18:6548
36. Patterson DM, Nazarova LA, Xie B, Kamber DN, Prescher JA (2012) J Am Chem Soc 134:18638
37. Devaraj N (2012) Synlett 23:2147
38. Yang J, Liang Y, Šečkutė J, Houk KN, Devaraj NK (2014) Chemistry 20:3365
39. Rossin R, van den Bosch SM, Ten Hoeve W, Carvelli M, Versteegen RM, Lub J, Robillard MS (2013) Bioconjugate Chem 24:1210
40. Taylor MT, Blackman ML, Dmitrenko O, Fox JM (2011) J Am Chem Soc 133:9646
41. Versteegen RM, Rossin R, ten Hoeve W, Janssen HM, Robillard MS (2013) Angew Chem Int Ed 52:14112
42. Royzen M, Yap GPA, Fox JM (2008) J Am Chem Soc 130:3760
43. Inoue Y, Kunitomi Y, Takamuku S, Sakurai H (1978) J Chem Soc Chem Commun 1024
44. Inoue Y, Takamuku S, Kunitomi Y, Sakurai H (1980) J Chem Soc Perkin Trans 2:1672
45. Zhang J, Matta ME, Martinez H, Hillmyer MA (2013) Macromolecules 46:2535

3 Statement of Contribution

I. Strain-Promoted Alkyne Azide Cycloaddition

Manuscript #1

The research subject of manuscript #1 was independently initiated by the applicant (D. Svatunek). Computational studies were performed by D. Svatunek. Kinetic NMR experiments and data analyses were conducted by N. Houszka in the course of her bachelor thesis under supervision by the applicant (D. Svatunek). The data was assembled and the manuscript was written by the applicant. All authors contributed to discussion, proofreading and revision.

Manuscript #2

The research subject was initiated by H. Mikula. Synthetic work was conducted by the applicant, G. Eilenberger, and C. Denk. G. Eilenberger and C. Denk developed the protocol for kinetic ATR-IR measurements. The applicant conducted the main part of kinetic measurements including subsequent data analysis. Results and data were assembled and the manuscript written by the applicant. All authors contributed to manuscript discussion, proofreading and revision.

Manuscript #3

Radiochemical procedures of this project were developed by C. Denk. The main part of synthetic work was performed by C. Denk. Compounds **7-10** were synthesized by M. Wilkovitsch during his bachelor thesis (under supervision of H. Mikula and C. Denk). The applicant (D. Svatunek) provided additional “cold” reference material and proposed structure **4**. P. Skrinjar contributed to the project by proposing structure **5**. *In vivo* experiments were performed at AIT in the group of C. Kuntner. The manuscript was written by C. Denk. D. Svatunek contributed to manuscript discussion, proofreading and revision.

II. Tetrazine Ligation

Manuscript #4

The main part of the synthesis and characterization of all substances presented in manuscript #4 as well as development of radiochemical protocols was done by Christoph Denk. The applicant (D. Svatunek) contributed to synthetic work with the preparation of additional precursor material. Computational studies were conducted by D. Svatunek. Animal studies were performed in collaboration with our cooperation partners at AIT.D. Svatunek contributed to radio synthesis and radio TLC of blood samples. The data was assembled and the manuscript was written by H. Mikula, C. Denk and D. Svatunek. All authors contributed to the manuscript discussion, proofreading and revision.

Manuscript #5

The lead structures of manuscript #5 were proposed and the main part of synthetic work was performed by C. Denk. The applicant (D. Svatunek) contributed to synthetic work by preparation of reference material. Computational studies and kinetic investigations as well as data analysis was conducted by D. Svatunek. Radiochemical method development and radiosynthesis were done by C. Denk. PET experiments and data analysis were performed by the group of C. Kuntner. The data was assembled and the manuscript was written by C. Denk. D. Svatunek contributed to the manuscript discussion, proofreading and revision.

Manuscript #6

The main part of the synthesis and characterization of substances presented in manuscript #6 as well as the development of radiochemical protocols was done by Christoph Denk. The applicant (D. Svatunek) contributed to synthetic work with the preparation of additional precursor and reference material. Computational studies and reaction kinetics investigations were carried out by the D. Svatunek. Animal studies were performed in collaboration with cooperation partners at AIT. The data was assembled and the manuscript was written by H. Mikula, C. Denk and D. Svatunek. All authors contributed to the manuscript discussion, proofreading and revision.

Manuscript #7

Synthesis and characterization of a tetrazine-modified RGD-peptide, preparation of conjugated reference material (^{19}F-labeled compounds), and kinetic investigations were conducted by the applicant (D. Svatunek) at University of Delaware in course of a research stay funded by the Austrian Marshall Plan Foundation. Synthesis and characterization of precursor for ^{18}F-labeled s-TCO was done by Y. Liu and replicated by D. Svatunek for the preparation of sufficient material for further studies. Radiolabeling and subsequent animal studies were performed at University of South Carolina at Chapel Hill by the group of Z. Li. The manuscript was written and composed by J. Fox, Z. Li, M. Whang and D. Svatunek. All authors contributed to the manuscript discussion, proofreading and revision.

Manuscript #8

The described photo flow reactor was designed and built by C. Denk and V. Rosecker. Synthesis of *trans*-cyclooctenes and kinetic measurements of photoisomerizations were performed by C. Denk, D. Svatunek, B. Sohr, and V. Rosecker. Characterization of the reactor was done by D. Svatunek. The applicant assembled and analyzed the data and results, and wrote the manuscript. All authors contributed to manuscript discussion, proofreading and revision.

4 Appendix

Supporting Information

Manuscript #1

Dennis Svatunek, Nicole Houszka, Christoph Denk, Christian Hametner, Günter Allmaier and Hannes Mikula*; Reactivity of Secondary and Tertiary Azides in Strain-Promoted Alkyne Azide Cycloadditions, manuscript draft.

Supporting Information

Reactivity of Secondary and Tertiary Azides in Strain-Promoted Alkyne Azide Cycloadditions

Dennis Svatunek, Nicole Houszka, Christoph Denk, Christian Hametner, Günter Allmaier and Hannes Mikula*[a]

---

1. Materials and Methods 2
2. Synthesis 2
3. Kinetic experiments 3
4. Quantum Chemical calculations 5
5. Literature 10

1. Materials and Methods

Unless otherwise noted, all reagents were purchased from commercial suppliers and used without further purification. BCN[1] and 2-Azidoethanol[2] were prepared following known procedures. ADIBO, was purchased from Click Chemistry Tool (Scottsdale, AZ, USA). DCM and THF were dried using PURESOLV-columns (Innovative Technology Inc.). All other solvents were distilled prior to use. Drying of organic solvents after extraction was performed using anhydrous Na_2SO_4 and subsequent filtration. Reactions were carried out under an atmosphere of argon in air-dried glassware with magnetic stirring. Sensitive liquids were transferred via syringe. Thin layer chromatography was performed using TLC alumina plates (Merck, silica gel 60, fluorescence indicator F254, or Merck, aluminium oxide neutral, fluorescence indicator F254). Preparative normal phase column chromatography was performed using a Büchi Sepacore Flash System (2 x Büchi Pump Module C-605, Büchi Pump Manager C-615, Büchi UV Photometer C-635, Büchi Fraction Collector C-660) or on a Grace Reveleris X2 Prep using silica gel 60 (40-63 µm) as obtained from Merck and distilled or redistilled solvents.

^1H and ^{13}C NMR spectra were recorded on a Bruker AC 200, Bruker Avance UltraShield 400 spectrometer at 20 °C or Bruker Bruker Avance III HD 600 (600 MHz). Chemical shifts are reported in ppm (δ) relative to tetramethylsilane and calibrated using solvent residual peaks. Data are shown as follows: Chemical shift, multiplicity (s = singlet, d = doublet, t = triplet, q = quartet, quin = quintet, m = multiplet, br = broad signal), coupling constant (J, Hz) and integration. Thermo Fischer Exactive Plus Orbitrap (LC-ESI+) was used for high resolution mass spectrometry.

2. Synthesis

2-azidopropan-1-ol (2)



2

Potassium carbonate (1.21 eq., 4.52 g, 32.7 mmol) and copper sulfate pentahydrate (0.01 eq., 0.07 g, 0.27 mmol) were added to a stirring solution of 2-aminopropanol (1 eq., 2 g, 26.63 mmol) in 135 mL anhydrous methanol under argon atmosphere. Imidazole-1-sulfonyl azide hydrochloride (1.2 eq., 6.7 g, 57.25 mmol) was added and the mixture stirred for 3.5 h at room temperature. Afterwards methanol was removed *in vacuo*, the residue diluted with water (400 mL), acidified with conc. HCl until pH 5, extracted with ethyl acetate (3x200 mL), dried over $MgSO_4$, filtered and concentrated. The crude product was filtered over a pad of silica (hexanes:diethyl ether, 2:1) to obtain **7** (2.03 g, 75% of theory) as a yellowish oil. Rf (PE:Et_2O = 2:1) = 0.16; NMR data matched previously reported data. [3]

2-azido-2-methylpropan-1-ol (3)

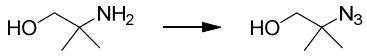

3

To a stirred mixture of 2-amino-2-methyl-propan-1-ol (1 eq., 4.25 g, 47.7 mmol), potassium carbonate (1.2 eq., 8.0 g, 58 mmol) and $CuSO_4$ x 5 H_2O (0.01 eq., 119 mg, 0.48 mmol) in 200 mL methanol was added imidazol-1-sulfonyl azide hydrochloride (1.2 eq., 10 g, 57.25 mmol) in portions. The mixture was stirred overnight at room temperatureand the majority of MeOH was carefully removed on the rotary evaporator. The residue was taken up in 500 mL water, acidified (pH 4) with HCl, and the solution was extracted three times with ethyl acetate. Combined extracts were dried over $MgSO_4$ and the solvent was removed on the rotary evaporator (50 mbar). The residue was purified by filtration over a plug of SiO2 using PE:Et_2O = 2:1 as eluent. Stripping of solvent afforded 3.47 g tertiary azide **3** as colorless liquid (63% of theory). TLC-Rf (PE:Et_2O = 2:1) = 0.4, ^{1}H NMR (200 MHz, $CDCl_3$) δ = 1.27 (s, 6 H) 2.54 (br. s, 1 H) 3.42 (s, 2 H) ppm, ^{13}C NMR (50.32 MHz, $CDCl_3$): δ = 22.5, 62.4, 70.0 ppm

3. Kinetic experiments

NMR kinetic experiments were performed on a Bruker Bruker Avance III HD 600 (600 MHz) at 298K. $CDCl_3$ (euriso-top) was used a solvent. All experiments were performed in triplicates.

Solutions of azides **1**, **2** and **3** as well as cyclooctynes BCN (**4**) and ADIBO (**5**) in $CDCl_3$, containing an internal standard, were prepared. In case of **4** biphenyl was used as an internal standard. For reactions with **5** CH_2Cl_2 was used as internal standard. Solutions of azides and cyclooctynes (approx. 0.3 mL each) were mixed in the NMR tube and after vigorously shaking the tube it was inserted into the NMR machine. Unless otherwise noted measurements were done every 2 minutes, using 16 scans over 2 minutes per measurement. Time point of first measurement was used as t=0 and using the internal standard concentration of starting material at the first measurement was adopted as starting concentration. Concentration of both reactants was determined by following the decline of a characteristic signal of either azide or cyclooctyne over time. Decline in concentration was used for calculation of second order rate constants. Data Analysis was done using TopSpin 3.2. Results are shown in Table S1.

Table S1: measured reaction rates of reaction between azides **1**,**2** and **3** and cyclooctynes **4** and **5**, used intervals for measurements as well as results of HRMS measurements of the reaction products

Reaction	**1+4**	**2+4**	**3+4**	**1+5**	**2+5**	**3+5**
k [$M^{-1}s^{-1}$] first measurement	0.0245	0.013	0.0117	0.8276	0.3087	$4.716 \cdot 10^{-6}$
k [$M^{-1}s^{-1}$] second measurement	0.0248	0.0125	0.0108	0.8794	0.2035	$4.626 \cdot 10^{-6}$
k [$M^{-1}s^{-1}$] third measurement	0.0229	0.0123	0.0121	0.9946	0.2324	$4.674 \cdot 10^{-6}$
mean k [$M^{-1}s^{-1}$]	**0.0241**	**0.0126**	**0.0115**	**0.9005**	**0.2482**	**$4.672 \cdot 10^{-6}$**
standard deviation	0.0008	0.0003	0.0005	0.0698	0.0444	$3.665 \cdot 10^{-8}$
Points	10	16	30	10	14	12
Time between measurements [min]	2	2	2	2	2	30
Total measurement time [min]	20	32	60	20	28	360
HRMS of product: $[M+H]^+$ calculated	238.1550	252.1707	266.1863	364.1768	378.1925	392.2081
HRMS of product: $[M+H]^+$ found	238.1559	252.1714	266.1876	364.1761	378.1936	392.2090

4. Quantum Chemical calculations

All SCS-MP2 calculations were performed using NWChem 6.6.[4] Geometry optimizations to energy minima or transition states as well as subsequent frequency analyses at 298.15 K of all considered compounds and intermediates were achieved with the 6-311G(d,p) basis set.[5] Imaginary frequencies corresponding to the desired reaction coordinates were obtained only in the case of transition state calculations. ΔE values were calculated by performing SCS-MP2 calculations using the 6-311+G(2d,2p) basis set on SCS-MP2/6-311G(d,p) optimized structures as proposed by van Delft and Coworkers.[6] In addition, counterpoise correction was applied to transition state structures.

Distortion/Interaction analysis was performed as introduced by Bickelhaupt[7] and Houk.[8] Therefore energy of both cyclooctyne and azide at transition state geometry were calculated. Energy difference between these distorted molecules and relaxed geometry is taken as ΔE_{dist}. By adding up $\Delta E_{dist,azide}$ and $\Delta E_{dist,octyne}$ one can calculate the total distortion energy $\Delta E_{dist,total}$. Difference between $\Delta E_{dist,total}$ and $\Delta E^{\ddagger}$ is attributed to interaction energy, ΔE_{int}. Formula S1 shows the connection between these energies and Figure S1 provides a graphical representation.

Formula S1:

$$\Delta E^{\ddagger} = \left(\Delta \mathrm{E}_{\mathrm{dist,azide}} + \Delta \mathrm{E}_{\mathrm{dist,azide}}\right) + \Delta \mathrm{E}_{\mathrm{int}}$$

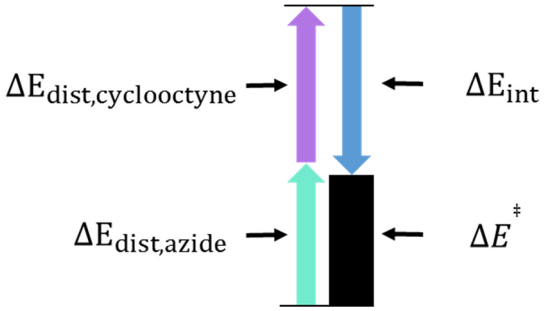

Figure S1: Graphical representation of interaction/distortion energies

Data analysis was done using Avogadro[9] and PyMol.[10]

Model structures were used in this study (Figure S2).

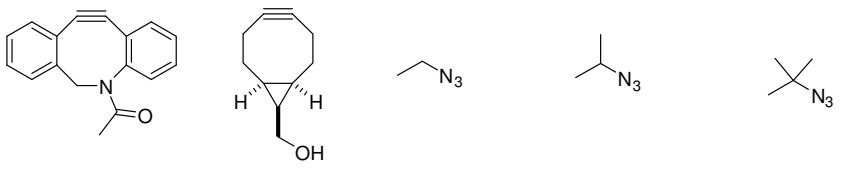

ADIBO **BCN** **ethyl azide** **isopropyl azide** **t.-butyl azide**

Figure S2: Used model structures

Calculated energies are shown in Table S2 and S3, cartesian coordinates of all structures are listed below.

Table S2: Energies of ground state geometries

Structure	E [hartree]
ADIBO	-783.57739
BCN	-463.43006
ethyl azide	-242.84779
isopropyl azide	-282.05923
t.-butyl azide	-321.2713

Table S3: Energies of transition state structures as well as distorted reactants

cyclooctyne	azide	E [hartree] of transition state structure	E [hartree] of azide at transition state structure	E [hartree] of cyclooctyne at transition state structure
ADIBO	ethyl azide	-1026.4131	-242.81331	-783.57195
	isopropyl azide	-1065.6245	-282.02378	-783.57178
	t.-butyl azide	-1104.8309	-321.22745	-783.56836
BCN	ethyl azide	-706.26081	-242.81584	-463.42645
	isopropyl azide	-745.47207	-282.02643	-463.42637
	t.-butyl azide	-784.68185	-321.23176	-463.4243

Cartesian Coordinates

SCS-MP2/6-311G(d,p) optimized structures

ADIBO, **5**

C	-1.85011	0.54587	0.36772
C	-1.79409	-0.68600	0.41205
C	0.38711	-0.54992	-1.23154
H	-0.44720	-0.13397	-1.80442
H	1.23168	-0.72063	-1.90828
C	-1.25593	1.81386	0.13455
C	0.12175	1.74510	-0.22278
C	0.80222	2.92359	-0.55232
H	1.83952	2.85975	-0.86934
C	0.15400	4.15935	-0.47869
H	0.69643	5.06722	-0.72636
C	-1.19488	4.22627	-0.10768
H	-1.69760	5.18775	-0.05914
C	-1.90159	3.05951	0.18448
H	-2.95193	3.09716	0.45779
C	-1.21184	-1.95609	0.15451
C	-1.65312	-3.18735	0.66287
H	-2.56222	-3.22530	1.25580
C	-0.92681	-4.34533	0.38384
H	-1.26571	-5.30141	0.77256
C	0.25622	-4.27182	-0.36175
H	0.82858	-5.17344	-0.56053
C	-0.02294	-1.87247	-0.61951
C	0.69745	-3.04400	-0.86460
H	1.62540	-2.98129	-1.42631
N	0.77861	0.48752	-0.25061
C	1.93827	0.22194	0.45862
C	2.31346	1.19685	1.55790
H	2.97834	1.97241	1.16817
H	1.44188	1.68101	2.00193
H	2.85812	0.62918	2.31342
O	2.59272	-0.78415	0.22130

BCN, **4**

C	1.07097	-2.20169	-0.15149
C	-0.11019	-2.51678	-0.22752
C	-1.00158	0.00024	0.78827
H	-1.43539	-0.30859	1.73933
C	-1.66480	-0.70232	-0.38250
H	-1.20947	-0.40505	-1.33158
H	-2.72509	-0.41565	-0.41960
C	-1.54850	-2.24481	-0.27083
C	2.18599	-1.26185	-0.01712
C	1.54709	0.14582	-0.13643
H	1.13598	0.24538	-1.14570
H	2.31507	0.92075	-0.02212
H	-2.04760	-2.59762	0.63982
H	-2.04122	-2.72587	-1.12290
H	2.94789	-1.40219	-0.79162
H	2.68152	-1.37190	0.95504
C	0.47199	0.37047	0.90918
C	-0.57324	1.45853	0.77045
H	0.85464	0.25572	1.92305
H	-0.78420	2.03375	1.66843
C	-0.63378	2.28349	-0.48265
H	-1.58134	2.84100	-0.50556
H	-0.59718	1.64642	-1.37417
O	0.47949	3.17751	-0.45451
H	0.38195	3.75498	-1.21647

ethyl azide

N	0.13751	-2.46147	0.00000
N	-0.53181	-0.16637	0.00000
N	-0.11448	-1.33339	0.00000
C	0.52681	0.87240	0.00000
C	-0.15525	2.22799	0.00000
H	-0.78279	2.33547	0.88705
H	-0.78279	2.33547	-0.88705
H	0.59342	3.02451	0.00000
H	1.15897	0.75618	0.88890
H	1.15897	0.75618	-0.88890

isopropyl azide

N	0.07552	2.60180	0.13121
N	-0.70544	0.38706	-0.32366
N	-0.25180	1.50692	-0.04688
C	-0.00152	-0.74825	0.34058
C	-0.80521	-1.99474	0.01147
H	-0.81546	-2.15317	-1.07048
H	-1.83501	-1.89062	0.35968
H	-0.35495	-2.86801	0.49160
H	-0.01819	-0.57677	1.42605
C	1.44256	-0.83848	-0.14028
H	1.46024	-0.98999	-1.22315
H	1.99560	0.07632	0.09311
H	1.95100	-1.67799	0.34335

tert.-butyl azide

N	0.11168	2.68371	0.00000
N	-0.90071	0.51554	0.00000
N	-0.31581	1.60799	0.00000
C	0.00478	-0.68263	0.00000
C	0.86770	-0.66284	-1.26034
H	1.51911	0.21747	-1.27347
H	0.23292	-0.64079	-2.15044
H	1.49999	-1.55560	-1.29872
C	0.86770	-0.66284	1.26034
H	1.51911	0.21747	1.27347
H	0.23292	-0.64079	2.15044
H	1.49999	-1.55560	1.29872
C	-0.93915	-1.87736	0.00000
H	-1.57610	-1.85592	-0.88832
H	-0.36185	-2.80694	0.00000
H	-1.57610	-1.85592	0.88832

Transition state: ADIBO (**5**) + ethyl azide

C	-1.27321	0.18800	0.35278
N	-3.28868	-0.40035	0.71048
C	-0.63322	-0.90144	0.42279
N	-2.09385	-2.37145	0.74519
C	1.26633	0.27417	-1.26975
H	0.31026	0.22569	-1.80015
H	2.06210	0.51115	-1.98530
N	-3.07139	-1.56846	0.73141
C	-1.25842	1.59771	0.10489
C	-0.01246	2.17955	-0.25458
C	0.05070	3.53759	-0.59165
H	1.00157	3.95148	-0.91634
C	-1.08479	4.34530	-0.50077
H	-1.01985	5.40029	-0.75129
C	-2.30829	3.78220	-0.11907
H	-3.19593	4.40472	-0.05115
C	-2.39753	2.42160	0.17367
H	-3.34490	1.97510	0.45357
C	0.60024	-1.61269	0.26800
C	0.88556	-2.81352	0.94407
H	0.14843	-3.21041	1.63646
C	2.11373	-3.44770	0.75374
H	2.33321	-4.36967	1.28533
C	3.06195	-2.89544	-0.11588
H	4.02068	-3.38590	-0.25872
C	1.56826	-1.03878	-0.59402
C	2.79314	-1.68860	-0.76825
H	3.54393	-1.22911	-1.40484
N	1.15458	1.37780	-0.29536
C	2.32553	1.71755	0.36130
C	2.21715	2.73837	1.47769
H	2.97282	2.47597	2.21968
H	2.44366	3.73952	1.10124
H	1.22622	2.75562	1.93441
O	3.38186	1.16992	0.07448
C	-2.10715	-3.40560	-0.31933
H	-1.18796	-3.97400	-0.17005
H	-2.95379	-4.07305	-0.12929
C	-2.16277	-2.81196	-1.72022
H	-2.19105	-3.61418	-2.46366
H	-3.05378	-2.19027	-1.84705
H	-1.27993	-2.19481	-1.90301

Transition state: ADIBO (**5**) + isopropyl azide

C	-1.18825	-0.03417	-0.34776
N	-2.92432	1.13678	-0.70349
C	-0.24642	0.80900	-0.41739
N	-1.18410	2.64634	-0.73370
C	1.20796	-0.89206	1.27066
H	0.31309	-0.55406	1.80222
H	1.89440	-1.36085	1.98512
N	-2.36229	2.18440	-0.72365
C	-1.60223	-1.38169	-0.09862
C	-0.59244	-2.31628	0.25781
C	-0.94605	-3.62862	0.59646
H	-0.16600	-4.31314	0.91875
C	-2.27388	-4.05166	0.50773
H	-2.53343	-5.07600	0.75942
C	-3.26817	-3.14182	0.12916
H	-4.30355	-3.46385	0.06315
C	-2.93847	-1.81913	-0.16514
H	-3.70503	-1.10465	-0.44278
C	1.14618	1.10764	-0.26649
C	1.78378	2.16181	-0.94721
H	1.20121	2.76459	-1.63841
C	3.14803	2.38897	-0.76256
H	3.63769	3.19836	-1.29729
C	3.88449	1.57378	0.10546
H	4.94804	1.74660	0.24375
C	1.89520	0.26544	0.59303
C	3.26104	0.50831	0.76160
H	3.83725	-0.15881	1.39641
N	0.76367	-1.90883	0.29644
C	1.77463	-2.59333	-0.35709
C	1.36015	-3.53336	-1.47278
H	1.28150	-4.55715	-1.09718
H	0.40645	-3.25461	-1.92379
H	2.15542	-3.50665	-2.21936
O	2.94778	-2.39641	-0.06896
C	-0.88480	3.65261	0.32242
H	0.19595	3.79412	0.23478
C	-1.21827	3.11772	1.70959
H	-0.94419	3.85610	2.46943
H	-2.29103	2.91445	1.79506
H	-0.67152	2.19146	1.90455
C	-1.59896	4.96119	-0.00050
H	-1.29128	5.73828	0.70602
H	-1.35889	5.28824	-1.01492
H	-2.68240	4.82770	0.07687

Transition state: ADIBO (**5**) + tert.butyl azide

C	-1.16272	0.09495	0.40045
N	-2.71484	-1.03617	0.89336
C	-0.16285	-0.69012	0.41746
N	-1.03160	-2.57604	0.71768
C	1.16904	1.08697	-1.29892
H	0.29561	0.66397	-1.80434
H	1.80944	1.58205	-2.03774
N	-2.20615	-2.11476	0.85743
C	-1.65205	1.42086	0.13888
C	-0.71689	2.40291	-0.28587
C	-1.16274	3.67922	-0.65304
H	-0.43597	4.39568	-1.02644
C	-2.51058	4.02430	-0.53965
H	-2.83988	5.02250	-0.81360
C	-3.43093	3.07135	-0.08925
H	-4.48251	3.32901	-0.00052
C	-3.01088	1.78039	0.22968
H	-3.72538	1.03554	0.55934
C	1.25866	-0.84092	0.31519
C	1.97837	-1.75951	1.10014
H	1.43275	-2.38637	1.79901
C	3.36394	-1.85332	0.97123
H	3.91654	-2.56031	1.58417
C	4.04149	-1.03710	0.05694
H	5.12082	-1.10992	-0.04293
C	1.94684	0.01950	-0.57488
C	3.33436	-0.09604	-0.69754
H	3.86014	0.58209	-1.36341
N	0.66467	2.09644	-0.34583
C	1.62957	2.88085	0.26459
C	1.16432	3.80639	1.37269
H	0.98851	4.81164	0.98044
H	0.24995	3.45703	1.85495
H	1.97805	3.86298	2.09746
O	2.80783	2.78008	-0.05084
C	-0.93418	-3.60092	-0.38729
C	0.50085	-4.10833	-0.44084
H	0.55339	-4.91994	-1.17406
H	1.19539	-3.32312	-0.74296
H	0.81015	-4.49791	0.53292
C	-1.87855	-4.75340	-0.03667
H	-2.91798	-4.41454	-0.02185
H	-1.77545	-5.54654	-0.78456
H	-1.62765	-5.16016	0.94707
C	-1.32594	-2.94865	-1.71274
H	-0.64186	-2.12685	-1.94440
H	-1.27619	-3.68796	-2.51922
H	-2.34540	-2.55196	-1.66891

Transition state: BCN (**4**) + ethyl azide

C	-0.14435	0.97154	-0.46844
C	1.08312	0.88478	-0.23927
C	-0.64826	-1.65774	0.72275
C	2.28507	0.08618	0.05335
C	0.84474	-1.76973	0.98256
C	1.91937	-1.40965	-0.02245
H	3.08792	0.32068	-0.65531
H	-1.22331	-1.32667	1.58723
H	2.66619	0.33004	1.05383
H	1.13189	-1.51122	2.00156
C	-1.45246	0.31249	-0.63810
H	-1.91560	0.60932	-1.58738
H	-2.14308	0.61861	0.16111
C	-1.25997	-1.21559	-0.58906
H	-2.22577	-1.71993	-0.71783
H	-0.63043	-1.51063	-1.43424
H	1.59559	-1.62678	-1.04454
H	2.81607	-2.01480	0.17179
C	-0.01099	-3.02177	0.88990
H	-0.22009	-3.52704	1.82947
C	0.07697	-3.96154	-0.27763
H	0.75387	-4.79091	-0.02623
H	0.48168	-3.45369	-1.16078
O	-1.24265	-4.44544	-0.53304
H	-1.15813	-5.10800	-1.22405
N	1.78437	2.93097	-0.38270
N	0.71293	3.39967	-0.58762
N	-0.47834	3.05701	-0.84134
C	-1.52092	3.62991	0.03390
H	-1.64748	4.68942	-0.21361
H	-2.43723	3.11209	-0.25962
C	-1.22757	3.43827	1.51640
H	-0.30512	3.95512	1.79555
H	-2.04620	3.84084	2.12032
H	-1.10313	2.37682	1.74442

Transition state: BCN (**4**) + isopropyl azide

C	0.00140	0.64480	-0.43812
C	1.22526	0.46327	-0.24615
C	-0.66311	-1.95542	0.73893
C	2.37162	-0.42753	0.00030
C	0.82404	-2.18255	0.95299
C	1.89259	-1.89076	-0.08026
H	3.16797	-0.24453	-0.73057
H	-1.18637	-1.59257	1.62332
H	2.80031	-0.22602	0.99092
H	1.15953	-1.95890	1.96544
C	-1.35614	0.08605	-0.57621
H	-1.82315	0.42964	-1.50776
H	-1.99808	0.43264	0.24678
C	-1.27705	-1.45254	-0.54976
H	-2.28074	-1.88264	-0.65631
H	-0.69474	-1.78192	-1.41589
H	1.52371	-2.07027	-1.09434
H	2.74688	-2.56337	0.08038
C	-0.12610	-3.36545	0.87322
H	-0.34562	-3.86499	1.81348
C	-0.14254	-4.29499	-0.30557
H	0.48034	-5.17378	-0.08414
H	0.26989	-3.80672	-1.19614
O	-1.50096	-4.67982	-0.52337
H	-1.48634	-5.33555	-1.22586
N	2.07158	2.44800	-0.37848
N	1.03351	3.00043	-0.54678
N	-0.18638	2.74697	-0.77040
C	-1.16501	3.40591	0.12614
H	-2.10562	2.90210	-0.12065
C	-1.28435	4.88646	-0.22384
H	-1.49703	5.00998	-1.28816
H	-2.08821	5.34931	0.35744
H	-0.34629	5.40053	0.00692
C	-0.82360	3.17311	1.59389
H	-0.71613	2.10480	1.79943

H	0.12234	3.66570	1.84221
H	-1.60753	3.58599	2.23639

Transition state: BCN (**4**) + tert.butyl azide

C	0.06557	0.44976	-0.32995
C	1.29358	0.20042	-0.22300
C	-0.60987	-2.20978	0.80246
C	2.41036	-0.75136	-0.05662
C	0.87553	-2.49288	0.93340
C	1.88768	-2.19539	-0.15182
H	3.17678	-0.57120	-0.81932
H	-1.08027	-1.85861	1.72042
H	2.89283	-0.59035	0.91689
H	1.27406	-2.31458	1.93171
C	-1.30255	-0.10389	-0.40274
H	-1.82460	0.28131	-1.28711
H	-1.88699	0.21360	0.47213
C	-1.25610	-1.64217	-0.44161
H	-2.27437	-2.04221	-0.52672
H	-0.71618	-1.95081	-1.34210
H	1.45740	-2.33740	-1.14728
H	2.73351	-2.89125	-0.06187
C	-0.11726	-3.64067	0.86575
H	-0.30688	-4.16103	1.80121
C	-0.22680	-4.53242	-0.33696
H	0.37602	-5.43773	-0.17461
H	0.15502	-4.03087	-1.23372
O	-1.60726	-4.86533	-0.49329
H	-1.65207	-5.49854	-1.21485
N	2.25358	1.96055	-0.44426
N	1.31618	2.68545	-0.56432
N	0.06191	2.57982	-0.69904
C	-0.76518	3.50379	0.13077
C	-2.21365	3.27758	-0.28849
H	-2.53684	2.25959	-0.06432
H	-2.86172	3.97198	0.25542
H	-2.32747	3.45552	-1.36166
C	-0.35372	4.94423	-0.18187
H	0.68272	5.12245	0.11756
H	-0.44642	5.13806	-1.25420
H	-1.00347	5.63831	0.36189
C	-0.55396	3.18234	1.60985
H	-1.16537	3.84319	2.23386
H	-0.82841	2.14357	1.81477
H	0.49738	3.31898	1.88306

5. Literature

[1] C. a DeForest, D. a Tirrell, *Nat. Mater.* **2015**, *14*, 523–531.

[2] H. R. Pfaendler, V. Weimar, *Synthesis* **1996**, *1996*, 1345–1349.

[3] F. W. HOFFMANN, *J. Org. Chem.* **1949**, *14*, 105–110.

[4] M. Valiev, E. J. Bylaska, N. Govind, K. Kowalski, T. P. Straatsma, H. J. J. Van Dam, D. Wang, J. Nieplocha, E. Apra, T. L. Windus, et al., *Comput. Phys. Commun.* **2010**, *181*, 1477–1489.

[5] R. Ditchfield, W. J. Hehre, J. A. Pople, *J. Chem. Phys.* **1971**, *54*, 724.

[6] J. Garcia-Hartjes, J. Dommerholt, T. Wennekes, F. L. Van Delft, H. Zuilhof, *Eur. J. Org. Chem.* **2013**, *6*, 3712–3720.

[7] W.-J. van Zeist, F. M. Bickelhaupt, *Org. Biomol. Chem.* **2010**, *8*, 3118–3127.

[8] D. H. Ess, K. N. Houk, *J. Am. Chem. Soc.* **2007**, *129*, 10646–10647.

[9] M. D. Hanwell, D. E. Curtis, D. C. Lonie, T. Vandermeersch, E. Zurek, G. R. Hutchison, *J. Cheminform.* **2012**, *4*, 17.

[10] The PyMOL Molecular Graphics System, Version 1.8 Schrödinger, LLC.

Supporting Information

Manuscript #2

Dennis Svatunek, Gottfried Eilenberger, Christoph Denk, Daniel Lumpi, Christian Hametner, Günter Allmaier and Hannes Mikula*; Monitoring of Strain-Promoted Alkyne Azide Cycloadditions in Biological Media by Inline ATR-IR spectroscopy, manuscript draft.

Supporting Information

Monitoring of Strain-Promoted Alkyne Azide Cycloadditions in Biological Media by Inline ATR-IR spectroscopy

Dennis Svatunek, Gottfried Eilenberger, Christoph Denk, Daniel Lumpi, Christian Hametner, Günter Allmaier and Hannes Mikula*

Contents

Materials and Methods 2
Synthesis 2
1-((1R*,8S*,9S*)-Bicyclo[6.1.0]non-4-yn-9-yl)-17,17,17-triphenyl-2,4,7,10,13,16-hexaoxa-3-heptadecanone (**10**) 3
15-((1R*,8S*,9S*)-Bicyclo[6.1.0]non-4-yn-9-yl)-13-oxo-3,6,9,12,14-pentaoxa-1-pentadecanol (**8**) 3
Setup 4
Kinetic experiments 6
General procedure 6
Data Analysis 6
Calibration curves in acetonitrile, water and human blood plasma 6
Measurements at different concentrations 8
Measurements at different temperatures 10
Comparison between NMR and ATR-IR 11
Monitoring in human blood plasma 12
Literature 13

Materials and Methods

Unless otherwise noted, all reagents were purchased from commercial suppliers and used without further purification. Cyclooctyne (**4**),[1] BCN (**6**),[2] 13,13,13-triphenyl-3,6,9,12-tetraoxatridecanol (**9**)[4] and 2-azidoethanol (**7**)[5] were prepared following known procedures. DCM was dried using PURESOLV-columns (Innovative Technology Inc.). All other solvents were distilled prior to use. Drying of organic solvents after extraction was performed using anhydrous Na_2SO_4 and subsequent filtration. Reactions were carried out under an atmosphere of argon in air-dried glassware with magnetic stirring. Sensitive liquids were transferred via syringe. Thin layer chromatography was performed using TLC alumina plates (Merck, silica gel 60, fluorescence indicator F254, or Merck, aluminium oxide neutral, fluorescence indicator F254). Preparative normal phase column chromatography was performed using a Büchi Sepacore Flash System (2 x Büchi Pump Module C-605, Büchi Pump Manager C-615, Büchi UV Photometer C-635, Büchi Fraction Collector C-660) using silica gel 60 (40-63 µm) as obtained from Merck and distilled or redistilled solvents.

^1H and ^{13}C NMR spectra were recorded on a Bruker AC 200 or a Bruker Avance UltraShield 400. Chemical shifts are reported in ppm (δ) relative to tetramethylsilane and calibrated using solvent residual peaks. Data are shown as follows: Chemical shift, multiplicity (s = singlet, d = doublet, t = triplet, q = quartet, quin = quintet, m = multiplet, br = broad signal), coupling constant (J, Hz) and integration. HRMS measurements were done on a Thermo Scientific MALDI LTQ Orbitrap mass spectrometer using α-cyano-4-hydroxycinnamic acid (CHCA) as matrix.

Synthesis

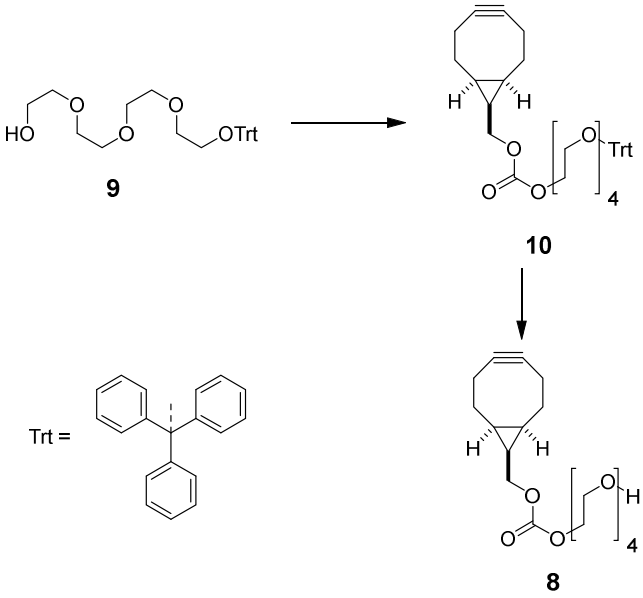

Scheme S-1: Synthesis of water soluble BCN derivative **8**

1-((1R*,8S*,9S*)-Bicyclo[6.1.0]non-4-yn-9-yl)-17,17,17-triphenyl-2,4,7,10,13,16-hexaoxa-3-heptadecanone (**10**)

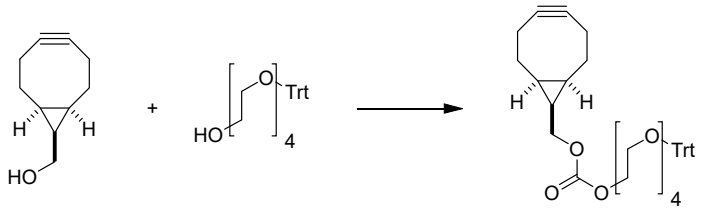

6 **9** **10**

To a stirred solution of triphosgene (0.19 g, 0.65 eq., 0.65 mmol) and pyridine (0.47 g, 6 eq., 6 mmol) in dry CH_2Cl_2 (2 mL) at -20 °C was dropwise added a solution of 6 (0.87 g, 2 eq., 2 mmol) in CH_2Cl_2 (2 mL). After stirring at -20 °C the mixture was allowed to reach RT. Subsequently BCN (0.15 g, 1 eq., 1 mmol) was added. After stirring at RT over night the reaction mixture was diluted with CH_2Cl_2 and washed twice with water. The organic phase was dried over Na_2SO_4 and concentrated *in vacuo*. The residual oil was purified by column chromatography (90g silica gel, hexanes:ethyl acetate = 3:1) to afford 152 mg of 10 (25%) as yellowish oil.

^{1}H NMR (200MHz, $CDCl_3$): δ = 7.02 - 7.56 (m, 15 H), 4.04 - 4.25 (m, 4 H), 3.44 - 3.72 (m, 12 H), 3.16 (t, J=5.18 Hz, 2 H), 1.97 - 2.37 (m, 5 H), 0.66 - 1.63 (m, 6 H) ppm

^{13}C NMR (50 MHz, $CDCl_3$): δ = 155.18 (s, 1 C), 144.02 (s, 3 C), 128.61 (d, 6 C), 127.66 (d, 6 C), 128.62 (d, 3 C), 98.67 (s, 1 C), 86.43 (s, 2 C), 70.70 (t, 1 C), 70.67 (t, 1 C), 70.59 (t, 3 C), 68.84 (t, 1 C), 66.81 (t, 1 C), 66.14 (t, 1 C), 63.23 (t, 1 C), 28.91 (t, 2 C), 21.28 (t, 2 C), 20.16 (d, 2 C), 17.31 (d, 1 C)

HRMS: calcd. for $[M+Na]^+$: 635.2979, found: 635.2990

15-((1R*,8S*,9S*)-Bicyclo[6.1.0]non-4-yn-9-yl)-13-oxo-3,6,9,12,14-pentaoxa-1-pentadecanol (**8**)

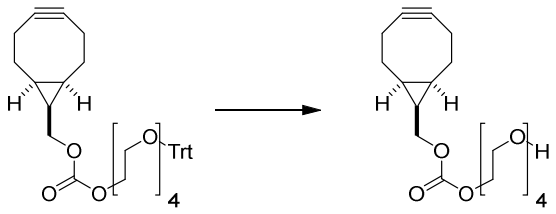

10 **8**

A solution of 10 (66 mg, 1 eq., 127 µmol) in 80% acetic acid (2 mL) was stirred at 40 °C for 2.5 h and subsequently cooled to 0 °C. The white precipitate was filtered of and washed with water. The combined filtrates were lyophilized to afford 34 mg of 8 (85%) as colorless oil.

^{1}H NMR (200MHz, DMSO-d6): δ = 4.58 (br. s., 1 H), 4.11 - 4.25 (m, 4 H), 3.12 - 3.72 (m, 14 H), 1.93 - 2.36 (m, 6 H), 0.73 - 1.71 (m, 5 H) ppm

13C NMR (50 MHz, DMSO-d6): δ = 154.71 (s, 1 C), 98.96 (s, 2 C), 72.35 (t, 1 C), 69.82 (t, 1 C), 69.75 (t, 4 C), 68.19 (t, 1 C), 66.64 (t, 1 C), 65.66 (t, 1 C), 60.21 (t, 1 C), 28.50 (t, 2 C), 20,80 (t, 2 C), 19.73 (d, 2 C), 17.13 (d, 1 C)

HRMS: calcd. for [M+Na]+: 393.1884, found: 393.1893

Setup

For ATR-IR kinetic experiments a ReactIR 15 System from METTLER TOLEDO was used in combination with an DST Series AgX Fiber SiComp probe. As a reaction vessel a custom made flask was used (Figure S-2). A double mantle enables connection to thermostats for accurate temperature control. A NS14 joint on top is used for insertion of the probe (Figure S-1) and a second joint is used for adding of reagents.



Figure S-1: Used reactor with inserted ATR-IR probe; **a)** overview; **b)** close-up of reaction solution in the reactor

Stirring can be realized by using magnetic stirring, a volume of 1 mL is sufficient for measurements (Manuscript Figure 1b).

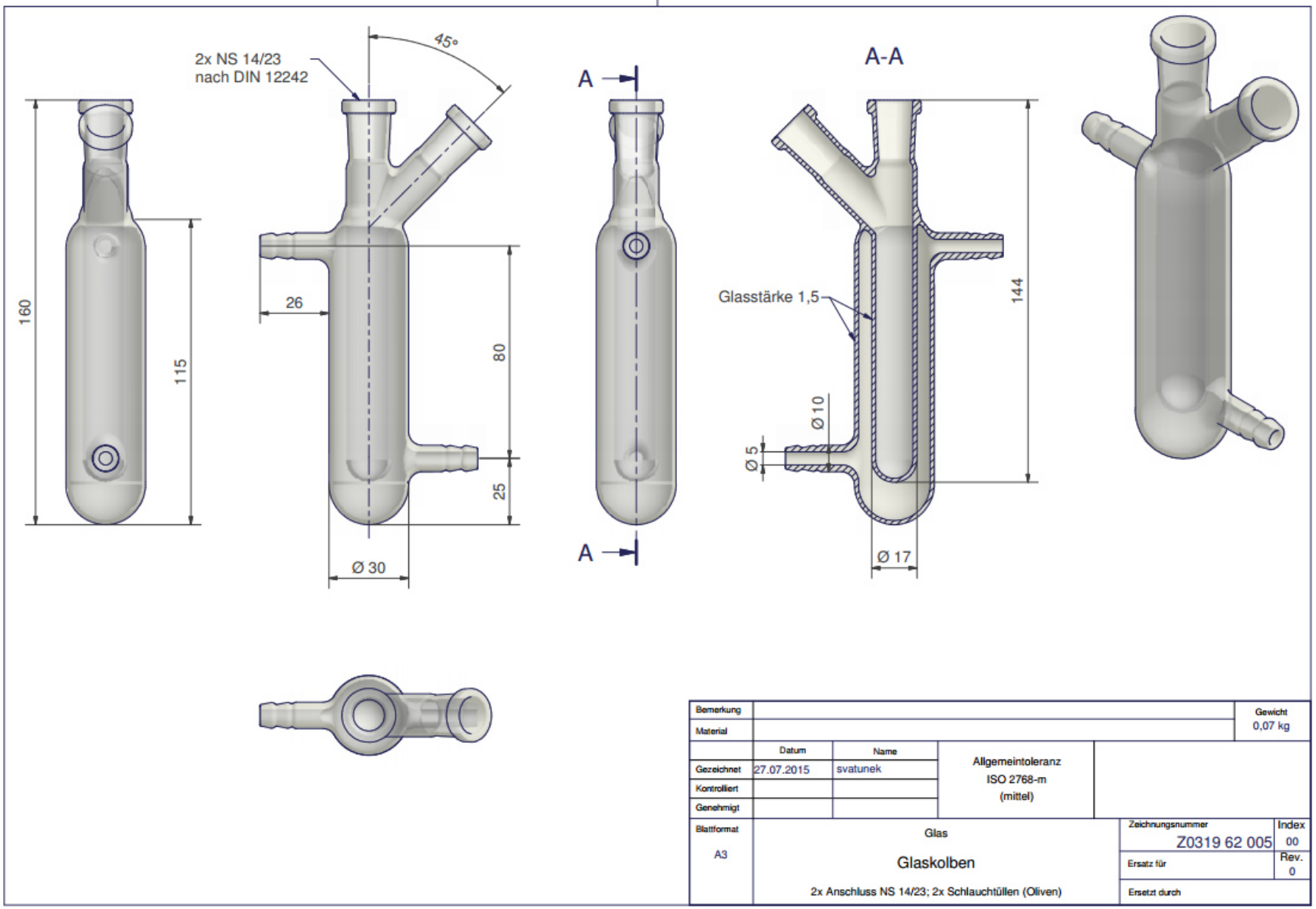

Figure S-2: Construction drawings of the used reactor. Values in mm

Kinetic experiments

General procedure

Baseline of pure solvent at the reaction temperature was recorded as background. 0.9 mL of azide solution was put in the reactor, stirred and the ATR-IR probe was immersed. After reaching constant temperature the measurement was started. Then 0.1 mL of 1,3-dipolarophile solution was added and this time point was set to t=0 for data analysis.

Data Analysis

Data was recorded using iC IR Software 4.3 (Mettler Toledo). Full Scans were performed every 20 seconds to 1 min depending on reaction speed. Base line offset was performed using the value at 2000 cm^{-1}. Solvent background was subtracted and signal region was drawn around the azide signal at ~2100 cm^{-1}. Both “Area to zero” and “Height to zero” time curves of that signal were exported. For determination of rate constants these curves were linearized by plotting 1/[azide] against time in seconds leading to a slope equal to second order rate constants of the reaction (Formula S-1).

Formula S-1:

$$\frac{1}{[azide]} = \frac{1}{[azide_{t=0}]} + k * t$$

Calibration curves in acetonitrile, water and human blood plasma

Calibration curves were prepared for azides in acetonitrile, water and human blood plasma at 37 °C. Benzyl azide (**2**) was used for calibration in acetonitrile and 2-azidoethanol (**7**) for calibration in water and human blood plasma. Calibration was done for height of the signal and area of the signal. Data analysis was performed sing PRISM 6 (Graphpad).

benzyl azide (2) in acetonitrile

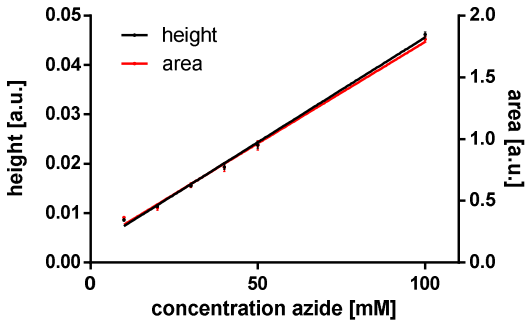

	height based	*area based*
Best-fit values		
Slope	0.0004243 ± 6.727e-006	0.01644 ± 0.0003216
Y-intercept when X=0.0	0.003141 ± 0.0003419	0.1429 ± 0.01635
X-intercept when Y=0.0	-7.402	-8.691
1/slope	2357	60.83
95% Confidence Intervals		
Slope	0.0004101 to 0.0004386	0.01576 to 0.01712
Y-intercept when X=0.0	0.002416 to 0.003866	0.1082 to 0.1775
X-intercept when Y=0.0	-9.377 to -5.538	-11.19 to -6.362
Goodness of Fit		
R square	0.9960	0.9939

2-azidoethanol (7) in water

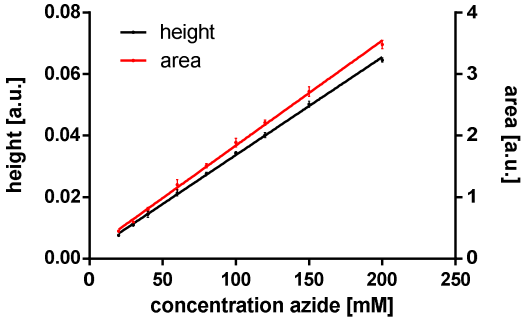

	height based	*area based*
Best-fit values		
Slope	0.0003185 ± 2.744e-006	0.01707 ± 0.0002119
Y-intercept when X=0.0	0.001842 ± 0.0002889	0.1320 ± 0.02231
X-intercept when Y=0.0	-5.785	-7.732
1/slope	3140	58.57
95% Confidence Intervals		
Slope	0.0003128 to 0.0003241	0.01664 to 0.01751
Y-intercept when X=0.0	0.001247 to 0.002438	0.08604 to 0.1780
X-intercept when Y=0.0	-7.772 to -3.858	-10.66 to -4.932
Goodness of Fit		
R square	0.9981	0.9962

2-azidoethanol (7) in human blood plasma

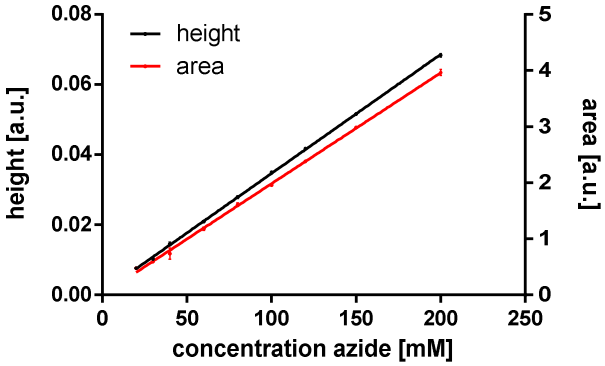

	height based	*area based*
Best-fit values		
Slope	0.0003397 ± 1.487e-006	0.01976 ± 0.0001702
Y-intercept when X=0.0	0.0006990 ± 0.0001566	0.008287 ± 0.01792
X-intercept when Y=0.0	-2.058	-0.4194
1/slope	2944	50.61
95% Confidence Intervals		
Slope	0.0003366 to 0.0003427	0.01941 to 0.02011
Y-intercept when X=0.0	0.0003765 to 0.001021	-0.02863 to 0.04520
X-intercept when Y=0.0	-3.030 to -1.100	-2.323 to 1.428
Goodness of Fit		
R square	0.9995	0.9981

Measurements at different concentrations

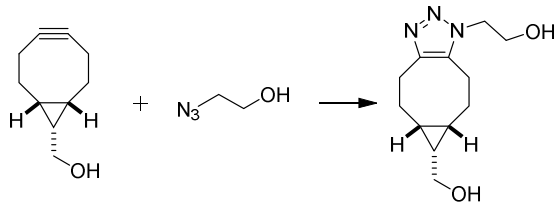

6 **7** **11**

The reaction between BCN (**6**) and 2-azidoethanol (**7**) in acetonitrile was used for determination of possible concentration range. Therefore, measurements were conducted at 10, 25, 50 and 100 mM concentration of both reagents at 37 °C (Figure S-3).

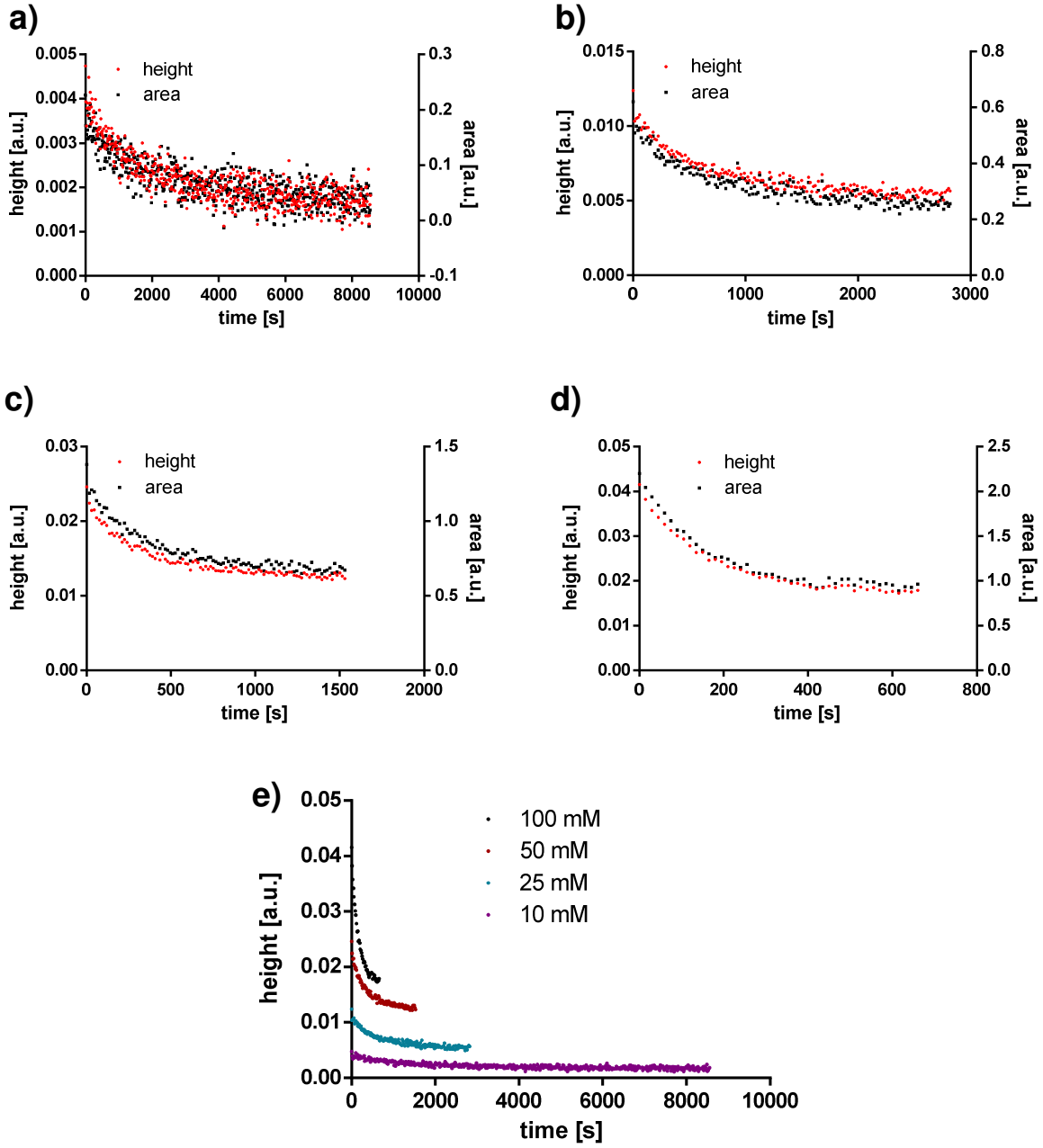

Figure S-3: Reaction between **6** and **7** in acetonitrile at 37 °C with both reagents at **a)** 10 mM **b)** 25 mM **c)** 50 mM and **d)** 100 mM concentration; **e)** Comparison of measurements at different concentrations based on peak height.

Table S-1: determined rate constants of reaction between **6** and **7** in acetonitrile at 37 °C

Concentration [mM]	**second order rate constant [$M^{-1}s^{-1}$]**
10	4.61×10^{-2}
25	4.75×10^{-2}
50	5.03×10^{-2}
100	4.80×10^{-2}

In case of 10 mM and 25 mM concentration the signal-to-noise ratio is too low to get reliable results. Starting concentration of 50 mM and higher are optimal for measurements using this setup.

Measurements at different temperatures

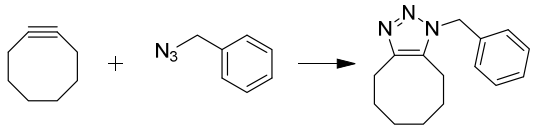

4 **2** **5**

The reaction between cyclooctyne (**4**) and benzyl azide (**2**) was monitored at different temperatures. 100 mM was chosen as starting concentration for both reagents and measurements were done in acetonitrile at 0, 20 and 37 °C as well as in DMSO at 37 and 60 °C.

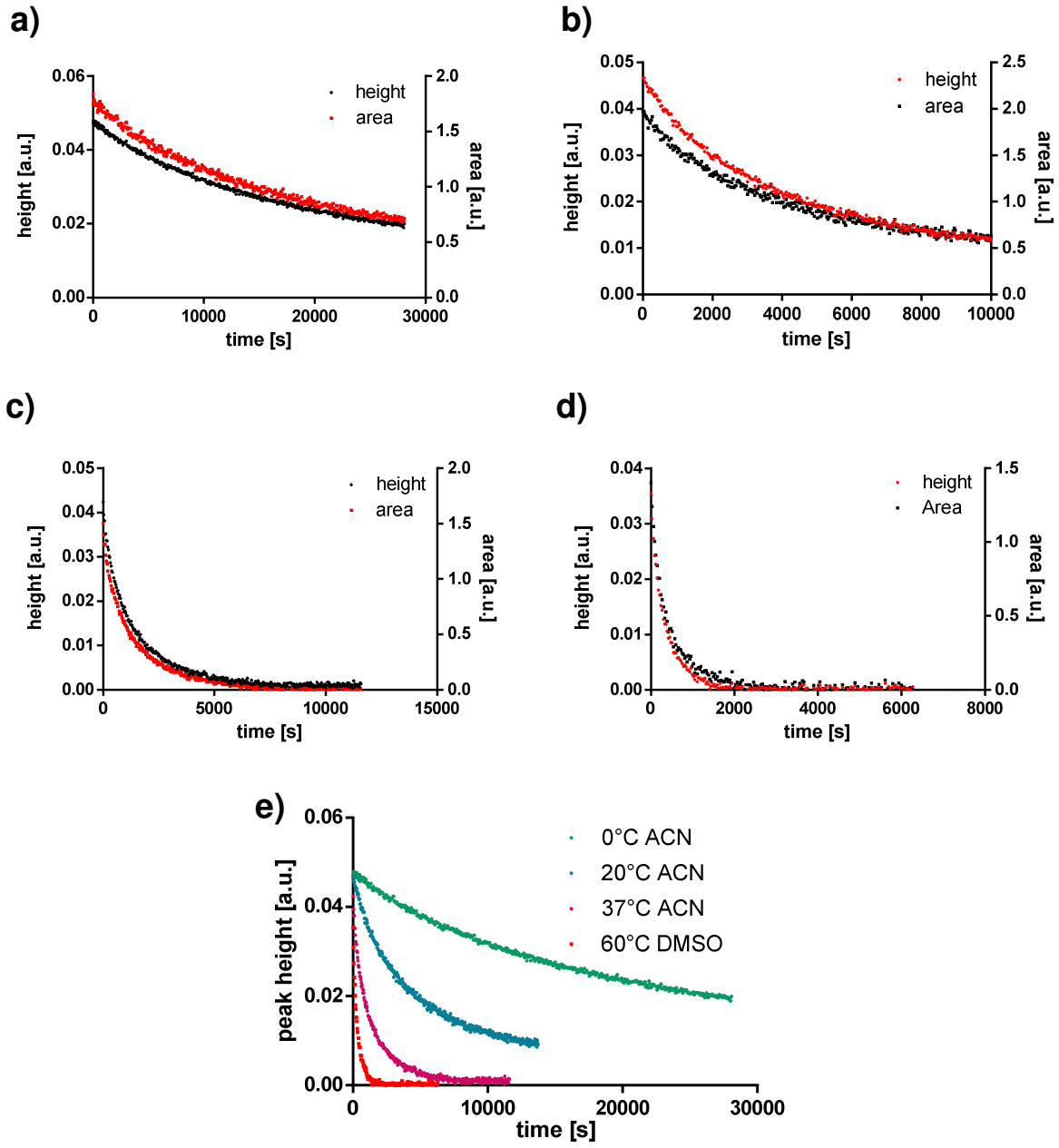

Figure S-4: Reaction between **2** and **4** at 100 mM starting concentration of both reagents at **a)** 0 °C in acetonitrile **b)** 20 °C in acetonitrile **c)** 37 °C in acetonitrile and **d)** 60 °C in DMSO; **e)** Comparison of measurements at different temperatures based on peak height.

Table S-2: determined rate constants of reaction between **2** and **4** at 100 mM

Temperature [°C]	solvent	second order rate constant [$M^{-1}s^{-1}$]
0	acetonitrile	4.99×10^{-4}
20	acetonitrile	2.79×10^{-3}
37	acetonitrile	1.35×10^{-2}
37	DMSO	1.52×10^{-2}
60	DMSO	5.83×10^{-2}

Comparison between NMR and ATR-IR

For comparison with NMR kinetic experiments the reaction between cyclooctyne (**4**) and benzyl azide (**2**) was performed in acetonitrile and d3-acetonitrile for IR and NMR experiments respectively.

NMR kinetic experiments were performed on a Bruker Avance UltraShield 400 at 37 °C. A NMR tube containing 0.6 mL of a 100 mM solution of benzyl azide (**2**) in dry acetonitrile-d3 was put into the temperated NMR machine and shimmed. The tube was removed and one equivalent of cyclooctyne (**4**) was added neat. After shaking vigorous the tube was reinserted into the NMR and ^{1}H spectra were measured with an interval of 2 minutes. To determine the conversion of benzyl azide the singlets of the two hydrogen aliphatic hydrogen atoms beside the phenyl residue were integrated and put in relation. Their chemical shift is 4.42 ppm for benzyl azide and 5.48 ppm for the resulting triazole. ATR-IR kinetic experiment was performed as described above at 100 mM starting concentration and at 37 °C.

In case of ATR-IR measurements data points could be obtained during and right after addition of reaction partner while in case of NMR measurements the first point could be obtained after 2 minutes (Figure S-5). Both modalities show very similar results.

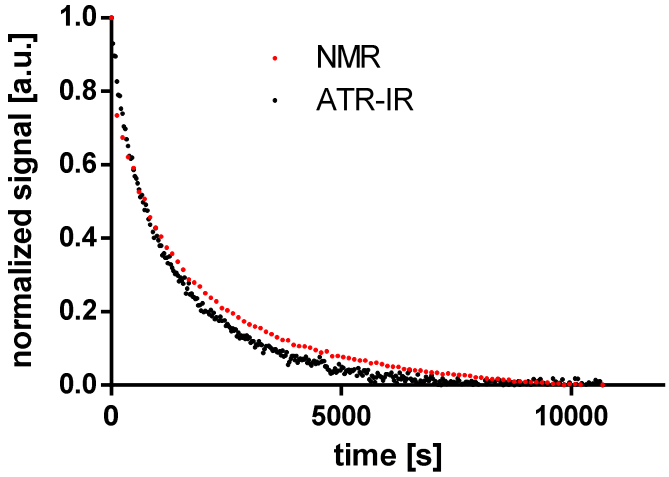

Figure S-5: Comparison between ATR-IR measured reaction based on signal height and NMR derived curve

Table S-3: determined rate constants of reaction between **2** and **4** at 100 mM in acetonitrile by NMR and ATR-IR

Modality	second order rate constant [$M^{-1}s^{-1}$]
NMR	1.11×10^{-2}
ATR-IR	1.35×10^{-2}

Monitoring in human blood plasma

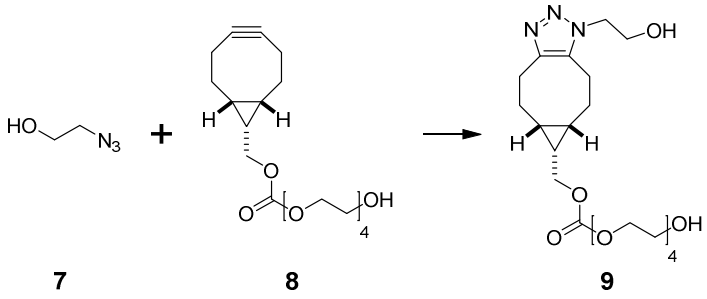

7 **8** **9**

Reaction between water soluble BCN derivative **8** and water soluble azide **7** was monitored in human blood plasma at 50 mM starting concentration and 37 °C and at 100 mM starting concentration and 20 °C (Figure S-6). In case of blood plasma signal-to-noise ratio is significantly lower and 100 mM starting concentration should be used. Both measurements could be used for determination of rate constants (Table S-4).

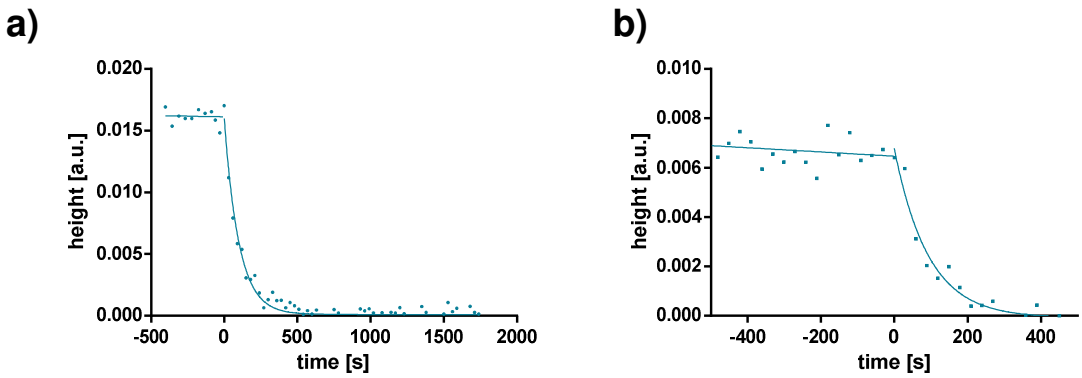

Figure S-6: Signal height based reaction monitoring of reaction between **7** and **8** in human blood plasma at a) 50 mM starting concentration and 37 °C and b) 100 mM and 20 °C.

Table S-4: Determined rate constants of reaction between **7** and **8** in human blood plasma

Temperature [°C]	Concentration [mM]	second order rate constant [$M^{-1}s^{-1}$]
37	50	5.68×10^{-2}
20	100	1.90×10^{-1}

Literature

[1] H. Meier, E. Voigt, *Tetrahedron* **1972**, *28*, 187–198.
[2] C. a DeForest, D. a Tirrell, *Nat. Mater.* **2015**, *14*, 523–531.
[3] Z. Cheng, D. R. Elias, N. P. Kamat, E. D. Johnston, A. Poloukhtine, V. Popik, D. A. Hammer, A. Tsourkas, *Bioconjug. Chem.* **2011**, *22*, 2021–2029.
[4] D. Lumpi, C. Braunshier, C. Hametner, E. Horkel, B. Zachhuber, B. Lendl, J. Fŕhlich, *Tetrahedron Lett.* **2009**, *50*, 6469–6471.
[5] H. R. Pfaendler, V. Weimar, *Synthesis* **1996**, *1996*, 1345–1349.

Supporting Information

Manuscript #3

Christoph Denk, Martin Wilkovitsch, Philipp Skrinjar, Dennis Svatunek, Severin Mairinger, Claudia Kuntner, Thomas Filip, Johannes Fröhlich, Thomas Wanek, Hannes Mikula*; Investigation of Small [^{18}F]-Fluoroalkylazides for Rapid Radiolabeling and *In Vivo* Click Chemistry, *Bioconjugate Chemistry* **2016**, submitted manuscript.

Investigation of Small [^{18}F]-Fluoroalkylazides for Rapid Radiolabeling and *In Vivo* Click Chemistry

Christoph Denk[a], Martin Wilkovitsch[a], Dennis Svatunek[a], Severin Mairinger[b], Philipp Skrinjar[a], Claudia Kuntner[b], Thomas Filip[b], Johannes Fröhlich[a], Thomas Wanek[b] and Hannes Mikula[a*]

a) Institut für Angewandte Synthesechemie, Technische Universität Wien (TUW) (Austria) E-mail: hannes.mikula@tuwien.ac.at b) Health and Environment Department, Biomedical Systems, Austrian Institute of Technology (AIT) Seibersdorf (Austria)

Supporting Information

Content

1. NMR Spectra 2

2. HPLC Data 14

3. LC/MS Data 19

4. TLC Data 21

1. NMR Spectra

^{1}H-NMR spectrum of **1** (as solution in DMF)

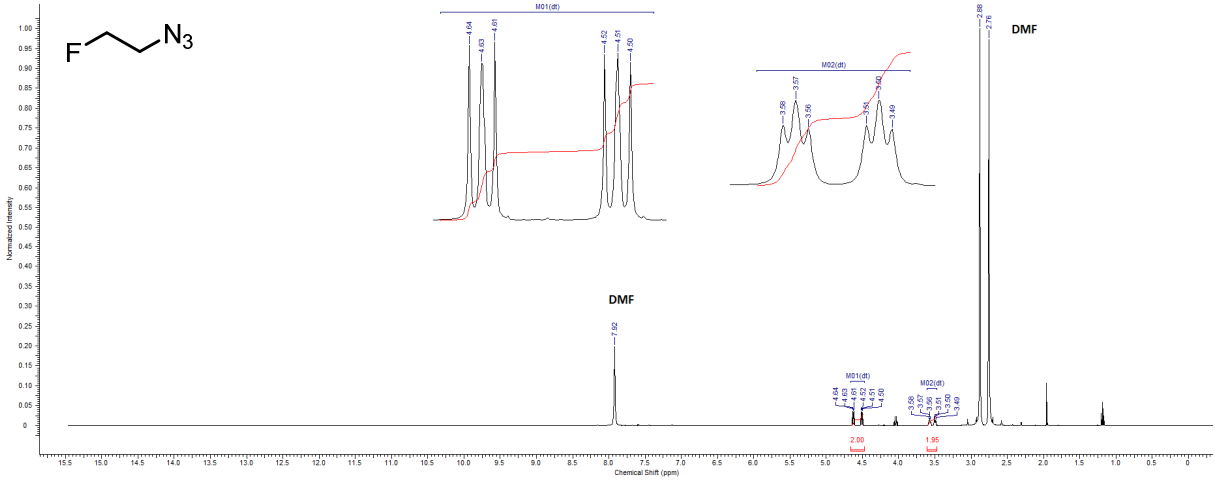

^{13}C-NMR spectrum of **1** (as solution in CD_3CN)

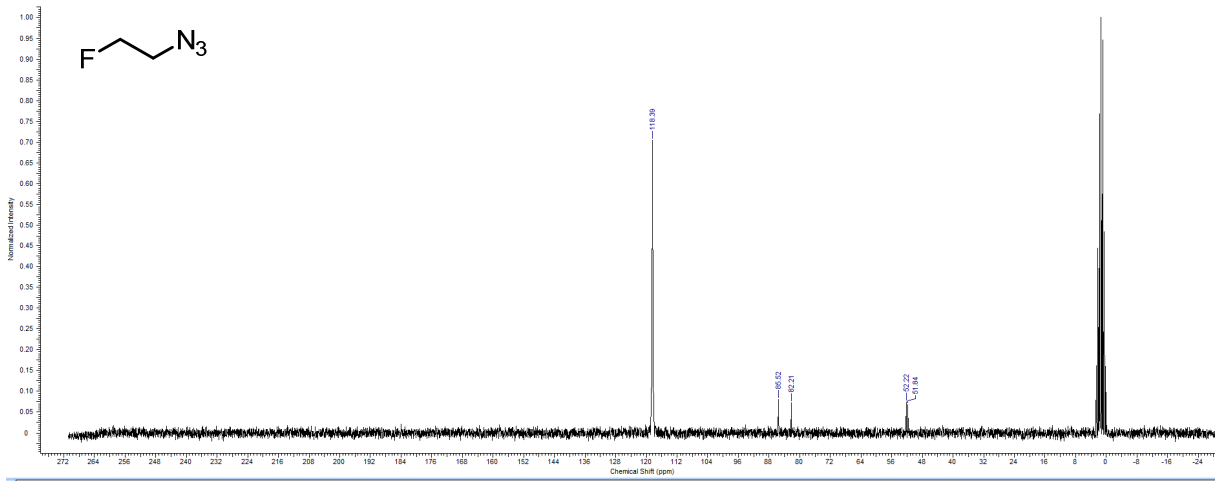

^{19}F-NMR spectrum of **1**

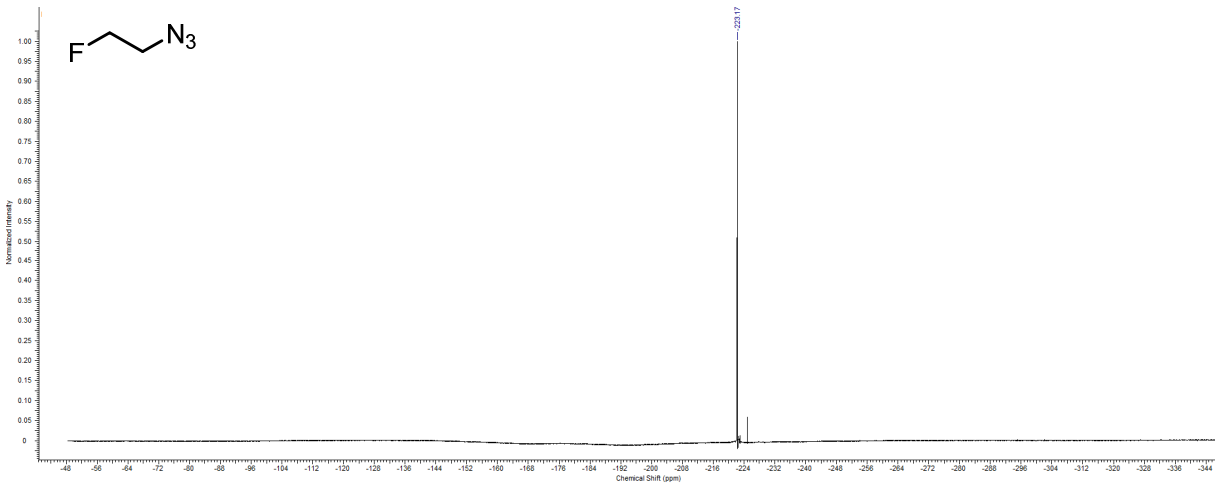

^{1}H-NMR spectrum of **2**

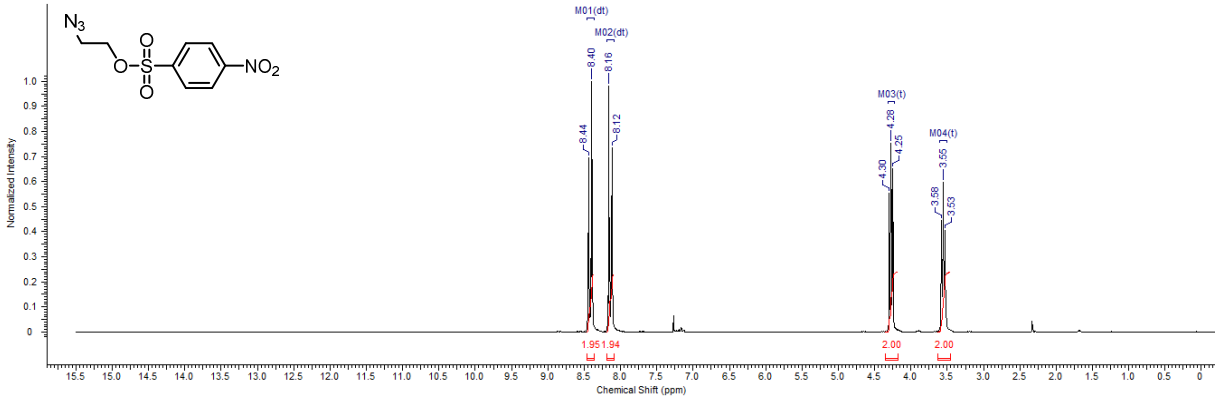

^{13}C-NMR spectrum of **2**

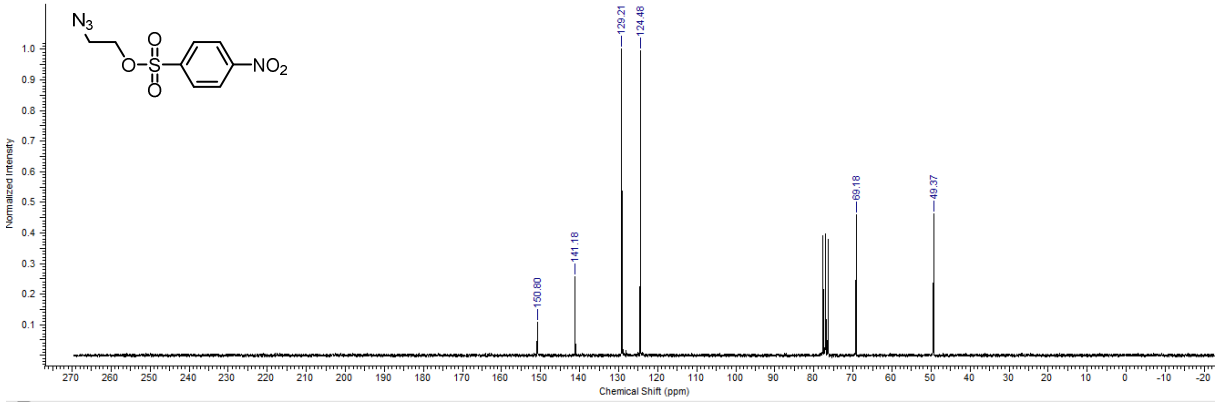

^{1}H-NMR spectrum of **3**

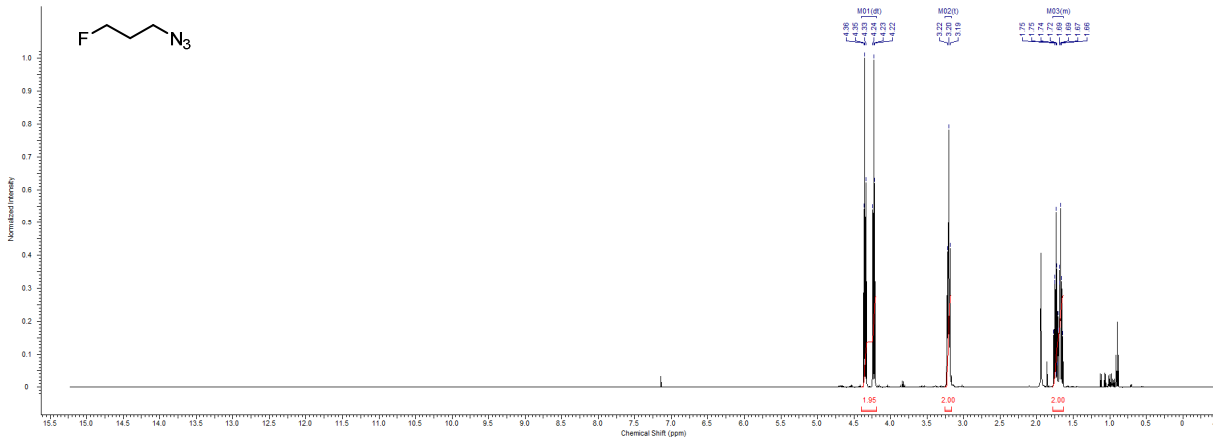

^{13}C-NMR spectrum of **3**

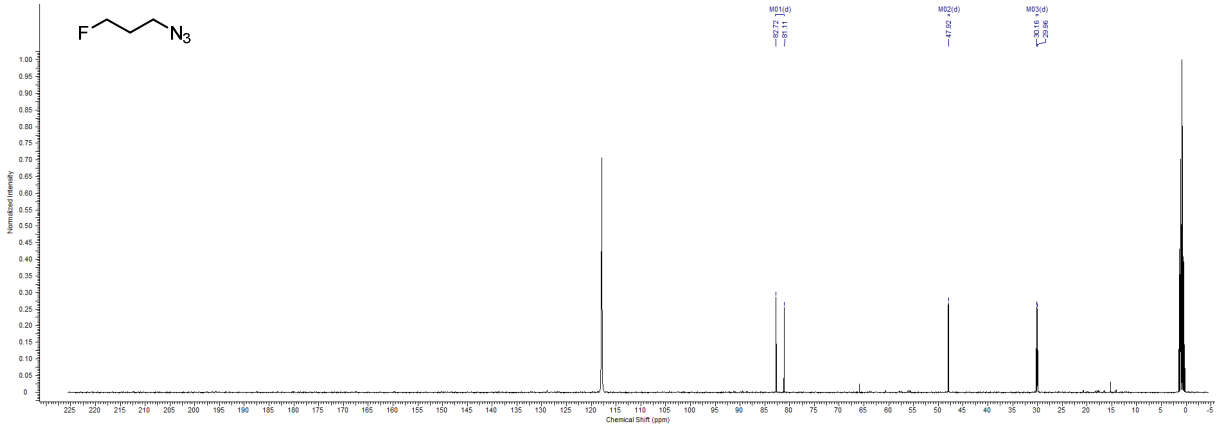

^{19}F-NMR spectrum of **3**

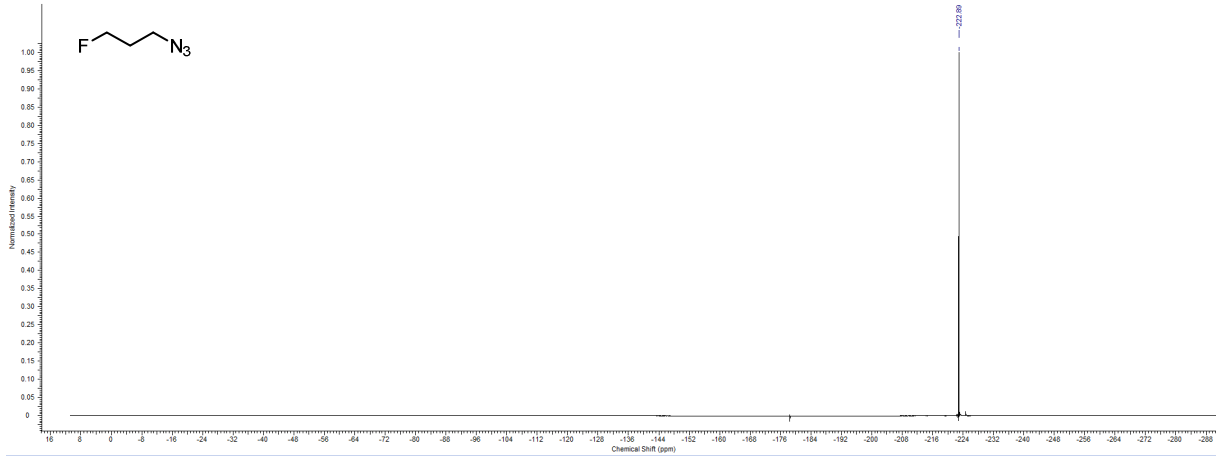

^{1}H-NMR spectrum of **4** (as solution in DMF)

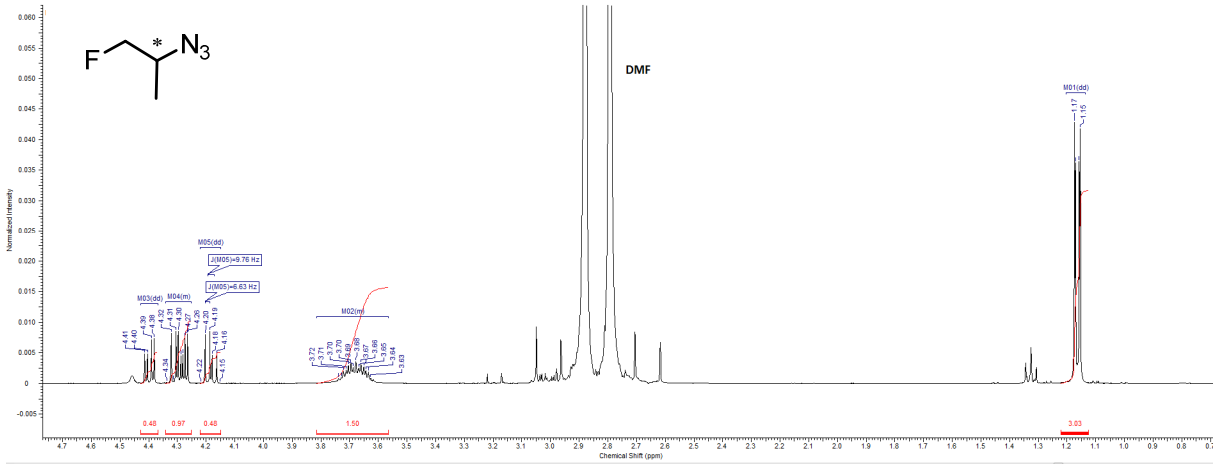

^{13}C-NMR spectrum of **4** (as solution in DMF)

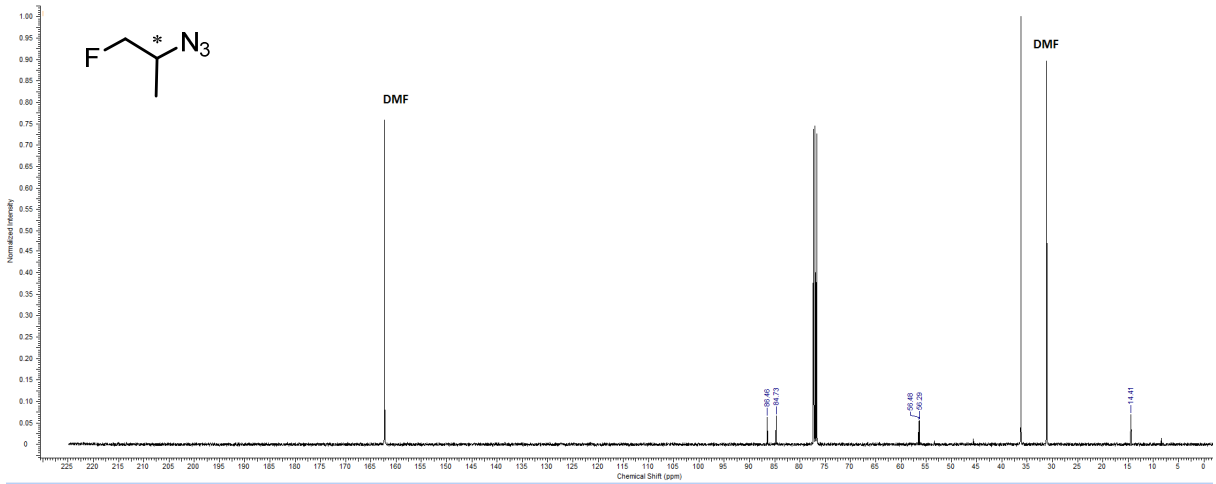

^{19}F-NMR spectrum of **4**

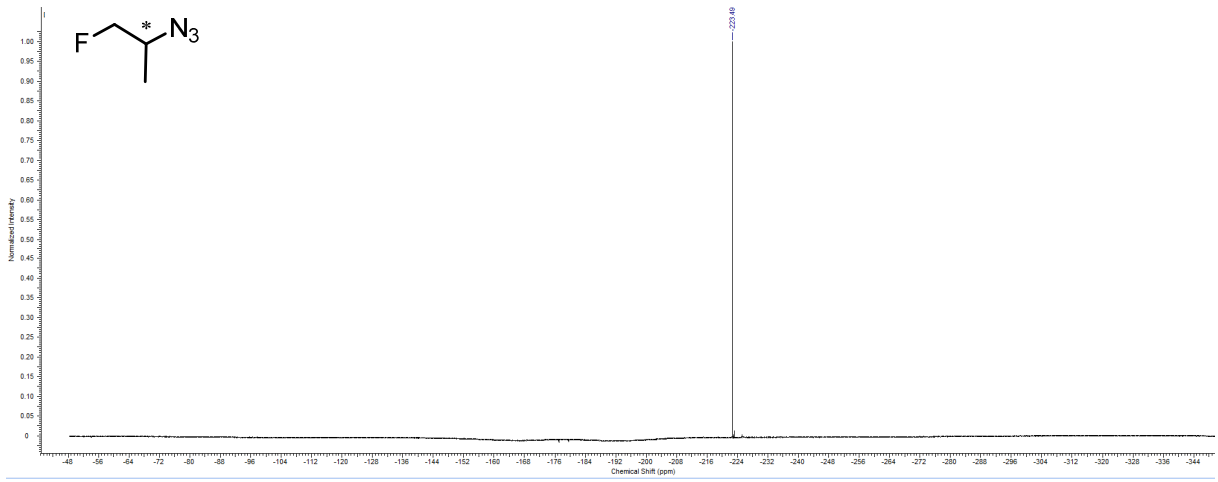

^{1}H-NMR spectrum of **6**

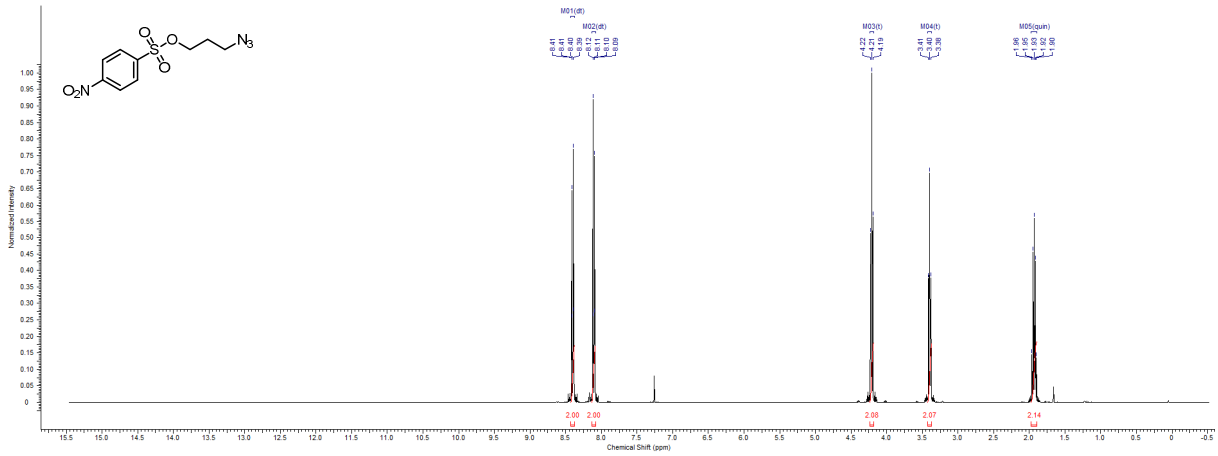

^{13}C-NMR spectrum of **6**

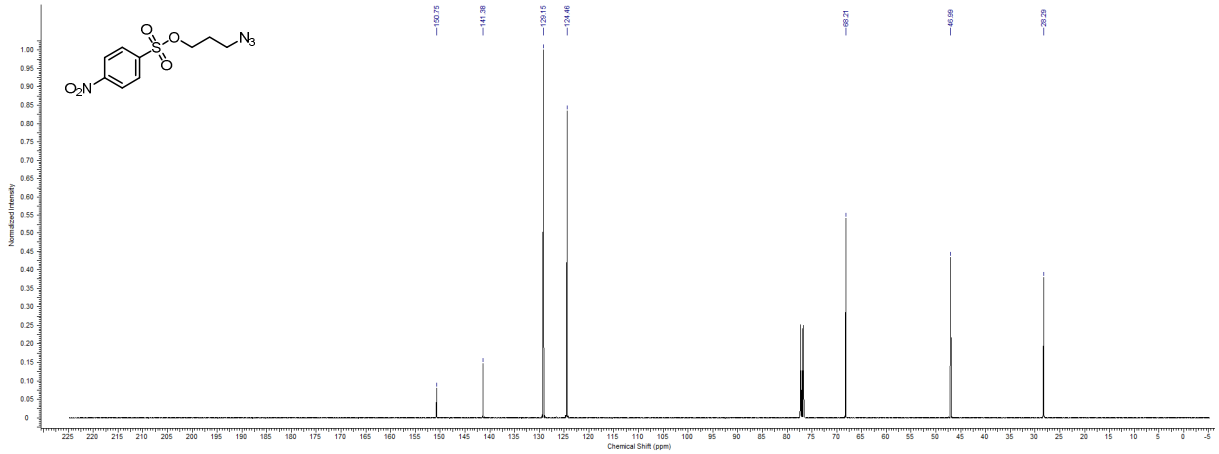

^{1}H-NMR spectrum of **8**

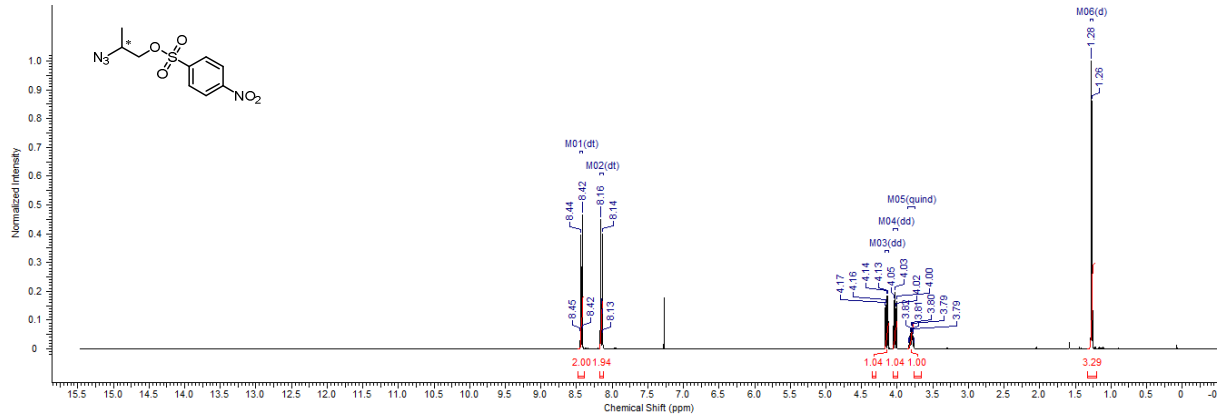

^{13}C-NMR spectrum of **8**

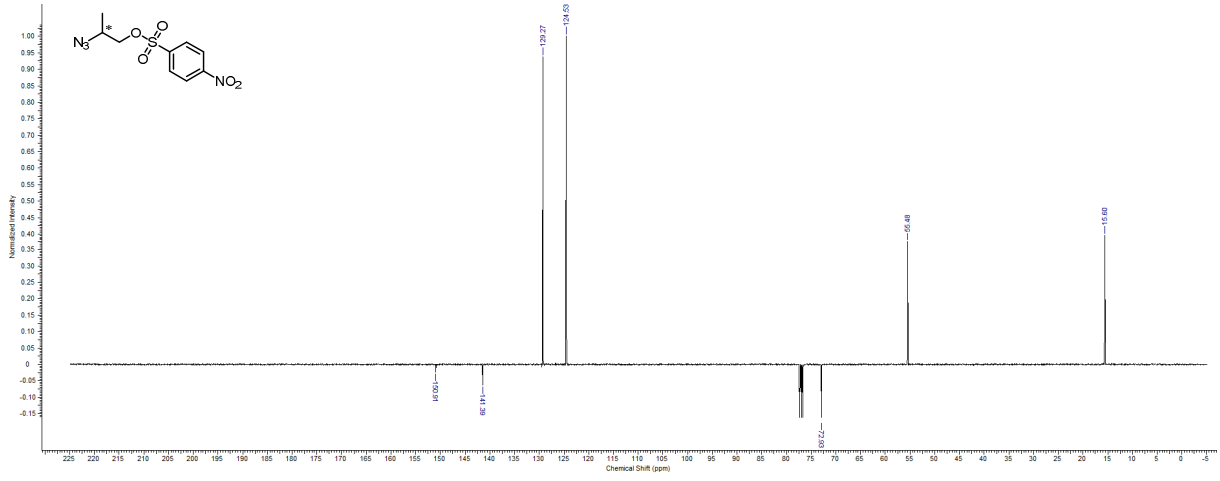

^{1}H-NMR spectrum of **9**

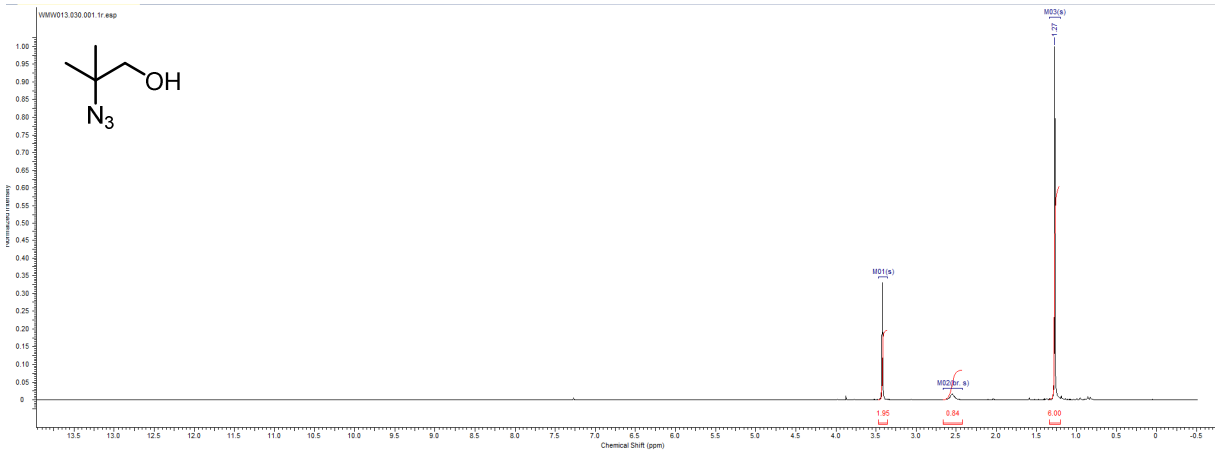

^{13}C-NMR spectrum of **9**

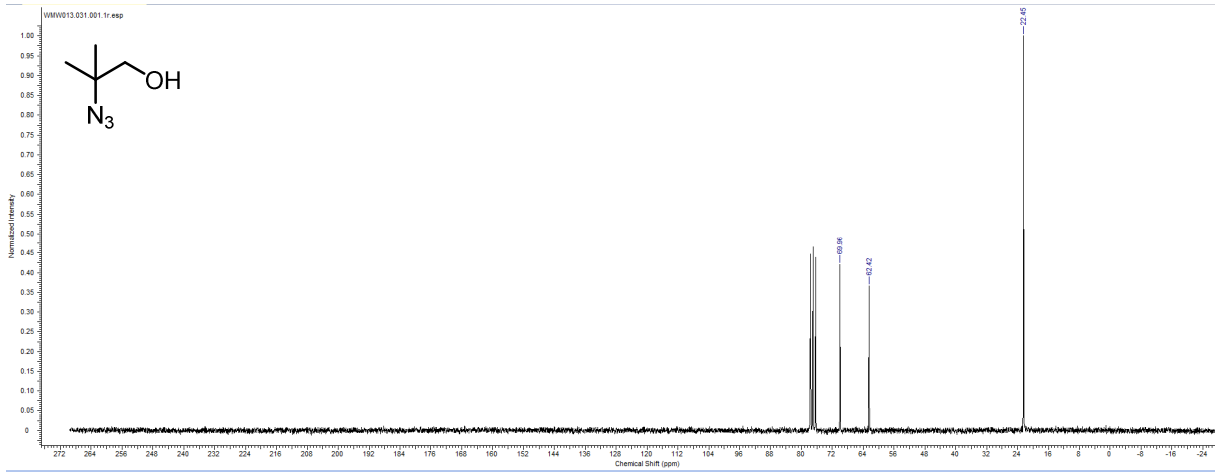

^{1}H-NMR spectrum of **10**

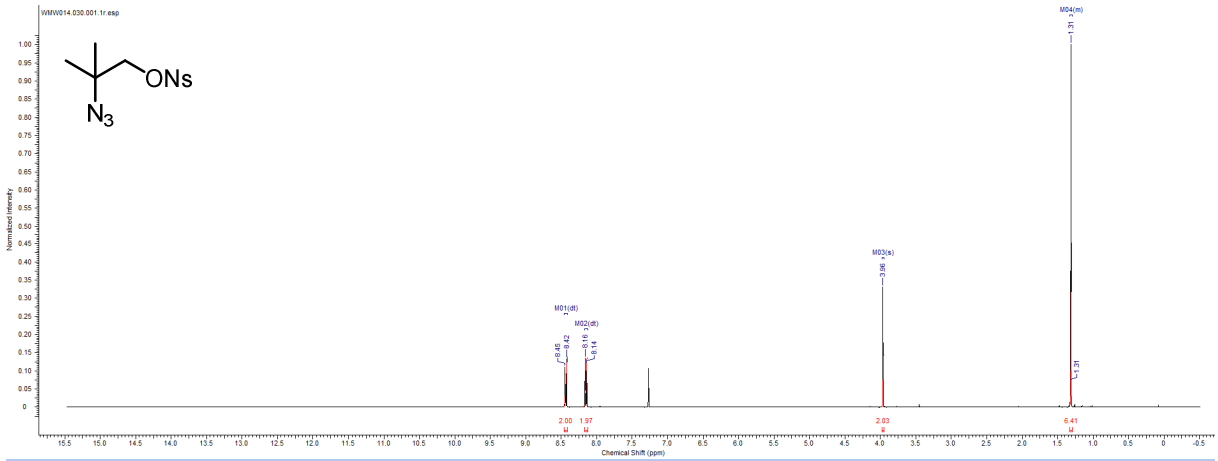

^{13}C-NMR spectrum of **10**

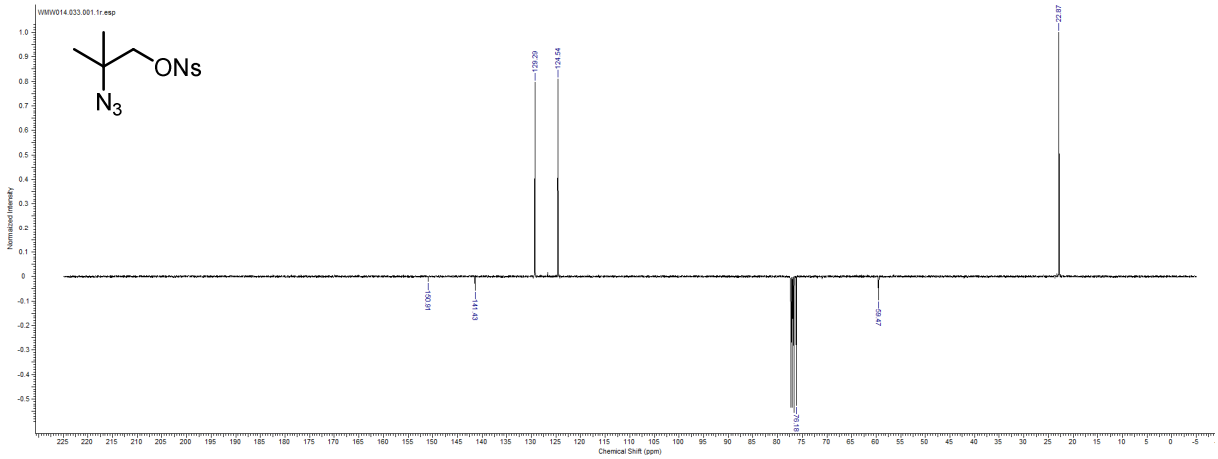

^{1}H-NMR spectrum of **13**

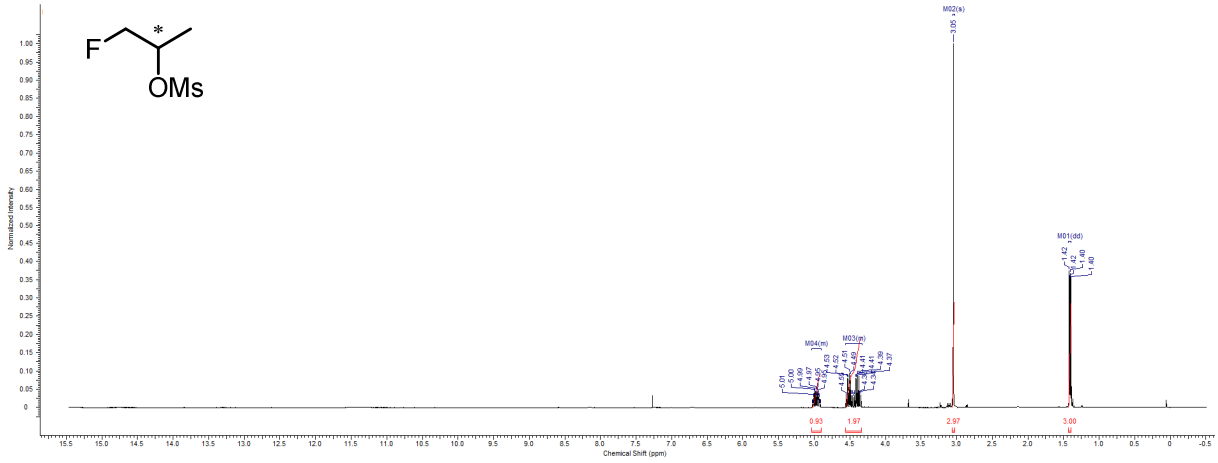

^{13}C-NMR spectrum of **13**

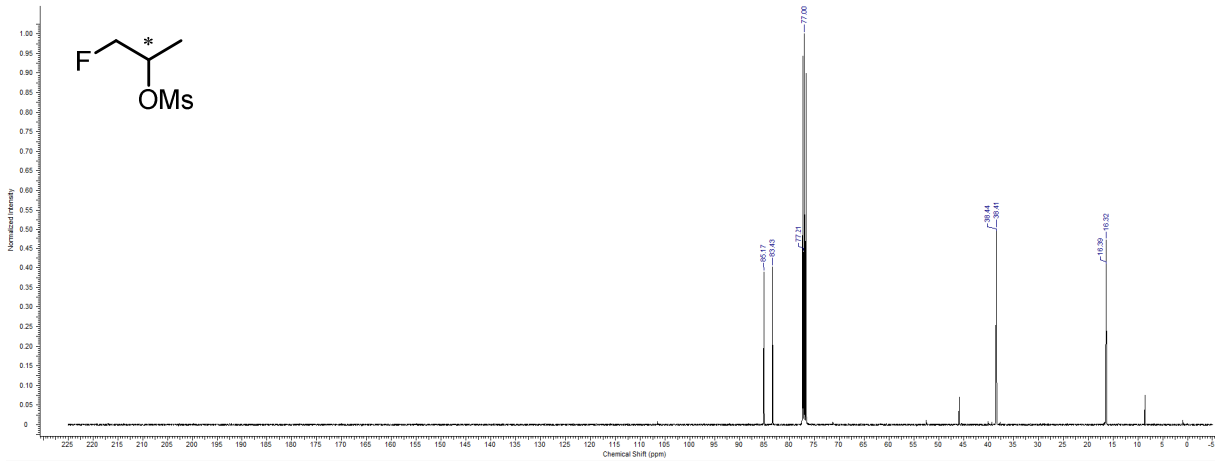

^{19}F-NMR spectrum of **13**

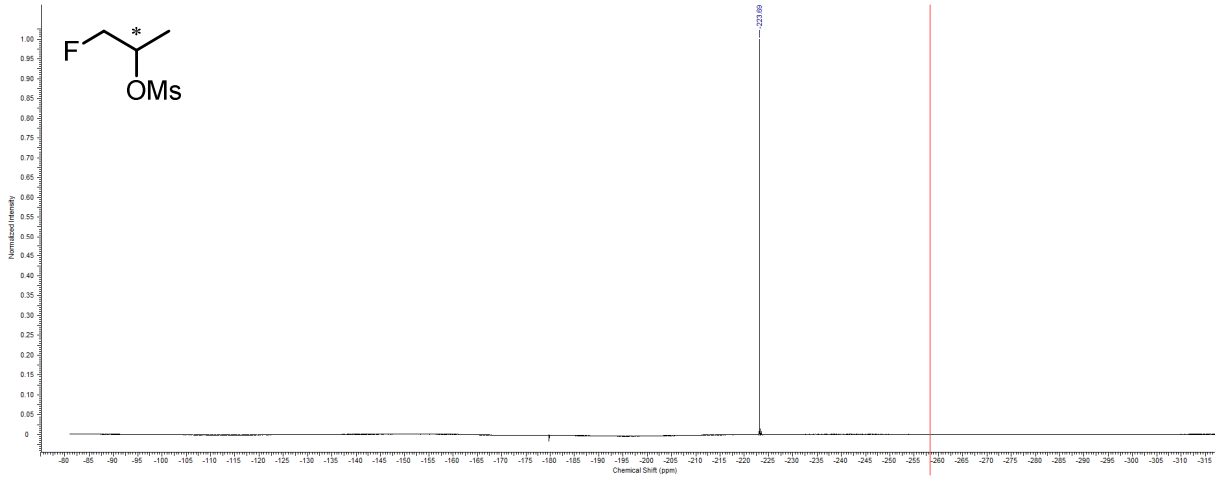

^{1}H-NMR spectrum of **15**

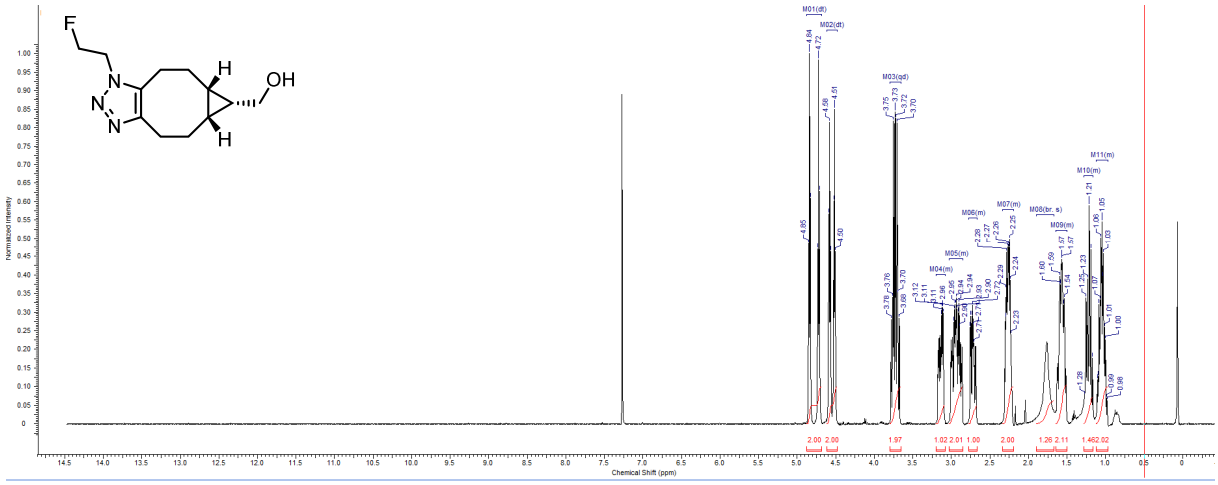

^{13}C-NMR spectrum of **15**

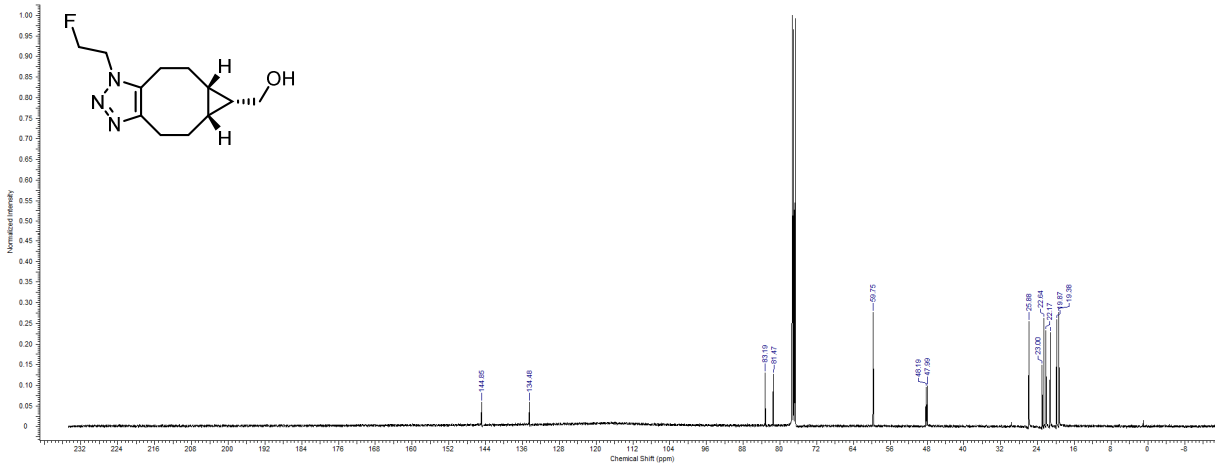

^{1}H-NMR spectrum of **16**

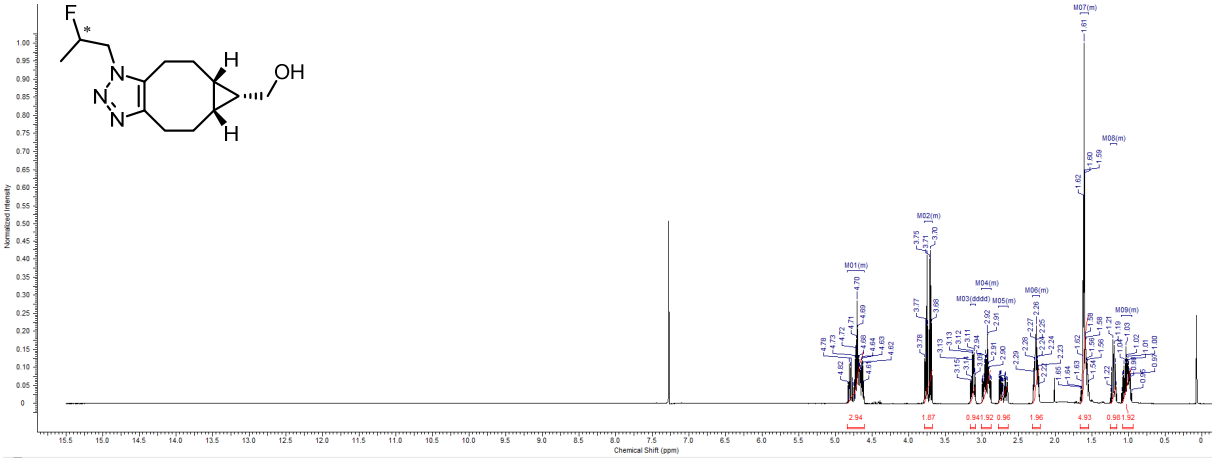

^{13}C-NMR spectrum of **16**

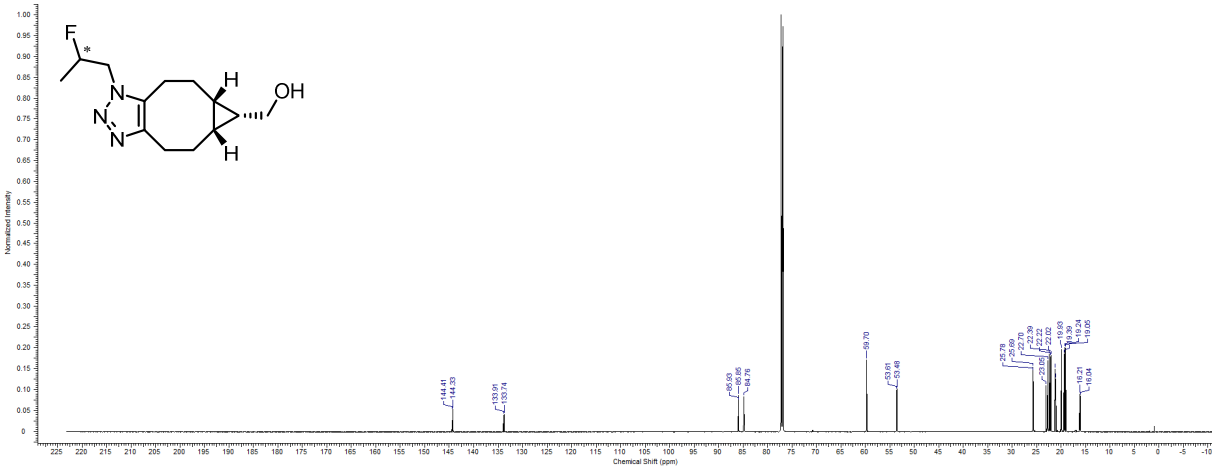

^{19}F-NMR spectrum of **16**

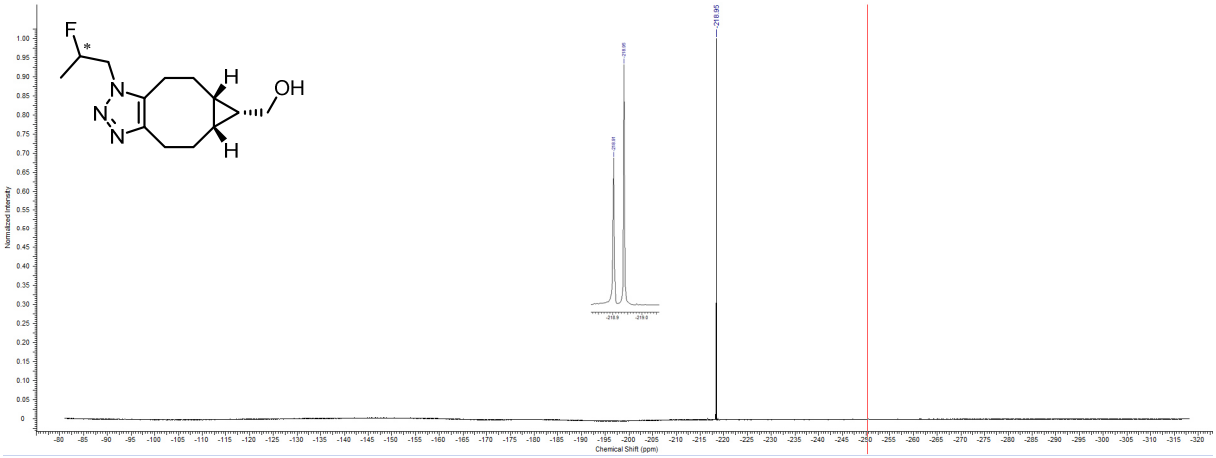

^{1}H-NMR spectrum of **17**

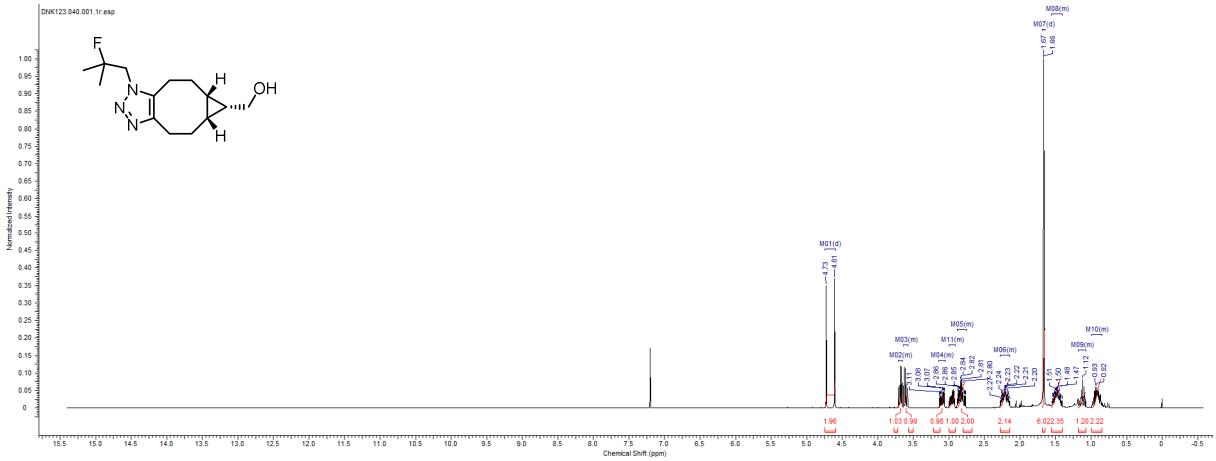

^{13}C-NMR spectrum of **17**

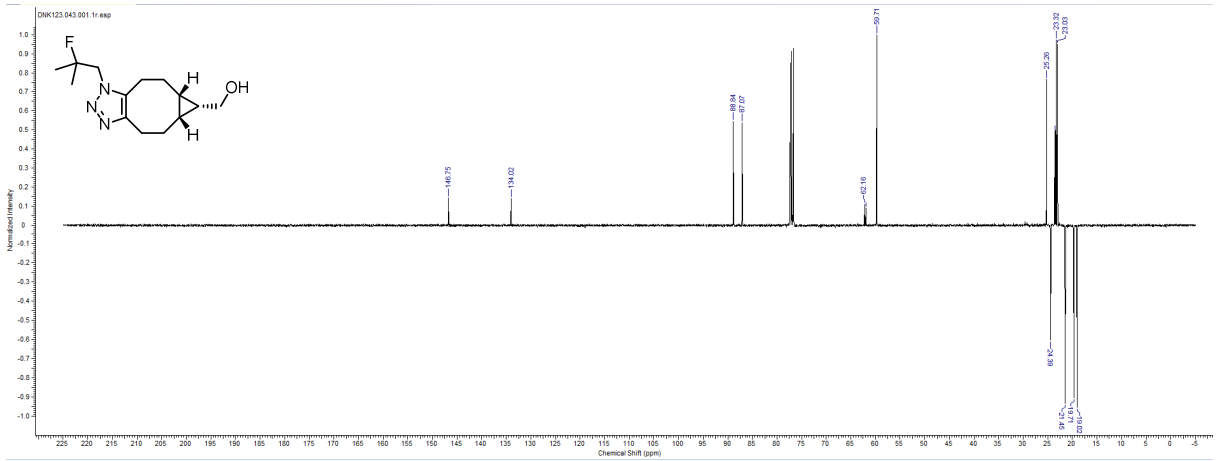

^{19}F-NMR spectrum of **17**

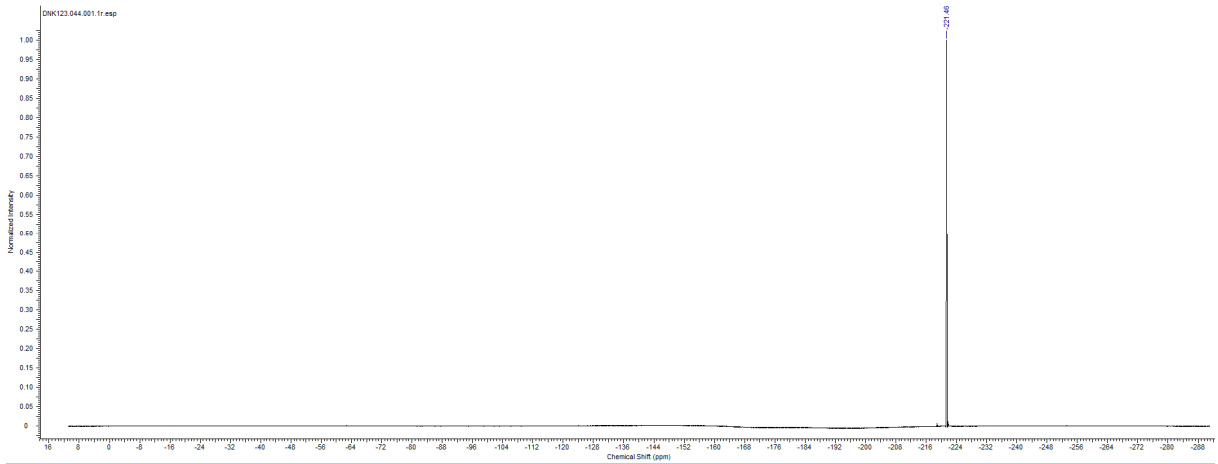

^{1}H-NMR spectrum of **18**

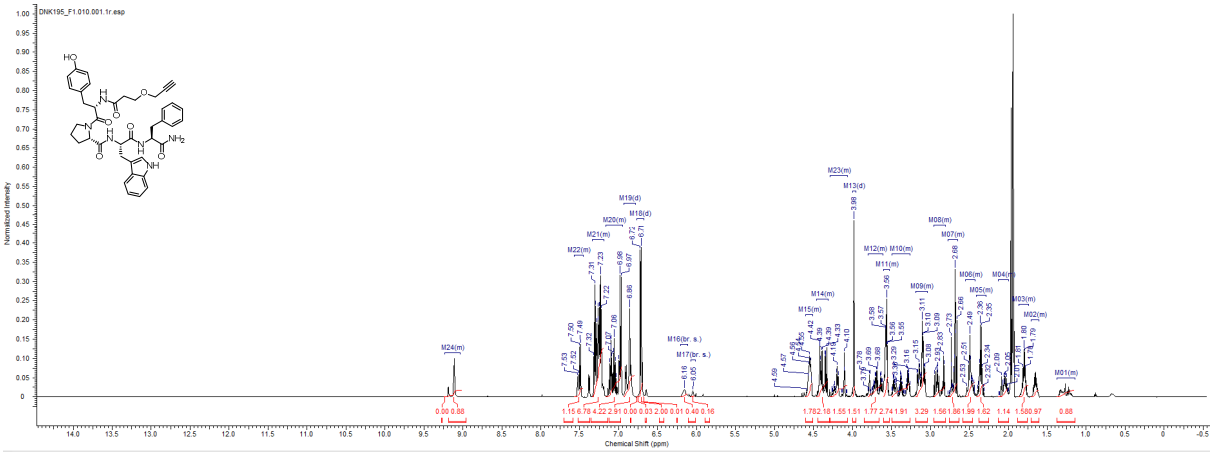

^{13}C-NMR spectrum of **18**

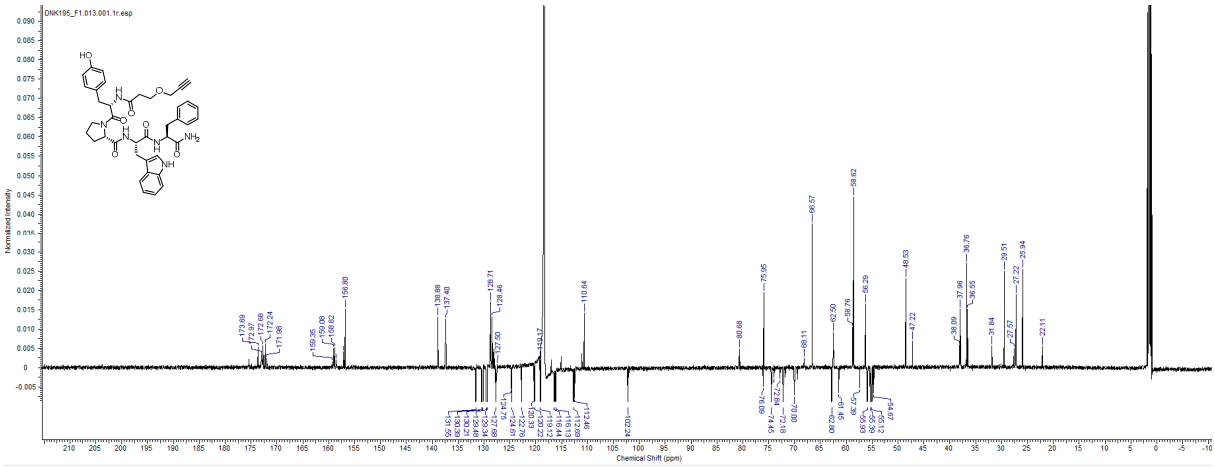

^{19}F-NMR spectrum of **19**

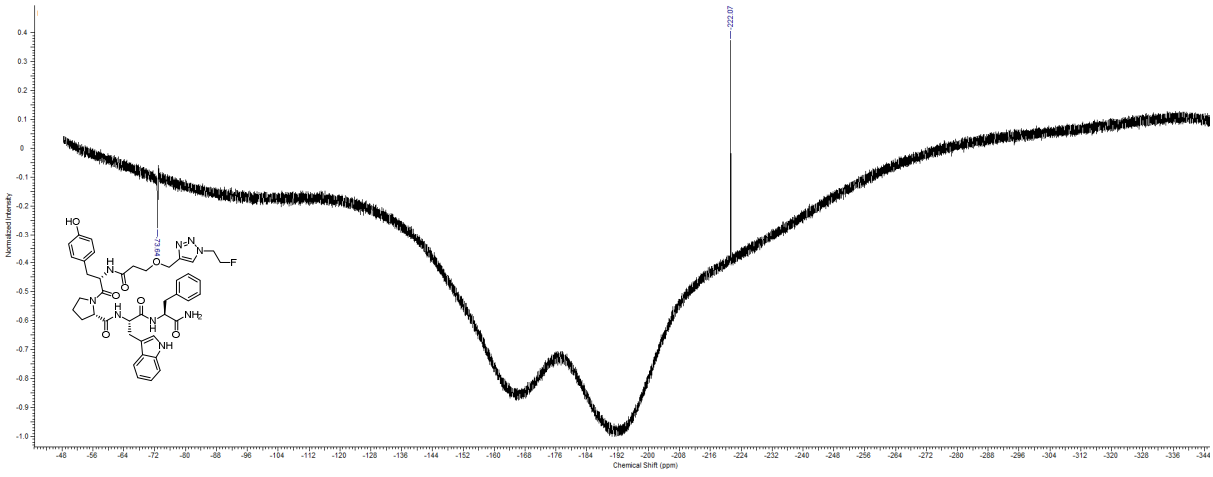

^{19}F-NMR spectrum of **20**

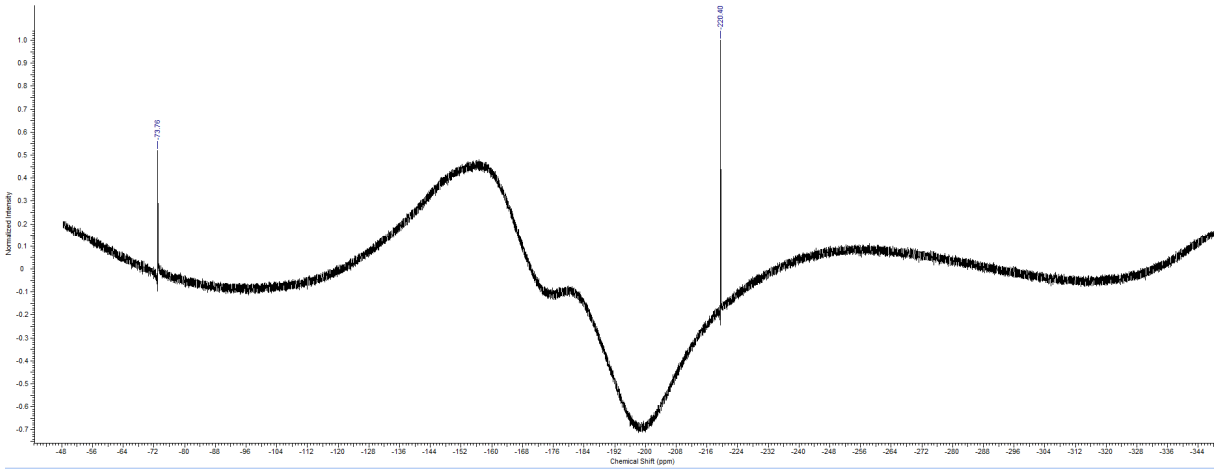

2. HPLC Data

Radiochromatogram of [^{18}F]**1** (HPLC Conditions A)

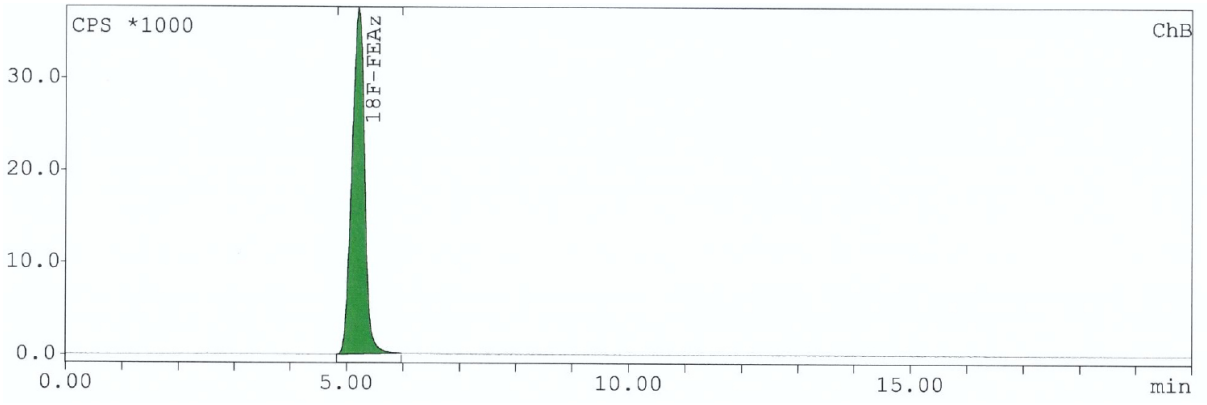

Radiochromatogram of [^{18}F]**15** (HPLC Conditions A)

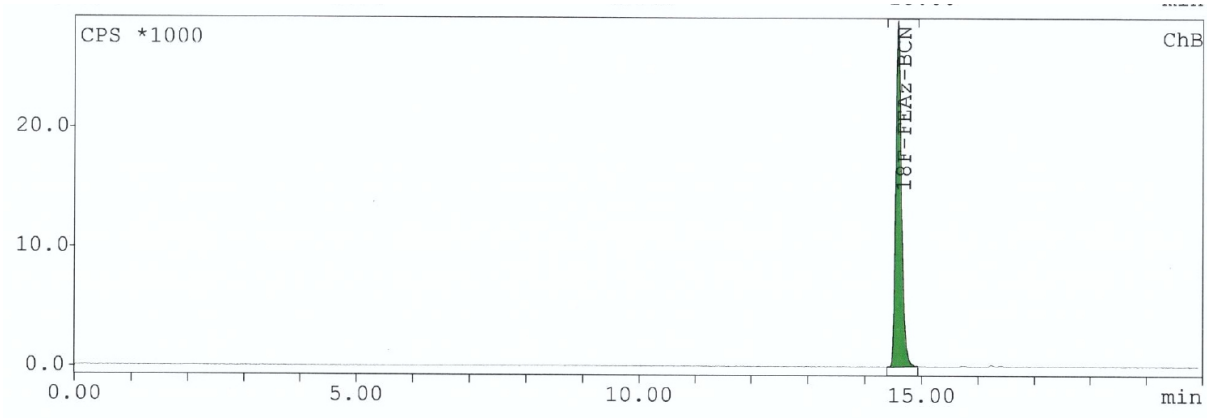

Chromatogram of **15** (230 nm, HPLC conditions A)

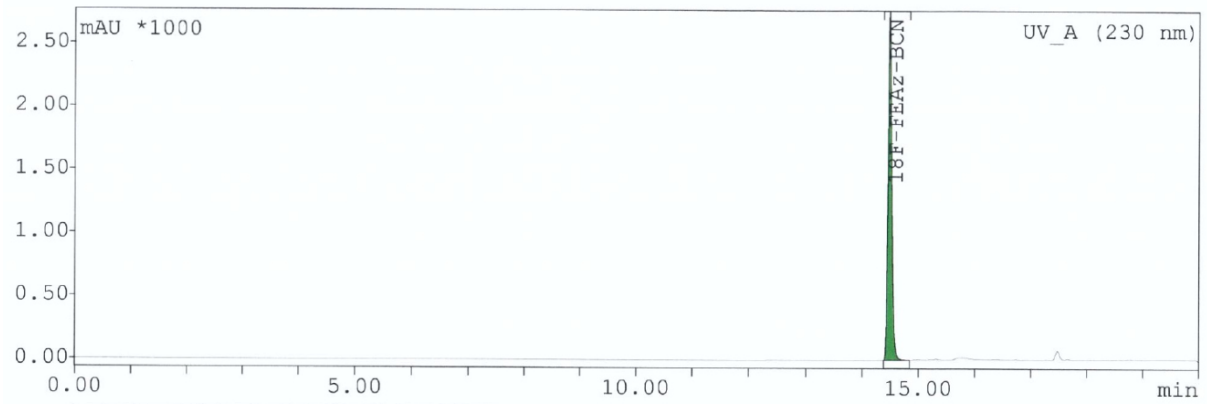

Chromatogram of **3** (216 nm, HPLC conditions A)

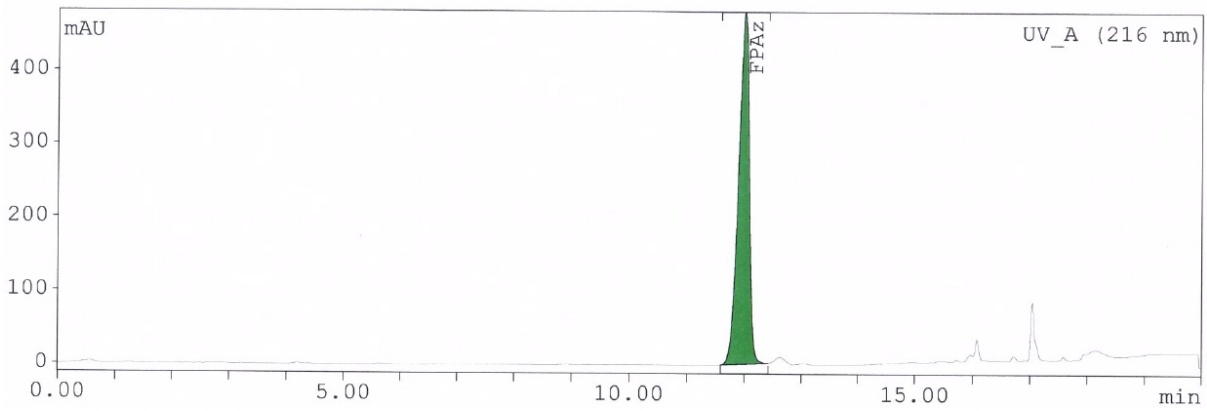

Radiochromatogram of [^{18}F]**3** (HPLC Conditions A)

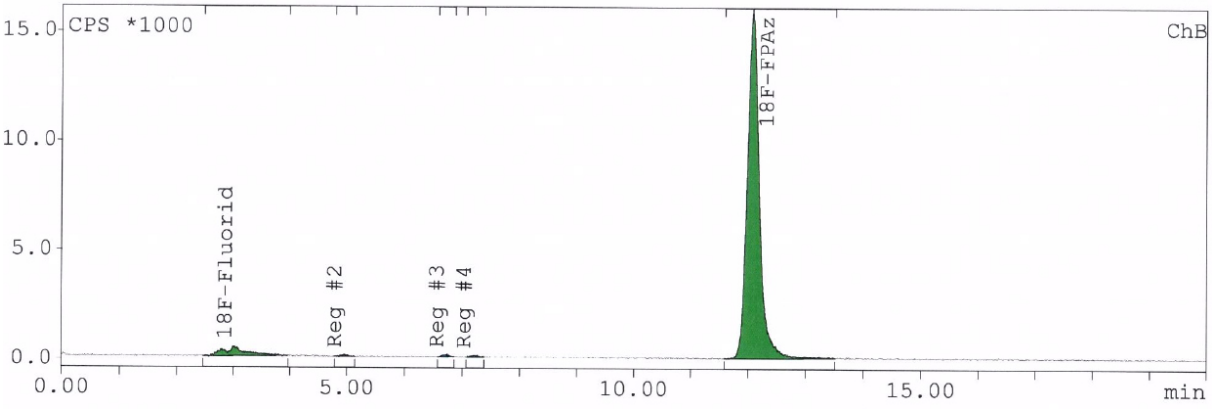

Chromatogram of **4** (solution in DMF, 216 nm, HPLC conditions A)

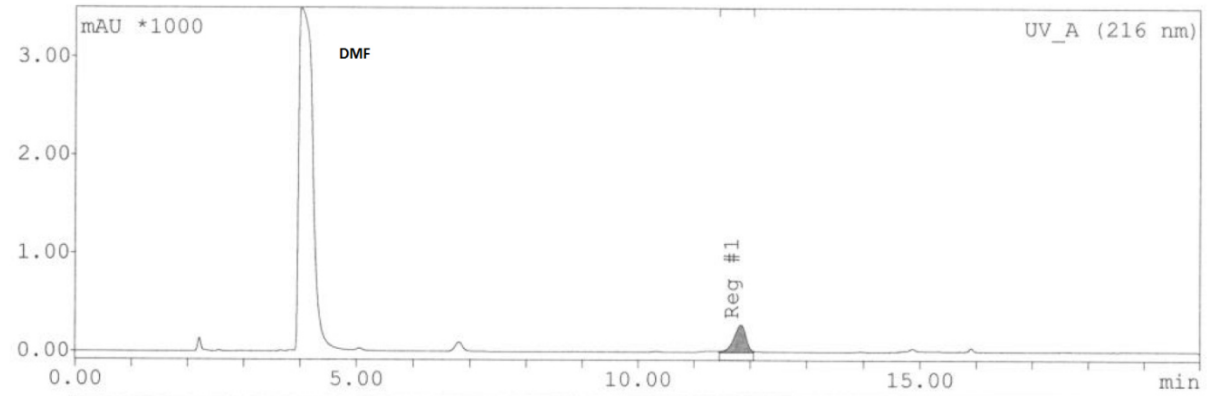

Radiochromatogram of [^{18}F]**4** (HPLC Conditions A)

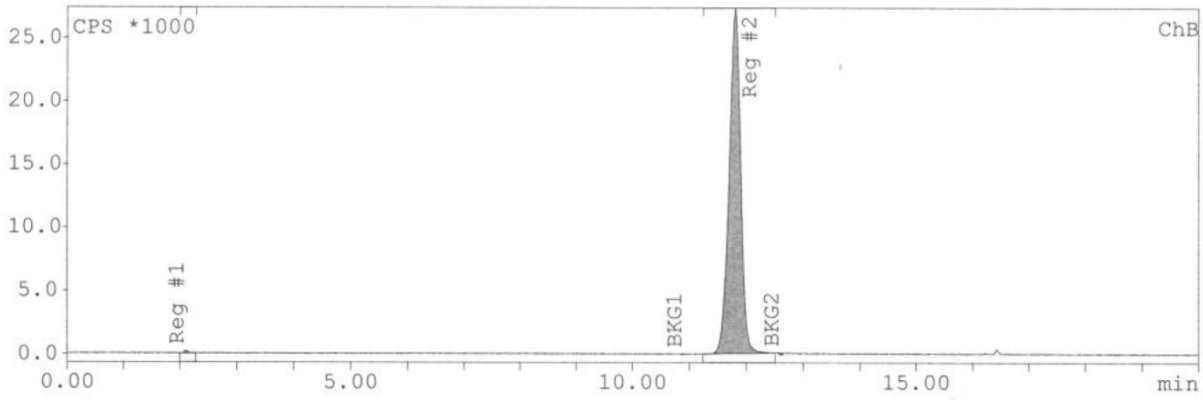

Chromatogram of **16** (230 nm, HPLC conditions A)

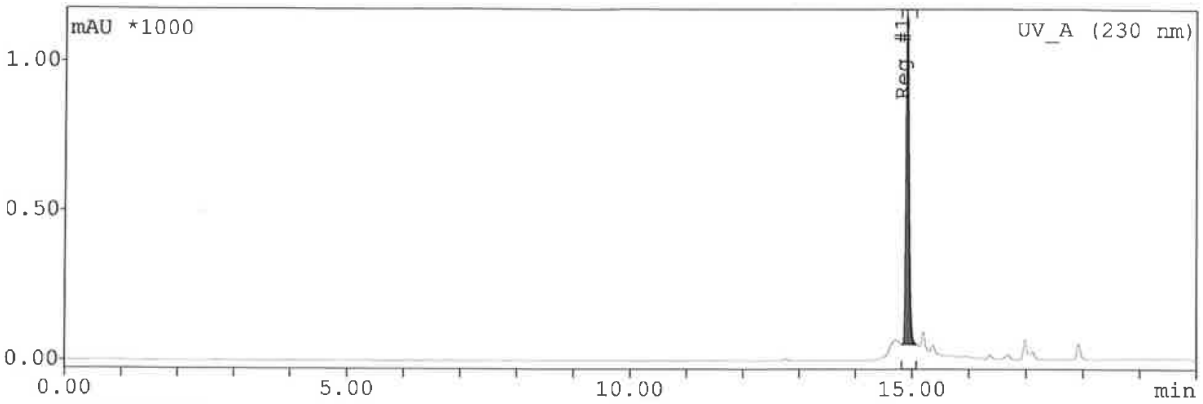

Radiochromatogram of [^{18}F]**16** (HPLC Conditions A)

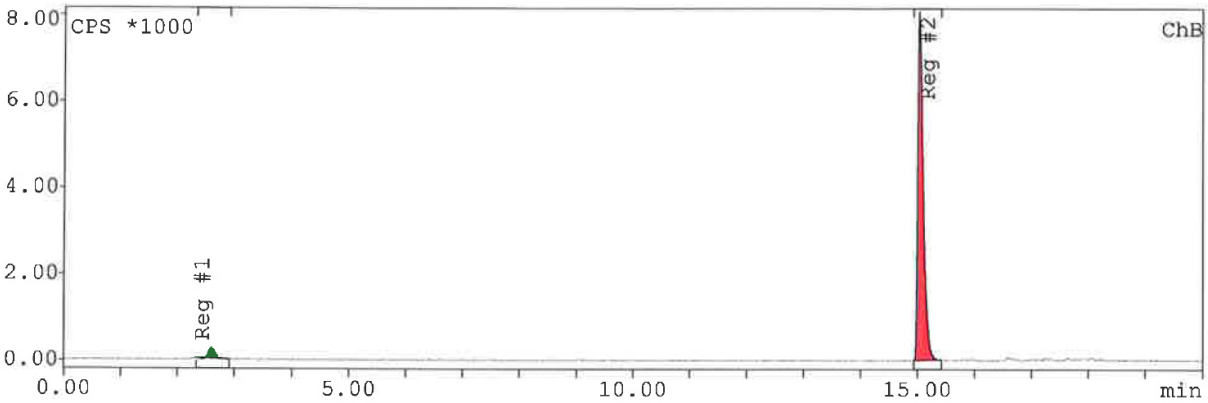

Chromatogram of **19** (280 nm, HPLC conditions B)

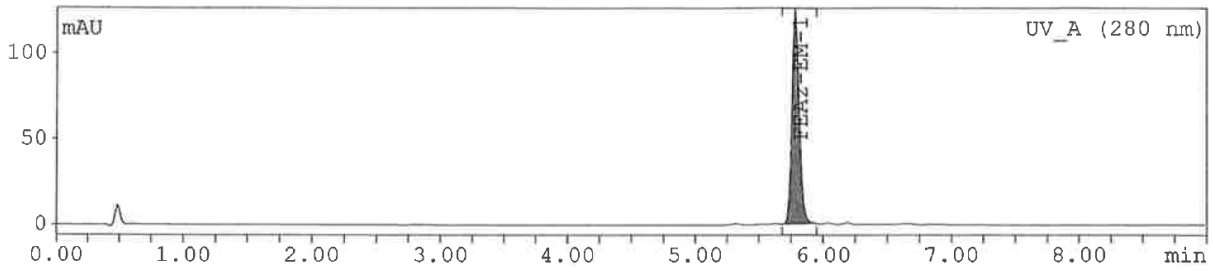

Chromatogram of **20** (280 nm, HPLC conditions B)

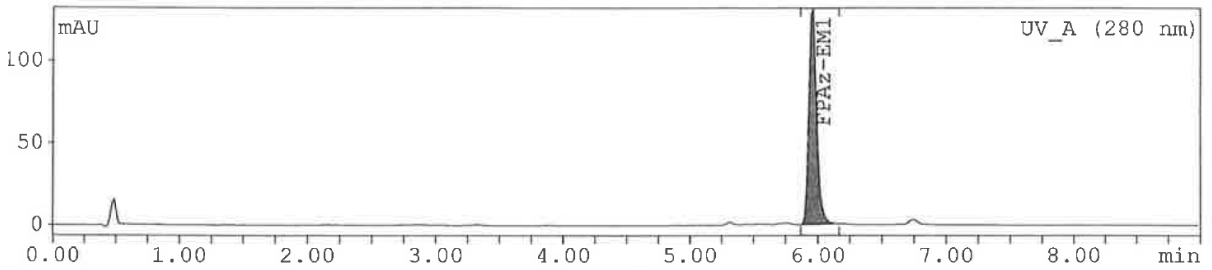

Chromatogram of **21** (280 nm, HPLC conditions B)

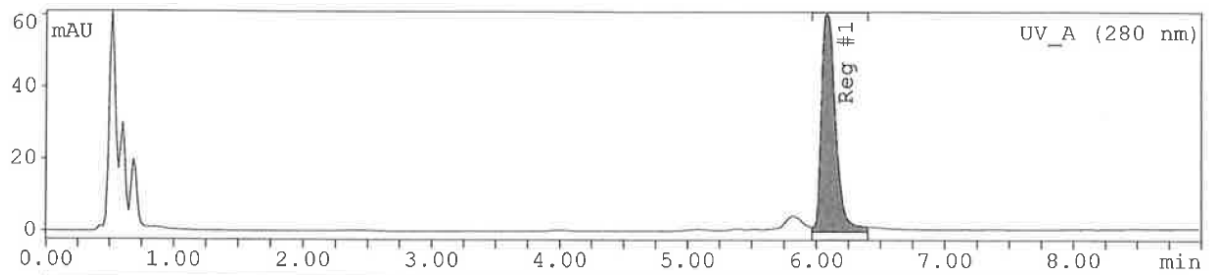

Radiochromatogram of [^{18}F]-**19** (quenched reaction mixture, HPLC conditions B)

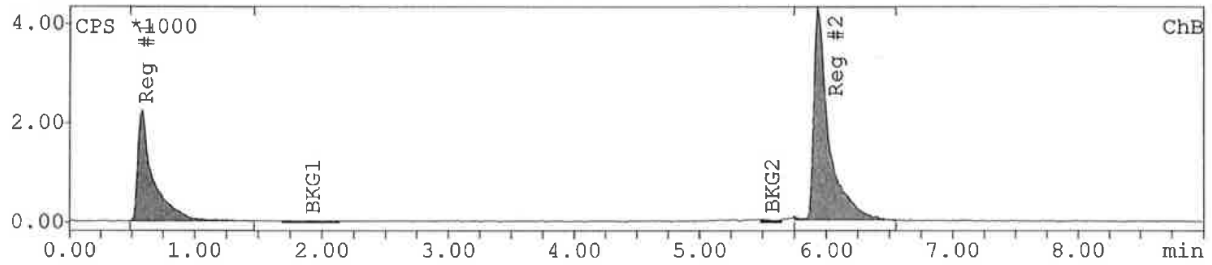

Radiochromatogram of [^{18}F]-**20** (quenched reaction mixture, HPLC conditions B)

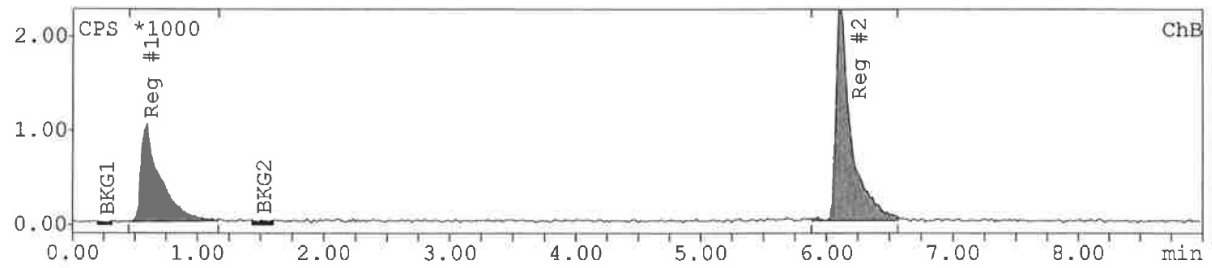

Radiochromatogram of [^{18}F]-**21** (quenched reaction mixture, HPLC conditions B)

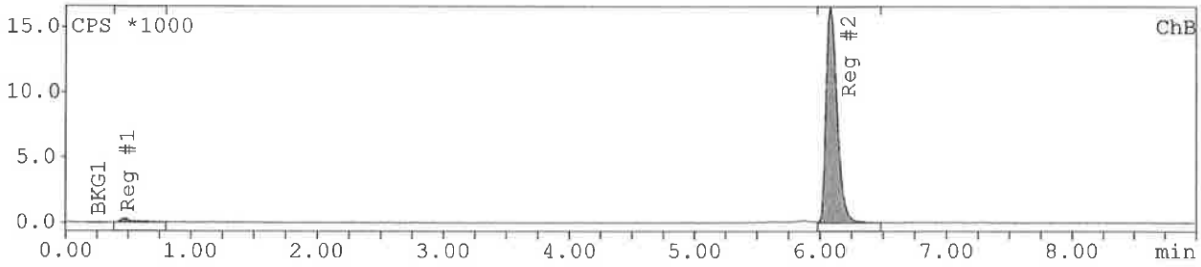

3. LC/MS Data

LC/ESI-MS of substance **15**
(green: DAD 230 nm, purple: TIC+)

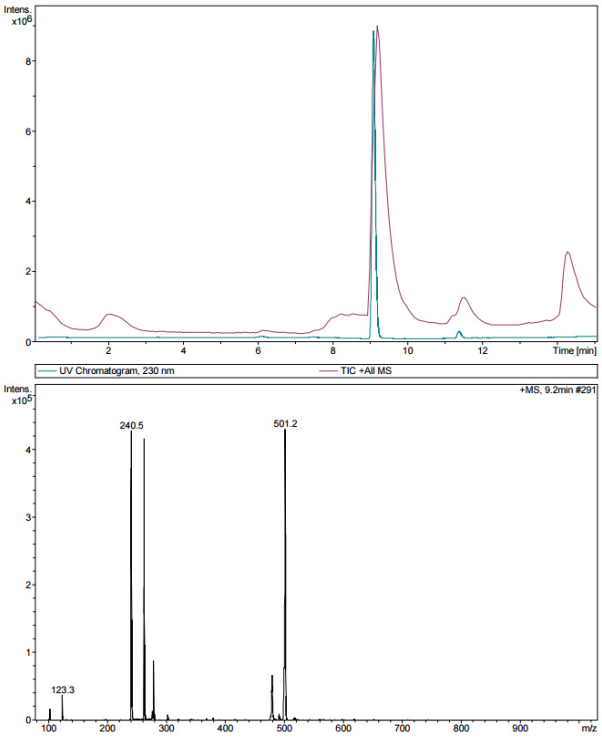

LC/ESI-MS of substance **16**
(yellow: DAD 230 nm, purple : TIC+)

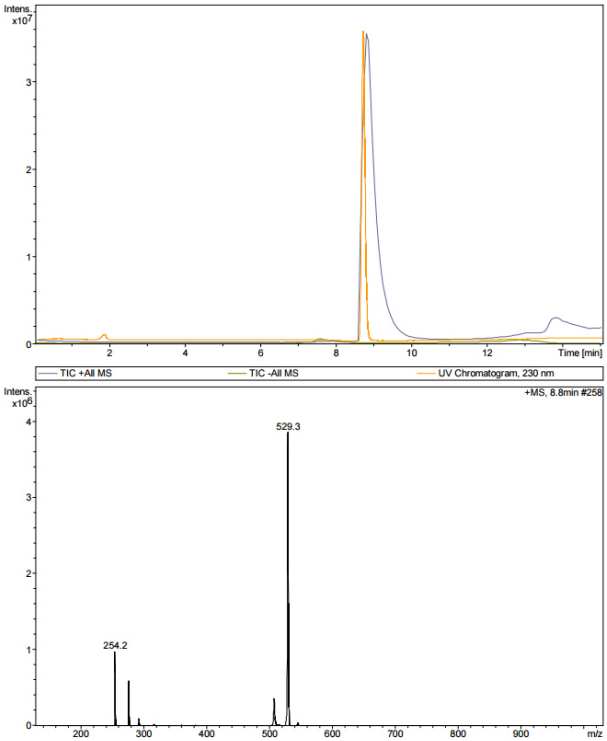

LC/ESI-MS of substance **17**
(green: DAD 230 nm, purple: TIC+)

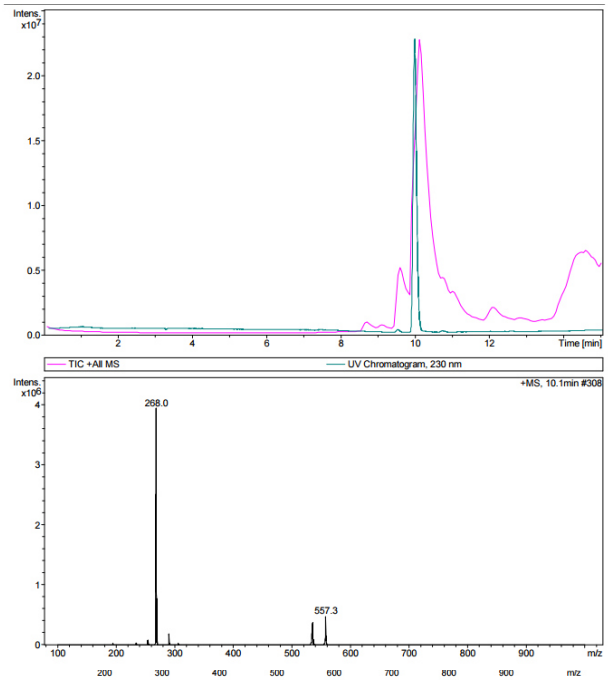

LC/ESI-MS of substance **18**
(red: DAD 280 nm, yellow: TIC-)

LC/ESI-MS of substance **19**
(red: DAD 280 nm, blue: TIC-)

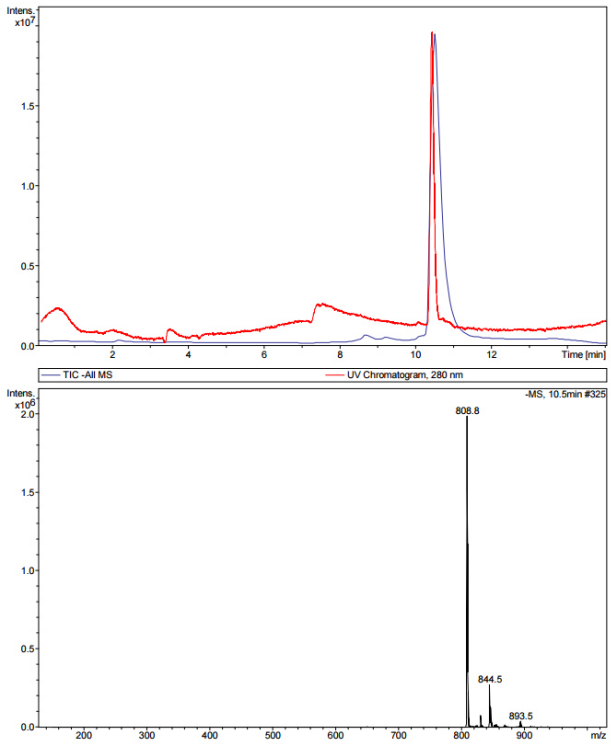

LC/ESI-MS of substance **20**
(black: DAD 280 nm, purple: TIC-)

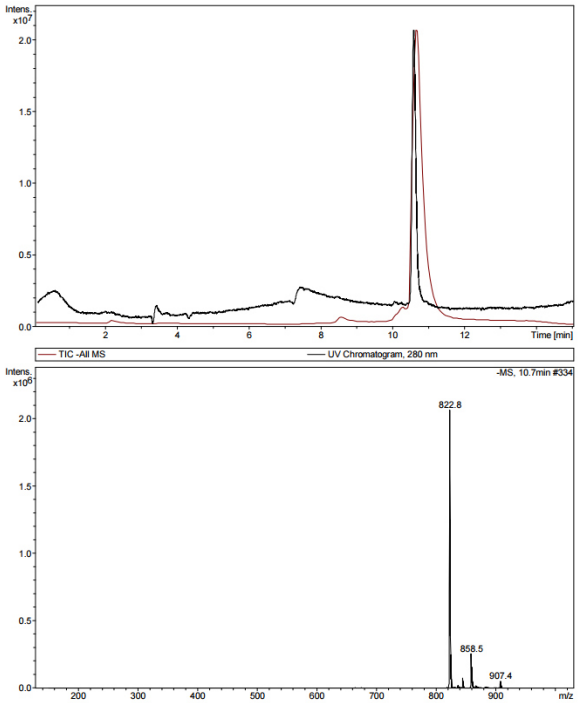

LC/ESI-MS of substance **21**
(red: DAD 280 nm, blue: TIC-)

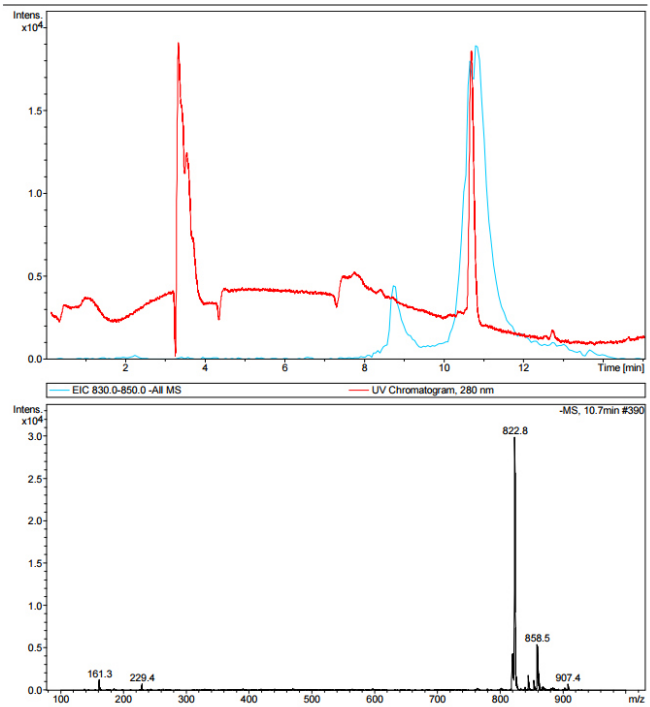

4. TLC Data

Plasma stability of [^{18}F] endomorphin-1 conjugates [^{18}F]-**14**, [^{18}F]-**15** or [^{18}F]-**16**

TLC conditions: 50% MeCN in H_2O + 0.1% TFA, RP18-Silica

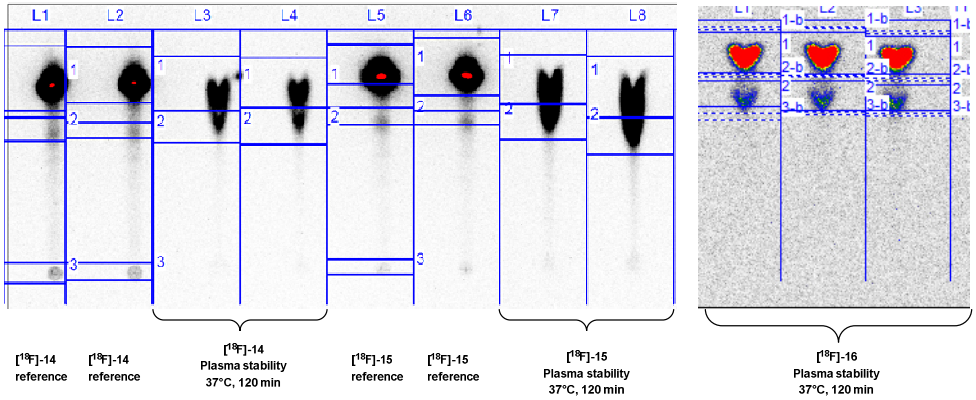

Supporting Information

Manuscript #4

Christoph Denk, Dennis Svatunek, Thomas Filip, Thomas Wanek, Daniel Lumpi, Johannes Fröhlich, Claudia Kuntner*, Hannes Mikula*; Development of a ^{18}F-Labeled Tetrazine with Favorable Pharmacokinetics for Bioorthogonal PET Imaging, *Angew. Chem. Int. Ed.* **2014**, 53, 9655–9659.

(with permission from John Wiley & Sons)

Angewandte Chemie
Eine Zeitschrift der Gesellschaft Deutscher Chemiker

Supporting Information

© Wiley-VCH 2014

69451 Weinheim, Germany

Development of a ^{18}F-Labeled Tetrazine with Favorable Pharmacokinetics for Bioorthogonal PET Imaging**

Christoph Denk, Dennis Svatunek, Thomas Filip, Thomas Wanek, Daniel Lumpi, Johannes Fröhlich, Claudia Kuntner, and Hannes Mikula**

anie_201404277_sm_miscellaneous_information.pdf

Supporting Information

Table of Contents

1.	Materials and Methods	S1
2.	Chemical Synthesis and Radiochemistry	S2
3.	Reaction kinetics	S6
4.	In vitro and in vivo investigations	S8
5.	NMR Spectra	S10
6.	Quantum Chemical Calculations	S12
7.	References	S27

1. Materials and Methods

Unless otherwise noted, all reagents were purchased from commercial suppliers and used without further purification. DCM and 1,4-dioxane were dried using PURESOLV-columns (Innovative Technology Inc.). Dry acetonitrile (Sigma Aldrich) and dry DMF (Acros) were commercially obtained and stored under argon. Tetrazine **2**[1], trans-cyclooctene (**3**)[2] and s-TCO **4**[3] were prepared following known procedures. Anhydrous hydrazine was prepared by the vacuum thermolysis of hydrazine cyanurate.[4] All other solvents were distilled prior to use. Drying of organic solvents after extraction was performed using anhydrous Na_2SO_4 or $MgSO_4$ (Sigma Aldrich) and subsequent filtration. Human Plasma for research purposes was purchased from the Austrian Red Cross blood donation service. Reactions were carried out under an atmosphere of argon in air-dried glassware with magnetic stirring. Sensitive liquids were transferred via syringe. Thin layer chromatography was performed using TLC alumina plates (Merck, silica gel 60, fluorescence indicator F254, or Merck, aluminium oxide neutral, fluorescence indicator F254). Preparative column chromatography was performed using a Büchi Sepacore Flash System (2 x Büchi Pump Module C-605, Büchi Pump Manager C-615, Büchi UV Photometer C-635, Büchi Fraction Collector C-660) using silica gel 60 (40-63 μm) as obtained from Merck and distilled or redistilled solvents. ^{1}H, ^{13}C and ^{19}F NMR spectra were recorded on a Bruker AC 200 or Bruker Avance UltraShield 400 spectrometer at 20 °C. Chemical shifts are reported in ppm (δ) relative to tetramethylsilane and calibrated using solvent residual peaks. Data are shown as follows: Chemical shift, multiplicity (s = singlet, d = doublet, t = triplet, q = quartet, quin = quintet, m = multiplet, br = broad signal), coupling constant (J, Hz) and integration. UV/VIS spectrophotometry was done on a UV-1800 Spectrophotometer (Shimadzu) and a temperature-controlled Applied Photophysics 05-19 system was used for stopped flow measurements. A Thermo Scientific LTQ Orbitrap XL hybrid FTMS (Fourier Transform Mass Spectrometer) equipped with Thermo Scientific MALDI Interface or Thermo Fischer Exactive Plus Orbitrap (LC-ESI+) and a Shimadzu IT-TOF Mass Spectrometer were used for high resolution mass spectrometry. α-Cyano-4-hydroxycinnamic acid was used as matrix for MALDI measurements. Aqueous [^{18}F]-fluoride (n.c.a.) was produced in a General Electrics PETtrace cyclotron (General Electric Healthcare, Uppsala, Sweden) via the $^{18}O(p,n)^{18}F$ nuclear reaction by irradiation of a 2.5 mL water target containing 95.9% enriched [^{18}O]H_2O (IASON, Graz, Austria) with a 16.5 MeV proton beam. Typical irradiation times were 65 min with a beam current of 45 μA, which yielded a [^{18}F]-fluoride amount of about 110 GBq at end of bombardment. A remote controlled GE Tracerlab FX module with 2.5 mL glass reactor housed in a lead castle was used for automated radiolabeling experiments. HPLC analysis was performed on a 1200 series system (Agilent Technologies) using a Zorbax SB-AQ (5 μm, 4.6 x 250 mm) column and H_2O/MeCN gradient elution (flow rate: 1.2 mL/min, 0-2 min: 5% MeCN, 2-10 min: 5 to 20% MeCN linear gradient, 10-16 min: 20 to 90% MeCN linear gradient). For radio-HPLC a GABI* radioactivity detector (Raytest) was used. Retention times were 17.2 min for precursor **8**, 12.4 min for [^{18}F]-**1** and 16.0 min/16.7 min for the ligation products [^{18}F]-**9** and [^{18}F]-**10**, respectively (see Manuscript, Figure 1). Preparative HPLC separation was done on an 1100 Series preparative HPLC system (Agilent Technologies) using a VP250/8 Nucleosil 100-5 C18 HD column (Macherey Nagel) and H_2O/EtOH gradient elution (flow rate 2.5 mL/min, 0-12 min: 8% EtOH, 12-32 min: 8 to 50% EtOH linear gradient) in combination with a K-2001 UV detector (Knauer) and a radioactivity detector from the Tracerlab Fx synthesis module.

2. Chemical Synthesis and Radiochemistry

2.1. Synthesis of tetrazine **1** and the precursor **8**

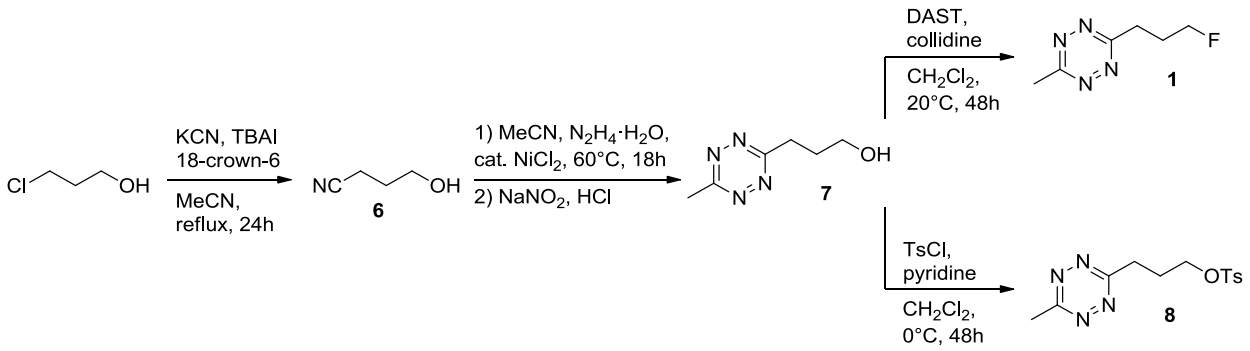

4-Hydroxybutanenitrile (6)



A mixture of 3-chloropropanole (1 eq., 25.7 ml, 307 mmol), potassium cyanide (1 eq., 20.0 g, 307 mmol), 18-crown-6 (0.003 eq., 244 mg, 0.92 mmol) and tetrabutylammonium iodide (0.003 eq., 340 mg, 0.92 mmol) in 50 mL MeCN was refluxed for 24 h. The reaction mixture was diluted with diethyl ether (100 mL), filtered and the solid residue was rinsed with additional Et_2O. Pooled filtrates were washed with water and brine, dried over Na_2SO_4 and concentrated. The residue was purified by distillation to yield **6** as colorless liquid (12.6 g, 48%); bp 128 °C / 25 mbar; ^{1}H NMR (200 MHz, $CDCl_3$) δ 3.61 (t, *J*=5.9 Hz, 2 H), 3.17 (brs, 1 H), 2.41 (t, *J*=7.0 Hz, 2 H), 1.86-1.71 (m, 2 H); ^{13}C NMR (50 MHz, $CDCl_3$) δ 119.6, 59.7, 27.7,13.4.

3-(6-Methyl-1,2,4,5-tetrazin-3-yl)propan-1-ol (7)

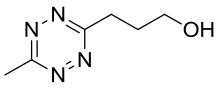

Procedure A (anhydrous hydrazine): A mixture of compound **6** (1 eq., 0.4 g, 4.7 mmol), MeCN (7 eq., 1.34 g, 32.6 mol) and $Zn(OTf)_2$ (0.85 g, 2.34 mmol) was treated dropwise with anhydrous hydrazine (36 eq., 5.4 g, 168.7 mmol). After stirring for 4 hours at 65°C a solution of sodium nitrite (8 eq., 2.58 g, 38 mmol) in 25 ml water was added followed by slow addition of 2 N HCl until gas evolution ceased. The pH was adjusted to 7 with $NaHCO_3$ and the mixture extracted with EtOAc (6 x 25 mL). Drying over Na_2SO_4 and removal of the solvent yielded the crude product, which was purified by column chromatography (25 g SiO_2, 15-50% EtOAc in hexanes) to yield **7** as a red liquid (160 mg, 21% of theory); R_f (hexanes/EtOAc, 3/1) 0.08; ^{1}H NMR (400 MHz, $CDCl_3$) δ 3.80 (q, *J*=5.8 Hz, 2 H), 3.43 (t, *J*=7.5 Hz, 2 H), 3.04 (s, 3 H), 2.22 (quin, *J*=6.7 Hz, 2 H), 1.61 (t, *J*=5.3 Hz, 1 H); ^{13}C NMR (101 MHz, $CDCl_3$) δ 169.8, 167.4, 61.8, 31.4, 30.6, 21.1; HR-ESI-TOF-MS $[M+H]^+$ *m/z* calcd. 155.0927 for $C_6H_{11}N_4O^+$, found 155.0924.

Procedure B (hydrazine monohydrate): A stirred mixture of compound **6** (1 eq., 5 g, 58.8 mmol), MeCN (7 eq., 16.9 g, 0.411 mol) and anhydrous $NiCl_2$ (5 mol%, 3.05 g, 23.5 mmol) was treated dropwise with hydrazine monohydrate (25 eq., 73.5 g, 1.47 mol). The purple reaction mixture was stirred at 60°C for 18 hours. Afterwards a solution of $NaNO_2$ (14.5 eq., 58.8 g, 0.85 mol) in 400 ml H_2O was carefully added. 2N HCl was added until the evolution of nitrous oxides ceased. The dark red solution was extracted with ethyl acetate for three hours using a continuous extractor. The extract was dried over Na_2SO_4 and concentrated. The residue was purified by column chromatography (100 g SiO_2, 30-45% EtOAc in hexanes) to give **7** as a red liquid (1.62 g, 18%); for characterization data see Procedure A.

3-(3-Fluoropropyl)-6-methyl-1,2,4,5-tetrazine (1)

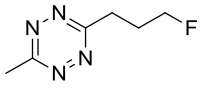

To a stirred solution of 3-(6-methyl-1,2,4,5-tetrazin-3-yl)propan-1-ol (**7**) (1 eq., 70 mg, 0.454 mmol) and 2,4,6-collidine (2.7 eq., 150 mg, 1.23 mmol) in dry DCM (2 mL) cooled to -10°C a solution of DAST (1.5 eq., 110 mg, 0.68 mmol) in dry DCM (1 mL) was dropwise added. After stirring for 48 h at room temperature, the reaction was quenched by addition of MeOH (200 µL) and concentrated. Column chromatography (8 g SiO_2, Et_2O/hexanes gradient elution) afforded **1** as a purple liquid (16 mg, 23%); Rf (hexanes/EtOAc, 3/1) 0.62; ^{1}H NMR (400 MHz, $CDCl_3$) δ 4.61 (dt, *J*=47.1, 5.60 Hz, 2 H), 3.46 (t, *J*=7.6 Hz, 2 H), 3.05 (s, 3 H), 2.45-2.28 (m, 2 H); ^{13}C NMR (101 MHz, $CDCl_3$) δ 169.2, 167.6, 82.9 (d, $^1J_{13C\text{-}19F}$ =167.2 Hz), 30.8 (d, $^3J_{13C\text{-}19F}$ =5.4 Hz), 28.5 (d, $^2J_{13C\text{-}19F}$ =20.7 Hz), 21.1; ^{19}F NMR (376.5 MHz, $CDCl_3$) δ -220.0; HR-ESI-FTMS $[M+H]^+$ *m/z* calcd. 157.0884 for $C_6H_{10}FN_4^+$, found 157.0883.

3-(6-Methyl-1,2,4,5-tetrazin-3-yl)propyl p-tolylsulfonate (8)

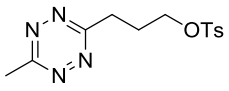

A stirred solution of 3-(6-methyl-1,2,4,5-tetrazin-3-yl)propan-1-ol (**7**) (1 eq., 18 mg, 0.117 mmol) and tosyl chloride (4 eq., 89 mg, 0.47 mmol) in dry DCM (2 mL) was treated with pyridine (4 eq., 37 mg, 0.47 mmol) at 0°C. The mixture was stirred at 0 °C for 48 hours, diluted with DCM (30 mL) and washed with cold 1N HCl followed by cold aq. 2% $NaHCO_3$ and water. The organic layer was dried over $MgSO_4$ and concentrated. Column chromatography (8 g SiO_2, 10-50% EtOAc in hexanes) afforded **8** as a red solid (29.8 mg, 83%); Rf (hexanes/EtOAc, 3/1) 0.28; ^{1}H NMR (400 MHz, CD_2Cl_2) δ 7.76 (d, *J*=8.2 Hz, 2 H), 7.36 (d, *J*=8.2 Hz, 2 H), 4.17 (t, *J*=6.1 Hz, 2 H), 3.33 (t, *J*=7.5 Hz, 2 H), 3.00 (s, 3 H), 2.45 (s, 3 H), 2.31 (quin, *J*=6.7 Hz, 2 H); ^{13}C NMR (101 MHz, CD_2Cl_2) δ 169.3, 168.2, 145.7, 133.3, 130.5, 128.4, 69.9, 31.3, 27.3, 21.9, 21.5; HR-ESI-TOF-MS $[M+H]^+$ *m/z* calcd. 309.1016 for $C_{13}H_{17}N_4O_3S^+$, found 309.1011.

2.2. Synthesis of s-TCO derivative **5**

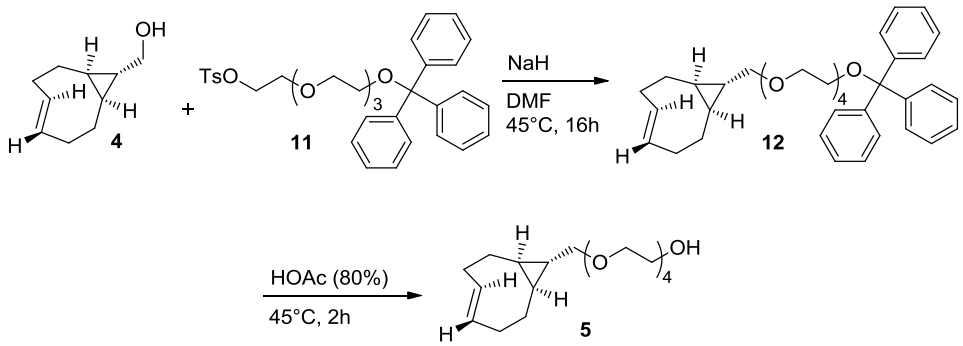

15-(*(1R*,8S*,9R*,E)*-Bicyclo[6.1.0]non-3-en-9-yl)-1,1,1-triphenyl-2,5,8,11,14-pentaoxapentadecane (12)

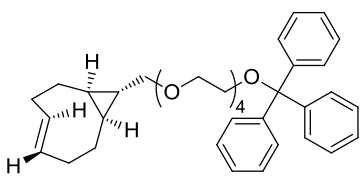

To a dispersion of sodium hydride (6 eq., 410 mg, 10.25 mmol) in dry DMF (0.6 mL) was dropwise added a solution of s-TCO **4**[3] (1 eq., 260 mg, 1.71 mmol) in dry DMF (1.8 mL). After stirring for 30 minutes at room temperature tosylate **11**[5] (1.1 eq., 1.1 g, 1.86 mmol) dissolved dry DMF (1.5 mL) was added dropwise. The resulting brownish reaction mixture was stirred at 45°C for 16 hours, then poured into ice/NH_4Cl and extracted with DCM. The combined organic layer was washed with brine, dried over $MgSO_4$ and concentrated. The residue was purified by column chromatography (90g SiO_2, 5-40% EtOAc in hexanes) to yield **12** as a yellowish oil (318 mg, 33%); Rf (hexanes/EtOAc, 1/1) 0.68; ^{1}H NMR (200 MHz, $CDCl_3$) δ 7.46-7.32 (m, 6 H) 7.29-7.06 (m, 9 H) 5.92-5.66 (m, 1 H) 5.14-4.95 (m, 1 H) 3.68-3.43 (m, 16 H) 3.16 (t, *J*=5.3 Hz, 3 H) , 2.41-2.02 (m, 5 H) 1.92-1.67 (m, 2 H) 0.63-0.90 (m, 2 H); ^{13}C NMR (50 MHz, $CDCl_3$) δ 144.1, 138.4, 131.2, 128.7, 127.7, 126.7, 75.6, 70.8, 70.7, 70.6, 69.4, 63.3, 38.7, 33.9, 32.6, 27.8, 25.2, 21.8, 20.8.

1-((*1R*,8S*,9R*,E)*-Bicyclo[6.1.0]non-3-en-9-yl)-2,5,8,11-tetraoxatridecan-13-ol (5)

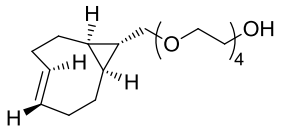

A solution of **12** (1 eq., 250 mg, 0.438 mmol) in 80% HOAc (4 mL) was stirred at 45°C for 2 h leading to precipitation of triphenylmethanol. The reaction mixture was poured into ice-water (10 mL) and filtrated. The removed solid was thoroughly washed with water and the combined filtrate was lyophilized to yield **5** as a yellowish oil (110 mg, 77%); Rf (hexanes/EtOAc, 1/1) 0.16; ^{1}H NMR (200 MHz, D_2O) δ 5.99-5.58 (m, 1 H), 5.23-4.93 (m, 1 H), 3.82-3.45 (m, 16 H), 3.37 (d, *J*=5.7 Hz, 2 H), 2.62-1.33 (m, 6 H), 0.98-0.24 (m, 4 H); ^{13}C NMR (50 MHz, D_2O) δ 138.3, 131.3, 75.4, 71.9, 69.8, 69.6, 69.0, 60.4, 38.5, 33.8, 32.4, 27.6, 24.8, 21.8, 20.7; HR-MALDI-FTMS $[M+Na]^+$ calcd. 351.2142 for $C_{18}H_{32}NaO_5^+$, found 351.2151.

2.3. Radiosynthesis of [^{18}F]-**1**

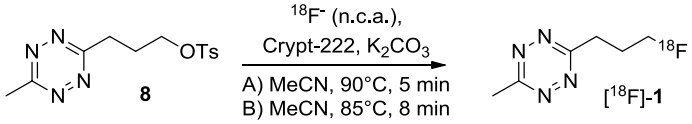

Procedure A (manual radiolabeling)[1]: 319 MBq (8.62 mCi) [^{18}F]-HF in water (500 µL) was added to a HCO_3^- anion exchange cartridge (^{18}F separation cartridge) previously conditioned with H_2O (5 mL). The radioactivity was eluted with a solution of [2.2.2]cryptand (14.4 mg) in MeCN (900 µL) to which a 3.5% aq. K_2CO_3 solution (100 µL) had been added. The eluate was collected in a 2.5 mL vial with stir bar and septum. Volatiles were removed at 90°C under a stream of argon, and the residue was azeotropically dried twice by addition and subsequent evaporation of dry MeCN (2 x 900 µL) at 90°C heating block temperature. Precursor **8** (10 mg, 32.4 µmol) dissolved in dry MeCN (700 µL) was added and after stirring for 5 min at 90 °C a sample was analyzed by radio-HPLC to determine the radiochemical yield of [^{18}F]-**1** (16 ± 2% decay corrected).

Procedure B (automated labeling – non-optimized): A remote controlled GE Tracerlab FX module (Figure S1) with 2.5 mL glass reactor housed in a lead castle was used for automated labeling experiments. In a typical labeling experiment [^{18}F]-fluoride (109 GBq) was produced in the cyclotron target by bombardment of ^{18}O-enriched water with a 16.5 MeV proton beam. The activity was transferred into the synthesis module and trapped on a preconditioned Waters QMA light cartridge. The radioactivity was eluted with a solution of [2.2.2]cryptand (14.8 mg) in MeCN (900 µl) to which a 3.5% aq. K_2CO_3 (100 µL) solution had been added. After addition of dry MeCN (500 µL) volatiles were removed in vacuo at a temperature of 60-120 °C. After cooling to 60 °C the precursor **8** (9.8 mg, 31.8 µmol) in dry MeCN (800 µL) was added, and the reaction mixture was heated to 85°C for 8 minutes. The reaction product was separated by preparative HPLC cutting the peak at retention time 15 min. Last traces of [^{18}F]-fluoride were removed by passing over a SepPAK Alumina-N cartridge, yielding 3.9 GBq [^{18}F]-**1** (5.2% decay corrected). The product was brought to physiological osmolality (320 mmol/kg) by addition of 10% aq. NaCl solution. Starting from 370.8 MBq/mL almost no radiolysis of [^{18}F]-**1** (< 1%) was observed after 4 h as determined by radio-HPLC.

[1] Procedures using other solvents (e.g. DMSO) or fluorination reagents (e.g. TBAF) afforded [^{18}F]-**1** in radiochemical yields below 11%.

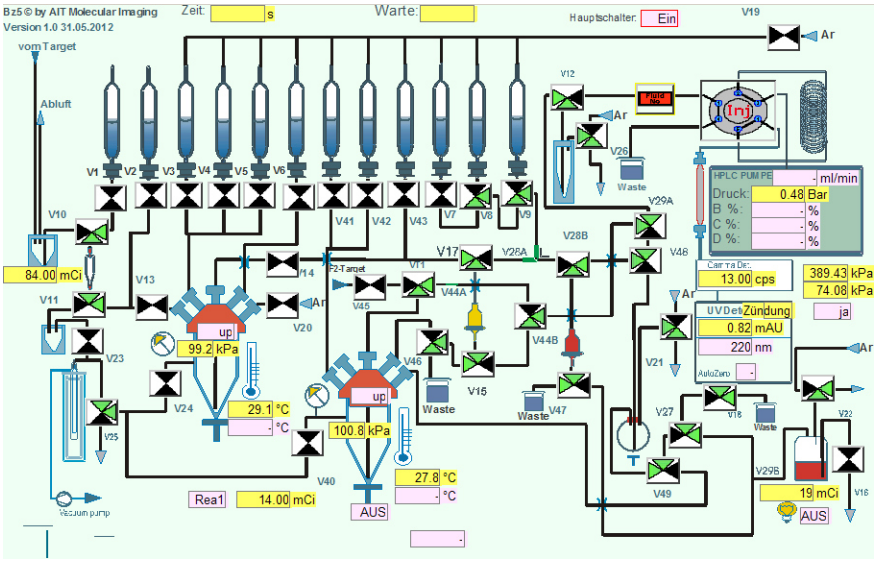

Figure S1. Schematic flow chart of automated labeling.

2.4. IEDDA-initiated conjugations

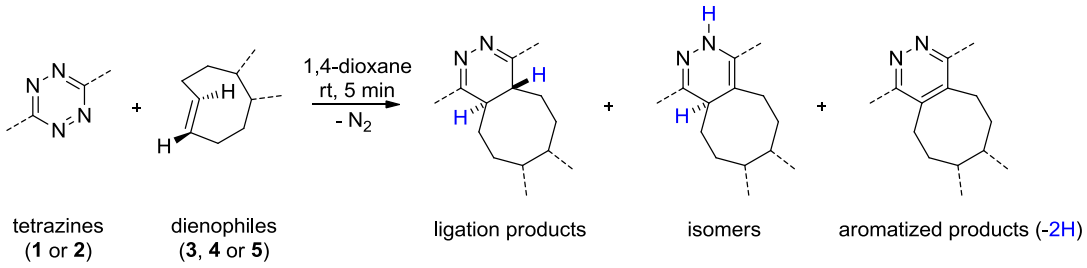

General procedure: To a 3 mM solution of tetrazine **1** or **2** in dry 1,4-dioxane (1 mL) was added a 3 mM solution of dienophile **3**, **4**, or **5** (1 eq.) in dry 1,4-dioxane (1 mL) and the resulting mixture was stirred for 1-5 min at room temperature. Due to the fast isomerization and aromatization known for tetrazine/TCO-ligation products, these samples were directly subjected to LC/HR-ESI-FTMS analysis for characterization (Table S1).

Table S1. Results of IEDDA-initiated conjugations of tetrazines (**1** and **2**) and dienophiles (**3**, **4**, and **5**).

Tetrazine	Dienophile	Products	Product formula	Product Calcd. mass	Found mass (HR-ESI-FTMS)
	3	-	$C_{14}H_{23}FN_2$	$[M+H]^+$ 239.1918	$[M+H]^+$ 239.1917
1	**4**	**9** + **10**	$C_{16}H_{25}FN_2O$	$[M+H]^+$ 281.2024	$[M+H]^+$ 281.2025
	5	**11** + **12**	$C_{24}H_{41}FN_2O_5$	$[M+H]^+$ 457.3072	$[M+H]^+$ 457.3069
2	**3**	-	$C_{17}H_{22}N_2O$	$[M+H]^+$ 271.1805	$[M+H]^+$ 271.1810

3. Reaction kinetics

The tetrazine (**1** or **2**) was weighted into a volumetric flask and filled with solvent (absolute 1,4-dioxane or human plasma) to generate a 3 mM solution. The dienophile was weighted into a volumetric flask and filled with solvent (absolute 1,4-dioxane or human plasma) to generate a 30 mM solution. The reactant solutions were transferred into the driver syringes of the stopped flow apparatus (Applied Photophysics, Surrey, UK). Upon temperature constancy (± 0.1°C of aimed value) triggering of driver syringe pneumatics caused mixing of equal reactant volumes. Depending on reaction rate time intervals between 0.1 to 1000 s were chosen to collect 4000 data points at 540 nm. All measurements were made in duplicate or triplicate. Reactions in 1,4-dioxane were monitored at 20°C, 37 °C and 60°C, reactions in human plasma were conducted at 37°C only. The pseudo first order rate constant (k_{obs}) was determined by linearization of the decay curve followed by linear fitting. The second order rate constant (k) was calculated from the pseudo-first order rate constant. Linearization and direct fitting to the Eyring equation (Equation 1) was used to calculate the enthalpy of activation ($\Delta H^{\ddagger}$) and the entropy of activation ($\Delta S^{\ddagger}$). Equation 2 gave rise to free energy of activation at 298.15 K ($\Delta G^{\ddagger}$). Results are summarized in Table S2 (rate constants) and Table S3 (thermodynamic data). Selected plots of kinetic measurements and Eyring linearization are shown in Figure S2.

$$\ln\left(\frac{k}{T}\right) = -\left(\frac{\Delta H^{\ddagger}}{R}\right) * \left(\frac{1}{T}\right) + \ln\left(\frac{K_b}{h}\right) + \left(\frac{\Delta S^{\ddagger}}{R}\right) \quad (1)$$

$$\Delta G^{\ddagger} = \Delta H^{\ddagger} - \mathrm{T}\Delta S^{\ddagger} \quad (2)$$

Table S2. Results of kinetic measurements (rate constants).

Reaction	Solvent	T (°C)	k_{obs} (s^{-1})	k ($M^{-1}s^{-1}$)
1 + **3**	1,4-dioxane	20	(13.0 ± 0.1) · 10^{-3}	0.81 ± 0.01
		37	(23.9 ± 0.2) · 10^{-3}	1.49 ± 0.01
		60	(46.3 ± 0.4) · 10^{-3}	2.89 ± 0.03
1 + **4**	1,4-dioxane	20	0.90 ± 0.02	60.1 ± 0.9
		37	1.28 ± 0.04	85.5 ± 2.3
		60	1.86 ± 0.03	124.2 ± 1.5
1 + **5**	Human plasma	37	123.0 ± 4.5	8200 ± 300
2 + **3**	1,4-dioxane	20	0.74 ± 0.01	49.0 ± 0.7
		37	1.19 ± 0.02	79.2 ± 1.3
		60	1.98 ± 0.01	131.8 ± 0.7

Table S3. Results of kinetic measurements (thermodynamic data).

Reaction	Solvent	$\Delta H^{\ddagger}$ (kcal/mol)	$\Delta S^{\ddagger}$ (kcal/mol)	$\Delta G^{\ddagger}$ (kcal/mol)
1 + **3**	1,4-dioxane	5.54	-0.040	17.5
1 + **4**	1,4-dioxane	2.89	-0.040	15.0
2 + **3**	1,4-dioxane	4.17	-0.036	15.1

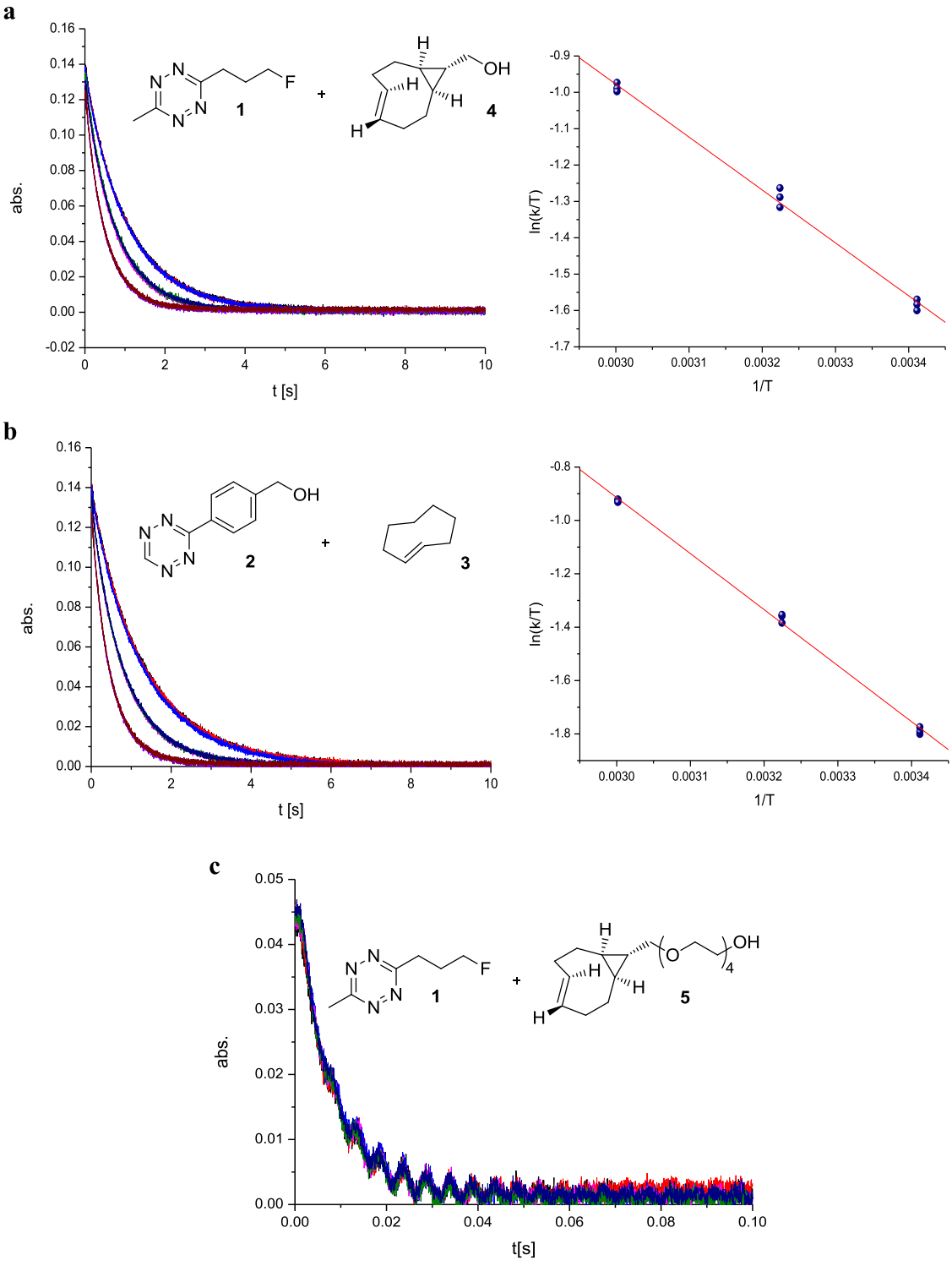

Figure S2. Selected data and plots of kinetic investigations: a) **1**+**4** in 1,4-dioxane at 20, 37 and 60 °C. b) **2**+**3** in 1,4-dixoane at 20, 37 and 60 °C. c) **1**+**5** in human plasma at 37 °C (abs. = absorbance).

4. In vitro and in vivo investigations

4.1. In vitro stability of tetrazine **1** and s-TCO derivative **5** in human plasma

Freshly prepared solutions of **1** and **5** in human plasma (3 mM) were incubated at 37 °C for 12 h and 24 h, respectively. The amount of degradation was determined by UV/VIS spectrophotometry and HPLC (both used for **1**) and titration with a tetrazine standard solution followed by UV/VIS (used for **5**). Recoveries: 99% **1**, 85 ± 5% **5** (n = 2).

4.2. In vivo experiments

Animals. Female BALB/c mice were scanned at a weight of 19.4±1.6 g and housed in groups of up to five individuals under controlled environmental conditions (22±1°C, 40-70% humidity) with a 12 h light-dark cycle (lights on at 6:00) and ad libitum access to food and water. Before PET scanning, an adaptation period of at least one week was accorded to each animal. The study was authorized by the institutional animal care and use committees, and all study procedures were performed in accordance with the European Communities Council Directive of November 24, 1986 (86/609/EEC). Every effort was made to minimize both the suffering and the number of animals used in this study. Anesthesia (2.0% isoflurane mixed in oxygen) was induced and the animals were warmed at 38°C to prevent hypothermia. Anesthesia and warming was maintained during the whole experimental procedure. Body temperature and respiratory rate were constantly monitored during the whole experiment using an MR compatible small animal monitoring and gating system (SA Instruments Inc., Stony Brook, NY). A humidifier was used to moisten the gas mixture before supplying it to the animal, thus preventing impairment of air passages.

PET/MR imaging. For imaging experiments animals were divided into two groups. In the first group (n=4), mice were scanned in prone position on a dual animal bed. In the second group (n=2) mice underwent a sequential PET/MRI scan on two stand-alone scanners. MRI was performed using a Bruker ICON 1T system (Bruker BioSpin, Ettlingen, Germany) and the animal holder mounted with the mouse body bed and mouse whole body RF coil. The whole body coil covers an axial field of view (FOV) of around 8 cm which is very similar to the PET axial FOV (7.6 cm). Images were acquired using a T1-weighted gradient echo sequence (FLASH-nav-3D) with the following parameters: field of view 76x28x24 mm, matrix 253x93x32, resolution 0.3x0.3x0.75 mm, repetition time 25 ms, echo time 4.7 ms, flip angle 25 deg., 5 repetitions, total scan time 6 min 15 sec. For the PET scan, a catheter, placed into a lateral tail vein, was used for i.v. administration of [^{18}F]-**1**. At the beginning of tracer administration (4.9±1.4 MB in 100 µL), dynamic PET imaging was initiated for 120 min using a µPET Focus220 scanner (Siemens Medical Solutions, Knoxville, TN, USA). Prior to the PET scan, a transmission scan using a ^{57}Co point source was recorded over 10 min. At the end of the scan the animals were sacrificed, organ samples and blood were extracted, weighted and counted for activity in a 1-detector Wallac gamma counter (Perkin Elmer Instruments, Wellesley, USA), which had been cross-calibrated with the PET camera. Organ activity data and blood were corrected for radioactive decay and normalized to injected dose per gram body weight and expressed as standardized uptake value (SUV = (radioactivity per mL/injected radioactivity) x body weight). PET data from the 120-min dynamic scans were sorted into three-dimensional sinograms according to the following frame sequence: 8×5 s, 2×10 s, 2×30 s, 3×60 s, 2×150 s, 2×300 s, 4×600 s and 3x1200 s. PET images were reconstructed by Fourier rebinning followed by 2-dimensional filtered back projection with a ramp filter resulting in a voxel size of 0.4x0.4x0.8 mm³. The standard data correction protocol (normalization, attenuation and decay correction) was applied to the data. For the PET/MRI group, images were aligned using a fixed transformation matrix. Different volumes of interest (brain, liver, muscle, kidneys, urinary bladder, and heart) were manually outlined on multiple planes using the image analysis software Amide[6] and time-activity curves (TACs), expressed as SUV, were calculated.

Analysis of murine plasma metabolites – In vivo stability of [^{18}F]-1. Direct after imaging experiments (120 min) murine plasma was obtained by centrifugation and proteins were precipitated with acetonitrile and removed by centrifugation. Supernatant solution was spotted on SiO_2 TLC plates and developed using DCM as mobile phase. [^{18}F]-**1** was spotted as reference. After development radioactivity was quantified using a Hewlett Packard Cyclone Phosphor Imager autoradiography system (Figure S3).

a)

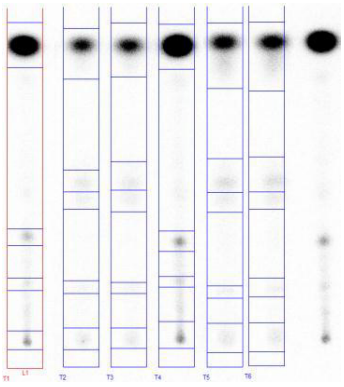

b)

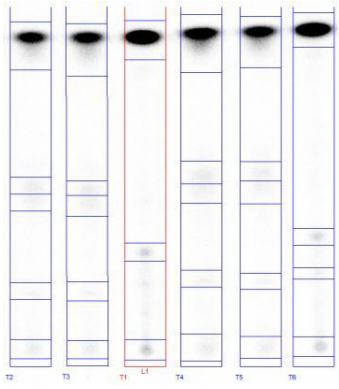

c)

In vivo stability of [^{18}F]-**1**	**#41**	**#42**	**#43**	**#44**
Unchanged [^{18}F]-**1** in plasma [%]	82.0	82.2	88.7	89.8

Figure S3. In vivo stability of [^{18}F]-**1** as determined by TLC radiochromatography of murine plasma after imaging experiments**:** a) Lane 1: Reference [^{18}F]-**1**; Lane 2 & Lane 3: Plasma metabolites mouse #41; Lane 4: Reference [^{18}F]-**1**; Lane 5 & Lane 6: Plasma metabolites mouse #42; Lane 7: Reference [^{18}F]-**1**. b) Lane 1 & Lane 2: Plasma metabolites mouse #43; Lane 3: Reference [^{18}F]-**1**; Lane 4 & Lane 5: Plasma metabolites mouse #44; Lane 6: Reference [^{18}F]-**1**. c) Results after quantification.

In vivo click reaction. For in vivo click experiments a third group of female BALB/c mice (n=4) was used. A lateral tail vein was used for i.v. administration of [^{18}F]-**1** (2.5 ± 0.5 MBq, 100 µl). After 20 min uptake time three mice received water-soluble s-TCO derivative **5** i.v. (10.5 mg/kg, 2.1 mg/mL in 0.9% NaCl). A control mouse received 0.9% NaCl instead. Retroorbital blood was collected 5, 15 (+ control) and 30 min after administration of **5**. 200 µl of blood were quenched immediately after blood retrieval with 107 µg of tetrazine **2** in 214 µl water (saturated solution). Murine plasma was obtained by centrifugation and proteins were precipitated with acetonitrile and removed by centrifugation. Supernatant solution was spotted on SiO_2 TLC plates and developed using 5% MeOH and 1% triethylamine in DCM as mobile phase (Figure S4).

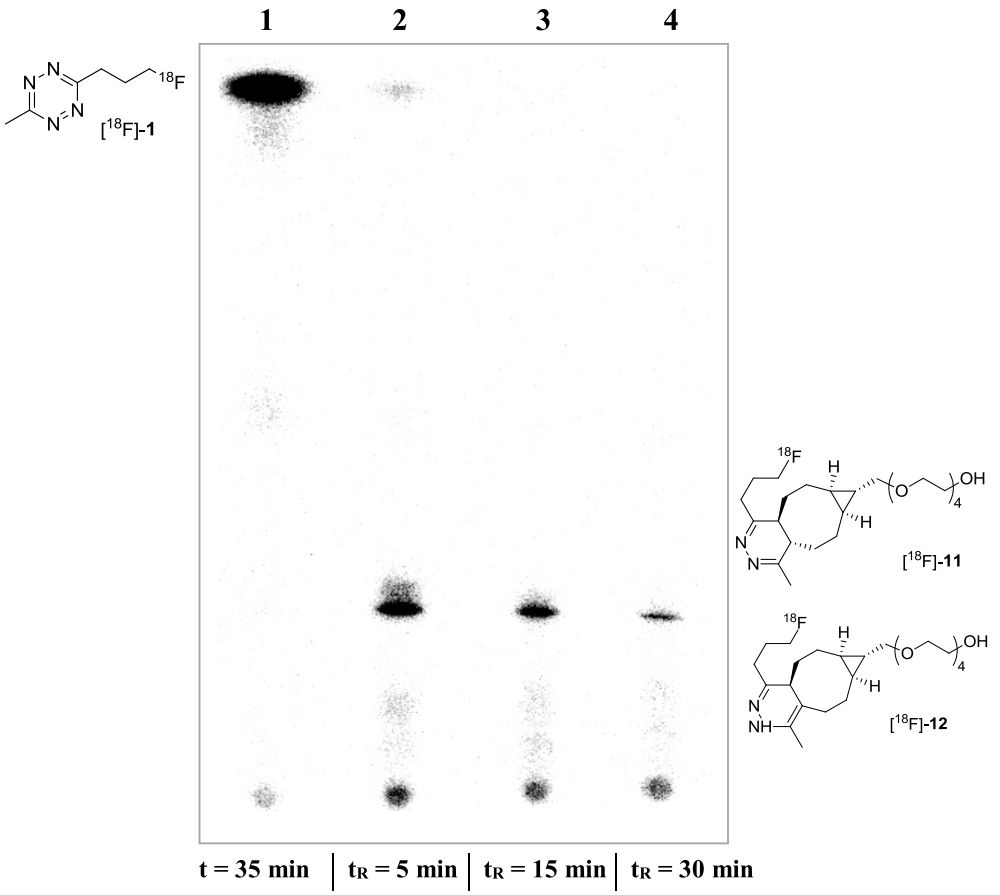

Figure S4. Radio-TLC after in vivo reaction of [^{18}F]-**1** and **5**. Lane 1: control, 35 min biodistribution of [^{18}F]-**1**. Lane 2: 5 min reaction time. Lane 3: 15 min reaction time. Lane 4: 30 min reaction time. For lanes 2-4, [^{18}F]-**1** was administered 20 min prior to **5** ($t = t_R + 20$ min).

5. NMR Spectra

^{1}H spectrum of compound **6**

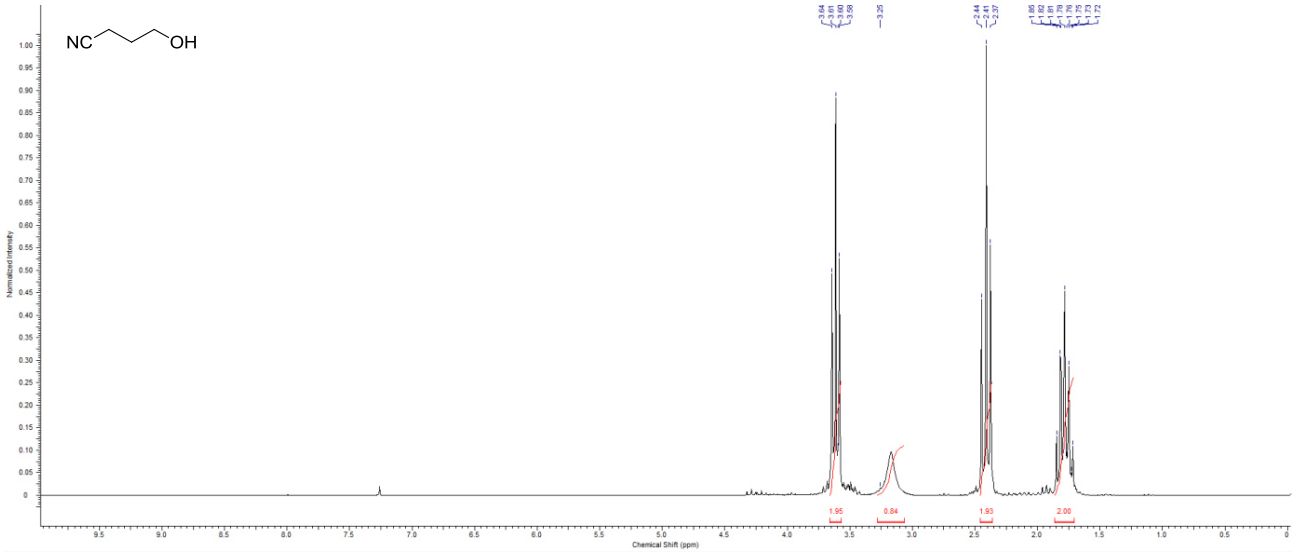

^{13}C spectrum of compound **6**

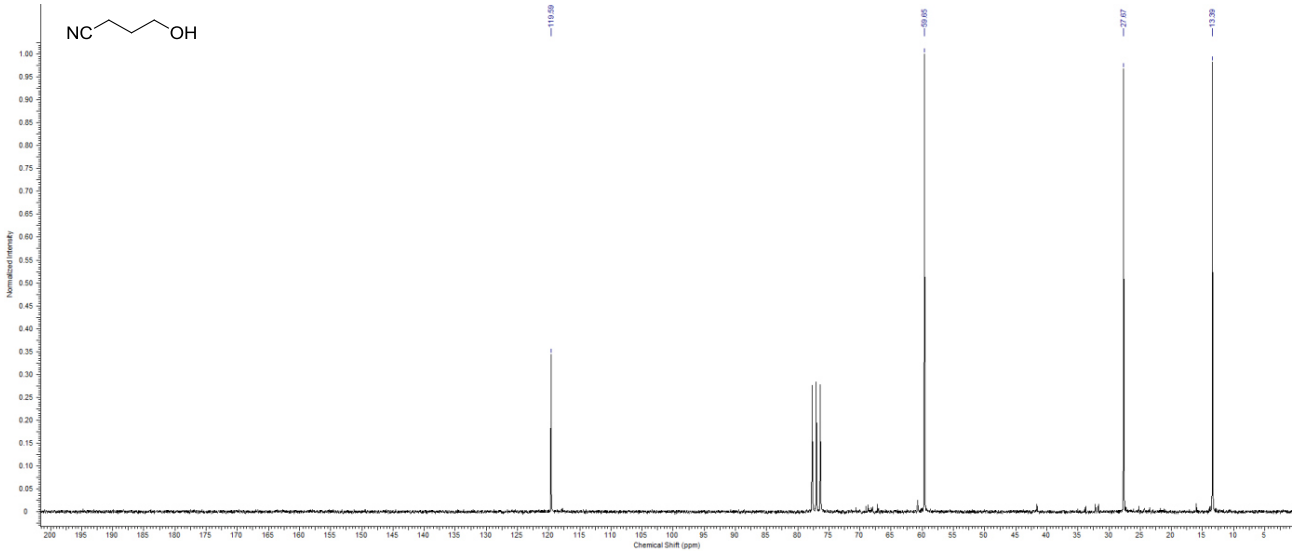

^{1}H spectrum of compound **7**

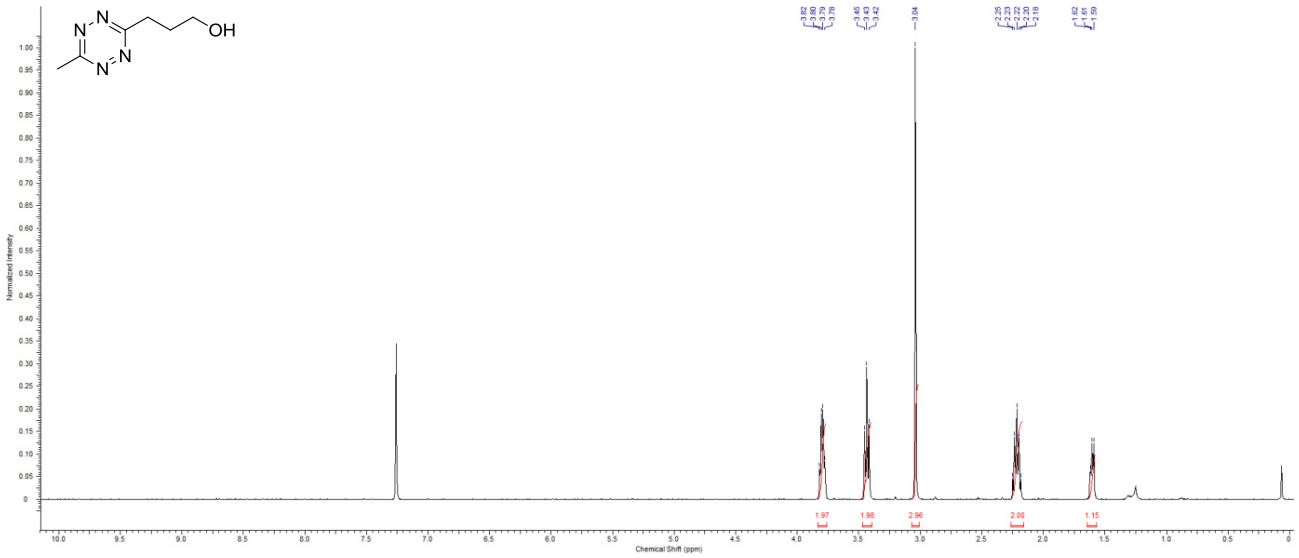

^{13}C spectrum of compound **7**

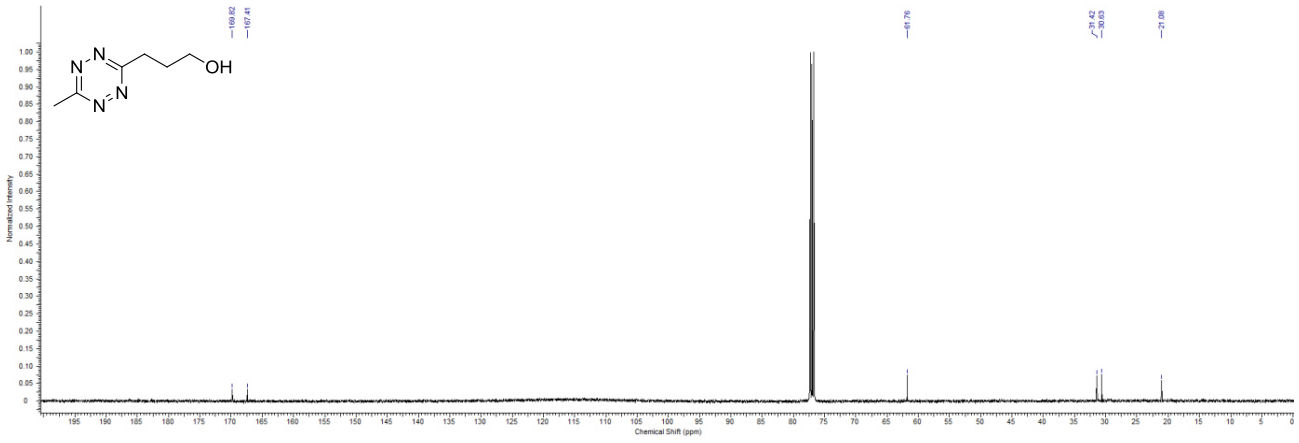

^{1}H spectum of compound **8**

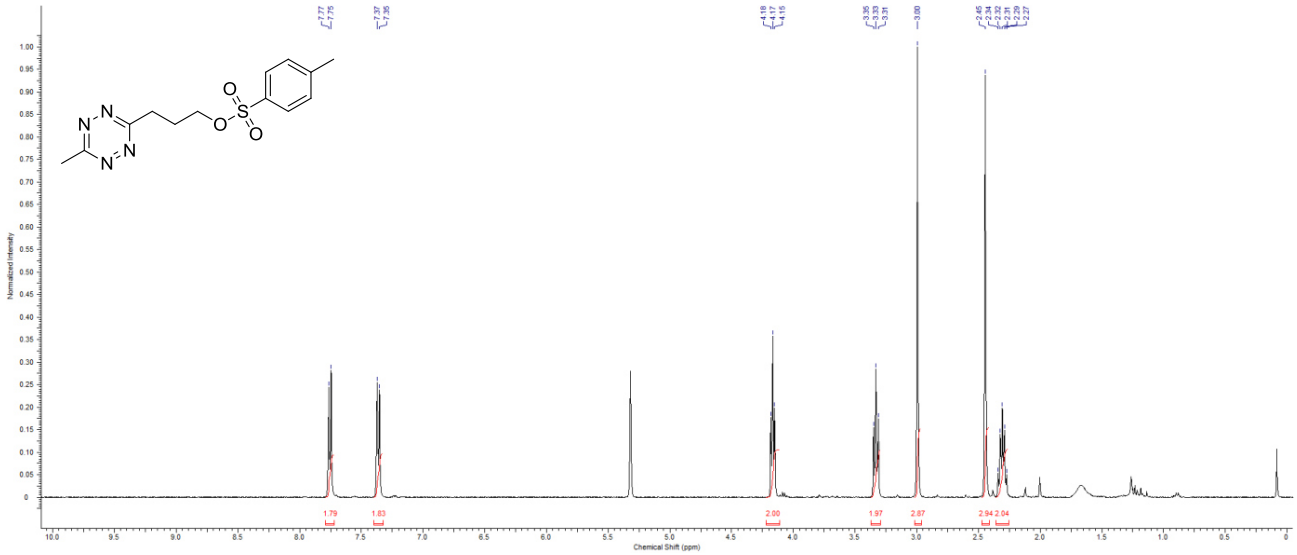

^{13}C spectum of compound **8**

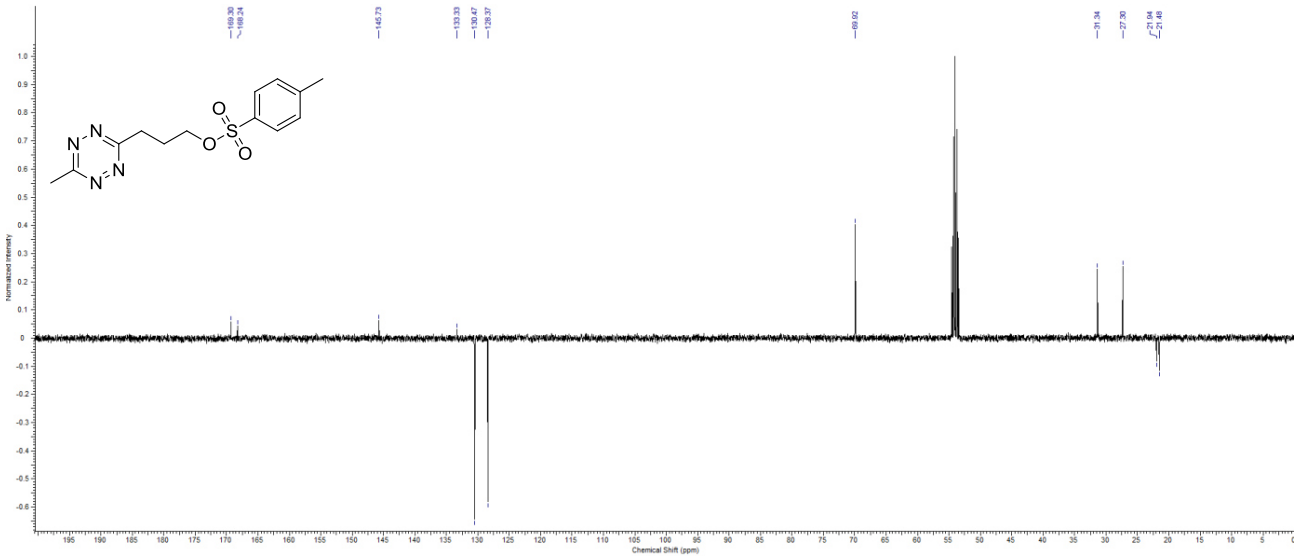

^{1}H spectrum of compound **1**

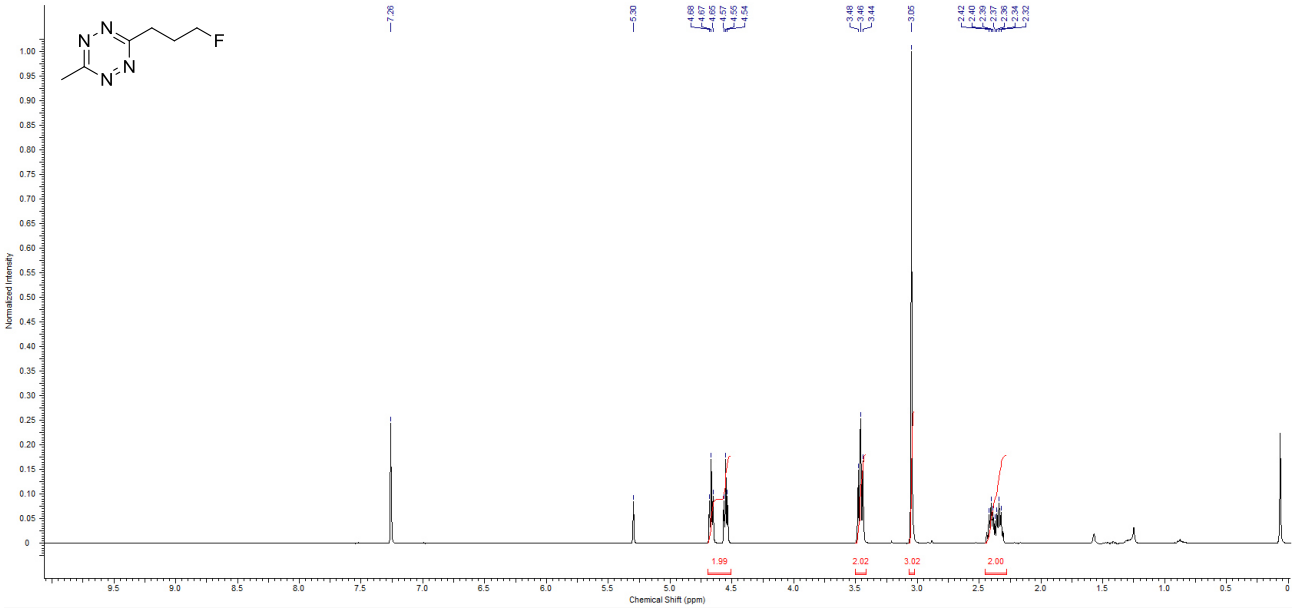

^{13}C spectrum of compound **1**

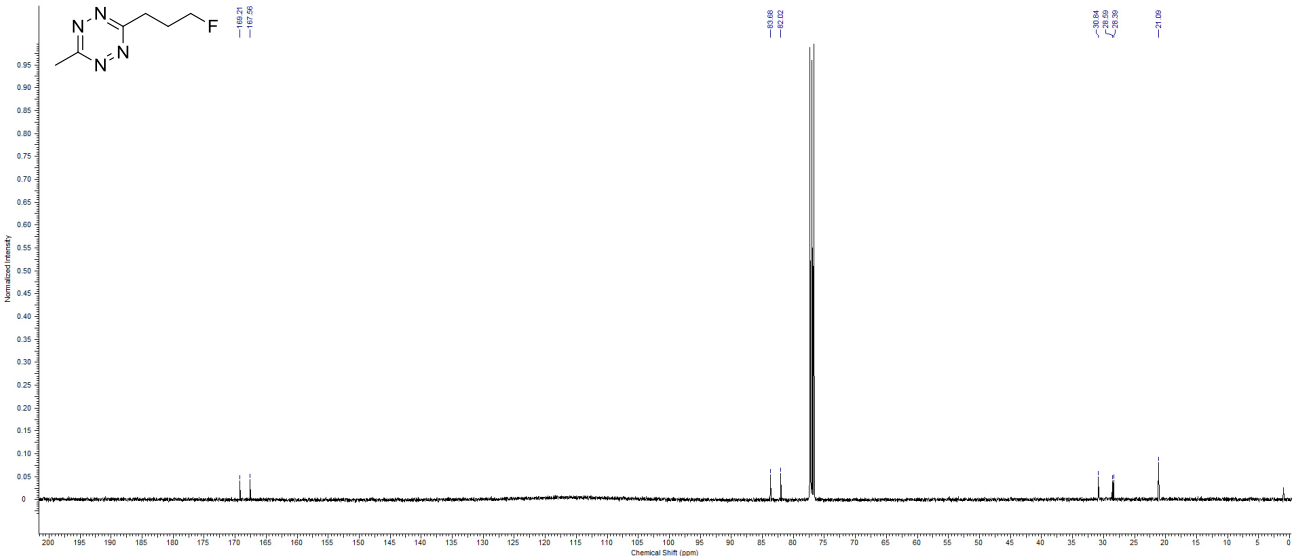

^{1}H spectrum of compound **12**

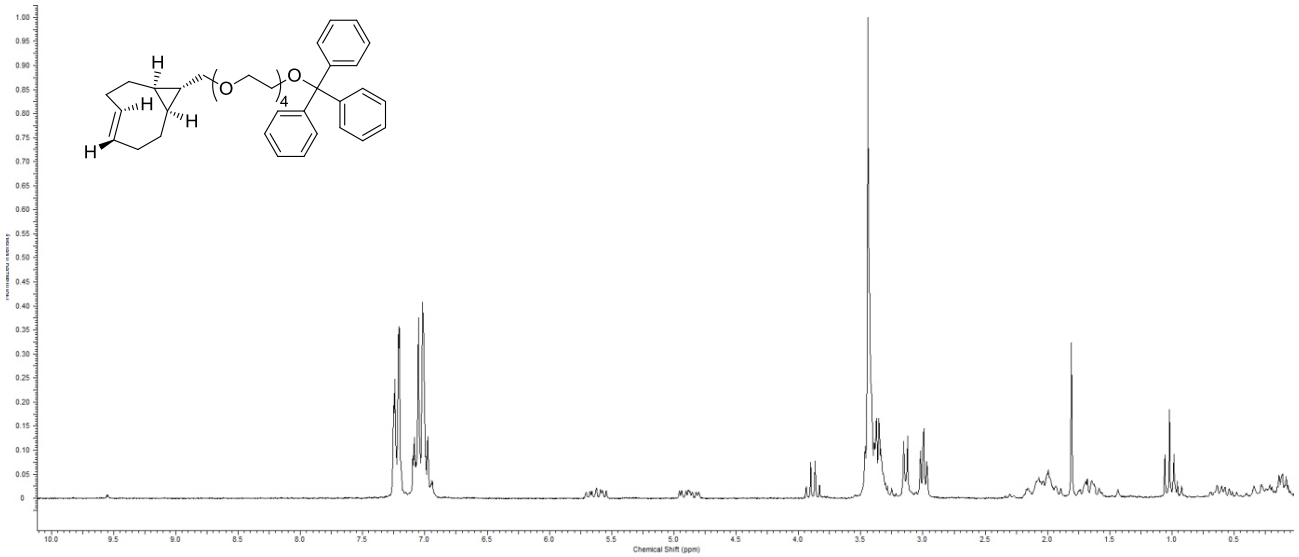

^{13}C spectrum of compound **12**

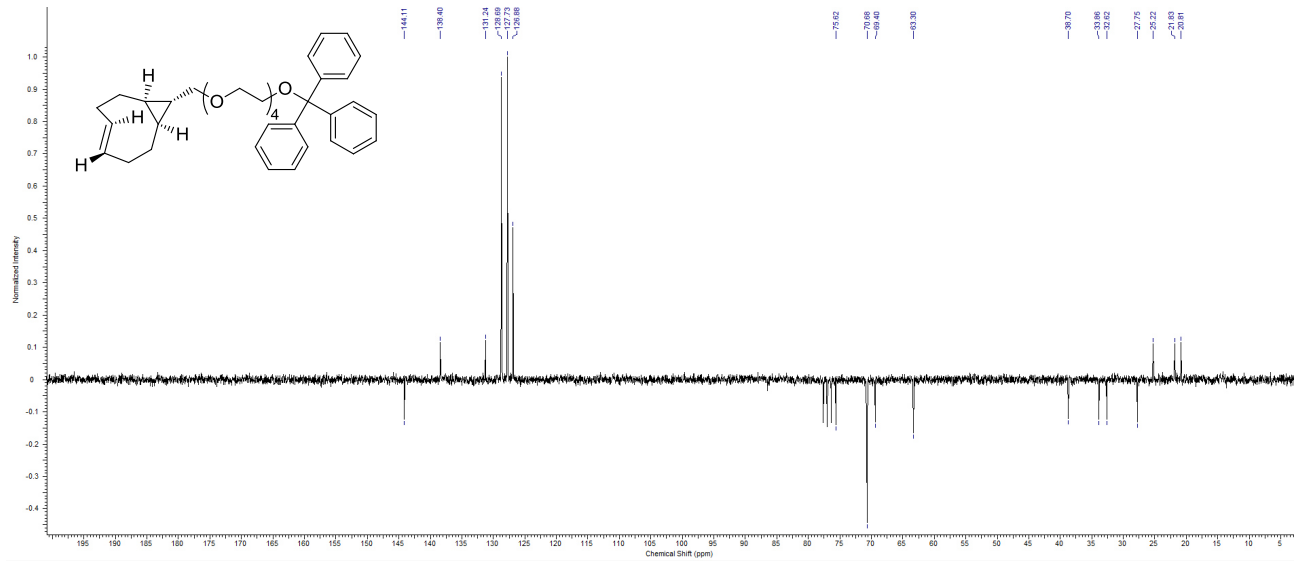

^{1}H spectrum of compound **5**

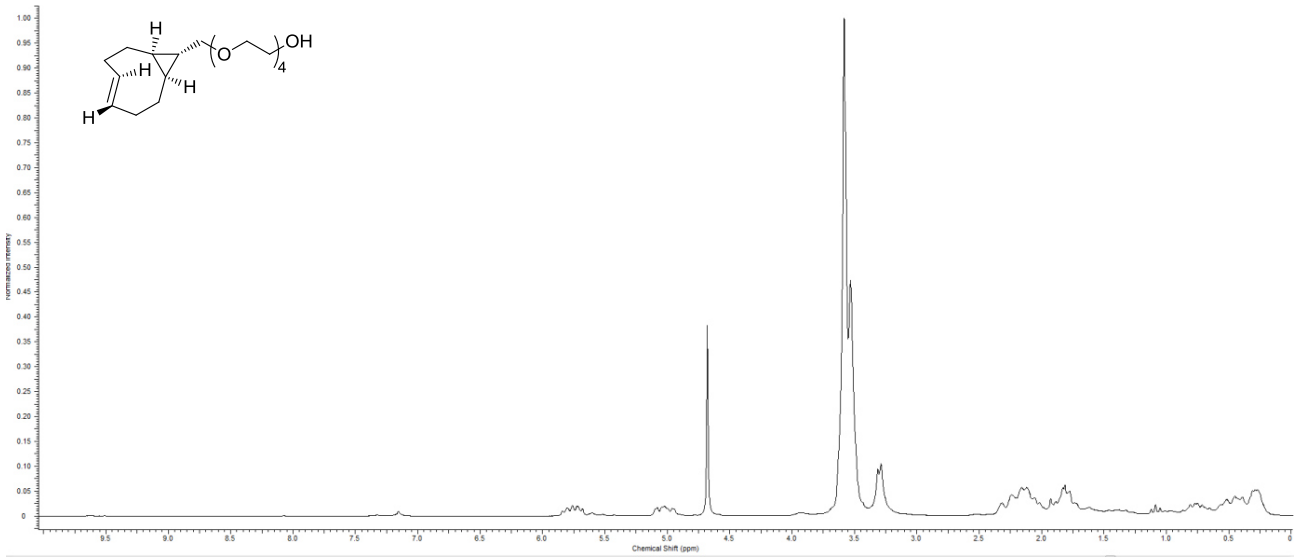

^{13}C spectrum of compound **5**

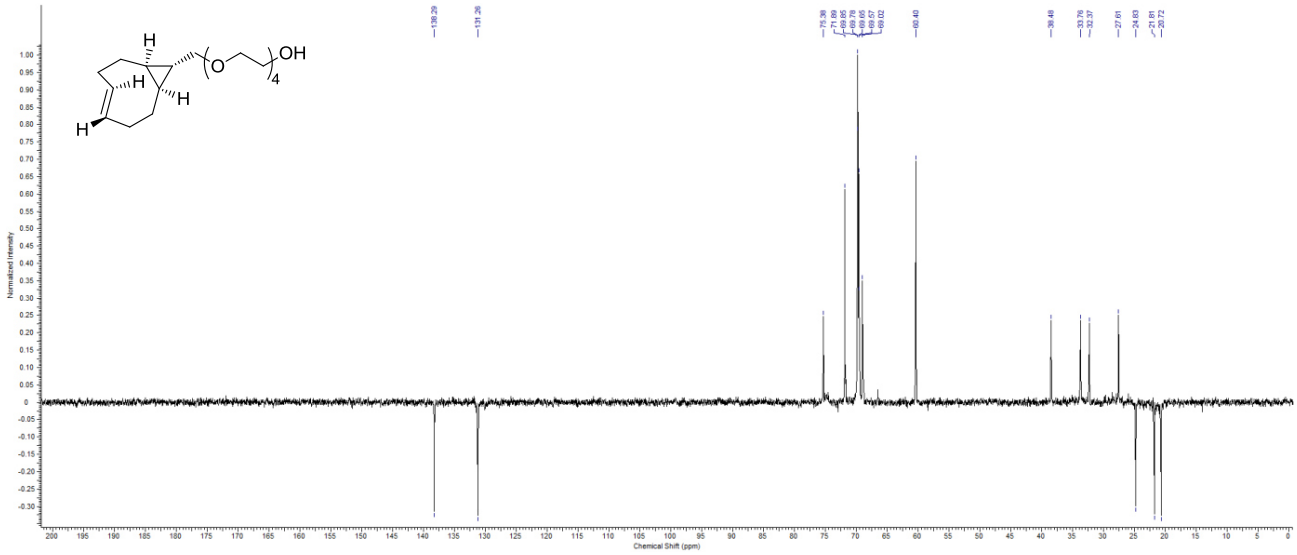

6. Quantum Chemical Calculations

All DFT calculations were performed using the Gaussian 09 (Rev. A.1) program package.[7] Geometry optimizations to energy minima or transition states as well as subsequent frequency analyses at 298.15 K of all considered compounds and intermediates were achieved with 6-31G(d,p)[8] basis set using the M06-2X density functional[9] as implemented in Gaussian 09, which has been found to give relatively accurate energy profiles for cycloadditions.[10] For calculations in water and 1,4-dioxane the polarizable continuum model (PCM)[11] using the CPCM polarizable conductor calculation model[12] with UFFI radii was applied. Imaginary frequencies corresponding to the desired reaction coordinates were obtained only in the case of transition state calculations. Data analysis was done using GaussView 5 (Gaussian, Inc.).

Full energy profiles for reactions of tetrazine **1** and **2** with TCO **3** are shown in Figure S5. $\Delta G^{\ddagger}$ for the first step (inverse electron demand Diels Alder) are 18.73 and 15.26 kcal/mol, respectively, whereas $\Delta G^{\ddagger}$ values for the second step (retro Diels Alder) are 10.57 and 12.97 kcal/mol, showing that the first step is rate determining. Therefore, $\Delta G^{\ddagger}$ values of the first step were considered to determine reaction activation barriers (see Manuscript) at 298.15 K. Optimized geometries of all starting materials and the transition states of the IEDDA cycloaddition are shown in Figure S6 and original data is summarized in Table S4 followed by listing of Cartesian coordinates of all relevant structures.

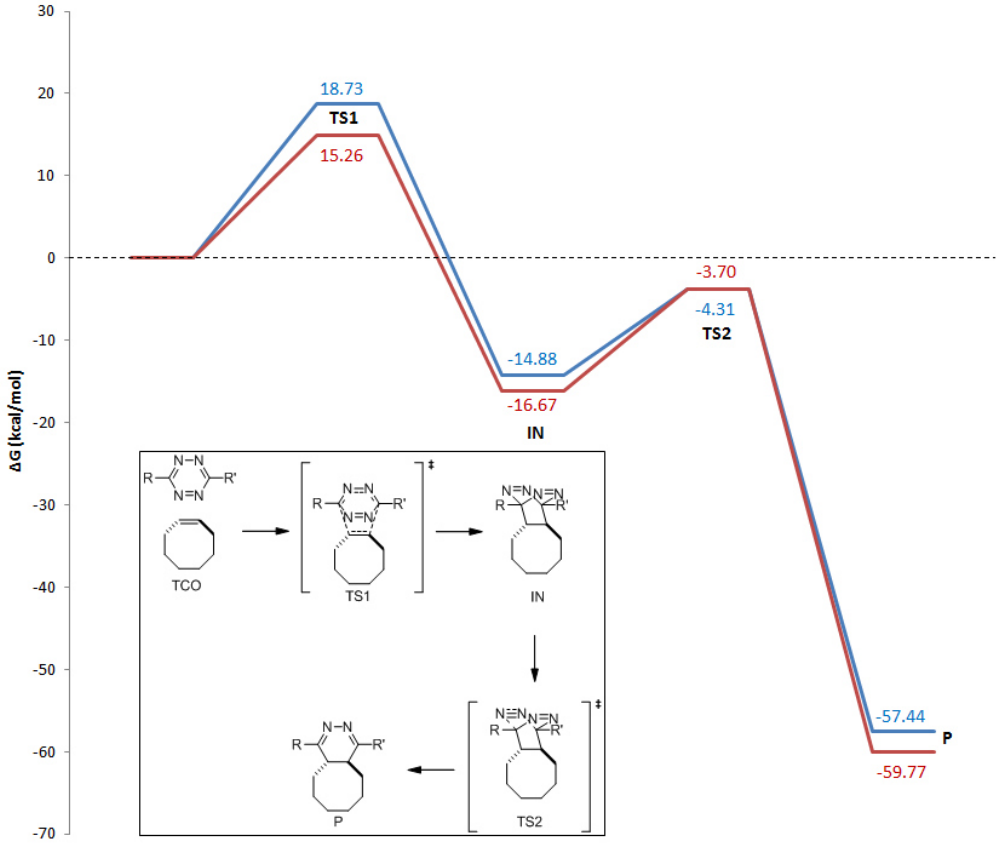

Figure S5. M06-2X/6-31G(d,p) calculated Gibbs free energies of IEDDA initiated ligations of tetrazine **1** (blue) and tetrazine **2** (red) with TCO **3** in gas phase relative to the Gibbs free energies of the starting materials.

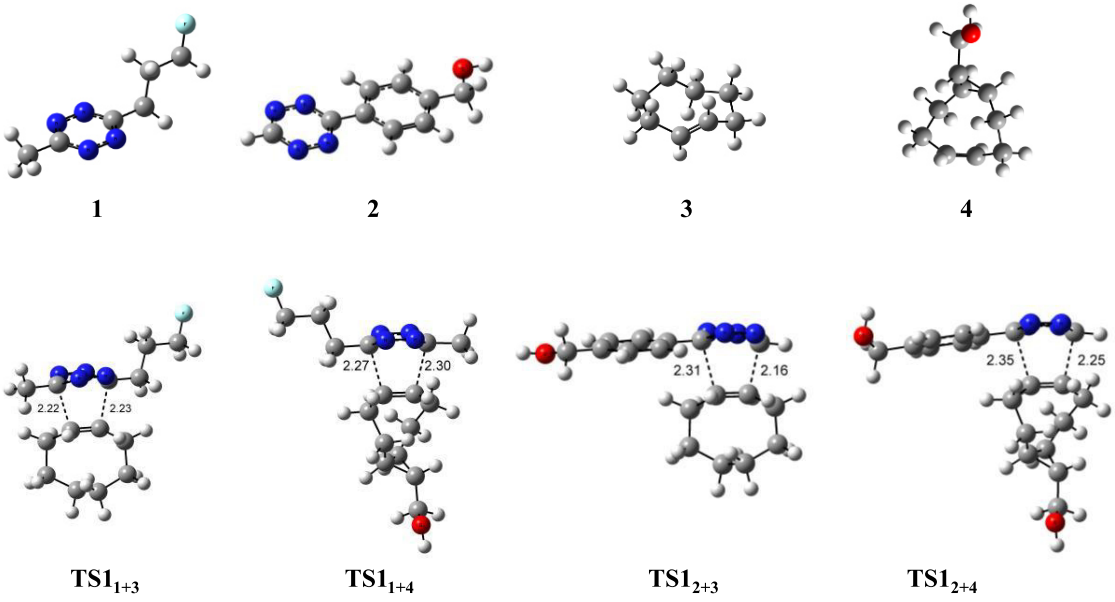

Figure S6. Optimized geometries (M06-2X/6-31G(d,p), gas phase) of tetrazines (**1** and **2**), dienophiles (**3** and **4**) and corresponding transition states of IEDDA cycloaddition.

Table S4. Selected original data from Gaussian calculations (E: total electronic energy, ZPE: zero point energy).

Compound	Calculated in	E (hartree)	H (hartree)[a]	G (hartree)[a]	S (J/(mol*K))[a]	ZPE (hartree)[a]
1	gas phase	-552.60350	-552.43287	-552.48402	107.653	-552.44466
	1,4-dioxane	-552.60855	-552.43803	-552.48962	108.567	-552.44987
	water	-552.61306	-552.44261	-552.49426	108.701	-552.45444
2	gas phase	-641.66272	-641.48295	-641.53351	106.395	-641.49515
	1,4-dioxane	-641.66881	-641.48914	-641.53993	106.903	-641.50137
3	gas phase	-313.10240	-312.88840	-312.92808	83.507	-313.06245
	1,4-dioxane	-313.10306	-312.88924	-312.92893	83.531	-312.89773
4	gas phase	-465.62872	-465.37225	-465.42029	101.107	-465.38401
	water	-465.63523	-465.37910	-465.42711	101.038	-465.39087
	1,4-dioxane	-465.63215	-465.37586	-465.42388	101.059	-465.38762
TS1$_{1+3}$	gas phase	-865.70338	-865.31706	-865.38225	137.190	-865.33618
	1,4-dioxane	-865.70950	-865.32337	-865.38860	137.297	-865.34251
TS1$_{1+4}$	gas phase	-1018.23454	-1017.80590	-1017.88035	156.698	-1017.82842
	water	-1018.25100	-1017.82280	-1017.89724	156.667	-1017.84538
	1,4-dioxane	-1018.24310	-1017.81469	-1017.88909	156.598	-1017.83722
TS1$_{2+3}$	gas phase	-954.76435	-954.36931	-954.43726	143.019	-954.38933
	1,4-dioxane	-954.77176	-954.37691	-954.44502	143.347	-954.39697
TS1$_{2+4}$	gas phase	-1107.29658	-1106.85907	-1106.93554	160.953	-1106.88228
	1,4-dioxane	-1107.30608	-1106.86886	-1106.94542	161.134	-1106.89221

[a] calculated for T = 298.15 K

Cartesian coordinates

TCO **3**, gas phase

C	-0.5319740	-1.3578980	-0.4009380
C	0.5319750	-1.3579000	0.4009390
C	1.8698840	-0.9014570	-0.0815100
C	-1.8698850	-0.9014570	0.0815090
C	1.8818250	0.6352820	0.1353760
C	-1.8818250	0.6352830	-0.1353780
C	-0.6505410	1.3762610	0.4300970
C	0.6505410	1.3762620	-0.4300940
H	-0.3725530	-1.3346870	-1.4809250
H	0.3725550	-1.3346940	1.4809260
H	2.7154270	-1.3581900	0.4428170
H	1.9792520	-1.1137950	-1.1515330
H	-2.7154260	-1.3581900	-0.4428210
H	-1.9792550	-1.1137960	1.1515320
H	2.7903930	1.0481690	-0.3184690
H	1.9561630	0.8413180	1.2111750
H	-2.7903940	1.0481700	0.3184640
H	-1.9561580	0.8413170	-1.2111770
H	-0.9508090	2.4184330	0.5838000
H	-0.4299190	0.9856240	1.4317690
H	0.9508100	2.4184350	-0.5837940
H	0.4299180	0.9856290	-1.4317680

1,4-dioxane

C	0.5323020	-1.3580770	0.4009860
H	0.3731520	-1.3329450	1.4810650
C	-0.5323020	-1.3580780	-0.4009850
H	-0.3731520	-1.3329490	-1.4810640
C	-1.8700870	-0.9014460	0.0821540
H	-2.7157920	-1.3572480	-0.4428260
H	-1.9796150	-1.1124530	1.1524500
C	1.8700870	-0.9014460	-0.0821530
H	2.7157920	-1.3572480	0.4428280
H	1.9796150	-1.1124540	-1.1524480
C	-1.8814500	0.6353650	-0.1357310
H	-2.7902340	1.0477190	0.3181550
H	-1.9549930	0.8401980	-1.2117080
C	1.8814500	0.6353650	0.1357300
H	2.7902340	1.0477180	-0.3181560
H	1.9549930	0.8401990	1.2117080
C	0.6504440	1.3761190	-0.4302620
H	0.9507390	2.4183430	-0.5839040
H	0.4298420	0.9846280	-1.4315770
C	-0.6504440	1.3761190	0.4302600
H	-0.9507380	2.4183440	0.5839000
H	-0.4298420	0.9846310	1.4315760

sTCO **4**, gas phase			
C	1.2755100	-0.3310120	-0.1709970
C	0.2659260	-0.8284380	0.8168240
C	0.4891150	0.6835330	0.6218020
H	0.9721390	-0.3839270	-1.2169120
H	0.7416980	-1.1163880	1.7558430
H	1.0385810	1.0798220	1.4747650
C	-0.8650550	-1.8337730	0.5538230
H	-0.3999340	-2.8281040	0.5391790
H	-1.5106670	-1.8316780	1.4399200
C	-0.2857170	1.7901490	-0.1133580
H	0.2553440	2.7283780	0.0570810
H	-0.2249230	1.5928800	-1.1876220
C	-1.7936530	1.9551820	0.2110670
H	-2.2549200	2.5855490	-0.5568590
H	-1.9508760	2.4394620	1.1787310
C	-1.7502900	-1.6841250	-0.6965960
H	-2.5827830	-2.3958410	-0.6322980
H	-1.1800230	-1.9680350	-1.5881460
C	-2.1725750	-0.2449530	-0.8521330
H	-2.0534880	0.2100540	-1.8359750
C	-2.3006220	0.5438130	0.2128880
H	-2.3733300	0.0810150	1.1948480
C	2.7472580	-0.5225660	0.0520950
H	3.0674580	-1.4993510	-0.3423980
H	2.9417800	-0.5252020	1.1372570
O	3.4343200	0.5363470	-0.5896650
H	4.3800140	0.3737200	-0.5125840

water			
C	1.2770130	-0.3265590	-0.1720290
C	0.2680210	-0.8247750	0.8160720
C	0.4864140	0.6874680	0.6195330
H	0.9722290	-0.3837460	-1.2176030
H	0.7447390	-1.1101530	1.7552390
H	1.0328670	1.0865230	1.4732960
C	-0.8601740	-1.8335720	0.5541170
H	-0.3917860	-2.8262590	0.5393730
H	-1.5048600	-1.8330520	1.4407810
C	-0.2932010	1.7898180	-0.1172500
H	0.2439700	2.7310870	0.0501380
H	-0.2364350	1.5894420	-1.1912880
C	-1.8006710	1.9520890	0.2109920
H	-2.2638580	2.5816850	-0.5564210
H	-1.9559990	2.4358120	1.1791860
C	-1.7466680	-1.6875490	-0.6957810
H	-2.5758050	-2.4030560	-0.6303840
H	-1.1765290	-1.9681460	-1.5883120
C	-2.1744370	-0.2496800	-0.8509040
H	-2.0549100	0.2059810	-1.8345130
C	-2.3045460	0.5392050	0.2143880
H	-2.3752270	0.0765400	1.1966890
C	2.7484190	-0.5193130	0.0540280
H	3.0693380	-1.4956820	-0.3387980
H	2.9425990	-0.5195260	1.1384900
O	3.4426510	0.5377180	-0.5885190
H	4.3874320	0.3680210	-0.5067180

1,4-dioxane			
C	1.2770130	-0.3265590	-0.1720290
C	0.2680210	-0.8247750	0.8160720
C	0.4864140	0.6874680	0.6195330
H	0.9722290	-0.3837460	-1.2176030
H	0.7447390	-1.1101530	1.7552390
H	1.0328670	1.0865230	1.4732960
C	-0.8601740	-1.8335720	0.5541170
H	-0.3917860	-2.8262590	0.5393730
H	-1.5048600	-1.8330520	1.4407810
C	-0.2932010	1.7898180	-0.1172500
H	0.2439700	2.7310870	0.0501380
H	-0.2364350	1.5894420	-1.1912880
C	-1.8006710	1.9520890	0.2109920
H	-2.2638580	2.5816850	-0.5564210
H	-1.9559990	2.4358120	1.1791860
C	-1.7466680	-1.6875490	-0.6957810
H	-2.5758050	-2.4030560	-0.6303840
H	-1.1765290	-1.9681460	-1.5883120
C	-2.1744370	-0.2496800	-0.8509040
H	-2.0549100	0.2059810	-1.8345130
C	-2.3045460	0.5392050	0.2143880
H	-2.3752270	0.0765400	1.1966890
C	2.7484190	-0.5193130	0.0540280
H	3.0693380	-1.4956820	-0.3387980
H	2.9425990	-0.5195260	1.1384900
O	3.4426510	0.5377180	-0.5885190
H	4.3874320	0.3680210	-0.5067180

Tetrazine **1**, gas phase				water				1,4-dioxane			
C	-0.2218010	0.2202470	0.5196200	C	-0.2175960	0.2050270	0.5324700	C	-0.2196930	0.2021440	0.5314190
C	-2.6616510	-0.0851050	-0.1948560	C	-2.6654050	-0.0777140	-0.2007890	C	-2.6630720	-0.0767910	-0.2001400
N	-2.1241970	1.1334720	-0.3132390	N	-2.1157620	1.1374130	-0.2970420	N	-2.1158670	1.1396240	-0.2928810
N	-0.8718500	1.2893830	0.0527440	N	-0.8645540	1.2810680	0.0770220	N	-0.8643610	1.2816100	0.0810250
N	-2.0039090	-1.1607990	0.2689710	N	-2.0111860	-1.1599430	0.2536850	N	-2.0111710	-1.1624920	0.2489620
N	-0.7583680	-1.0051090	0.6323500	N	-0.7670920	-1.0165020	0.6253160	N	-0.7666270	-1.0206660	0.6204010
C	-4.0886550	-0.2712960	-0.6004390	C	-4.0898660	-0.2519410	-0.6154680	C	-4.0885450	-0.2485560	-0.6149810
C	1.2176940	0.3798450	0.8992620	C	1.2213480	0.3504740	0.9166490	C	1.2196030	0.3462860	0.9162920
H	1.3975720	1.4338550	1.1285890	H	1.4068260	1.3950770	1.1799150	H	1.4031890	1.3905540	1.1833780
H	1.4090020	-0.2149460	1.7980990	H	1.4140930	-0.2708270	1.7962880	H	1.4113740	-0.2798420	1.7930620
H	-4.1636400	-1.0525930	-1.3599240	H	-4.1649780	-1.0262780	-1.3818150	H	-4.1648030	-1.0205860	-1.3836180
H	-4.4843590	0.6648190	-0.9920550	H	-4.4804150	0.6873760	-1.0041140	H	-4.4772710	0.6934550	-0.9992500
H	-4.6827140	-0.5890150	0.2598080	H	-4.6906110	-0.5683360	0.2405020	H	-4.6893110	-0.5692840	0.2394400
C	2.1339320	-0.0849100	-0.2390180	C	2.1336080	-0.0789300	-0.2396530	C	2.1334480	-0.0781030	-0.2402790
H	1.9261720	-1.1338640	-0.4744280	H	1.9254090	-1.1202190	-0.5071290	H	1.9257910	-1.1183190	-0.5119450
H	1.9351460	0.5036500	-1.1410250	H	1.9319500	0.5386240	-1.1212900	H	1.9323830	0.5424250	-1.1199500
C	3.5946640	0.0616980	0.1358880	C	3.5935370	0.0563490	0.1392360	C	3.5938370	0.0559830	0.1382650
H	3.8339790	-0.5405850	1.0206790	H	3.8395050	-0.5769850	0.9982800	H	3.8379110	-0.5791590	0.9974300
H	3.8404980	1.1087920	0.3507380	H	3.8439140	1.0945220	0.3822510	H	3.8423070	1.0940860	0.3866480
F	4.3835020	-0.3668470	-0.9110030	F	4.3811890	-0.3407550	-0.9322690	F	4.3812390	-0.3361830	-0.9301340

Tetrazine **2**, gas phase

C	-1.6804960	-0.0052510	-0.0000110
C	-4.2252090	-0.1713360	0.0000320
N	-3.5389400	-1.3156700	0.0001970
N	-2.2335910	-1.2309670	0.0002000
N	-2.3886010	1.1378490	-0.0001710
N	-3.6943830	1.0521940	-0.0001210
C	-0.2084140	0.0906470	-0.0000540
C	0.4140580	1.3448350	0.0000980
C	1.7970370	1.4276820	0.0001050
H	-0.1956860	2.2408890	0.0002170
C	1.9610940	-0.9755680	-0.0002090
C	2.5824660	0.2713230	-0.0000390
H	2.2763410	2.4038880	0.0002520
H	2.5735990	-1.8691520	-0.0003090
C	0.5739590	-1.0670900	-0.0002080
H	0.0858270	-2.0352430	-0.0003180
H	-5.3067180	-0.2424760	0.0000400
C	4.0853900	0.3990940	0.0000210
H	4.3885880	0.9790720	-0.8853450
H	4.3885140	0.9790920	0.8853990
O	4.6691380	-0.8828650	0.0000410
H	5.6257440	-0.7830050	0.0005940

1,4-dioxane

C	1.6809430	-0.0049220	0.0000100
C	4.2300680	-0.1711840	-0.0000070
N	3.5411520	-1.3139630	0.0000430
N	2.2359220	-1.2295540	0.0000590
N	2.3905590	1.1370760	-0.0000610
N	3.6961240	1.0511270	-0.0000580
C	0.2088690	0.0905410	0.0000060
C	-0.4155820	1.3443200	0.0000410
C	-1.7987760	1.4273650	0.0000400
H	0.1908600	2.2425070	0.0000820
C	-1.9612390	-0.9757820	-0.0000250
C	-2.5847570	0.2705770	0.0000040
H	-2.2780460	2.4032630	0.0000740
H	-2.5706790	-1.8714730	-0.0000390
C	-0.5738240	-1.0672900	-0.0000350
H	-0.0887040	-2.0368520	-0.0000620
H	5.3112830	-0.2420940	0.0000140
C	-4.0875620	0.3989530	0.0000050
H	-4.3908210	0.9789870	0.8844610
H	-4.3908180	0.9790300	-0.8844230
O	-4.6734890	-0.8830590	-0.0000260
H	-5.6303010	-0.7771630	-0.0000110

Cartesian coordinates

TCO **3**, gas phase

C	-0.5319740	-1.3578980	-0.4009380
C	0.5319750	-1.3579000	0.4009390
C	1.8698840	-0.9014570	-0.0815100
C	-1.8698850	-0.9014570	0.0815090
C	1.8818250	0.6352820	0.1353760
C	-1.8818250	0.6352830	-0.1353780
C	-0.6505410	1.3762610	0.4300970
C	0.6505410	1.3762620	-0.4300940
H	-0.3725530	-1.3346870	-1.4809250
H	0.3725550	-1.3346940	1.4809260
H	2.7154270	-1.3581900	0.4428170
H	1.9792520	-1.1137950	-1.1515330
H	-2.7154260	-1.3581900	-0.4428210
H	-1.9792550	-1.1137960	1.1515320
H	2.7903930	1.0481690	-0.3184690
H	1.9561630	0.8413180	1.2111750
H	-2.7903940	1.0481700	0.3184640
H	-1.9561580	0.8413170	-1.2111770
H	-0.9508090	2.4184330	0.5838000
H	-0.4299190	0.9856240	1.4317690
H	0.9508100	2.4184350	-0.5837940
H	0.4299180	0.9856290	-1.4317680

1,4-dioxane

C	0.5323020	-1.3580770	0.4009860
H	0.3731520	-1.3329450	1.4810650
C	-0.5323020	-1.3580780	-0.4009850
H	-0.3731520	-1.3329490	-1.4810640
C	-1.8700870	-0.9014460	0.0821540
H	-2.7157920	-1.3572480	-0.4428260
H	-1.9796150	-1.1124530	1.1524500
C	1.8700870	-0.9014460	-0.0821530
H	2.7157920	-1.3572480	0.4428280
H	1.9796150	-1.1124540	-1.1524480
C	-1.8814500	0.6353650	-0.1357310
H	-2.7902340	1.0477190	0.3181550
H	-1.9549930	0.8401980	-1.2117080
C	1.8814500	0.6353650	0.1357300
H	2.7902340	1.0477180	-0.3181560
H	1.9549930	0.8401990	1.2117080
C	0.6504440	1.3761190	-0.4302620
H	0.9507390	2.4183430	-0.5839040
H	0.4298420	0.9846280	-1.4315770
C	-0.6504440	1.3761190	0.4302600
H	-0.9507380	2.4183440	0.5839000
H	-0.4298420	0.9846310	1.4315760

sTCO **4**, gas phase			
C	1.2755100	-0.3310120	-0.1709970
C	0.2659260	-0.8284380	0.8168240
C	0.4891150	0.6835330	0.6218020
H	0.9721390	-0.3839270	-1.2169120
H	0.7416980	-1.1163880	1.7558430
H	1.0385810	1.0798220	1.4747650
C	-0.8650550	-1.8337730	0.5538230
H	-0.3999340	-2.8281040	0.5391790
H	-1.5106670	-1.8316780	1.4399200
C	-0.2857170	1.7901490	-0.1133580
H	0.2553440	2.7283780	0.0570810
H	-0.2249230	1.5928800	-1.1876220
C	-1.7936530	1.9551820	0.2110670
H	-2.2549200	2.5855490	-0.5568590
H	-1.9508760	2.4394620	1.1787310
C	-1.7502900	-1.6841250	-0.6965960
H	-2.5827830	-2.3958410	-0.6322980
H	-1.1800230	-1.9680350	-1.5881460
C	-2.1725750	-0.2449530	-0.8521330
H	-2.0534880	0.2100540	-1.8359750
C	-2.3006220	0.5438130	0.2128880
H	-2.3733300	0.0810150	1.1948480
C	2.7472580	-0.5225660	0.0520950
H	3.0674580	-1.4993510	-0.3423980
H	2.9417800	-0.5252020	1.1372570
O	3.4343200	0.5363470	-0.5896650
H	4.3800140	0.3737200	-0.5125840

water			
C	1.2770130	-0.3265590	-0.1720290
C	0.2680210	-0.8247750	0.8160720
C	0.4864140	0.6874680	0.6195330
H	0.9722290	-0.3837460	-1.2176030
H	0.7447390	-1.1101530	1.7552390
H	1.0328670	1.0865230	1.4732960
C	-0.8601740	-1.8335720	0.5541170
H	-0.3917860	-2.8262590	0.5393730
H	-1.5048600	-1.8330520	1.4407810
C	-0.2932010	1.7898180	-0.1172500
H	0.2439700	2.7310870	0.0501380
H	-0.2364350	1.5894420	-1.1912880
C	-1.8006710	1.9520890	0.2109920
H	-2.2638580	2.5816850	-0.5564210
H	-1.9559990	2.4358120	1.1791860
C	-1.7466680	-1.6875490	-0.6957810
H	-2.5758050	-2.4030560	-0.6303840
H	-1.1765290	-1.9681460	-1.5883120
C	-2.1744370	-0.2496800	-0.8509040
H	-2.0549100	0.2059810	-1.8345130
C	-2.3045460	0.5392050	0.2143880
H	-2.3752270	0.0765400	1.1966890
C	2.7484190	-0.5193130	0.0540280
H	3.0693380	-1.4956820	-0.3387980
H	2.9425990	-0.5195260	1.1384900
O	3.4426510	0.5377180	-0.5885190
H	4.3874320	0.3680210	-0.5067180

1,4-dioxane			
C	1.2770130	-0.3265590	-0.1720290
C	0.2680210	-0.8247750	0.8160720
C	0.4864140	0.6874680	0.6195330
H	0.9722290	-0.3837460	-1.2176030
H	0.7447390	-1.1101530	1.7552390
H	1.0328670	1.0865230	1.4732960
C	-0.8601740	-1.8335720	0.5541170
H	-0.3917860	-2.8262590	0.5393730
H	-1.5048600	-1.8330520	1.4407810
C	-0.2932010	1.7898180	-0.1172500
H	0.2439700	2.7310870	0.0501380
H	-0.2364350	1.5894420	-1.1912880
C	-1.8006710	1.9520890	0.2109920
H	-2.2638580	2.5816850	-0.5564210
H	-1.9559990	2.4358120	1.1791860
C	-1.7466680	-1.6875490	-0.6957810
H	-2.5758050	-2.4030560	-0.6303840
H	-1.1765290	-1.9681460	-1.5883120
C	-2.1744370	-0.2496800	-0.8509040
H	-2.0549100	0.2059810	-1.8345130
C	-2.3045460	0.5392050	0.2143880
H	-2.3752270	0.0765400	1.1966890
C	2.7484190	-0.5193130	0.0540280
H	3.0693380	-1.4956820	-0.3387980
H	2.9425990	-0.5195260	1.1384900
O	3.4426510	0.5377180	-0.5885190
H	4.3874320	0.3680210	-0.5067180

Tetrazine **1**, gas phase				water				1,4-dioxane			
C	-0.2218010	0.2202470	0.5196200	C	-0.2175960	0.2050270	0.5324700	C	-0.2196930	0.2021440	0.5314190
C	-2.6616510	-0.0851050	-0.1948560	C	-2.6654050	-0.0777140	-0.2007890	C	-2.6630720	-0.0767910	-0.2001400
N	-2.1241970	1.1334720	-0.3132390	N	-2.1157620	1.1374130	-0.2970420	N	-2.1158670	1.1396240	-0.2928810
N	-0.8718500	1.2893830	0.0527440	N	-0.8645540	1.2810680	0.0770220	N	-0.8643610	1.2816100	0.0810250
N	-2.0039090	-1.1607990	0.2689710	N	-2.0111860	-1.1599430	0.2536850	N	-2.0111710	-1.1624920	0.2489620
N	-0.7583680	-1.0051090	0.6323500	N	-0.7670920	-1.0165020	0.6253160	N	-0.7666270	-1.0206660	0.6204010
C	-4.0886550	-0.2712960	-0.6004390	C	-4.0898660	-0.2519410	-0.6154680	C	-4.0885450	-0.2485560	-0.6149810
C	1.2176940	0.3798450	0.8992620	C	1.2213480	0.3504740	0.9166490	C	1.2196030	0.3462860	0.9162920
H	1.3975720	1.4338550	1.1285890	H	1.4068260	1.3950770	1.1799150	H	1.4031890	1.3905540	1.1833780
H	1.4090020	-0.2149460	1.7980990	H	1.4140930	-0.2708270	1.7962880	H	1.4113740	-0.2798420	1.7930620
H	-4.1636400	-1.0525930	-1.3599240	H	-4.1649780	-1.0262780	-1.3818150	H	-4.1648030	-1.0205860	-1.3836180
H	-4.4843590	0.6648190	-0.9920550	H	-4.4804150	0.6873760	-1.0041140	H	-4.4772710	0.6934550	-0.9992500
H	-4.6827140	-0.5890150	0.2598080	H	-4.6906110	-0.5683360	0.2405020	H	-4.6893110	-0.5692840	0.2394400
C	2.1339320	-0.0849100	-0.2390180	C	2.1336080	-0.0789300	-0.2396530	C	2.1334480	-0.0781030	-0.2402790
H	1.9261720	-1.1338640	-0.4744280	H	1.9254090	-1.1202190	-0.5071290	H	1.9257910	-1.1183190	-0.5119450
H	1.9351460	0.5036500	-1.1410250	H	1.9319500	0.5386240	-1.1212900	H	1.9323830	0.5424250	-1.1199500
C	3.5946640	0.0616980	0.1358880	C	3.5935370	0.0563490	0.1392360	C	3.5938370	0.0559830	0.1382650
H	3.8339790	-0.5405850	1.0206790	H	3.8395050	-0.5769850	0.9982800	H	3.8379110	-0.5791590	0.9974300
H	3.8404980	1.1087920	0.3507380	H	3.8439140	1.0945220	0.3822510	H	3.8423070	1.0940860	0.3866480
F	4.3835020	-0.3668470	-0.9110030	F	4.3811890	-0.3407550	-0.9322690	F	4.3812390	-0.3361830	-0.9301340

Tetrazine **2**, gas phase

C	-1.6804960	-0.0052510	-0.0000110
C	-4.2252090	-0.1713360	0.0000320
N	-3.5389400	-1.3156700	0.0001970
N	-2.2335910	-1.2309670	0.0002000
N	-2.3886010	1.1378490	-0.0001710
N	-3.6943830	1.0521940	-0.0001210
C	-0.2084140	0.0906470	-0.0000540
C	0.4140580	1.3448350	0.0000980
C	1.7970370	1.4276820	0.0001050
H	-0.1956860	2.2408890	0.0002170
C	1.9610940	-0.9755680	-0.0002090
C	2.5824660	0.2713230	-0.0000390
H	2.2763410	2.4038880	0.0002520
H	2.5735990	-1.8691520	-0.0003090
C	0.5739590	-1.0670900	-0.0002080
H	0.0858270	-2.0352430	-0.0003180
H	-5.3067180	-0.2424760	0.0000400
C	4.0853900	0.3990940	0.0000210
H	4.3885880	0.9790720	-0.8853450
H	4.3885140	0.9790920	0.8853990
O	4.6691380	-0.8828650	0.0000410
H	5.6257440	-0.7830050	0.0005940

1,4-dioxane

C	1.6809430	-0.0049220	0.0000100
C	4.2300680	-0.1711840	-0.0000070
N	3.5411520	-1.3139630	0.0000430
N	2.2359220	-1.2295540	0.0000590
N	2.3905590	1.1370760	-0.0000610
N	3.6961240	1.0511270	-0.0000580
C	0.2088690	0.0905410	0.0000060
C	-0.4155820	1.3443200	0.0000410
C	-1.7987760	1.4273650	0.0000400
H	0.1908600	2.2425070	0.0000820
C	-1.9612390	-0.9757820	-0.0000250
C	-2.5847570	0.2705770	0.0000040
H	-2.2780460	2.4032630	0.0000740
H	-2.5706790	-1.8714730	-0.0000390
C	-0.5738240	-1.0672900	-0.0000350
H	-0.0887040	-2.0368520	-0.0000620
H	5.3112830	-0.2420940	0.0000140
C	-4.0875620	0.3989530	0.0000050
H	-4.3908210	0.9789870	0.8844610
H	-4.3908180	0.9790300	-0.8844230
O	-4.6734890	-0.8830590	-0.0000260
H	-5.6303010	-0.7771630	-0.0000110

TS1$_{1+3}$, gas phase			
C	-0.4486110	2.2438020	0.3462180
C	1.2012590	0.3792600	0.1204820
C	-0.7906720	-0.6208040	0.0062830
H	-0.5339730	-0.9855930	-0.9897300
C	-1.6899860	0.4210090	0.0737250
H	-2.1459040	0.6085340	1.0474660
N	1.0438120	0.9004130	1.3768170
N	0.1933220	1.8535800	1.4927200
N	1.0474740	1.1928510	-0.9701140
N	0.2036680	2.1520380	-0.8552220
C	-2.5376290	0.7498180	-1.1226810
H	-2.8559680	1.7963260	-1.1438780
H	-1.9616260	0.5621900	-2.0361420
C	-0.7626670	-1.6419700	1.1084750
H	0.2068930	-2.1390040	1.2039470
H	-0.9744310	-1.1477760	2.0638510
C	-3.7891100	-0.1543820	-1.0948690
H	-4.3443810	0.0113120	-2.0247720
H	-4.4479870	0.1764770	-0.2815260
C	-1.8404840	-2.7087190	0.8152590
H	-1.8872110	-3.3839160	1.6769300
H	-1.5121110	-3.3206780	-0.0348470
C	-3.2502830	-2.1673900	0.5176480
H	-3.9548480	-2.9790560	0.7246530
H	-3.4964290	-1.3790980	1.2407840
C	-3.5140100	-1.6597390	-0.9284750
H	-4.3877230	-2.1907810	-1.3193390
H	-2.6815500	-1.9498940	-1.5827950
C	2.1901090	-0.7416960	-0.0257410
C	-1.4659080	3.3366560	0.4924190
H	-2.3395120	2.9923210	1.0508960
H	-1.7733650	3.6920290	-0.4910570
H	-1.0215060	4.1673800	1.0458490
H	1.9083900	-1.3612810	-0.8847930
H	2.1508390	-1.3600370	0.8755560
C	3.6088000	-0.1940870	-0.2137860
H	3.6404800	0.4442870	-1.1016120
H	3.8792330	0.4222900	0.6497660
C	4.6177830	-1.3143890	-0.3608770
H	4.3892940	-1.9345550	-1.2366200
H	4.6243460	-1.9575520	0.5279170
F	5.8810640	-0.7822570	-0.5215990

1,4-dioxane			
C	-0.4510940	2.2505260	0.3467880
C	1.2053250	0.3852740	0.1166960
C	-0.7941350	-0.6229390	0.0086110
H	-0.5329750	-0.9916990	-0.9847230
C	-1.6946030	0.4173980	0.0706000
H	-2.1527260	0.6097810	1.0422750
N	1.0487040	0.9083380	1.3718400
N	0.1960410	1.8602400	1.4898060
N	1.0480880	1.2018360	-0.9705940
N	0.2024830	2.1600920	-0.8534360
C	-2.5380340	0.7432880	-1.1291860
H	-2.8586800	1.7889210	-1.1535770
H	-1.9614480	0.5501850	-2.0411900
C	-0.7641110	-1.6375400	1.1164430
H	0.2060150	-2.1322950	1.2162940
H	-0.9836920	-1.1405330	2.0686410
C	-3.7885160	-0.1630090	-1.0990440
H	-4.3418730	-0.0008180	-2.0305990
H	-4.4477020	0.1704980	-0.2873040
C	-1.8386870	-2.7079550	0.8226300
H	-1.8853270	-3.3800470	1.6866000
H	-1.5055860	-3.3203640	-0.0250740
C	-3.2489480	-2.1702520	0.5206020
H	-3.9517020	-2.9833810	0.7278980
H	-3.4985270	-1.3805860	1.2411190
C	-3.5108400	-1.6673520	-0.9276710
H	-4.3835300	-2.2005030	-1.3178900
H	-2.6769560	-1.9583340	-1.5798480
C	2.1903140	-0.7383280	-0.0326900
C	-1.4747310	3.3365780	0.4950880
H	-2.3412870	2.9877810	1.0612130
H	-1.7945960	3.6845910	-0.4869350
H	-1.0327770	4.1749160	1.0391630
H	1.9083180	-1.3527490	-0.8947210
H	2.1471620	-1.3624370	0.8641150
C	3.6120600	-0.1955070	-0.2139990
H	3.6509990	0.4441260	-1.1008100
H	3.8828770	0.4174010	0.6520190
C	4.6155480	-1.3203480	-0.3605120
H	4.3902200	-1.9365340	-1.2387380
H	4.6205890	-1.9638670	0.5269130
F	5.8843020	-0.7885110	-0.5171440

TS1$_{1+4}$, gas phase			
C	-3.9612780	-0.5611950	0.1339090
C	-2.9416510	-0.6319390	1.2284710
C	-2.7740960	-1.4728400	-0.0440470
H	-3.9182150	0.3311260	-0.4910680
H	-3.2654720	-1.2920370	2.0342350
H	-2.9944940	-2.5166980	0.1746180
C	-2.2026950	0.5456000	1.8670180
H	-2.9101260	1.0247690	2.5553510
H	-1.4157930	0.1295140	2.5068180
C	-1.8774950	-1.3323870	-1.2762460
H	-2.0977830	-2.1818400	-1.9321240
H	-2.1758810	-0.4412670	-1.8356170
C	-0.3561300	-1.2363710	-1.0331920
H	0.1456630	-0.9754700	-1.9727370
H	0.0485450	-2.1936090	-0.6910100
C	-1.5740930	1.6416760	0.9902250
H	-0.9643310	2.2787030	1.6424280
H	-2.3530400	2.2808730	0.5612010
C	-0.7673650	1.0422070	-0.1420710
H	-1.0794460	1.3070330	-1.1513910
C	-0.1566100	-0.1724850	0.0189110
H	-0.0328830	-0.5347540	1.0374260
C	0.9763150	2.5195700	-0.3820840
C	2.0666250	0.2835080	-0.1052900
C	2.6798370	-1.0757830	0.0652430
C	0.2491870	3.8180500	-0.5512250
N	1.5432170	2.2670150	0.8338090
N	2.0589540	0.8021720	-1.3668360
N	2.0992570	1.1150500	0.9757750
N	1.4895130	1.9474030	-1.5088720
H	0.9734980	4.6253260	-0.6907760
H	-0.3922650	3.7779190	-1.4329750
H	-0.3450730	4.0437140	0.3347850
H	2.2866120	-1.5288660	0.9821350
H	2.3819200	-1.6986780	-0.7841170
C	-5.3450710	-1.1140140	0.3161870
H	-5.9999010	-0.3536540	0.7687820
H	-5.2963720	-1.9657180	1.0142800
O	-5.8277270	-1.5141610	-0.9523650
H	-6.7413180	-1.8012690	-0.8539520
C	4.2071700	-0.9807580	0.1364490
H	4.4957310	-0.3401300	0.9756140
H	4.5877040	-0.5206830	-0.7812370
C	4.8381500	-2.3474320	0.3071020
H	4.4988090	-2.8228160	1.2359270
H	4.5828540	-3.0047960	-0.5333240
F	6.2112760	-2.2208130	0.3591500

water			
C	-3.9674610	-0.5703200	0.1230310
C	-2.9459680	-0.6316440	1.2165250
C	-2.7708160	-1.4737360	-0.0536630
H	-3.9295590	0.3247960	-0.4990480
H	-3.2649650	-1.2926020	2.0229830
H	-2.9782030	-2.5195150	0.1689760
C	-2.2169910	0.5527860	1.8546010
H	-2.9320220	1.0317560	2.5346030
H	-1.4339920	0.1414950	2.5020160
C	-1.8725320	-1.3256430	-1.2841430
H	-2.0843960	-2.1747220	-1.9437400
H	-2.1683820	-0.4309730	-1.8395870
C	-0.3512610	-1.2291970	-1.0360980
H	0.1493140	-0.9657120	-1.9754920
H	0.0537540	-2.1856500	-0.6942230
C	-1.5880400	1.6489210	0.9778550
H	-0.9896530	2.2937410	1.6328470
H	-2.3646960	2.2823810	0.5377390
C	-0.7724760	1.0468270	-0.1461380
H	-1.0721790	1.3168200	-1.1579540
C	-0.1637980	-0.1667290	0.0189960
H	-0.0399050	-0.5304970	1.0370980
C	0.9905960	2.5407860	-0.3773270
C	2.0862540	0.2954870	-0.0961150
C	2.6814710	-1.0707770	0.0762400
C	0.2500130	3.8305340	-0.5470130
N	1.5574130	2.2840380	0.8366570
N	2.0840080	0.8208530	-1.3538660
N	2.1142870	1.1309570	0.9805200
N	1.5139330	1.9671930	-1.4976800
H	0.9630860	4.6450500	-0.7029100
H	-0.4069010	3.7767100	-1.4163840
H	-0.3368790	4.0556870	0.3438060
H	2.2839910	-1.5178790	0.9932490
H	2.3727710	-1.6930170	-0.7690540
C	-5.3472350	-1.1285700	0.3213400
H	-6.0005150	-0.3725680	0.7800900
H	-5.2900900	-1.9816410	1.0147560
O	-5.8545180	-1.5320150	-0.9424090
H	-6.7654470	-1.8218100	-0.8173960
C	4.2109670	-0.9993320	0.1420450
H	4.5150130	-0.3678090	0.9829920
H	4.5972600	-0.5441200	-0.7759490
C	4.8166680	-2.3775860	0.3057730
H	4.4817030	-2.8493030	1.2359500
H	4.5521690	-3.0277360	-0.5351700
F	6.2001150	-2.2676540	0.3493560

1,4-dioxane			
C	-3.9643560	-0.5659780	0.1282810
C	-2.9439070	-0.6310430	1.2225080
C	-2.7722020	-1.4733550	-0.0482830
H	-3.9239630	0.3273090	-0.4958750
H	-3.2653090	-1.2910640	2.0290620
H	-2.9859500	-2.5181240	0.1729140
C	-2.2101800	0.5506020	1.8599150
H	-2.9215320	1.0301770	2.5436530
H	-1.4251680	0.1377050	2.5039710
C	-1.8745020	-1.3294970	-1.2794800
H	-2.0903920	-2.1790400	-1.9369260
H	-2.1714420	-0.4367980	-1.8372830
C	-0.3532460	-1.2331850	-1.0336760
H	0.1480050	-0.9716890	-1.9732770
H	0.0514820	-2.1898530	-0.6909930
C	-1.5815810	1.6461040	0.9823120
H	-0.9783230	2.2880150	1.6356810
H	-2.3595310	2.2815170	0.5466170
C	-0.7693970	1.0448030	-0.1448970
H	-1.0749420	1.3112720	-1.1558250
C	-0.1596460	-0.1692900	0.0192440
H	-0.0363670	-0.5316300	1.0378590
C	0.9828190	2.5297600	-0.3798350
C	2.0758630	0.2892470	-0.0999630
C	2.6807860	-1.0732200	0.0718630
C	0.2497300	3.8242500	-0.5499170
N	1.5492670	2.2753670	0.8354140
N	2.0713430	0.8110250	-1.3597760
N	2.1057320	1.1229930	0.9787710
N	1.5016480	1.9566600	-1.5031370
H	0.9690960	4.6344220	-0.6986060
H	-0.3999160	3.7770780	-1.4252120
H	-0.3402400	4.0506810	0.3386470
H	2.2859200	-1.5229580	0.9892010
H	2.3773650	-1.6962750	-0.7750990
C	-5.3460760	-1.1217810	0.3186790
H	-6.0004540	-0.3635360	0.7737680
H	-5.2930010	-1.9737800	1.0148980
O	-5.8407940	-1.5244050	-0.9473070
H	-6.7531520	-1.8129130	-0.8357680
C	4.2092870	-0.9894770	0.1396120
H	4.5059610	-0.3534880	0.9796130
H	4.5921040	-0.5315750	-0.7783120
C	4.8276830	-2.3620300	0.3061720
H	4.4910890	-2.8357650	1.2357570
H	4.5674460	-3.0155130	-0.5345990
F	6.2061320	-2.2440780	0.3533860

TS1$_{2+3}$, gas phase			
C	0.0506210	-1.5579120	-0.0906270
C	-1.3252380	0.3024670	-0.0537890
H	-0.9746730	0.4823500	0.9639350
C	-2.5901160	-0.2207180	-0.2056490
H	-3.0157720	-0.1748610	-1.2097230
N	-0.3045150	-1.9633200	-1.3489440
N	-1.5088370	-2.3803930	-1.4984900
N	-0.5266100	-2.1583630	0.9980350
N	-1.7295530	-2.5799590	0.8527980
C	-3.5796700	-0.1248280	0.9234160
H	-4.3386470	-0.9138720	0.8852300
H	-3.0506420	-0.2273470	1.8777360
C	-0.7474000	1.1857000	-1.1169150
H	0.3466750	1.1683350	-1.1277430
H	-1.1010330	0.8499380	-2.0993550
C	-4.2692560	1.2542400	0.8481550
H	-4.9036520	1.3638810	1.7348350
H	-4.9460250	1.2676640	-0.0158750
C	-1.2312100	2.6305120	-0.8527080
H	-0.9045730	3.2532050	-1.6928750
H	-0.7166190	3.0191820	0.0354050
C	-2.7498840	2.7924290	-0.6595600
H	-2.9938460	3.8355880	-0.8847250
H	-3.2751280	2.2012340	-1.4211250
C	-3.3164160	2.4602940	0.7508580
H	-3.8670280	3.3357290	1.1096940
H	-2.4905470	2.3248550	1.4611110
C	1.3807720	-0.9419720	0.0952130
C	1.8055320	-0.5752000	1.3766180
C	2.2103170	-0.6918890	-0.9999720
C	3.0399040	0.0328680	1.5501860
H	1.1631080	-0.7807130	2.2267900
C	3.4498960	-0.0859950	-0.8182760
H	1.8754640	-0.9824000	-1.9901100
C	3.8736410	0.2812100	0.4570480
H	3.3621200	0.3193410	2.5486530
H	4.0980550	0.1113490	-1.6640740
C	-2.2841640	-2.3512020	-0.3743710
H	-3.3201230	-2.6472000	-0.4979360
C	5.2230700	0.9178740	0.6807500
H	5.1016440	1.7865550	1.3461540
H	5.8691060	0.1971330	1.2061450
O	5.7809200	1.2919960	-0.5588680
H	6.6789810	1.6010750	-0.4072670

1,4-dioxane			
C	0.0552290	-1.5668440	-0.0860160
C	-1.3299540	0.3070440	-0.0571430
H	-0.9739890	0.4903430	0.9581420
C	-2.5947560	-0.2149750	-0.2020190
H	-3.0244060	-0.1792320	-1.2047290
N	-0.3029220	-1.9769380	-1.3409140
N	-1.5088660	-2.3929520	-1.4879250
N	-0.5223370	-2.1652280	1.0024080
N	-1.7270150	-2.5857060	0.8591790
C	-3.5795870	-0.1167170	0.9303080
H	-4.3388750	-0.9053360	0.8971030
H	-3.0473550	-0.2097640	1.8838970
C	-0.7524910	1.1797690	-1.1284490
H	0.3416060	1.1596060	-1.1433540
H	-1.1126070	0.8415370	-2.1075930
C	-4.2686160	1.2628650	0.8470580
H	-4.9005330	1.3777650	1.7346880
H	-4.9463070	1.2701810	-0.0160630
C	-1.2326030	2.6272150	-0.8686340
H	-0.9072770	3.2446420	-1.7130570
H	-0.7148990	3.0178520	0.0166630
C	-2.7507100	2.7914630	-0.6725730
H	-2.9932630	3.8339430	-0.9020530
H	-3.2783000	2.1971490	-1.4300580
C	-3.3144640	2.4672980	0.7410300
H	-3.8639770	3.3450550	1.0956490
H	-2.4873610	2.3351800	1.4505270
C	1.3823280	-0.9446460	0.0977480
C	1.7965100	-0.5517190	1.3754940
C	2.2206280	-0.7131810	-0.9949400
C	3.0289090	0.0608550	1.5485420
H	1.1463920	-0.7346180	2.2250350
C	3.4584260	-0.1028730	-0.8137650
H	1.8962840	-1.0184840	-1.9839650
C	3.8725490	0.2892190	0.4577990
H	3.3413580	0.3681750	2.5435750
H	4.1115690	0.0776500	-1.6594900
C	-2.2855740	-2.3595790	-0.3656770
H	-3.3233420	-2.6487510	-0.4872730
C	5.2176210	0.9352570	0.6816130
H	5.0857210	1.8204320	1.3217710
H	5.8588610	0.2319690	1.2342510
O	5.7914800	1.2789530	-0.5605780
H	6.6861660	1.5961380	-0.4005200

TS1$_{2+4}$, gas phase

C	-4.0224090	-1.3331360	0.0456020
C	-3.0924930	-0.8456140	1.1156580
C	-2.5533970	-1.6440830	-0.0783520
H	-4.3661790	-0.5779670	-0.6613840
H	-3.1099970	-1.5002550	1.9879590
H	-2.2925510	-2.6540320	0.2350700
C	-2.9555880	0.5943700	1.6186620
H	-3.8393800	0.7977780	2.2361640
H	-2.1064510	0.6241180	2.3116670
C	-1.7876660	-1.2227740	-1.3335510
H	-1.6551040	-2.1202870	-1.9479790
H	-2.4130150	-0.5431270	-1.9205810
C	-0.4285930	-0.5200480	-1.1099290
H	-0.0666280	-0.1104150	-2.0611080
H	0.3293600	-1.2112650	-0.7310630
C	-2.7984950	1.7507090	0.6226610
H	-2.6457050	2.6729530	1.1957210
H	-3.7272390	1.8860610	0.0567990
C	-1.6910150	1.4849360	-0.3810140
H	-1.9550130	1.6152840	-1.4305780
C	-0.7149940	0.5648730	-0.1097630
H	-0.5452450	0.2955820	0.9302620
C	-0.5752400	3.4383480	-0.3902150
C	1.2782320	1.8067530	-0.0885440
N	-0.0465630	3.3697280	0.8612540
N	1.1425900	2.3523170	-1.3322450
N	0.9094180	2.5221230	1.0152540
N	0.1873100	3.1994440	-1.4900580
C	-5.0231070	-2.4192530	0.3146230
H	-5.9581660	-1.9861940	0.7013090
H	-4.6204300	-3.0861870	1.0946260
O	-5.2447140	-3.1189860	-0.8953160
H	-5.9547430	-3.7536780	-0.7543150
C	2.2478000	0.7052460	0.0853050
C	2.4886550	0.1791410	1.3579880
C	2.8995970	0.1559470	-1.0220600
C	3.3744350	-0.8785140	1.5154190
H	1.9906780	0.6200700	2.2153340
C	3.7798960	-0.9064950	-0.8559030
H	2.7118140	0.5732960	-2.0054950
C	4.0248300	-1.4348550	0.4123120
H	3.5686990	-1.2743740	2.5093190
H	4.2906390	-1.3377370	-1.7110600
C	4.9706460	-2.6037030	0.5821460
H	4.4118500	-3.5440360	0.5219510
H	5.4234830	-2.5639670	1.5841130
O	5.9496800	-2.6800290	-0.4299770
H	6.4472160	-1.8538490	-0.4176000
H	-1.4334700	4.0879800	-0.5225010

1,4-dioxane

C	-3.9941490	-1.3660690	0.0292240
C	-3.0723580	-0.8300650	1.0836390
C	-2.5157630	-1.6315930	-0.0997890
H	-4.3695120	-0.6338070	-0.6858760
H	-3.0654930	-1.4691740	1.9673330
H	-2.2176340	-2.6267530	0.2279190
C	-2.9766820	0.6232370	1.5594330
H	-3.8750480	0.8181080	2.1579910
H	-2.1399940	0.6860780	2.2654670
C	-1.7675940	-1.2002880	-1.3617920
H	-1.6276820	-2.0945920	-1.9796500
H	-2.4020300	-0.5217540	-1.9408040
C	-0.4139250	-0.4836530	-1.1417570
H	-0.0585190	-0.0689400	-2.0929590
H	0.3504170	-1.1676250	-0.7623580
C	-2.8321270	1.7612690	0.5419910
H	-2.7405180	2.7042940	1.0937450
H	-3.7460100	1.8435030	-0.0573670
C	-1.6899480	1.5159330	-0.4272620
H	-1.9170860	1.6715860	-1.4822100
C	-0.7235400	0.5927380	-0.1409780
H	-0.5805400	0.3116130	0.8998580
C	-0.5562460	3.4830740	-0.3510660
C	1.2930470	1.8368020	-0.0534620
N	-0.0524740	3.3773610	0.9066650
N	1.1811710	2.4155640	-1.2831850
N	0.9012510	2.5246780	1.0585670
N	0.2301800	3.2696250	-1.4380950
C	-4.9566870	-2.4769920	0.3353240
H	-5.8987680	-2.0664230	0.7275800
H	-4.5218750	-3.1161730	1.1200190
O	-5.1794460	-3.2113340	-0.8566510
H	-5.8395970	-3.8885480	-0.6725690
C	2.2457350	0.7201890	0.1099720
C	2.4340750	0.1392060	1.3685340
C	2.9292840	0.2051440	-0.9944760
C	3.2997260	-0.9363290	1.5145950
H	1.9068650	0.5452700	2.2257030
C	3.7903790	-0.8753650	-0.8403130
H	2.7800520	0.6574280	-1.9688440
C	3.9826830	-1.4575040	0.4130610
H	3.4498170	-1.3762330	2.4973500
H	4.3236850	-1.2784290	-1.6951190
C	4.8982570	-2.6517040	0.5747700
H	4.3076870	-3.5732980	0.5317900
H	5.3678550	-2.6189140	1.5682950
O	5.8598390	-2.7647700	-0.4517880
H	6.4192600	-1.9791300	-0.4186910
H	-1.4143590	4.1319710	-0.4846440

7. References

[1] S. A. Lang, B. D. Johnson, E. Cohen, *J. Heterocyclic Chem.* **1975**, *12*, 1143-1153.

[2] M. Royzen, G. P. A. Yap, J. M. Fox, *J. Am. Chem. Soc.* **2008**, *130*, 3760-3761.

[3] M. T. Taylor, M. L. Blackman, O. Dmitrenko, J. M. Fox, *J. Am. Chem. Soc.* **2011**, *133*, 9646-9649.

[4] E. Nachbaur, G. Leiseder, *Monatsh. Chem.* **1971**, *102*, 1718-1723.

[5] D. Lumpi, C. Braunshier, C. Hametner, E. Horkel, B. Zachhuber, B. Lendl, J. Fröhlich, *Tetrahedron Lett.* **2009**, *50*, 6469-6471.

[6] A. M. Loening, S. S. Gambhir, *Mol. Imaging* **2003**, *2*, 131-137.

[7] M. J. T. Frisch, G. W.; Schlegel, H. B.; Scuseria, G. E.; Robb, M. A.; Cheeseman, J. R.; Scalmani, G.; Barone, V.; Mennucci, B.; Petersson, G. A.; Nakatsuji, H.; Caricato, M.; Li, X.; Hratchian, H. P.; Izmaylov, A. F.; Bloino, J.; Zheng, G.; Sonnenberg, J. L.; Hada, M.; Ehara, M.; Toyota, K.; Fukuda, R.; Hasegawa, J.; Ishida, M.; Nakajima, T.; Honda, Y.; Kitao, O.; Nakai, H.; Vreven, T.; Montgomery, Jr., J. A.; Peralta, J. E.; Ogliaro, F.; Bearpark, M.; Heyd, J. J.; Brothers, E.; Kudin, K. N.; Staroverov, V. N.; Kobayashi, R.; Normand, J.; Raghavachari, K.; Rendell, A.; Burant, J. C.; Iyengar, S. S.; Tomasi, J.; Cossi, M.; Rega, N.; Millam, J. M.; Klene, M.; Knox, J. E.; Cross, J. B.; Bakken, V.; Adamo, C.; Jaramillo, J.; Gomperts, R.; Stratmann, R. E.; Yazyev, O.; Austin, A. J.; Cammi, R.; Pomelli, C.; Ochterski, J. W.; Martin, R. L.; Morokuma, K.; Zakrzewski, V. G.; Voth, G. A.; Salvador, P.; Dannenberg, J. J.; Dapprich, S.; Daniels, A. D.; Farkas, Ö.; Foresman, J. B.; Ortiz, J. V.; Cioslowski, J.; Fox, D. J, *Gaussian 09, Revision A.1*, Gaussian Inc, Wallingford CT, **2009**.

[8] R. Ditchfield, W. J. Hehre, J. A. Pople, *J. Chem. Phys.* **1971**, *54*, 724-728.

[9] Y. Zhao, D. Truhlar, *Theor. Chem. Acc.* **2008**, *120*, 215-241.

[10] a) Y. Lan, L. Zou, Y. Cao, K. N. Houk, *J. Phys. Chem. A* **2011**, *115*, 13906-13920; b) R. S. Paton, J. L. Mackey, W. H. Kim, J. H. Lee, S. J. Danishefsky, K. N. Houk, *J. Am. Chem. Soc.* **2010**, *132*, 9335-9340.

[11] J. Tomasi, B. Mennucci, R. Cammi, *Chem. Rev.* **2005**, *105*, 2999-3094.

[12] a) V. Barone, M. Cossi, *J. Phys. Chem. A* **1998**, *102*, 1995-2001; b) M. Cossi, N. Rega, G. Scalmani, V. Barone, *J. Comput. Chem.* **2003**, *24*, 669-681.

Supporting Information

Manuscript #5

Christoph Denk, Dennis Svatunek, Severin Mairinger, Claudia Kuntner, Thomas Filip, Michael Sauberer, Johannes Fröhlich, Thomas Wanek, Hannes Mikula*; A Tale of 3-[^{18}F]Fluoropropyl-1,2,4,5-tetrazines, manuscript draft

A Tale of 3-[^{18}F]Fluoropropyl-1,2,4,5-Tetrazines

Christoph Denk[a], Dennis Svatunek[a], Severin Mairinger[b], Claudia Kuntner[b], Thomas Filip[b], Michael Sauberer[b,] Johannes Fröhlich[a], Thomas Wanek[b] and Hannes Mikula[a*]

a) Institut für Angewandte Synthesechemie, Technische Universität Wien (TUW) (Austria) E-mail: hannes.mikula@tuwien.ac.at b) Health and Environment Department, Biomedical Systems, Austrian Institute of Technology (AIT) Seibersdorf (Austria)

Supporting Information

Contents

1. *In vivo* Data 2

2. NMR Spectra 7

3. HPLC Data 26

4. Determination of Specific Activity 29

5. Kinetic Measurements 31

6. Quantum Chemical Calculations 42

7. References 50

1. *In vivo* Data

[^{18}F]**2**

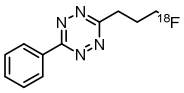

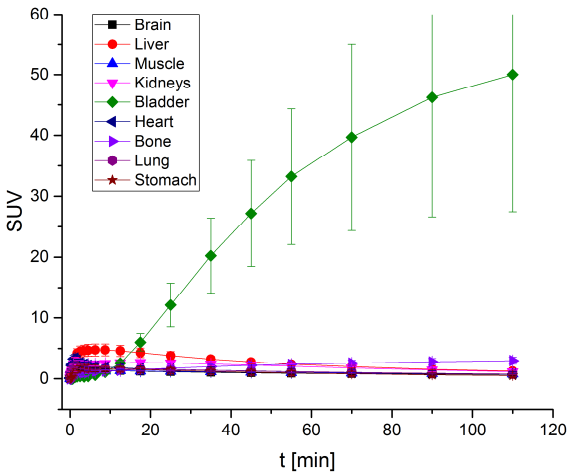

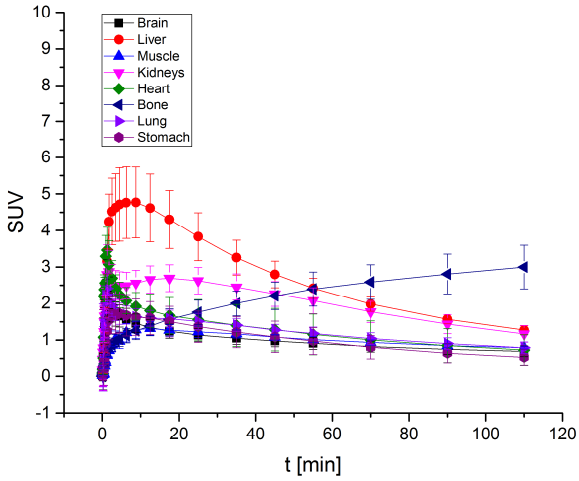

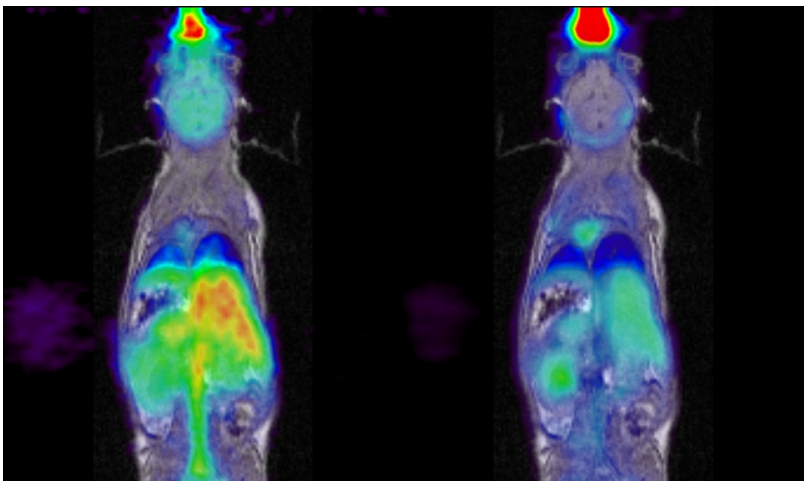

0-5 min **5-120 min**

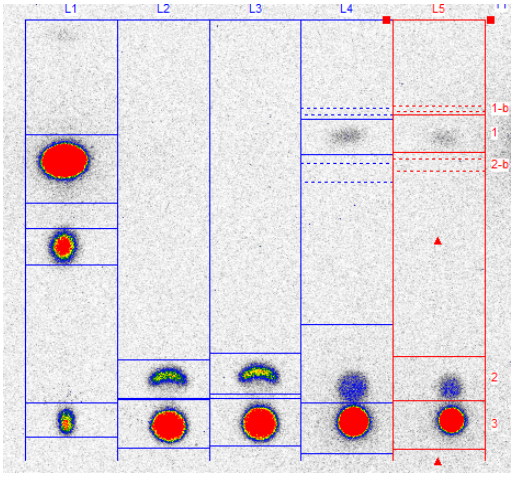

Radio-TLC metabolite analysis:

Eluent: DCM

Lane 1: Reference [^{18}F]**2**
Lane 2: Plasma
Lane 3: Plasma
Lane 4: Urine
Lane 5: Urine

[^{18}F]3

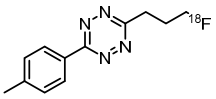

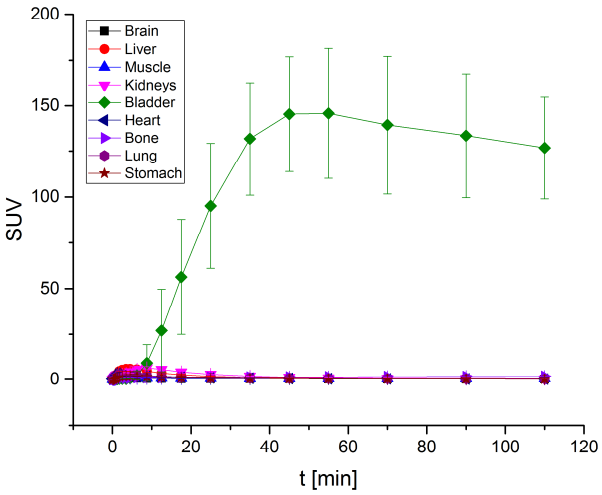

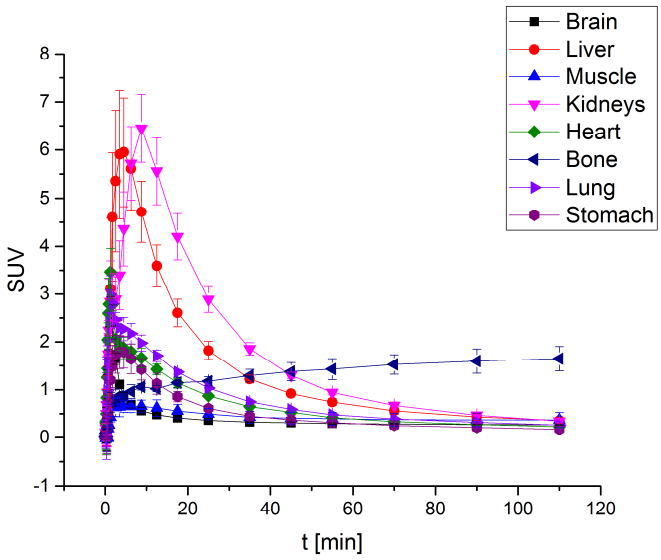

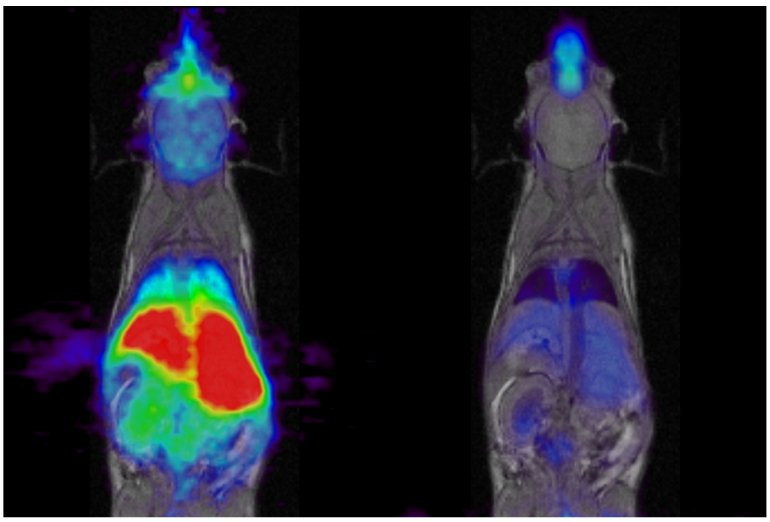

0-5 min **5-120 min**

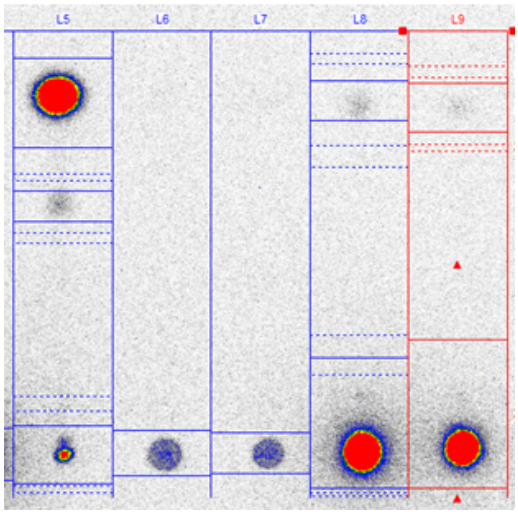

Radio-TLC metabolite analysis:

Eluent: DCM

Lane 1: Reference [^{18}F]**3**
Lane 2: Plasma
Lane 3: Plasma
Lane 4: Urine
Lane 5: Urine

[^{18}F]**5**

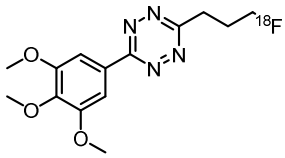

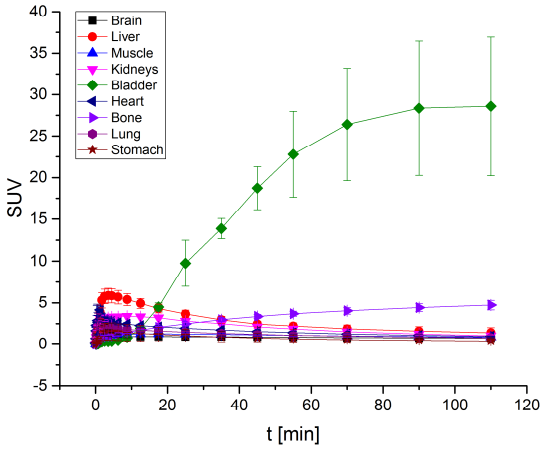

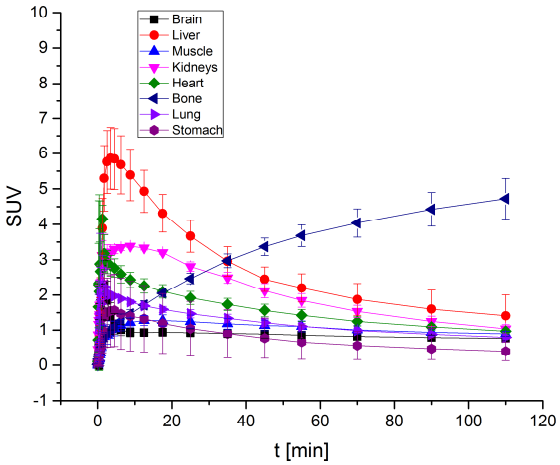

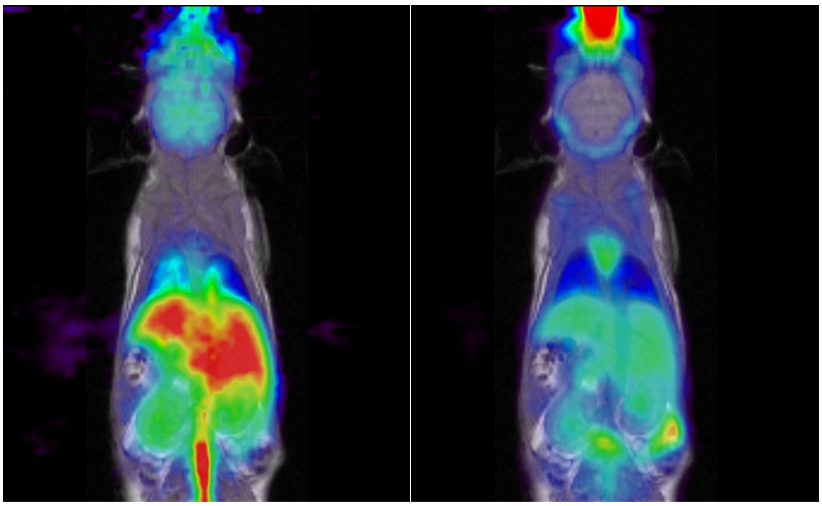

0-5 min **5-120 min**

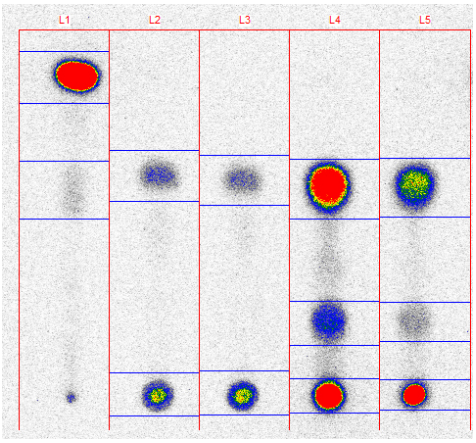

Radio-TLC metabolite analysis:

Eluent: 3% MeOH in DCM

Lane 1: Reference [^{18}F]**5**
Lane 2: Plasma
Lane 3: Plasma
Lane 4: Urine
Lane 5: Urine

[^{18}F]**6**

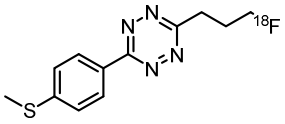

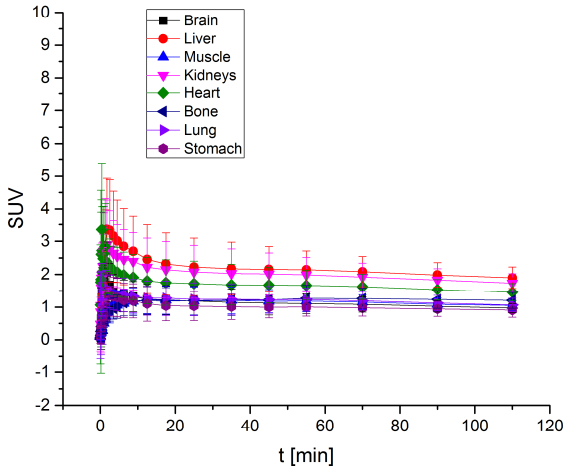

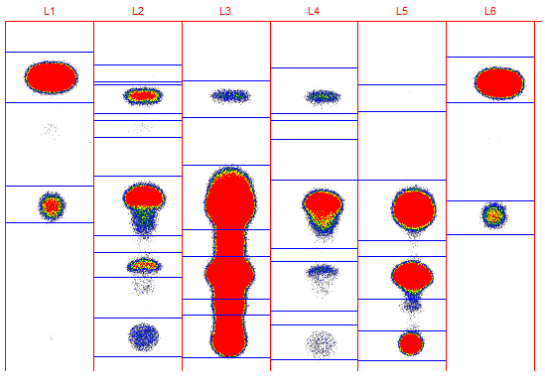

Radio-TLC metabolite analysis 120 min post administration:

Eluent: 5% MeOH in DCM

Lane 1: Reference [^{18}F]**6**
Lane 2: Plasma
Lane 3: Urine
Lane 4: Plasma
Lane 5: Urine
Lane 6: Reference [^{18}F]**6**

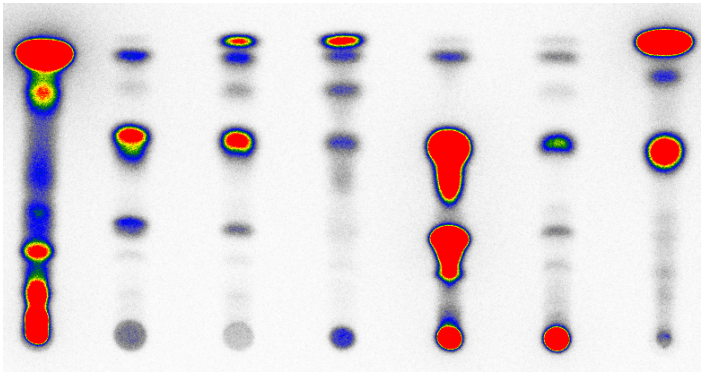

Radio-TLC metabolite analysis 60 min post administration:

Eluent: 5% MeOH in DCM

Lane 1: Reference [^{18}F]**7** (Sulfone derivative)
Lane 2: Plasma
Lane 3: CNS extract
Lane 4: Liver extract
Lane 5: Urine
Lane 6: Bile
Lane 7: Reference [^{18}F]**6**

[^{18}F]**7**

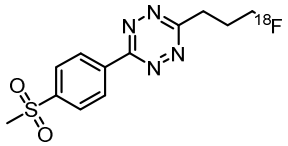

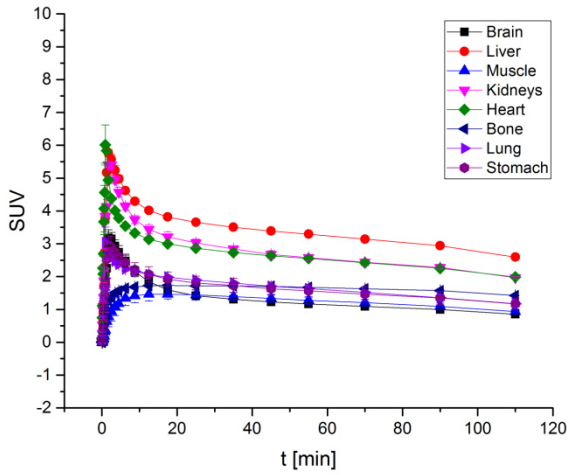

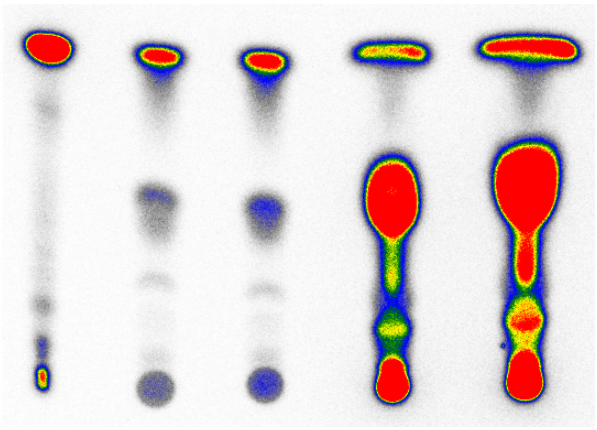

Radio-TLC metabolite analysis 120 min post administration:

Eluent: 5% MeOH in DCM

Lane 1: Reference [^{18}F]**7**
Lane 2: Plasma
Lane 3: Plasma
Lane 4: Urine
Lane 5: Urine
Lane 6: Reference [^{18}F]**6**

2. NMR Spectra

^{1}H Spectrum of compound **2**

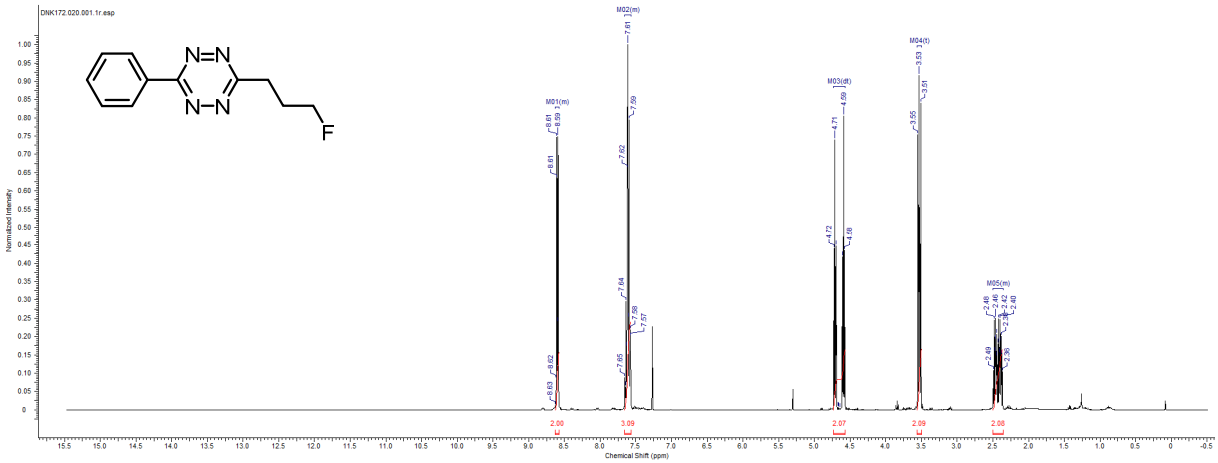

^{13}C Spectrum of compound **2**

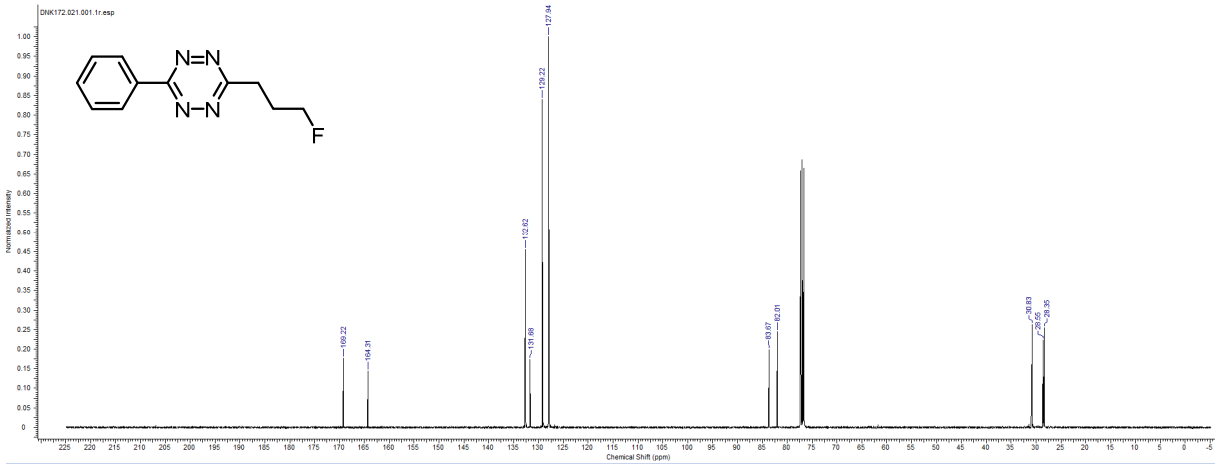

^{19}F Spectrum of compound **2**

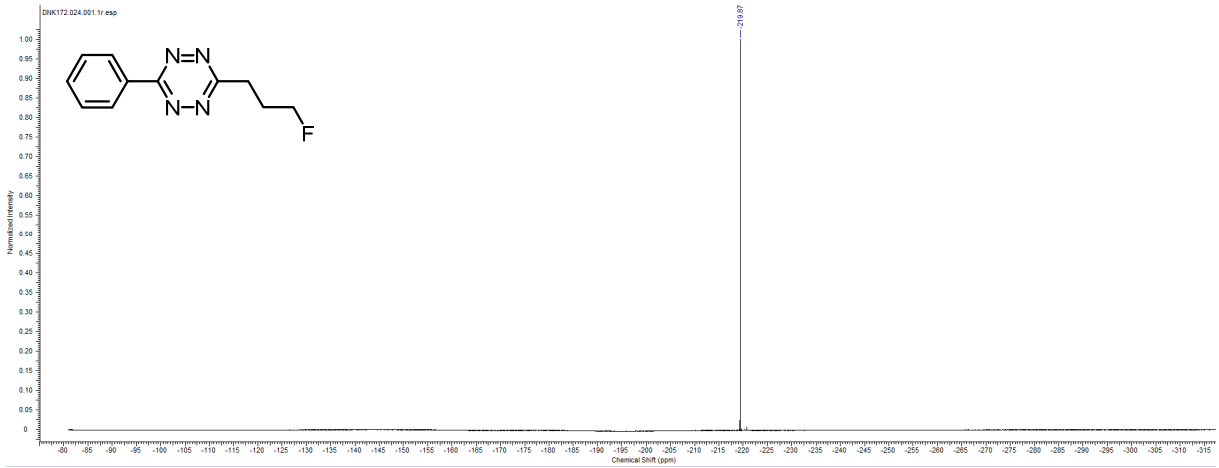

^{1}H Spectrum of compound **3**

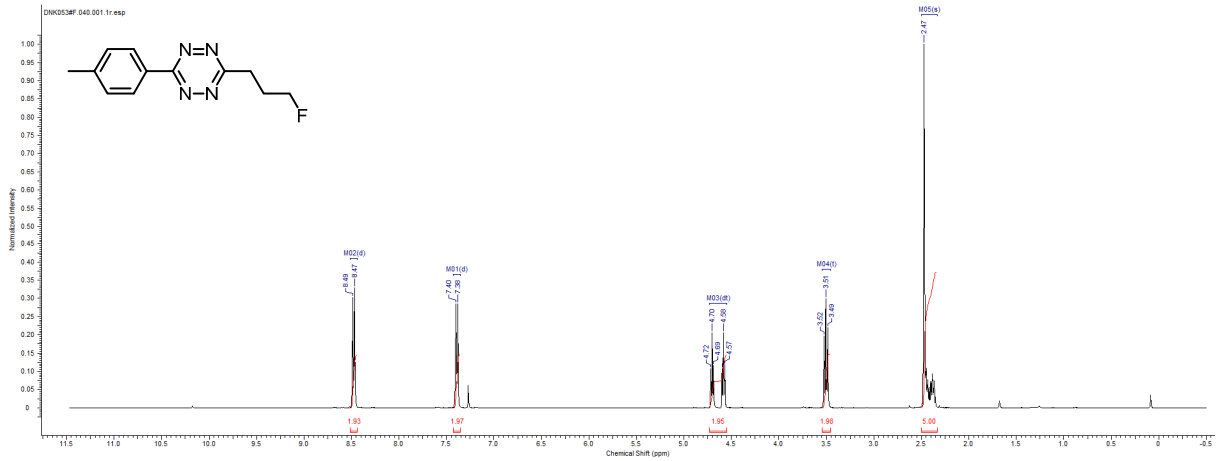

^{13}C Spectrum of compound **3**

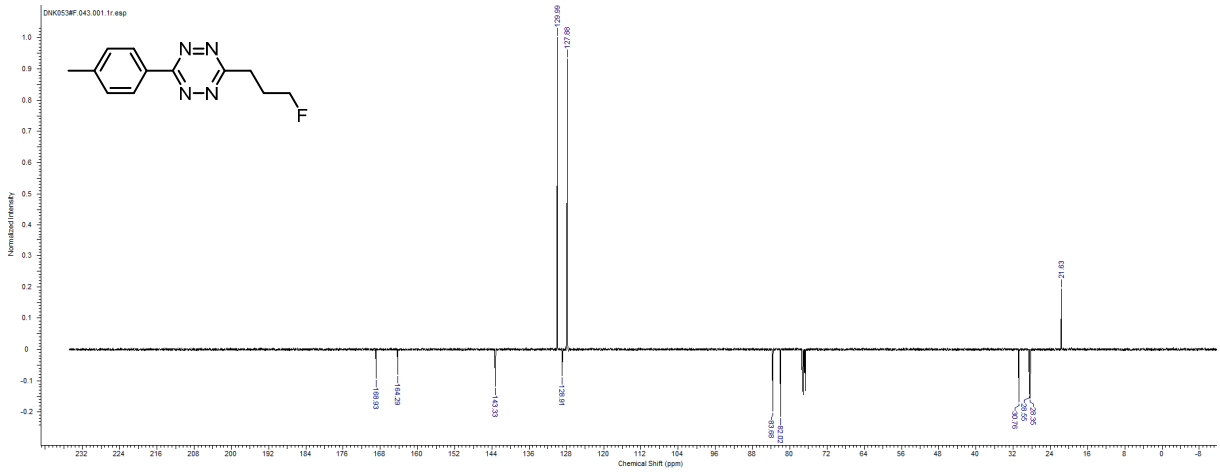

^{19}F Spectrum of compound **3**

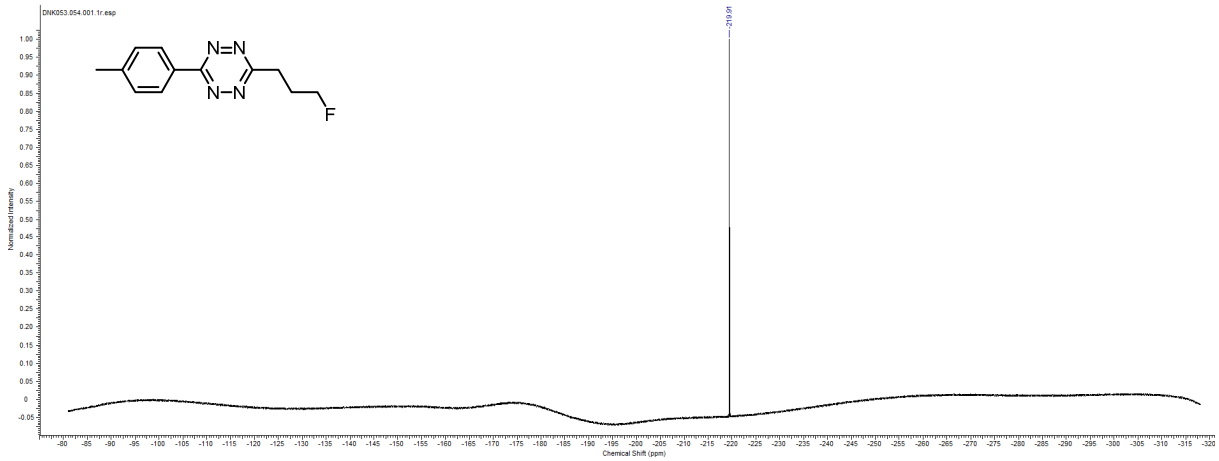

^{1}H Spectrum of compound **4**

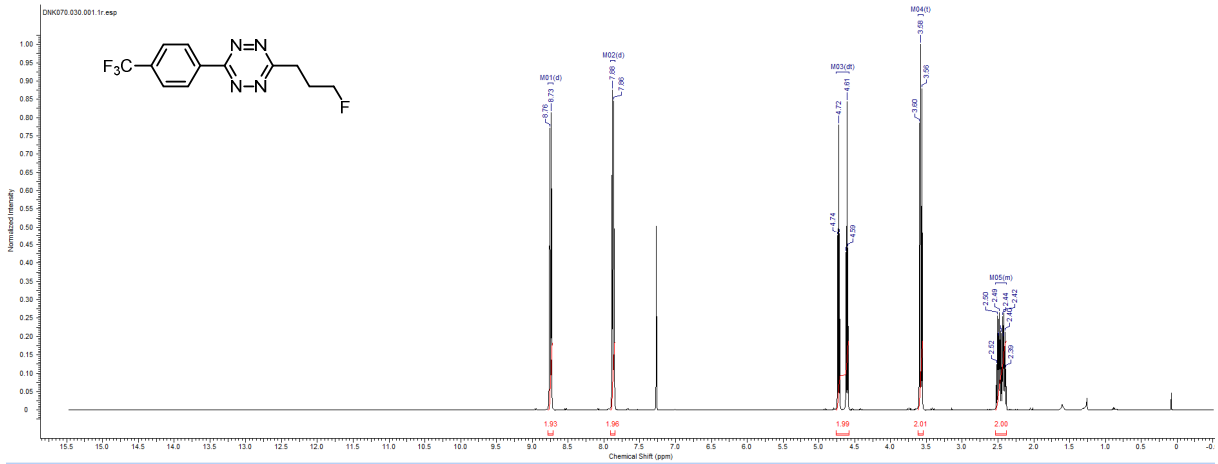

^{13}C Spectrum of compound **4**

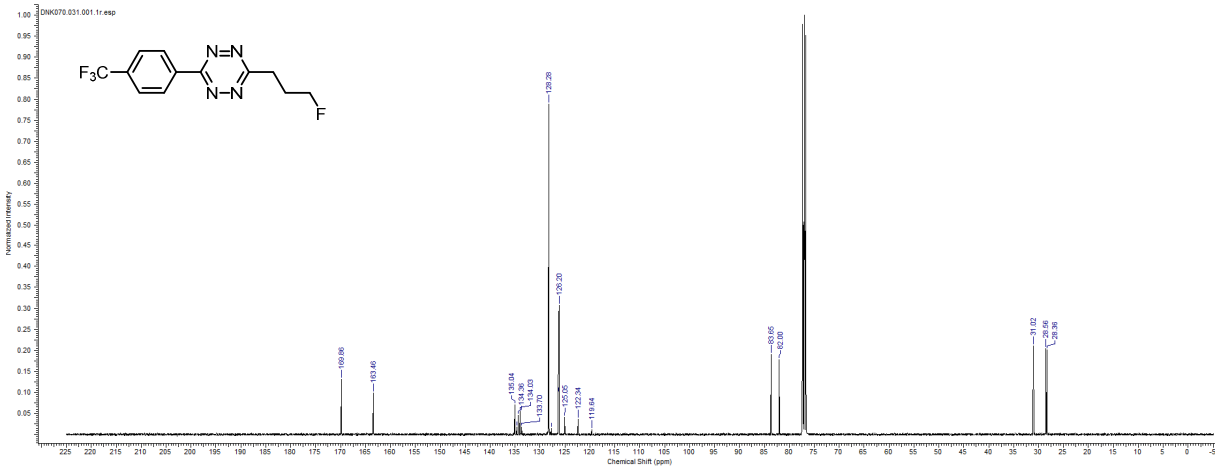

^{19}F Spectrum of compound **4**

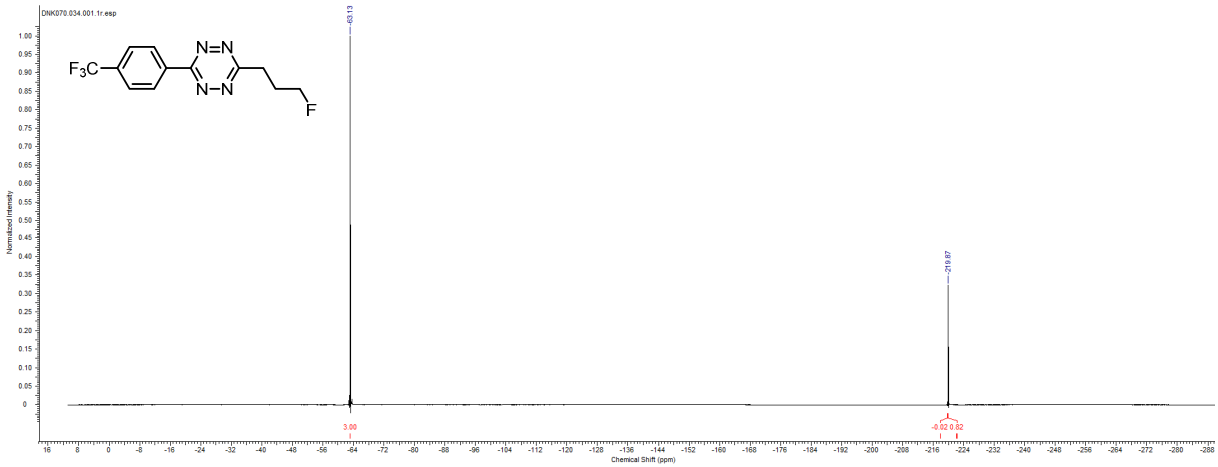

^{1}H Spectrum of compound **5**

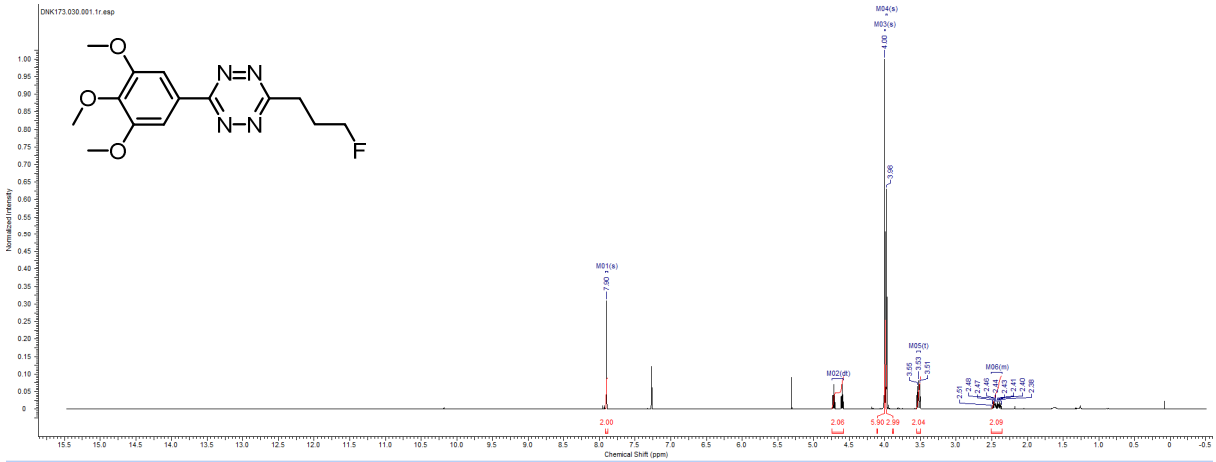

^{13}C Spectrum of compound **5**

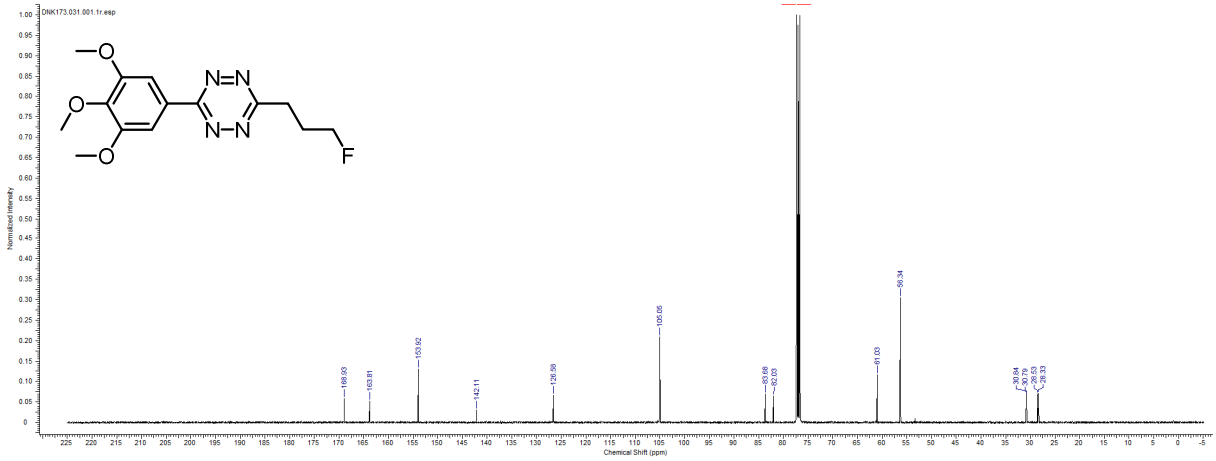

^{19}F Spectrum of compound **5**

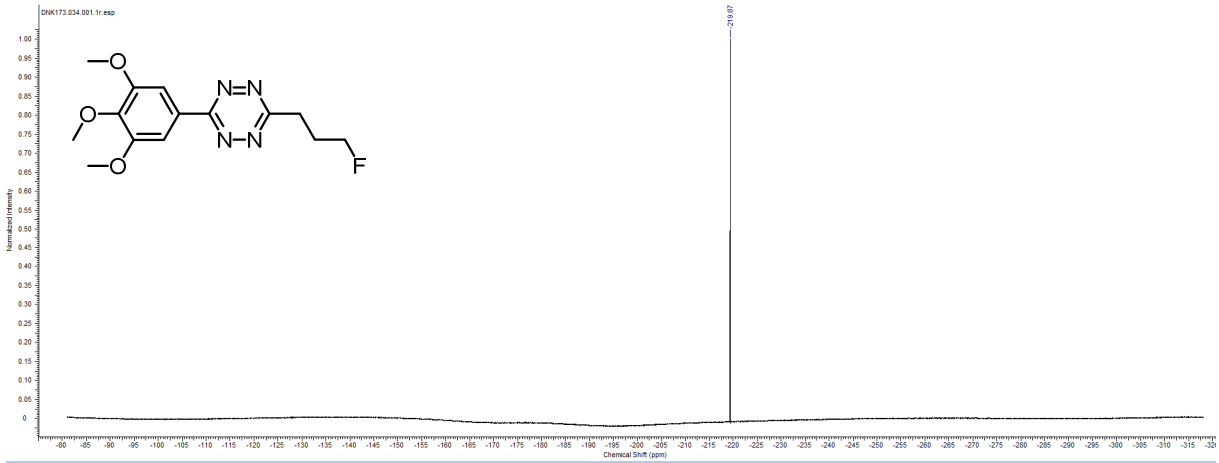

^{1}H Spectrum of compound **6**

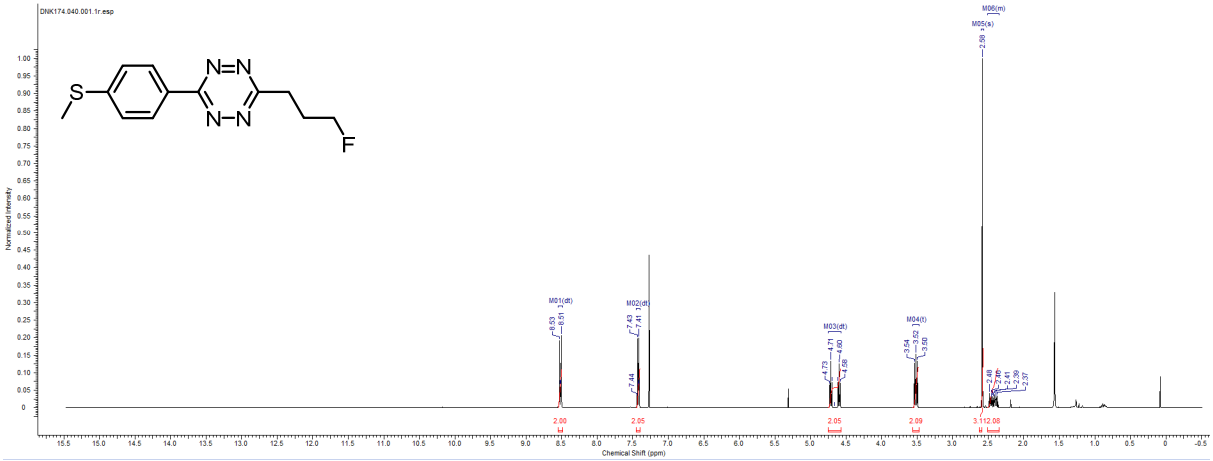

^{13}C Spectrum of compound **6**

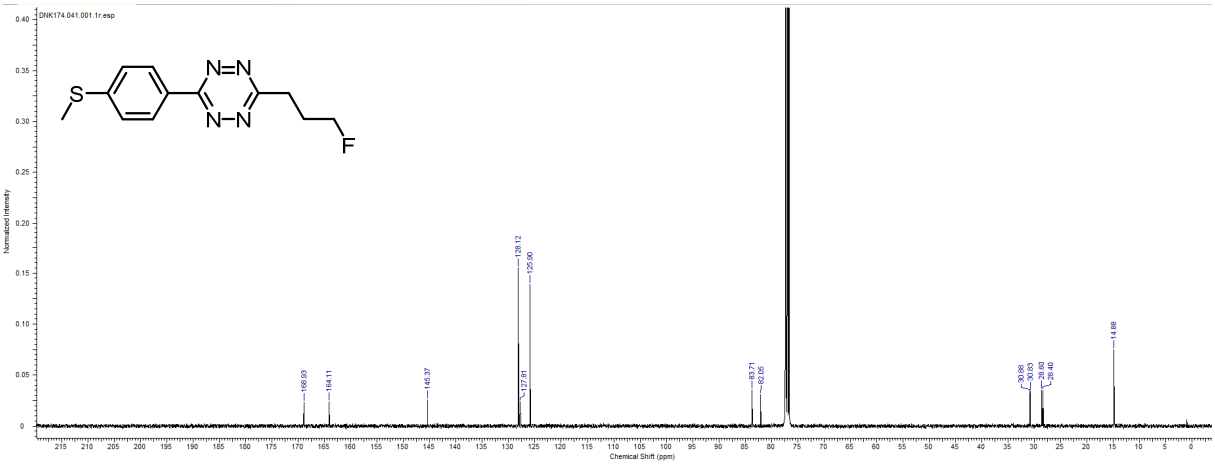

^{19}F Spectrum of compound **6**

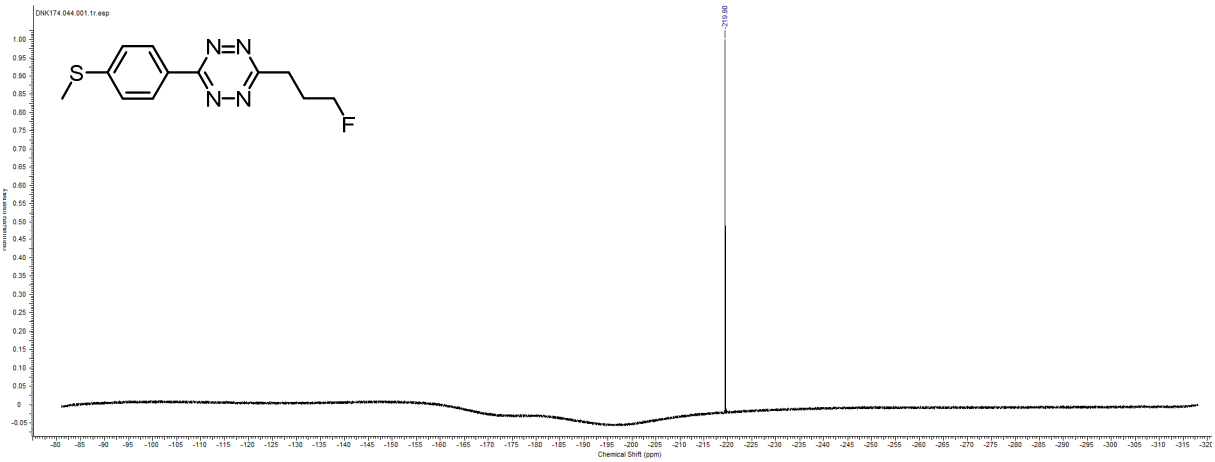

^{1}H Spectrum of compound **7**

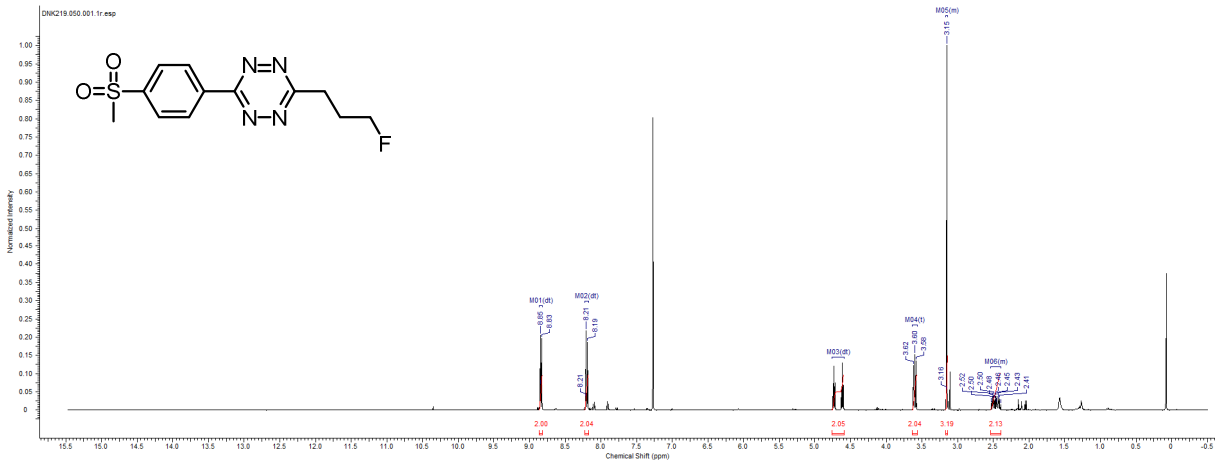

^{13}C Spectrum of compound **7**

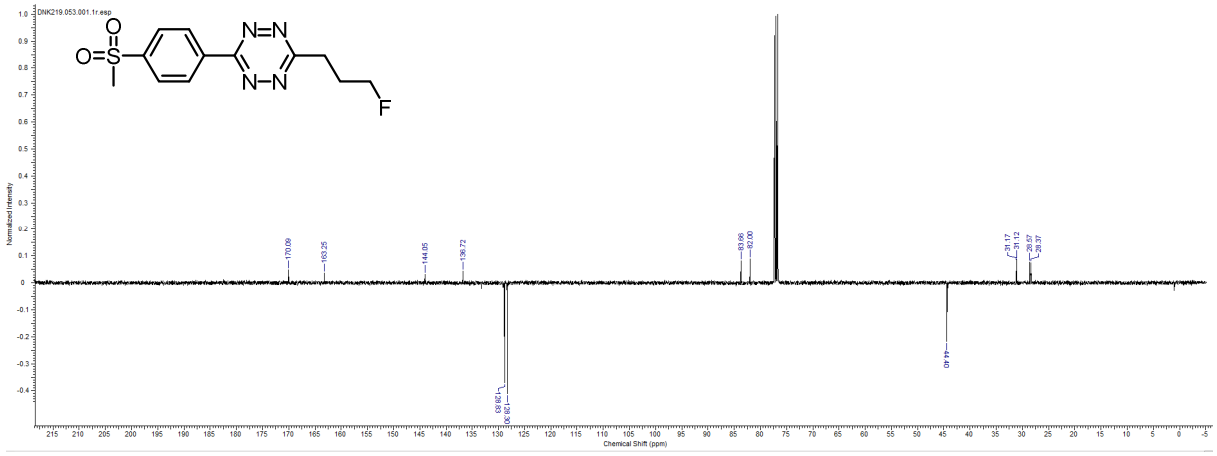

^{19}F Spectrum of compound **7**

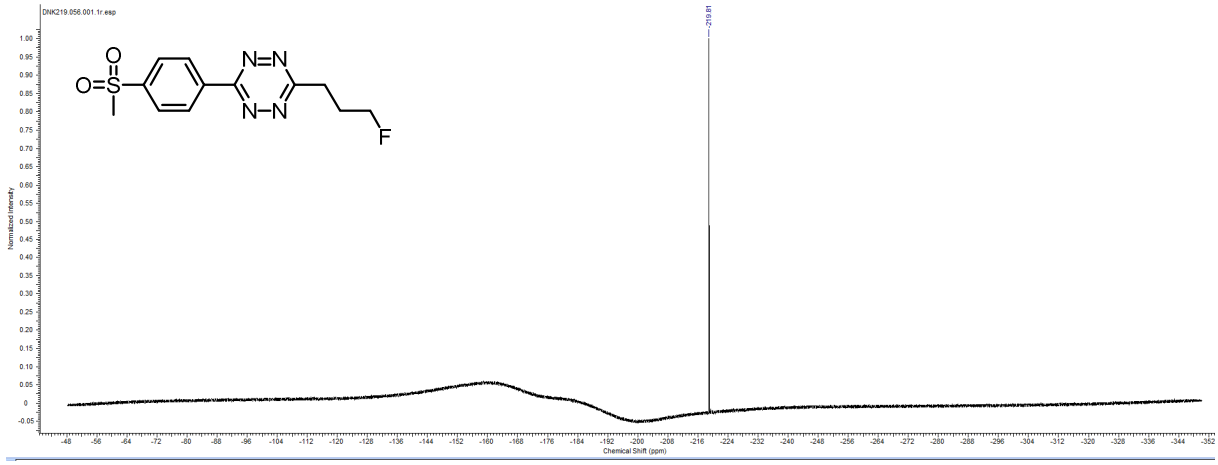

^{1}H Spectrum of compound **8**

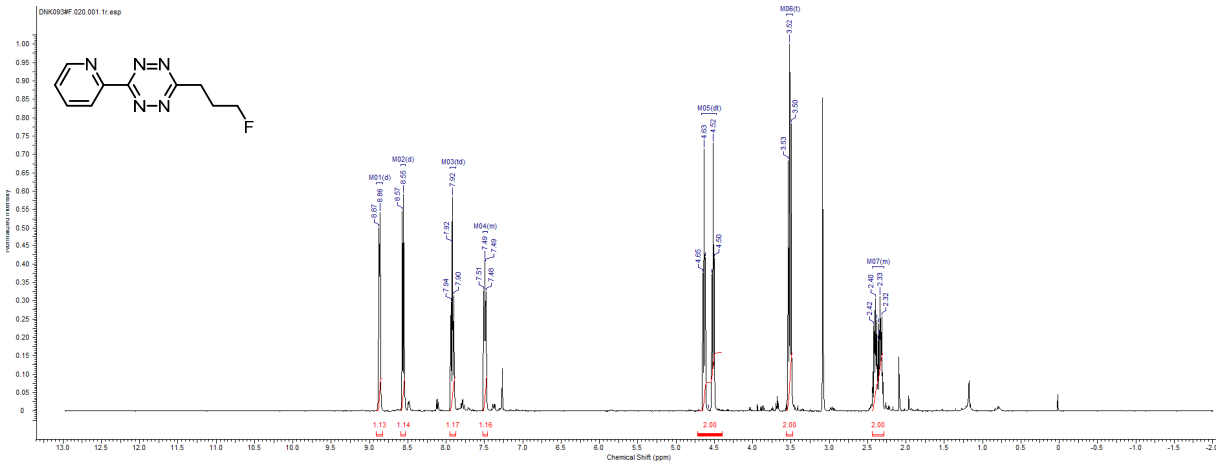

^{13}C Spectrum of compound **8**

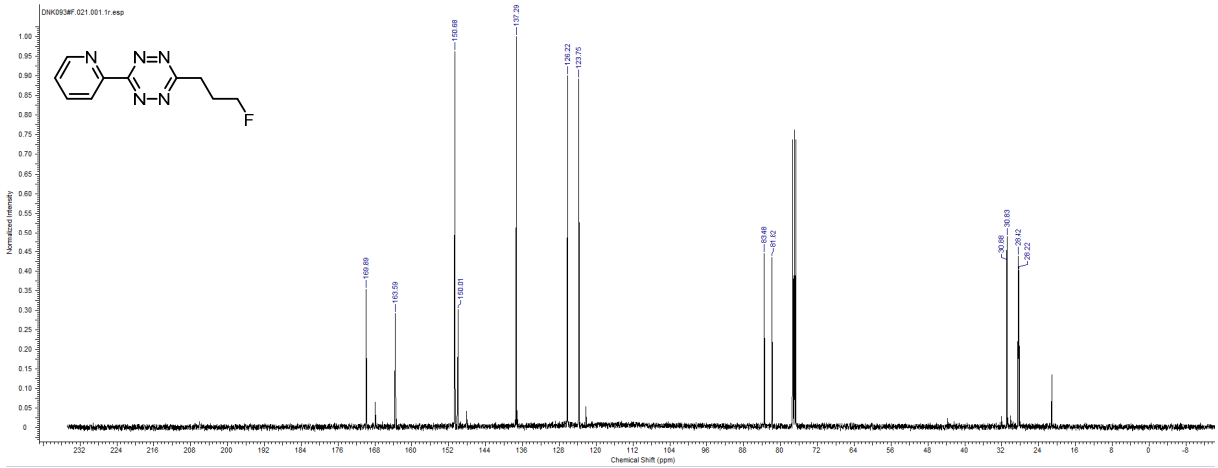

^{19}F Spectrum of compound **8**

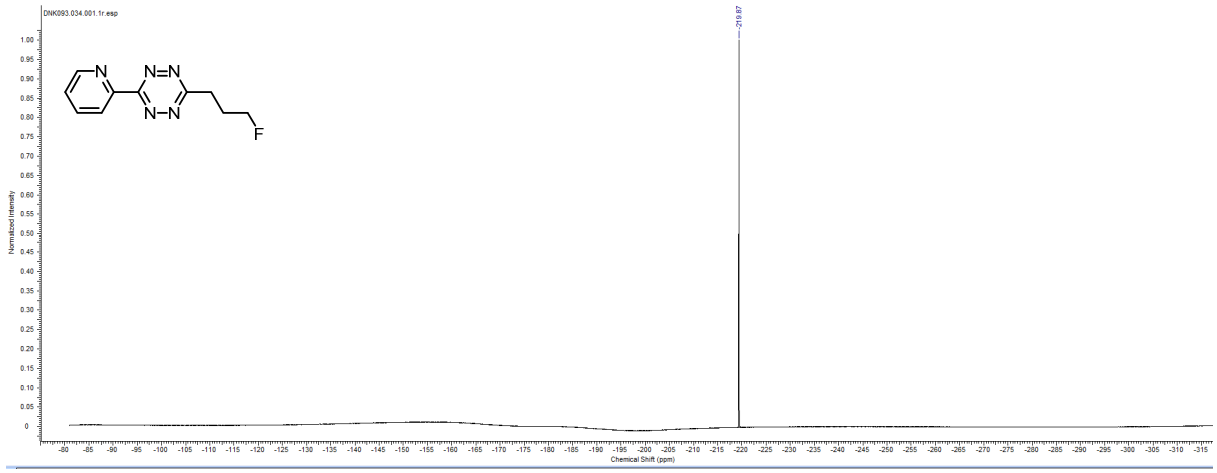

^{1}H Spectrum of compound **9**

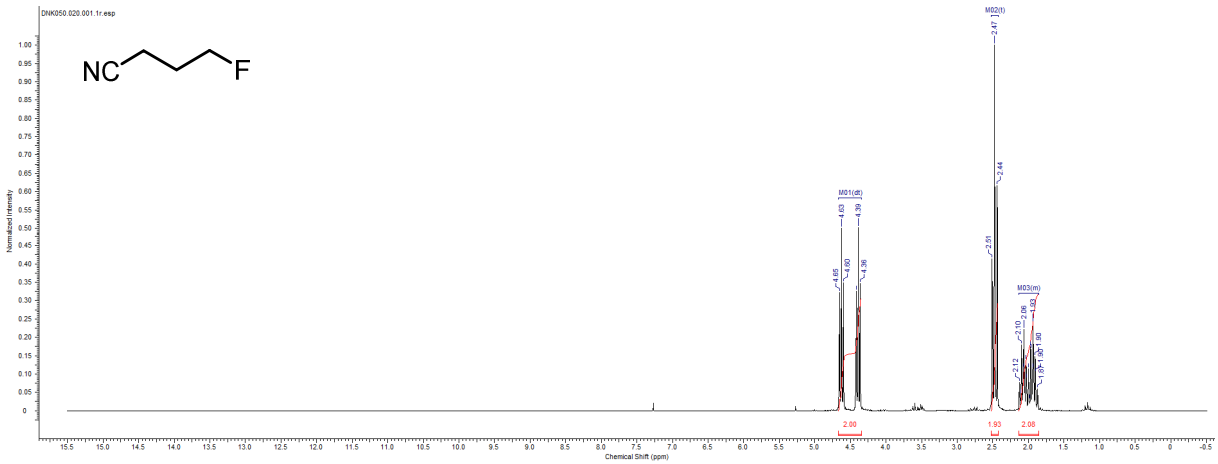

^{13}C Spectrum of compound **9**

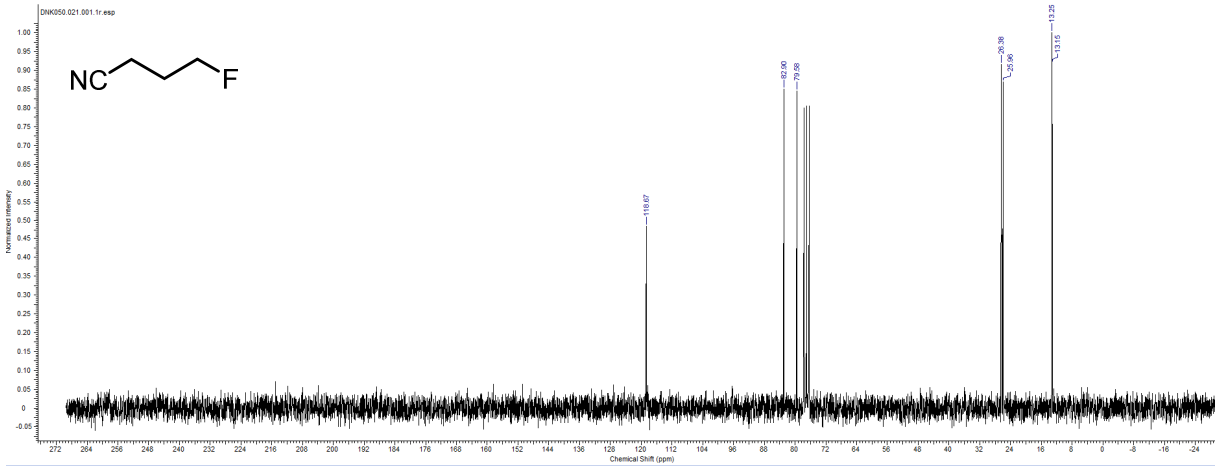

^{1}H Spectrum of compound **11**

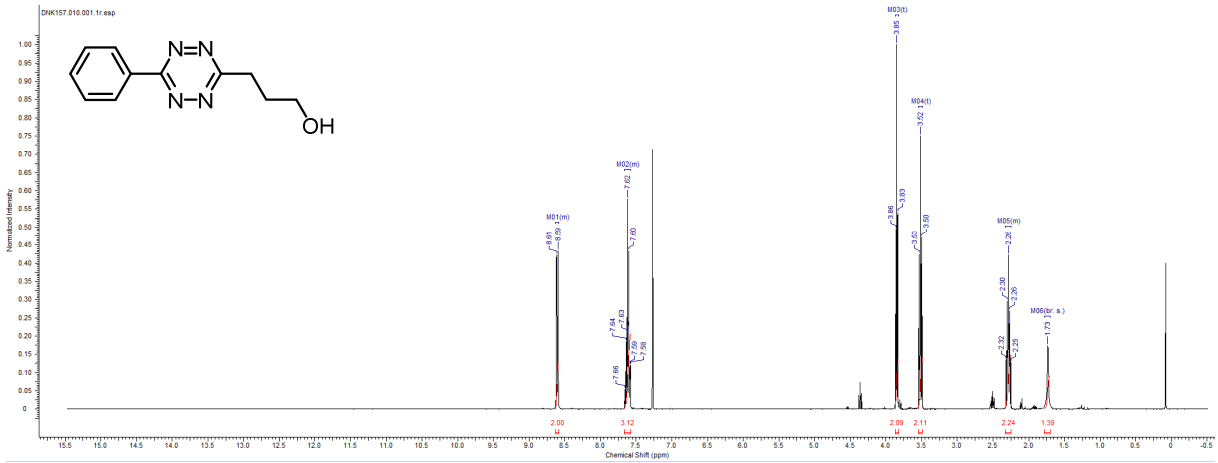

^{13}C Spectrum of compound **11**

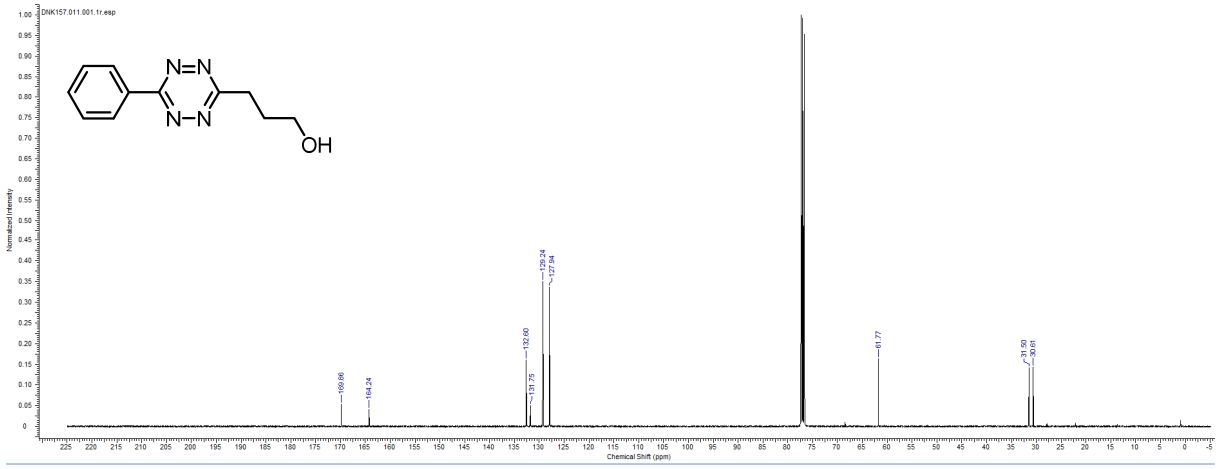

^{1}H Spectrum of compound **12**

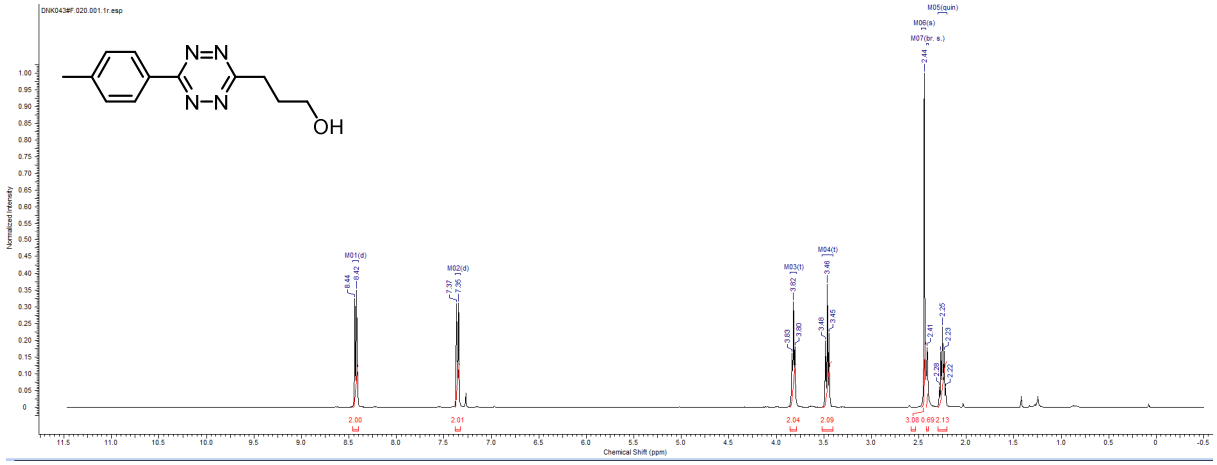

^{13}C Spectrum of compound **12**

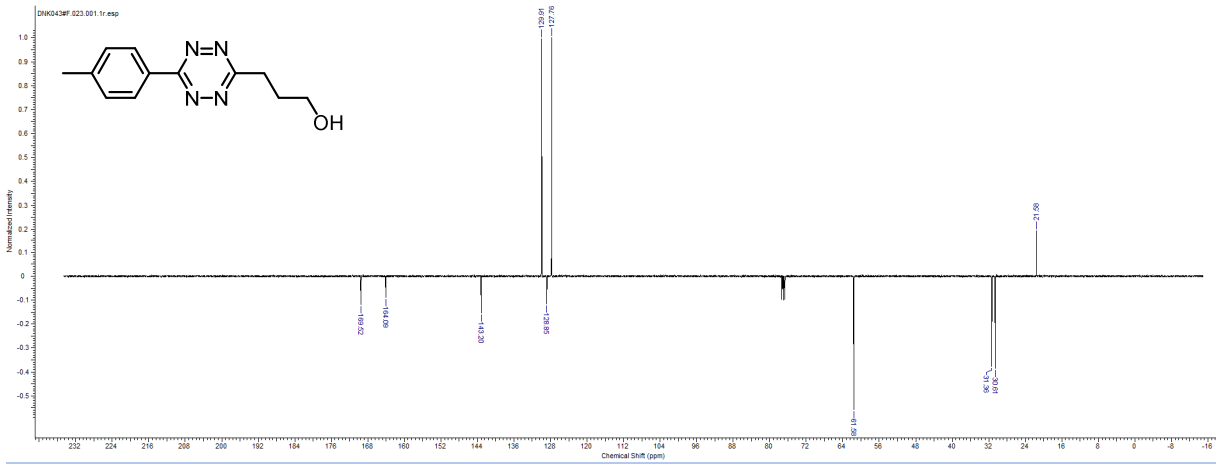

^{1}H Spectrum of compound **13**

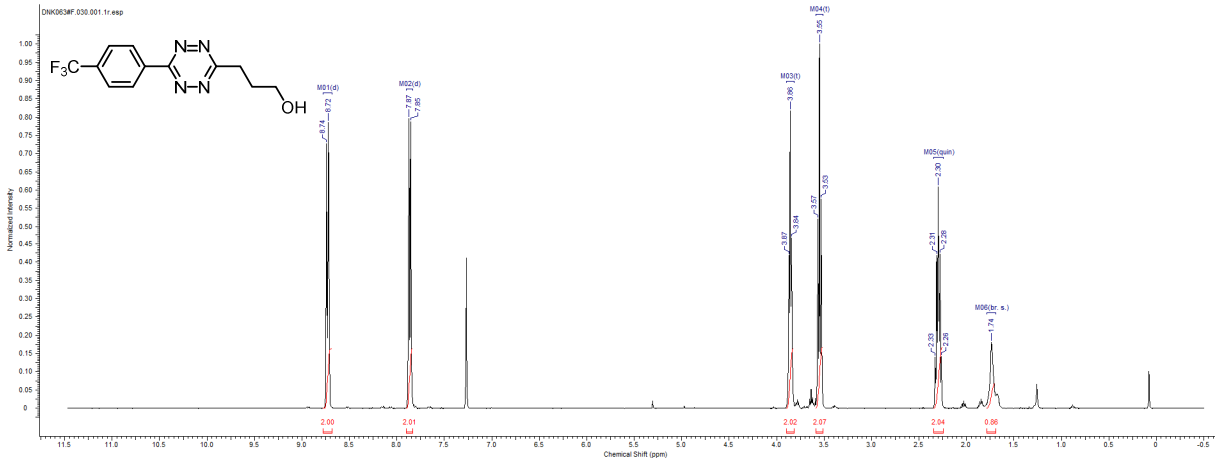

^{13}C Spectrum of compound **13**

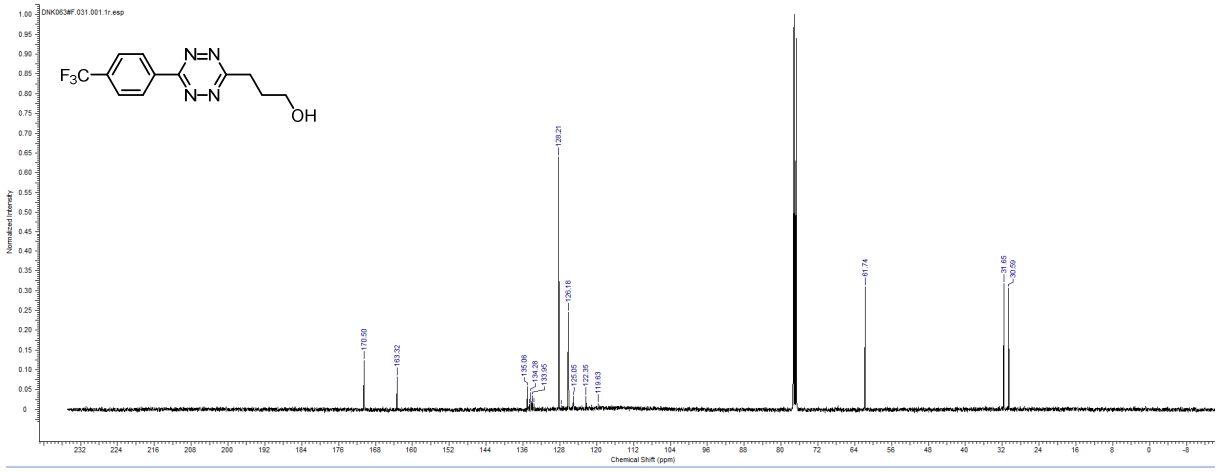

^{19}F Spectrum of compound **13**

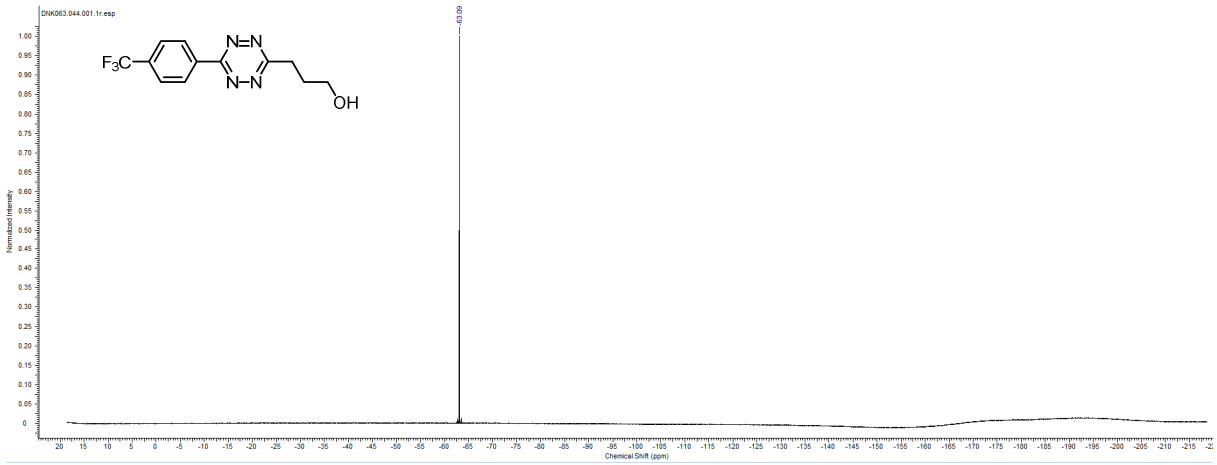

^{1}H Spectrum of compound **14**

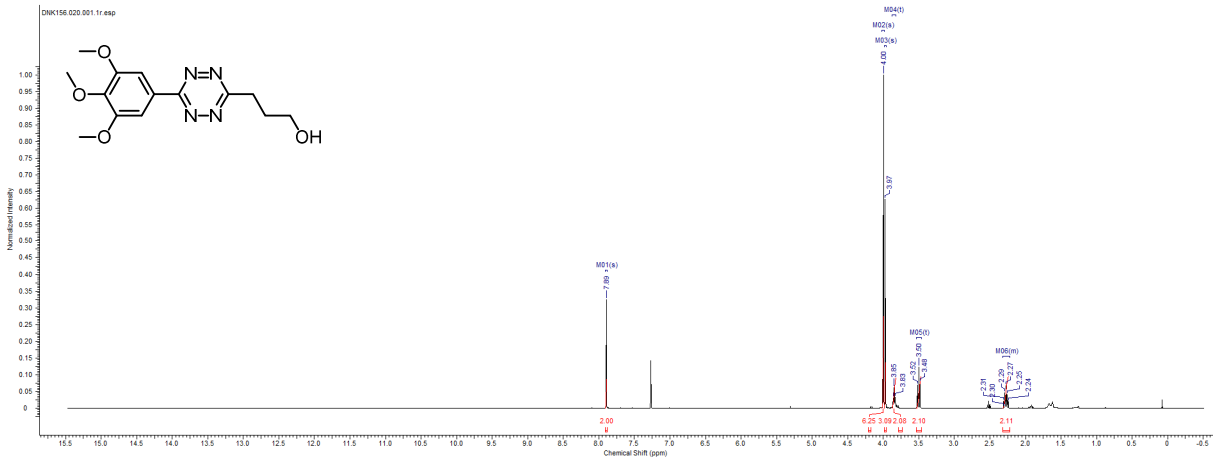

^{13}C Spectrum of compound **14**

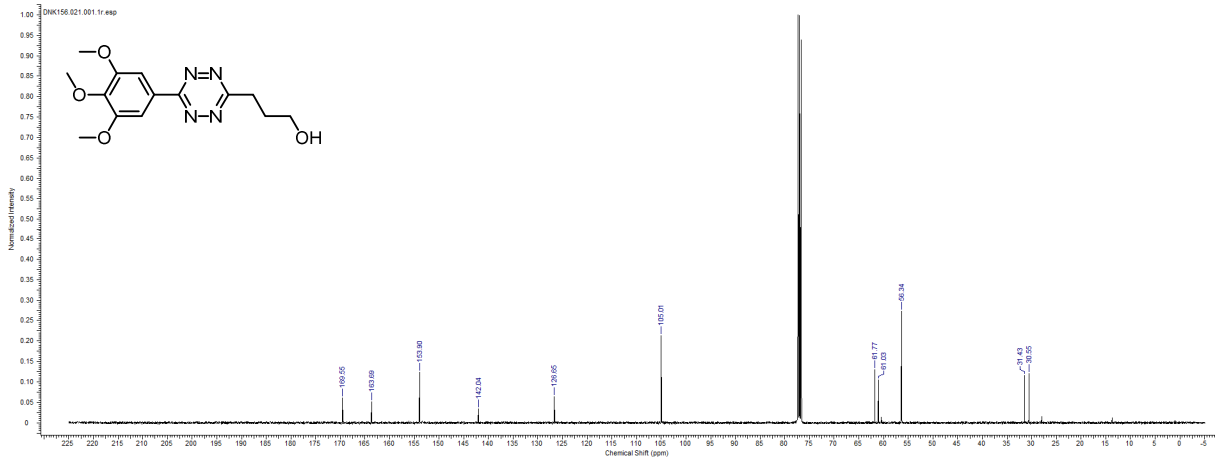

^{1}H Spectrum of compound **15**

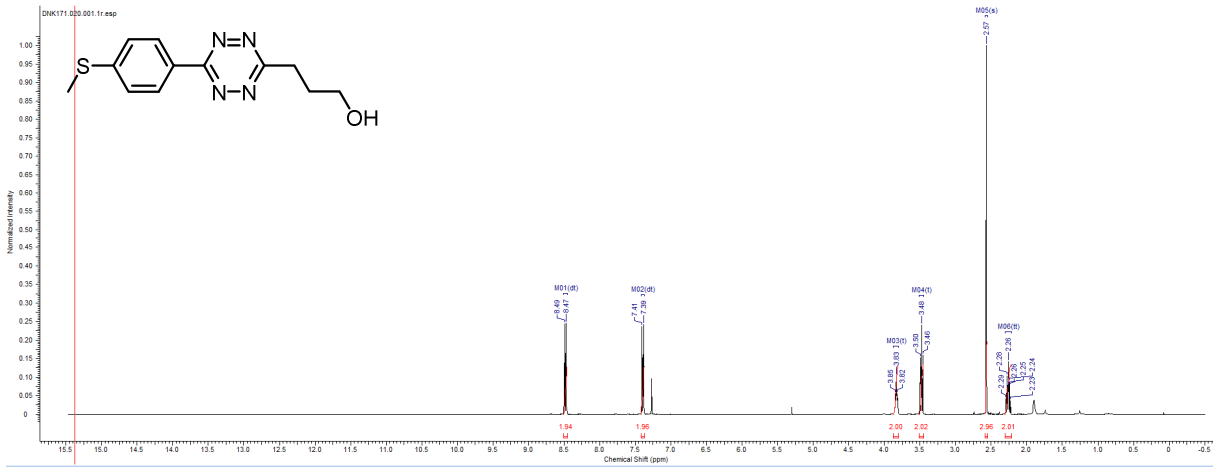

^{13}C Spectrum of compound **15**

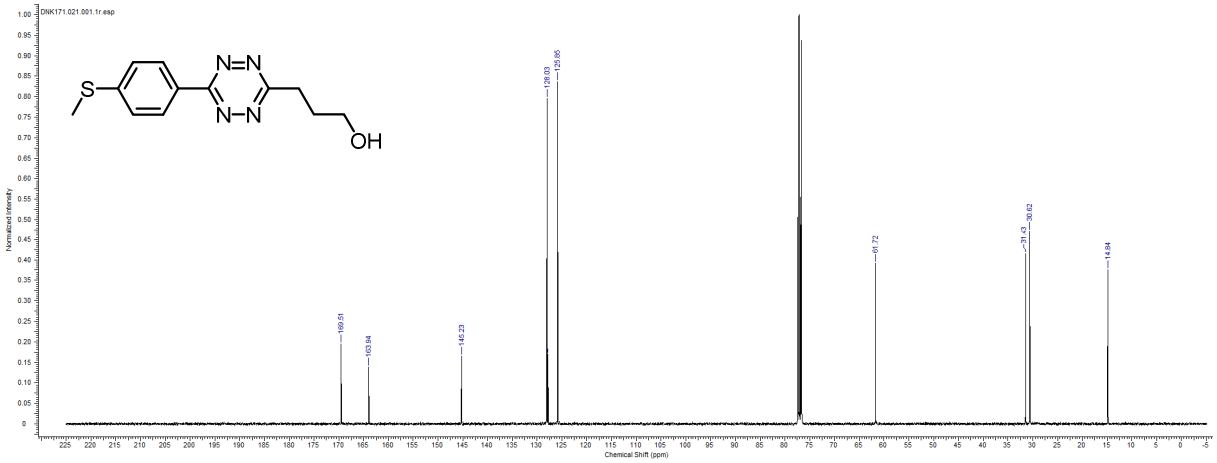

^{1}H Spectrum of compound **16**

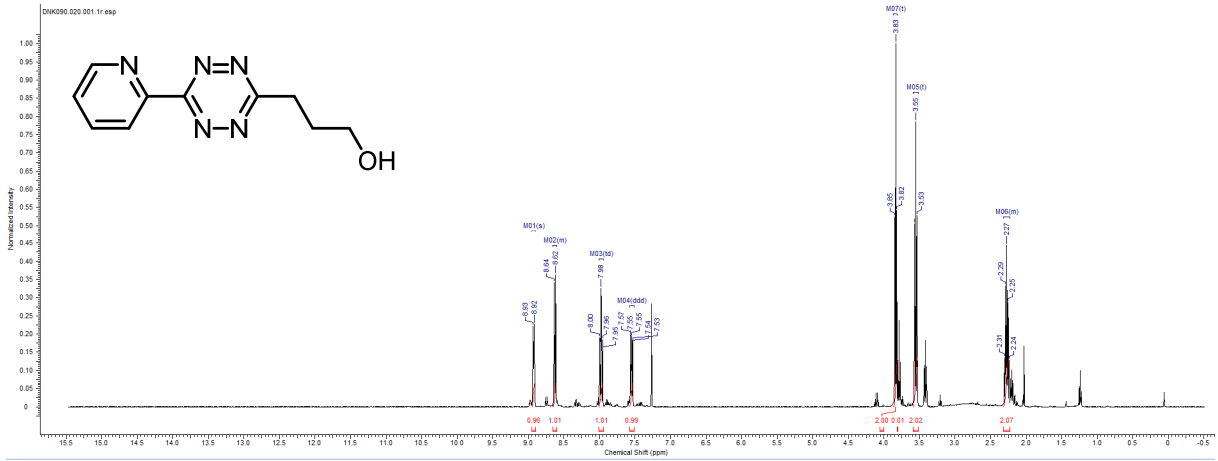

^{13}C Spectrum of compound **16**

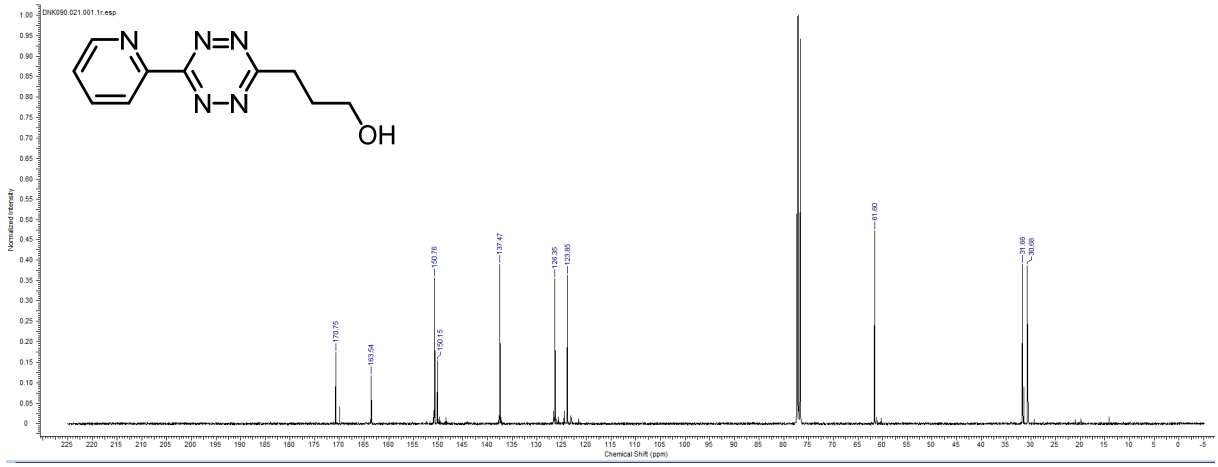

^{1}H Spectrum of compound **17**

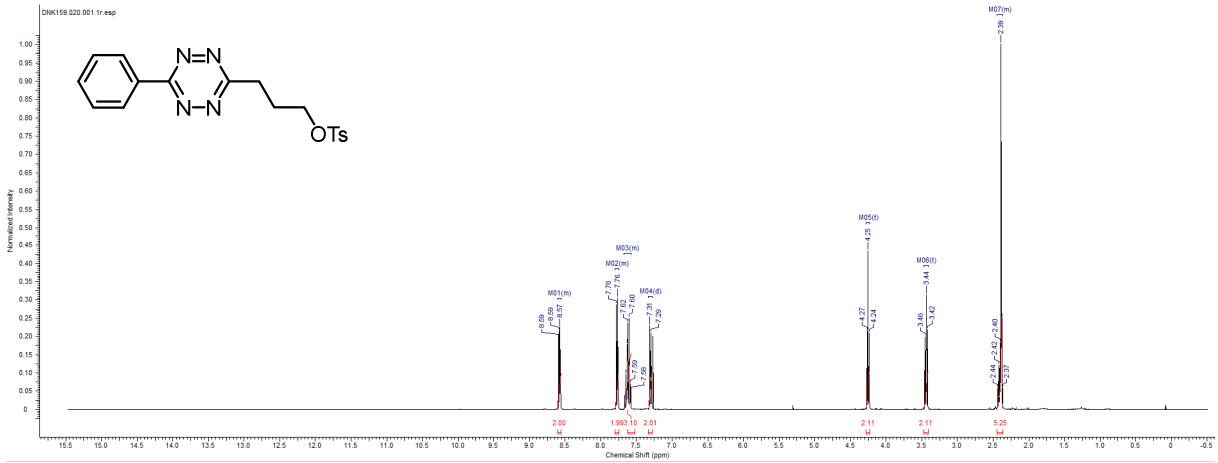

^{13}C Spectrum of compound **17**

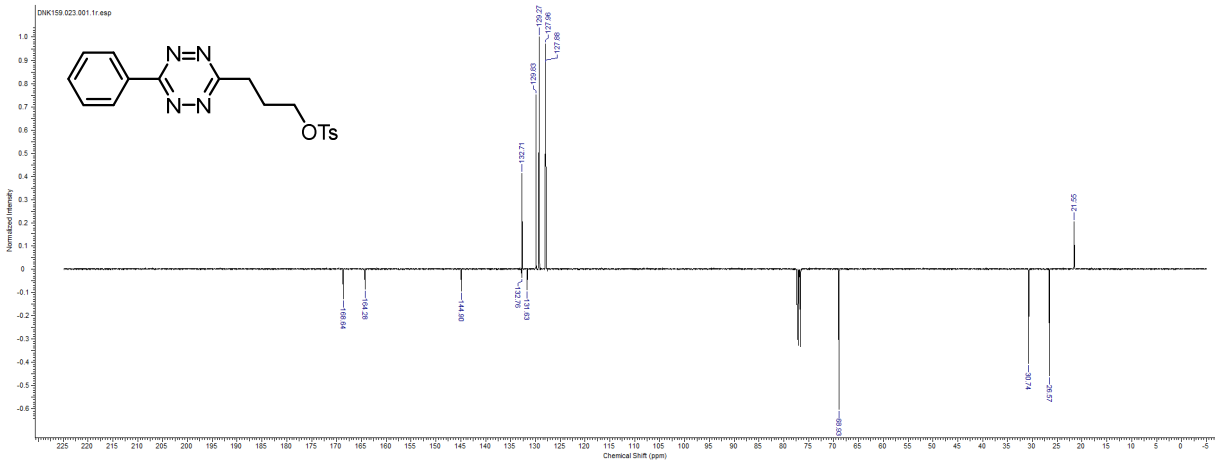

^{1}H Spectrum of compound **18**

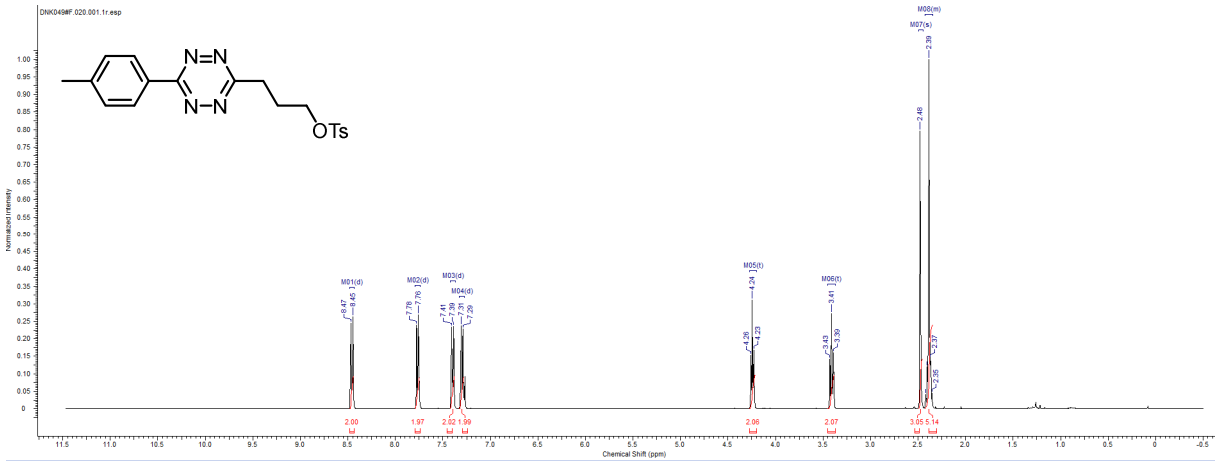

^{13}C Spectrum of compound **18**

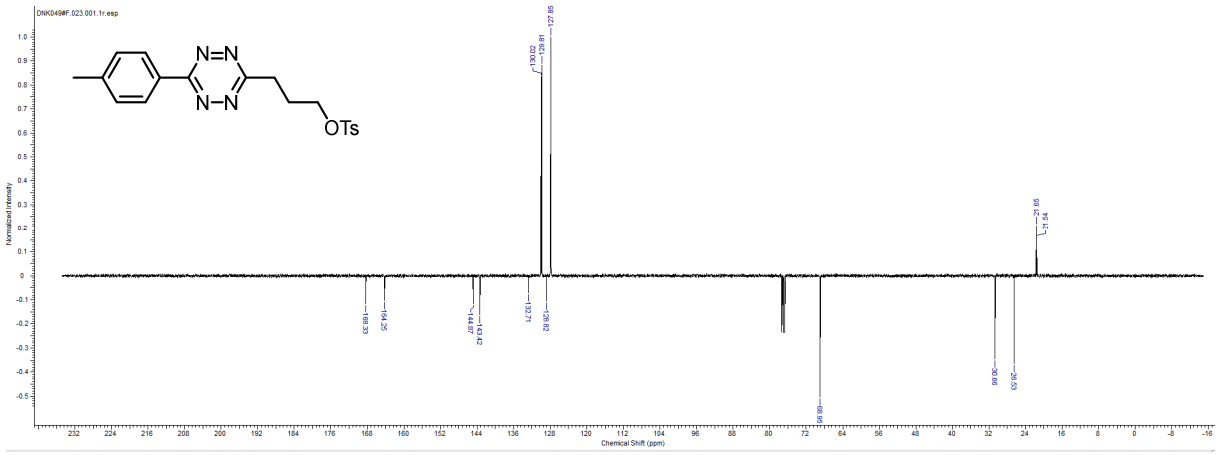

^{1}H Spectrum of compound **19**

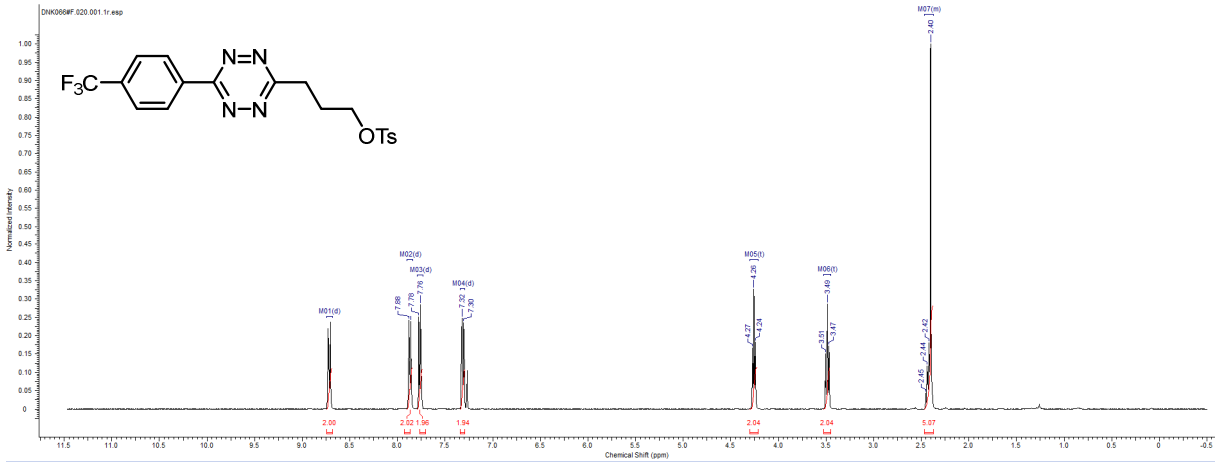

^{13}C Spectrum of compound **19**

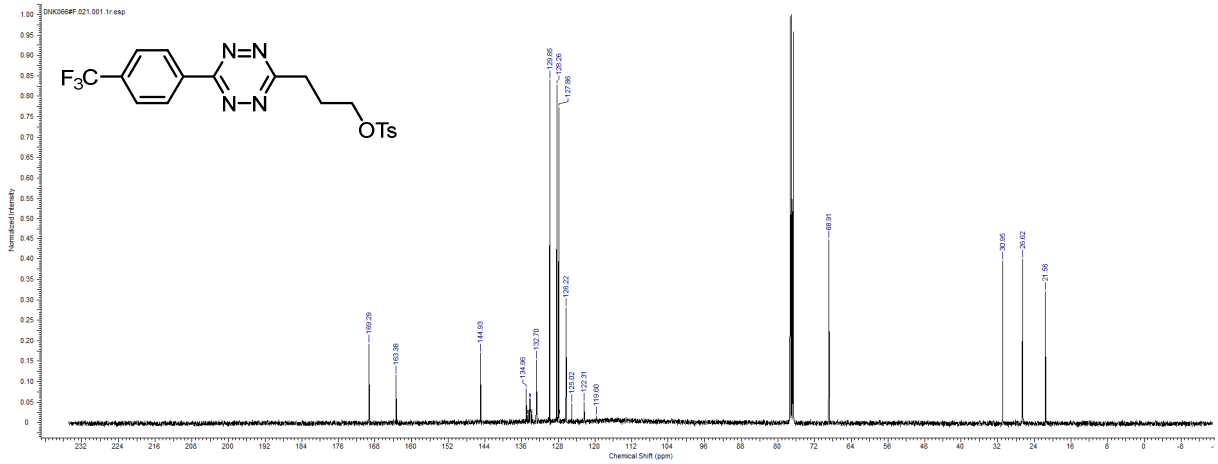

^{1}H Spectrum of compound **20**

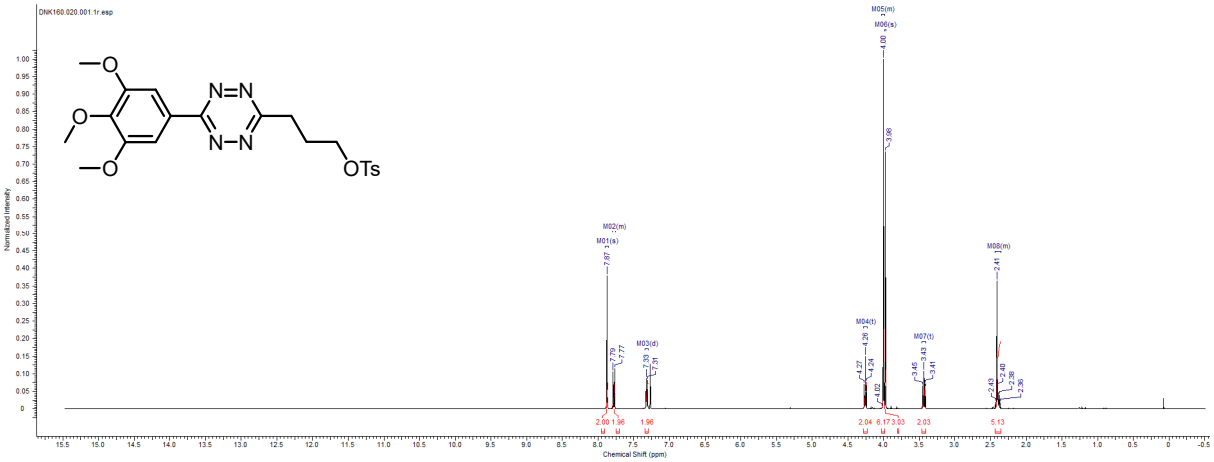

^{13}C Spectrum of compound **20**

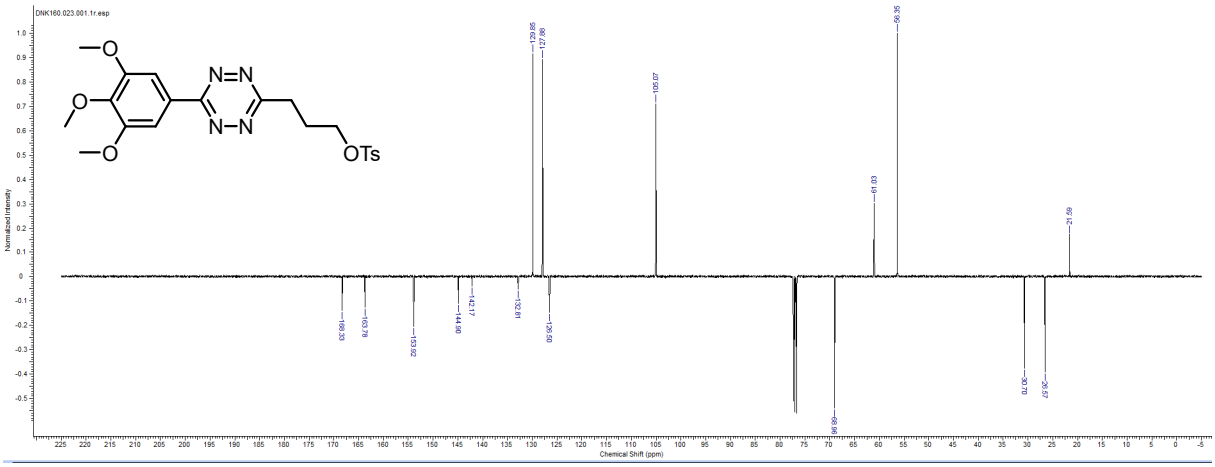

^{1}H Spectrum of compound **21**

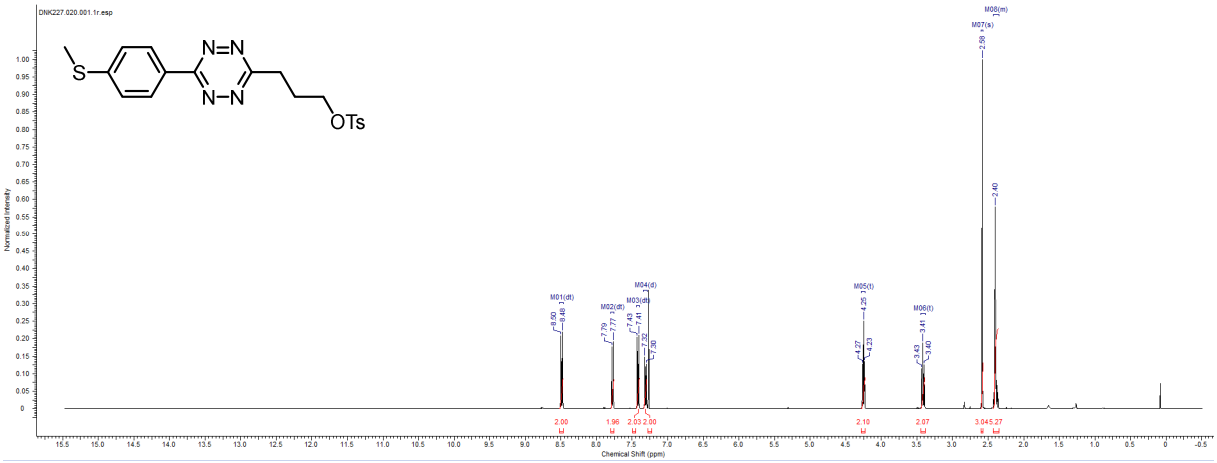

^{13}C Spectrum of compound **21**

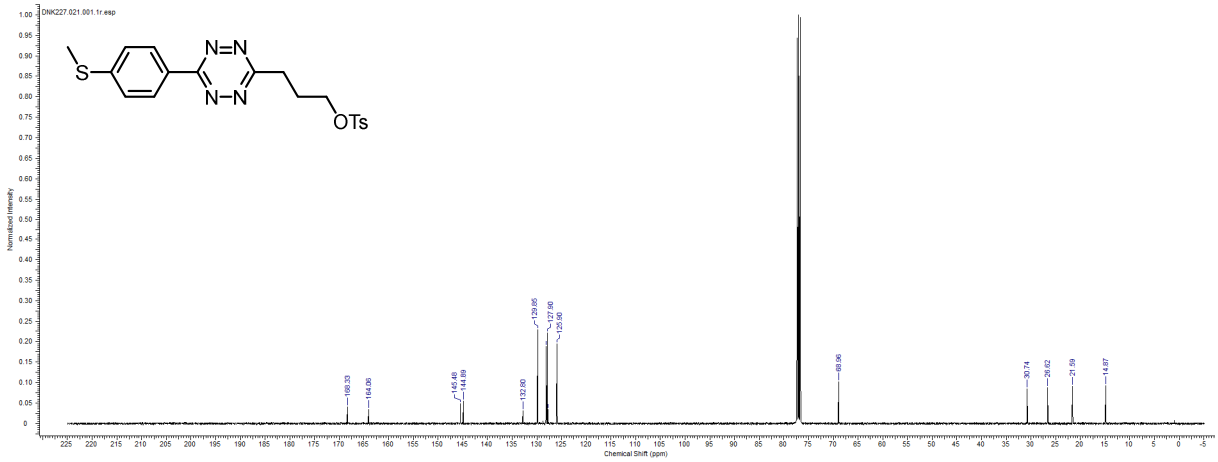

^{1}H Spectrum of compound **22**

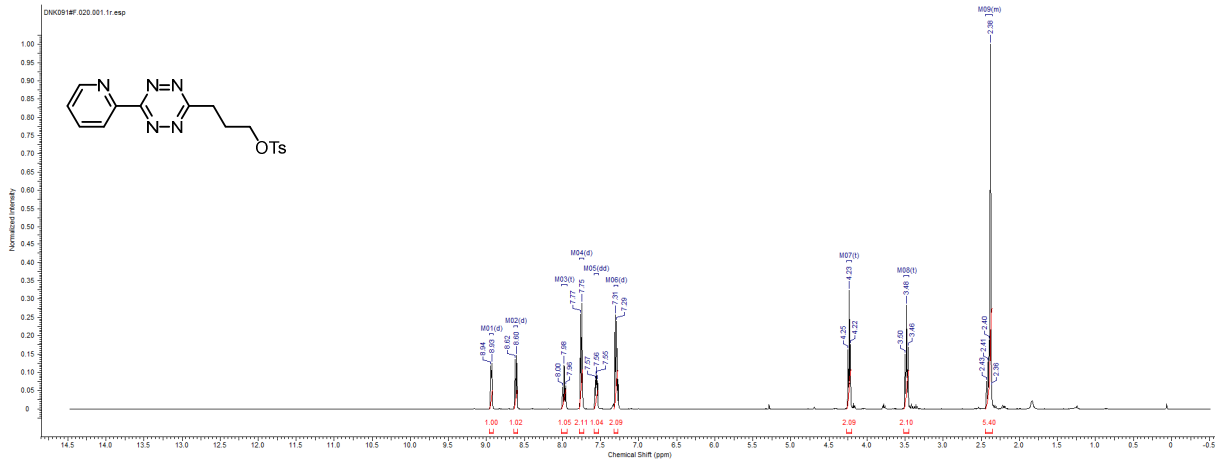

^{13}C Spectrum of compound **22**

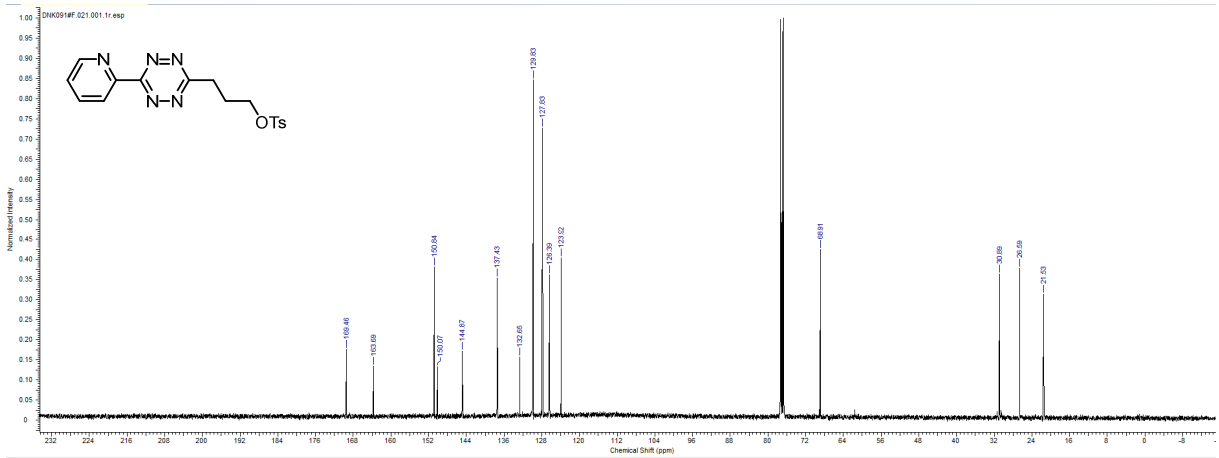

^{1}H Spectrum of compound **23**

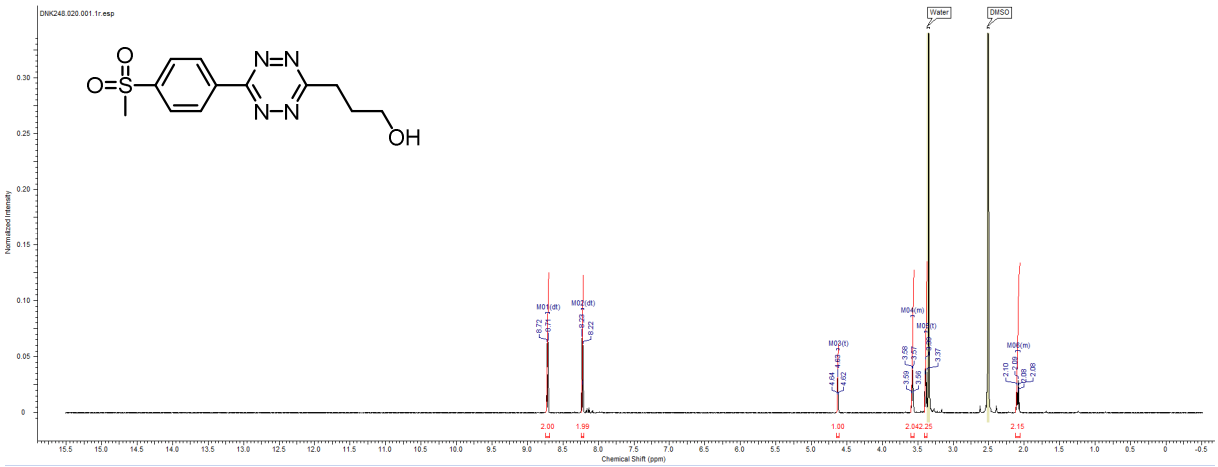

^{13}C Spectrum of compound **23**



^{1}H Spectrum of compound **24**

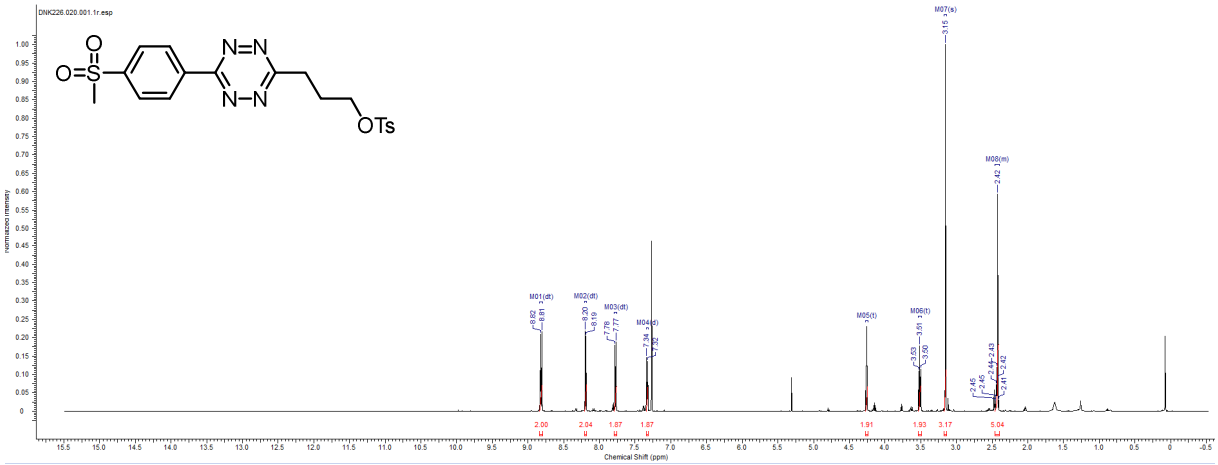

^{13}C Spectrum of compound **24**

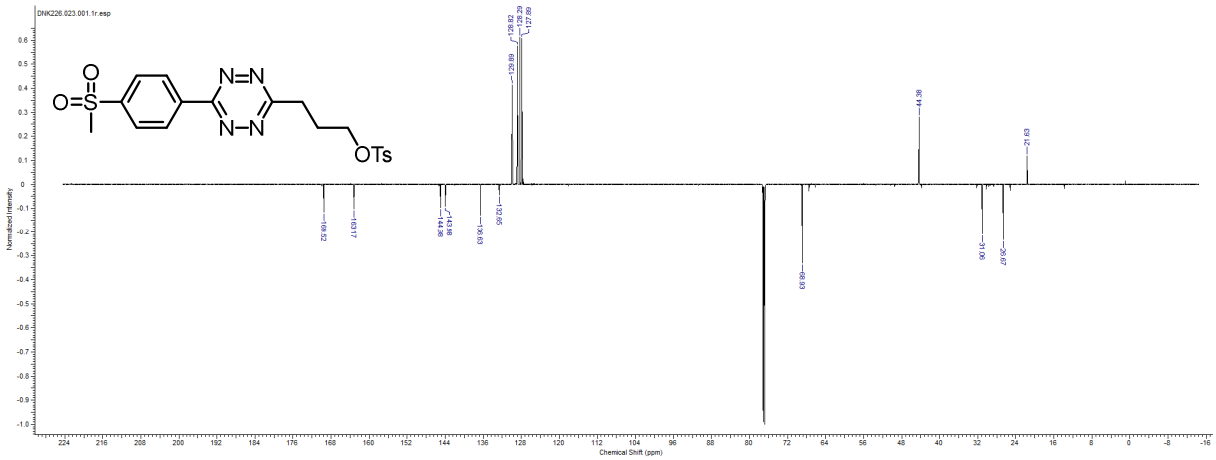

^{1}H Spectrum of compound **25**

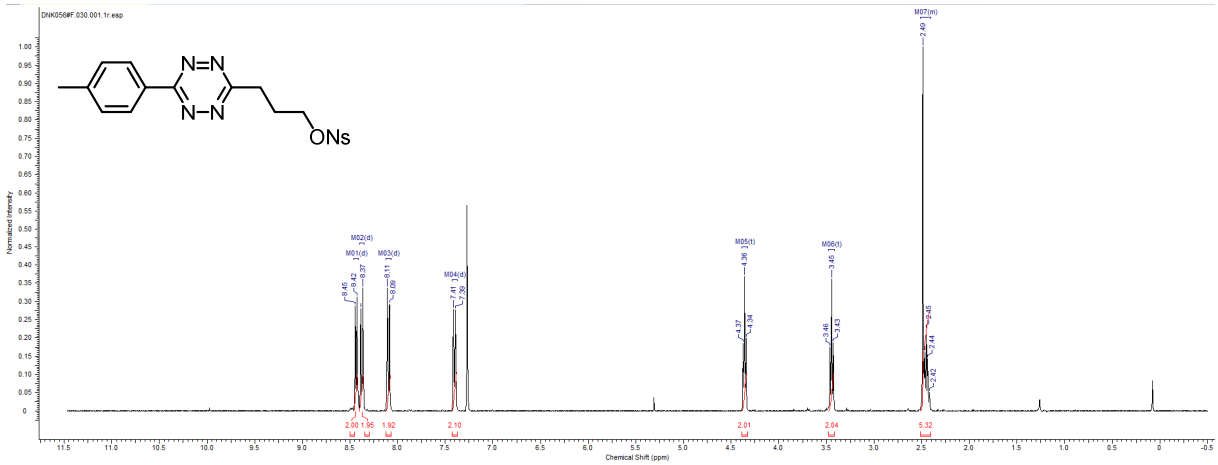

^{13}C Spectrum of compound **25**

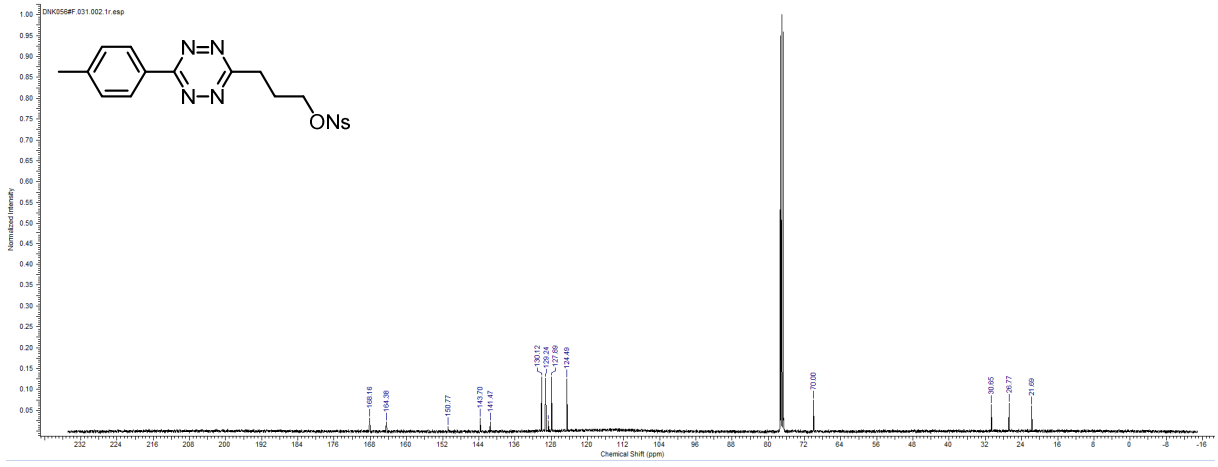

^{1}H Spectrum of compound **26**

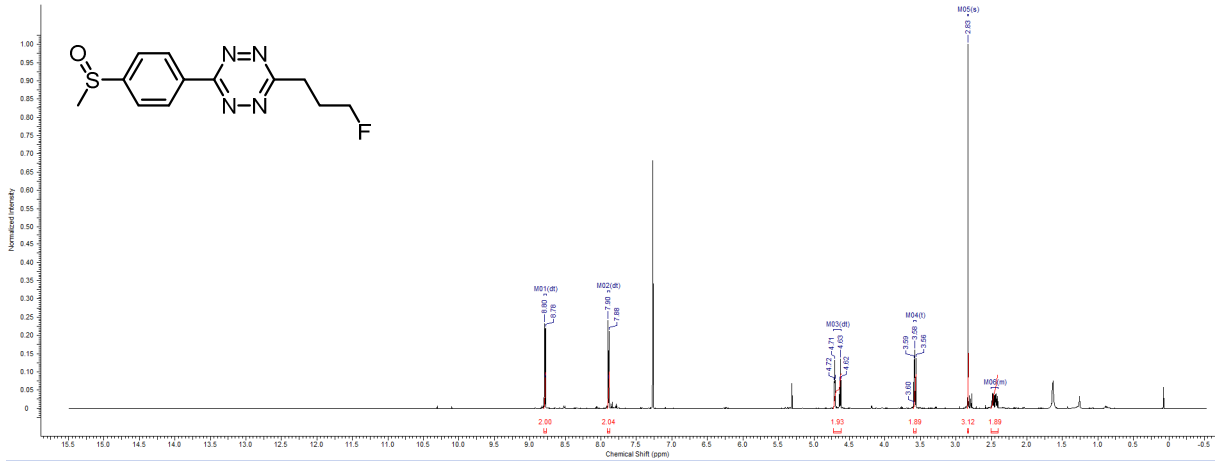

^{13}C Spectrum of compound **26**

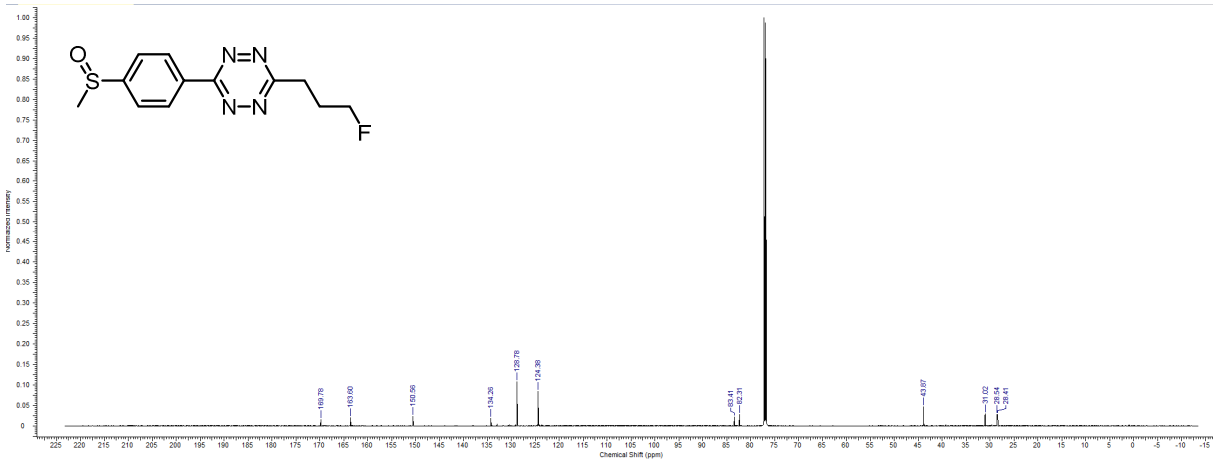

^{19}F Spectrum of compound **26**

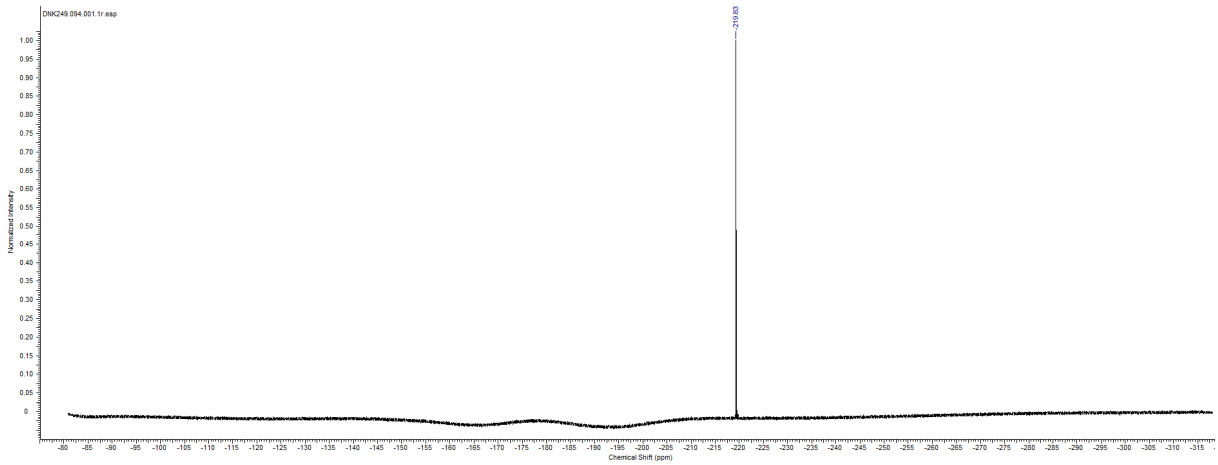

3. HPLC Data

Chromatogram of **2** (254 nm, HPLC conditions A)

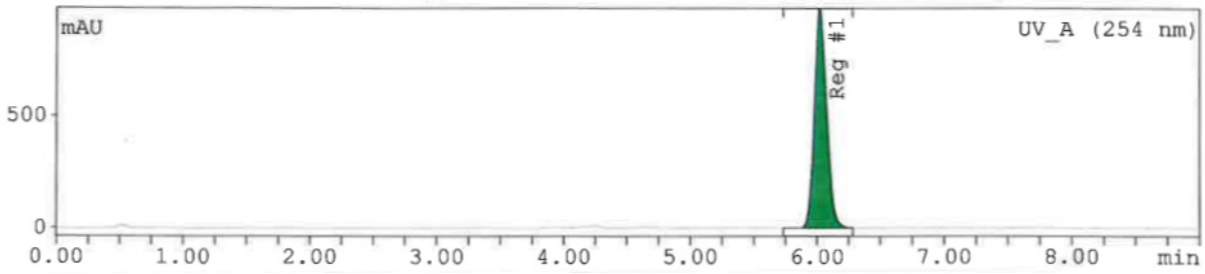

Radio-Chromatogram of [^{18}F]**2** (HPLC conditions A)

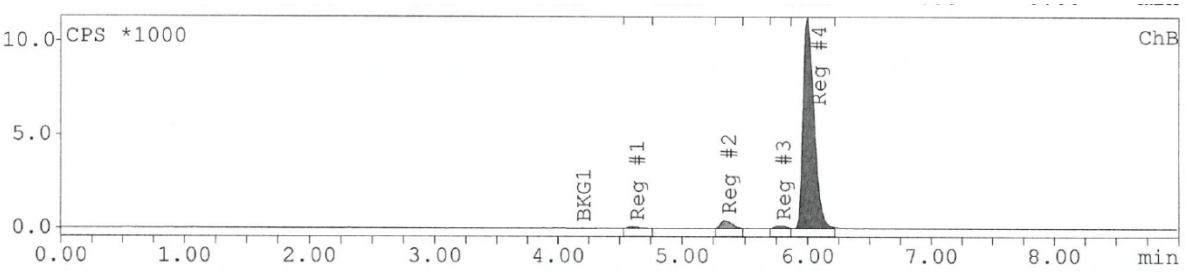

Chromatogram of **3** (540 nm, HPLC conditions B)

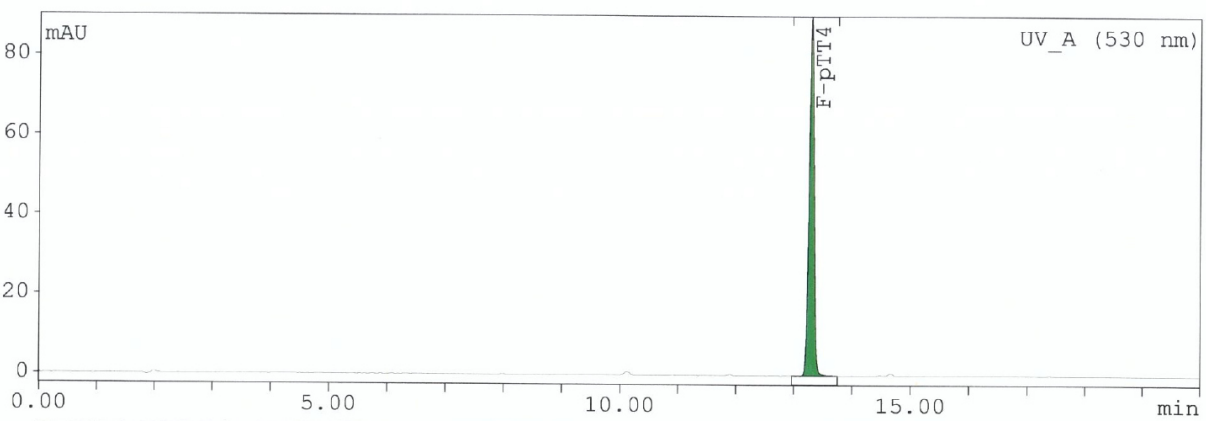

Radio-Chromatogram of [^{18}F]**3** (HPLC conditions B)

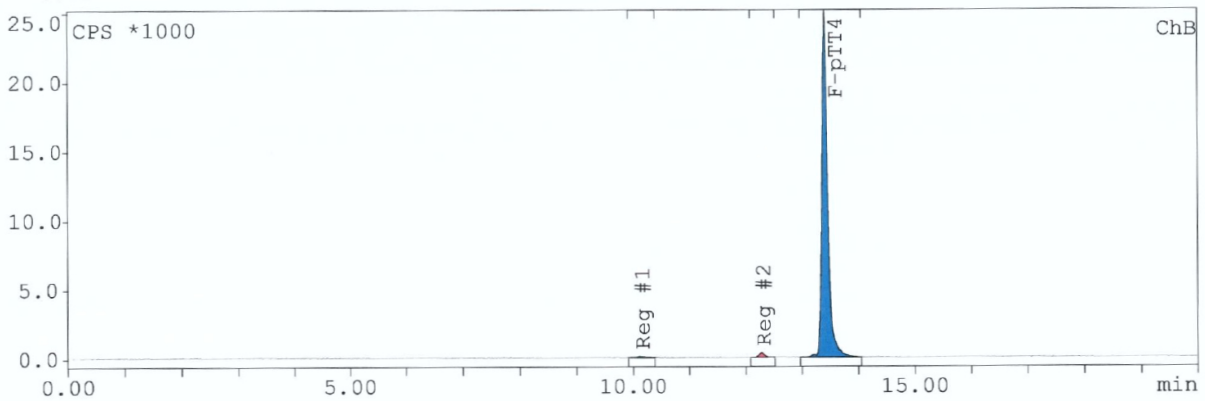

Chromatogram of **5** (254 nm, HPLC conditions A)

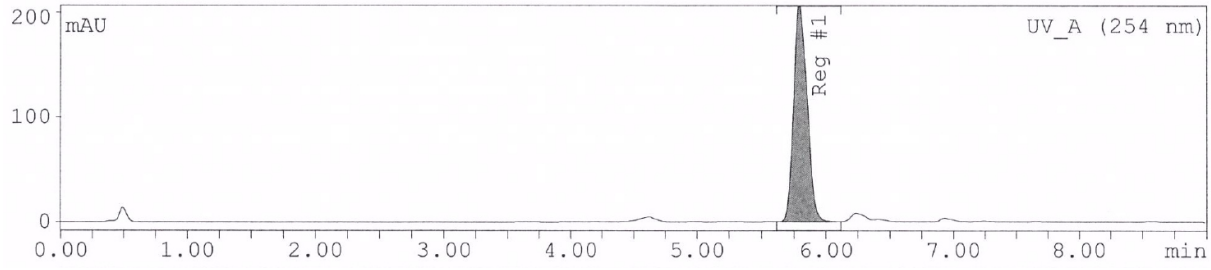

Radio-Chromatogram of [^{18}F]**5** (HPLC conditions A)

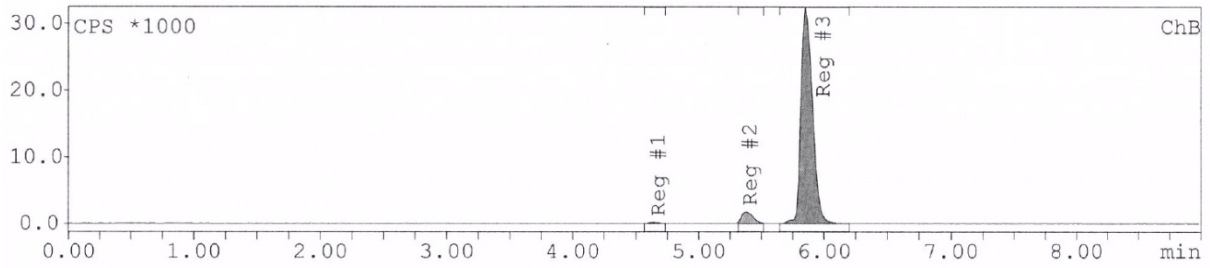

Chromatogram of **6** (254 nm, HPLC conditions A)

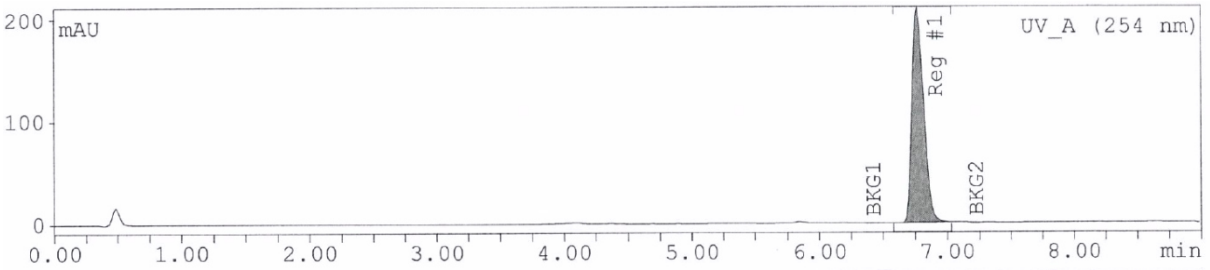

Radio-Chromatogram of [^{18}F]**6** (HPLC conditions A)

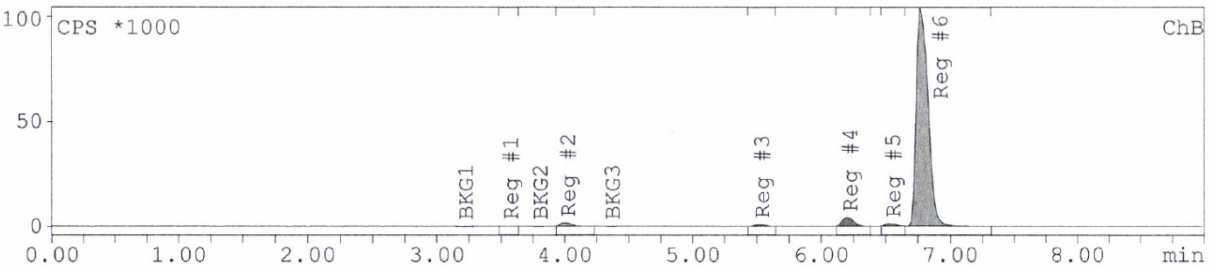

Chromatogram of **7** (254 nm, HPLC conditions A)

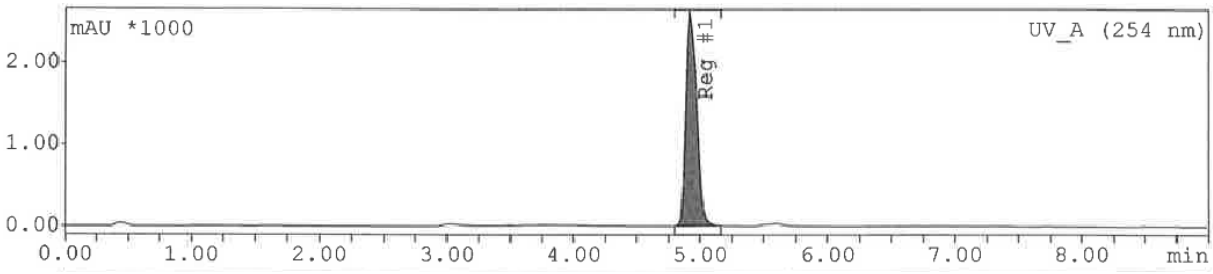

Radio-Chromatogram of [^{18}F]**7** (HPLC conditions A)

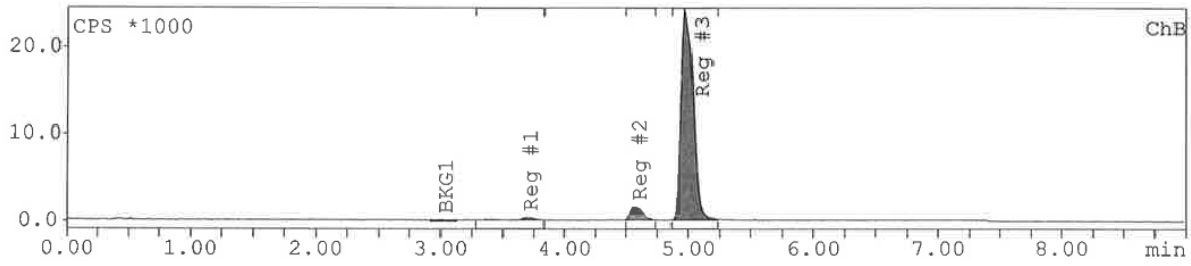

4. Determination of Specific Activity

The specific activity of [^{18}F]**2**, [^{18}F]**6** and [^{18}F]**7** was determined by injection of a dilution series of authentic standard materials into the analytical HPLC system in combination with UV-detection (254 nm). A sample of the radiotracer preparation was also injected into the same HPLC system. Linear regression was used, and the linear equation was furthermore employed to calculate the concentration of according tetrazine in the radiotracer preparation. Radioactivity in a aliquot (1 ml) of the radiotracer preparation was furthermore determined in a Capintec CRC-15 dose calibrator. The specific activity is expressed in GBq/µmol.

[^{18}F]**2**

Concentration	Response
[mmol/ml]	[mAu*s]
0,000458211	6641
4,58211E-05	701,3
4,58211E-06	66,72
0	0

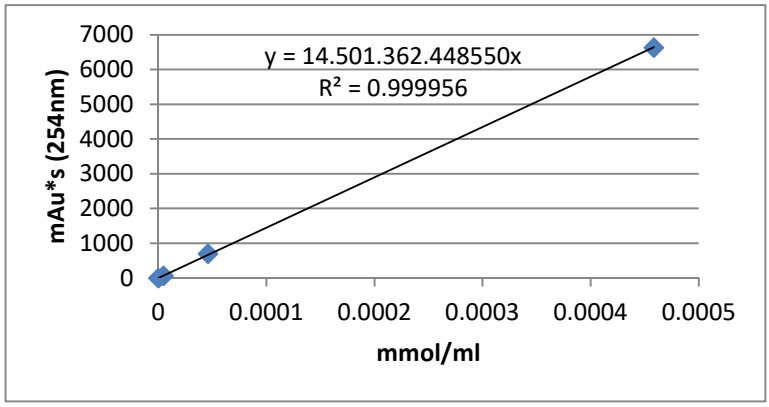

Detector response sample : 74.94 mAu*s

Activity Concentration : 511.7 MBq/ml

Specific activity : 99.0 GBq/µmol

[^{18}F]**6**

Concentration	Response
[mmol/ml]	[mAu*s]
0,000378329	1333,1
3,78329E-05	146,42
3,78329E-06	14,475
0	0

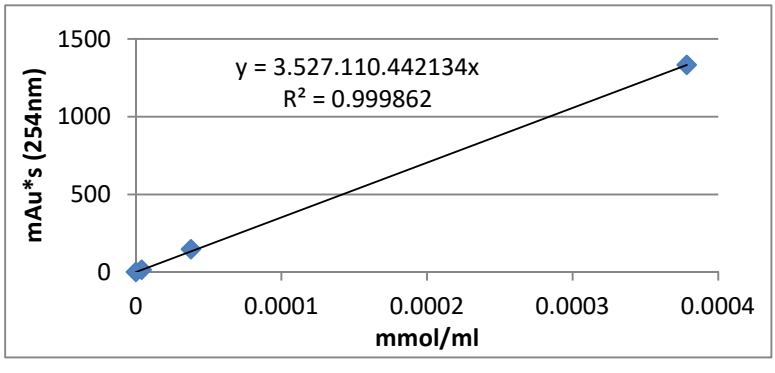

Detector response sample : 12.226 mAu*s

Activity Concentration : 795.5 MBq/ml

Specific activity : 229 GBq/µmol

[^{18}F]**7**

Concentration	Response
[mmol/ml]	[mAu*s]
0,00149838	16116,96667
0,00074919	8284,593333
0,000149838	1670,5
0	0

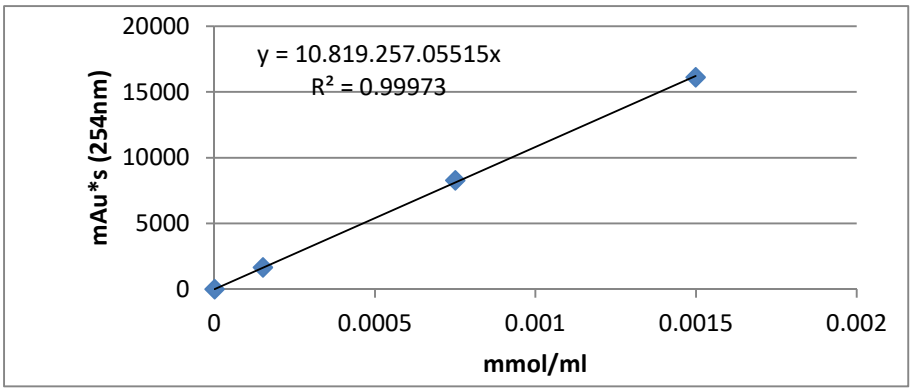

Detector response sample : 73.54 mAu*s

Activity Concentration : 381.8 MBq/ml

Specific activity : 56.2 GBq/µmol

5. Kinetic Measurements

Reaction rates of the Tetrazine ligation between *trans*-Cyclooctene (**10**) and tetrazines **1-8** and **26** in 1,4-dioxane were determined using a SX20 stopped flow spectrophotometer system (Applied Photophysics, Surrey, UK) equipped with a 535 nm LED light source. Pseudo first order conditions were used. An approximately 4 mM solution of **10** as well as an approx. 0.1 mM solution of the corresponding tetrazine were prepared in anhydrous 1,4-dioxane (Note: for correct measurements it is of utmost importance to use anhydrous 1,4-dioxane, since even small amounts of water will accelerate the reaction, leading to irreproducible data). These solutions were loaded into the driver syringes and equal volumes of both solutions were mixed, resulting in concentrations of approx. 2 mM and 0.05 mM respectively. The reaction progress was followed by measuring the absorption around 535 nm. Measurements were performed in sixtuplicates at 25 ± 0.16 °C, 37 ± 0.16 °C and 50 ± 0.16 °C. Observed reaction konstants (k_{obs}) were determined by non-linear regression (one-phase-decay) using Prism 6 (Graphpad) and second order rate constants were calculated from k_{obs}. Table S1shows k_{obs}, k as well as thermodynamic data for all observed reactions. Original data from stopped flow measurements is attached in the last part of this section.

Furthermore relative reaction values (RRVs) were assigned, which allows for easy comparison of reactivity of different tetrazines. We propose using reaction rates determined in anhydrous 1,4-dioxane at 25, 37 and 50 °C with TCO **10** and comparing them to the rates of tetrazine **1**. RRVs can be calculated as described in Formula S1.

$$RRV = \frac{\frac{k_{25°C}}{1.1077} + \frac{k_{37°C}}{1.5713} + \frac{k_{50°C}}{2.1962}}{3}$$

Formula S1

Using these RRVs and computational data described in chapter 6 (Supporting Information) we were able to find a good correlation between calculated $\Delta E^{\ddagger}$ (M06-2X/6-311+G(d,p), gas phase) and measured RRVs of alkly-aryl tetrazines **2-8**. This correlation can be used for prediction of RRVs of aryl-alkyl substituted tetrazines using Formula S2, whereas $\Delta E^{\ddagger}$ is the calculated value from M06-2X/6-311+G(d,p) gas phase calculation in kcal/mol.

$$RRV_{predicted} = e^{-0.8273 * \Delta E^{\ddagger} + 1.3728}$$

Formula S2

This was done for tetrazine **26**, where a $\Delta E^{\ddagger}$ value of 0.55 kcal/mol was calculated, which results in a $RRV_{predicted}$ of 2.50. This is in excellent agreement with observed RRV of 2.62.

reaction	k_{obs} [$M^{-1}s^{-1}$]			Initial concentration TCO [mM]	k [$M^{-1}s^{-1}$]			ΔS	ΔH	ΔG^a	RRV
	25°C	37°C	50°C		25°C	37°C	50°C	kcal/(mol*K)	kcal/mol	kcal/mol	
1+10	0.002141 ± 0.000003	0.003037 ± 0.000003	0.004245 ± 0.000021	3.87	1.108 ± 0.002	1.571 ± 0.001	2.196 ± 0.011	-0.0428	4.63	17.39	1.00
2+10	0.003280 ± 0.000002	0.004777 ± 0.000003	0.006627 ± 0.000034	4.16	1.576 ± 0.001	2.296 ± 0.002	3.185 ± 0.016	-0.0416	4.77	17.18	1.44
3+10	0.002646 ± 0.000002	0.003977 ± 0.000002	0.006107 ± 0.000003	4.19	1.262 ± 0.001	1.897 ± 0.001	2.913 ± 0.001	-0.0387	5.79	17.32	1.22
4+10	0.007797 ± 0.000011	0.011530 ± 0.000027	0.016210 ± 0.000006	4.03	3.870 ± 0.005	5.723 ± 0.014	8.047 ± 0.003	-0.0391	4.99	16.65	3.60
5+10	0.002046 ± 0.000002	0.002961 ± 0.000024	0.004027 ± 0.000015	4.10	0.998 ± 0.001	1.444 ± 0.012	1.964 ± 0.007	-0.0432	4.57	17.45	0.90
6+10	0.002697 ± 0.000001	0.004101 ± 0.000018	0.005269 ± 0.000004	4.16	1.296 ± 0.001	1.971 ± 0.009	2.532 ± 0.002	-0.0428	4.51	17.28	1.19
7+10	0.009852 ± 0.000004	0.014510 ± 0.000024	0.017080 ± 0.000003	3.87	5.097 ± 0.002	7.507 ± 0.012	8.837 ± 0.001	-0.0432	3.60	16.47	4.47
8+10	0.030670 ± 0.000004	0.043800 ± 0.000011	0.065150 ± 0.000139	4.19	14.631 ± 0.002	20.895 ± 0.005	31.080 ± 0.066	-0.0359	5.15	15.87	13.55
26+10	0.005805 ± 0.000004	0.0083 ± 0.000012	0.01066 ± 0.000034	3.92	2.962 ± 0.002	4.235 ± 0.006	5.439 ± 0.017	-0.0428	4.04	16.80	2.62

Table S1: *Kinetic data from stopped flow measurements of the reaction between **10** and tetrazines **1-8** and **26**. [a] ΔG was calculated for 298.15 K.*

Reactants 1+10

25°C

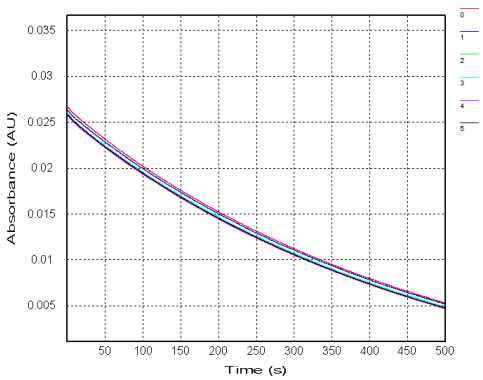

37°C

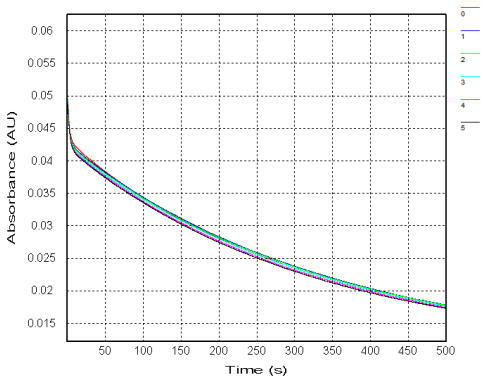

50°C

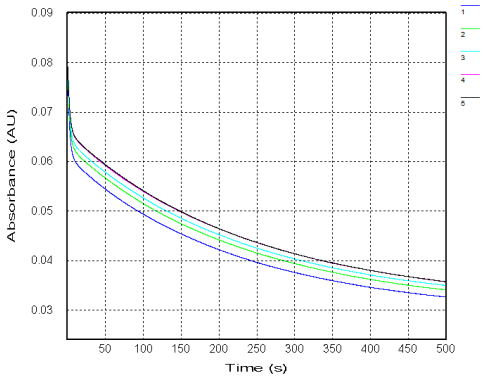

Reactants 2+10

25°C

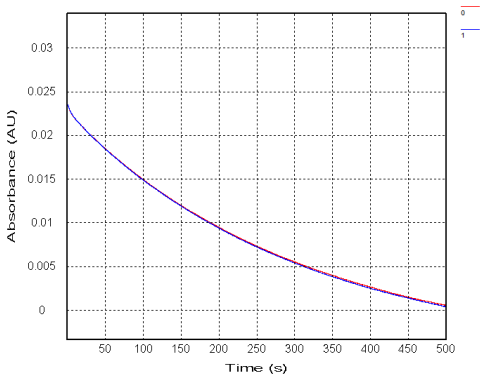

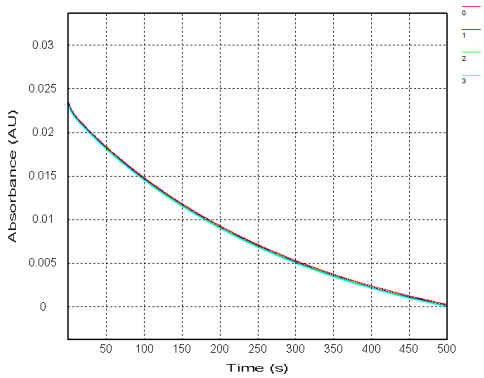

37°C

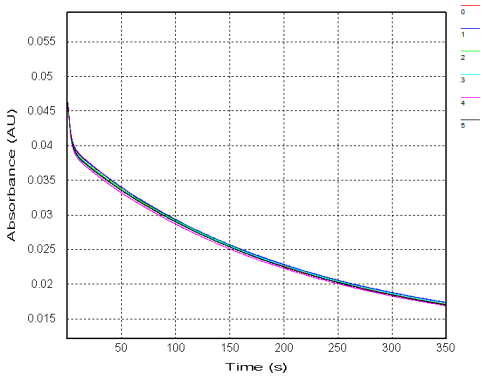

50°C

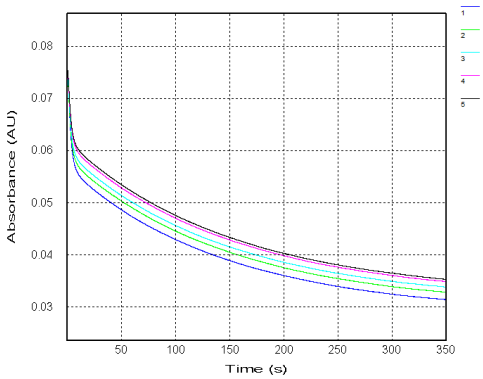

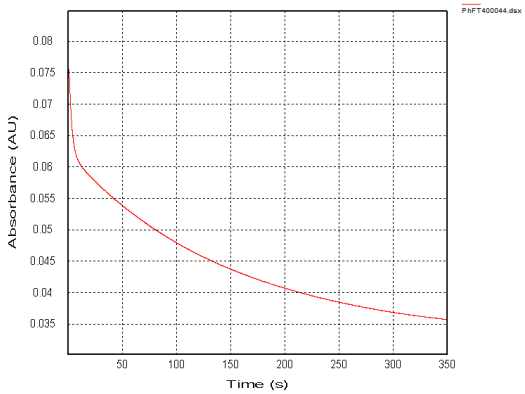

Reactants 3+10

25°C

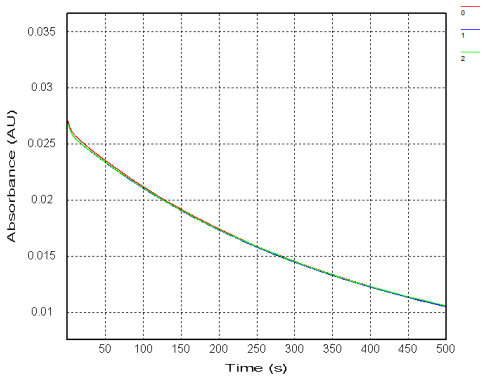

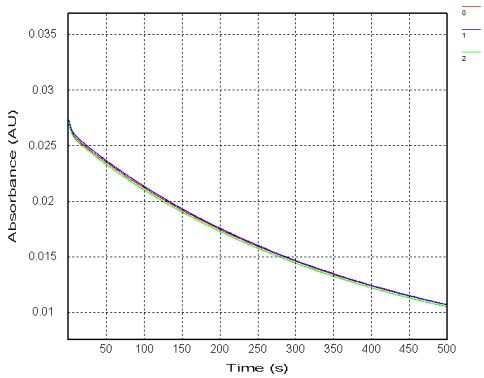

37°C

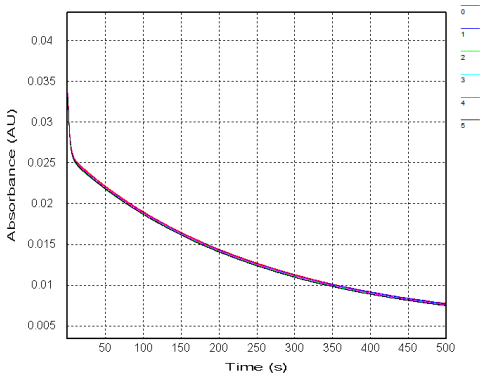

50°C

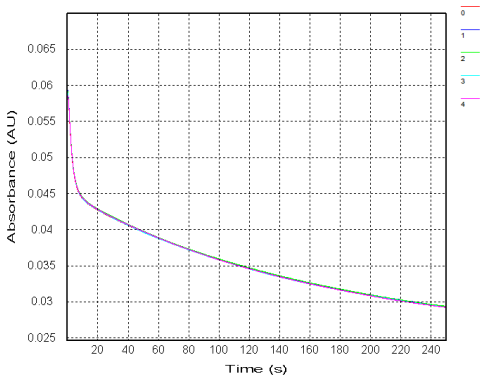

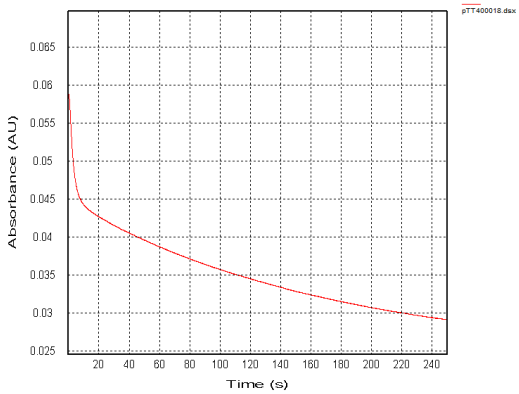

Reactants 4+10

25°C

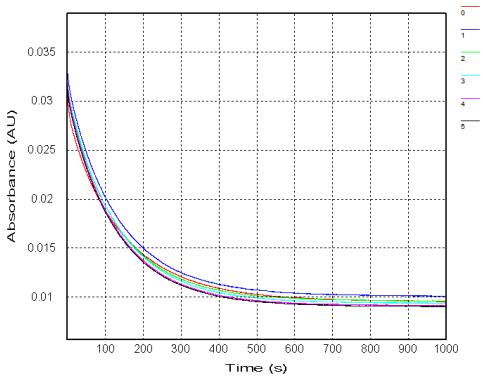

37°C

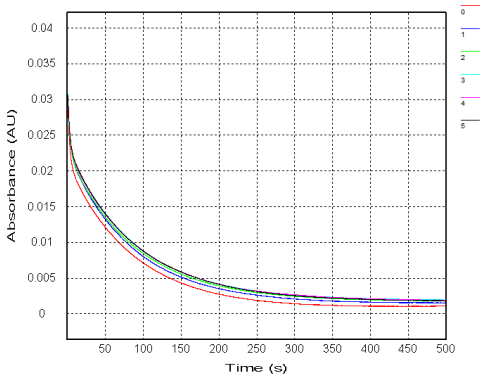

50°C

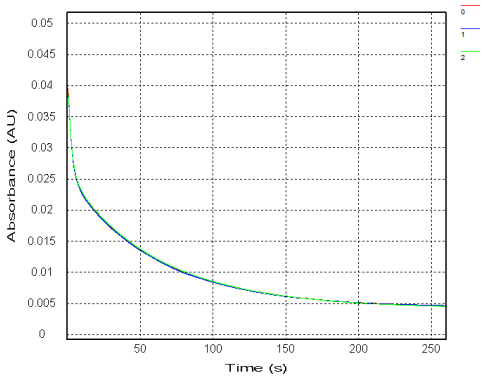

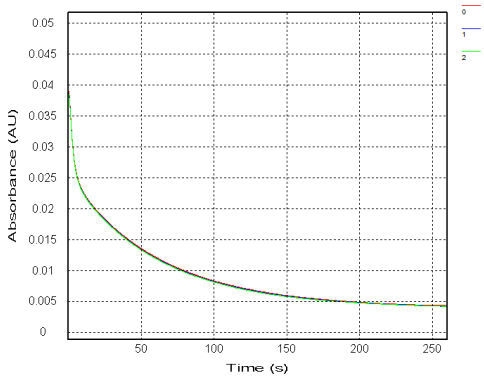

Reactants 5+10

25°C

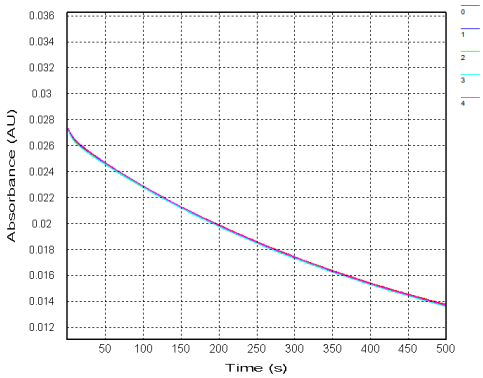

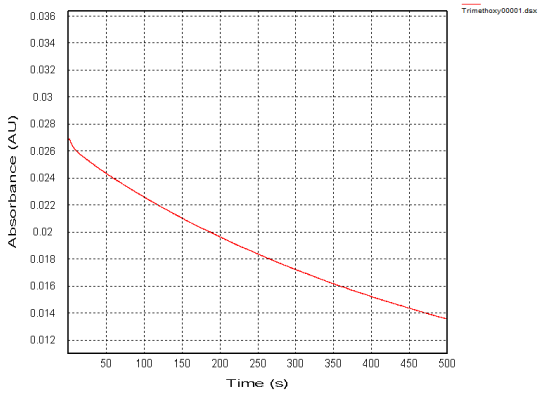

37°C

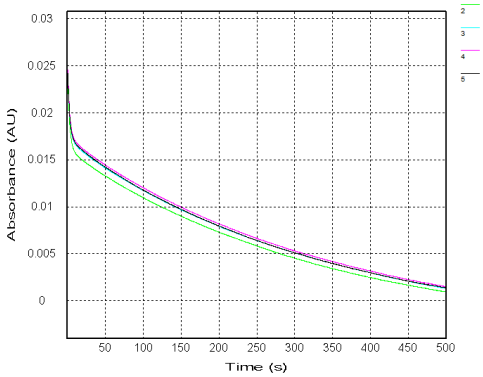

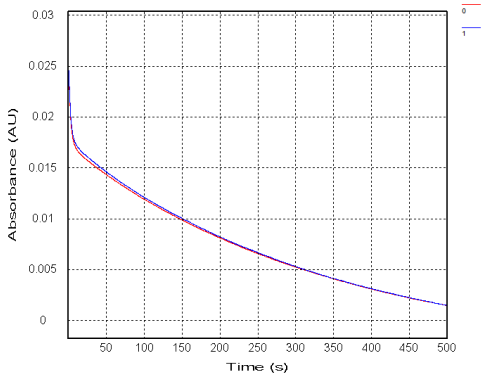

50°C

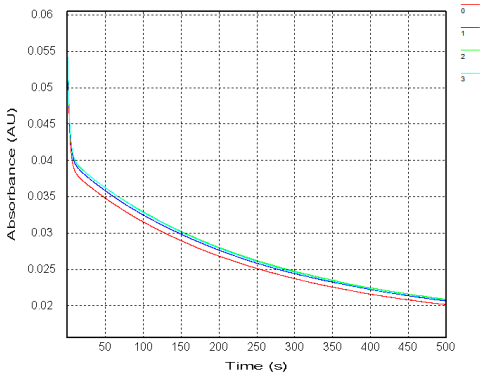

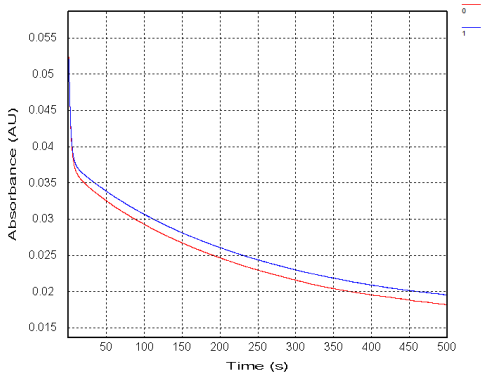

Reactants 6+10

25°C

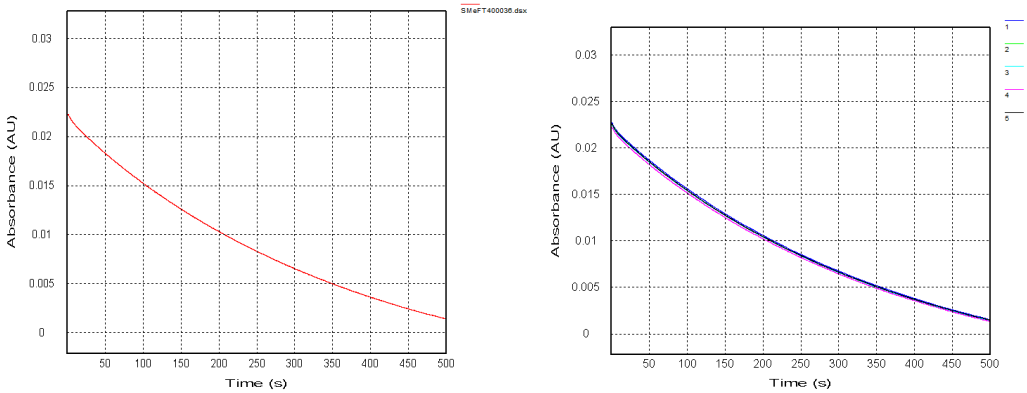

37°C

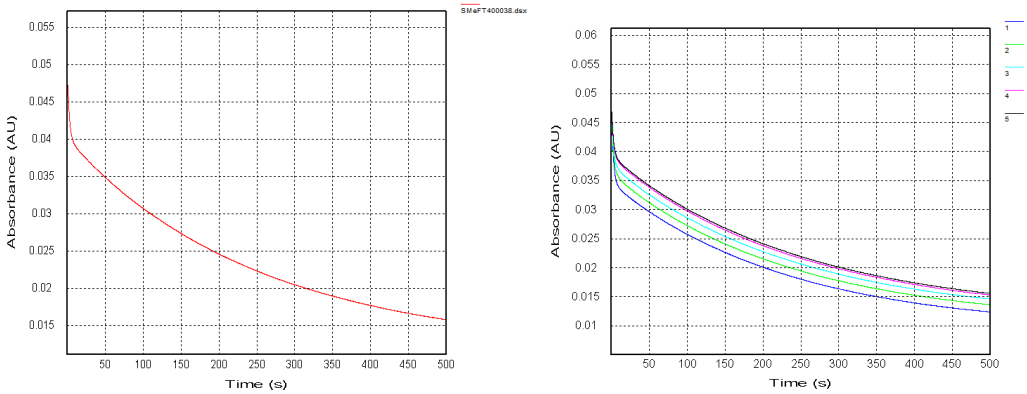

50°C

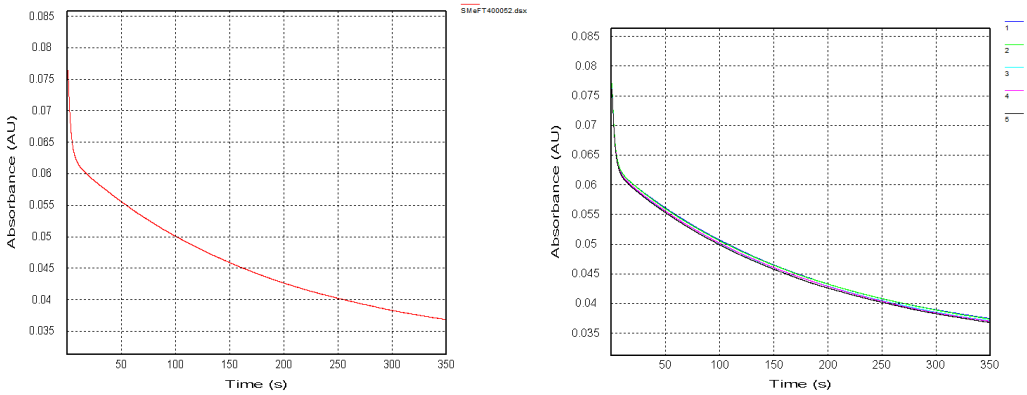

Reactants 7+10

25°C

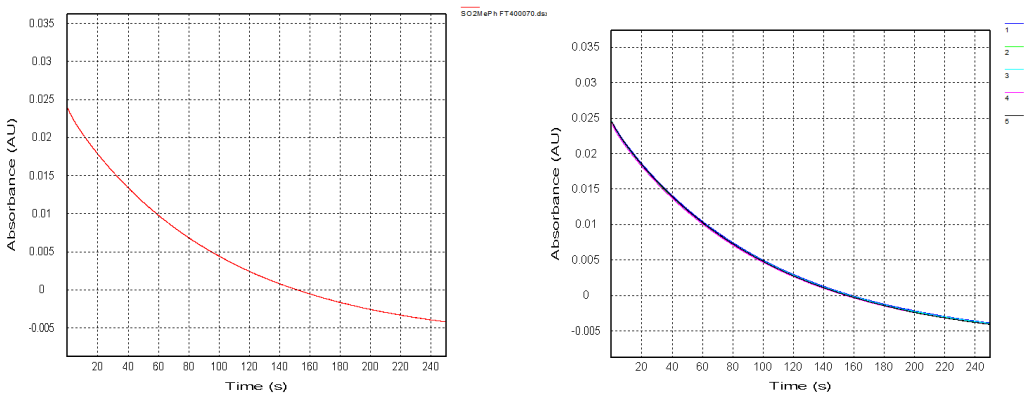

37°C

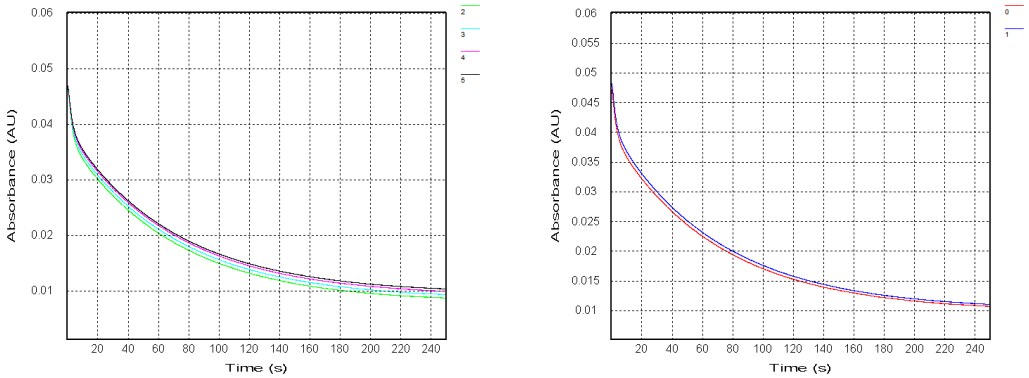

50°C

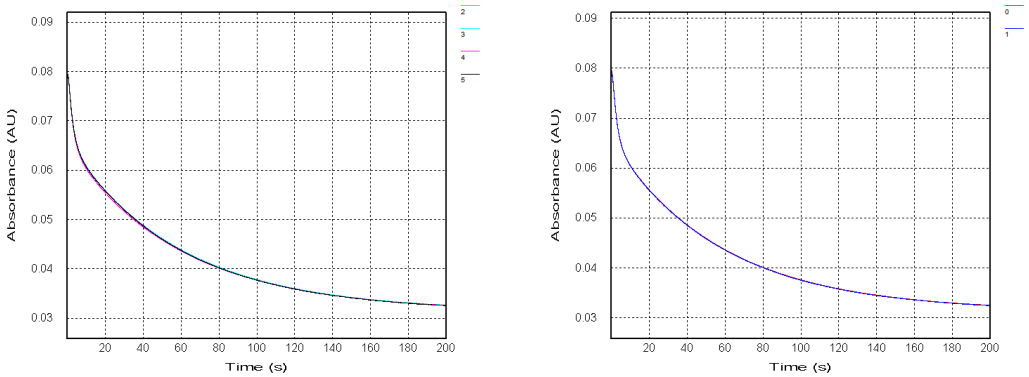

Reactants 8+10

25°C

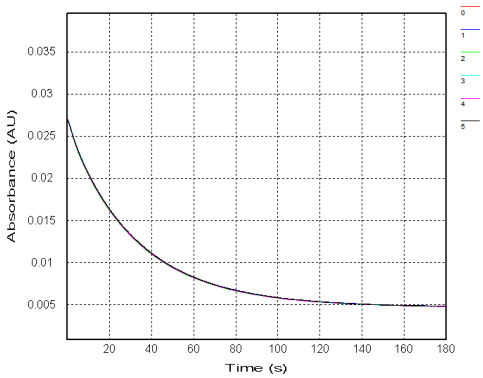

37°C

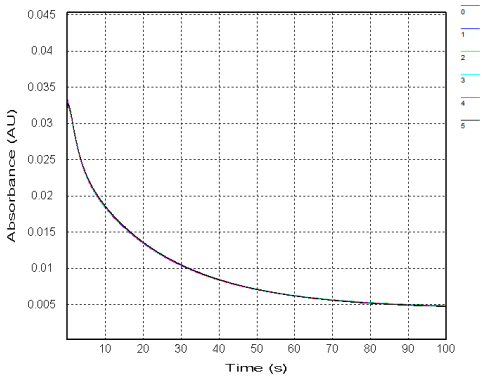

50°C

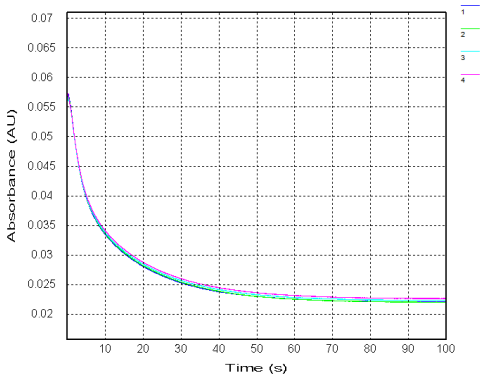

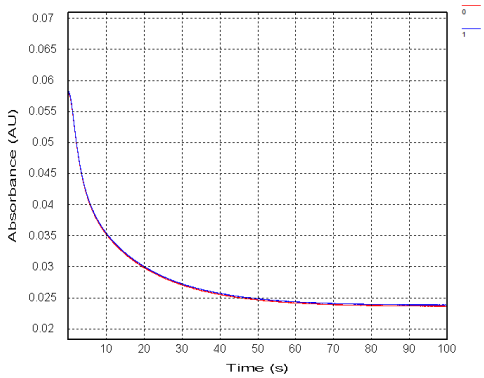

Reactants 26+10

25°C

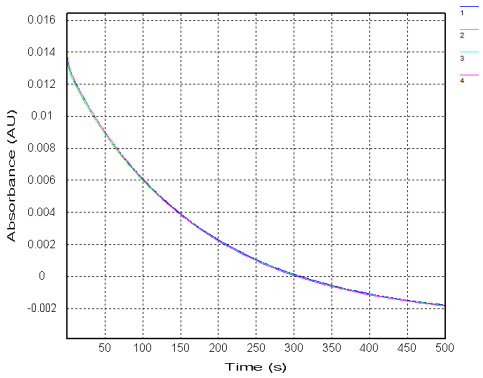

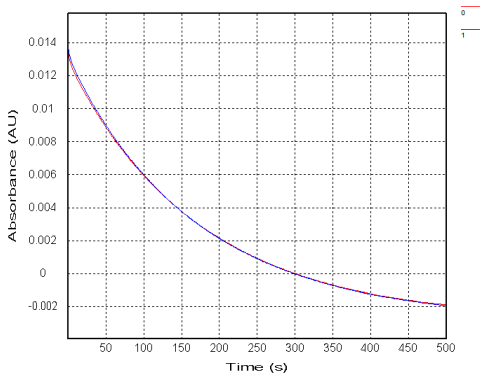

37°C

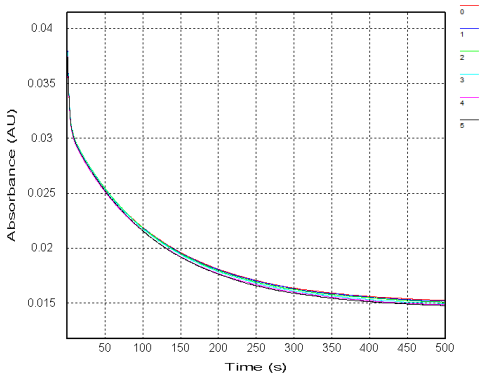

50°C

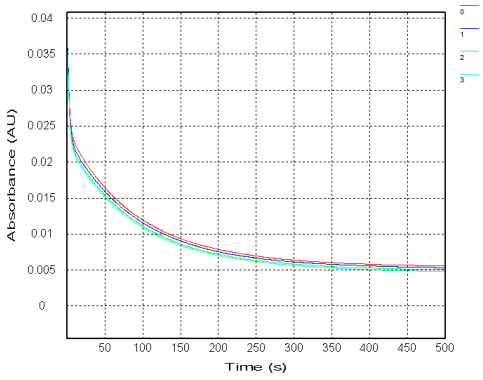

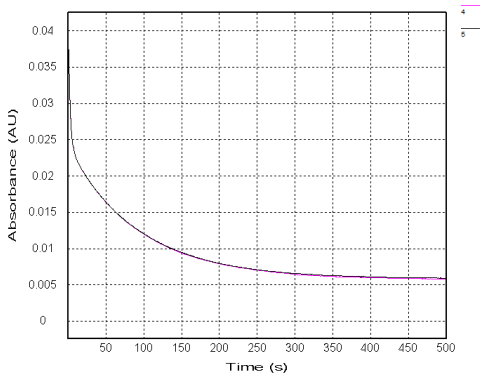

6. Quantum Chemical Calculations

All DFT calculations were performed on the Vienna Scientific Cluster 3 using the Gaussian 09 (Rev. D.01) program package.[1] Geometry optimizations to energy minima or transition states as well as subsequent frequency analyses at 298.15 K of all considered compounds and intermediates were achieved using the M06-2X density functional[2] in combination with the 6-311+G(d,p)[3] basis set as implemented in Gaussian 09, which has been found to give relatively accurate energy profiles for cycloadditions.[4,5] Imaginary frequencies corresponding to the desired reaction coordinates were obtained only in the case of transition state calculations. Data analysis was done using GaussView 5 (Gaussian, Inc.).

The reaction of tetrazines with strained dienophiles proceeds in two steps, the first being an inverse electron demand Diels-Alder (IEDDA)-initiated reaction leading to an intermediate that subsequently undergoes retro-Diels-Alder reaction with the loss of N_2 (Scheme S1).

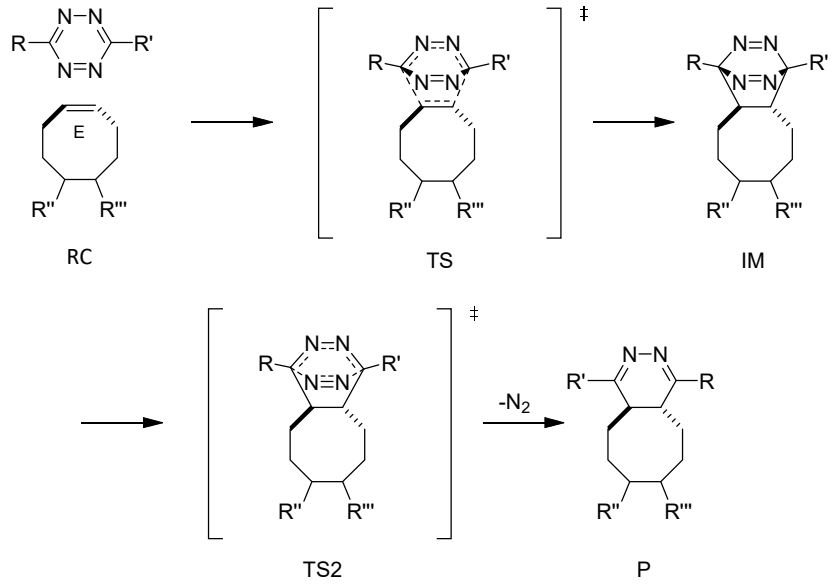

Scheme S1: *General mechanism of the tetrazine ligation (RC = reactant complex, TS = transition state, IM = intermediate, P = product).*

The first step of this reaction (RC → TS), the inverse electron demand Diels-Alder reaction, is the rate-determining step and is therefore used for prediction of reaction rates.[19,20]

Original data is summarized in Tables S2 – S4 followed by listing of Cartesian coordinates of all relevant structures.

$\Delta G^{\ddagger}$ was used to predict relative rates, compared to the reaction between **1** and **10**, which are shown in table S5. However, correlation between these calculated values and experimental values was poor and M06-2X/6-311+G(d,p) calculated $\Delta G^{\ddagger}$ values should not be used for prediction of RRVs of alkyl-aryl tetrazines, instead above described method (See chapter "Kinetic Investigations" in the main manuscript) using M06-2X/6-311+G(d,p) calculated $\Delta E^{\ddagger}$ values provides very accurate results.

	TCO	Tetrazines								
	10	**1**	**2**	**3**	**4**	**5**	**6**	**7**	**8**	**26**
E (hartree)	-313.172677	-552.754462	-744.464487	-783.771996	-1081.51571	-1087.99437	-1181.95319	-1332.32808	-760.498963	-1257.12132
G (hartree)[a]	-312.999391	-552.634625	-744.295682	-783.579015	-1081.34784	-1087.73633	-1181.76109	-1332.12846	-760.342988	-1256.92684

Table S2: *M06-2X/6-311+G(d,p) calculated energies of TCO 10 and Tetrazines 1-8 and 26 (E: total electronic energy, [a] calculated for 298.15 K)*

	Transition States								
	1+10	**2+10**	**3+10**	**4+10**	**5+10**	**6+10**	**7+10**	**8+10**	**26+10**
E (hartree)	-865.924139	-1057.63536	-1096.94238	-1394.6878	-1401.16446	-1495.12347	-1645.50103	-1073.67414	-1570.293123
G (hartree)[a]	-865.604288	-1057.26854	-1096.55074	-1394.31978	-1400.70963	-1494.73171	-1645.1013	-1073.31944	-1569.898486

Table S3: *M06-2X/6-311+G(d,p) calculated energies of transition states between TCO 10 and Tetrazines 1-8 and 26 (E: total electronic energy, [a] calculated for 298.15 K)*

	Energies of activation								
	1+10	**2+10**	**3+10**	**4+10**	**5+10**	**6+10**	**7+10**	**8+10**	**26+10**
$\Delta E^{‡}$ (kcal/mol)	1.88	1.13	1.44	0.36	1.62	1.51	-0.17	-1.57	0.55
$\Delta G^{‡}$ (kcal/mol)[a]	18.65	16.65	17.36	17.22	16.37	18.05	16.66	14.40	17.41

Table S4: *Resulting energies of activation for the reaction between TCO 10 and Tetrazines 1-8 and 26 (E: total electronic energy, [a] calculated for 298.15 K)*

	Predicted RRV values using $\Delta G^{‡}$							
	1+10	**2+10**	**3+10**	**4+10**	**5+10**	**6+10**	**7+10**	**8+10**
RRV	1.00	7.44	3.65	4.19	9.81	1.83	7.34	70.69

Table S5: *Predicted relative reactivity values based on $\Delta G^{‡}$, calculated using M06-2X/6-311+G(d,p)*

Cartesian Coordinates

Tetrazines 1-8 and 26

1

C	2.6541930	0.0002870	-0.2232200
C	0.2201670	-0.0006280	0.5745190
C	-1.2178290	-0.0010960	0.9854390
H	-1.4060680	-0.8913470	1.5895580
H	-1.4061070	0.8878670	1.5914420
C	-2.1230580	0.0002210	-0.2533710
H	-1.9147170	0.8850880	-0.8612390
H	-1.9147810	-0.8833880	-0.8630860
C	-3.5828140	-0.0001300	0.1459580
H	-3.8375600	-0.8917360	0.7253640
H	-3.8375030	0.8903450	0.7271200
F	-4.3762250	0.0010110	-0.9909940
N	0.8145320	-1.1815150	0.3763060
N	2.0561370	-1.1814510	-0.0303980
N	2.0558240	1.1815710	-0.0286960
N	0.8142170	1.1806900	0.3780560
C	4.0818810	0.0007640	-0.6607650
H	4.2946430	0.8973360	-1.2405390
H	4.7337370	-0.0014270	0.2165170
H	4.2941590	-0.8934190	-1.2444350

2

C	-3.1521940	1.2090240	0.1404990
C	-4.5190400	1.2049210	0.3849500
C	-5.2046490	0.0000520	0.5077510
C	-4.5190490	-1.2048500	0.3851040
C	-3.1522160	-1.2090010	0.1406520
C	-2.4630470	0.0000040	0.0163490
H	-2.6109410	2.1412800	0.0432690
H	-5.0496500	2.1445310	0.4801930
H	-5.0496850	-2.1444330	0.4804720
H	-2.6109580	-2.1412670	0.0435370
C	-1.0079330	-0.0000290	-0.2468120
C	1.5140220	-0.0000660	-0.7211310
C	2.9912560	-0.0000730	-0.9519580
H	3.2502480	-0.8893680	-1.5309750
H	3.2502400	0.8891560	-1.5310810
C	3.7429490	0.0000130	0.3851970
H	3.4652680	0.8841140	0.9657830
H	3.4653050	-0.8840400	0.9658740
C	5.2397730	0.0000330	0.1607860
H	5.5604310	-0.8912350	-0.3856240
H	5.5603940	0.8912680	-0.3857010
F	5.8932640	0.0000990	1.3830140
N	0.8972530	-1.1808030	-0.6020580
N	-0.3842910	-1.1809240	-0.3622390
N	-0.3842460	1.1808620	-0.3622290
N	0.8972830	1.1807020	-0.6020450
H	-6.2712480	0.0000730	0.6988000

3

C	-2.7026230	1.2062180	0.0284130
C	-4.0734120	1.1985780	0.2435920
C	-4.7808230	0.0000290	0.3502500
C	-4.0721900	-1.1984910	0.2408390
C	-2.7022580	-1.2050210	0.0254940
C	-2.0058440	0.0012520	-0.0840000
H	-2.1635070	2.1415790	-0.0515770
H	-4.6040630	2.1405090	0.3325970
H	-4.6027480	-2.1408280	0.3277410
H	-2.1625100	-2.1397950	-0.0568590
C	-0.5473400	0.0016690	-0.3121950
C	1.9861470	0.0021230	-0.7255670
C	3.4685800	0.0022100	-0.9220460
H	3.7403890	-0.8857600	-1.4972760
H	3.7408980	0.8925620	-1.4933250
C	4.1900000	-0.0010640	0.4315110
H	3.9000810	0.8820560	1.0076040
H	3.8987920	-0.8860890	1.0040270
C	5.6914930	-0.0018280	0.2410090
H	6.0238060	-0.8923680	-0.2996340
H	6.0251840	0.8902800	-0.2961920
F	6.3174790	-0.0046890	1.4777450
N	1.3664050	-1.1785680	-0.6241810
N	0.0796490	-1.1793800	-0.4150590
N	0.0800790	1.1829660	-0.4097010
N	1.3668050	1.1826180	-0.6188540
C	-6.2725170	-0.0043320	0.5512460
H	-6.7863510	-0.0853490	-0.4108850
H	-6.5839480	-0.8509830	1.1650610
H	-6.6091650	0.9148590	1.0322880

4

C	-1.5884940	1.2097790	-0.1007950
C	-2.9648340	1.2090920	0.0720820
C	-3.6462980	-0.0001400	0.1563520
C	-2.9647830	-1.2091260	0.0691290
C	-1.5884340	-1.2093710	-0.1036970
C	-0.8962290	0.0003220	-0.1916220
H	-1.0429350	2.1420250	-0.1657500
H	-3.5076720	2.1431710	0.1477180
H	-3.5076340	-2.1433900	0.1424570
H	-1.0428770	-2.1414640	-0.1708470
C	0.5724420	0.0005530	-0.3805030
C	3.1116740	0.0010090	-0.7289640
C	4.5977370	0.0012060	-0.8890430
H	4.8837400	-0.8875720	-1.4558910
H	4.8837110	0.8911860	-1.4539910
C	5.2827210	-0.0003270	0.4835290
H	4.9779130	0.8833960	1.0509670
H	4.9774180	-0.8849940	1.0492250
C	6.7892070	-0.0006360	0.3332450
H	7.1361720	-0.8914980	-0.1975590
H	7.1368080	0.8912710	-0.1953750
F	7.3790050	-0.0023480	1.5866330
N	2.4900020	-1.1803940	-0.6400800
N	1.1982000	-1.1799830	-0.4635570
N	1.1978370	1.1813680	-0.4633510
N	2.4895830	1.1822500	-0.6398740
C	-5.1437330	-0.0004340	0.2796970
F	-5.5937270	-1.0809190	0.9311820
F	-5.7343990	-0.0003270	-0.9271820
F	-5.5941980	1.0795530	0.9316590

5

C	-1.4724740	1.2312030	-0.0025240
C	-2.8485250	1.2341470	0.2158810
C	-3.5447140	0.0252510	0.3410170
C	-2.8573860	-1.1891150	0.2197720
C	-1.4827300	-1.1999970	-0.0025220
C	-0.8027020	0.0128780	-0.1082760
H	-0.9120710	2.1494100	-0.0957410
H	-0.9303370	-2.1233350	-0.0930820
C	0.6556140	0.0065410	-0.3401360
C	3.1897640	-0.0047630	-0.7549980
C	4.6724200	-0.0109450	-0.9493870
H	4.9418480	-0.9008930	-1.5226380
H	4.9490210	0.8773250	-1.5219010
C	5.3917960	-0.0140830	0.4051930
H	5.1026440	0.8702030	0.9798980
H	5.0981250	-0.8978300	0.9784440
C	6.8936530	-0.0178320	0.2174020
H	7.2252170	-0.9091110	-0.3225150
H	7.2299270	0.8734460	-0.3196050
F	7.5170930	-0.0214860	1.4551980
N	2.5637490	-1.1824020	-0.6570490
N	1.2771000	-1.1771210	-0.4478120
N	1.2893520	1.1847040	-0.4372410
N	2.5757440	1.1784470	-0.6472940
O	-4.8737860	0.0377790	0.6148620
O	-3.6035840	2.3509060	0.3178260
O	-3.6231150	-2.2996320	0.3320870
C	-5.6969710	-0.1329560	-0.5345130
H	-5.4993600	-1.0987730	-1.0069690
H	-6.7267060	-0.0997800	-0.1837950
H	-5.5250070	0.6786600	-1.2474580
C	-2.9729280	-3.5534120	0.2531280
H	-2.2247060	-3.6591740	1.0440590
H	-3.7505270	-4.3018430	0.3860420

H	-2.4954170	-3.6896850	-0.7219880
C	-2.9422060	3.5975950	0.2286060
H	-2.4621280	3.7215120	-0.7470260
H	-3.7137300	4.3536450	0.3536250
H	-2.1940470	3.7047100	1.0195740

6

C	-1.8590560	1.3845800	0.0595180
C	-3.2281710	1.4008130	0.2465410
C	-3.9699580	0.2128850	0.1873920
C	-3.3066110	-0.9899720	-0.0633870
C	-1.9309730	-1.0029470	-0.2515310
C	-1.1936560	0.1791520	-0.1929100
H	-1.2917580	2.3053730	0.1061570
H	-3.7348830	2.3393740	0.4408350
H	-3.8487030	-1.9243430	-0.1151830
H	-1.4205660	-1.9378000	-0.4456940
C	0.2664170	0.1587420	-0.3908520
C	2.8106130	0.1211560	-0.7307540
C	4.2985370	0.0887230	-0.8743560
H	4.5607980	-0.7077460	-1.5744730
H	4.6281840	1.0458690	-1.2843680
C	4.9622330	-0.1630080	0.4858810
H	4.6863180	0.6317550	1.1844820
H	4.6086580	-1.1117460	0.8990630
C	6.4688180	-0.2074000	0.3494020
H	6.7848250	-1.0176360	-0.3134570
H	6.8629990	0.7399540	-0.0284430
F	7.0430000	-0.4346380	1.5907950
N	2.1475660	-1.0377220	-0.8169200
N	0.8560820	-1.0193930	-0.6454700
N	0.9350380	1.3186640	-0.3113550
N	2.2274360	1.2986160	-0.4833540
S	-5.7105570	0.3568620	0.4391630
C	-6.2773980	-1.3535760	0.3004270
H	-7.3545580	-1.3171100	0.4569990
H	-6.0779460	-1.7578780	-0.6917930
H	-5.8290690	-1.9821560	1.0695880

7

C	-1.2567830	1.2122850	-0.0826130
C	-2.6314930	1.2149090	0.1083940
C	-3.3000040	-0.0000510	0.1920610
C	-2.6313830	-1.2149120	0.1078140
C	-1.2566750	-1.2120780	-0.0832060
C	-0.5688740	0.0001590	-0.1835690
H	-0.7084350	2.1430310	-0.1468490
H	-3.1832430	2.1419510	0.2130190
H	-3.1830410	-2.1420580	0.2120070
H	-0.7082560	-2.1427500	-0.1478970
C	0.8986760	0.0002830	-0.3872050
C	3.4366310	0.0004410	-0.7420300
C	4.9230290	0.0004600	-0.8970650
H	5.2111490	-0.8887770	-1.4620690
H	5.2112250	0.8902230	-1.4611960
C	5.6021260	-0.0002510	0.4785930
H	5.2949170	0.8837340	1.0443230
H	5.2946230	-0.8846300	1.0435470
C	7.1093170	-0.0004090	0.3346350
H	7.4586720	-0.8917430	-0.1938080
H	7.4588810	0.8910830	-0.1934060
F	7.6934500	-0.0007650	1.5904250
N	2.8142010	-1.1810770	-0.6569120
N	1.5229310	-1.1802960	-0.4771880
N	1.5228720	1.1808840	-0.4763480
N	2.8142020	1.1818280	-0.6560960
S	-5.0780080	-0.0001800	0.3901790
O	-5.4573770	-1.2689480	0.9933070
O	-5.4575160	1.2684290	0.9935310
C	-5.6787240	-0.0000650	-1.2945900
H	-6.7662520	-0.0002430	-1.2205420
H	-5.3243940	0.9022250	-1.7899140
H	-5.3241270	-0.9021330	-1.7901300

8

C	4.4084840	-1.2021110	0.2704090
C	5.1636470	-0.0514040	0.4833620
C	4.5152010	1.1754160	0.4571360
C	3.1477890	1.2057880	0.2206510
C	2.4863800	-0.0074820	0.0245560
H	4.8801360	-2.1798850	0.2794480
H	5.0624740	2.0965590	0.6179130
H	2.5948690	2.1344560	0.1860080
C	1.0175010	-0.0198160	-0.2274670
C	-1.4956100	-0.0022670	-0.7050320
C	-2.9697570	-0.0022560	-0.9536280
H	-3.2202160	0.8798350	-1.5466610
H	-3.2233440	-0.8988940	-1.5242110
C	-3.7364270	0.0109660	0.3750630
H	-3.4571840	-0.8624240	0.9706470
H	-3.4733820	0.9057120	0.9461300
C	-5.2304720	-0.0047340	0.1332920
H	-5.5514560	0.8729830	-0.4344620
H	-5.5379840	-0.9091120	-0.3988740
F	-5.8981470	0.0146880	1.3476910
N	-0.8577890	1.1703040	-0.6871870
N	0.4262120	1.1578760	-0.4449670
N	0.3731540	-1.1944550	-0.2177950
N	-0.9066080	-1.1810740	-0.4622480
H	6.2287890	-0.1233740	0.6632790
N	3.0993460	-1.1898870	0.0466980

26

C	1.6016290	-1.1634990	0.0180620
C	2.9850510	-1.1061390	0.1381100
C	3.6335280	0.0890170	-0.1318540
C	2.9366580	1.2219790	-0.5392830
C	1.5566930	1.1621180	-0.6565970
C	0.8841650	-0.0318940	-0.3754670
H	1.0702300	-2.0834320	0.2256400
H	3.5747020	-1.9686220	0.4300610
H	3.4638450	2.1412370	-0.7735910
H	0.9916220	2.0306110	-0.9692980
C	-0.5884310	-0.0943560	-0.5020600
C	-3.1412400	-0.2007490	-0.7209570
C	-4.6334310	-0.2495200	-0.7951220
H	-4.9658490	0.4566240	-1.5592210
H	-4.9319510	-1.2585090	-1.0882140
C	-5.2454210	0.1120350	0.5644350
H	-4.8913300	-0.5873140	1.3269100
H	-4.9289550	1.1170630	0.8571200
C	-6.7572190	0.0628940	0.5057870
H	-7.1513990	0.7774940	-0.2218730
H	-7.1139320	-0.9396450	0.2544510
F	-7.2801160	0.3954880	1.7451640
N	-2.5366160	0.9625040	-0.9850170
N	-1.2383020	1.0160540	-0.8739390
N	-1.1973510	-1.2584650	-0.2401970
N	-2.4950830	-1.3123930	-0.3504240
C	5.4846340	1.0871920	1.5466080
H	6.5342200	1.1907180	1.8188750
H	5.0342680	2.0654540	1.3783240
H	4.9448980	0.5271780	2.3100390
S	5.4374590	0.1227530	0.0072310
O	5.8578880	-1.2725840	0.3782090

Trans-Cyclooctene **10**

C	0.5318520	-1.3589840	0.3996640
H	0.3744330	-1.3388160	1.4781560
C	-0.5318840	-1.3585380	-0.3995650
H	-0.3742230	-1.3368990	-1.4780190
C	-1.8690770	-0.9025640	0.0834010
H	-2.7109740	-1.3589110	-0.4431120
H	-1.9793480	-1.1138860	1.1513860
C	1.8688930	-0.9026020	-0.0836680
H	2.7109760	-1.3589910	0.4424710
H	1.9787600	-1.1140400	-1.1516990
C	-1.8811540	0.6346470	-0.1369480
H	-2.7888180	1.0457230	0.3159040
H	-1.9547410	0.8378520	-1.2114020
C	1.8812090	0.6344950	0.1367650
H	2.7887720	1.0455390	-0.3163480
H	1.9551820	0.8376990	1.2111940
C	0.6517960	1.3791870	-0.4284790
H	0.9536840	2.4199210	-0.5751010

H	0.4327970	0.9945680	-1.4305910
C	-0.6516990	1.3789050	0.4288570
H	-0.9534390	2.4195610	0.5763670
H	-0.4326710	0.9934100	1.4306360

Transition states

TS_{1+10}

C	-0.4598930	2.2404580	0.3446990
C	1.1972770	0.3836430	0.1175860
C	-0.7854570	-0.6163260	0.0087090
H	-0.5286230	-0.9843530	-0.9839530
C	-1.6880720	0.4221870	0.0713870
H	-2.1482380	0.6078670	1.0414010
N	1.0405830	0.9077220	1.3716170
N	0.1891350	1.8536100	1.4877050
N	1.0410400	1.2005900	-0.9688360
N	0.1979850	2.1541100	-0.8531000
C	-2.5356940	0.7422390	-1.1271580
H	-2.8589280	1.7849630	-1.1503770
H	-1.9611100	0.5534030	-2.0390390
C	-0.7566410	-1.6334830	1.1142560
H	0.2127220	-2.1253260	1.2129990
H	-0.9747400	-1.1396910	2.0662200
C	-3.7843400	-0.1659420	-1.0950830
H	-4.3388970	-0.0040260	-2.0240270
H	-4.4423080	0.1641310	-0.2831040
C	-1.8268060	-2.7074540	0.8190150
H	-1.8705430	-3.3797940	1.6809250
H	-1.4934410	-3.3174170	-0.0284050
C	-3.2395280	-2.1754820	0.5195030
H	-3.9377630	-2.9909010	0.7237870
H	-3.4918300	-1.3902720	1.2408280
C	-3.5042290	-1.6701120	-0.9273840
H	-4.3752420	-2.2034540	-1.3160430
H	-2.6720330	-1.9579560	-1.5797760
C	2.1887060	-0.7333330	-0.0300460
H	1.9088380	-1.3500350	-0.8895690
H	2.1518860	-1.3512450	0.8692640
C	3.6066850	-0.1812620	-0.2160880
H	3.6409660	0.4522930	-1.1051750
H	3.8750560	0.4336220	0.6471170
C	4.6041850	-1.3100800	-0.3573240
H	4.3857960	-1.9267090	-1.2339470
H	4.6182950	-1.9455740	0.5327590
F	5.8817180	-0.7936140	-0.5192230
C	-1.4759740	3.3321050	0.4939300
H	-1.0176350	4.1735120	1.0167010
H	-1.8094130	3.6679080	-0.4861620
H	-2.3308040	2.9963980	1.0828700

TS_{2+10}

C	0.7311520	-1.2454520	0.1233070
C	-1.6618810	-0.5248010	0.0806020
C	-0.5554150	1.3545970	-0.0064830
H	-1.0311280	1.5856570	-0.9591670
C	0.7724160	0.9830220	-0.0581610
H	1.3336740	1.0200930	0.8744720
N	-1.1790680	-0.9612620	1.2867610
N	0.0469450	-1.3148650	1.3101420
N	-1.1702080	-1.0924280	-1.0687350
N	0.0501080	-1.4615430	-1.0462900
C	1.5668860	1.2252480	-1.3067160
H	2.3983850	0.5251830	-1.4136560
H	0.9156820	1.1130200	-2.1795790
C	-1.0447240	2.1456290	1.1753080
H	-2.1154050	2.0281420	1.3507300
H	-0.5237880	1.8091680	2.0769810
C	2.1283050	2.6637560	-1.2517150
H	2.6111550	2.8691190	-2.2115740
H	2.9197070	2.7054160	-0.4949650
C	-0.7479730	3.6396040	0.9217890
H	-1.0137750	4.1909900	1.8285360
H	-1.4169000	4.0055770	0.1344910
C	0.7044110	3.9714380	0.5355400
H	0.8710520	5.0219850	0.7859750
H	1.3867230	3.4065300	1.1806750
C	1.0964000	3.7661230	-0.9557530
H	1.5128990	4.7056930	-1.3273260
H	0.1967010	3.5895730	-1.5564360
C	-3.1055630	-0.1125790	0.0460440
H	-3.2552750	0.6097980	-0.7621660
H	-3.3479100	0.3718990	0.9938510
C	-4.0168830	-1.3278130	-0.1568790
H	-3.7758060	-1.8164250	-1.1034530
H	-3.8490450	-2.0497660	0.6467920
C	-5.4708350	-0.9087240	-0.1589980
H	-5.6801950	-0.2004000	-0.9659110
H	-5.7600070	-0.4591070	0.7952910
F	-6.2803690	-2.0171840	-0.3581690
C	2.1743870	-1.5765140	0.1588270
C	2.8252280	-2.0485540	-0.9824600
C	2.8958650	-1.3923870	1.3395880
C	4.1853290	-2.3324390	-0.9383900
H	2.2570770	-2.1954090	-1.8926590
C	4.2556330	-1.6739940	1.3768890
H	2.3805740	-1.0413220	2.2259840
C	4.9035120	-2.1443820	0.2381630
H	4.6841460	-2.7047490	-1.8252800
H	4.8090440	-1.5301130	2.2971520
H	5.9637980	-2.3658620	0.2685960

TS_{3+10}

C	0.5660430	-1.0728470	0.0959220
C	-1.8927100	-0.6218930	0.0733100
C	-1.0098700	1.3665800	-0.0050320
H	-1.5167330	1.5512640	-0.9515690
C	0.3510160	1.1454790	-0.0698110
H	0.9117560	1.2370050	0.8594170
N	-1.3563740	-1.0103760	1.2735120
N	-0.0987610	-1.2258170	1.2867620
N	-1.3493460	-1.1261650	-1.0830210
N	-0.0956640	-1.3559480	-1.0713670
C	1.1049970	1.4809630	-1.3218080
H	2.0058340	0.8746960	-1.4386970
H	0.4626880	1.3052620	-2.1907520
C	-1.5710880	2.0902530	1.1884720
H	-2.6222660	1.8596170	1.3691180
H	-1.0112420	1.7995500	2.0828060
C	1.5073110	2.9713820	-1.2591490
H	1.9548040	3.2375370	-2.2211830
H	2.2963940	3.0932000	-0.5087140
C	-1.4348110	3.6109560	0.9529950
H	-1.7455290	4.1193750	1.8705120
H	-2.1477270	3.9154860	0.1781490
C	-0.0308690	4.0984170	0.5546050
H	0.0253270	5.1586240	0.8138880
H	0.7160930	3.6050460	1.1863800
C	0.3626710	3.9496590	-0.9426660
H	0.6672980	4.9326140	-1.3103980
H	-0.5187430	3.6776040	-1.5342420
C	-3.3757090	-0.3848870	0.0468160
H	-3.6155130	0.2974420	-0.7743190
H	-3.6709300	0.0838560	0.9874300
C	-4.1317970	-1.7070350	-0.1278970
H	-3.8271520	-2.1839490	-1.0620620
H	-3.8788910	-2.3824890	0.6936700
C	-5.6263260	-1.4722650	-0.1432140
H	-5.9187580	-0.8179770	-0.9695260
H	-5.9745000	-1.0378750	0.7982180
F	-6.2900050	-2.6788680	-0.3145920
C	2.0358400	-1.2420230	0.1194090
C	2.7321060	-1.6217740	-1.0284760
C	2.7449660	-1.0015050	1.2974750
C	4.1145020	-1.7565000	-0.9918760
H	2.1816710	-1.8198210	-1.9400680
C	4.1257820	-1.1360400	1.3216810
H	2.2041550	-0.7266870	2.1956260
C	4.8339250	-1.5125030	0.1780760
H	4.6444100	-2.0613030	-1.8883150
H	4.6645900	-0.9515300	2.2452860
C	6.3352320	-1.6292490	0.2051310
H	6.6839570	-2.0012860	1.1699530
H	6.6923130	-2.3049300	-0.5732130
H	6.8004870	-0.6533750	0.0389550

TS_{4+10}

C	0.1146240	-0.9075410	-0.0734930
C	2.6064060	-0.7485250	-0.0797570
C	1.9540780	1.3424440	0.0034160
H	2.4867060	1.4664620	0.9457210
C	0.5781420	1.2792140	0.0799810
H	0.0248010	1.4324850	-0.8457300
N	2.0137640	-1.0686440	-1.2733270
N	0.7392580	-1.1353640	-1.2716570
N	2.0204840	-1.1812890	1.0841960
N	0.7483700	-1.2638650	1.0866930
C	-0.1205230	1.7045450	1.3365830
H	-1.0863480	1.2114060	1.4671960
H	0.5044540	1.4590500	2.2010780
C	2.5877960	1.9883620	-1.1976280
H	3.6038040	1.6353450	-1.3814370
H	1.9928630	1.7601980	-2.0873590
C	-0.3476470	3.2314980	1.2672280
H	-0.7532450	3.5524810	2.2309140
H	-1.1247720	3.4385320	0.5230240
C	2.6319750	3.5155580	-0.9683400
H	2.9951790	3.9788950	-1.8903740
H	3.3811230	3.7364310	-0.1994590
C	1.2979990	4.1674630	-0.5642280
H	1.3676100	5.2260320	-0.8262240
H	0.4939950	3.7664020	-1.1915260
C	0.8985130	4.0709690	0.9360030
H	0.7084100	5.0838860	1.2992440
H	1.7482680	3.7071270	1.5250580
C	4.1059800	-0.6771280	-0.0692320
H	4.4279670	-0.0185190	0.7429770
H	4.4417710	-0.2531240	-1.0172600
C	4.7103180	-2.0744710	0.1120590
H	4.3570070	-2.5088300	1.0498090
H	4.3823810	-2.7226510	-0.7050030
C	6.2222760	-2.0086120	0.1215460
H	6.5902610	-1.3992280	0.9521510
H	6.6121980	-1.6068430	-0.8180050
F	6.7446540	-3.2840510	0.2771220
C	-1.3671080	-0.9091230	-0.0799890
C	-2.0814130	-1.2164950	1.0788970
C	-2.0518600	-0.5835340	-1.2524240
C	-3.4697090	-1.1952460	1.0662750
H	-1.5409980	-1.4783470	1.9796510
C	-3.4383420	-0.5580890	-1.2653970
H	-1.4903920	-0.3660290	-2.1529770
C	-4.1420620	-0.8644060	-0.1045690
H	-4.0289740	-1.4433160	1.9599040
H	-3.9745910	-0.3124180	-2.1739720
C	-5.6405400	-0.7769860	-0.1070870
F	-6.1627250	-1.1243350	-1.2915670
F	-6.0612210	0.4759820	0.1457670
F	-6.1947100	-1.5654520	0.8233670

TS_{5+10}

C	-0.2227370	-0.8475380	0.2432790
C	-2.7156860	-0.6500380	0.1766290
C	-2.0382330	1.3653060	-0.2717230
H	-2.5521880	1.3260760	-1.2318550
C	-0.6611080	1.2760290	-0.3082500
H	-0.1208320	1.5861610	0.5850390
N	-2.1458800	-0.7607710	1.4191130
N	-0.8732790	-0.8453740	1.4517000
N	-2.1211620	-1.2987080	-0.8781620
N	-0.8511430	-1.3991260	-0.8439060
C	0.0677790	1.4644370	-1.6049450
H	1.0264290	0.9414450	-1.6199740
H	-0.5440830	1.0771380	-2.4261230
C	-2.6820900	2.2306810	0.7770800
H	-3.7053850	1.9288240	1.0066890
H	-2.1035070	2.1661340	1.7037940
C	0.3167520	2.9754370	-1.8051820
H	0.7504640	3.1131140	-2.8000720
H	1.0787590	3.3061420	-1.0904560
C	-2.7033390	3.6895470	0.2706840
H	-3.0787880	4.3183940	1.0834330
H	-3.4338780	3.7724770	-0.5421880
C	-1.3540040	4.2461440	-0.2162830
H	-1.4168570	5.3354640	-0.1536280
H	-0.5674240	3.9598420	0.4910270
C	-0.9241990	3.8740400	-1.6640930
H	-0.7136220	4.8016540	-2.2019300
H	-1.7652450	3.4137030	-2.1950670
C	-4.2152050	-0.5707960	0.1343280
H	-4.5243100	-0.0575600	-0.7813500
H	-4.5544900	0.0129240	0.9920780
C	-4.8335320	-1.9720820	0.1909410
H	-4.4940310	-2.5604350	-0.6643270
H	-4.5032210	-2.4794570	1.1013360
C	-6.3446030	-1.8922610	0.1830150
H	-6.7144420	-1.4156380	-0.7294590
H	-6.7213360	-1.3443200	1.0515480
F	-6.8828920	-3.1699270	0.2319340
C	1.2574840	-0.8659180	0.2713260
C	1.9635420	-1.3604600	-0.8232890
C	1.9194600	-0.3524610	1.3846200
C	3.3572110	-1.3457120	-0.7961580
H	1.4145060	-1.7550770	-1.6659260
C	3.3133060	-0.3376620	1.4039120
H	1.3376350	0.0046070	2.2227380
C	4.0383340	-0.8435890	0.3183540
O	5.3962910	-0.8839920	0.3705130
O	4.0587260	0.1459120	2.4246210
O	4.1455810	-1.7926550	-1.8031740
C	3.3742770	0.6114430	3.5701530
H	4.1448130	0.9193920	4.2732120
H	2.7365740	1.4682300	3.3299400
H	2.7669420	-0.1815800	4.0162930
C	6.0245960	0.2067890	-0.2922620
H	5.7413790	1.1521170	0.1806460
H	7.0977480	0.0548590	-0.1904120
H	5.7534770	0.2184370	-1.3515500
C	3.5063540	-2.3497710	-2.9351060
H	2.8709870	-1.6114610	-3.4343470
H	4.3044230	-2.6573960	-3.6067980
H	2.9048430	-3.2205160	-2.6587840

TS_{6+10}

C	0.1000860	-0.9375810	-0.0037410
C	-2.3886690	-0.7174340	0.0926120
C	-1.7009040	1.3399550	0.0138870
H	-2.2614860	1.4927900	-0.9076690
C	-0.3285640	1.2503900	-0.1108020
H	0.2598430	1.3800160	0.7963840
N	-1.7630110	-1.0738380	1.2600190
N	-0.4920160	-1.1717140	1.2127200
N	-1.8550080	-1.1515170	-1.0967030
N	-0.5865920	-1.2631590	-1.1459240
C	0.3364400	1.6781510	-1.3848970
H	1.2859140	1.1649510	-1.5507590
H	-0.3216600	1.4558220	-2.2308870
C	-2.2784770	1.9864570	1.2434680
H	-3.2944920	1.6525070	1.4597800
H	-1.6574970	1.7353880	2.1087490
C	0.5967570	3.1990430	-1.3086180
H	0.9739840	3.5227700	-2.2828440
H	1.4029560	3.3840250	-0.5901070
C	-2.2971500	3.5165130	1.0347540
H	-2.6159370	3.9773460	1.9742510
H	-3.0670280	3.7645950	0.2953210
C	-0.9626250	4.1404650	0.5907170
H	-0.9935170	5.1963800	0.8703960
H	-0.1472110	3.7077220	1.1807240
C	-0.6221660	4.0553910	-0.9244080
H	-0.4317190	5.0692300	-1.2848630
H	-1.4979960	3.7076410	-1.4835760
C	-3.8871360	-0.6213350	0.1383350
H	-4.2279790	0.0609880	-0.6461980
H	-4.1791670	-0.2118930	1.1070260
C	-4.5257630	-2.0023370	-0.0486740
H	-4.2245300	-2.4198780	-1.0117240
H	-4.1728790	-2.6765250	0.7361870
C	-6.0346460	-1.9072450	0.0135960
H	-6.4270610	-1.2639280	-0.7790810
H	-6.3728920	-1.5285110	0.9821780
F	-6.5927180	-3.1657910	-0.1581350
C	1.5765850	-0.9752930	-0.0513600
C	2.2504600	-1.2549810	-1.2445350
C	2.3197690	-0.7078800	1.0957870
C	3.6337360	-1.2654930	-1.2821670
H	1.6780630	-1.4721030	-2.1378510

C	3.7093780	-0.7141450	1.0624740
H	1.8035170	-0.5054370	2.0269640
C	4.3804960	-0.9926440	-0.1292320
H	4.1459200	-1.4915510	-2.2107580
H	4.2552380	-0.5035630	1.9722650
S	6.1394080	-1.0288720	-0.2992500
C	6.7080160	-0.6928600	1.3824980
H	6.3621780	-1.4592070	2.0758810
H	7.7956770	-0.7230520	1.3352910
H	6.3963440	0.2963170	1.7171860

TS_{7+10}

C	0.3278320	-0.8534810	-0.0551720
C	2.8230410	-0.7988760	-0.0793820
C	2.2577990	1.3200370	-0.0063170
H	2.8025400	1.4274390	0.9311560
C	0.8811710	1.3169330	0.0812780
H	0.3277690	1.4877750	-0.8413940
N	2.2091500	-1.1014760	-1.2668340
N	0.9329470	-1.1145780	-1.2560960
N	2.2279050	-1.2002030	1.0910280
N	0.9535560	-1.2295600	1.1026210
C	0.2110940	1.7816320	1.3395470
H	-0.7738620	1.3313280	1.4819960
H	0.8318020	1.5177310	2.2016560
C	2.9092080	1.9291310	-1.2171640
H	3.9069500	1.5299340	-1.4067770
H	2.2968550	1.7219640	-2.1001780
C	0.0487040	3.3163860	1.2573030
H	-0.3383140	3.6620430	2.2199700
H	-0.7229020	3.5497390	0.5152990
C	3.0229550	3.4541610	-0.9984590
H	3.4003250	3.8945040	-1.9260680
H	3.7864970	3.6461340	-0.2360450
C	1.7222970	4.1677340	-0.5902090
H	1.8384580	5.2205140	-0.8587090
H	0.8966350	3.8006450	-1.2101980
C	1.3281520	4.0983050	0.9130720
H	1.1846400	5.1207720	1.2706360
H	2.1646920	3.7014760	1.4998660
C	4.3241340	-0.7871740	-0.0792940
H	4.6775980	-0.1331090	0.7234390
H	4.6695950	-0.3865650	-1.0339420
C	4.8752400	-2.2049440	0.1125540
H	4.5138740	-2.6156870	1.0578520
H	4.5157200	-2.8488230	-0.6945790
C	6.3885900	-2.1971520	0.1083810
H	6.7873640	-1.5954810	0.9303240
H	6.7850120	-1.8182570	-0.8379210
F	6.8627150	-3.4903390	0.2702240
C	-1.1524840	-0.7889050	-0.0508930
C	-1.8677000	-1.0552760	1.1188620
C	-1.8275530	-0.4261160	-1.2188920
C	-3.2535610	-0.9655360	1.1218830
H	-1.3292260	-1.3290760	2.0173070
C	-3.2117010	-0.3289940	-1.2221610
H	-1.2607800	-0.2242220	-2.1198500
C	-3.9062270	-0.6046610	-0.0500700
H	-3.8272010	-1.1502360	2.0228040
H	-3.7540160	-0.0249170	-2.1100980
S	-5.6901540	-0.5127210	-0.0576920
O	-6.1313980	-0.3033170	1.3138790
O	-6.0853280	0.3978380	-1.1229660
C	-6.1908800	-2.1603750	-0.5412690
H	-5.8194820	-2.8675470	0.1983630
H	-7.2807180	-2.1478440	-0.5540400
H	-5.7935550	-2.3661000	-1.5337280

TS_{8+10}

C	0.6919500	-1.2634430	0.1513560
C	-1.6838140	-0.5206690	0.0821400
C	-0.4988620	1.3761270	-0.0438210
H	-0.9710820	1.5949480	-1.0013730
C	0.8104710	0.9567870	-0.0783390
H	1.3699420	0.9675300	0.8557300
N	-1.2084850	-0.9288280	1.2993910
N	0.0138790	-1.2982080	1.3403980
N	-1.1984780	-1.1152670	-1.0493650
N	0.0196500	-1.5047560	-1.0102240
C	1.6182050	1.1403330	-1.3292200
H	2.4211690	0.4049930	-1.4253830
H	0.9680050	1.0422030	-2.2044600
C	-0.9737650	2.1890980	1.1266490
H	-2.0507640	2.1157460	1.2888990
H	-0.4752740	1.8400680	2.0359710
C	2.2359130	2.5567180	-1.2886050
H	2.7283990	2.7354720	-2.2490130
H	3.0251560	2.5745450	-0.5286840
C	-0.6134810	3.6690120	0.8632680
H	-0.8604300	4.2381170	1.7643860
H	-1.2620560	4.0565850	0.0692520
C	0.8541630	3.9342130	0.4824460
H	1.0647000	4.9788750	0.7249870
H	1.5074330	3.3453440	1.1357210
C	1.2444940	3.6998590	-1.0056360
H	1.6966530	4.6197540	-1.3847880
H	0.3410170	3.5504530	-1.6081010
C	-3.1091000	-0.0550690	0.0337560
H	-3.2307840	0.6451730	-0.7980700
H	-3.3318650	0.4687320	0.9651890
C	-4.0653070	-1.2420570	-0.1296600
H	-3.8422190	-1.7706340	-1.0590620
H	-3.9240680	-1.9419360	0.6982590
C	-5.5024200	-0.7691340	-0.1462960
H	-5.6887590	-0.0870770	-0.9809360
H	-5.7702020	-0.2703270	0.7895820
F	-6.3540970	-1.8536620	-0.2974780
C	2.1405060	-1.6042580	0.1870870
C	2.6961320	-2.4279080	-0.7915910
C	4.1444660	-1.3523210	1.2430310
C	4.0520720	-2.7145720	-0.7144820
H	2.0676860	-2.8248110	-1.5774560
C	4.7957840	-2.1697240	0.3239720
H	4.6926980	-0.9004030	2.0640050
H	4.5186020	-3.3560280	-1.4528830
H	5.8557200	-2.3659260	0.4240160
N	2.8466850	-1.0667110	1.1819690

TS_{26+10}

C	0.0854050	-0.8462950	-0.0125420
C	2.5810250	-0.7904700	-0.0899860
C	2.0215050	1.3199910	-0.0034180
H	2.5883590	1.4270170	0.9207240
C	0.6467750	1.3169200	0.1164840
H	0.0708510	1.4908150	-0.7913880
N	1.9420650	-1.0957040	-1.2640110
N	0.6666670	-1.1094850	-1.2262170
N	2.0116110	-1.1943500	1.0923970
N	0.7375400	-1.2238730	1.1312760
C	0.0060640	1.7741360	1.3927320
H	-0.9754400	1.3226990	1.5523540
H	0.6456310	1.5024580	2.2384990
C	2.6435580	1.9332030	-1.2277930
H	3.6368430	1.5362430	-1.4429530
H	2.0104610	1.7282520	-2.0963830
C	-0.1550120	3.3097050	1.3278680
H	-0.5122650	3.6492150	2.3041840
H	-0.9460760	3.5520730	0.6098130
C	2.7592190	3.4579810	-1.0083690
H	3.1079510	3.9033420	-1.9445370
H	3.5423060	3.6514140	-0.2665710
C	1.4661450	4.1621080	-0.5618840
H	1.5647290	5.2158380	-0.8335350
H	0.6260840	3.7873370	-1.1568940
C	1.1177760	4.0877530	0.9521090
H	0.9919920	5.1089120	1.3198510
H	1.9680610	3.6803420	1.5104890
C	4.0821780	-0.7827790	-0.1246790
H	4.4569260	-0.1314180	0.6704660
H	4.4051130	-0.3806980	-1.0865240
C	4.6349640	-2.2020110	0.0506290
H	4.3033510	-2.6108240	1.0074610
H	4.2473470	-2.8453730	-0.7436460
C	6.1474100	-2.1974080	-0.0019320
H	6.5726470	-1.5855690	0.7986800
H	6.5138460	-1.8316290	-0.9651730
F	6.6263180	-3.4887150	0.1621810
C	-1.3938560	-0.7839880	0.0228160
C	-2.0861410	-1.0541020	1.2069740
C	-2.0969340	-0.4215370	-1.1270290
C	-3.4708080	-0.9638760	1.2362060

H	-1.5308250	-1.3319420	2.0938940
C	-3.4834670	-0.3275790	-1.1027650
H	-1.5505790	-0.2226350	-2.0414430
C	-4.1537590	-0.6083620	0.0782990
H	-4.0099570	-1.1609380	2.1574810
H	-4.0581900	-0.0356790	-1.9751790
C	-6.2952930	-2.2390830	0.0699170
H	-5.8878410	-2.6963780	0.9714860
H	-7.3780770	-2.3530530	0.0379900
H	-5.8394130	-2.6570770	-0.8273620
S	-5.9558410	-0.4539380	0.0882240
O	-6.3441160	0.0558430	-1.2736200

7. References

(1) Frisch, M. J. G., Trucks, W., Schlegel, H. B., Scuseria, G. E., Robb, M. A., Cheeseman, J. R., Scalmani, G., Barone, V., Mennucci, B., Petersson, G. A., Nakatsuji, H., Caricato, M., Li, X., Hratchian, H. P., Izmaylov, A. F., Bloino, J., Zheng, G., and Sonnenberg, J. L. (2009) Gaussian 09, Revision D.01. *Inc. Wallingford, CT*.

(2) Zhao, Y., and Truhlar, D. G. (2008) The M06 suite of density functionals for main group thermochemistry, thermochemical kinetics, noncovalent interactions, excited states, and transition elements: Two new functionals and systematic testing of four M06-class functionals and 12 other function. *Theor. Chem. Acc. 120*, 215–241.

(3) Ditchfield, R., Hehre, W. J., and Pople, J. A. (1971) Self-Consistent Molecular-Orbital Methods. IX. An Extended Gaussian-Type Basis for Molecular-Orbital Studies of Organic Molecules. *J. Chem. Phys. 54*, 724.

(4) Lan, Y., Zou, L., Cao, Y., and Houk, K. N. (2011) Computational methods to calculate accurate activation and reaction energies of 1,3-dipolar cycloadditions of 24 1,3-dipoles. *J. Phys. Chem. A 115*, 13906–13920.

(5) Liu, F., Paton, R. S., Kim, S., Liang, Y., and Houk, K. N. (2013) Diels-Alder reactivities of strained and unstrained cycloalkenes with normal and inverse-electron-demand dienes: activation barriers and distortion/interaction analysis. *J. Am. Chem. Soc. 135*, 15642–9.

Supporting Information

Manuscript #6

Christoph Denk, Dennis Svatunek, Severin Mairinger, Johann Stanek, Thomas Filip, Dominik Matscheko, Claudia Kuntner, Thomas Wanek, Hannes Mikula*; Design, Synthesis, and Evaluation of a Low-Molecular-Weight ^{11}C-Labeled Tetrazine for Pretargeted PET Imaging Applying Bioorthogonal *in Vivo* Click Chemistry, *Bioconjugate Chem.* **2016**, 27, 1707-1712.

(with permission from American Chemical Society. Copyright 2016 American Chemical Society)

Supplementary Material

Design, Synthesis and Evaluation of a Low-Molecular-Weight ^{11}C-Labeled Tetrazine for Pretargeted PET Imaging applying Bioorthogonal *in Vivo* Click Chemistry

Christoph Denk,[†] Dennis Svatunek,[†] Severin Mairinger,[‡] Johann Stanek,[‡] Thomas Filip,[‡] Dominik Matscheko,[†] Claudia Kuntner,[‡] Thomas Wanek,[‡] and Hannes Mikula*[,†]

[†]Institute of Applied Synthetic Chemistry, Vienna University of Technology (TU Wien), Vienna, Austria

[‡]Health and Environment Department, Biomedical Systems, Austrian Institute of Technology (AIT), Seibersdorf, Austria

Corresponding Author

*hannes.mikula@tuwien.ac.at

Table of Contents

1. Materials and Methods S2
2. Chemical Synthesis and Radiolabeling S3
3. Reaction Kinetics S15
4. *In vitro* and *in vivo* Investigations S17
5. NMR Spectra S21
6. Quantum Chemical Calculations S27
7. References S35

1. Materials and Methods

Unless otherwise noted, all reagents were purchased from commercial suppliers and used without further purification. DCM and 1,4-dioxane were dried using PURESOLV-columns (Innovative Technology Inc.). Dry acetonitrile (Sigma Aldrich) was commercially obtained and stored under argon. Boc protected aminoacetonitrile and dienophiles *s*-TCO **4** and s-TCO-OPNP were prepared following known procedures.[1,2] Anhydrous hydrazine was prepared by the vacuum thermolysis of hydrazine cyanurate.[3] All other solvents were distilled prior to use. Drying of organic solvents after extraction was performed using anhydrous Na_2SO_4 or $MgSO_4$ (Sigma Aldrich) and subsequent filtration. Human Plasma for research purposes was purchased from the Austrian Red Cross blood donation service. Reactions were carried out under an atmosphere of argon in air-dried glassware with magnetic stirring. Sensitive liquids were transferred via syringe. Thin layer chromatography was performed using TLC alumina plates (Merck, silica gel 60, fluorescence indicator F254, or Merck, aluminium oxide neutral, fluorescence indicator F254). Detection in radio-TLC was performed by placing the TLC plates on multisensitive phosphor screens (Perkin-Elmer Life Sciences, Waltham, MA). The screens were scanned at 300 dpi resolution using a PerkinElmer Cyclone® Plus Phosphor Imager (Perkin-Elmer Life Sciences). Preparative column chromatography was performed using a Büchi Sepacore Flash System (2 x Büchi Pump Module C-605, Büchi Pump Manager C-615, Büchi UV Photometer C-635, Büchi Fraction Collector C-660) using silica gel 60 (40-63 µm) as obtained from Merck and distilled or redistilled solvents. ^{1}H, ^{13}C and ^{19}F NMR spectra were recorded on a Bruker Avance IIIHD 600 MHz spectrometer equipped with a Prodigy BBO cryo probe or on a Bruker Avance UltraShield 400 spectrometer at 20 °C. Chemical shifts are reported in ppm (δ) relative to tetramethylsilane and calibrated using solvent residual peaks. Data are shown as follows: Chemical shift, multiplicity (s = singlet, d = doublet, t = triplet, q = quartet, quin = quintet, m = multiplet, br = broad signal) and integration. UV/VIS spectrophotometry was done on a UV-1800 Spectrophotometer (Shimadzu) and temperature-controlled Applied Photophysics 05-19 and SX20 (535 nm LED light source) stopped flow spectrophotometer systems (Applied Photophysics, Surrey, UK) were used for stopped flow measurements. Fluorescence measurements were done on an Edinburgh FLS920 system (Livingston, UK) using Suprasil glass cuvettes. ESI-MS was performed on an HCT ion trap mass spectrometer (Bruker, Germany). A Thermo Fischer Exactive Plus Orbitrap (LC-ESI+) Mass Spectrometer was used for high-resolution mass spectrometry. [^{11}C]Methane was produced *via* the $^{14}N(p, \alpha)^{11}C$ nuclear reaction by irradiating nitrogen gas containing 10% hydrogen using a PETtrace cyclotron equipped with a methane target system (GE Healthcare, Uppsala, Sweden). [^{11}C]Methyl iodide was prepared *via* the gas-phase method in a TracerLab FXC Pro synthesis module (GE Healthcare) and converted into [^{11}C]methyl triflate by passage through a column containing silver-triflate impregnated graphitized carbon.[4,5] HPLC analysis was performed on a 1200 series system (Agilent Technologies) using a Phenomenex Luna SCX (5 µm, 4.6 x 250 mm) column and 9:1 50 mM phosphate buffer pH=2.4:EtOH (flow rate: 1.5 mL/min). For radio-HPLC a GABI* radioactivity detector (Raytest) was used. Retention times were 12.3 min for precursor **8** and 16 min for [^{11}C]-**1**. Preparative HPLC separation was done on the built in HPLC system on the TracerLab FXC pro synthesis module using a Phenomenex Luna SCX (5 µm, 4.6 x 250 mm) column and 9:1 50 mM phosphate buffer pH=2.4:EtOH (flow rate: 1.5 mL/min) in combination with a K-2001 UV detector (Knauer) and radioactivity detector.

2. Chemical Synthesis and Radiolabeling

(E)-cyclooct-4-en-1-yl (2-(2-(2-(2-hydroxyethoxy)ethoxy)ethoxy)ethyl)carbamate (6)

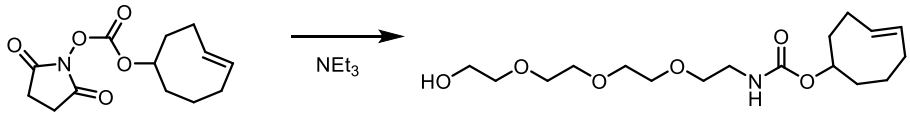

2-(2-(2-(2-aminoethoxy)ethoxy)ethoxy)ethan-1-ol (27 mg, 0.14 mmol, 1.5 eq.) in 200 µl anhydrous DMF was treated with triethyl amine (39 µl, 0.28 mmol, 3 eq.), followed by TCO-O(CO)NHS [6] (25 mg, 0.093 mmol, 1 eq.) in 800 µl anhydrous DMF. The mixture was stirred at room temperature for 22 hours, diluted with 1.25 mL DMSO and 1.25 mL water and loaded onto 30 g C18-silica. The column was eluted with a gradient of acetonitril in water (5-80%). Freeze drying of the product containing fraction yielded 28 mg of title compound as colorless oil (87% of theory). ^{1}H NMR (400 MHz, D_2O) ^{1}H NMR (400 MHz, D_2O) d = 1.54 - 1.71 (m, 3 H) 1.84 - 2.07 (m, 4 H) 2.22 - 2.37 (m, 3 H) 3.25 (t, *J*=5.27 Hz, 2 H) 3.55 (t, *J*=5.27 Hz, 2 H) 3.58 - 3.62 (m, 2 H) 3.63 - 3.72 (m, 10 H) 4.25 (d, *J*=8.20 Hz, 1 H) 5.45 - 5.58 (m, 1 H) 5.59 - 5.74 (m, 1 H) ppm; ^{13}C NMR (100 MHz, D_2O) □ = 30.6, 32.1, 33.7, 37.9, 40.4, 60.4, 69.4, 69.5, 69.6, 69.7, 71.7, 81.9, 133.4, 135.7, 158.3 ppm; ESI-MS $[M+H]^+$ calcd. 346.2 for $C_{17}H_{32}NO_6^+$, found 346.3.

((1R,8S,9r,E)-bicyclo[6.1.0]non-4-en-9-yl)methyl (2-(2-(2-(2-hydroxyethoxy)ethoxy)ethoxy)ethyl) carbamate (7)

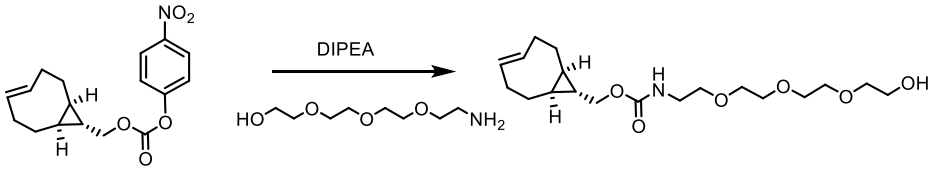

2-(2-(2-(2-aminoethoxy)ethoxy)ethoxy)ethan-1-ol (50 mg, 0.259 mmol, 1.1 eq.) in anhydrous DMF was treated with s-TCO-OC(O)PNP[1] (75 mg, 0.235 mmol, 1 eq.) in one portion followed by diisopropyl ethyl amine (76 mg, 0.59 mmol, 2.5 eq.) causing intense yellow coloration. The mixture was stirred at room temperature for 2 hours, diluted with 1.25 mL DMSO and 1.25 mL water and loaded onto a preparative HPLC column (Phenomenex Luna C18, 21.2x250 mm, 10 µm). Elution with a gradient from 10 to 90% MeCN in water followed by freeze drying of the product fraction yielded 55 mg of title compound as colorless oil (63% of theory). ^{1}H NMR (400 MHz, D_2O) δ = 0.38 - 0.49 (m, 2 H) 0.49 - 0.63 (m, 2 H) 0.77 - 0.90 (m, 1 H) 1.82 - 1.96 (m, 2 H) 2.11 - 2.27 (m, 3 H) 2.32 (d, *J*=12.10 Hz, 1 H) 3.28 (t, *J*=5.27 Hz, 2 H) 3.55 (t, *J*=5.46 Hz, 2 H) 3.58 - 3.71 (m, 13 H) 3.91 (d, *J*=5.07 Hz, 2 H) 5.08 - 5.18 (m, 1 H) 5.81 - 5.93 (m, 1 H); ^{13}C NMR (100 MHz, D_2O) δ = 20.8, 21.9, 24.4, 27.5, 32.3, 33.6, 38.4, 40.12, 60.5, 69.5, 69.6, 69.7, 69.8, 71.9, 131.6, 138.7, 158.1 ppm; ESI-MS $[M+Na]^+$ calcd. 394.2 for $C_{19}H_{33}NNaO_6^+$, found 394.2.

***tert*-butyl N-cyanomethyl-N-methylcarbamate (8)**

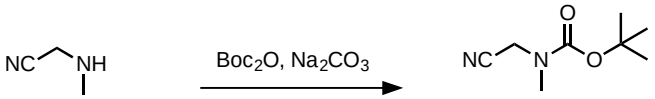

8

N-Methylaminoacetonitrile hydrochloride (1 eq., 1.44 g, 13.51 mmol) was dissolved in a mixture of MeOH (12 mL) and water (4 mL). The solution was treated with sodium carbonate (1.15 eq., 1.64 g, 15.5 mmol). Afterwards Boc_2O (1.5 eq., 4.42 g, 20.2 mmol) was added in one portion. The reaction mixture was stirred for 3 h at room temperature and concentrated. The residue was dissolved in dichloromethane and washed with water. The aqueous phase was re-extracted twice with DCM. The combined organic layer was dried over sodium sulfate and concentrated. Purification by column chromatography (40 g SiO_2, 25% ethyl acetate in hexanes + 0.1% Et_3N) yielded the title compound (2.3 g, 13.5 mmol, 99%) as a white solid. ^{1}H NMR data matched that previously reported.[7]

***tert*-butyl N-methyl-N-((6-methyl-1,2,4,5-tetrazin-3-yl)methyl)carbamate (9)**

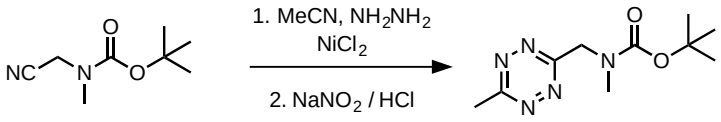

8 **9**

To a stirred mixture of Boc-protected N-methylaminoacetonitrile **8** (1 eq., 0.6 g, 3.5 mmol), dry acetonitrile (7 eq., 0.98 g, 24 mmol) and nickel chloride (0.4 eq., 0.18 g, 1.4 mmol) was carefully added anhydrous hydrazine (36 eq., 4 g, 125 mmol) while cooling using an ice/salt bath. After finished addition the mixture was heated to 42°C for 18 hours. Afterwards the mixture was cooled to 0°C and a ~10% solution of sodium nitrite (2 eq., 0.5 g, 7 mmol) in water was added. While cooling 1N HCl was added slowly until gas evolution ceased. The mixture was extracted ten times with diethyl ether, combined extracts dried over Na_2SO_4, and concentrated. Column chromatography (90 g SiO_2, 50% Et_2O in hexanes + 1% Et_3N) afforded **9** (238 mg, 28%) as a pink oil that crystallized in the freezer.^{1}H NMR (600 MHz, C_6D_6) δ 4.74 (s, 1.2 H), 4.53 (s, 0.8 H), 2.91 (s, 1.3 H), 2.81 (s, 1.7 H), 2.47 (s, 1.3 H), 2.39 (s, 1.7 H), 1.42 (s, 5 H), 1.30 (s, 4 H); ^{13}C NMR (151 MHz, C_6D_6) δ 168.9, 168.7, 167.6, 167.4, 156.4, 155.4, 80.2, 80.1, 52.2, 52.0, 36.1, 36.0, 28.7, 28.6, 21.0 ppm (NMR spectra show a mixture of rotamers); Attempted HR-ESI-FTMS resulted in fragmentation and detection of deprotected substance **1** as $[M+H]^+$ ion (for MS data of **1** see below).

N-methyl-1-(6-methyl-1,2,4,5-tetrazin-3-yl)methanamine (1)

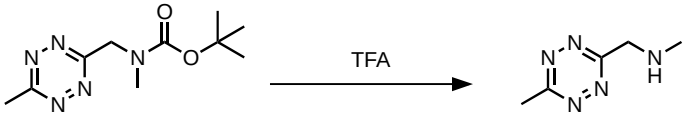

9 **1**

To a stirred solution of **9** (1 eq., 137 mg, 0.573 mmol) in dry DCM (5 mL) was added trifluoroacetic acid (11.4 eq., 0.5 mL, 6.5 mmol) at 0°C. The mixture was stirred at 0°C until TLC indicated complete consumption of starting material (3h). The reaction mixture was partitioned between water and DCM. The organic layer was extracted twice with water and the combined aqueous phases were made alkaline by addition of NaOH. The mixture was extracted several times with DCM and the combined organic layer was washed with water and dried over sodium sulfate. Removal of solvent afforded **1** (40 mg, 51%) as a pink solid. ^{1}H NMR (600 MHz, CD_2Cl_2) δ 4.32 (s, 2 H), 3.03 (s, 3 H), 2.49 (s, 3 H), 1.93 (br. s, 1 H); ^{13}C NMR (151 MHz, CD_2Cl_2) δ 168.8, 168.4, 54.3, 36.2, 21.6 ppm; HR-ESI-FTMS $[M+H]^+$ calcd. 140.0931 for $C_5H_{10}N_5^+$, found 140.0926.

N-methyl-1-(6-methyl-1,2,4,5-tetrazin-3-yl)methanamine trifluoroacetate (1·TFA)

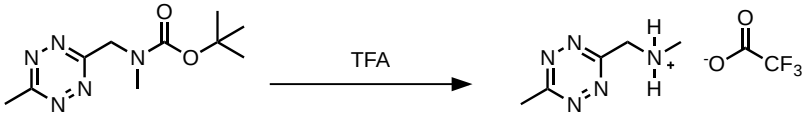

9 **1·TFA**

To a stirred solution of **9** (1 eq., 36 mg, 0.15 mmol) in dry DCM (1 mL) was added trifluoroacetic acid (8.7 eq., 0.1 mL, 1.3 mmol) at 0°C. The mixture was stirred at 0°C until TLC indicated complete consumption of starting material. The reaction mixture was evaporated to dryness on the rotary evaporator. The dark red residue was dissolved in 5 mL water, frozen and lyophilized to obtain **1·TFA** as red oil in quantitative yield. No signs of degradation were noted even after prolonged storage at room temperature. ^{1}H NMR (400 MHz, D_2O) δ 4.90 (s, 2 H), 3.02 (s, 3 H), 2.90 (s, 3 H); ^{13}C NMR (101 MHz, D_2O) δ 169.3, 162.9 (q, J = 35.3 Hz), 162.1, 116.3 (q, J = 292 Hz), 49.6, 33.2, 20.4; ^{19}F NMR (376.5 MHz, D_2O) δ -75.6 ppm.

***tert*-butyl N-((6-methyl-1,2,4,5-tetrazin-3-yl)methyl)carbamate (10)**

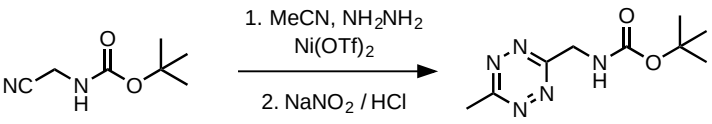

10

To a stirred mixture of tert-butyl (cyanomethyl)carbamate (1 eq., 0.62 g, 4 mmol), dry acetonitrile (7 eq., 1.46 mL, 28 mmol) and nickel trifluoromethanesulfonate (0.52 eq., 0.74 g, 2.08 mmol) was carefully added anhydrous hydrazine (36 eq., 4.5 mL, 144 mmol) while cooling using an ice/salt bath. After finished addition the mixture was heated to 65°C for 20 hours. Afterwards the mixture was cooled to 0°C and a ~10% solution of sodium nitrite (2 eq., 0.55 g, 8 mmol) in water was added. While cooling 1N HCl was added slowly until gas evolution ceased (pH 3). The mixture was extracted three

times with diethyl ether, combined extracts dried over Na_2SO_4, and the solvent removed. Column chromatography (90 g SiO_2, 50% Et_2O in hexanes) afforded **10** (260 mg, 29%) as a pink oil. ^1H and ^{13}C NMR data matched that previously reported.[8]

(6-methyl-1,2,4,5-tetrazin-3-yl)methanamine (11)

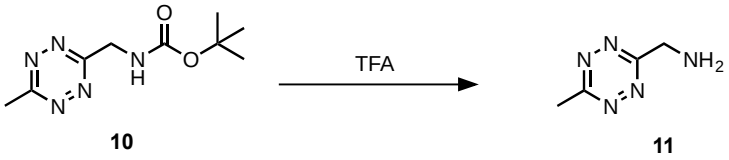

To a stirred solution of **10** (1 eq., 315 mg, 1.4 mmol) in dry DCM (8 mL) was added trifluoroacetic acid (4.6 eq., 0.5 mL, 6.5 mmol) at 0°C. The mixture was stirred at room temperature for 26 h. The reaction mixture was diluted with DCM (40 mL) and 25% NH_4OH (30 mL). Brine (~40 mL) was added, the organic phase was separated and the aqueous phase extracted five times with DCM. The combined organic layer was dried over sodium sulfate and concentrated to yield 156 mg **11** (89%) as a pink-red solid. Even though purity of the raw product was high according to ^1H-NMR the product was further purified (column chromatography over SiO_2 using 5% MeOH in DCM) prior to ^{11}C labeling and NMR measurements. ^1H NMR (600 MHz, $CDCl_3$) δ 4.51 (s, 2 H), 3.08 (s, 3 H), 1.85 (br. s, 2 H); ^{13}C NMR (151 MHz, $CDCl_3$) δ 169.3, 168.1, 45.3, 21.2 ppm; HR-ESI-FTMS $[M+H]^+$ calcd. 126.0774 for $C_4H_8N_5^+$, found 126.0772.

(6-methyl-1,2,4,5-tetrazin-3-yl)methanamine trifluoroacetate (11·TFA)

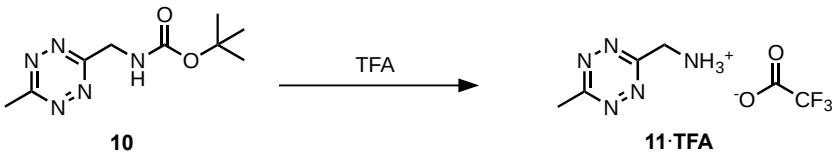

To a stirred solution of **10** (1 eq., 20.1 mg, 0.089 mmol) in dry DCM (1 mL) was added trifluoroacetic acid (14.6 eq., 0.1 mL, 1.3 mmol) at 0°C. The mixture was stirred at 0°C until TLC indicated complete consumption of starting material. The reaction mixture was evaporated to dryness on the rotary evaporator. The dark red residue was redissolved in 5 mL water, frozen and lyophilized to obtain **11·TFA** as a pink solid. No signs of degradation were noted even after prolonged storage at room temperature. ^1H NMR (400 MHz, D_2O) δ 4.91 (s, 2 H), 3.08 (s, 3 H); ^{13}C NMR (101 MHz, D_2O) δ 169.2, 163.0 (q, J = 35.3 Hz), 162.8, 116.3 (q, J = 292 Hz), 41.0, 20.4; ^{19}F NMR (376.5 MHz, D_2O) δ -75.6 ppm

methyl 4-(6-(pyrimidin-2-yl)-1,2,4,5-tetrazin-3-yl)benzoate

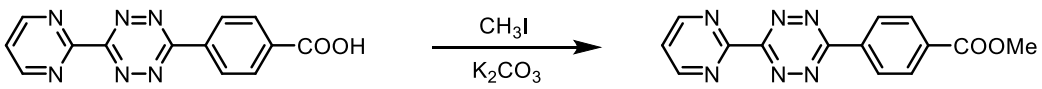

4-(6-(pyrimidin-2-yl)-1,2,4,5-tetrazin-3-yl)benzoic acid [9] (1 eq., 0.56 g, 2 mmol) and potassium carbonate (2 eq., 0.55 g, 4 mmol) were stirred in 37 mL anhydrous DMF under an argon atmosphere. Methyl iodide (1.1 eq., 0.311 g, 2.20 mmol) was added in one portion, and the reaction was stirred at room temperature for 16 h after which TLC showed full conversion. The reaction mixture was diluted with 300 mL EtOAc, washed twice with H_2O and brine, dried over $MgSO_4$, and the solvent was removed on the rotary evaporator. Flash chromatography with 5% MeOH in DCM over a pad of silica yielded the title compound (520 mg, 88.3% of theory) as a deep purple solid. Rf (5% MeOH in DCM) = 0.76, ^{1}H NMR (600 MHz, DMSO-d_6) d = 3.94 (s, 3 H) 7.85 (t, *J*=4.84 Hz, 1 H) 8.26 - 8.29 (m, 2 H) 8.72 - 8.74 (m, 2 H) 9.21 (d, *J*=4.69 Hz, 2 H) ppm; ^{13}C NMR (150 MHz, DMSO-d_6) d = 52.6, 123.1, 128.5, 130.2, 133.2, 135.8, 158.6, 159.0, 162.9, 163.1, 165.7 ppm; FT-MS [M+H$^+$] calcd. 295.0938, found 295.0946

Radiosynthesis of N-[^{11}C]methyl-1-(6-methyl-1,2,4,5-tetrazin-3-yl)methanamine ([^{11}C]-1)

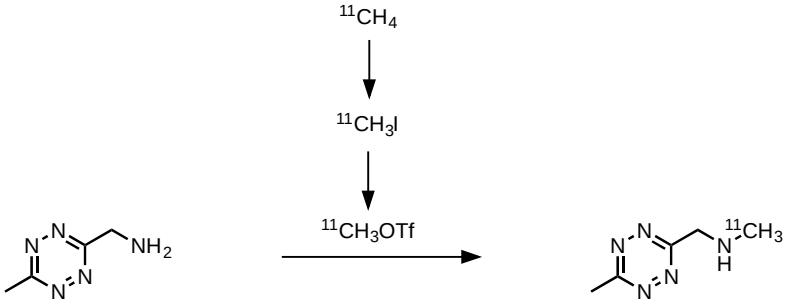

11 [^{11}C]-**1**

[^{11}C]methyl triflate was bubbeled through a solution of compound **11** (0.5 mg, 4 µmol) dissolved in anhydrous MeCN (400 µL) using a TracerLab FXC Pro synthesis module. The reaction mixture was heated for 5 min to 75°C, followed by cooling to 25°C and dilution with HPLC eluent (500 µL, 50 mM phosphate buffer pH = 2.4/ EtOH, 9/1, v/v) and injected into a built-in HPLC system. A Phenomenex Luna SCX 250 x 4.6 mm was eluted with 50 mM phosphate buffer pH=2.4 (solvent A) and EtOH (solvent B), A:B= 9:1 (v/v) at a flow rate of 1.5 mL/min. The HPLC eluate was monitored in series for radioactivity and ultraviolet (UV) absorption at a wavelength of 280 nm. On this system, radiolabeling precursor **11** and product [^{11}C]-**1** eluted with retention times of 11.5—13.5 min and 16-18 min, respectively.

The product fraction from HPLC was collected and evaporated to dryness on a rotary evaporator, followed by reformulation in 0.1 M Na_2HPO_4 at an approximate concentration of 37 MBq/mL for intravenous (IV) injection into animals. The formulated product had a pH of 6 and an osmolarity of 485 mmol/kg.

[^{11}C]-**1** ready for IV injection was obtained in a decay-corrected radiochemical yield based on $^{11}CH_3OTf$ of 52 ± 6% (*n* = 3) in a total synthesis time of 30 min. Radiochemical purity of [^{11}C]-**1** was

determined by analytical radio-HPLC using a Phenomenex Luna SCX column (5 µm, 4.6 x 250 mm) and elution with 50 mM phosphate buffer pH=2.4 (solvent A) and EtOH (solvent B), A:B= 9:1 (v/v) at a flow rate of 1.5 mL/min. UV detection was performed at a wave-length of 530 nm. The retention time of [^{11}C]-**1** was 16 min on this HPLC system. The identity of [^{11}C]-**1** was confirmed by HPLC-comparison injecting unlabeled **1**. Radiochemical purity of [^{11}C]-1 was > 95%. The specific activity of [^{11}C]-**1** was determined by measuring radioactivity of a 1 mL aliquot (using a Capintec Dose calibrator) and by HPLC quantification of **1** (conditions described above ; dilution series**:** 0.01 mM, 0.1 mM, 0.5 mM). The Specific activity was determined to be 10 ± 5.4 GBq/µmol (n=4).

Radiosynthesis of N-[^{11}C]methyl-1-(6-methyl-1,2,4,5-tetrazin-3-yl)methanamine ([^{11}C]-1) using 8·TFA as precursor

The general labeling procedure was followed using 1.2 mg **11·TFA** (5.3 µmol) in 400 µl anhydrous MeCN. Prior to labeling 1 µl diisopropylethyl amine (5.75 µmol, 1.08 eq) was added to the reaction mixture. [^{11}C]-**1** was obtained in 34.6% (n = 1) decay corrected radiochemical yield and in >98% radiochemical purity.

Synthesis of mesoporous silica nanoparticles (MSNs) [10]

1 g (2.74 mmol) cetyltrimethylammonium bromide (CTAB) was suspended in 490 mL 15 mM NaOH. The mixture was stirred using a mechanical stirrer at 300 rpm and heated to 80°C which resulted in a homogenous solution. Tetraethylorthosilicate (TEOS, 6.7 ml, 30.23 mmol) was added within 10 seconds and the turbid mixture was stirred at 80°C for additional 2 hours. The mixture was allowed to reach room temperature, the stirring was turned off and the precipitate was allowed to settle. The supernatant was decanted off and the precipitate was collected by centrifugation (10 m, 3000 x g). The pellet was resuspended in 50 mL distilled water, vortexed for 60 seconds followed by centrifugation (10 m, 3000 x g). This washing cycle was repeated twice with water and once with methanol. Drying in vacuo yielded 1.5 g MSNs as white powder (83% of theory). The surfactant was removed by heating in air using the following temperature program: 20°C → 300°C (2°C/min), 300°C (2 h), 300°C → 550°C (2°C/min), 550°C (16 h). The size of the particles was in the range of 120-145 nm (determined by SEM, Fig. S1).

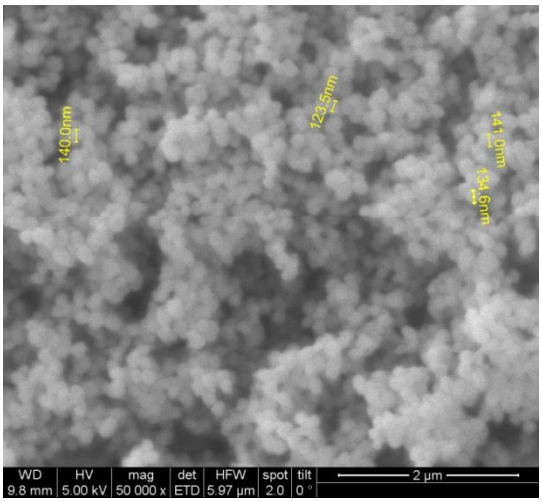

Figure S1: *Electron microscopy of mesoporous silica nanoparticles*

Amino-functionalization of MSNs[11]

357 mg of MSNs were suspended in 20 mL anhydrous toluene and heated on a dean stark trap for 2 h to remove traces of moisture. The dean stark trap was removed and 3-aminopropyltrimethoxysilane (APTMS, 80 µl, 0.458 mmol) was added. The mixture was refluxed for additional 3 h and allowed to cool and settle. The majority of toluene was decanted off and the solids were collected by centrifugation (5 min, 3000 x g). The pellet was resuspended in MeOH, and the solids again collected by centrifugation. Drying in vacuo at 60°C afforded 223 mg amino-grafted MSNs as white powder. The modification did not influence particle size as determined by SEM (Fig. S2).

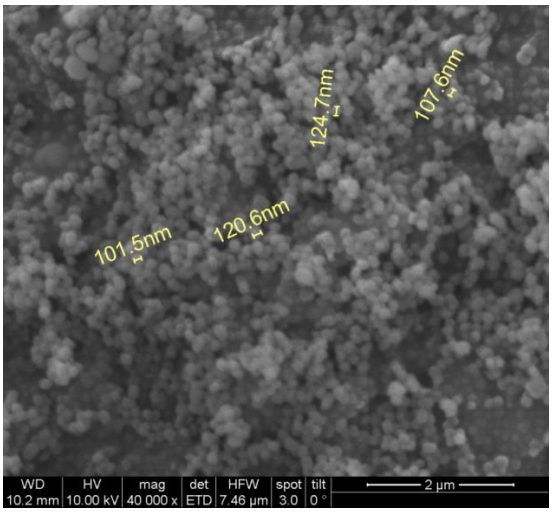

Figure S2: *Electron microscopy of amino-functionalized MSNs*

Determination of amine surface modification

The Fluram (4'-phenylspiro[2-benzofuran-3,2'-furan]-1,3'-dione) assay was chosen for analysis of the degree of surface functionalization with amines.[12] Fluram forms highly fluorescent adducts with primary amines. A stock solution was made by dissolving 14.98 mg native MSNs in 30 g 0.02 N NaOH

followed by the addition of 6.07 mg APTMS (2.26 mmol amine/g MSNs). This stock solution was diluted 1:1, 1:9, 1:99 with a matrix solution (containing 0.5 mg/g native MSNs in 0.02N NaOH) giving solutions corresponding to 1.13 mmol/g, 0.226 mmol/g and 0.0226 mmol/g amine surface modification). The analyte (amino modified MSNs) was also dissolved in dilute NaOH (0.495 mg/g 0.02N NaOH; total 11.22 mg). The blank contained only matrix solution. 100 µl of standard, blank or sample solution were treated with 2 mL 200 mM phosphate buffer pH 8 in a quartz cuvette followed by 1 mL 1 mM fluram solution in acetone. The samples were measured 5 min after fluram addition at 22°C in an Edinburgh FLS920 fluorometer (excitation: 366 nm, emission: 480 nm). Results are summarized in Table S1.

Table S1: *Dilution series concentrations and measured fluorescence intensities*

mmol NH_2/g	cts
blank	1.21E+05
0.022586	1.24E+05
0.22586	1.81E+05
1.1293	3.82E+05
2.2586	6.04E+05

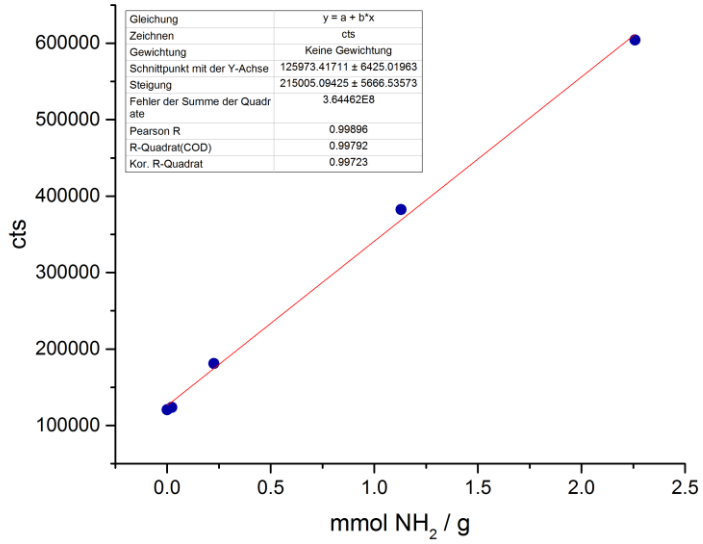

Figure S3: *Linear regression of dilution series data points*

Results of standard and blank measurements were fitted by a linear regression. The sample was found to have **a functionalization degree of 0.92 mmol NH_2/g MSNs**. (3.24E+05 cts; calculated from linear regression shown in Fig. S3).

s-TCO modification of amino-MSNs

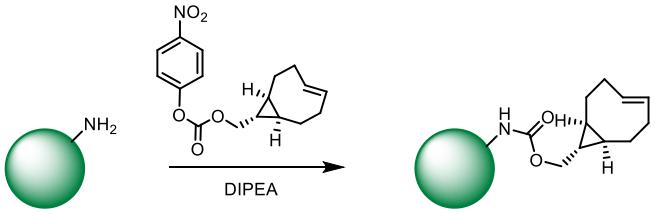

600 µl anhydrous DMF and 30 µl diisopropyl ethyl amine (0.172 mmol) were added to 8 mg of amino-MSNs (7.36 µmol amine). 5 mg of s-TCO-OC(O)PNP[1] (15.75 µmol, 2.14 eq) were added in one portion resulting in intense yellow coloration. The reaction mixture was shaken for 16 hours at room temperature and the particles harvested by centrifugation (13.4krpm, 3 min). The supernatant was discarded and the pellet resuspended in 1.5 mL DMF by vortexing. The solvent was again removed following centrifugation. These washing cycles were repeated three times with DMF and once with EtOH. The particles were dried in high vacuum at ambient temperature using a speedvac system.

TCO-modification of amino-MSNs

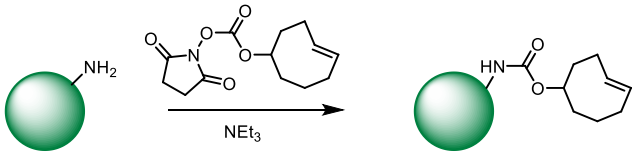

100 µl anhydrous DMF and 15 µl triethyl amine (0.108 mmol) were added to 5.8 mg of amino-MSNs (5.3 µmol amine). 1 mg of TCO-O(CO)NHS[6] (3.74 µmol, 0.81 eq) in 200 µl anhydrous DMF was added in one portion. The reaction mixture was shaken for 16 hours at room temperature and the particles harvested by centrifugation (13.4 krpm, 3 min). The supernatant was discarded and the pellet resuspended in 1.5 mL DMF by vortexing. The solvent was again removed following centrifugation. These washing cycles were repeated three times with DMF and twice with water. The pellet was resuspended in 1.2 mL 0.9% saline.

Analysis of reactive dienophile loading on s-TCO-MSNs and TCO-MSNs

Highly reactive tetrazine methyl 4-(6-(pyrimidin-2-yl)-1,2,4,5-tetrazin-3-yl)benzoate (15.43 mg, 52.43 µmol) was dissolved in MeOH (100 mL) to obtain a 0.524 mM solution. The stock solution and a dilution series (1:1, 1:3, 1:9: 1:19, stock solution diluted with MeOH) were analyzed by HPLC (isocratic, 30% MeCN in 10 mM phosphate buffer pH 6, Agilent Extend-C18 column 3.0 x 100 mm, 3.5 µm, 1.3 ml/min), monitoring the absorption at 530 nm. The tetrazine eluted at 1.6-1.7 min. A linear regression was calculated based on HPLC results (Fig. S4). A defined mass (1-1.45 mg) of nanoparticles (s-TCO-MSNs, TCO-MSNs, Amino-MSNs) was weighted into 1.5 mL tubes and treated with tetrazine stock solution (400-500 µl, corresponding to 210 – 262 nmol). The vials were vortexed for 60 s and shaken for additional 10 min at 37°C to allow for quantitative IEDDA reaction. Following

centrifugation (13.3 krpm, 5 min) excess tetrazine in the supernatant was analyzed by HPLC using the method described above. The calibration factor was obtained by linear regression of HPLC data arising from the dilution series (Table S2, Fig. S4).

Table S2: *Dilution series concentrations and detector response*

Dilution	c [µmol/ml]	Mean area [mAu*s]
Stock	0.524	185.34
1:1	0.262	91.69
1:3	0.131	48.25
1:9	0.052	18.47
1:19	0.026	9.63

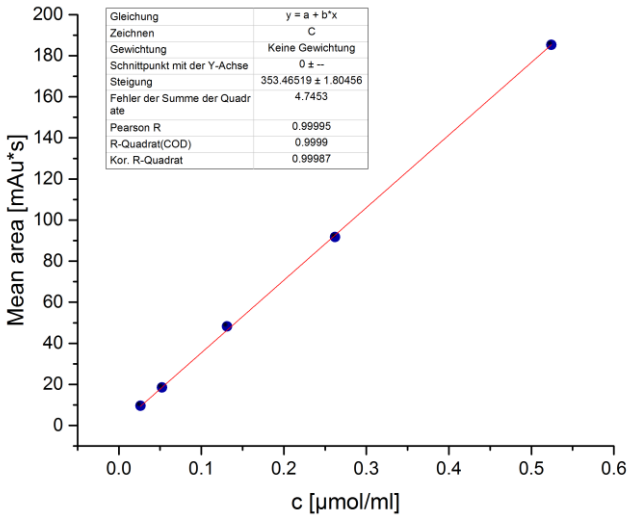

Figure S4: *Linear regression of dilution series data points used for dienophile loading assay*

The dienophile-loading in µmol/g was calculated using the following formula. Results are summarized in Table S3.

$$TCO\ loading\ \left[\frac{\mu mol}{g}\right] = \frac{1000 * V_{stock}\ [ml]}{m\ NP\ [mg]} * \left(0.52435 - \frac{area\ [mAu * s]}{calibration\ factor}\right)$$

Table S3: *Results of dienophile loading assay*

Particle	mass [mg]	V_{stock} [ml]	Mean area [mAu*s]	Dienophile [µmol/g]

Amino-MSNs	1.450	0.50	184.26	**1**
s-TCO-MSNs	1.160	0.40	63.41	**119**
TCO-MSNs	0.500	0.50	144.21	**116**

Synthesis of ^{11}C-labeled MSNs

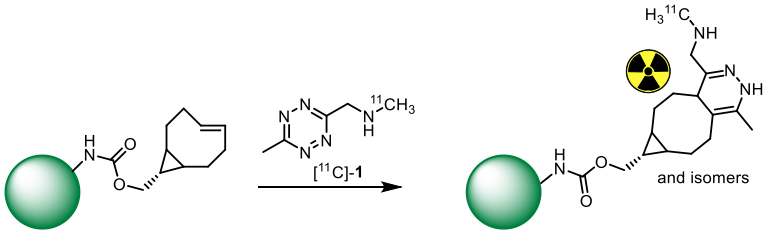

[^{11}C]-**1** (70.3 MBq in 1.5 mL phosphate buffer pH 5.9) was added to 1.48 mg s-TCO-MSNs (176 nmol s-TCO) and vortexed briefly. After 5 min standing at room temperature the suspension was centrifuged (13.3 krpm, 2 min). The supernatant was discarded and the pellet consisting of [^{11}C]MSNs (44.4 MBq, 80% decay-corrected yield) was resuspended in 300 µl 0.9% saline to obtain a suspension ready for i.v. administration.

IEDDA-initiated conjugations

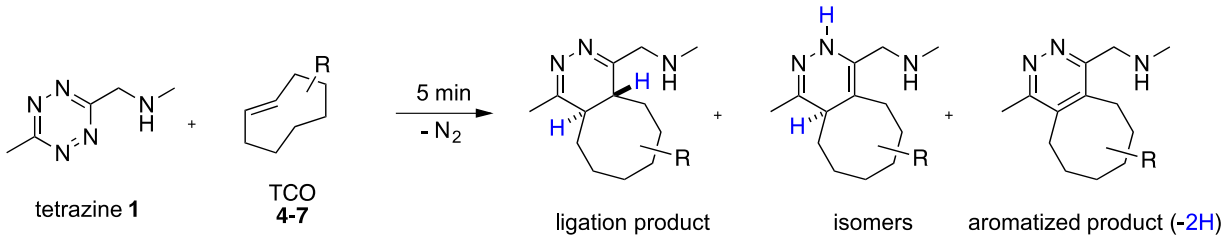

To a 3 mM solution of tetrazine **1** in dry 1,4-dioxane (for **1**+**4** and **1**+**5**) (1 mL) or PBS (for **1**+**6** and **1**+**7**) was added a 3 mM solution of TCO-derivative (1 eq.) in dry 1,4-dioxane (**4** and **5**) or water (**6** and **7**) (1 mL) and the resulting mixture was stirred for 5 min at room temperature. Due to the fast isomerization and aromatization known for the tetrazine/TCO-ligation products, the sample was directly subjected to LCMS analysis for characterization (Table S4).

Table S4. IEDDA-initiated conjugation of tetrazine (**1)** and TCO-derivatives **4**-**7**

Tetrazine	Dienophile	Product formula	Product Calcd. mass	Found mass
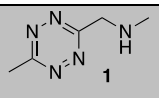 **1**	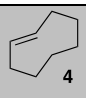 **4**	$[M+H]^+$ $C_{13}H_{24}N_3^+$	$[M+H]^+$ 222.2	$[M+H]^+$ 222.0
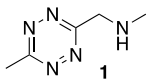 **1**	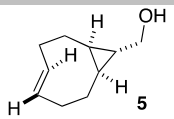 **5**	$[M+H]^+$ $C_{15}H_{26}N_3O^+$	$[M+H]^+$ 264.2	$[M+H]^+$ 264.2
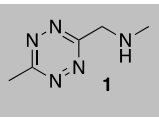 **1**	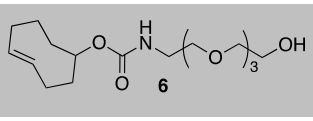 **6**	$[M+H]^+$ $C_{22}H_{39}N_4O_6^+$ (aromatized)	$[M+H]^+$ 455.3	$[M+H]^+$ 455.3
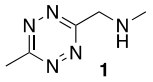 **1**	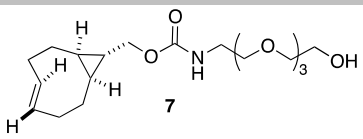 **7**	$[M+H]^+$ $C_{24}H_{41}N_4O_6^+$ (aromatized)	$[M+H]^+$ 481.3	$[M+H]^+$ 481.5

IEDDA initiated conjugation of [^{11}C]-1 with dienophile 5

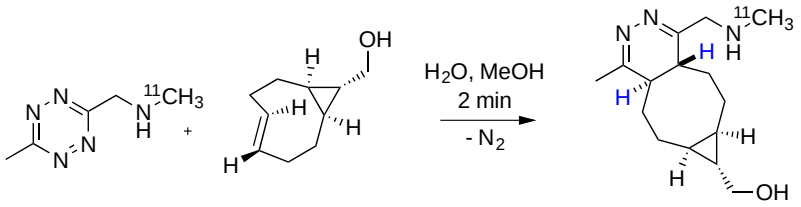

tetrazine [^{11}C]-**1** | s-TCO (**5**) | ligation products + isomers [^{11}C]-**12** + [^{11}C]-**13**

To prove IEDDA reactivity of tetrazine [^{11}C]-**1**, a solution of s-TCO (**5**) (0.5 mg, 3.3 µmol) in MeOH (5 µL) was added to 37 MBq of tetrazine [^{11}C]-**1** dissolved in a mixture of 50 mM phosphate buffer pH=2.4 (solvent A) and EtOH (solvent B), A:B= 9:1 (v/v), 200 µL. The reaction was stirred for 2 min and ~0.5 µL were spotted on SiO_2 plates (together with [^{11}C]-**1** as reference) and TLCs were developed with 10% MeOH + 1% triethylamine in DCM. Analysis of radioactivity distribution on the TLC plates using a Cyclone Phospho Imager indicated complete consumption of [^{11}C]-**1** and the formation of more hydrophilic ligation products [^{11}C]-**12** and [^{11}C]-**13** (Manuscript Fig. 2c).

3. Reaction kinetics

Tetrazine **1** was weighted into a volumetric flask and filled with dry 1,4-dioxane to generate a 3 mM solution. Dienophiles TCO **(4)** and s-TCO (**5**) were weighted into a volumetric flask and filled with dry 1,4-dioxane to generate a 30 mM solution. The reactant solutions were transferred into the driver syringes of the stopped-flow apparatus (Applied Photophysics, Surrey, UK). Upon temperature constancy (± 0.1°C of aimed value) triggering of driver syringe pneumatics caused mixing of equal reactant volumes. Depending on reaction rate time intervals between 10 to 200 s were chosen to collect 4000 data points at 530 nm. All measurements were made in duplicate or triplicate. Reactions in 1,4-dioxane were monitored at 20°C, 37 °C and 60°C. The pseudo first order rate constant (k_{obs}) was determined by linearization of the decay curve followed by linear fitting. The second order rate constant (k) was calculated from the pseudo-first order rate constant. Linearization and direct fitting to the Eyring equation (Equation 1) was used to calculate the enthalpy of activation ($\Delta H^{\ddagger}$) and the entropy of activation ($\Delta S^{\ddagger}$). Equation 2 gave rise to free energy of activation at 298.15 K ($\Delta G^{\ddagger}$). Results are summarized in Table S5 (rate constants) and Table S6 (thermodynamic data). Selected plots of kinetic measurements and Eyring linearization are shown in Fig. S5.

$$\ln\left(\frac{k}{T}\right) = -\left(\frac{\Delta H^{\ddagger}}{R}\right) * \left(\frac{1}{T}\right) + \ln\left(\frac{K_b}{h}\right) + \left(\frac{\Delta S^{\ddagger}}{R}\right) \qquad (1)$$

$$\Delta G^{\ddagger} = \Delta H^{\ddagger} - \mathrm{T}\Delta S^{\ddagger} \qquad (2)$$

Table S5. Results of kinetic measurements (rate constants).

Reaction	Solvent	T (°C)	k_{obs} (s^{-1})	k ($M^{-1}s^{-1}$)
1 + **4**	1,4-dioxane	20	$(8.6 \pm 0.1) \cdot 10^{-3}$	0.57 ± 0.01
		37	$(15.6 \pm 0.5) \cdot 10^{-3}$	1.04 ± 0.03
		60	$(29.9 \pm 0.4) \cdot 10^{-3}$	1.99 ± 0.03
1 + **5**	1,4-dioxane	20	0.99 ± 0.03	65.9 ± 2
		37	1.34 ± 0.02	89.5 ± 1.3
		60	2.026 ± 0.03	135.1 ± 2

Table S6. Results of kinetic measurements (thermodynamic data).

Reaction	Solvent	$\Delta H^{\ddagger}$ (kcal/mol)	$\Delta S^{\ddagger}$ (kcal/mol)	$\Delta G^{\ddagger}$ (kcal/mol)
1 + **4**	1,4-dioxane	5.44	-0.041	17.67
1 + **5**	1,4-dioxane	2.65	-0.041	14.92

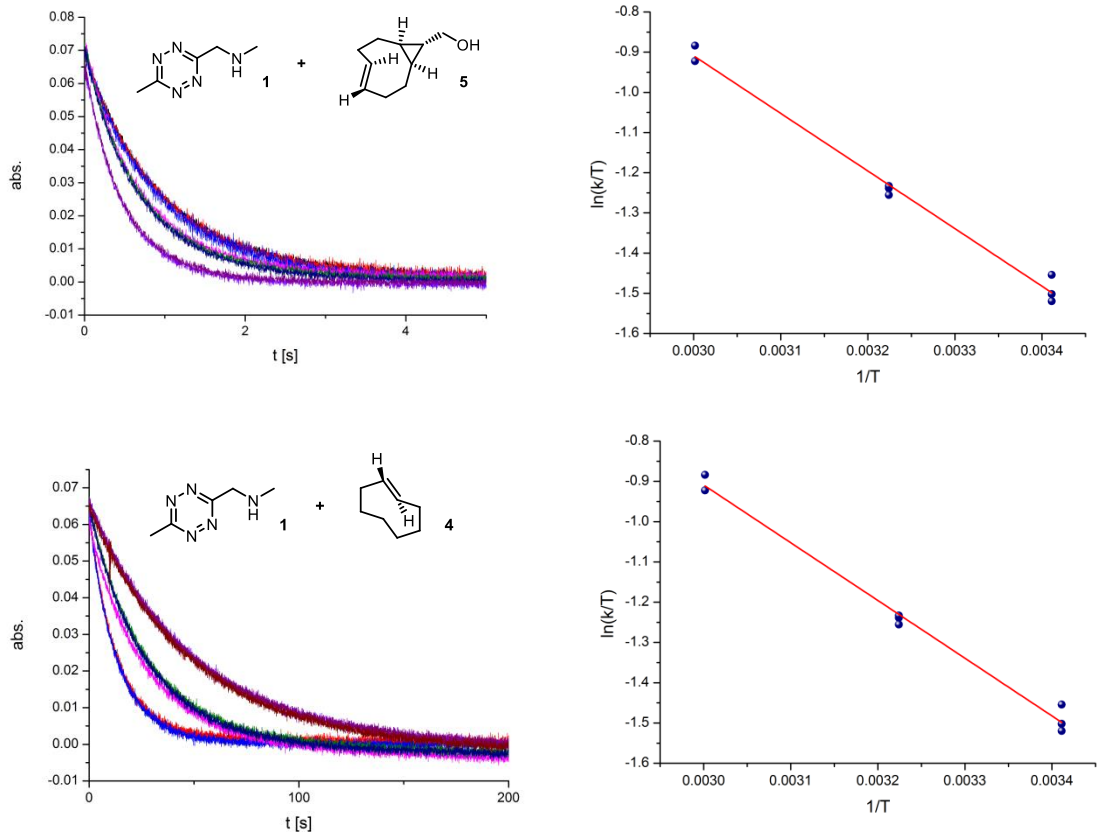

Figure S5. Stopped flow measurements of **1** + **5** and **1** + **4** at 20°C, 37°C and 60°C (left) and Eyring linearization (right)

Reaction rates of **1** with water-soluble dienophiles **6** and **7** were determined in PBS (Fluka, pH 7.4) using a SX20 stopped flow spectrophotometer system (Applied Photophysics, Surrey, UK) equipped with a 535 nm LED light source and a cell temperature of 37.00 ± 0.05 °C. Measurements were done under pseudo-first order conditions with a starting concentration of 1 mM for **1** (as trifluoroacetate), 10.0 mM for **6** and 16.6 mM for **7**. Equal volumes of Tz and TCO solutions were mixed, resulting in concentrations of 0.5 mM for **1**, 5.0 mM for **6** and 8.3 for **7**. Measurements were performed in quintuplicates. The pseudo first order rate constants (k_{obs}) were determined by linearization of the decay curve followed by linear fitting. The second order rate constant (k) was calculated from the pseudo-first order rate constant. Results are summarized in Table S7.

Table S7. Results of kinetic measurements (rate constants).

Reaction	Solvent	T (°C)	k_{obs} (s^{-1})	k ($M^{-1}s^{-1}$)
1 + **6**	PBS	37.00 ± 0.05	0.88 ± 0.01	175.4 ± 1.2
1 + **7**			352.7 ± 25.8	42500 ± 3100

4. *In vitro* and *in vivo* investigations

4.1 Plasma stability of 1

Plasma stability was determined by absorbance measurement. A 5.3 mM solution of **1** in human blood plasma was incubated at 37°C and absorbance at 530 nm was followed over a period of 120 min revealing > 90% recovery (Fig. S6). Identity of remaining **1** was verified by TLC.

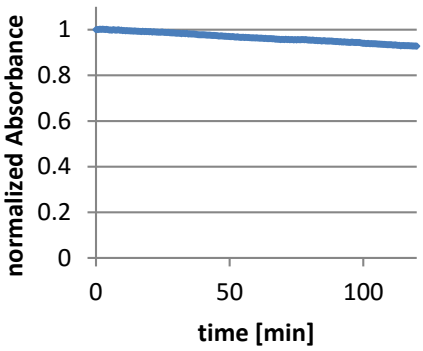

Figure S6. Absorbance of **1** in human blood plasma at 37°C over the course of 120 min

4.2 Animals

For the biodistribution experiments, female BALB/c mice weighting 21.6 ± 5.4 g were purchased from the Division of Laboratory Animal Science and Genetics, Medical University of Vienna, Himberg, Austria. All animals were housed in groups under individual ventilated cage (IVC) conditions in polysulfon type III cages. Environmental conditions were temperature: 22 ±3 °C, humidity: 40% to 70% and a 12-hour light/dark cycle (lights on at 6:00) with free access to standard laboratory diet (ssniff R/m-H, ssniff Spezialdiäten GmbH, Soest, Germany) and tap water. An acclimatization period of at least 1 week was allowed before the animals were used in the experiments. All studies involving laboratory animals were approved by national authorities (*Amt der Niederösterreichischen Landesregierung*) and all study procedures were performed in full accordance to the European Council Directive of September 22, 2010 (2010/63/EU). All efforts were made to comply with the 3R principle.

4.3 PET/MR Imaging – Biodistribution study

Two mice underwent PET scanning on a dual animal bed in a dedicated small-animal PET scanner and one mouse underwent sequential PET/MRI on two stand-alone scanners. Prior imaging, mice were pre-anesthetized in an induction chamber using isoflurane (2.5% in oxygen), placed in prone position on a heated animal bed (38°C) and the lateral tail vein was cannulated using a custom made tail vein catheter. Animal respiratory rate and body temperature were constantly monitored (SA Instruments Inc, Stony Brook, NY, USA) and the isoflurane level was adjusted (1.5-2.5% on oxygen) to achieve a constant depth of anesthesia. Anesthesia was maintained for the whole imaging period. A humidifier was used to moisten the gas mixture before supplying it to the animal(s). For anatomical magnetic resonance imaging (MRI) a single mouse body bed mounted with a mouse whole body RF coil was

used. The whole body coil covers an axial field of view (FOV) of about 8 cm that is very similar to the axial FOV of the PET scanner (7.6 cm). Images were acquired on a 1 Tesla benchtop MRI (ICON, Bruker Biospin GmbH, Ettlingen, Germany) using a modified 3D T_1-weighted gradient echo sequence (T1-FLASH) with the following imaging parameters: echo time (TE) = 5 ms; repetition time (TR) = 25 ms; flip angle (FA) = 25 °; field of view (FOV) = 7.6 x 2.6 x 2.4 cm; matrix = 253 x 93; 32 slices; slice thickness = 750 µm; 5 repetitions; total imaging time = 6 min 15 sec. After MRI, the animal bed was transferred into the gantry of a microPET scanner (Focus 220, Siemens Medical Solutions, Knoxville, TN, USA). Total anesthesia time prior start of PET scanning for mice that underwent PET scanning only was similar to that of the PET/MRI examined animal. Direct after positioning of the animal bed in the gantry of the PET scanner a 10 min transmission scan using a rotating ^{57}Co point source was recorded. Simultaneously with intravenous injection of 16.2 ± 5.9 Mbq [^{11}C]-**1**, dynamic PET imaging was initiated for 60 min using an energy window of 250-750 keV and a timing window of 6 ns. After completion of the imaging procedure, a terminal blood sample was withdrawn under isoflurane anesthesia from the retrobulbar venous plexus and the animals were sacrificed by cervical dislocation. Blood was centrifuged (17000 *g*, 4°C, 4 min) to obtain plasma, and organ samples as well as urine were collected. Aliquots of blood, plasma and urine as well as organ samples were transferred into pre-weighted tubes and measured for radioactivity in a gamma counter (Wizard 1470, Perkin-Elmer, Wellesley, MA, USA). The measured radioactivity data were corrected for radioactive decay and expressed as standardized uptake value ((radioactivity per g/injected radioactivity) x body weight). The 60 min dynamic emission PET data were sorted into 23 frames, which incrementally increased in time length from 5 seconds to 10 min. Images were reconstructed using Fourier rebinning of the 3D sonograms followed by two-dimensional filtered back projection with a ramp filter, resulting in an image voxel size of 0.4 x 0.4 x 0.796 mm^3. A standard data correction protocol (normalization, attenuation and decay correction) was applied to the PET data. The PET units were converted into units of radioactivity concentration by applying a calibration factor derived from imaging of a cylindrical phantom with a known ^{11}C-radioactivity concentration. Corresponding PET/MRI images were aligned using a pre-calculated, fixed transformation matrix. Using the image analysis software Amide,[13] different volumes of interest (brain, liver, kidneys, urinary bladder, heart, lung, bone (left humerus), muscle (right forearm muscle)) were manually outlined on multiple planes and time-radioactivity concentration curves (TACs), expressed in standardized uptake values, were derived.

4.4 Analysis of murine metabolites – *In vivo* stability of [^{11}C]-1

Urine and blood samples were harvested directly after imaging experiments (60 min post administration). Murine plasma was obtained by centrifugation. Proteins were precipitated with acetonitrile and removed by centrifugation. Supernatant solution was spotted on SiO_2 plates and TLCs were developed using 10% MeOH and 1% Et_3N in DCM as mobile phase. [^{11}C]-**1** was spotted as reference. Radioactivity was quantified using a Hewlett Packard Cyclone Phosphor Imager autoradiography system (Figure S7). Analysis showed 50% [^{11}C]-**1** in urine and 38% in plasma together with one main metabolite that is considered to be formed by oxidation of the methyl group at position 6 of the Tz scaffold (similar to the previously reported ^{18}F-labeled Tz[15]).

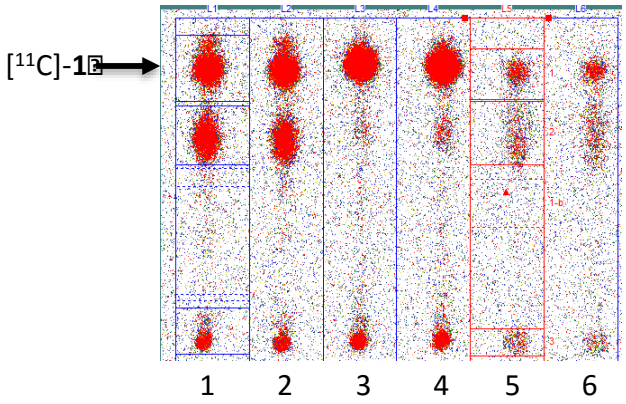

Figure S7. *In vivo* stability of [^{11}C]-**1** as determined by TLC radiochromatography of murine plasma and urine after imaging experiments**:** Lane 1 & 2: Urine metabolites ; Lane 3 & 4: Reference [^{11}C]-**1**; Lane 5 & Lane 6: Plasma metabolites.

4.5 *In vivo* click

For *in vivo* click experiments a group of female BALB/c mice (n=4) was used. A lateral tail vein was used for i.v. administration of water soluble s-TCO derivative **7** (11.8 mg/kg in 0.9% saline, n=2) or 0.9% saline (control group, n=2). After 5 min uptake time the mice were injected with of ^{11}C-[**1**] (mean 8.15 MBq). Retroorbital blood was collected 5 min after administration of ^{11}C-[**1**]. 200 µl of blood was quenched immediately after blood retrieval with 107 µg of tetrazine (4-(1,2,4,5-tetrazin-3-yl)phenyl)methanol in 214 µl water (saturated solution). Murine plasma was obtained by centrifugation and proteins were precipitated with acetonitrile and removed by centrifugation. Supernatant solution was spotted on SiO_2 TLC plates and developed using 20% MeOH in DCM as mobile phase (Fig. S8)

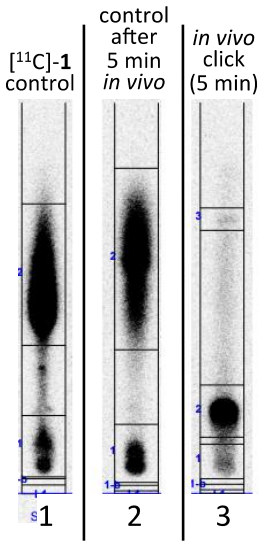

*Figure **S8**. Radio-TLC after in vivo reaction of [^{11}C]-**1** and **7**. Lane 1: [^{11}C]-**1**, Lane 2: control, 5 min biodistribution of [^{11}C]-**1**. Lane 3: after 5 min in vivo reaction .*

Results from this experiment indicate high *in vivo* reactivity between water-soluble s-TCO derivative **7** and [^{11}C]-**1**. After 5 min of *in vivo* reaction time only 1.5 % of total radioactivity originated from [^{11}C]-**1** while >90% of activity was encountered as a single ligation product (Fig. S8, lane 3). Most likely the dihydropyridazine isomers are rapidly oxidized to the appropriate pyridazine resulting in only one detectable aromatized ligation product when the reaction is carried out *in vivo*.

4.6 Biodistribution of [^{11}C]MSNs

The general method for PET data acquisition and reconstruction described under point 4.3 was followed. The nanoparticle suspension was sonicated prior to administration to minimize agglomeration of particles. Female BALB/c mice (n=2) were injected with ^{11}C-labeled MSNs (0.5 mg, 12.9 ± 1.8 MBq) via tail vein catheder and dynamic PET imaging performed for 60 min. PET data revealed rapid and high (18-25 SUV) uptake in the lungs (already after 5 min), while other organs showed much lower activity concentration (Fig. S9). These findings were also confirmed by gamma counter measurements (*ex vivo*).

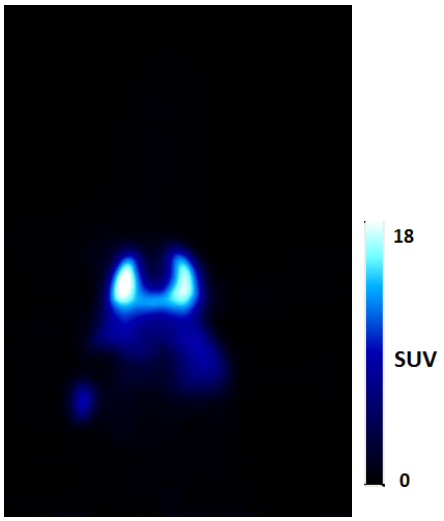

Figure S9. Coronal PET slice (0-60 min) showing high accumulation of [^{11}C]-MSNs in the lung.

4.7 Pretargeted imaging using TCO/s-TCO-MSNs

The general method for PET data acquisition and reconstruction described under point 4.3 was followed. Prior to PET imaging functionalized nanoparticles were administered using a tail vein catheter. The nanoparticle suspensions in 0.9% saline were vortexed and sonicated for 60 seconds prior to administration to minimize agglomeration of particles. Animals were divided into two study groups receiving s-TCO-MSNs (n=5, 0.5 mg, 59 nmol s-TCO) or TCO-MSNs (n=2, 0.5 mg, 58 nmol TCO) as suspension in 100 µL physiological saline. 5 min post nanoparticle administration PET data acquisition was started and the animals were dosed with [^{11}C]-**1** (15.4 ± 6.0 MBq, i.v., 100 µl). Dynamic PET scanning was conducted for 60 min. *Ex vivo* measurements were done using a gamma counter.

5. NMR Spectra

^{1}H spectrum of compound **6**

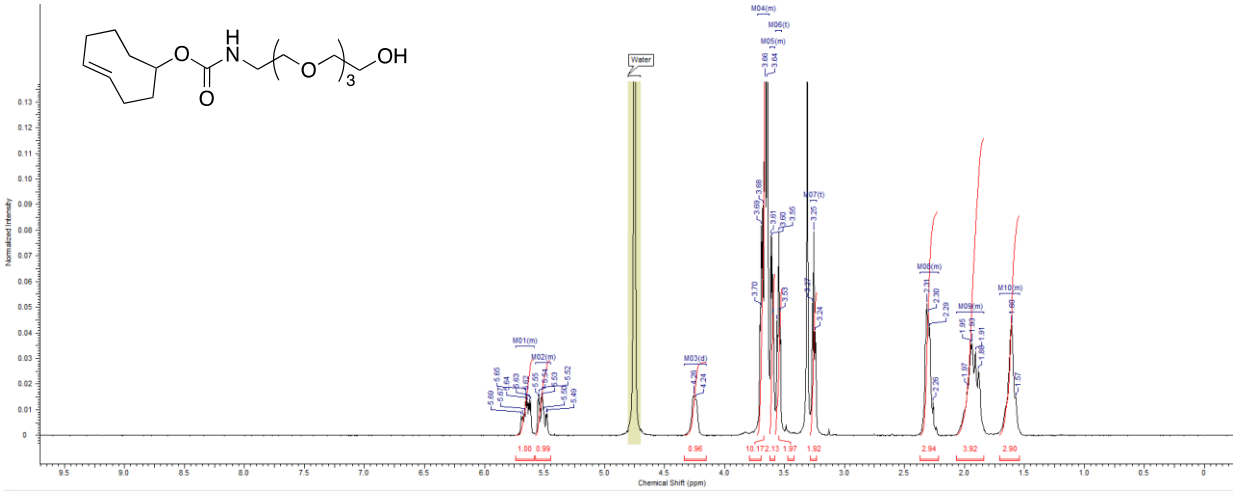

^{13}C spectrum of compound **6**

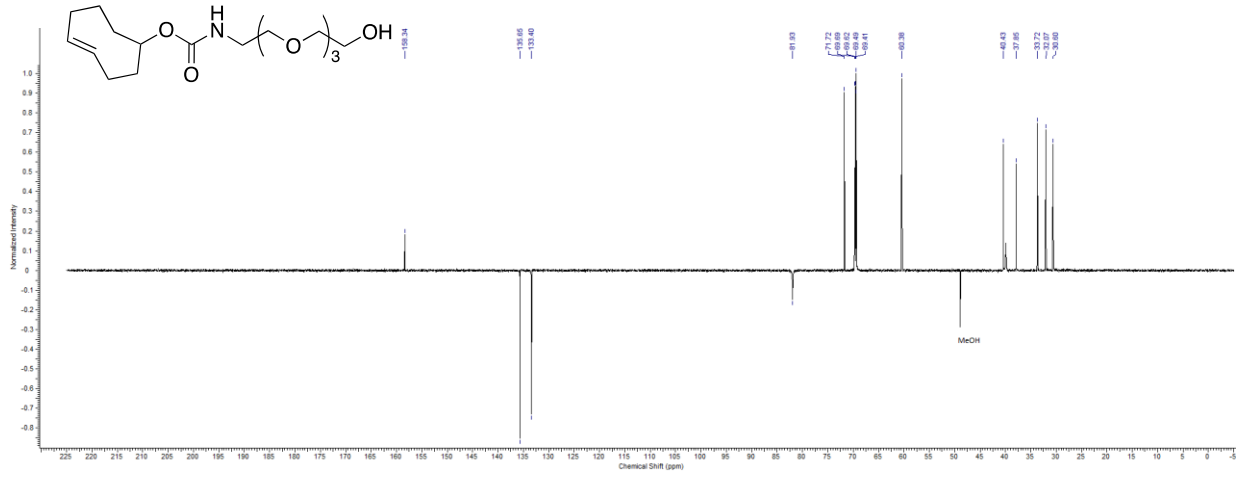

^{1}H spectrum of compound **7**

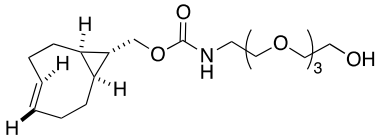

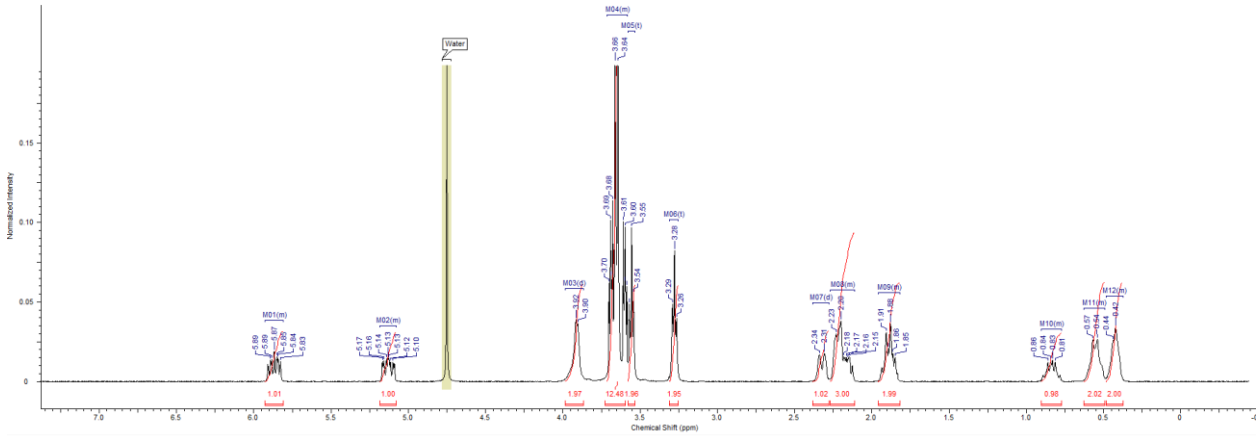

^{13}C spectrum of compound **7**

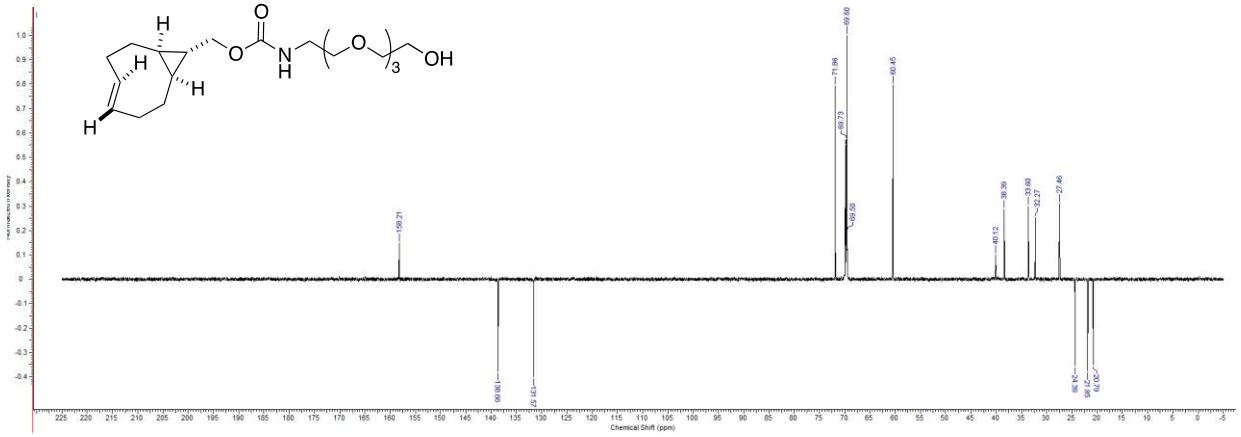

^{1}H spectrum of compound **9**

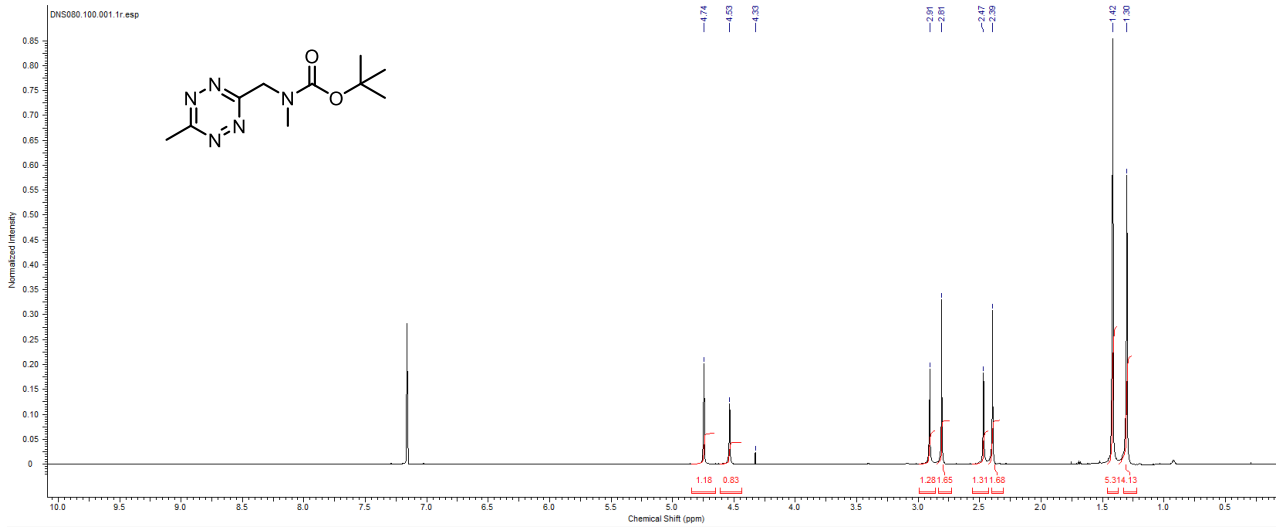

^{13}C spectrum of compound **9**

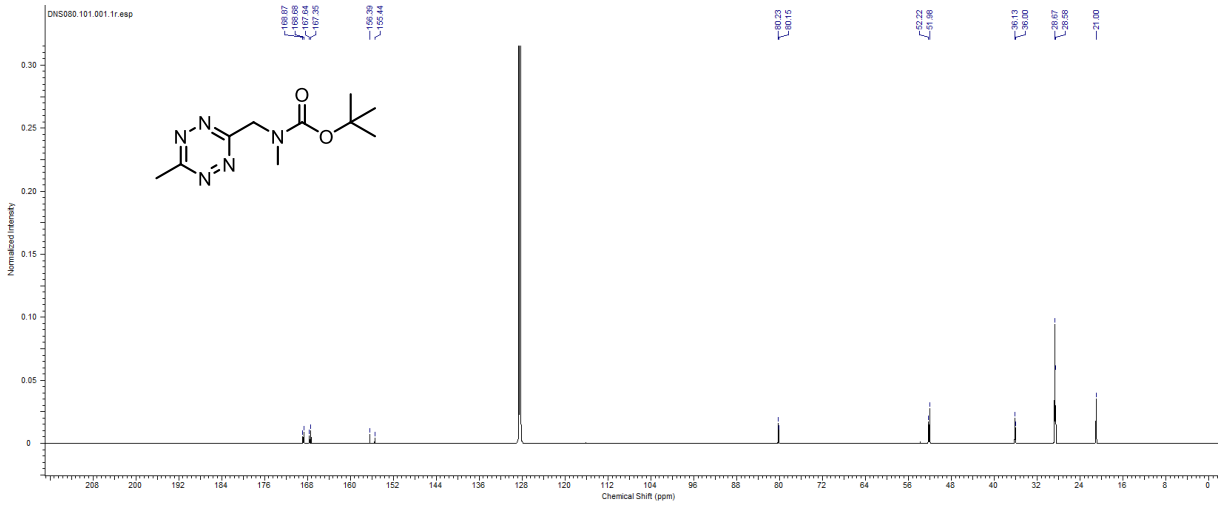

^{1}H spectrum of compound **1**

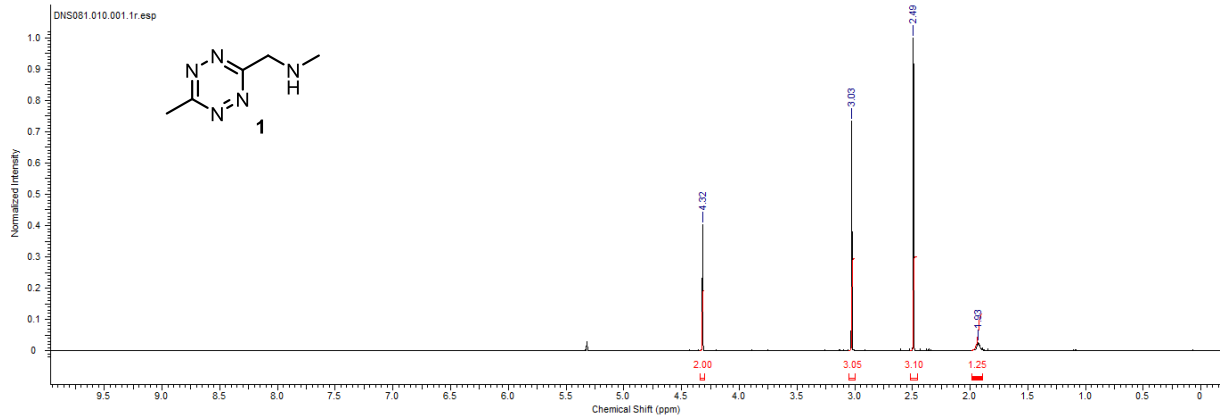

^{13}C spectrum of compound **1**

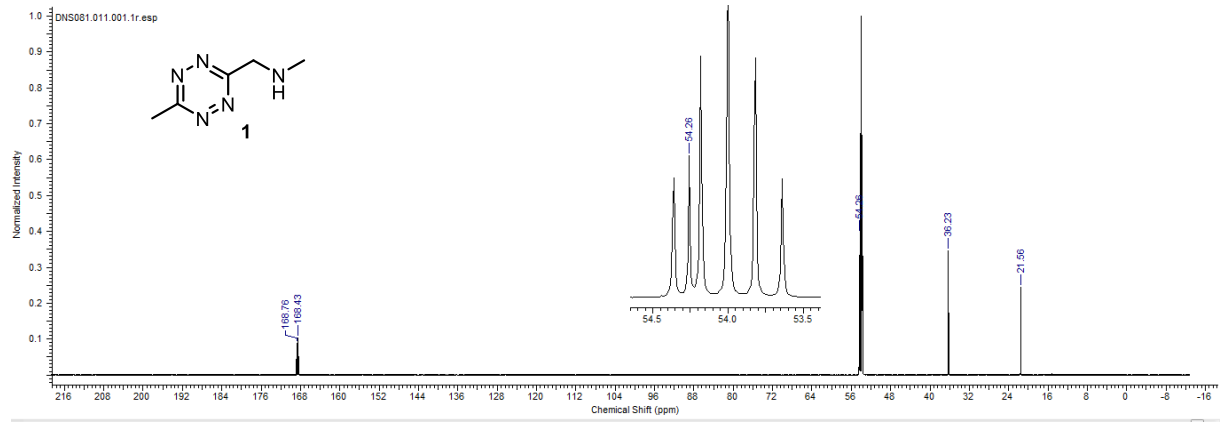

^{1}H spectrum of compound **1·TFA**

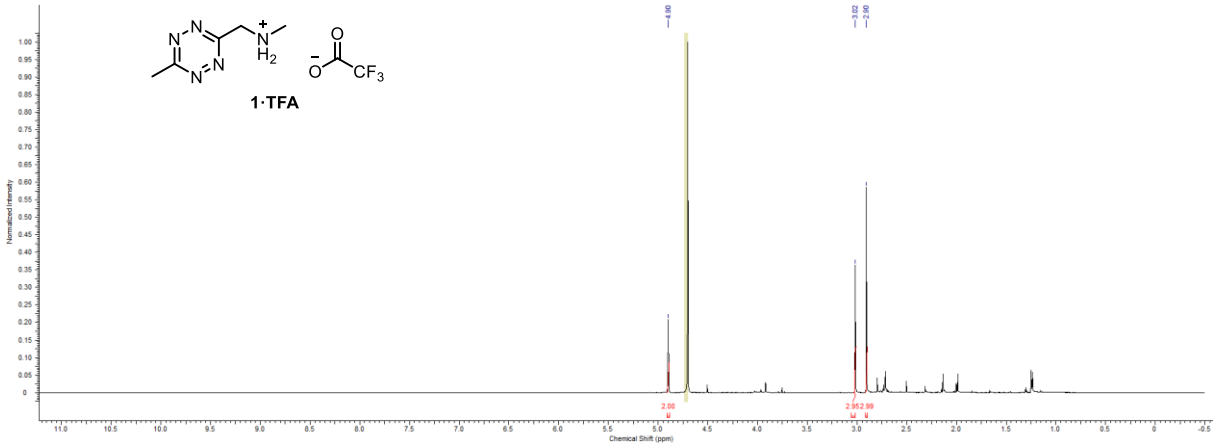

^{13}C spectrum of compound **1·TFA**

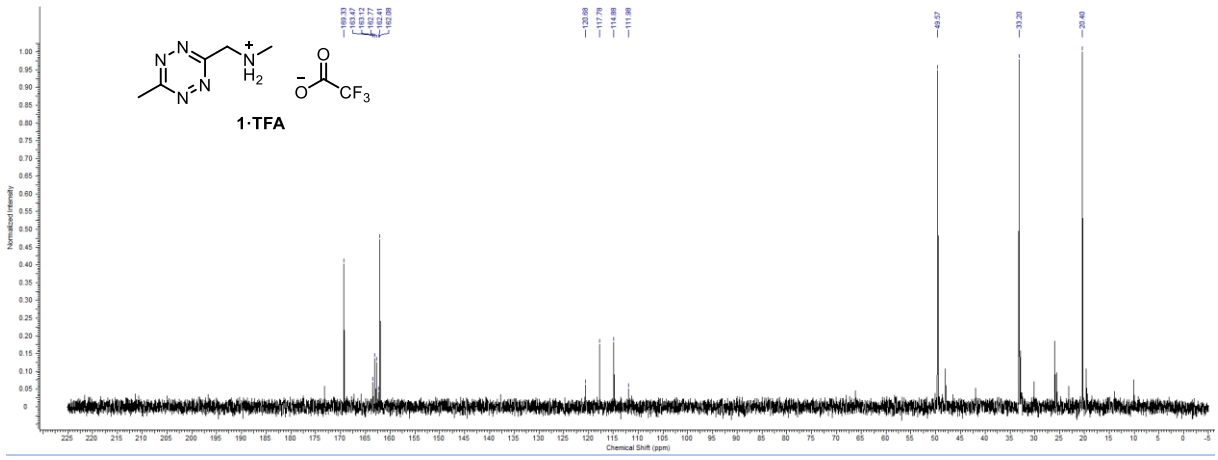

^{19}F spectrum of compound **1·TFA**

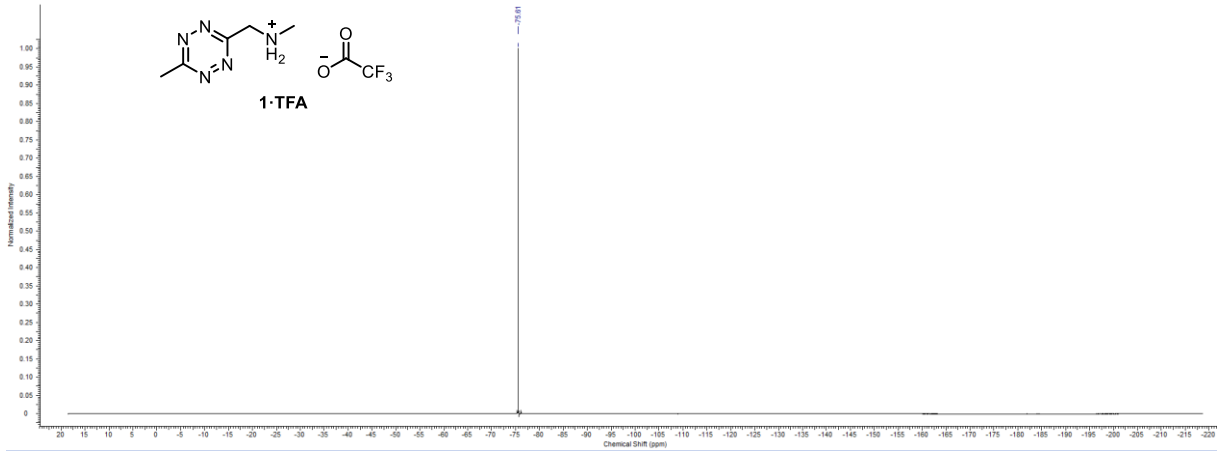

^{1}H spectrum of compound **11**

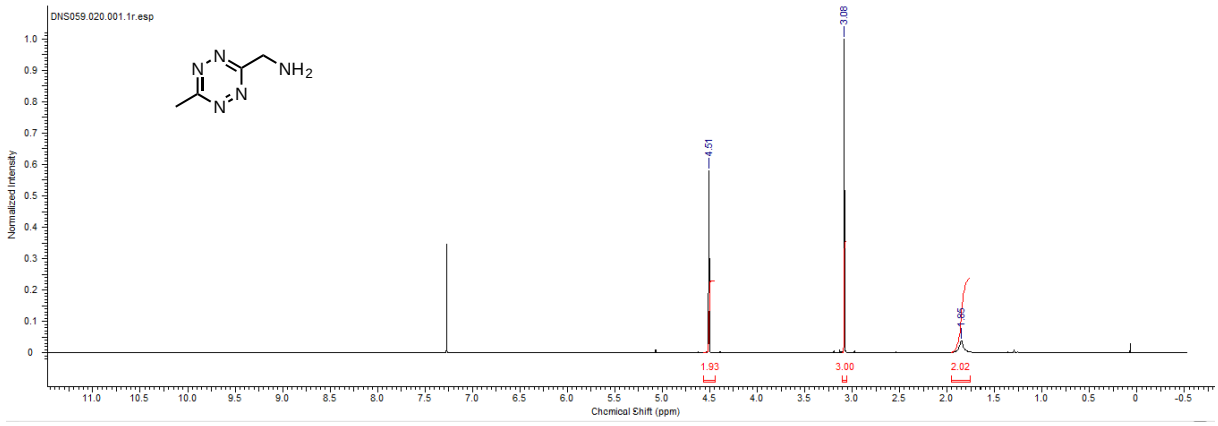

^{13}C spectrum of compound **11**

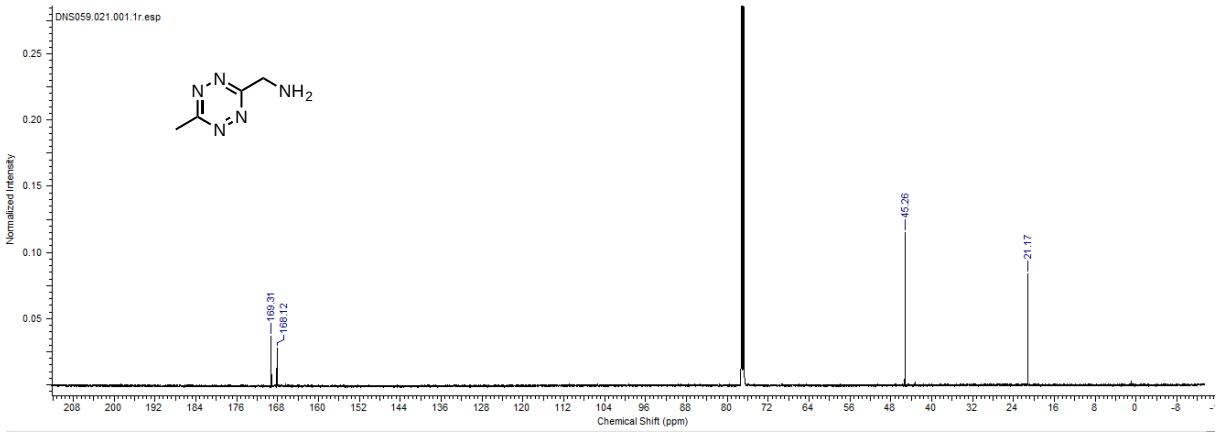

^{1}H spectrum of compound **11·TFA**

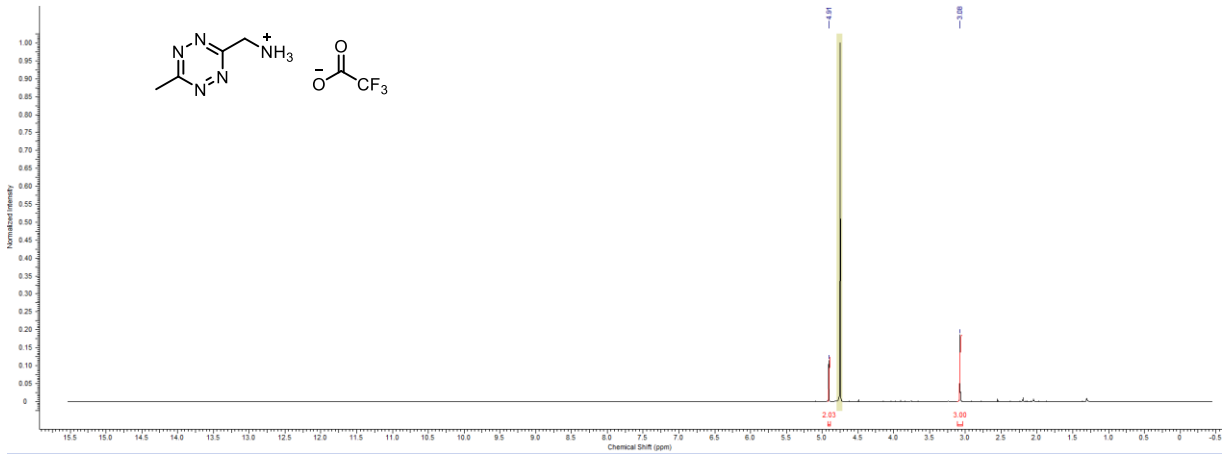

^{13}C spectrum of compound **11·TFA**

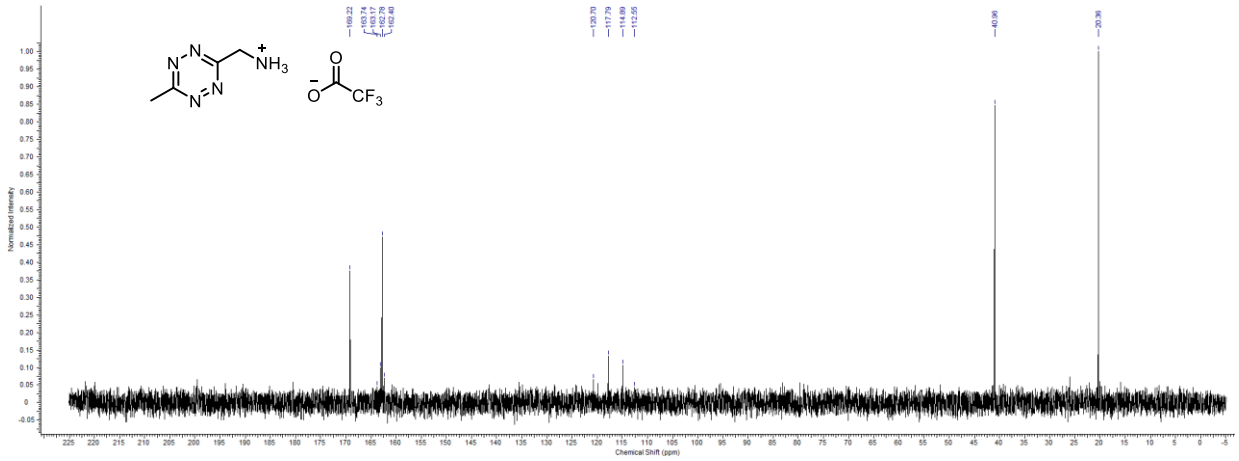

^{19}F spectrum of compound **11·TFA**

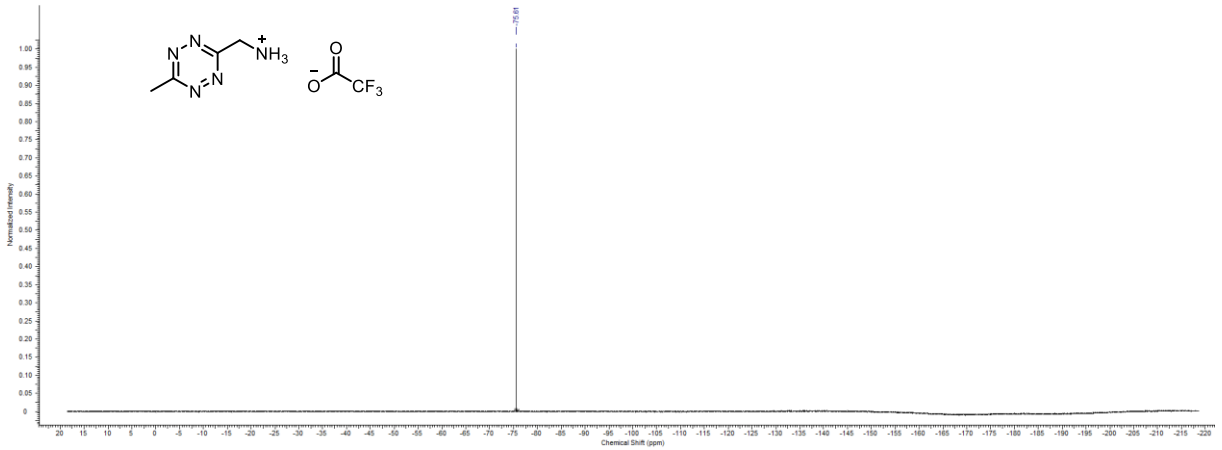

^{1}H spectrum of **methyl 4-(6-(pyrimidin-2-yl)-1,2,4,5-tetrazin-3-yl)benzoate**

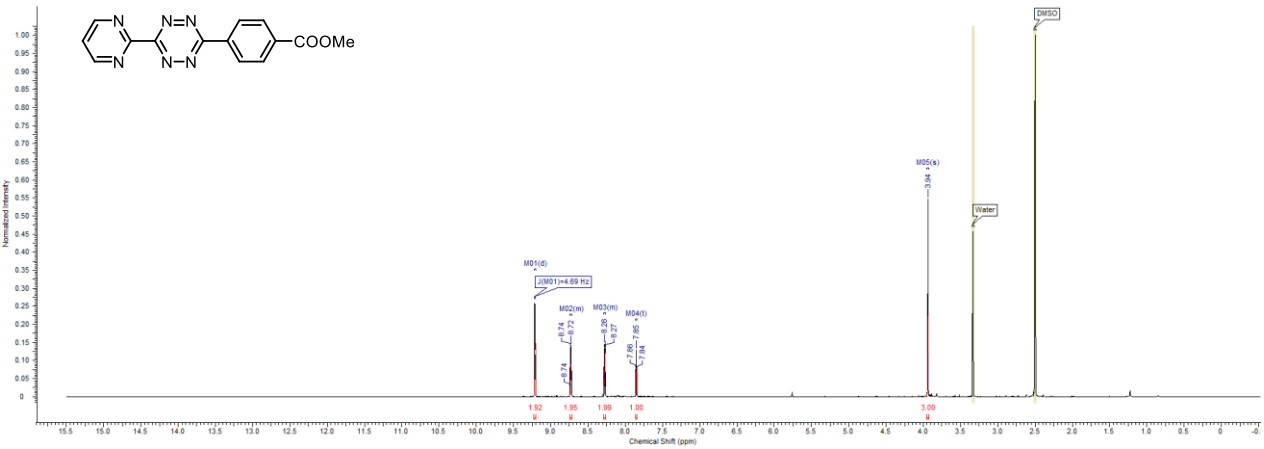

^{13}C spectrum of **methyl 4-(6-(pyrimidin-2-yl)-1,2,4,5-tetrazin-3-yl)benzoate**

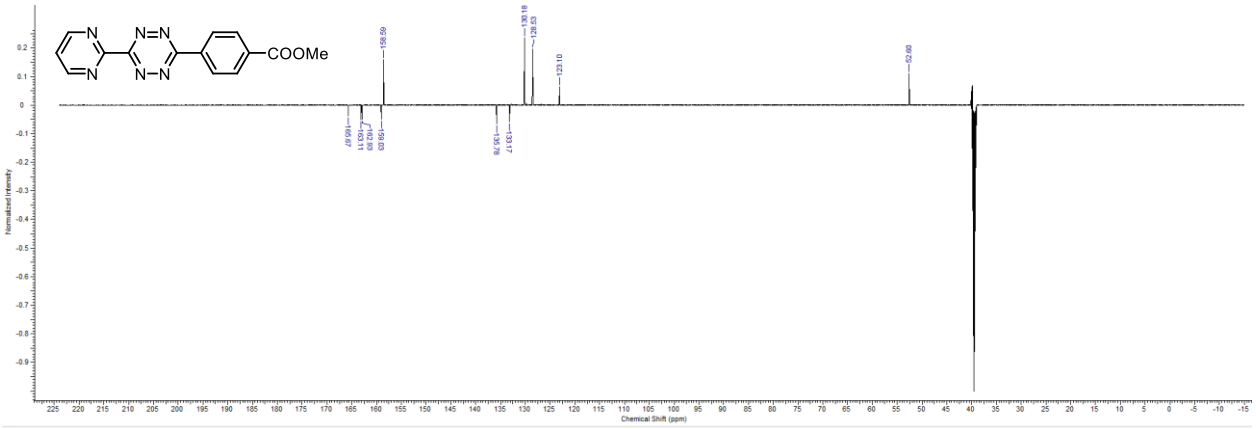
COOMe
158.59
130.18
128.53
123.10
52.60
165.67
153.11
152.93
159.03
136.78
133.17
Normalized Intensity
Chemical Shift (ppm)

6. Quantum chemical calculations

All DFT calculations were performed on the Vienna Scientific Cluster 3 using the Gaussian 09 (Rev. D.01) program package.[14] Geometry optimizations to energy minima or transition states as well as subsequent frequency analyses at 298.15 K of all considered compounds and intermediates were achieved using the M06-2X density functional[15] in combination with the 6-31G(d,p)[16] basis set as implemented in Gaussian 09, which has been found to give relatively accurate energy profiles for cycloadditions.[17,18] All calculations were performed in 1,4-dioxane applying the polarizable conductor calculation model (CPCM) as provided in Gaussian 09. Imaginary frequencies corresponding to the desired reaction coordinates were obtained only in the case of transition state calculations. Data analysis was done using GaussView 5 (Gaussian, Inc.).

The reaction of tetrazines with strained dienophiles proceeds in two steps, the first being an inverse electron demand Diels-Alder (IEDDA)-initiated reaction leading to an intermediate that subsequently undergoes retro-Diels-Alder reaction with the loss of N_2 (Scheme S1).

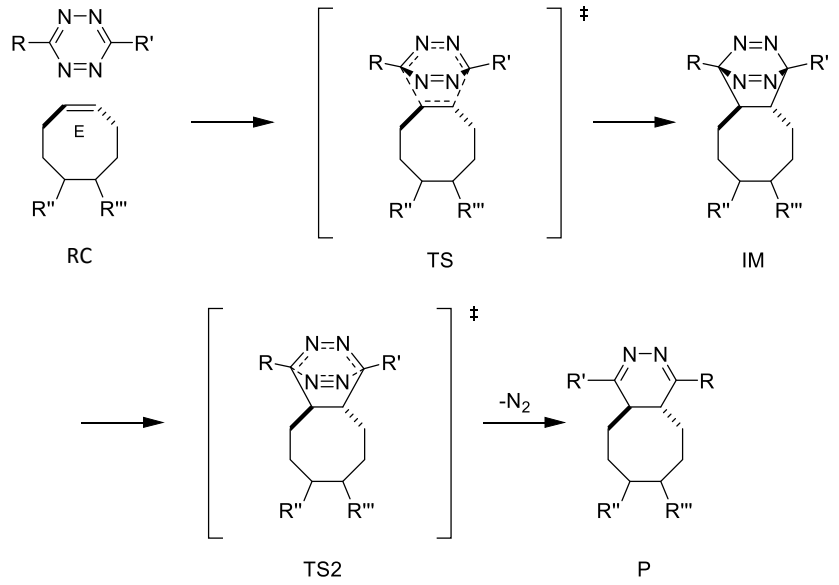

Scheme S1: General mechanism of the tetrazine ligation (RC = reactant complex, TS = transition state, IM = intermediate, P = product).

The first step of this reaction (RC → TS), the inverse electron demand Diels-Alder reaction, is the rate-determining step.[19,20] Therefore, $\Delta G^{\ddagger}$ values of this cycloaddition were considered to determine reaction activation barriers at 298.15 K. Original data is summarized in Table S8 followed by listing of Cartesian coordinates of all relevant structures.

Table S8: Selected original data from Gaussian calculations (E: total electronic energy, ZPE: zero point energy).

Structure	E (hartree)	H (hartree)[a]	G (hartree)[a]	S (Cal/(mol*K))[a]	ZPE (hartree)[a]
TS_{1+4}	-782.533302622	-782.152443	-782.215082	131.835	-782.170739
RC_{1+4}	-782.545771650	-782.164423	-782.234466	147.418	-782.184624
TS_{2+4}	-743.252237286	-742.901448	-742.959890	123.001	-742.918240
RC_{2+4}	-743.272434428	-742.921403	-742.989495	143.313	-742.940619
TS_{3+4}	-865.709502963	-865.323370	-865.388604	137.296	-865.342514
RC_{3+4}	-865.722926843	-865.336327	-865.408282	151.443	-865.357273
TS_{1+5}	-935.088736580	-934.665951	-934.735503	146.384	-934.687298
RC_{1+5}	-935.096619506	-934.673420	-934.749388	159.886	-934.696541
TS_{2+5}	-895.805512643	-895.412924	-895.478989	139.045	-895.432909
RC_{2+5}	-895.820924491	-895.427532	-895.501096	154.829	-895.449600
TS_{3+5}	-1018.26259416	-1017.834645	-1017.908032	154.455	-1017.857081
RC_{3+5}	-1018.27136121	-1017.842855	-1017.922242	167.085	-1017.866880

[a] calculated for T = 298.15

Cartesian Coordinates

TS_{1+4}

C	-0.8947280	2.2034350	-0.1678950
C	-1.8477810	-0.1115990	-0.3334160
C	0.3780830	-0.4376670	-0.2154100
H	0.2098390	-1.0263830	0.6854980
C	0.9026640	0.8240760	-0.0736050
H	1.2853020	1.3073030	-0.9745580
N	-1.8241150	0.6246260	-1.4875910
N	-1.3385720	1.8096960	-1.4014940
N	-2.0102210	0.5343410	0.8588830
N	-1.5150950	1.7180110	0.9481110
C	1.5710320	1.2068610	1.2153040
H	1.5585910	2.2854810	1.3989790
H	1.0536330	0.7190320	2.0498070
C	0.6699980	-1.2370890	-1.4509380
H	-0.1090160	-1.9725360	-1.6667040
H	0.7609670	-0.5667510	-2.3138350
C	3.0381230	0.7226840	1.1567650
H	3.4914380	0.9013430	2.1382270
H	3.5903110	1.3494700	0.4446060
C	2.0034310	-1.9807250	-1.2157500
H	2.2807110	-2.4845420	-2.1485160
H	1.8335500	-2.7725250	-0.4748440
C	3.1743460	-1.0980510	-0.7460670
H	4.0988140	-1.6231450	-1.0068990
H	3.1873730	-0.1734610	-1.3379230
C	3.2282430	-0.7553970	0.7710460
H	4.2071550	-1.0633440	1.1523110
H	2.4974070	-1.3662910	1.3163880
C	-2.4186190	-1.5080600	-0.4525410
C	-0.2702080	3.5631660	-0.0791380
H	0.6468570	3.6121930	-0.6700730
H	-0.0516920	3.8065980	0.9604360
H	-0.9667070	4.3063080	-0.4756250
H	-2.3273870	-1.7968120	-1.5020940
H	-3.4968850	-1.4247340	-0.2272420
N	-1.7572550	-2.5042050	0.3790700
H	-1.9737860	-3.4179540	-0.0051650
C	-2.1746670	-2.4729850	1.7784920
H	-3.2688590	-2.4980280	1.9059700
H	-1.7411870	-3.3303130	2.2982620
H	-1.8091210	-1.5600890	2.2530520

RC_{1+4}

C	-1.6153570	2.0906250	-0.2399240
C	-2.3769350	-0.3532520	-0.2083010
C	0.7691130	-0.3635000	-0.0911220
H	0.6675230	-1.0964170	0.7109460
C	1.1558760	0.8779620	0.2094500
H	1.3067410	1.5872480	-0.6091210
N	-2.0726510	0.1907830	-1.3920760
N	-1.6876250	1.4428200	-1.4100440
N	-2.4208770	0.3316750	0.9434590
N	-2.0260350	1.5778070	0.9295530
C	1.8529210	1.1843950	1.4943950
H	1.7115520	2.2107780	1.8505400
H	1.5088450	0.5022240	2.2808910
C	0.9282680	-0.9162850	-1.4678680
H	0.1925180	-1.6915820	-1.7012500
H	0.8390550	-0.1148030	-2.2116950
C	3.3579570	0.9257630	1.2142460
H	3.9091760	0.9995980	2.1589350
H	3.7406500	1.7279540	0.5700120
C	2.3651940	-1.5016470	-1.5045290
H	2.5978050	-1.7996350	-2.5336270
H	2.3862220	-2.4213180	-0.9053080
C	3.4682520	-0.5486600	-0.9923900
H	4.4131790	-0.8952820	-1.4248950
H	3.3001900	0.4491410	-1.4170940
C	3.6643590	-0.4351030	0.5512020
H	4.7116570	-0.6663140	0.7740530
H	3.0788760	-1.2148360	1.0548380
C	-2.7481470	-1.8116790	-0.1783430
C	-1.0926790	3.4903670	-0.2338490
H	-0.2426850	3.5601590	0.4497290
H	-1.8630220	4.1802050	0.1187980
H	-0.7797400	3.7726810	-1.2384240
H	-3.0276620	-2.0947620	-1.1951140
H	-3.6252590	-1.9281920	0.4793880
N	-1.6131540	-2.6267000	0.2430990
H	-1.7638730	-3.5749420	-0.0847920
C	-1.4308220	-2.6395830	1.6896650
H	-2.3316780	-2.9540090	2.2405910
H	-0.6084920	-3.3127470	1.9429770
H	-1.1671730	-1.6362580	2.0358970

TS_{2+4}

C	-1.1426650	1.7907920	-0.3240800
C	-1.8486690	-0.5978000	-0.0624200
C	0.3379150	-0.5716970	-0.0165180
H	0.3110750	-0.9808160	0.9951420
C	0.6937780	0.7608270	-0.1425640
H	1.0031140	1.0845100	-1.1383150
N	-1.9820530	-0.0580570	-1.3288630
N	-1.6199140	1.1566440	-1.4564530
N	-2.0472570	0.2205230	1.0261490
N	-1.6879390	1.4420110	0.8889290
C	1.4000400	1.4402400	1.0004320
H	1.2619890	2.5254290	0.9946360
H	1.0003240	1.0601330	1.9477840
C	0.6973940	-1.5510590	-1.0926260
H	-0.0071320	-2.3891920	-1.1186290
H	0.6733730	-1.0499290	-2.0678640
C	2.9092180	1.1313580	0.9074000
H	3.3913410	1.5577210	1.7942480
H	3.3275130	1.6660830	0.0447150
C	2.1197850	-2.0830560	-0.8206760
H	2.4079590	-2.7232600	-1.6620640
H	2.0954370	-2.7311440	0.0649080
C	3.1953390	-1.0011420	-0.6165460
H	4.1634760	-1.4626090	-0.8362300
H	3.0669350	-0.2183450	-1.3757190
C	3.2820730	-0.3577370	0.7965560
H	4.3147800	-0.4541640	1.1469460
H	2.6795860	-0.9367250	1.5085750
C	-0.7664060	3.2349790	-0.5046040
H	0.1340060	3.3351550	-1.1155000
H	-0.5987430	3.6993020	0.4673730
H	-1.5782670	3.7624870	-1.0107300
N	-2.1520650	-1.9310730	0.0621450
H	-2.5863140	-2.3087600	-0.7691140
C	-2.6199100	-2.4437910	1.3373120
H	-2.7506730	-3.5223150	1.2462930
H	-1.8706590	-2.2490510	2.1081740
H	-3.5618890	-1.9863170	1.6620290

RC_{2+4}

C	-1.8949710	1.7655720	-0.2336070
C	-2.2085400	-0.7702360	-0.1082070
C	0.7709130	-0.5718850	0.1742720
H	0.7635830	-0.8293680	1.2360780
C	0.9398460	0.7071280	-0.1681490
H	0.9899770	0.9636690	-1.2292030
N	-2.1458880	-0.2056080	-1.3408500
N	-1.9785780	1.0776200	-1.3909920
N	-2.2525910	-0.0807000	1.0452850
N	-2.0880090	1.2174800	0.9661880
C	1.5265810	1.6919650	0.7890210
H	1.2044530	2.7254790	0.6211740
H	1.2651050	1.4185400	1.8180070
C	1.0757840	-1.6789010	-0.7808860
H	0.5041760	-2.5955420	-0.5944230
H	0.8749490	-1.3553980	-1.8094030
C	3.0637110	1.5825770	0.6001400
H	3.5563190	2.1772730	1.3780810
H	3.3357940	2.0427410	-0.3585450
C	2.5931740	-1.9632530	-0.6130300
H	2.9075060	-2.6675440	-1.3920390
H	2.7518670	-2.4726600	0.3461750
C	3.4953710	-0.7110650	-0.6648160
H	4.4990780	-1.0551150	-0.9367560
H	3.1699820	-0.0719380	-1.4952750
C	3.6179890	0.1414240	0.6359530
H	4.6811670	0.2173980	0.8882440
H	3.1560200	-0.3957570	1.4739710
C	-1.6286880	3.2354250	-0.3213170
H	-0.7185970	3.4185100	-0.8984960
H	-1.5097700	3.6461860	0.6812420
H	-2.4521520	3.7482970	-0.8248600
N	-2.2939610	-2.1135440	-0.0602290
H	-2.1639530	-2.5898970	-0.9396200
C	-2.1869570	-2.8427230	1.1868270
H	-1.2334620	-2.6393240	1.6884200
H	-2.9955020	-2.5608280	1.8645730
H	-2.2586240	-3.9076200	0.9696320

TS_{3+4}

C	-0.4510910	2.2505400	0.3467970
C	1.2053330	0.3852900	0.1166910
C	-0.7941460	-0.6229410	0.0086290
H	-0.5329680	-0.9917220	-0.9846920
C	-1.6946110	0.4173940	0.0705840
H	-2.1527470	0.6098010	1.0422490
N	1.0487120	0.9083460	1.3718360
N	0.1960450	1.8602480	1.4898090
N	1.0480830	1.2018490	-0.9705960
N	0.2024760	2.1601050	-0.8534310
C	-2.5380150	0.7432730	-1.1292200
H	-2.8586500	1.7889100	-1.1536310
H	-1.9614140	0.5501560	-2.0412110
C	-0.7641340	-1.6375120	1.1164880
H	0.2059990	-2.1322460	1.2163860
H	-0.9837570	-1.1404860	2.0686660
C	-3.7884950	-0.1630250	-1.0990800
H	-4.3418410	-0.0008530	-2.0306450
H	-4.4476940	0.1704940	-0.2873550
C	-1.8386890	-2.7079450	0.8226660
H	-1.8853400	-3.3800260	1.6866430
H	-1.5055650	-3.3203600	-0.0250240
C	-3.2489510	-2.1702600	0.5206020
H	-3.9516970	-2.9834010	0.7278840
H	-3.4985620	-1.3805980	1.2411130
C	-3.5108230	-1.6673680	-0.9276800
H	-4.3835090	-2.2005210	-1.3179030
H	-2.6769310	-1.9583610	-1.5798420
C	2.1903100	-0.7383220	-0.0327060
C	-1.4747460	3.3365760	0.4950990
H	-2.3413340	2.9877450	1.0611570
H	-1.7945630	3.6846300	-0.4869250
H	-1.0328300	4.1748900	1.0392390
H	1.9083120	-1.3527180	-0.8947530
H	2.1471380	-1.3624450	0.8640870
C	3.6120650	-0.1955140	-0.2139940
H	3.6510160	0.4441350	-1.1007920
H	3.8828830	0.4173730	0.6520390
C	4.6155420	-1.3203620	-0.3605230
H	4.3902160	-1.9365310	-1.2387620
H	4.6205770	-1.9638960	0.5268910
F	5.8843050	-0.7885280	-0.5171400

RC_{3+4}

C	0.0134640	2.5858340	0.2722770
C	1.5415420	0.5365480	0.2078290
C	-1.1564470	-0.7594440	0.0138320
H	-0.8498360	-1.0395950	-0.9971760
C	-1.9447830	0.3075330	0.1652900
H	-2.2890350	0.5649100	1.1700130
N	1.2172750	1.0338060	1.4090100
N	0.4359820	2.0814320	1.4411400
N	1.2373790	1.1255860	-0.9556320
N	0.4544540	2.1729830	-0.9248860
C	-2.7401550	0.8466150	-0.9788480
H	-2.9660710	1.9159690	-0.9034310
H	-2.2047050	0.6791710	-1.9208420
C	-1.0850460	-1.8291850	1.0538610
H	-0.1331140	-2.3712730	1.0725580
H	-1.2512310	-1.3999570	2.0488120
C	-4.0605750	0.0300390	-0.9824430
H	-4.6290310	0.2880730	-1.8832720
H	-4.6741410	0.3464380	-0.1291330
C	-2.2403720	-2.8092660	0.7135090
H	-2.3303890	-3.5399160	1.5256080
H	-1.9674170	-3.3788920	-0.1840790
C	-3.6115250	-2.1385420	0.4794150
H	-4.3720150	-2.9090990	0.6445460
H	-3.7797800	-1.3887860	1.2627980
C	-3.8734690	-1.5012330	-0.9200390
H	-4.7880280	-1.9474300	-1.3251730
H	-3.0746260	-1.7911100	-1.6145300
C	2.3765800	-0.7054310	0.1592460
C	-0.9576700	3.7207790	0.3187200
H	-1.8541810	3.4180090	0.8657590
H	-1.2285930	4.0174670	-0.6940380
H	-0.5176040	4.5716020	0.8444690
H	1.9363030	-1.3898380	-0.5747020
H	2.3342680	-1.1815810	1.1430300
C	3.8248400	-0.3869610	-0.2292240
H	3.8416330	0.1083590	-1.2053670
H	4.2636270	0.3016220	0.5004220
C	4.6669380	-1.6443180	-0.2930860
H	4.2678500	-2.3482750	-1.0324490
H	4.7060390	-2.1436840	0.6817630
F	5.9582810	-1.3107380	-0.6627820

TS_{1+5}

C	-2.5956420	0.4068510	-0.5141960
C	-0.1805810	1.2820370	-0.8509890
C	-0.5201260	-1.7053070	1.2891840
C	0.3846330	0.2920350	0.1267220
C	0.0160180	-1.0222260	0.0559330
C	-1.6291040	1.5699780	-0.3828990
C	-1.8325270	-0.9712180	1.6593670
H	-0.1835370	0.8711470	-1.8679240
H	0.1935450	-1.6403440	2.1183470
H	0.6197690	0.7048770	1.1088520
H	-0.3776910	-1.3739470	-0.8983340
H	0.3829040	2.2189400	-0.8482480
H	-0.7253870	-2.7635220	1.1003820
H	-2.0326950	2.4091840	-0.9616210
H	-1.5751080	0.0008470	2.0957900
H	-1.5918760	1.9109370	0.6593140
H	-2.3768030	-1.5313550	2.4288670
N	2.6815160	-1.6652730	0.7634490
N	2.5325070	-0.4047970	-1.6115620
C	2.0040300	-2.1702830	-0.3050870
C	2.6447930	0.2524150	-0.4243280
N	2.2066130	-1.6480890	-1.5501260
N	3.0112150	-0.4204460	0.6988600
C	-2.7226910	-0.7615480	0.4488690
C	-3.7839340	0.2989780	0.4039760
H	-3.7897230	1.0007720	1.2371340
H	-2.9950520	-1.6951500	-0.0450500
H	-2.8028830	0.1393320	-1.5503490
C	1.5506970	-3.5954330	-0.2291430
C	2.9897860	1.7147480	-0.4800160
C	-5.1395240	-0.0056960	-0.1650490
H	-5.8050610	-0.3852020	0.6240590
H	-5.0378580	-0.7990650	-0.9221100
O	-5.6574960	1.1831260	-0.7382200
H	-6.5532390	1.0032550	-1.0439030
H	2.4724070	2.1619350	-1.3350420
H	4.0721630	1.7920360	-0.6930280
H	2.3337630	-4.2489870	-0.6233120
H	1.3556830	-3.8705610	0.8074580
H	0.6507840	-3.7450060	-0.8288800
N	2.6031760	2.3938960	0.7421820
H	3.0245230	1.8967900	1.5233930
C	3.0382900	3.7830170	0.7477250
H	2.5096300	4.3287410	-0.0404640
H	2.7824430	4.2427520	1.7044230
H	4.1193740	3.9094560	0.5759670

RC_{1+5}

C	-2.7867280	0.4070500	-0.5005950
C	-0.3806880	1.3735680	-0.6227120
C	-0.6891780	-1.9607790	0.9866150
C	0.1059330	0.2486620	0.2351940
C	-0.1871000	-1.0169520	-0.0714450
C	-1.8570320	1.5670840	-0.1748690
C	-2.0562400	-1.3602760	1.4215460
H	-0.3432770	1.1098740	-1.6868870
H	-0.0170440	-2.0093650	1.8515020
H	0.3253340	0.5062770	1.2741630
H	-0.4549560	-1.2478100	-1.1036810
H	0.1803690	2.2999400	-0.4642570
H	-0.8180820	-2.9779690	0.6021010
H	-2.2721380	2.4688660	-0.6411720
H	-1.8492400	-0.4904630	2.0561690
H	-1.8633410	1.7525770	0.9069010
H	-2.6233200	-2.0749850	2.0309510
N	2.9313680	-1.4955290	0.8647600
N	2.8099230	-0.3052590	-1.5605470
C	2.5695480	-2.1411720	-0.2506700
C	2.9714040	0.3723700	-0.4157020
N	2.6042570	-1.5908910	-1.4762720
N	3.1387050	-0.2054610	0.7769220
C	-2.9034990	-0.9206220	0.2366750
C	-3.9857910	0.1126180	0.3619050
H	-4.0134140	0.6531630	1.3075140
H	-3.1506490	-1.7464450	-0.4321000
H	-2.9744530	0.3085180	-1.5701560
C	2.2028870	-3.5862830	-0.1466340
C	3.0843890	1.8679090	-0.4982360
C	-5.3311050	-0.1077390	-0.2671330
H	-5.9900530	-0.6485110	0.4282610
H	-5.2072080	-0.7378360	-1.1621400
O	-5.8782450	1.1562310	-0.6047910
H	-6.7742350	1.0171740	-0.9303190
H	2.4668580	2.2019100	-1.3398070
H	4.1302290	2.1219510	-0.7551430
H	3.0493550	-4.2121450	-0.4432400
H	1.9300680	-3.8256700	0.8812660
H	1.3686080	-3.8050790	-0.8153280
N	2.6222600	2.4952140	0.7235690
H	3.1150830	2.0807450	1.5094060
C	2.8243350	3.9355500	0.6995730
H	2.1961200	4.3749990	-0.0823550
H	2.5167060	4.3627260	1.6560260
H	3.8662400	4.2352520	0.5005690

TS_{2+5}

C	2.5028470	-0.4292780	-0.4649670
C	0.1706670	-1.5102170	-0.7037850
C	0.2512310	1.6630290	1.1613240
C	-0.4862630	-0.5081130	0.1982350
C	-0.2546340	0.8339720	0.0040430
C	1.6345440	-1.6513800	-0.2227870
C	1.6184950	1.0706750	1.5758470
H	0.1516530	-1.1591240	-1.7427200
H	-0.4469070	1.6231660	2.0049570
H	-0.6345220	-0.8425950	1.2280560
H	0.1289850	1.1150430	-0.9774690
H	-0.3350730	-2.4794810	-0.6559660
H	0.3705590	2.7119220	0.8717930
H	2.1035140	-2.5020350	-0.7311320
H	1.4460180	0.1208280	2.0948590
H	1.6301430	-1.9010070	0.8459920
H	2.1157810	1.7373540	2.2902800
N	-2.8617620	1.2518810	0.6903460
N	-2.6504110	-0.2922800	-1.5078480
C	-2.2040900	1.6551570	-0.4405210
C	-2.6689840	-0.8014740	-0.2256040
N	-2.4143280	0.9584050	-1.6102370
N	-3.1013020	-0.0047890	0.8046820
C	2.5236460	0.8310860	0.3828290
C	3.6738590	-0.1325130	0.4329320
H	3.7370680	-0.7490400	1.3289240
H	2.7156830	1.7355540	-0.1957690
H	2.6890040	-0.2426950	-1.5226140
C	4.9998680	0.2357360	-0.1667570
H	5.6226680	0.7508620	0.5793050
H	4.8315080	0.9377470	-0.9986090
O	5.6272930	-0.9521540	-0.6194100
H	6.5066120	-0.7240490	-0.9401600
C	-1.9450390	3.1270110	-0.5871920
H	-2.7986750	3.6072640	-1.0724910
H	-1.8028070	3.5784930	0.3950590
H	-1.0605330	3.3046930	-1.2027760
N	-2.8174730	-2.1571230	-0.1097520
C	-3.3921710	-2.7253000	1.0950270
H	-2.7997840	-2.4242000	1.9620570
H	-4.4261990	-2.4034860	1.2667840
H	-3.3581730	-3.8117380	1.0125120
H	-3.0317790	-2.6092430	-0.9876890

RC_{2+5}

C	-2.6823310	0.4312540	-0.4290070
C	-0.3801880	1.6234710	-0.3375130
C	-0.4258190	-1.8680210	0.9268730
C	0.1808070	0.4720970	0.4378490
C	0.0183060	-0.7756580	-0.0042480
C	-1.8863570	1.6365860	0.0508050
C	-1.8641420	-1.4499010	1.3467470
H	-0.2719070	1.4603990	-1.4168530
H	0.2132230	-1.9403830	1.8142160
H	0.3223970	0.6349890	1.5097310
H	-0.1846980	-0.9231500	-1.0660000
H	0.0756980	2.5881630	-0.0885410
H	-0.4342450	-2.8473520	0.4373470
H	-2.3676790	2.5364250	-0.3511210
H	-1.7753030	-0.6371870	2.0771870
H	-1.9554280	1.7137370	1.1434600
H	-2.3818900	-2.2766740	1.8485140
N	3.2026280	-1.0578600	0.7924960
N	2.8660710	0.3248550	-1.5142310
C	2.8830460	-1.6377430	-0.3647860
C	3.0312800	0.9140630	-0.3035010
N	2.7822130	-0.9678890	-1.5308160
N	3.2853280	0.2491080	0.8380100
C	-2.7000170	-0.9697240	0.1692540
C	-3.8812870	-0.0588620	0.3394070
H	-3.9993690	0.3775850	1.3307220
H	-2.8365840	-1.7409570	-0.5900910
H	-2.8168090	0.4242430	-1.5110030
C	-5.1725230	-0.3357670	-0.3748210
H	-5.8070790	-0.9953650	0.2349550
H	-4.9537560	-0.8644800	-1.3160310
O	-5.8192310	0.9017800	-0.6233690
H	-6.6854320	0.7155700	-1.0017040
C	2.6962520	-3.1222490	-0.3994690
H	1.7927820	-3.3718290	-0.9604060
H	3.5423070	-3.6088730	-0.8925160
H	2.6112120	-3.5050720	0.6177140
N	3.0056310	2.2607590	-0.2727380
H	2.7073370	2.7088660	-1.1257630
C	2.9856280	2.9928330	0.9772290
H	2.9294870	4.0569790	0.7518510
H	2.1255370	2.7071090	1.5945830
H	3.8950210	2.7959400	1.5487320

TS_{3+5}

C	-3.0883090	-0.2794450	-0.5369970
C	-1.5781320	1.8121450	-0.7542370
C	-0.3155960	-0.8436990	1.4703580
C	-0.6282250	1.3275460	0.3048240
C	-0.1749170	0.0384140	0.2548150
C	-2.9659080	1.2269100	-0.3906040
C	-1.8352750	-0.9920400	1.7283360
H	-1.2626900	1.4554410	-1.7418720
H	0.1740700	-0.3958690	2.3425820
H	-0.7577160	1.7722780	1.2946010
H	-0.2355820	-0.4621910	-0.7118770
H	-1.6481460	2.9028890	-0.7914160
H	0.1303790	-1.8283830	1.2995050
H	-3.7284460	1.6891320	-1.0282030
H	-2.2115920	-0.0509120	2.1458050
H	-3.2093630	1.5231950	0.6375900
H	-2.0171100	-1.7688580	2.4801540
N	2.3221780	0.9933550	1.1417190
N	1.6201420	2.0717350	-1.2218680
C	2.1036160	0.2497310	0.0200250
C	1.2701560	2.6181340	-0.0221350
N	2.0501620	0.8583200	-1.1987240
N	1.8919770	2.2065040	1.1204850
C	-2.5961670	-1.3184210	0.4567710
C	-4.0652880	-1.0492450	0.3111490
H	-4.5254830	-0.4799520	1.1179220
H	-2.2547570	-2.2381670	-0.0198080
H	-3.0331590	-0.6120230	-1.5735010
C	2.5620390	-1.1787930	0.0458980
C	0.7042020	4.0046620	-0.0280090
C	-4.9679500	-2.0660700	-0.3257370
H	-5.3442240	-2.7661220	0.4343000
H	-4.3872900	-2.6514950	-1.0560680
O	-6.0347670	-1.3770430	-0.9551540
H	-6.6576510	-2.0308460	-1.2910560
H	0.2501950	4.2176110	-0.9958050
H	-0.0374070	4.1252000	0.7642550
H	1.5070000	4.7253080	0.1491710
H	2.3876330	-1.5812640	1.0480680
H	1.9637200	-1.7577070	-0.6663860
C	4.5183380	-2.7210640	-0.3008740
H	4.3690260	-3.1805910	0.6830040
H	3.9792900	-3.3133990	-1.0495680
C	4.0495620	-1.2809100	-0.3071190
H	4.6375860	-0.7077780	0.4173590
H	4.2236650	-0.8463870	-1.2963890
F	5.8691220	-2.7688100	-0.6001330

RC_{3+5}

C	-3.3779760	-0.2115390	-0.5392920
C	-1.7920550	1.8351970	-0.6793960
C	-0.5006070	-1.0659880	1.2494900
C	-0.8774010	1.1868430	0.3132390
C	-0.4641600	-0.0680620	0.1253420
C	-3.1956040	1.2806270	-0.3039780
C	-2.0135770	-1.2242280	1.5747180
H	-1.5347340	1.5413340	-1.7037020
H	0.0349060	-0.7113890	2.1376620
H	-0.9209290	1.5771050	1.3342520
H	-0.4887870	-0.4690160	-0.8892330
H	-1.8004330	2.9288460	-0.6280680
H	-0.0661030	-2.0274260	0.9557870
H	-3.9687480	1.8059910	-0.8773770
H	-2.3298150	-0.3336370	2.1305260
H	-3.3853950	1.5150280	0.7513470
H	-2.1850440	-2.0879730	2.2288640
N	2.4232140	0.9595480	1.2096830
N	1.8884980	2.1308170	-1.1697400
C	2.4817810	0.3074990	0.0397390
C	1.6613570	2.7271340	0.0090520
N	2.3105520	0.8926790	-1.1524520
N	2.0034910	2.1967760	1.1934900
C	-2.8672240	-1.3587640	0.3233280
C	-4.3290270	-1.0164590	0.3067700
H	-4.7008770	-0.5016820	1.1920750
H	-2.6070210	-2.2375490	-0.2684660
H	-3.4038350	-0.4664860	-1.5990820
C	2.8749070	-1.1368210	0.0544680
C	1.0623050	4.0960940	0.0090770
C	-5.3265530	-1.9284620	-0.3466650
H	-5.6926140	-2.6712920	0.3770890
H	-4.8279080	-2.4770580	-1.1610320
O	-6.3919460	-1.1351100	-0.8426490
H	-7.0703590	-1.7244680	-1.1900550
H	0.7814140	4.3759190	-1.0058050
H	0.1798300	4.1117250	0.6533140
H	1.7774070	4.8221650	0.4035160
H	2.6486980	-1.5444330	1.0441950
H	2.2665450	-1.6665300	-0.6866280
C	4.7588540	-2.7670290	-0.2975170
H	4.5763560	-3.2425440	0.6728890
H	4.1989710	-3.3114050	-1.0666260
C	4.3635670	-1.3051640	-0.2708620
H	4.9681810	-0.7831410	0.4781490
H	4.5783650	-0.8549080	-1.2454840
F	6.1084100	-2.8722560	-0.58543

7. References

(1) Taylor, M. T., Blackman, M. L., Dmitrenko, O., and Fox, J. M. (2011) Design and synthesis of highly reactive dienophiles for the tetrazine-trans-cyclooctene ligation. *J. Am. Chem. Soc. 133*, 9646–9649.

(2) Matt, T., and Seebach, D. (1998) C-Alkylation of Peptides Containing Aminomalonate and (Amino)(cyano)acetate Residues. *Helv. Chim. Acta 81*, 1845–1895.

(3) Nachbaur, E., and Leiseder, G. (1971) Über eine einfache und gefahrlose Methode zur Darstellung von wasserfreiem Hydrazin. *Monatsh. Chem. 102*, 1718–1723.

(4) Larsen, P., Ulin, J., Dahlstrøm, K., and Jensen, M. (1997) Synthesis of [11C]iodomethane by iodination of [^{11}C]methane. *Appl. Radiat. Isot. 48*, 153–157.

(5) Jewett, D. M. (1992) A simple synthesis of [^{11}C]methyl triflate. *Int. J. Radiat. Appl. Instrumentation. Part A. Appl. Radiat. Isot. 43*, 1383–1385.

(6) Devaraj, N. K., Upadhyay, R., Haun, J. B., Hilderbrand, S. A., and Weissleder, R. (2009) Fast and sensitive pretargeted labeling of cancer cells through a tetrazine/trans-cyclooctene cycloaddition. *Angew. Chem. Int. Ed. 48*, 7013–7016.

(7) Eisenbrand, G., Lauck-Birkel, S., and Tang, W. C. (1996) An Approach Towards More Selective Anticancer Agents. *Synthesis 1996*, 1246–1258.

(8) Yang, J., Karver, M. R., Li, W., Sahu, S., and Devaraj, N. K. (2012) Metal-Catalyzed One-Pot Synthesis of Tetrazines Directly from Aliphatic Nitriles and Hydrazine. *Angew. Chem. Int. Ed. 51*, 5222–5225.

(9) Beckmann, H. S. G., Niederwieser, A., Wiessler, M., and Wittmann, V. (2012) Preparation of Carbohydrate Arrays by Using Diels-Alder Reactions with Inverse Electron Demand. *Chem. Eur. J. 18*, 6548–6554.

(10) Ostafin, A., Nooney, R. I., Thirunavukkarasu, D., Chen, Y., Josephs, R., and Ostafin, A. E. (2015) Synthesis of Nanoscale Mesoporous Silica Spheres with Controlled Particle Size. *Chem. Mater. 14*, 4721–4728.

(11) Yokoi, T., Yoshitake, H., and Tatsumi, T. (2004) Synthesis of amino-functionalized MCM-41 via direct co-condensation and post-synthesis grafting methods using mono-, di- and tri-amino-organoalkoxysilanes. *J. Mater. Chem. 14*, 951–957.

(12) Ritter, H., Nieminen, M., Karppinen, M., and Brühwiler, D. (2009) A comparative study of the functionalization of mesoporous silica MCM-41 by deposition of 3-aminopropyltrimethoxysilane from toluene and from the vapor phase. *Microporous Mesoporous Mater. 121*, 79–83.

(13) Loening, A. M., and Gambhir, S. S. (2003) AMIDE: A Free Software Tool for Multimodality Medical Image Analysis. *Mol. Imaging 2*, 131–137.

(14) Frisch, M. J. G., Trucks, W., Schlegel, H. B., Scuseria, G. E., Robb, M. A., Cheeseman, J. R., Scalmani, G., Barone, V., Mennucci, B., Petersson, G. A., *et al.* (2009) Gaussian 09, Revision D.01. *Inc. Wallingford, CT*.

(15) Zhao, Y., and Truhlar, D. G. (2008) The M06 suite of density functionals for main group thermochemistry, thermochemical kinetics, noncovalent interactions, excited states, and transition elements: Two new functionals and systematic testing of four M06-class functionals and 12 other functionals. *Theor. Chem. Acc. 120*, 215–241.

(16) Ditchfield, R., Hehre, W. J., and Pople, J. A. (1971) Self-Consistent Molecular-Orbital Methods. IX. An Extended Gaussian-Type Basis for Molecular-Orbital Studies of Organic Molecules. *J. Chem. Phys. 54*, 724.

(17) Lan, Y., Zou, L., Cao, Y., and Houk, K. N. (2011) Computational methods to calculate accurate activation and reaction energies of 1,3-dipolar cycloadditions of 24 1,3-dipoles. *J. Phys. Chem. A 115*, 13906–13920.

(18) Liu, F., Paton, R. S., Kim, S., Liang, Y., and Houk, K. N. (2013) Diels-Alder reactivities of strained and unstrained cycloalkenes with normal and inverse-electron-demand dienes: activation barriers and distortion/interaction analysis. *J. Am. Chem. Soc. 135*, 15642–15649.

(19) Talbot, A., Devarajan, D., Gustafson, S. J., Fernández, I., Bickelhaupt, F. M., and Ess, D. H. (2015) Activation-Strain Analysis Reveals Unexpected Origin of Fast Reactivity in Heteroaromatic Azadiene Inverse-Electron-Demand Diels–Alder Cycloadditions. *J. Org. Chem. 80*, 548-558.

(20) Denk, C., Svatunek, D., Filip, T., Wanek, T., Lumpi, D., Fröhlich, J., Kuntner, C., and Mikula, H. (2014) Development of a ^{18}F-Labeled Tetrazine with Favorable Pharmacokinetics for Bioorthogonal PET Imaging. *Angew. Chem. Int. Ed. 53*, 9655–9659.

Supporting Information

Manuscript #7

Mengzhe Wang, Dennis Svatunek, Katarina Rohlfing, Yu Liu, Hui Wang, Ben Giglio, Hong Yuan, Zhanghong Wu, Zibo Li*, Joseph Fox*; Conformationally Strained *trans*-Cyclooctene (sTCO) Enables the Rapid Construction of ^{18}F-PET Probes via Tetrazine Ligation, *Theranostics* **2016**, 6, 887-895.

(with permission from Ivyspring Int. Publ.)

Conformationally Strained *trans*-Cyclooctene (sTCO) Enables the Rapid Construction of ^{18}F-PET Probes via Tetrazine Ligation Supplementary Information

Mengzhe Wang,[1] Dennis Svatunek,[2,3] Katarina Rohlfing,[2] Yu Liu,[2] Hui Wang,[1] Ben Giglio,[1] Hong Yuan,[1] Zhanghong Wu,[1] Zibo Li,*[, 1] and Joseph Fox*[, 2]

1. Department of Radiology and Biomedical Research Imaging Center, University of North Carolina at Chapel Hill, Chapel Hill, North Carolina, 27599, United States.

2. Brown Laboratories, Department of Chemistry and Biochemistry, University of Delaware, Newark, Delaware 19716, United States.

3. Institute of Applied Synthetic Chemistry, TU Wien, Vienna, 1060, Austria.

1. Synthetic Procedures

1.1. General Considerations: All reactions were carried out in glassware that was flame-dried under vacuum and cooled under nitrogen. All commercially available reagents and solvents were used as received. (rel-1R,8S,9S,4Z)-Bicyclo[6.1.0]non-4-ene-9-ylmethanol and 4-nitrophenyl 4-(6-phenyl-1,2,4,5-tetrazin-3-yl)benzyl carbonate were prepared following known procedures.[1,2] Reactions were monitored by thin layer chromatography (TLC) performed on SiliCycle silica gel GF 250 μm plates and were visualized with ultraviolet (UV) light (254 nm) and/or $KMnO_4$ staining. Flash chromatography was performed using normal phase SiliCycle silica gel (40-63D, 60Å). Deactivated silica gel was prepared by treating silica gel with $EtSiCl_3$.[3] ^{1}H, ^{13}C and ^{19}F nuclear magnetic resonance (NMR) chemical shifts are reported in ppm relative to $CHCl_3$, CH_2Cl_2 and MeOH (i.e. ^{1}H NMR δ = 7.26 and ^{13}C NMR = 77.0, ^{1}H NMR = 5.32 and ^{13}C NMR = 54.0, ^{1}H NMR = 3.31 and ^{13}C NMR = 49.1).

1.2. (rel-1R,8S,9S,4E)-Bicyclo[6.1.0]non-4-ene-9-ylmethanol (5)

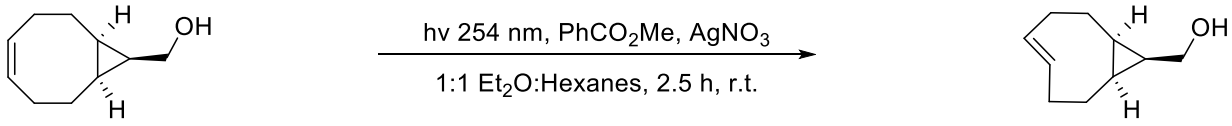

7 **5**

The flow photoisomerization procedure (ref 1) was followed using **7** (395 mg, 2.59 mmol) in 1:1 ether/hexanes (250 mL), methyl benzoate (705 mg, 5.18 mmol) and dodecane (491 mg, 2.88 mmol, standard for GC monitoring) in a 250 mL quartz tube. A 50 g Biotage® SNAP column was filled with normal silica gel (2.5 inches) and the remaining space was packed with 10% silver impregnated silica (5.70 g). The column was connected to a pump and flushed with 1:1 ether/hexanes (250 mL). Irradiation was carried out at 254 nm for 2.5 h at which GC monitoring

showed no more starting material. The column was flushed with 1:1 ether/hexanes (250 mL) and dried under air flow. The silica was placed into a flask and stirred in ammonium hydroxide (200 mL) and dichloromethane (200 mL) for 10 min. The silica was filtered and washed with additional ammonium hydroxide (100 mL) and dichloromethane (100 mL). The phases were separated and the aqueous layer was extracted an additional three times. The combined organic layers were washed twice with water, dried over Na_2SO_4, filtered and concentrated by rotary evaporation. Purification by column chromatography (25%, EtOAc : Hexanes) to yield 318 mg (2.09 mmol, 81%) of compound **5** as a colorless oil which was stored as a solution in MeOH at -15 °C. ^{1}H NMR (600 MHz, CD_3OD) δ: 5.88 (ddd, *J* = 16.2, 9.3, 6.2 Hz, 1H), 5.16 (dddd, *J* = 16.7, 10.6, 3.9, 1.1 Hz, 1H), 3.50 (d, *J* = 7.7 Hz, 2H), 2.31 (dtd, *J* = 11.4, 3.7, 2.4 Hz, 1H), 2.28 (ddd, *J* = 12.5, 8.4, 6.9 Hz, 1H), 2.21 – 2.15 (m, 1H), 2.13 – 2.09 (m, 1H), 1.96 – 1.86 (m, 2H), 1.20 (dt, *J* = 9.1, 7.7 Hz, 1H), 1.09 (tdd, *J* = 12.9, 11.2, 7.1 Hz, 1H), 0.85 – 0.71 (m, 2H), 0.60 (dtd, *J* = 13.0, 8.8, 4.6 Hz, 1H), (small peaks attributable to impurities were detected by ^{1}H NMR at 5.49, 4.09, 2.01, 1.29,1.24 and 0.90 ppm). ^{13}C NMR (151 MHz, CD_3OD) δ 139.4, 132.3, 59.5, 35.3, 34.8, 28.6, 28.3, 21.7, 20.2, 19.2; HRMS (EI) [M+H] *m/z*: calcd for $C_{10}H_{16}O$: 152.1201; found: 152.1181.

1.3. 2-(2-(2-((*syn*-(*E*)-bicyclo[6.1.0]non-4-en-9-yl)methoxy)ethoxy)ethoxy)ethyl 4-methylbenzenesulfonate (8)

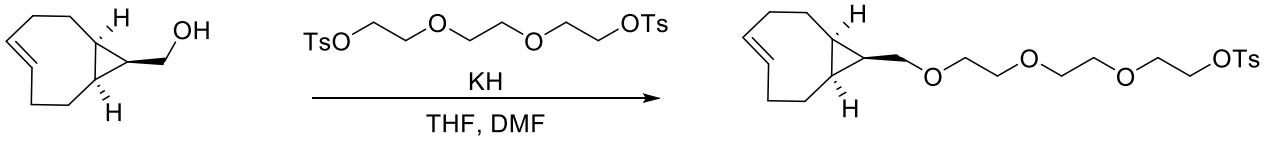

5 **8**

Triethylene glycol bis(*p*-toluenesulfonate) (972 mg, 2.12 mmol) was added into a flame-dried round bottom flask and dissolved in anhydrous THF (6.0 mL, 0.35M) and DMF (0.6 mL, 3.53M). **5** (100mg, 0.66 mmol) was added followed by potassium hydride (210 mg, 50% in paraffin, 2.63 mmol). The mixture was stirred at room temperature for 16 h after which saturated aqueous NH_4Cl solution was added followed by ether. The phases were separated and the aqueous layer was extracted an additional three times. The combined organic layers were dried over Na_2SO_4, filtered and concentrated by rotary evaporation. Purification by column chromatography (25 - 50%, EtOAc : Hexanes) yielded 85 mg (0.19 mmol, 30%) of desired compound **8** as a colorless oil which was stored as a solution in MeOH at -15 °C. ^{1}H NMR (600 MHz, CD_3OD) δ: 7.80 (d, *J* = 8.3 Hz, 2H) 7.45 (d, *J* = 8.4 Hz, 2H), 5.86 (ddd, *J* = 16.2, 9.3, 6.3 Hz, 1H), 5.16 (dddd, *J* = 16.8, 10.6, 3.9, 1.1 Hz, 1H), 4.18-4.12 (m, 2H), 3.68-3.34 (m, 2H), 3.60-3.52 (m, 8H), 3.46 – 3.41 (m, 2H), 2.46 (s, 3H), 2.34-2.27 (m, 1H), 2.26-2.19 (m, 1H), 2.19-2.11 (m, 1H), 2.11-2.04 (m, 1H), 1.98-1.84 (m, 2H), 1.30-1.19 (m, 1H), 1.14-1.01 (m, 1H), 0.87-0.69 (m, 2H) 0.65-0.55 (m, 1H), (small peaks attributable to impurities were detected by ^{1}H NMR at 4.63, 4.09, 2.01 and 1.24 ppm) ; ^{13}C APT NMR (100.6 MHz, CD_3OD) δ: 146.5, 139.4, 134.6, 132.4, 131.2, 129.2, 73.1, 71.7, 71.7, 71.6, 71.0, 69.9, 69.1, 35.5, 34.8, 28.8, 28.4, 21.7, 20.3, 19.3, 19.2, (a small peak attributable to dichloromethane was detected by ^{13}C at 54.9 ppm); HRMS (LIFDI-TOF) *m/z*: $[M]^+$ Calcd for $C_{23}H_{34}O_6S^+$ 438.2076; Found 438.2066.

1.4. *syn*-(*E*)-9-((2-(2-(2-fluoroethoxy)ethoxy)ethoxy)methyl)bicycle[6.1.0]non-4-ene (9)

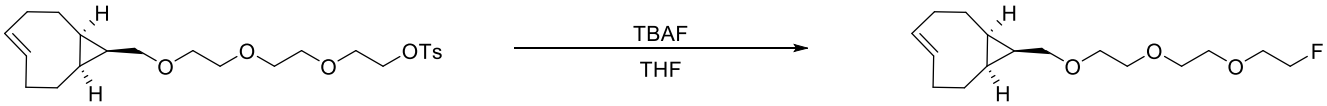

8 **9**

Tosylate **8** (10 mg, 0.02 mmol) was charged into a 4 dram vial and TBAF (0.5 mL, 1.0 M in THF) was added via syringe. The mixture was heated to 60 °C for 3.5 h and subsequently cooled to room temperature. The mixture was diluted with ethyl acetate, washed with saturated aqueous $NaHCO_3$ and dried over Na_2SO_4. The solution was filtered and concentrated by rotary evaporation. Purification by column chromatography (25%, EtOAc : Hexanes) yielded 5 mg (0.02 mmol, 76%) of **9** as a colorless oil that was stored as a solution in MeOH at -15 °C. ^{1}H NMR (600 MHz, CD_3OD) δ: 5.87 (ddd, J = 16.2, 9.3, 6.2 Hz, 1H), 5.17 (ddd, J = 14.0, 10.6, 3.8 Hz, 1H), 4.52 (dt, J_{CF} = 48 Hz, J_{HH} = 4.1 Hz, 2H), 3.72 (dt, J_{CF} = 30.1 Hz, J_{HH} = 4.0 Hz, 2H), 3.68-3.59 (m, 6H), 3.59-3.54 (m, 2H), 3.44 (d, J = 7.5 Hz, 2H), 2.34-2.28 (m, 1H), 2.28-2.21 (m, 1H), 2.19-2.13 (m, 1H), 2.11-2.06 (m, 1H), 1.99-1/84 (m, 2H), 1.27-1.21 (m, 1H), 1.14-1.04 (m, 1H), 0.86-0.80 (m, 1H), 0.79-0.71 (m, 1H), 0.65-0.57 (m, 1H), (small peaks attributable to the cis isomer (5.61 ppm) and an impurity (1.29, 0.90 ppm) were also detected by ^{1}H NMR); ^{13}C APT NMR (100.6 MHz, MeOD) δ: 139.4, 132.4, 84.2 (d, JCF = 168 Hz), 71.82, 71.76, 71.74 (d, JCF = 20 Hz), 71.65, 71.0, 69.1, 35.5, 34.8, 28.8, 28.4, 20.3, 19.4, 19.3; ^{19}F NMR (376 MHz, CD_3OD) δ: -224.7 (tt, J = 48.1, 30.0 Hz); HRMS (Orbitrap) *m/z*: $[M + Na]^+$ Calcd for $C_{16}H_{27}FO_3Na$ 309.18364; Found 309.18453.

1.5. 3-oxo-1-(4-(6-phenyl-1,2,4,5-tetrazin-3-yl)phenyl)-2,7,10,13,16,19,22,25,28,31,34,37,40-tridecaoxa-4-azatritetracontan-43-oic acid (11)

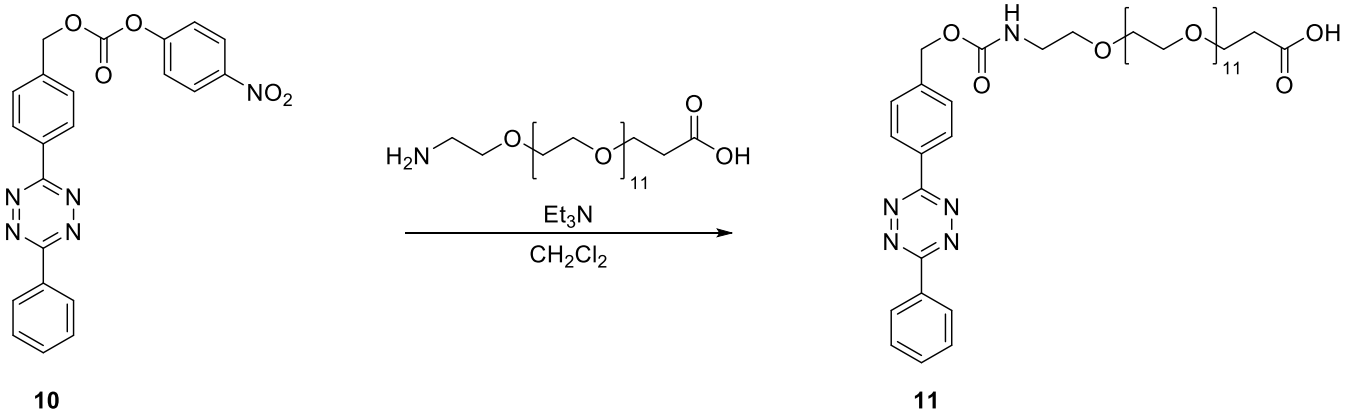

10 **11**

4-nitrophenyl 4-(6-phenyl-1,2,4,5-tetrazin-3-yl)benzyl carbonate (**10**) (43 mg, 0.10 mmol) and PEG12-Amino acid (31 mg, 0.05 mmol) were dissolved in anhydrous dichloromethane (4.0 mL, 0.01 M). Triethylamine (13.8 µL) was added and the reaction was stirred at room temperature for 30 h. 1N HCl (5 mL) was added and the aqueous phase was extracted with dichloromethane (3x). The combined organics were dried over Na_2SO_4, filtered and concentrated by rotary evaporation.

The crude was purified by column chromatography using deactivated silica gel (2.50 g, 0 - 5% MeOH : DCM) to yield 40 mg (0.04 mmol, 88%) of **11** as a purple solid. mp: 39 - 40 °C; ^{1}H NMR (400 MHz, $CDCl_3$) δ: 8.67-8.61 (m, 4H), 7.70-7.59 (m, 5H), 5.58 (t, J = 5.8 Hz, 1H), 5.22(m, 2H), 3.73 (t, J = 5.8 Hz, 2H), 3.66-3.54 (m, 48H), 3.39 (q, 5.4 Hz, 2H), 2.60 (bs, 2H); ^{13}C NMR (100 MHz, $CDCl_3$) δ: 173.3, 164.1, 163.8, 156.5, 141.8, 132.9, 131.8, 131.4, 129.5, 128.6, 128.2, 128.1, 70.8, 70.7 – 70.5 (19 C's), 70.4, 70.3, 70.1, 66.7, 66.0, 41.1, 35.1 (a peak attributed to CH_2Cl_2 was observed at 54 ppm); HRMS (LIFDI-TOF) *m/z*: $[M + Na]^+$ Calcd for $C_{43}H_{65}N_5O_{16}Na$ 930.4324; Found 930.4336.

1.6. 2,5-dioxopyrrolidin-1-yl 3-oxo-1-(4-(6-phenyl-1,2,4,5-tetrazin-3-yl)phenyl)-2,7,10,13,16,19,22,25,28,31,34,37,40-tridecaoxa-4-azatritetracontan-43-oate (11a)

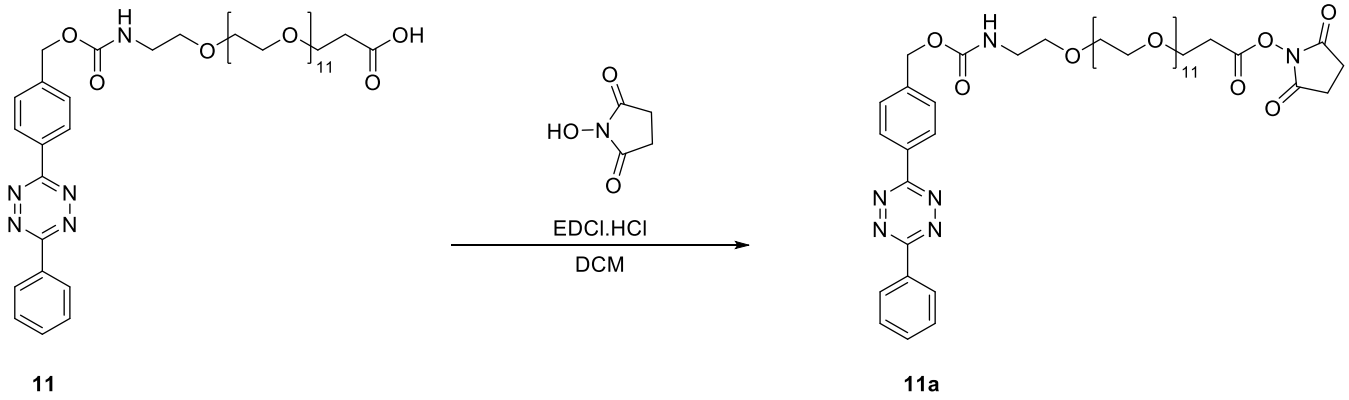

11 **11a**

Acid **11** (24 mg, 0.0264 mmol), N-hydroxysuccinimide (NHS) (5.0 mg, 0.0434 mmol) and 1-ethyl-3-(3-dimethylaminopropyl)carbodiimide hydrochloride (EDCl) (8.0 mg, 0.0417 mmol) were added to a flame-dried round bottom flask. The mixture was dissolved in anhydrous dichloromethane (2.0 mL, 0.02 M) and stirred at room temperature for 16 h. The solution was directly applied to a column of deactivated silica gel (2.50 g) and washed with large amounts of dichloromethane after which product was eluted with 5% MeOH : DCM. Further purification using HILIC (2.50 g silica gel, 5% H_2O : MeOH) yielded 19 mg (0.02 mmol, 72%) of **11a** as a purple solid. mp: 37 - 39 °C; ^{1}H NMR (400 MHz, CD_2Cl_2) δ: 8.67-8.60 (m, 4H), 7.70-7.59 (m, 5H), 5.54 (bs, 1H, NH), 5.22 (s, 2H), 3.83 (t, J = 6.3 Hz, 2H), 3.67-3.52 (m, 48H), 3.39 (m, 2H), 2.88 (t, J = 6.3 Hz, 2H), 2.84-2.76 (bs, 4H); ^{13}C NMR (100 MHz, CD_2Cl_2) δ: 169.5, 167.3, 164.4, 164.2, 156.5, 142.5, 133.0, 132.3, 131.8, 129.7, 128.7, 128.3, 128.2, 71.0, 70.9 – 70.7 (20 C's), 70.3, 66.0, 41.4, 32.5, 26.0; HRMS (LIFDI-TOF) *m/z*: $[M + Na]^+$ Calcd for $C_{47}H_{68}N_6O_{18}Na$ 1027.4488; Found 1027.4487, : $[M + K]^+$ Calcd for $C_{47}H_{68}N_6O_{18}K$ 1043.4227, Found 1043.4200.

1.7 RGDyK-Tz (12)

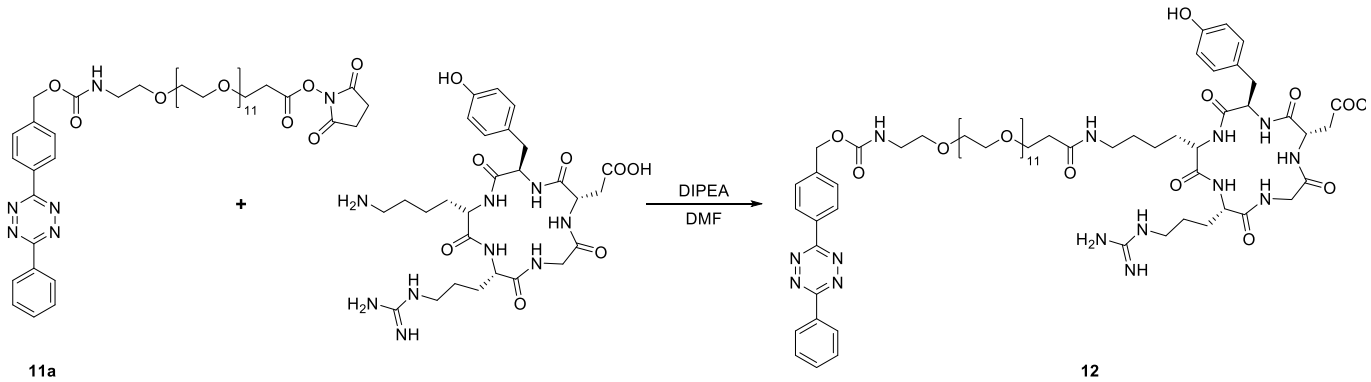

11a 12

RGDyK (3.0 mg, 0.0048 mmol) was added to a 4 dram vial followed by TzPEG12NHS (**11a**) (10 mg, 0.0099 mmol) as a solution in anhydrous dimethylformamide (400 µL, 0.01 M). *N,N*-diisopropylethylamine (3.0 mg, 0.02 mmol) was added as a solution in anhydrous dimethylformamide (100 µL, 0.20 M) and the reaction was allowed to stir at room temperature for 18 h. H_2O was added and the solvents were removed via freeze drying. The residue was purified by RP HPLC to yield 7.2 mg (**12**) (0.005 mmol, 99 %) as a pink solid. HRMS (LIFDI-TOF) *m/z* $[M + Na]^+$ Calcd for $C_{70}H_{104}N_{14}O_{23}Na$ 1531.7296; Found 1531.7279.

1.8 RGDyK-Tz-sTCOPEGF (15)

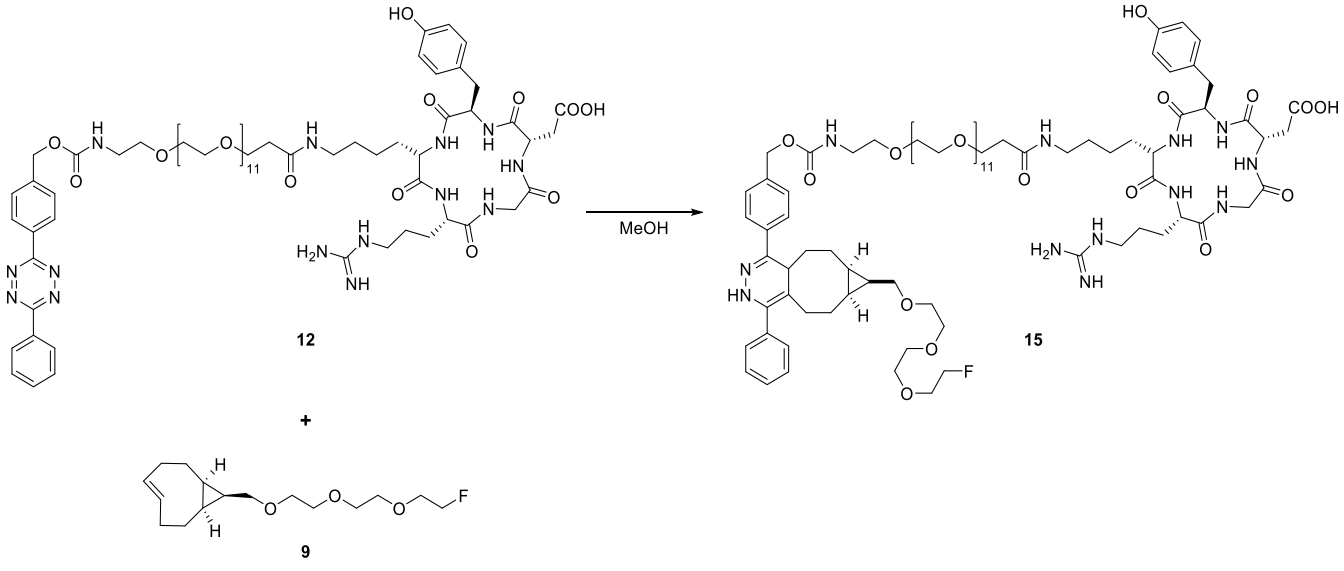

12 15

9

Tetrazine-RGD conjugate (**12**) (0.3 mg, 0.0002 mmol) was dissolved in methanol (0.5 mL) and sTCOPEGF (**9**) (23 µL of a 2.5 mg/mL solution in MeOH, 0.06 mg, 0.0002 mmol) was added dropwise. The reaction was monitored by UV/Vis and was complete within 1 min. The product (**15**) was purified by reverse phase HPLC (C-18 column, 10% ACN + 0.1% formic acid to 100% ACN + 0.1% formic acid).

1.9 General procedure for stop-flow kinetic analysis of sTCO's and 11 at variable concentrations

The reaction between sTCOs (**4** & **5**) and the PEGylated tetrazine **11** was measured under pseudo-first order conditions in water : methanol 45:55 by following the exponential decay of the tetrazine at 298 nm over time using an SX 18MV-R stoppedflow spectrophotometer (Applied Photophysics Ltd.). Solutions were prepared for the sTCO concentrations see table below (water : methanol 45:55) and the tetrazine (0.1 mM in water : methanol 45:55) and thermostatted in the syringes of the spectrophotometer before measuring. An equal volume of each was mixed by the stopped flow device (resulting concentrations shown in the table below). 400 data points were recorded over a period of 1 second, and performed in sextuplicate at 298 K. The k_{obs} was determined by nonlinear regression analysis of the data points using Prism software (v. 6.00, GraphPad Software Inc.)

	Resulting concentration Tetrazine [mM]	Initial concentration sTCO [mM]	Resulting concentration sTCO [mM]	k_{obs}	k_2 [$M^{-1}s^{-1}$]	Mean k_2 [$M^{-1}s^{-1}$]
syn sTCO	0.05	0.49	0.245	8.415	34347	36,100 +/− 1,400
		0.98	0.49	18.41	37571	
		1.96	0.98	35.08	35796	
		2.94	1.47	54.18	36857	
anti sTCO		0.5	0.25	7.458	29832	31,700 +/− 1,300
		1.0	0.5	15.84	31680	
		2.0	1	32.51	32510	
		3.0	1.5	48.98	32653	

Table 1. Rate constants for the reaction of *trans*-cyclooctenes (sTCO's **4** & **5**) with PEGylated tetrazine **11** at 25 °C in water : methanol (45:55) measured under pseudo first order conditions using SX 18MV-R stoppedflow spectrophotometer. Values were determined from an average of four runs.

References:

1. Taylor, M. T.; Blackman, M. L.; Dmitrenko, O.; Fox, J. M., *J. Am. Chem. Soc.* **2011**, *133*, 9646-9649.

2. Zhang, H.; Dicker, K. T.; Xu, X.; Jia, X.; Fox, J. M. *ACS Macro Lett.* **2014**, *3*, 727-731.

3. Panne, P.; Fox, J. M., *J. Am. Chem. Soc.* **2007**, *129*, 22-23.

Figure S1. LC-MS trace and mass spectra for **9**

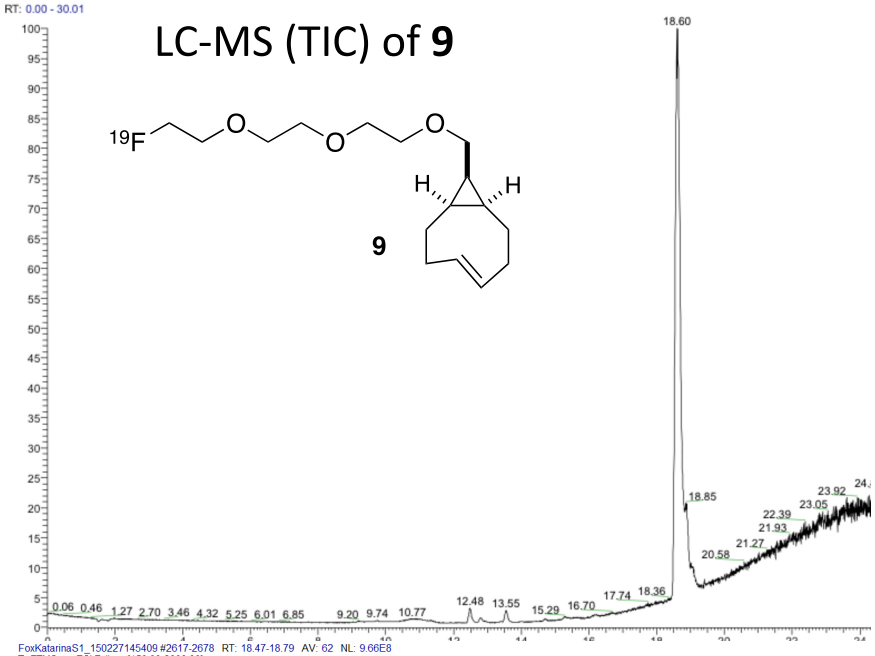

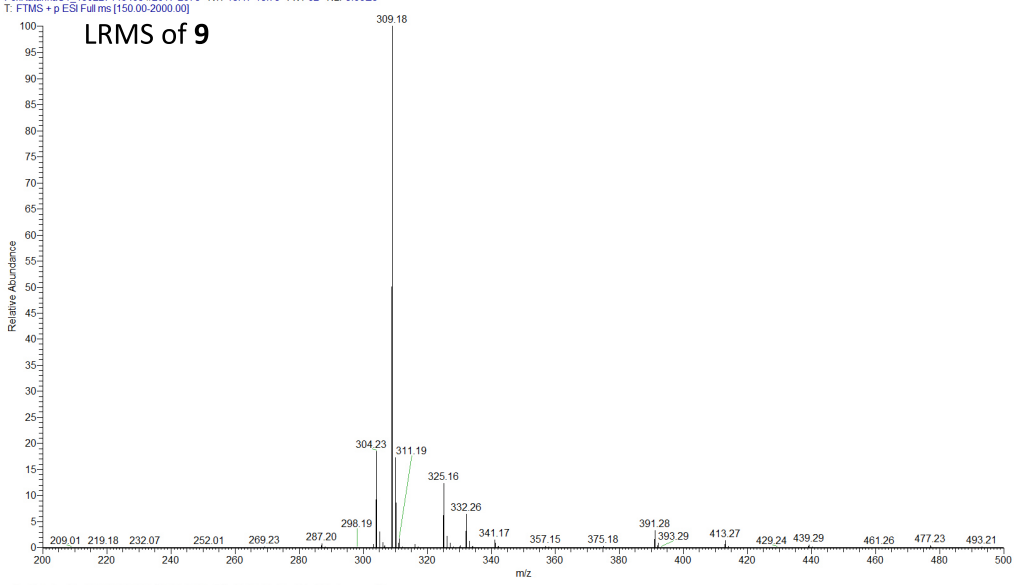

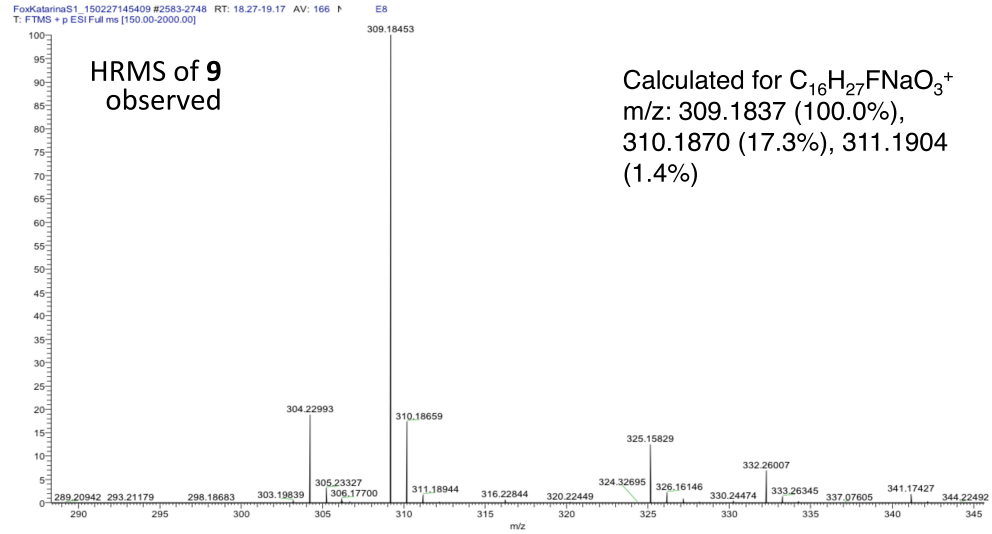

Calculated for $C_{16}H_{27}FNaO_3^+$
m/z: 309.1837 (100.0%), 310.1870 (17.3%), 311.1904 (1.4%)

Figure S2. LC-MS trace and mass spectra for crude **15**

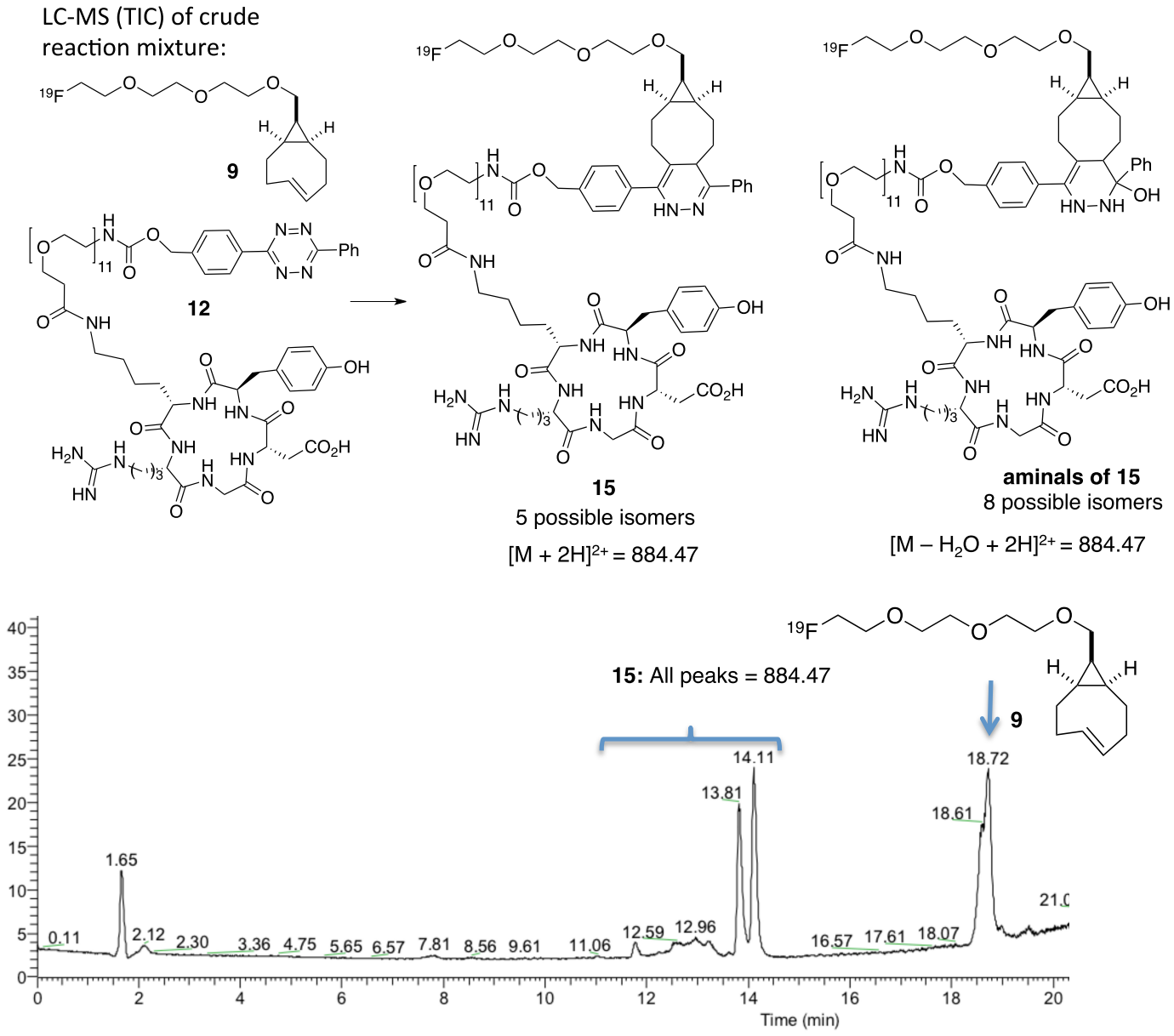

Figure S2 (continued). LC-MS trace and mass spectra for crude **15**

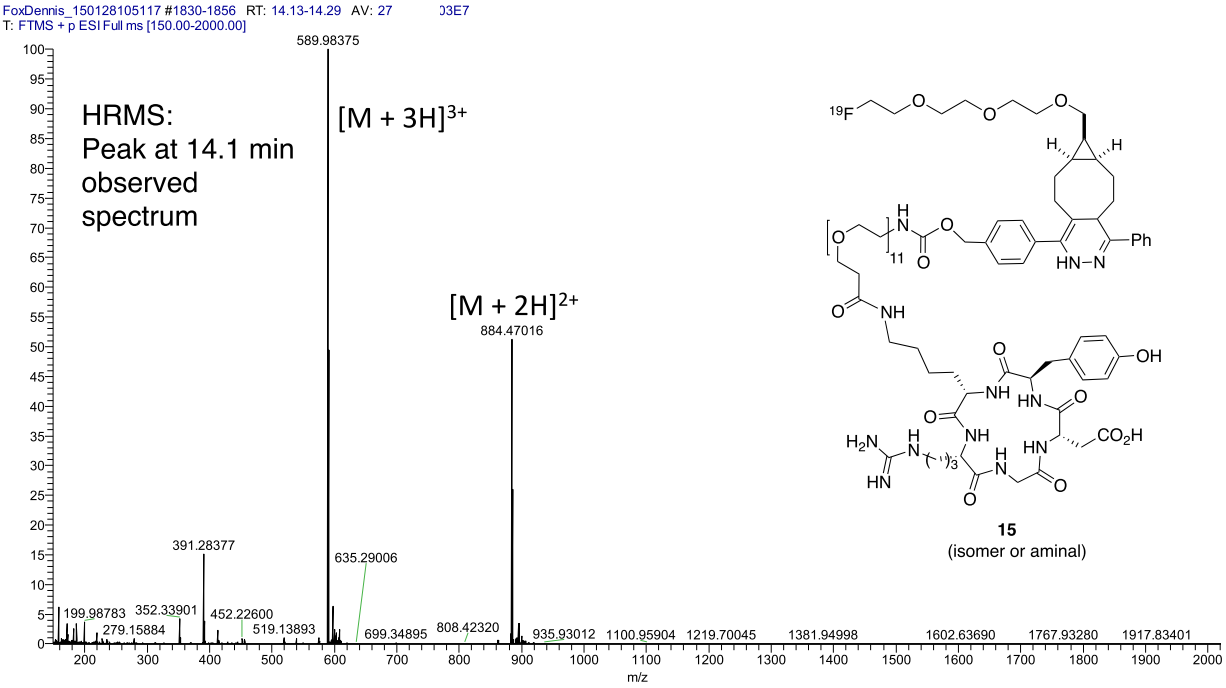

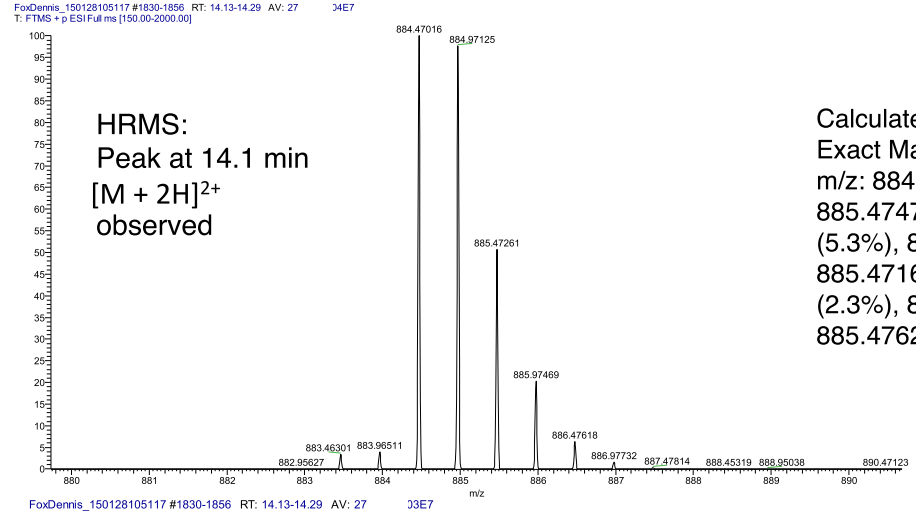

Calculated for $[M + 2H]^{2+}$, $C_{86}H_{133}FN_{12}O_{26}^{2+}$
Exact Mass: 1768.9427
m/z: 884.4714 (100.0%), 884.9731 (93.0%), 885.4747 (42.8%), 885.9764 (12.9%), 885.4735 (5.3%), 885.9752 (5.0%), 884.9699 (4.4%), 885.4716 (4.1%), 886.4781 (2.9%), 886.4769 (2.3%), 885.9732 (1.9%), 884.9745 (1.5%), 885.4762 (1.4%)

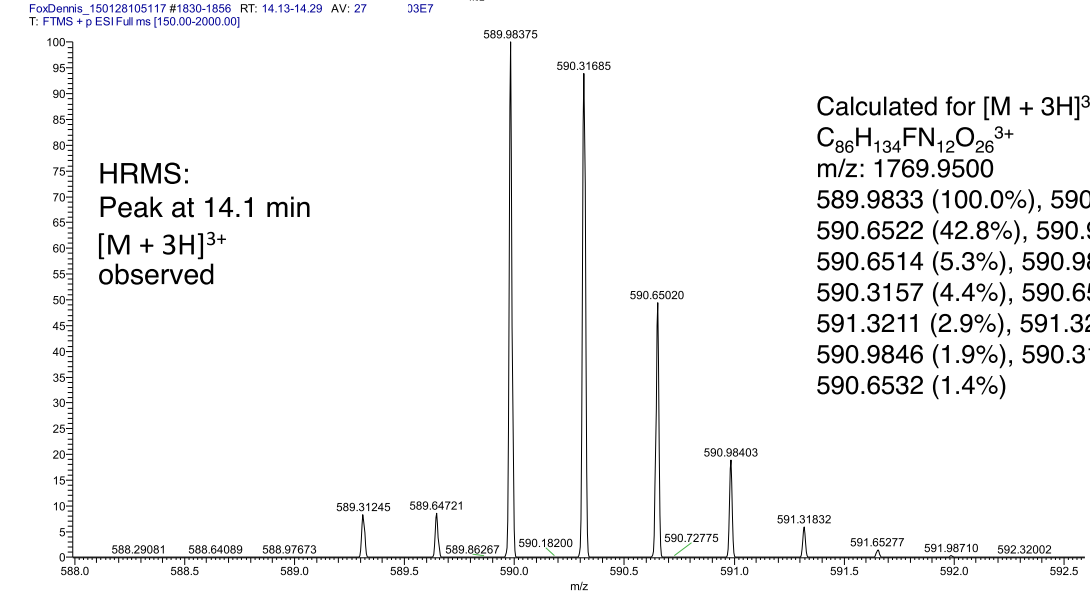

Calculated for $[M + 3H]^{3+}$,
$C_{86}H_{134}FN_{12}O_{26}^{3+}$
m/z: 1769.9500
589.9833 (100.0%), 590.3178 (93.0%), 590.6522 (42.8%), 590.9867 (12.9%), 590.6514 (5.3%), 590.9859 (5.0%), 590.3157 (4.4%), 590.6501 (4.1%), 591.3211 (2.9%), 591.3203 (2.3%), 590.9846 (1.9%), 590.3188 (1.5%), 590.6532 (1.4%)

Figure S2 (continued). LC-MS trace and mass spectra for crude **15**

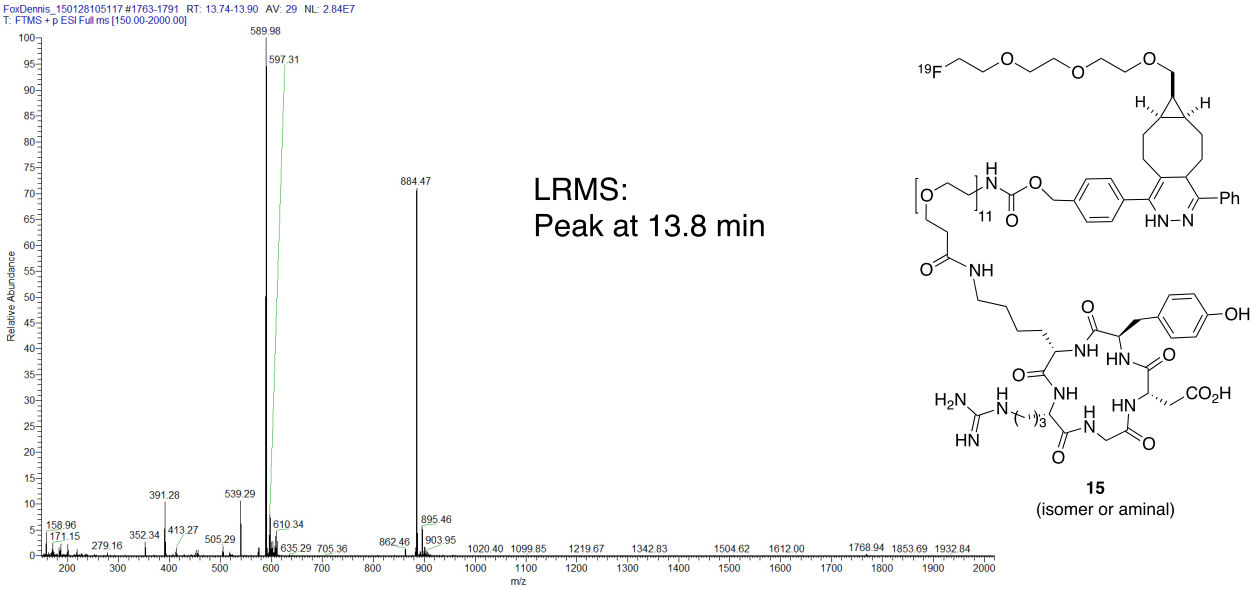

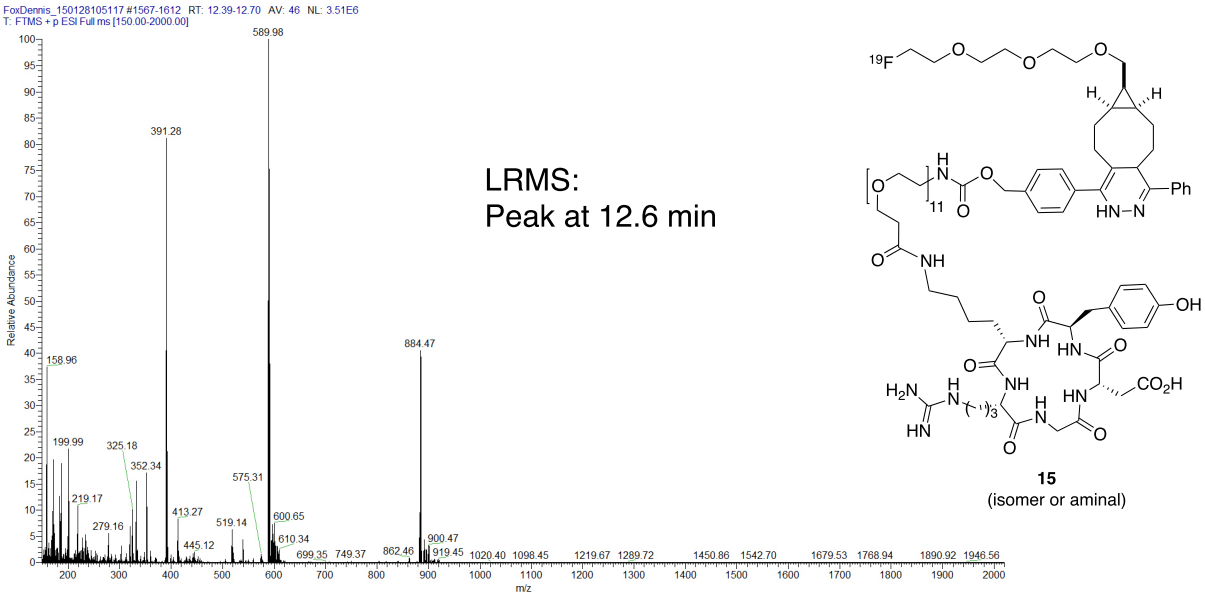

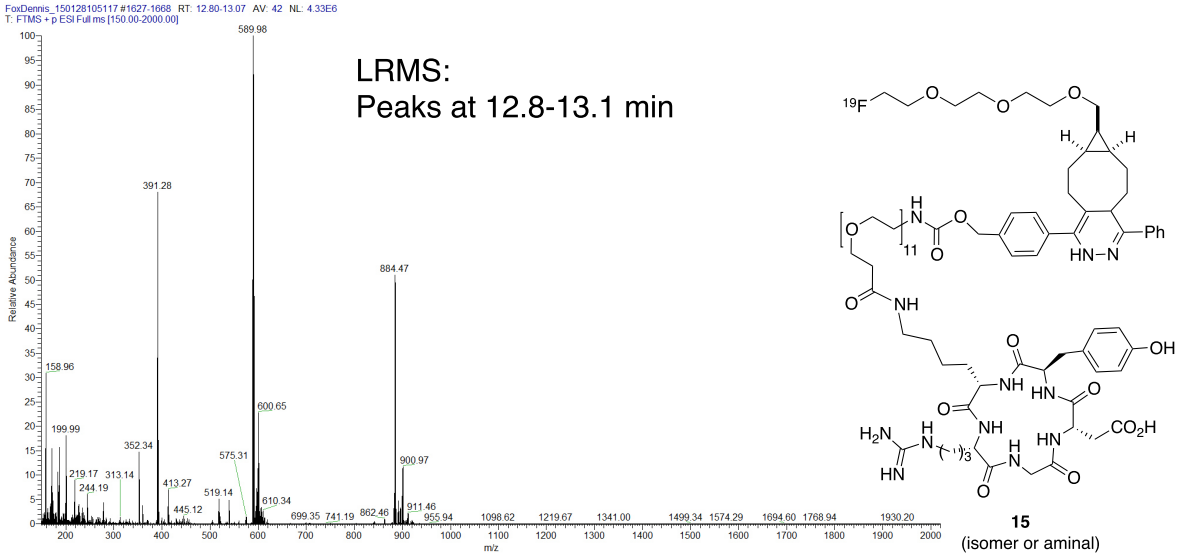

Figure S3. HPLC profile of ^{18}F-**9**. a) Radio channel and b) UV channel of ^{18}F-**9** (co-injection with standard). Radio profile of ^{18}F-**9** after c) 1h incubation and d) 2h incubation in 1xPBS at 37 °C.

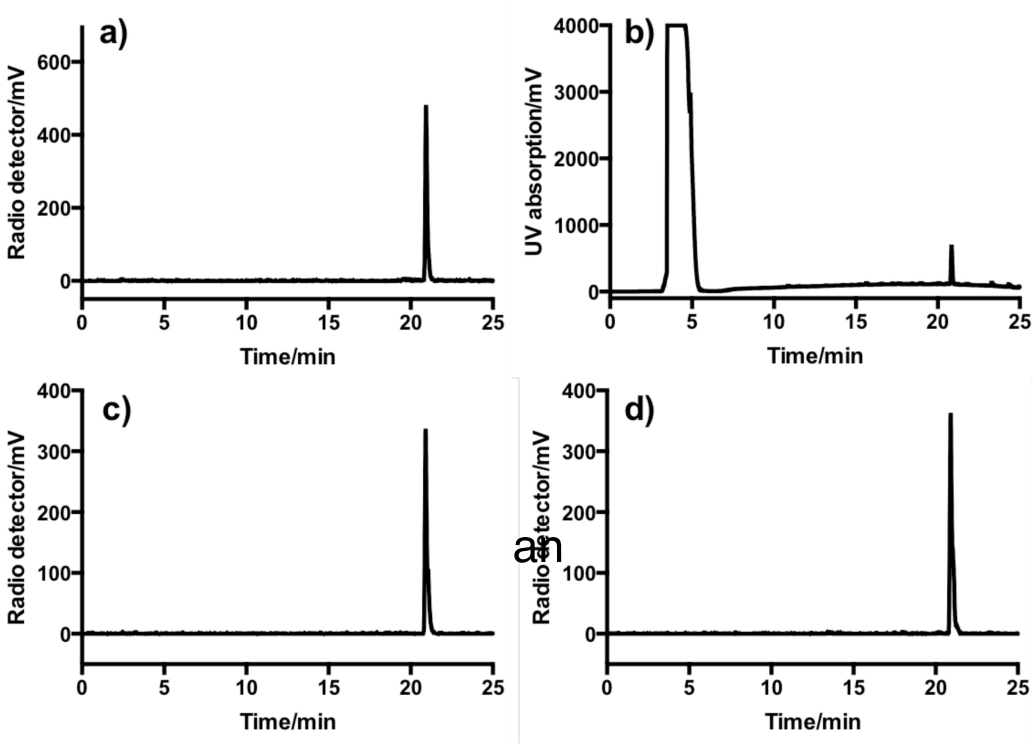

Figure S4. HPLC profile of crude reaction between ^{18}F-**9** and **12**. a) Radio channel and b) UV channel of the reaction when using excess amount of **12**. c) Radio channel and d) UV channel of the reaction when using excess amount of ^{18}F-**9** .

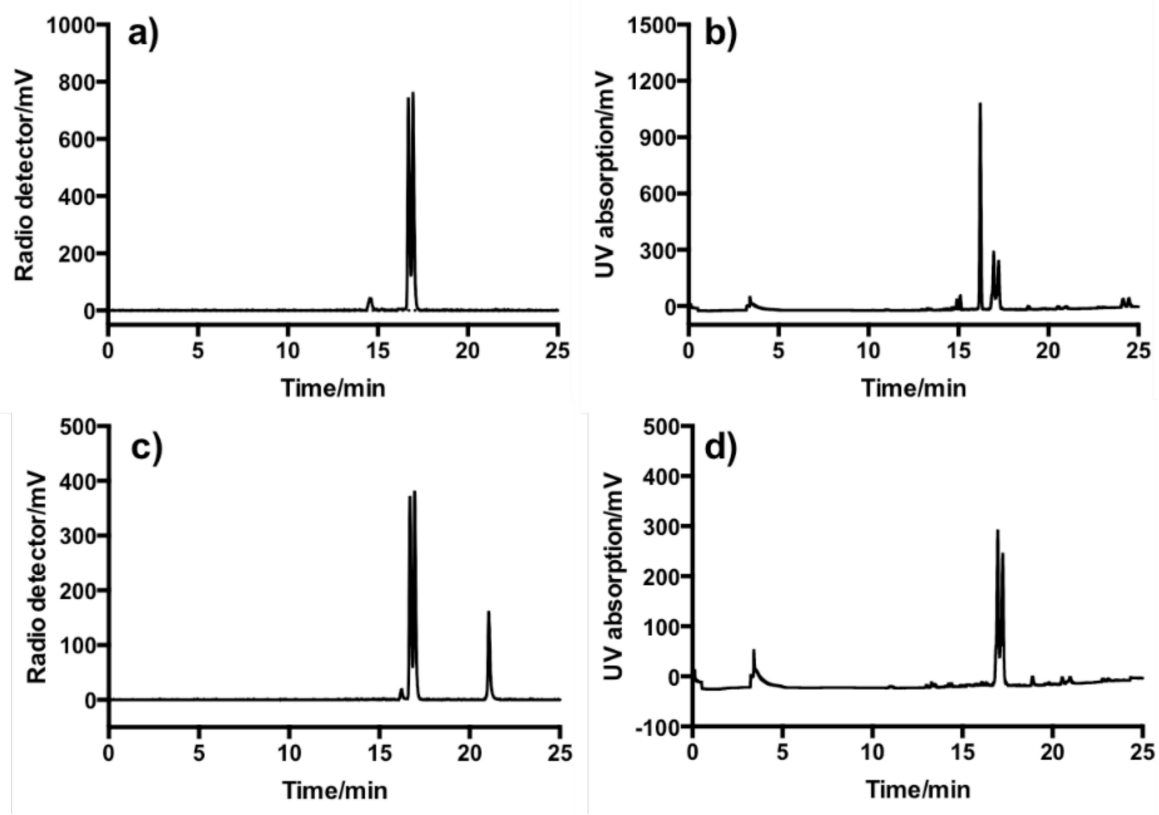

Figure S5. Reverse phase HPLC of purified **12.** Conditions: C18 Halo-column, 3.0 x 0.75 mm, 2.7μm. HPLC solvents were modified by 0.1% formic acid. The chromatogram was carried out with a gradient from 10% water in acetonitrile at t=0 min, to 100% acetonitrile at t=10 min, which was then held until the end of the run at t=20 min.

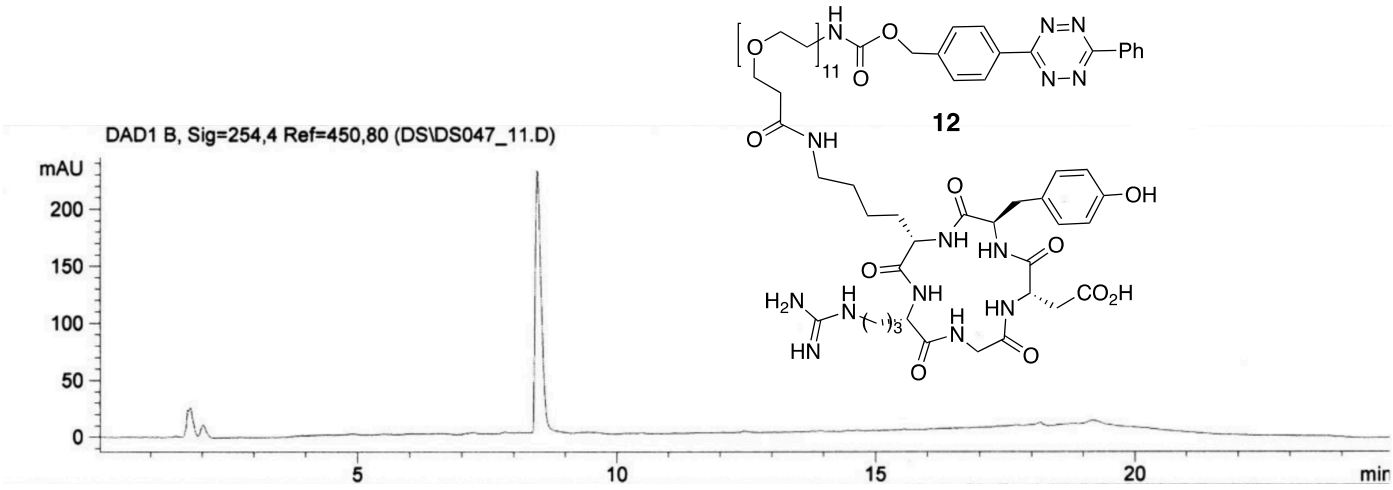

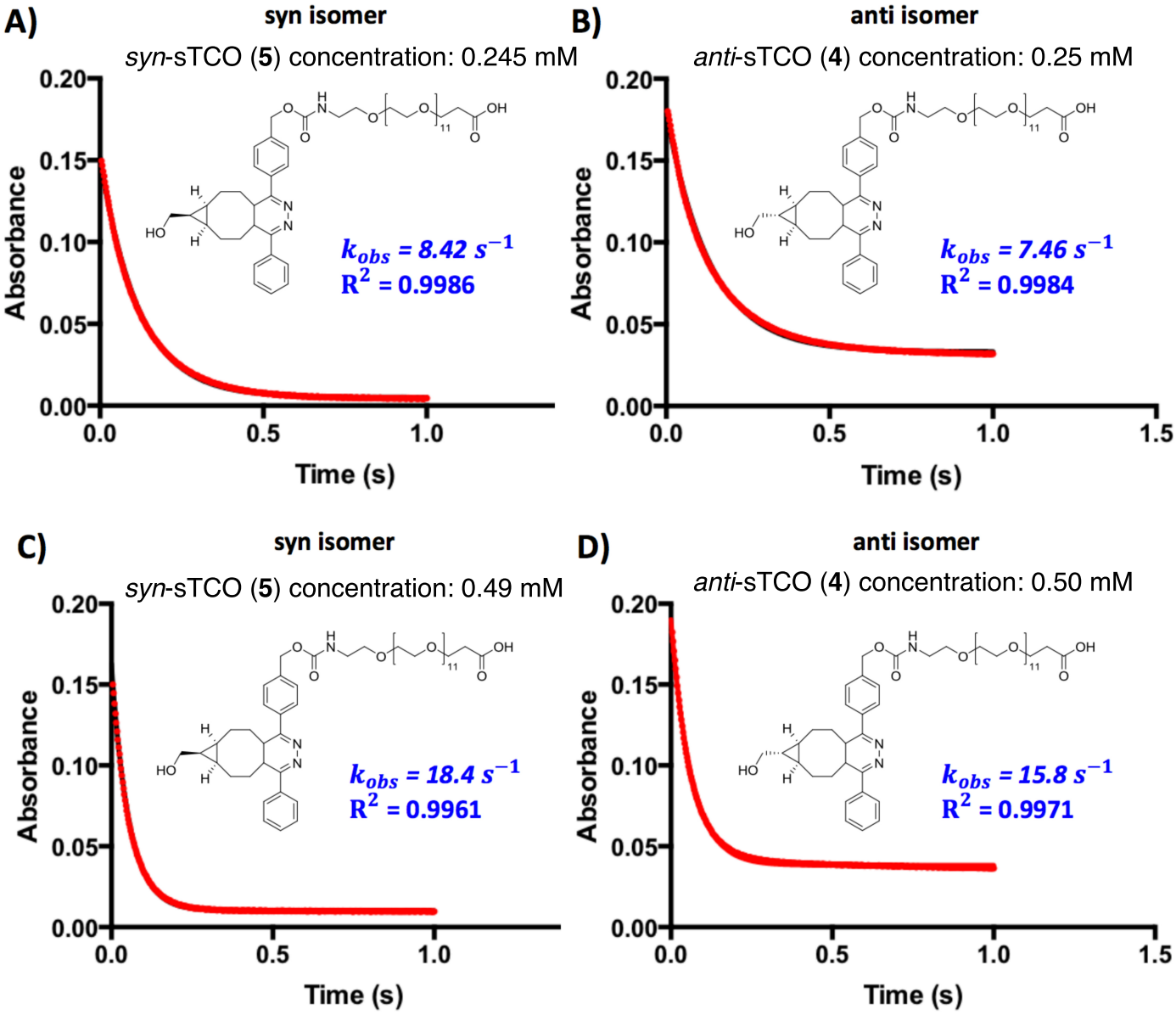

Figure S6. Stopped-flow monitored reaction of **11** (0.05 mM) with syn (**5**) and anti (**4**) diastereomers of sTCO. Each plot represents the average of 4 kinetic runs. The concentration of the sTCO used in each kinetic data set is given above each plot.

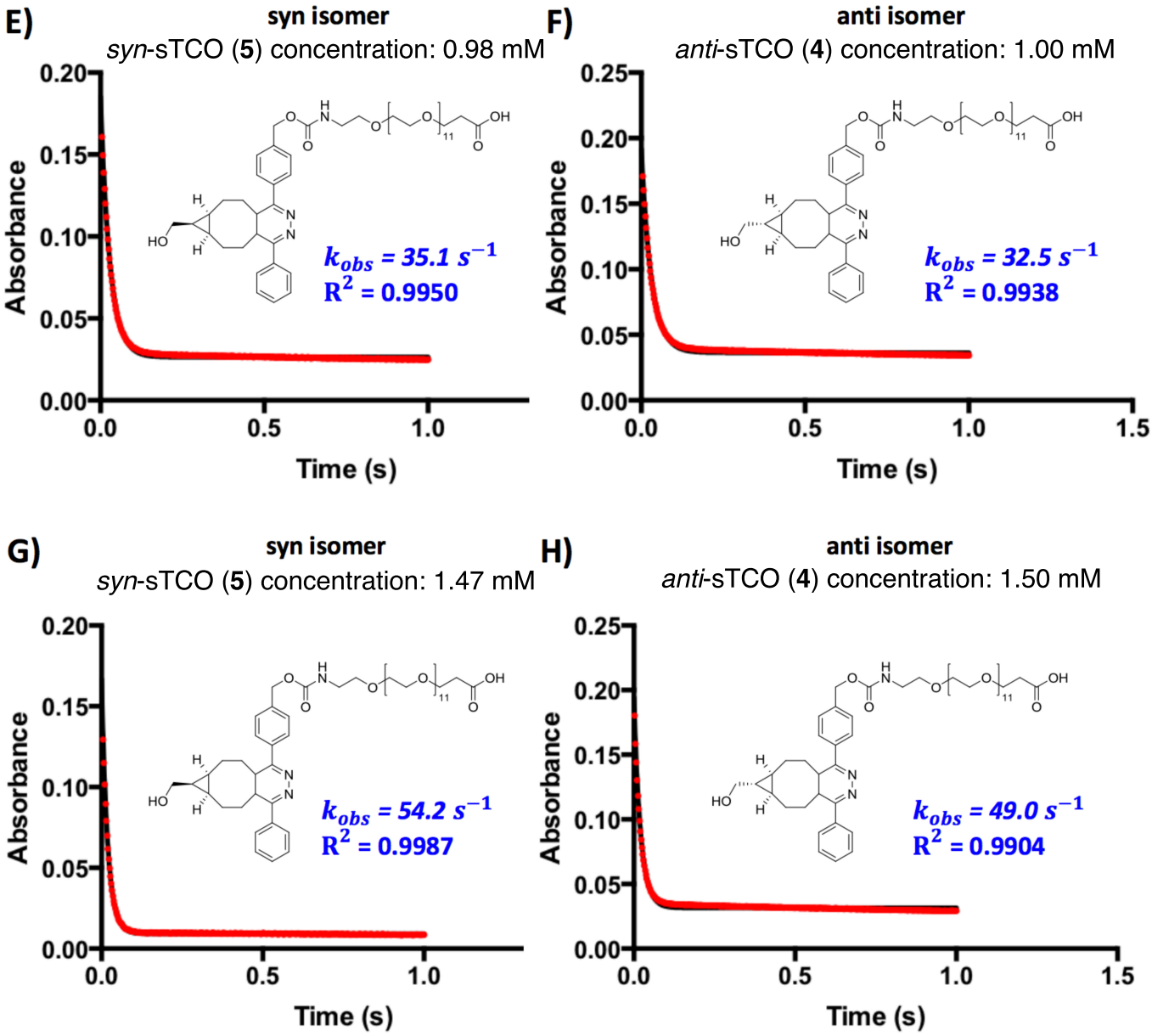

Figure S6 (continued)**.** Stopped-flow monitored reaction of **11** (0.05 mM) with syn (**5**) and anti (**4**) diastereomers of sTCO. Each plot represents the average of 4 kinetic runs. The concentration of the sTCO used in each kinetic data set is given above each plot.

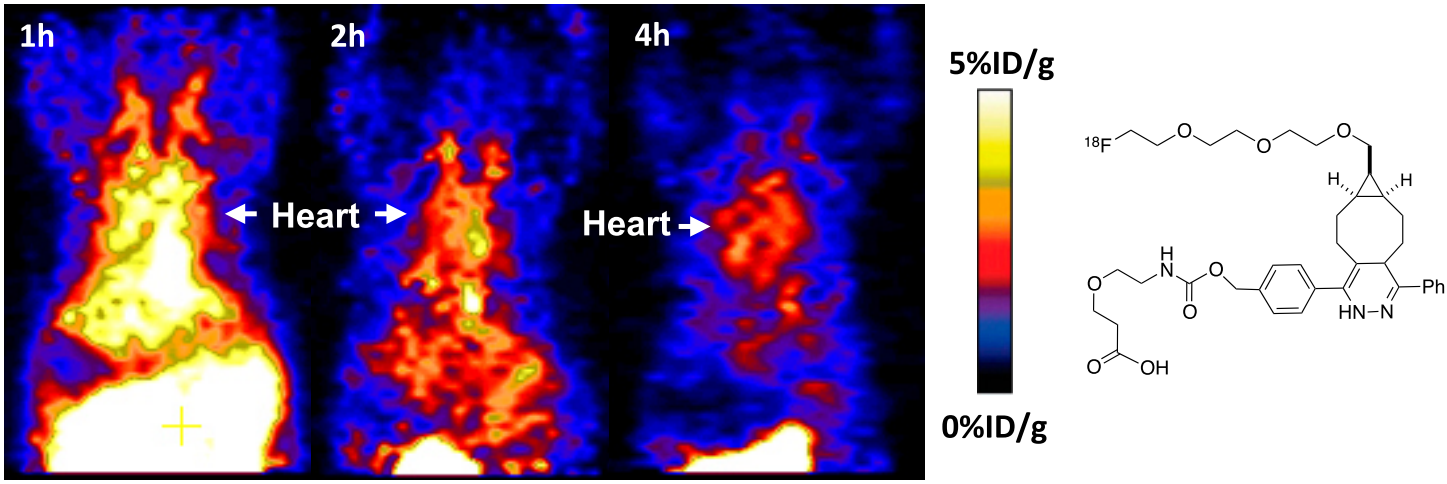

Figure S7. Small animal PET images for healthy mice injected with ^{18}F-sTCO-PEG-tetrazine conjugate (shown) and imaged at 1, 2, 4h post injection, respectively.

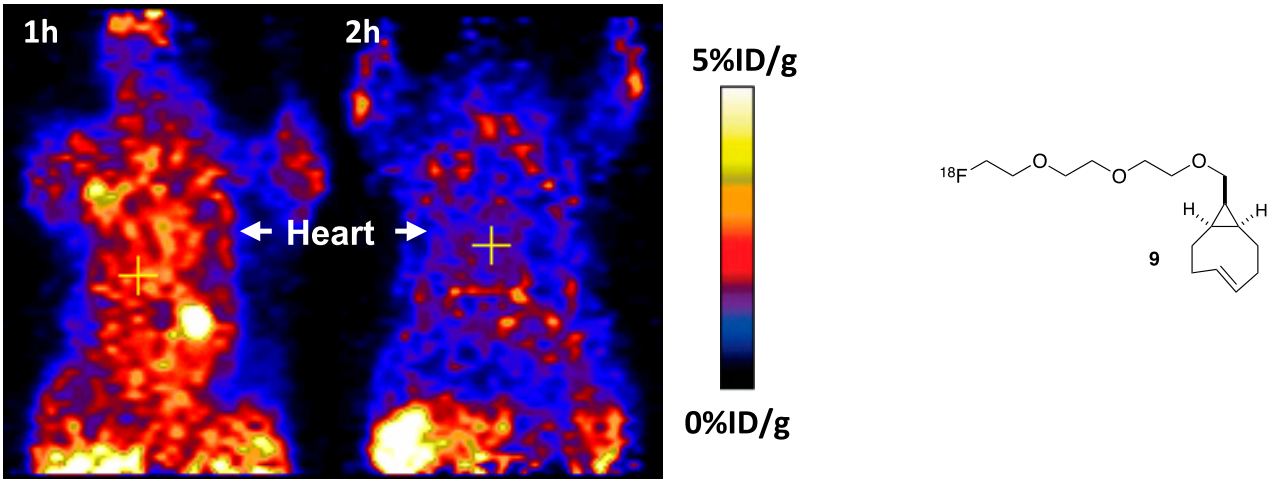

Figure S8. Small animal PET images for healthy mice injected with ^{18}F-sTCO **9** and imaged at 1 and 2 h post injection, respectively.

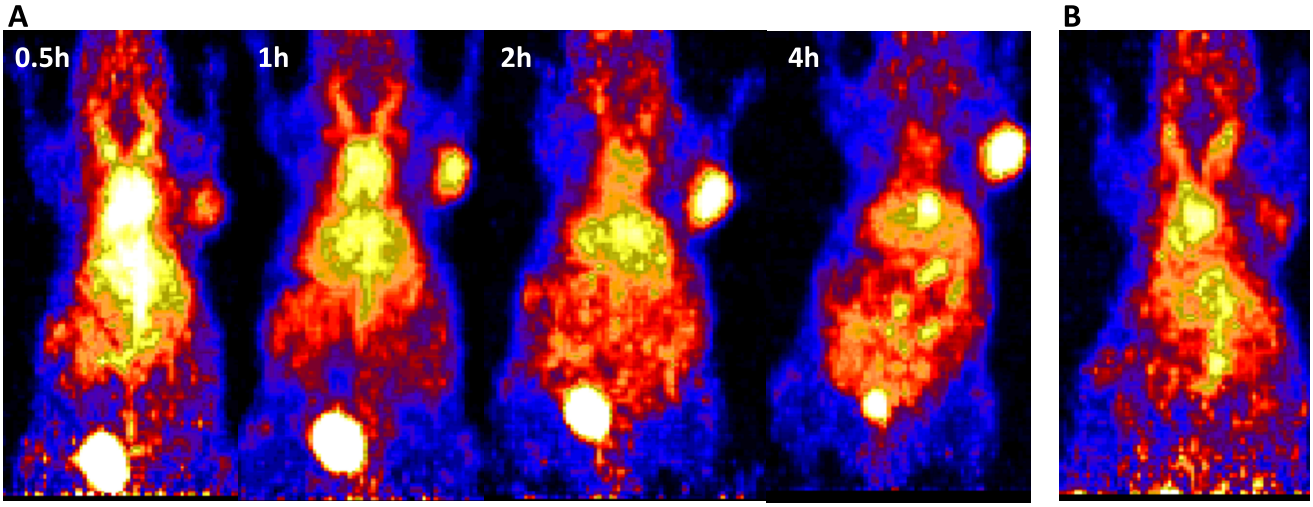

Figure S9. Two –dimensional maximum intensity projection of the mouse shown in Figure 2.

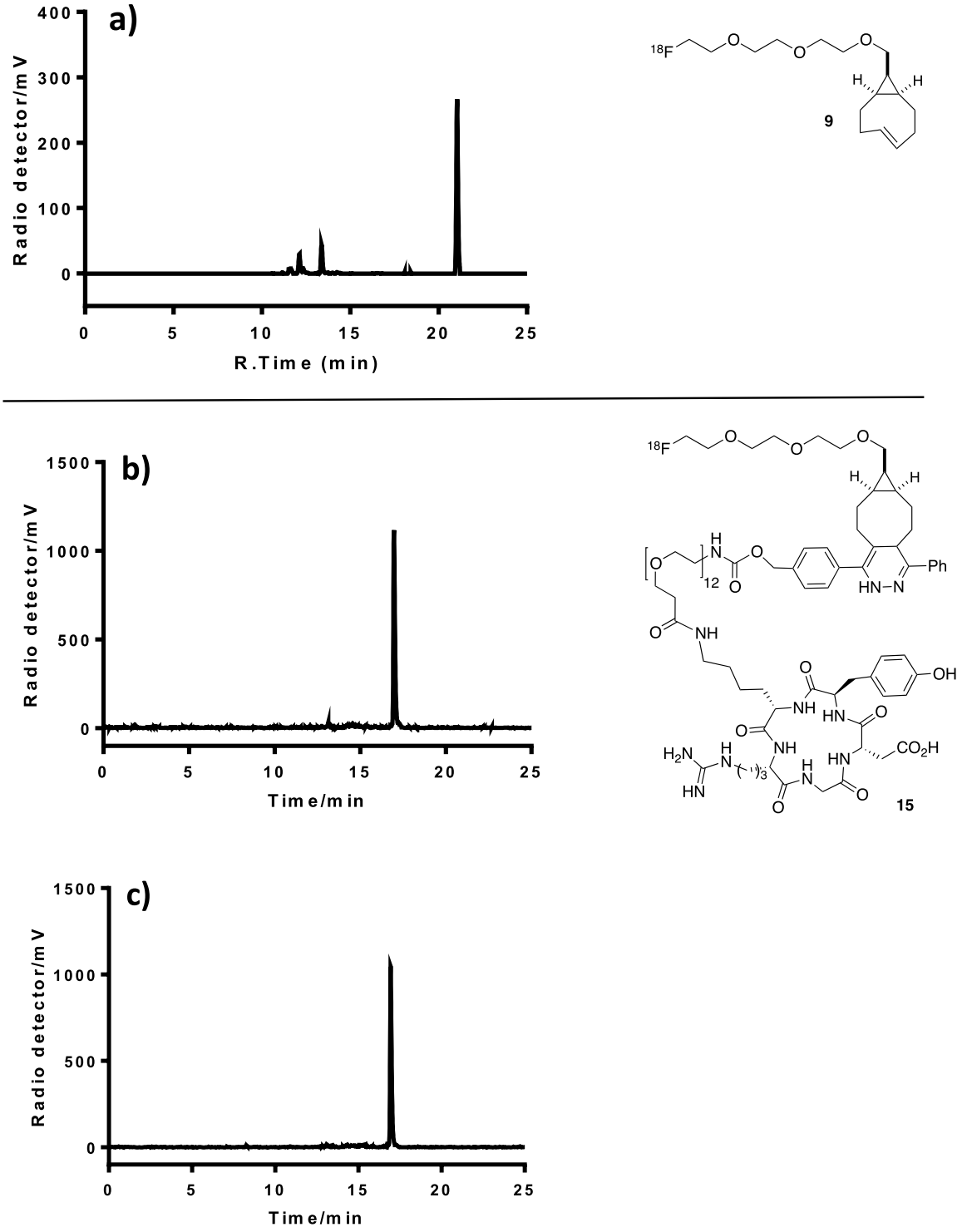

Figure S10. HPLC profile of serum stability test. a) 1h incubation of ^{18}F-**9** in FBS at 37°C. b) 2h and c) 4h incubation of ^{18}F-**15** in FBS at 37°C.

(rel-1R,8S,9S,4E)-Bicyclo[6.1.0]non-4-ene-9-ylmethanol (**5**) Svatunek, D. (2016)

^{1}H NMR (600 MHz, CD_3OD)

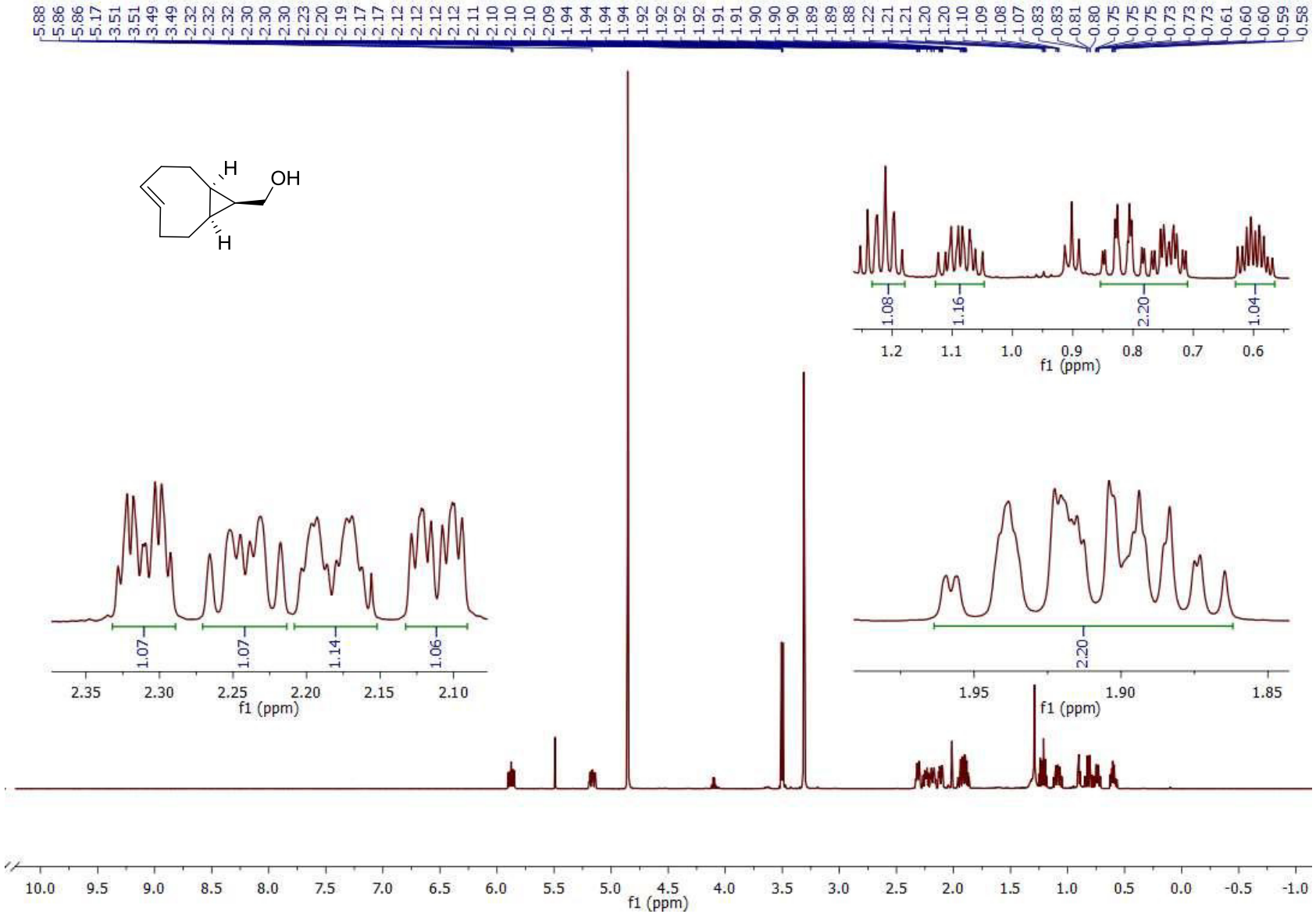

(rel-1R,8S,9S,4E)-Bicyclo[6.1.0]non-4-ene-9-ylmethanol (**5**) Svatunek, D. (2016)

^{1}H NMR (600 MHz, CD_3OD)

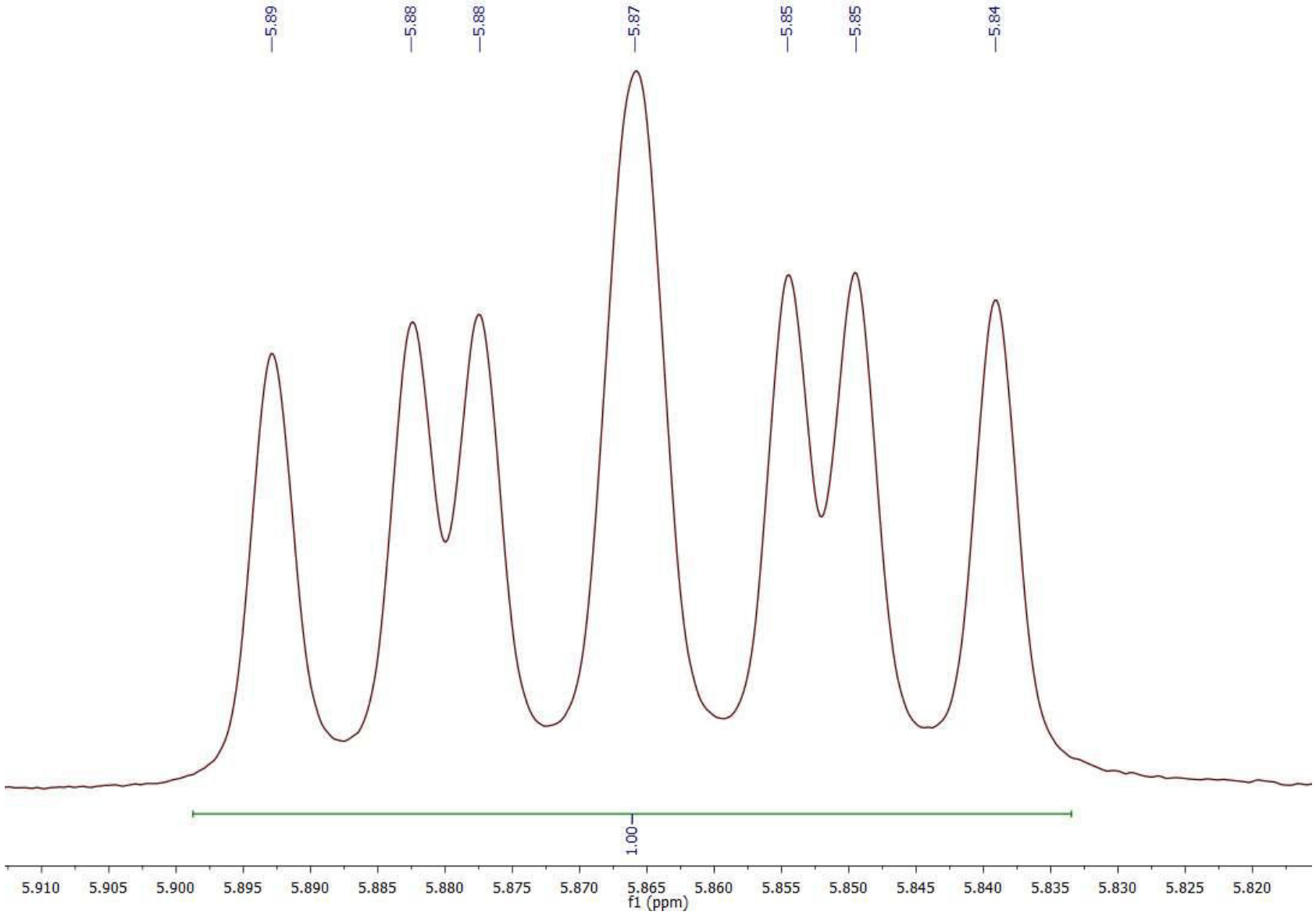

(rel-1R,8S,9S,4E)-Bicyclo[6.1.0]non-4-ene-9-ylmethanol (**5**)

^{1}H NMR (600 MHz, CD_3OD)

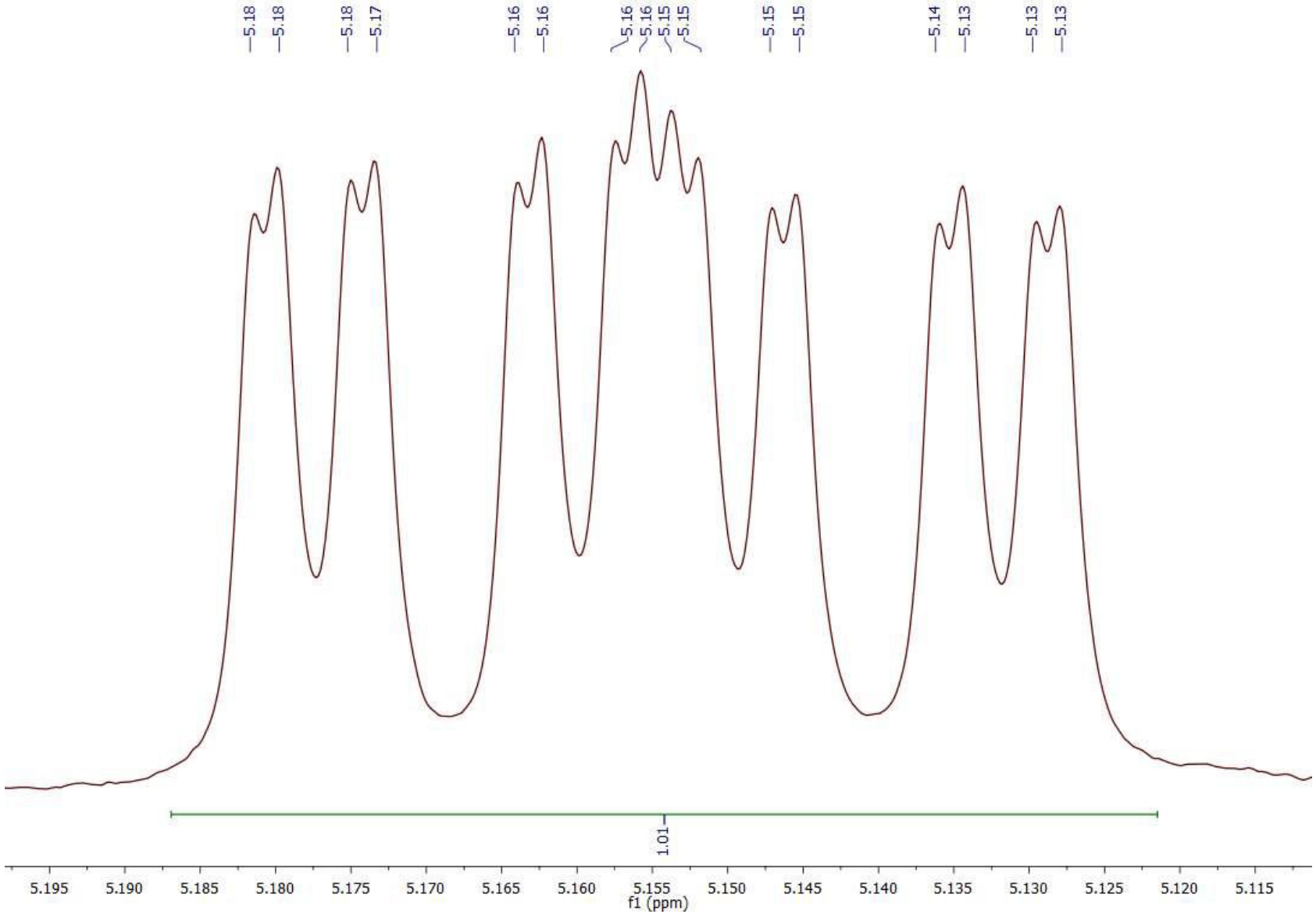

(rel-1R,8S,9S,4E)-Bicyclo[6.1.0]non-4-ene-9-ylmethanol (**5**)

^{1}H NMR (600 MHz, CD_3OD)

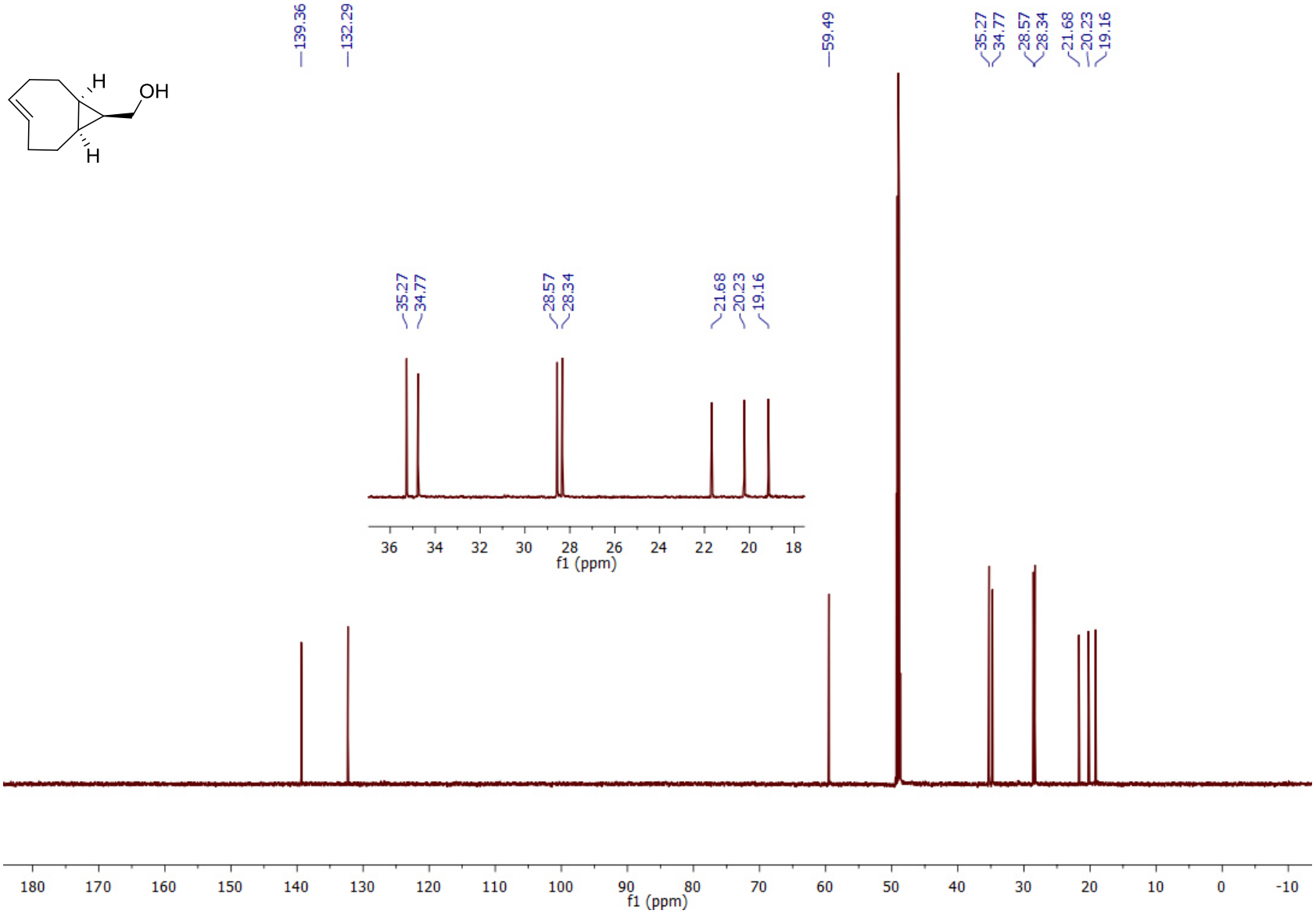

2-(2-(2-((*syn*-(*E*)-bicyclo[6.1.0]non-4-en-9-yl)methoxy)ethoxy)ethoxy)ethyl 4-methylbenzenesulfonate (**8**)

Svatunek, D. (2016)

^{1}H NMR (600 MHz, CD_3OD)

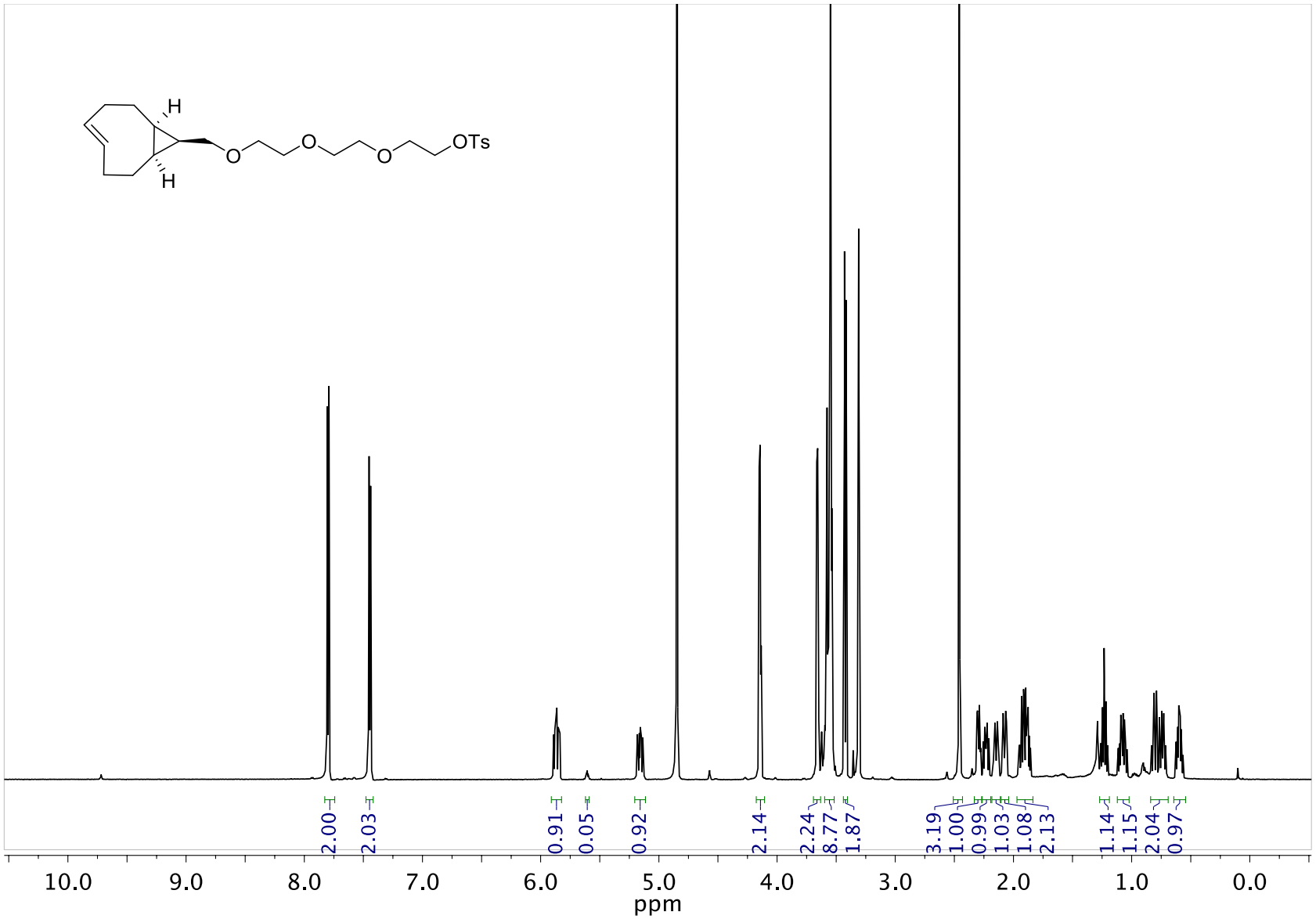

2-(2-(2-((*syn*-(*E*)-bicyclo[6.1.0]non-4-en-9-yl)methoxy)ethoxy)ethoxy)ethyl 4-methylbenzenesulfonate (8)

^{1}H NMR (400 MHz, CD_3OD)

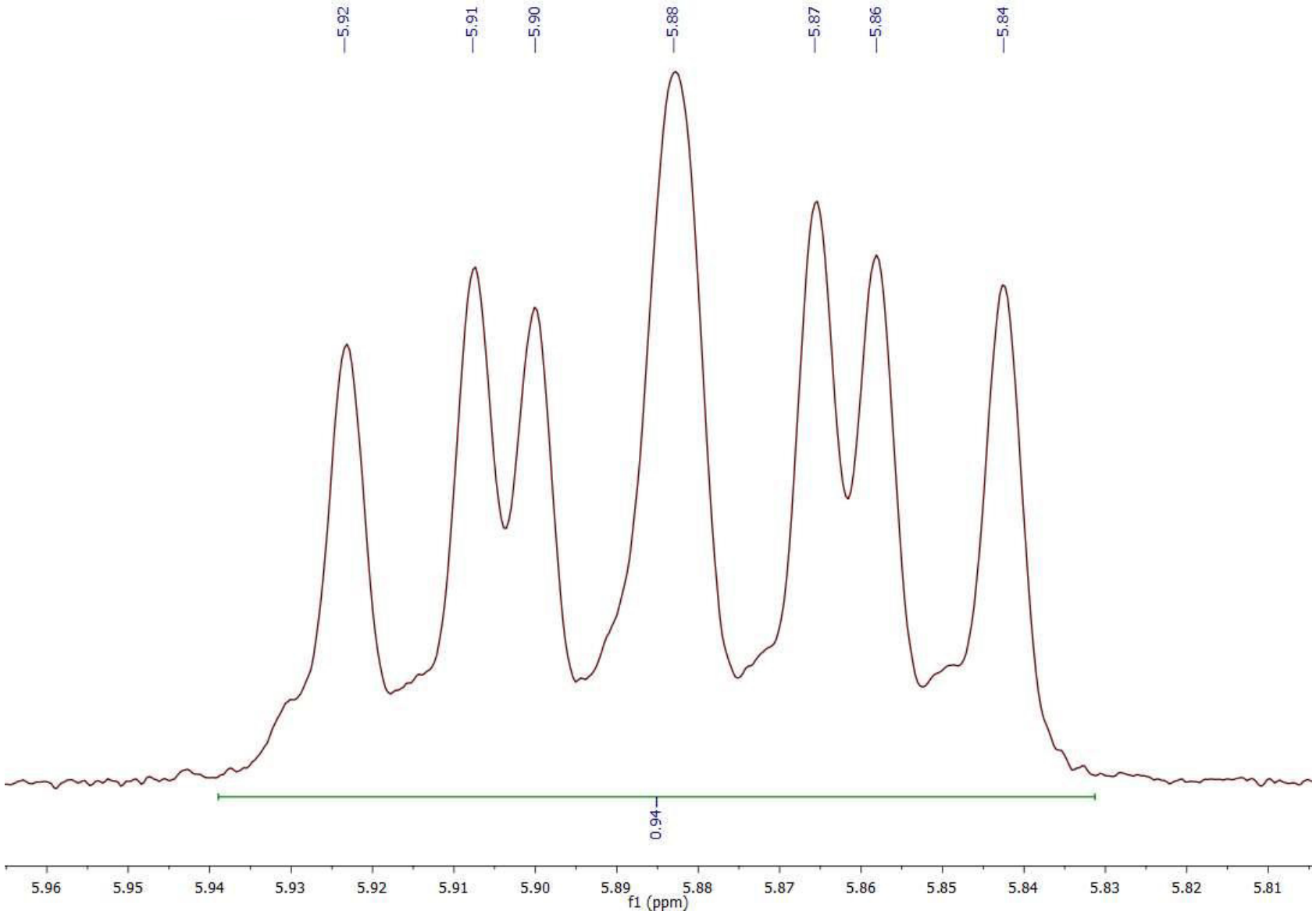

2-(2-(2-((*syn*-(*E*)-bicyclo[6.1.0]non-4-en-9-yl)methoxy)ethoxy)ethoxy)ethyl 4-methylbenzenesulfonate (8)

^{1}H NMR (400 MHz, CD_3OD)

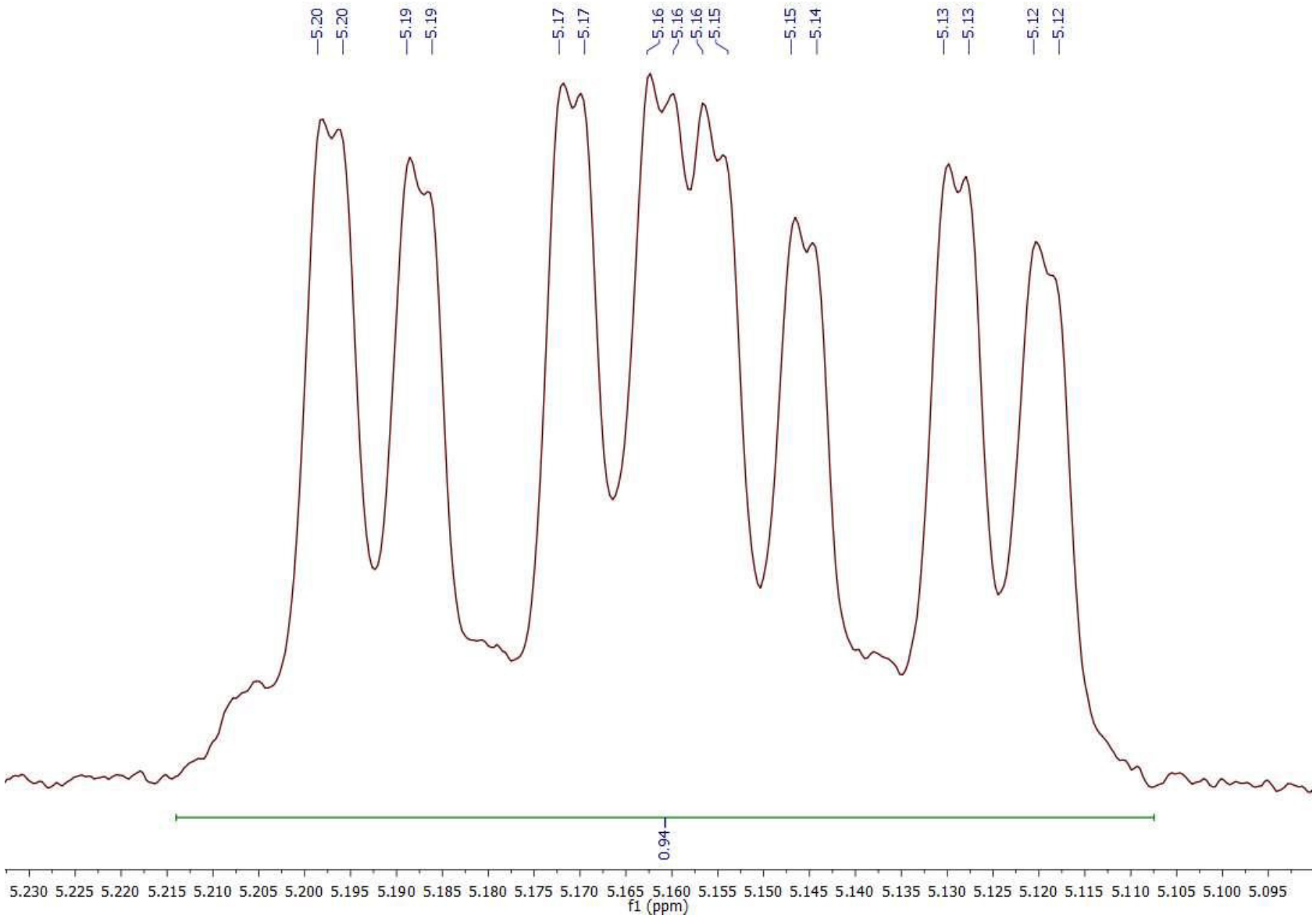

2-(2-(2-((*syn*-(*E*)-bicyclo[6.1.0]non-4-en-9-yl)methoxy)ethoxy)ethoxy)ethyl 4-methylbenzenesulfonate (8)

^{13}C APT NMR (100.6 MHz, CD_3OD)

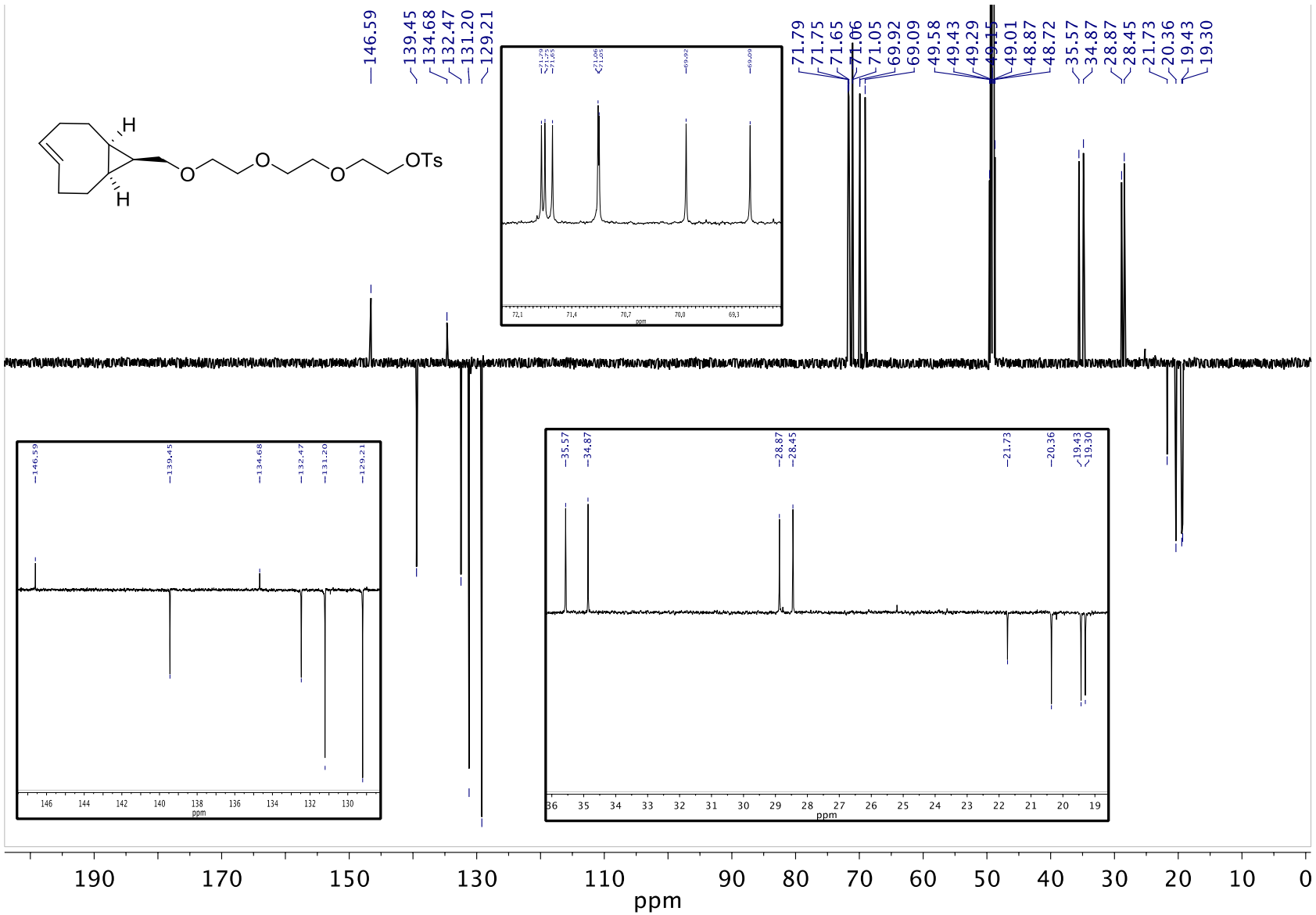

syn-(*E*)-9-((2-(2-(2-fluoroethoxy)ethoxy)ethoxy)methyl)bicyclo[6.1.0]non-4-ene (**9**)
Svatunek, D. (2016)

^{1}H NMR (600 MHz, CD_3OD)

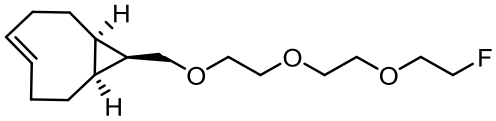

*Cis Isomer

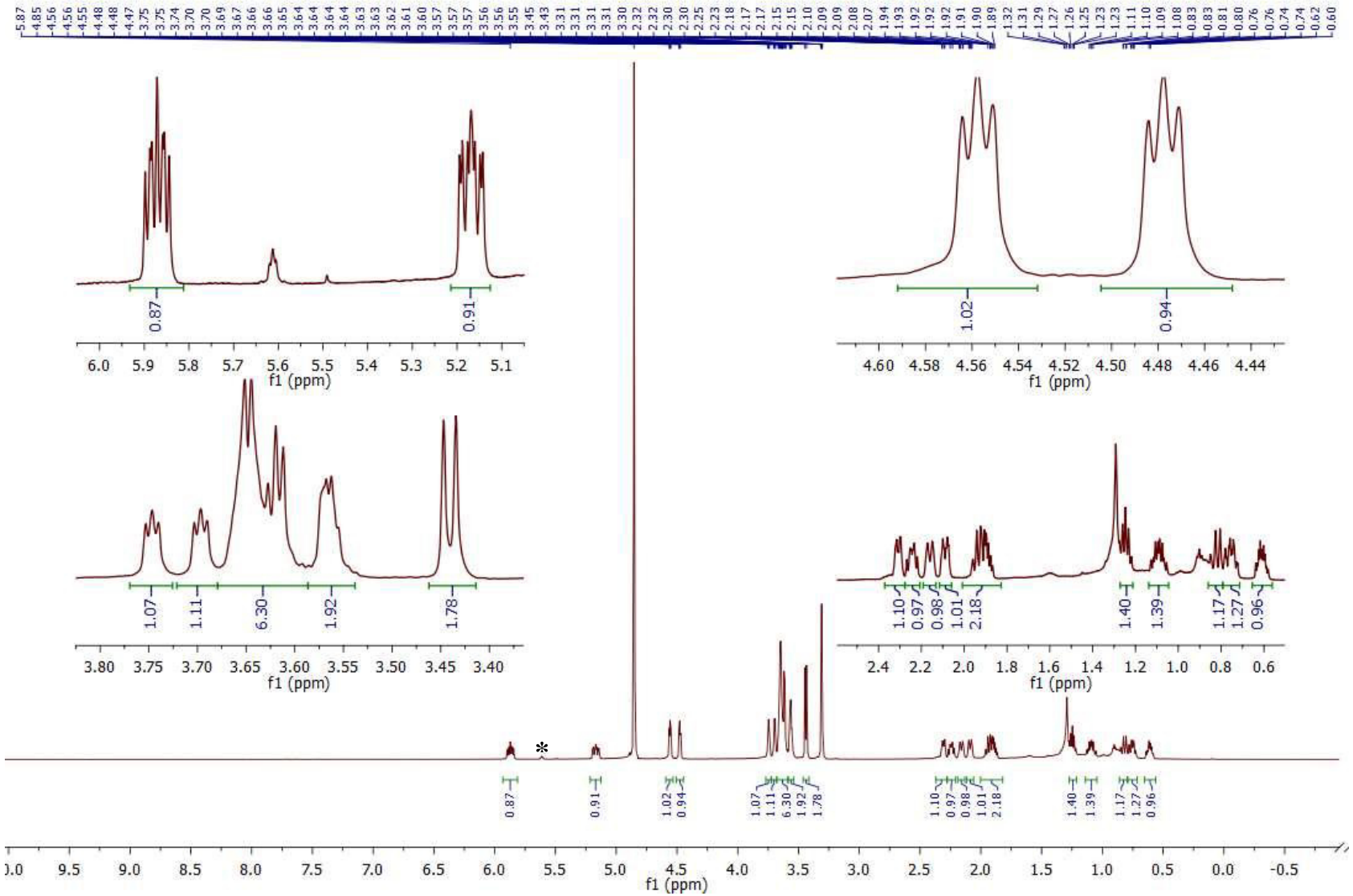

syn-(*E*)-9-((2-(2-(2-fluoroethoxy)ethoxy)ethoxy)methyl)bicyclo[6.1.0]non-4-ene (**9**)
Svatunek, D. (2016)

^{13}C APT NMR (100.6 MHz, CD_3OD)

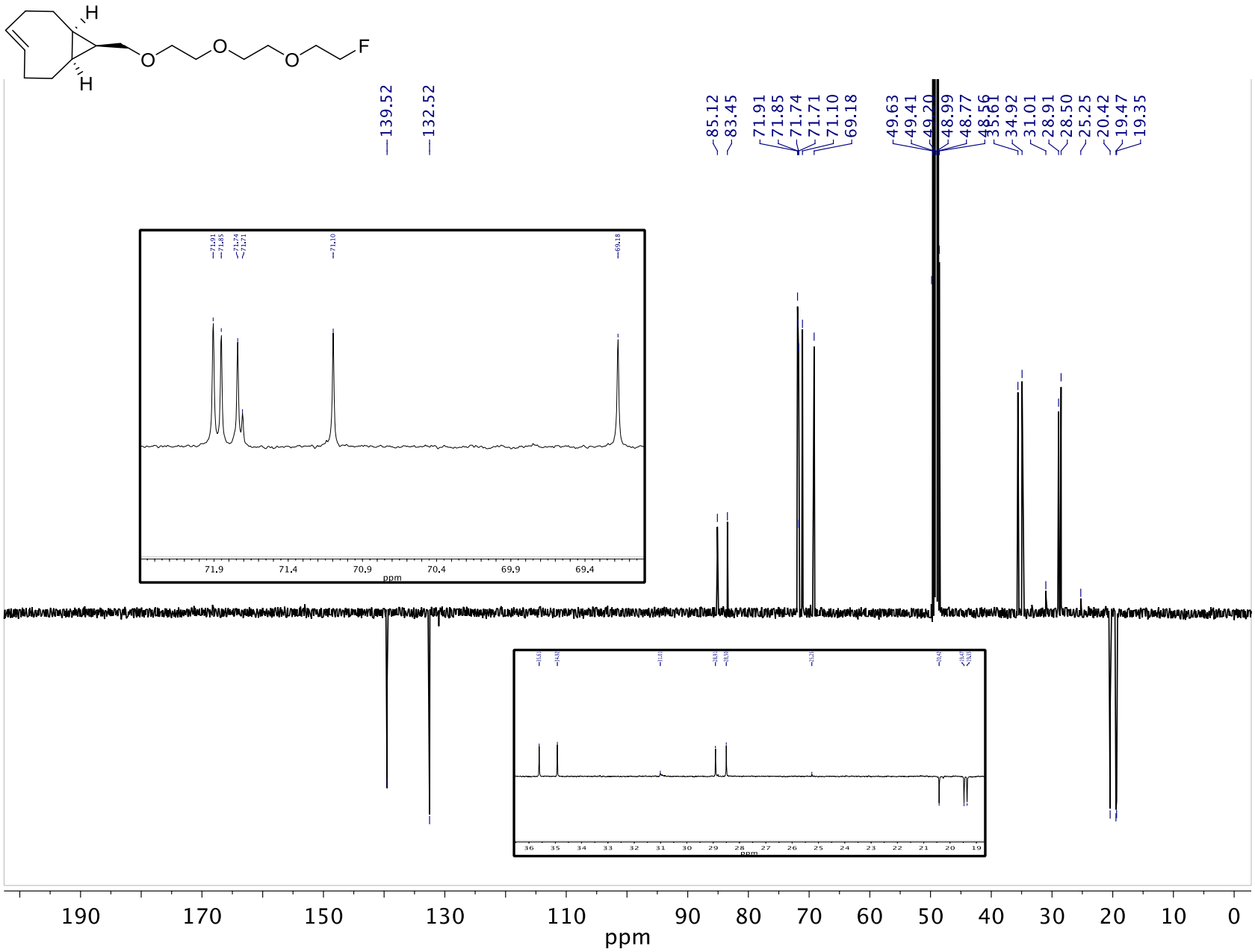

syn-(*E*)-9-((2-(2-(2-fluoroethoxy)ethoxy)ethoxy)methyl)bicyclo[6.1.0]non-4-ene (**9**)
^{19}F NMR

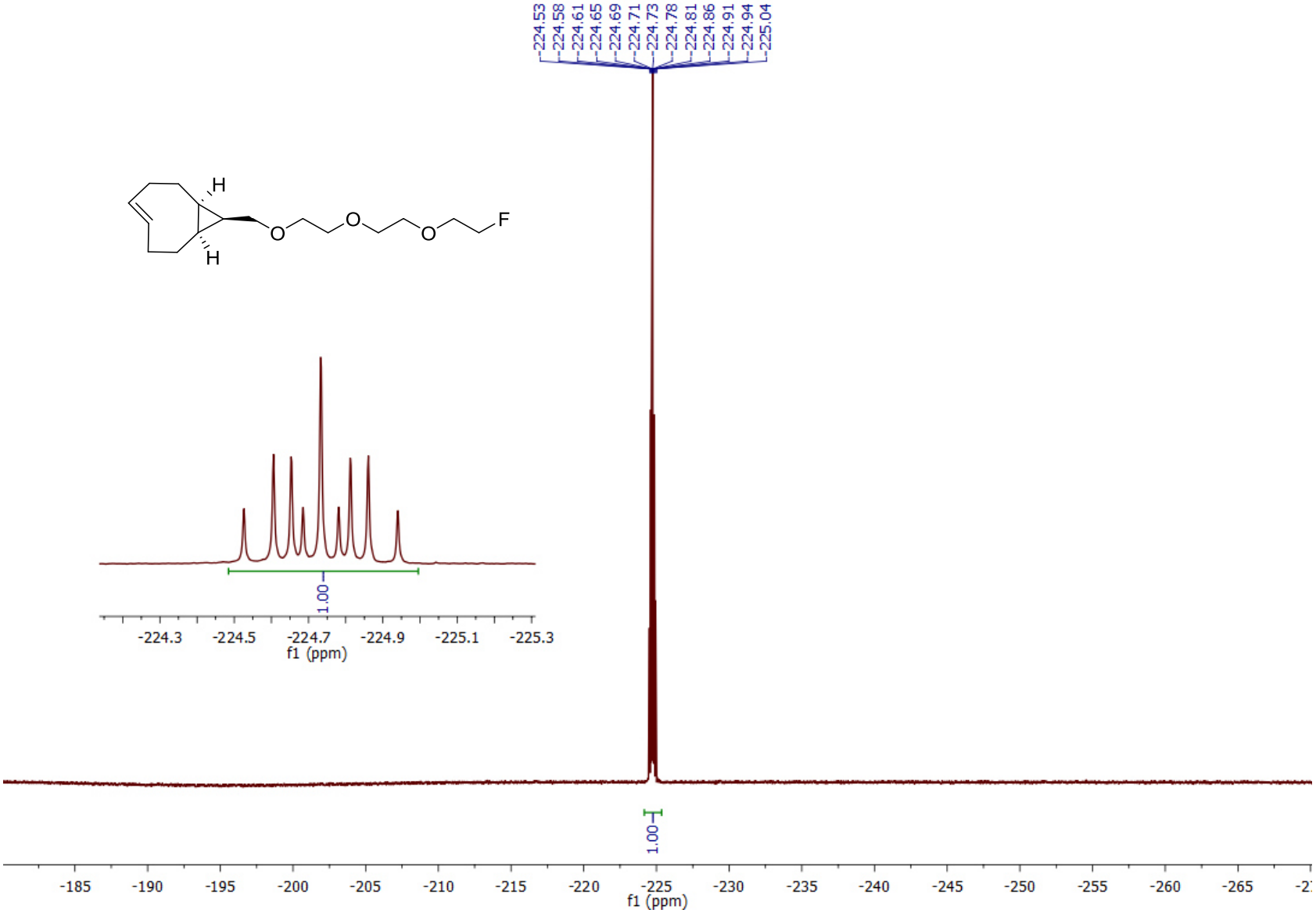

3-oxo-1-(4-(6-phenyl-1,2,4,5-tetrazin-3-yl)phenyl)-2,7,10,13,16,19,22,25,28,31,34,37,40-tridecaoxa-4-azatritetracontan-43-oic acid (**11**)

^{1}H NMR (400 MHz, CD_2Cl_2)

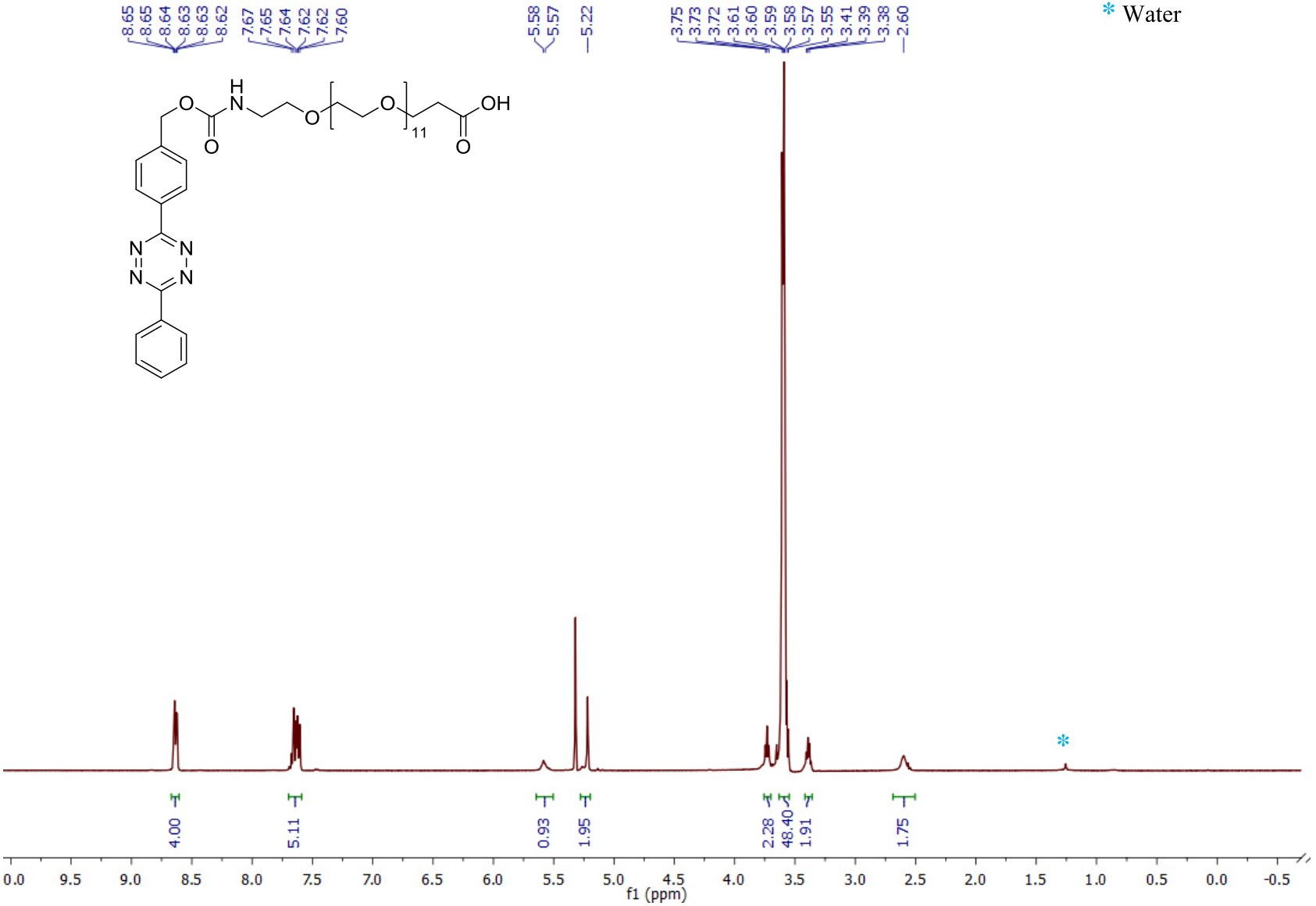

3-oxo-1-(4-(6-phenyl-1,2,4,5-tetrazin-3-yl)phenyl)-2,7,10,13,16,19,22,25,28,31,34,37,40-tridecaoxa-4-azatritetracontan-43-oic acid (**11**)

Svatunek, D. (2016)

^{13}C NMR (101 MHz, $CDCl_3$)

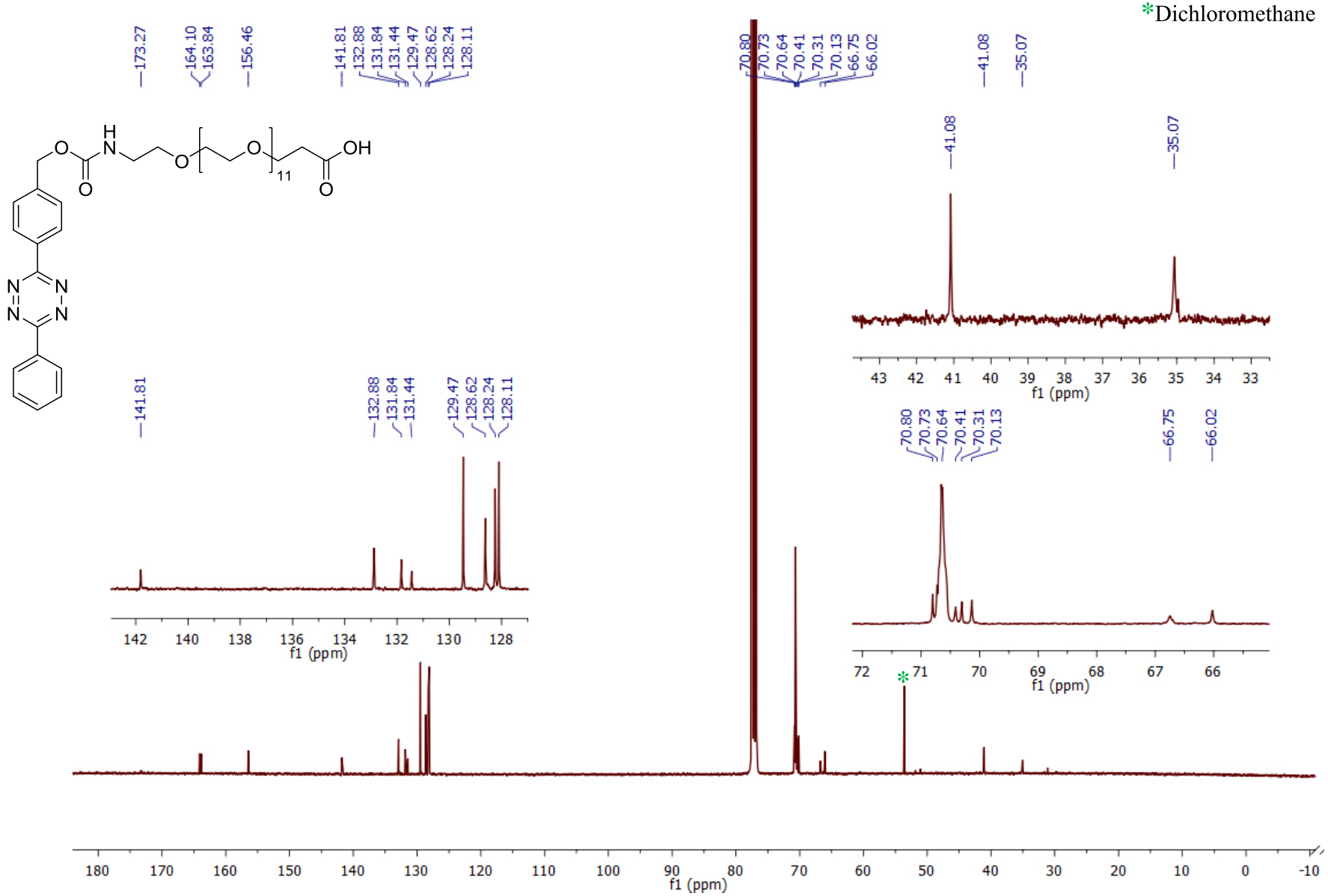

2,5-dioxopyrrolidin-1-yl 3-oxo-1-(4-(6-phenyl-1,2,4,5-tetrazin-3-yl)phenyl)-2,7,10,13,16,19,22,25,28,31,34,37,40-tridecaoxa-4-azatritetracontan-43-oate

Svatunek, D. (2016)

^{1}H NMR (400 MHz, CD_2Cl_2)

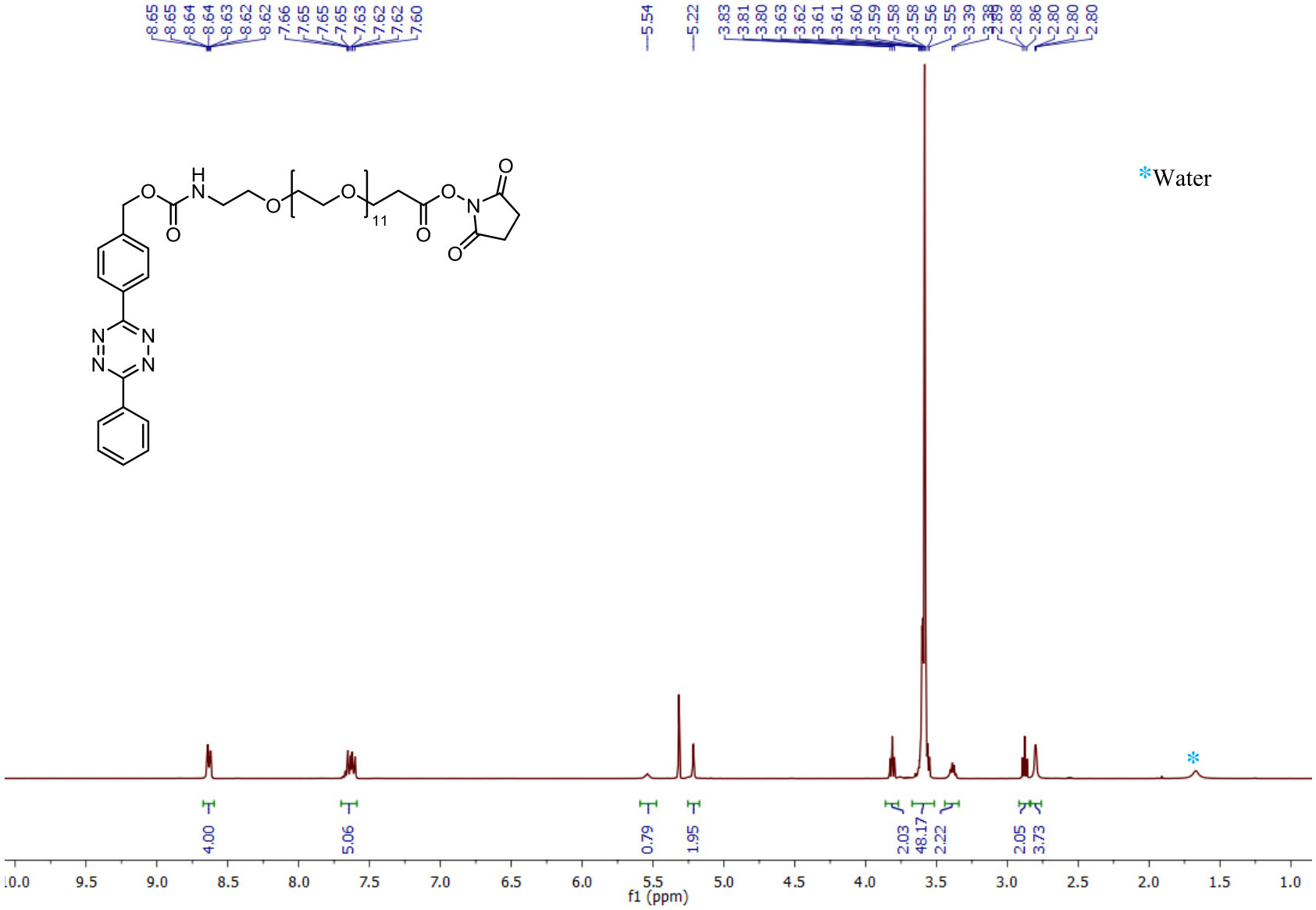

2,5-dioxopyrrolidin-1-yl 3-oxo-1-(4-(6-phenyl-1,2,4,5-tetrazin-3-yl)phenyl)-2,7,10,13,16,19,22,25,28,31,34,37,40-tridecaoxa-4-azatritetracontan-43-oate

Svatunek, D. (2016)

^{13}C NMR (101 MHz, CD_2Cl_2)

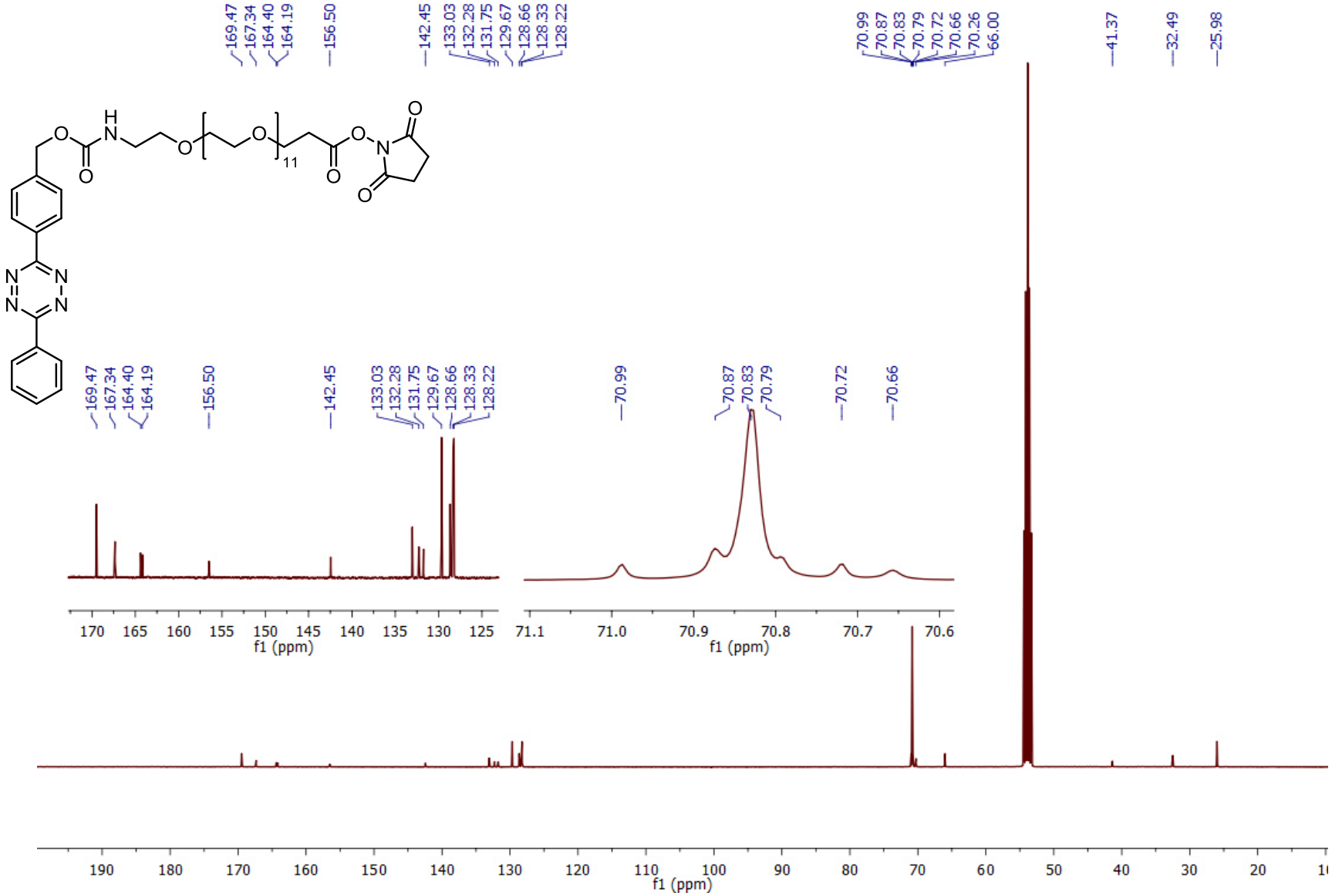

Supporting Information

Manuscript #8

Dennis Svatunek, Christoph Denk, Veronika Rosecker, Barbara Sohr, Christian Hametner, Günter Allmaier, Johannes Fröhlich, Hannes Mikula*; Efficient low-cost preparation of *trans*-cyclooctenes using a simplified flow setup for photoisomerization, *Monatsh Chem* **2016**, 147, 579–585.

(with permission from Springer Nature)

Supporting Information

Efficient low-cost preparation of *trans*-cyclooctenes using a simplified flow setup for photoisomerization

Dennis Svatunek[1, 2] ● Christoph Denk[1] ● Veronika Rosecker[1] ● Barbara Sohr[1] ● Christian Hametner[1] ● Günter Allmaier[2] ● Johannes Fröhlich[1] ● Hannes Mikula[1]

———

✉ Hannes Mikula

hannes.mikula@tuwien.ac.at

[1] Institute of Applied Synthetic Chemistry, TU Wien, Vienna, Austria

[2] Institute of Chemical Technologies and Analytics, TU Wien, Vienna, Austria

Flow reactor

Fig. S1 Flow photoreactor; 1) 55W OSRAM HNS 90 cm T8 OFR lamps; 2) Quartz tube



Photoisomerization setup

Fig. S2 Photoisomerization setup; **1**: Reservoir flask equipped with condenser and cooled with ice water; **2**) BESTA HPLC HD 2-2000 pump; **3**) Column filled with silica gel topped by $AgNO_3$ on silica gel (10%) ; **4**) Flow photo reactor

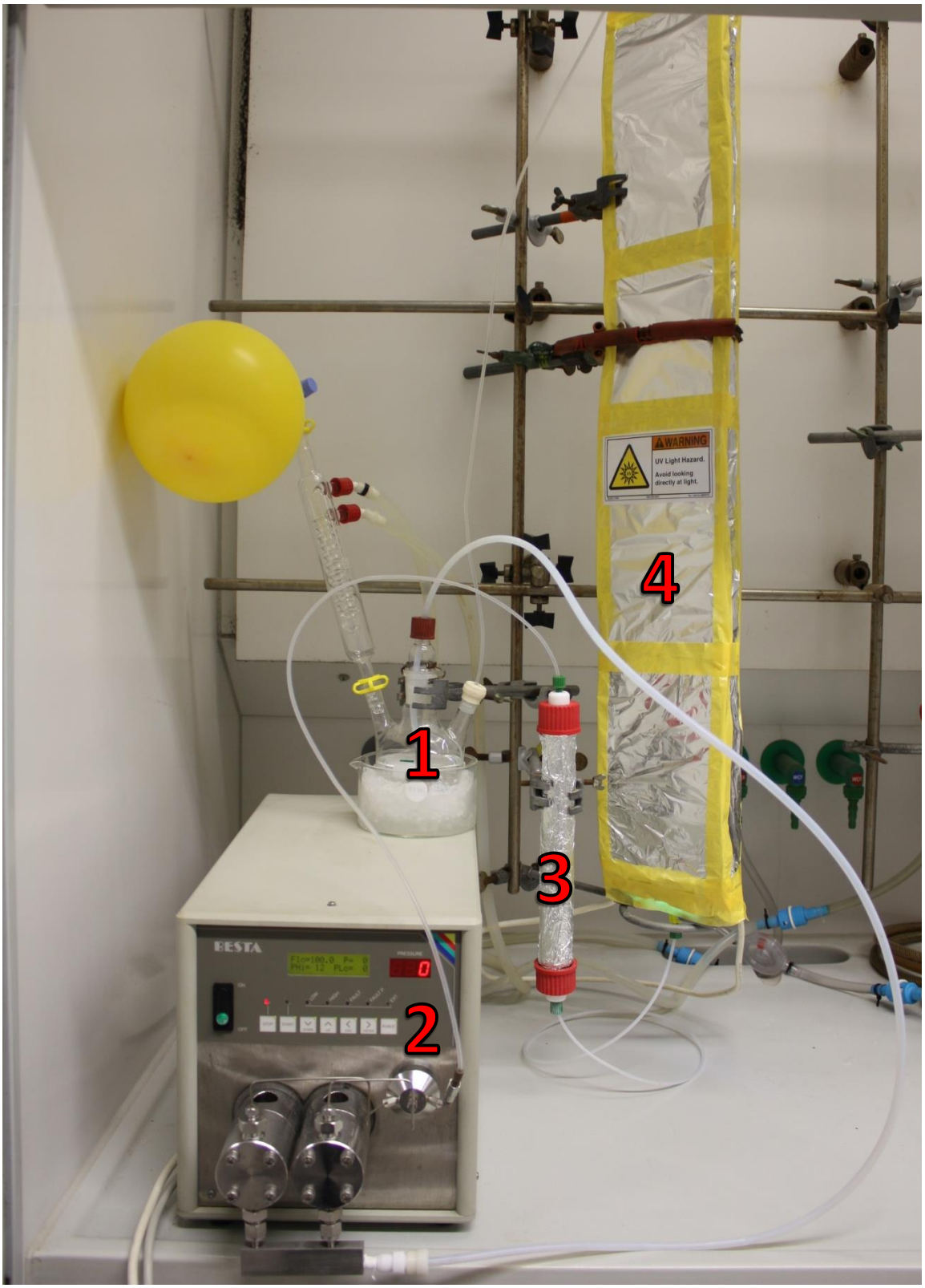

5 Curriculum Vitae

DENNIS SVATUNEK

Neustiftgasse 60/2
1070 Vienna Austria
0043 676 73 48 112
dennis.svatunek@tuwien.ac.at

EDUCATION

PhD studies **02.2013 - Present**
Vienna University of Technology
Doctoral program “Molecular and Elemental Imaging in Biosciences” (“MEIBIO”)
Supervision: Prof. Günther Allmaier, Co-supervision: Prof. Johannes Fröhlich

Marshall Plan Internship **08.2014 – 02.2015**
University of Delaware, USA, research group of Prof. Joseph M. Fox

"TUtheTop" **09.2012 - 06.2013**
High potential program of the Vienna University of Technology

MSc in Technical Chemistry – Synthesis **08.2011 - 01.2013**
Vienna University of Technology, passed with distinction
Diploma Thesis: Silylpropargylic Ethers as Protecting Groups for Carbohydrate Chemistry
Advisor: Prof. Johannes Fröhlich

BSc in Technical Chemistry **10.2007 - 08.2011**
Vienna University of Technology
Bachelor Thesis: Synthesis of Novel Diastereoselective Glucosyl Donors
Advisor: Prof. Johannes Fröhlich

HONORS & AWARDS

Young Scientists Best Paper Award **2016**
Monatshefte für Chemie/Chemical Monthly, Springer

Marshall Plan Fellowship **2014**
of the Austrian Marshall Plan Foundation

Diploma Thesis Award **2013**
of the Austrian Chemical Society

"Stiftungsstipendium der TU Wien" **2010 and 2013**
(scholarship of the foundation of the Vienna University of Technology) for excellence in studies

"Förderstipendium" **2012**
(supporting scholarship) of the Federal Ministry of Science and Research, Austria

"Leistungsstipendium" **2010 and 2012**
(merit scholarship) for excellence in studies of the Federal Ministry of Science and Research, Austria

PUBLICATIONS

M. Wang, D. Svatunek, K. Rohlfing, Y. Liu, H. Wang, B. Giglio, H. Yuan, Z. Wu, Z. Li, J. Fox
Conformationally Strained *trans*-Cyclooctene (sTCO) Enables the Rapid Construction of ^{18}F-PET Probes *via* Tetrazine Ligation
Theranostics, **2016**, 6, 887-895

D. Svatunek, C. Denk, V. Rosecker, B. Sohr, C. Hametner, G. Allmaier, J. Fröhlich, H. Mikula
Efficient low-cost preparation of *trans*-cyclooctenes using a simplified flow setup for photoisomerization
Monatsh Chem, **2016**, 147, 579–585

C. Denk, D. Svatunek, S. Mairinger, J. Stanek, T. Filip, D. Matscheko, J. Fröhlich, C. Kuntner, T. Wanek, H. Mikula
Design, Synthesis, and Evaluation of a Low-Molecular-Weight ^{11}C-Labeled Tetrazine for Pretargeted PET Imaging Applying Bioorthogonal *in Vivo* Click Chemistry
Bioconjugate Chem., **2016,** 27, 1707-1712

C. Denk, D. Svatunek, T. Filip, T. Wanek, D. Lumpi, J. Fröhlich, C. Kuntner, H. Mikula
Development of a ^{18}F-Labeled Tetrazine with Favorable Pharmacokinetics for Bioorthogonal PET Imaging
Angewandte Chemie International Edition, **2014**, 53, 9655-9659

H. Mikula, D. Svatunek, P. Skrinjar, E. Horkel, C. Hametner, J. Fröhlich
DFT study of the Lewis acid mediated synthesis of 3-acyltetramic acids
Journal of Molecular Modeling, **2014**, 20, 2181

H. Mikula, J. Weber, D. Svatunek, P. Skrinjar, G. Adam, R. Krska, C. Hametner, J. Fröhlich
Synthesis of Zearalenone-16-β,D-Glucoside and Zearalenone-16-Sulfate: A Tale of Protecting Resorcylic Acid Lactones for Regiocontrolled Conjugation
Beilstein Journal of Organic Chemistry, **2014**, 10, 1129-1134

H. Mikula, D. Svatunek, D. Lumpi, F. Glöcklhofer, C. Hametner, J. Fröhlich
Practical and Efficient Large-Scale Preparation of Dimethyldioxirane
Organic Process Research & Development, **2013**, 17, 313-316

ORAL CONTRIBUTIONS

D. Svatunek, H. Mikula, J. Fröhlich
Advanced synthesis of glycoconjugates and oligosaccharides
International Forum-Competition of Young Researches, Topical Issues of Rational Use of Natural Resources, 04/24/2013 - 04/26/2013, St. Petersburg, Russia

TEACHING/MENTORING EXPERIENCE

University Assistant **2014 - Present**
Vienna University of Technology, Institute of Applied Synthetic Chemistry, Austria
Main activities and responsibilities: Supervision of laboratory courses

Student assistant **10.2010 - 02.2013**
Vienna University of Technology, Institute of Applied Synthetic Chemistry, Austria
Main activities and responsibilities: Tutor in different laboratory courses

LANGUAGES

German - mother tongue
English - proficient user

PROFESSIONAL TRAINING

GÖCH Summerschool "1D- and 2D-NMR Spectroscopy in Liquids" **09.2012**
Niederöblarn, Austria

PROFESSIONAL MEMBERSHIPS

Austrian Chemical Society (GÖCH)

REFERENCES

Prof. Johannes Fröhlich
Vice rector for Research, Vienna University of Technology, Vienna, Austria

Prof. Joseph M. Fox
Department of Chemistry and Biochemistry, University of Delaware, Newark DE, USA

Dennis Svatunek
November 2016